AN INVESTIGATION OF THE WEAK LINKS IN THE SEISMIC LOAD PATH OF UNREINFORCED MASONRY BUILDINGS

Kevin Thomas Doherty
B.E. Hons (Civil) The University of Adelaide

A thesis submitted to the Faculty of Engineering at The University of Adelaide for the Degree of Doctor of Philosophy

Department of Civil and Environmental Engineering,
The University of Adelaide
AUSTRALIA

May 2000

Amendments To Thesis
'An Investigation of the Weak Links in the Seismic Load Path of Unreinforced Masonry Buildings'

A1 Replace on Page 53, Figure 4.2.1 the text 'Rigid Frame Fixed to Laboratory Strong Floor' with 'Stationary Reference Datum'.

A2 Insert the following regression coefficients to the figures indicated:

Figure 4.4.3 R = 0.999
Figure 4.4.4 R = 0.996
Figure 4.4.5 R = 0.997
Figure 4.4.6 R = 0.998
Figure 4.4.7 R = 0.999
Figure 4.4.8 R = 0.988

The regression coefficient R for the plots indicate a very good correlation of the test data with a straight line.

A3 Insert the following paragraph as a new second paragraph on page 106:
Under the assumption adopted of unreinforced masonry building systems having stiff shear wall and diaphragms the restrained translation of floors providing equal input motions at the base on top of wall specimens is appropriate. This is not the case however where floor diaphragms are flexible such as those constructed of timber. Where this is the case the response of the floor diaphragm may govern the wall response with possibly quite different inputs at the base and top of the wall. Here a different dynamic stability problem than that being investigated in the current research project may develop as it is possible that the walls will not crack at mid-height but will rock about their base after a crack forms at the base bed joint. Consequently these systems will have a much lower frequency than that of the individual wall panel.

A4 Insert the following paragraph as a new third paragraph on page 219:
The following points summarise the salient findings of the bending tests:

- Confirmation of mid-height cracking and dynamic stability problems
- Damping associated with the rocking walls was determined and generally found to be of the order of 5%. Rayleigh Damping was found to best approximate the damping by combining both stiffness and mass proportional damping components. Increases in damping where found at high and low frequencies.
- The force displacement relationship for URM walls cracked at mid height was assessed via push tests. Here the variation in the force displacement relationship with wall slenderness, boundary conditions, precompression and degradation due to rocking cycles where determined. A tri-linear approximation of the force displacement relationship was proposed to best approximate the true relationship with empirically derived points to define the initial stiffness and plateau for various levels of wall degradation.
- The effective resonant frequency associated with the frequency for maximum displacement amplification was determined for URM walls cracked at mid

height for various slenderness, boundary conditions, precompression and degradation due to rocking cycles.

- Both displacement and acceleration responses were recorded for walls subjected to transient, impulse and free vibration for later comparison with analytically derived response.

A5 Insert the following paragraph as the final paragraph on page 220:
Since the current research project has focussed on the one-way bending of unreinforced masonry walls to now take into account the two-way bending action which is often observed in seismic failure modes further research is required. Further as the assumption of the restrained translation of floors providing equal input motions at the base on top of wall specimens appropriate for unreinforced masonry building systems having stiff shear wall and diaphragms has been adopted further research is required to take into account flexible floor diaphragms and shear walls.

A6 Typographical errors:

page 9, line 14	replace 'earthquake' with 'earthquakes'
page 16, line 6	replace 'Masonry' with 'masonry'
page 43, line 3	replace 'Section 0' with 'Section 2.4'
page 47, line 8	replace 'Chapter 0' with 'Chapter 4'
page 49, line 11	replace 'f_{de}' with 'f_d'
page 51, title	replace 'Connection' with 'Connections'
page 221, 10th Citation	replace 'P.D.' with 'D.P.'
Throughout document	replace 'Nigel Priestly' with 'Nigel Priestley'

A7 Insert the following paragraph as the final paragraph on page 47.
Along with variations in local material properties the wide variety of test configurations discussed above may also be responsible for the wide scatter of reported results. In particular in-plane tests are seen to be particularly sensitive to variation in test configuration. Typically an average shear stress along the friction plane is used to determine the friction coefficient. Accordingly where three high brick prisms have been used for in plane testing the average shear stress and thus frictional coefficient determined may be significantly effected by the end conditions and the moment induced at the friction plane. By adopting wallets with multiple brick lengths the effect of the end conditions and the variation in normal stresses over the friction plane is reduced.

Insert the following paragraph as the final paragraph on page 54.
The results of the in plane tests presented in Figures 4.4.6 to 4.4.8 show a regression coefficient of near unity thus indicating a very good linear correlation. Although in plane tests are always difficult due to the nature of pure shear tests the good linear correlation indicates the assumption of a uniform shear stress for the derivation of the average friction coefficient is appropriate. In reality, due to the height of the lead weights a lever arm and thus overturning moment exists so that a triangular stress profile is likely. Here the increase in frictional resistance at the end subject to the increased vertical stress is offset by the decrease at the opposite

end. As a result the average frictional resistance is unaffected and thus the derivation of the average frictional resistance remains appropriate.

Due to the length of the four brick wallets any end effects are also not apparent in this test series.

A8 Add to Section 3.3.2 last paragraph on page 42: Expected differential movements associated with time dependant behaviour of URM walls including concrete shrinkage or clay masonry expansion are generally in the order of around 3mm per meter run of wall. This is dependant on many factors as has been briefly discussed.

Tests associated with the time dependant movement of URM connections containing DPC have recently been undertaken at the University of Newcastle, New South Wales, Australia. These tests have highlighted that under shrinkage creep the frictional resistance force appears to be less than under dynamic loading. Consequently, the connections have been observed to slip under the time dependant forces but are less likely to slip under dynamic loading.

A9 Insert the following paragraph as the final paragraph on page 49:
It is widely recognised that vertical accelerations associated with seismic loading may effectively reduce the gravitational force at the friction interface of DPC connections. As a result, the frictional resistance and thus the shear resistive capacity of the connection is also reduced. The SAA Masonry Code takes this reduction into account in the derivation of the frictional resistance in Equation 3.4.1 by the application of the 0.9 factor applied to the gravitiational force. The shear friction strength of the shear section under earthquake actions is thus defined by

$$V_{le} = 0.9\, G_g\, k_v$$

A10 Page 55, last paragraph replace 'Although these four specimen tests were carried out at only one value of vertical compressive stress (0.164MPa) both in-plane and out-of-plane shaking were examined so that a total of eight tests were undertaken.' With 'Since each of the four standard and centered connection specimen where tested at only one value of vertical compressive stress (0.164MPa) a total of eight tests were undertaken.'

Page 57, first paragraph replace 'The slip joint tests were performed over a range of three normal compression stresses being 0.04, 0.18 and 0.33 MPa conducted only in the in-plane direction.' With 'The slip joint tests were performed over a range of three normal compression stresses being 0.04, 0.18 and 0.33 MPa conducted both in the in-plane and out-of-plane directions.'

A11 It is noted that the term 'overburden' used throughout the document may be more commonly referred to as 'Pre-compression'.

A12 It is noted that in Section 6.3.1 the Characteristic bond strength should have been calculated taking into account the specimen size. Also the standard deviation

values reported being based on three tests are relatively meaningless however are provided as indicative for the quality of masonry.

A13 Page 115 second paragraph replace 'The brickwork modulus was then calculated for each specimen as the chord modulus between 5% and 33% of the ultimate brickwork compressive strength, f'_m.' with 'The brickwork modulus was then calculated for each specimen as the chord modulus associated with the linear portion of developed stress – strain curve.'

Page 115 last paragraph replace 'Table 6.3.2 presents a summary of the modulus test results ranging from 3,300 MPa to 16,000 MPa for the 110mm specimens and 6,700 MPa to 9,800 MPa for the 50mm specimens. While the results varied significantly the modulus values were typically found to be relatively high as expected of modern masonry.' With 'Table 6.3.2 presents a summary of the modulus test results ranging from 4,000 MPa to 10,000 MPa for the 110mm specimens and 5,000 MPa to 8,000 MPa for the 50mm specimens. It is suspected that the large apparent variation in the brickwork modulus is due to inconsistencies in the preparation of the five brick prisms. Here any slight eccentricity of construction causes non uniform loading of he prism so that the modulus calculation in some cases may have been slightly modified. The modulus results attained however are provided typically the results are quite high as would be expected of modern masonry.'

Replace Table 6.3.2 Brickwork Modulus Test Results with:

Table 6.3.2 Brickwork Modulus Test Results

Specimen No.	Specimen Thickness	Modulus E_m (MPa)	Ultimate Compressive Load (N)	Masonry Compressive Strength, f'_m (MPa)
1	110mm	-	330,000	13
2	110mm	10,000	332,000	13.1
3	110mm	5,000	336,000	13.3
4	110mm	4,000	333,000	13.1
5	110mm	9,000	360,000	14.2
6	110mm	-	338,000	13.4
7	110mm	9,000	313,000	12.4
8	110mm	5,400	245,000	9.7
11	110mm	8,000	359,000	14.2
12	110mm	11,000	397,000	15.7
13	110mm	-	397,000	15.7
AVERAGE	**110mm**	**7,700**	**339,000**	**13.4**
STANDARD DEVIATION		**2,500**	**41,528**	**1.64**
10	50mm	8,000	307,000	26.7
14	50mm	5,000	303,000	26.3
AVERAGE	**50mm**	**6,500**	**305,000**	**26.5**
STANDARD DEVIATION		**2,100**	**2,824**	**0.28**

TABLE OF CONTENTS

LIST OF FIGURES

LIST OF TABLES

ABSTRACT

A large proportion of domestic and low rise building stock in Australia is of unreinforced masonry (URM) construction and has not been designed to resist earthquake loads. Previous researchers have identified that under current Australian design conditions the two predominant weak links in the seismic load path for URM buildings are the shear connections between the walls and floor or roof and out-of-plane wall flexure.

This report documents the experimental and analytical research undertaken at The University of Adelaide aimed at providing the fundamental tools required to successfully avoid the identified brittle 'weak link' failures in the design of new and the assessment of existing URM buildings. This was achieved for the DPC connections through an extensive series of shaking table tests, which provided realistic data on the dynamic capacity of these connections. For the out-of-plane failure of walls in the upper stories of URM buildings, an extensive series of shaking table tests was used to develop a better understanding of the physical processes governing the collapse behaviour. Following this realistic analytical models were developed to provide accurate and reliable assessment of actual wall capacities. Since these were necessarily complex, a further refinement was undertaken to produce a more simplistic but rational analysis procedure for practical applications based on the 'Displacement-based' failure criteria.

DECLARATION

This thesis contains no material which has been accepted for the award of any other degree or diploma in any university or other tertiary institution and, to the best of my knowledge and belief, contains no material previously published or written by another person, except where due reference is made in the text.

I give consent to this copy of my thesis, when deposited in the University Library, being made available for loan or photocopying.

Kevin Thomas Doherty Date 24/5/00

ACKNOWLEDGMENT

I would firstly like to recognise the contributions made throughout the duration of this project by Associate Professor Mike Griffith of The University of Adelaide as his foresight and direction was largely responsible for the conception and success of this project. I am also indebted to my collaborative researchers, Dr. Nelson Lam and Dr. John Wilson of The University of Melbourne for valuable research meetings, ideas and discussions. I would also like to acknowledge the exceptional technical assistance provided by the Laboratory staff at the Chapman Structural Testing Laboratory at The University of Adelaide under the supervision of Mr. Greg Atkins.

Funding for this project was provided through an Australian Research Council grant as well as a University of Adelaide Postgraduate Scholarship Award for which I am appreciative.

I would also like to express my sincerest appreciation to my Mother and Father, Joan and Lindsay Doherty for their guidance and encouragement throughout both my under- and post-graduate careers. My Father, whom also being a structural engineer has spent many nights discussing with me issues related to structural and earthquake engineering providing me with motivation to succeed in my professional endeavors. Finally, I would like to acknowledge the contribution of my Fiancée Tammie. For her endless tolerance and support I am eternally indebted. The supports of these exceptional people have provided me with the inspiration and resolve to undertake this project for which I am extremely grateful.

1. INTRODUCTION

From the time of earliest civilisation, the use of masonry has provided a successful building technique. Examples of early stone masonry construction can be found dating as far back as c. 9000 BC in Israel and to the better known pyramids of Egypt constructed around c. 2800 – 2000 BC. Later, along with the emergent Roman Empire in around 700 BC, the use of masonry became widespread. Notable cities were established and developed throughout the colony comprising elaborate masonry palaces, churches, bridges and aqueducts. Over the centuries significant advancements have been made in the processes of masonry construction and to this day world cities have substantial building stock comprised of unreinforced masonry (URM).

The main characteristics of masonry that have enabled it to endure as a building medium through the ages are both the simplicity of laying stones or bricks on top of one another and the ready availability of materials and labour. Aesthetically, masonry is available in a vast array of colour and texture. Due to the small modular size of bricks and blocks it is also extremely versatile in application in that it can be used to form a great variety of shapes and sizes of walls, piers, arches, domes or chimneys. Furthermore masonry's exceptional fire resistance prompted Charles II to insist that all buildings built after the 1666 Great Fire of London be constructed of brick or stone. Durability, sound insulation and thermal mass are other advantageous characteristics of masonry construction.

In contrast, from its very foundation, the intrinsic drawback of masonry construction has been its poor seismic performance. While recent earthquakes have heightened modern awareness of this problem (Benuska 1990, Page 1990, Somers 1994, Pham 1995, Bruneau 1996, Spence 1999, Alcocer 1999, Pujol 1999) it is also evident that the problem existed even from the early days of the Roman Empire (Dobbins 1994). One remarkable example was the city of Pompeii. Located near the Bay of Naples in Italy, Pompeii,

having been incorporated as a Roman Colony in 80BC, had an estimated population of between 8,000 and 12,000 people. It is believed that the final years of the city were framed by two natural disasters. The first was a devastating earthquake in 62 AD which caused considerable damage to the city's masonry infrastructure requiring large scale rebuilding. The second, a cataclysmic eruption of Mount Versuvius 17 years later, destroyed Pompeii and the neighboring city of Herculaneum. The eruption of 79 AD is significant here as the resulting ash layer preserved much of the evidence of the earthquake damage that would have otherwise been obscured had Pompeii endured throughout antiquity. Figure 1.1.1 shows an ancient depiction taken from the house of Lucius Caecilius Iucundus of damage to the Temple of Jupiter and The Arch of Triumph at Pompeii during the 62 AD earthquake.

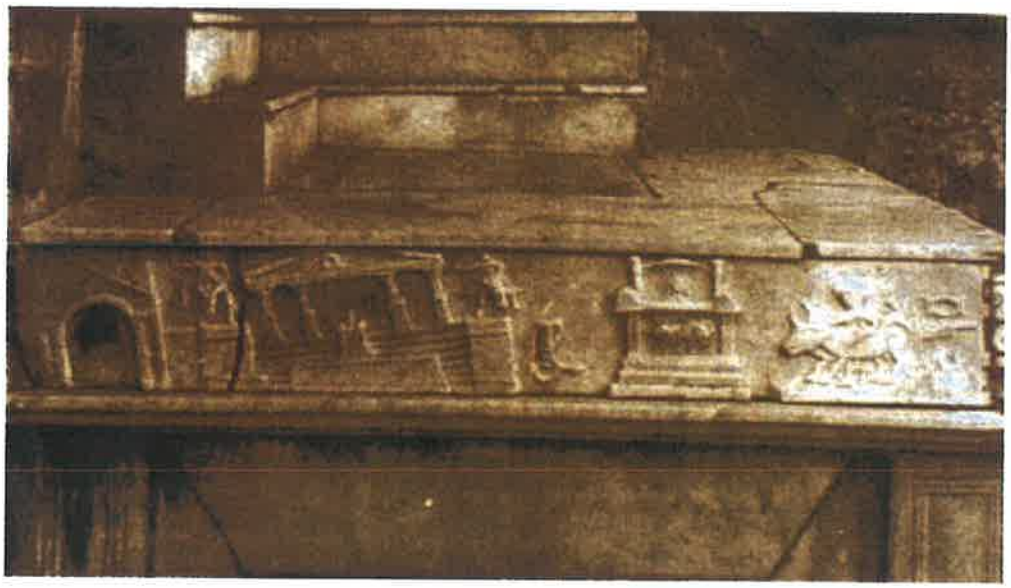

Figure 1.1.1 Depiction of Damage During the 62 AD Earthquake in Pompeii
(Kozak Collection, Earthquake Engineering Research Center, University of California, Berkeley)

Unlike modern steel and reinforced concrete construction it is clear that the development of masonry construction followed a different path. Throughout history, forms of structural masonry passed from generation to generation and evolved from trial and error as opposed to that of specialised research. As a consequence, methods have tended to be less sophisticated and more empirically based with generally little if any consideration

given to seismic action until comparatively recently. These buildings have thus tended to be at greater seismic risk than comparable new buildings. This is not only because they have not been designed for seismic loading requirements but also because they are less capable of dissipating energy through large inelastic deformations during an earthquake. Historically this has resulted in an abundance of seismically induced catastrophic masonry failures often with a high loss of life. For example 50 years ago it was customary to support floors on stone or masonry corbels. During an earthquake the floor and walls would vibrate typically eventuating in the floor slipping from the corbel and collapsing dramatically.

In response to the observed damage to un-engineered or poorly constructed buildings, public prejudice developed against the use of structural URM. A consequence has been its disappearance from modern construction in regions of high seismicity with a respective increase in the popularity of steel and concrete construction. Owing to this shift in focus comparatively little research has been undertaken on the ultimate dynamic behaviour of URM construction.

Although the performance of URM buildings when subjected to earthquake excitation has typically been poor there is also significant evidence suggesting that these buildings do not necessarily perform poorly in areas of low to moderate seismicity (Scrivener 1993, Tomazevic and Weiss 1994, Abrams 1995). This was highlighted in 1989 in Australia by the M_L5.6 Newcastle earthquake. Here it was reported (Melchers 1990, Griffith 1991, Page 1992, Murphy 1993) that while older masonry buildings, typically in poor condition and not having been designed with any consideration to lateral loading, suffered significant damage, many other masonry buildings performed well suffering only minor or no damage at all. These findings have placed an increased pressure on engineers in regions of low to moderate seismicity to continue taking advantage of the significant beneficial characteristics of masonry construction by designing and detailing URM buildings to perform adequately during an earthquake.

The current URM research focus is therefore twofold. Firstly, there is a need to rationalise the design of new URM buildings for regions of low to moderate seismicity. This involves the identification of weaknesses in masonry construction practices and correlating these to observed catastrophic failures. Consequent development and implementation of design guidelines would then prevent future occurrences of similar brittle failures occurring in newly designed structures.

Secondly, there is a need to assess the seismic vulnerability of the large numbers of URM building stock of unknown quality and condition in cities around the world. These structures were generally constructed prior to mandatory earthquake design requirements and due to the sporadic nature of earthquake loading many remain untested against seismic action. Earthquakes have repeatedly impressed the need to review the seismic adequacy of existing masonry buildings. As a recent example historically significant structures in Italy, having stood for hundreds of years, have failed dramatically under seismic loading. These failures clearly illustrate the potential risk in assuming age-old structures will last forever and the possible physical and social consequence of inaction. With these constant reminders owners are now recognising that they must reconcile the potential for structural retrofitting with the level of seismic risk.

The distinction is drawn between the development of analysis and design procedures for new and existing buildings since for the design of a new building a certain degree of conservatism may impose only a minor economic penalty. In contrast, the same degree of conservatism for the review of an existing structure may impose substantial economic penalty and hence cross the line of being economically viable to seismically retrofit. Should the imposed economic penalty be deemed too great historically or socially significant structures could be lost.

The research challenge therefore lay in establishing a better understanding of the physical processes governing the collapse behaviour thus permitting the development of realistic, accurate assessment methodologies for the determination of the dynamic capacity of URM buildings and their constituent components.

1.1. Study Objectives and Key Outcomes

The specific focus of the current research project was an investigation of the brittle 'weak links' in the seismic load path for Australian URM buildings under earthquake loading. As is discussed in more detail in Chapter (2) the 'weak links' are evident through the review of damage surveillance documentation and have been confirmed through an analytical study (Klopp 1998) as:

(1) The limited force capacity of connections between floors and walls, in particular the friction dependent connections containing damp proof course (DPC) membranes and

(2) *the out-of-plane failure of walls in the upper stories of URM buildings.*

The primary intention of the current project was therefore to provide the fundamental tools required to successfully avoid the identified brittle 'weak link' failures in the design of new and the assessment of existing URM buildings. This was achieved for the DPC connections through an extensive series of shaking table tests, which provided realistic data on the dynamic capacity of these connections. For the out-of-plane failure of walls in the upper stories of URM buildings, an extensive series of shaking table tests was used to develop a better understanding of the physical processes governing the collapse behaviour. Following this realistic analytical models were developed to provide accurate and reliable assessment of actual wall capacities. Since these were necessarily complex, a further refinement was undertaken to produce a more simplistic but rational analysis procedure for practical applications. To encourage the ready introduction and acceptance into the real design environment, where optimisation of design output is often the driving force, it was necessary that the simplified procedure be formulated through easily understood and familiar concepts while still encompassing the essential ingredients of the dynamic behaviour.

Since a building's structural capacity is related to its weakest link, by avoiding the identified brittle 'weak link' failure modes the overall effective structural capacity and thus seismic performance will improve. An additional benefit is that with a better

understanding of the physical process governing the dynamic collapse behaviour, designers will more readily be able to adopt the desirable 'Capacity' type design approach discussed further in Chapter (2). Where this enables more ductile failure modes to be activated, the structure's effective capacity and energy dissipating characteristics will be further enhanced.

Although specifically related to Australian construction practices and conditions, it is expected that these research outcomes are sufficiently general so that they will be easily extrapolated to other regions of similar seismicity and construction techniques.

1.2. Brief Outline of Report

To set the overall scene a general overview of earthquakes and URM is presented in Chapter (2) where the basic aspects of seismicity and URM performance, both internationally and in Australia are covered. Following this, a brief review of the development of seismic design criteria and URM construction practices in Australia are presented as these dictate the standard of the existing URM building stock. This includes the results of a survey performed as part of the current research project to catalogue typical URM wall connections and levels of applied overburden stress based on Australian masonry construction. A review of the vulnerability of URM failure modes from reconnaissance documentation is then presented to confirm the typical weak link URM failure patterns in areas of moderate intensity shaking.

Chapters (3) and (4) are devoted to the shear capacity of URM connections containing DPC membranes being, the first of the previously identified weak links. Chapter (3) commences with a general description of connections containing DPC membranes. A specific literature survey covering previous experimental and related work is then presented. Chapter (3) concludes with the specific research requirement to be undertaken within the scope of this project being the experimental determination of dynamic friction data for DPC connections typically used in Australian masonry construction.

Chapter (4) presents the results of a series of dynamic friction tests for DPC connections. Here the experimentally determined dynamic friction coefficients are compared with static test results (Page 1995, Griffith et al 1998) for connections of the same configuration and concludes with recommendations on the suitability of current codified friction coefficients.

Chapters (5) to (8) are devoted to the out-of-plane failure of walls in the upper stories of URM buildings being the second of the weak links to be investigated. This is specifically related to the dynamic stability of simply supported URM walls subjected to transient out-of-plane forces.

Chapter (5) introduces the physical considerations that must be assessed for out-of-plane analysis including boundary conditions and dynamic stabilising effects. Following this a specific literature review is presented which highlights key aspects of previous related experimental and analytical work. Further to the literature review a critical assessment of currently available analysis and design methodologies for face-loaded URM walls under one-way bending action subjected to transient excitations is presented. Here it is found that the existing methods have serious limitations for the realistic prediction of the ultimate dynamic wall capacity.

In Chapter (6) the key results of an extensive series of static push and shaking table tests on simply supported face loaded URM walls are presented. Here the results of static, impulse and free vibration tests are used to examine the non-linear force-displacement (F-Δ), frequency-displacement (f-Δ) and damping characteristics of URM walls. Harmonic and transient excitations are also used to examine the dynamic response at various excitation frequency and amplitude content and for later confirmation of the comprehensive analytical model.

Chapter (7) describes the development of a comprehensive analytical model for the semi-rigid rocking response of post cracked URM walls subjected to out-of-plane forces. The computer software ROWMANRY, developed as part of the current research project to

the highly non-linear time-history analysis (THA), is also presented. Results of experimental work as described in Chapter (6) are then used to calibrate and confirm the accuracy of the analytical results.

In Chapter (8) a rational simplistic displacement-based (DB) analysis procedure is presented for the prediction of the ultimate capacity of face loaded URM walls. A brief description of the displacement-based design methodology is provided and followed by key aspects as it is applied to rocking URM walls. In order to confirm the effectiveness of the linearised DB analysis, comparisons with experimental and comprehensive THA results are presented. Similar comparisons are also made with currently available ultimate analysis methodologies where it is concluded that the linearised DB methodology provides the most effective estimate of ultimate wall capacity.

Chapter (9) summarises the results of the study, highlighting key outcomes, design recommendations and future research requirements.

2. EARTHQUAKES AND UNREINFORCED MASONRY

2.1. Introduction

Earthquakes pose a substantial threat to life with an average fatality rate this century of around 10,000 deaths per year (McCue 1992). Damage to unreinforced masonry (URM) buildings and elements is a ubiquitous aspect of many earthquakes and as such URM has a poor seismic performance record throughout the world. It has been reported (Scrivener 1993), however, that the poor overall public perception of URM can generally be attributed to media reports not mentioning typical causes of the failures such as:

- buildings not designed to any engineering code, let alone an earthquake code;
- poorly constructed of adobe, mud brick or weak clay bricks with weak mortar of mud or earth or with insufficient cement; and
- un-connected structural elements often with heavy roofs

In many instances the damage level has been enormous with masonry littering streets and in larger earthquakes the complete collapse of URM buildings. This severe damage has often been responsible for a non-commensurable loss of life and injury during earthquake, which is both unacceptable and unnecessary. The spectacular nature of the damage has therefore tended to obscure the satisfactory performance of many other URM buildings in earthquakes. This is supported by research (Griffith 1991, Page 1992, Schrivener 1993, Tomazevic and Weiss 1994, Abrams 1995) indicating that URM buildings can satisfactorily withstand moderate levels of ground shaking if designed, detailed and constructed with consideration to seismic loading.

This Chapter provides a general overview of the seismicity, URM construction and seismic performance in Australia. Aspects which are applicable for Australian conditions are clarified and vulnerable weak links in URM buildings designed to current practices

are identified. To quantify the performance of URM buildings in areas of moderate seismicity, a summary of observed damage patterns for Australian and relevant international earthquakes is presented. This section concludes with the specific research focus to be addressed within the scope of this report.

2.2. Australian Seismicity

While it is possible for an earthquake to occur at any location their occurrence frequency is unevenly distributed over the earth. The majority of earthquakes are found to occur along relatively narrow continuous belts at the convergent boundaries of the major crustal plates. Here, inter-plate earthquakes contribute more than 90% of the earth's release of seismic energy (Bolt 1996) with the remaining released as interior or intra-plate type events. Further, approximately 75% of the total energy release is believed to occur along the edges of the Pacific ocean, where the thinner Pacific plate is being forced beneath the thicker continental crust (BGS 1999). This is demonstrated in active inter-plate regions such as Japan, California or Papua New Guinea where the major plates interact at velocities of up to 100 mm/year. As a consequence, it can take only tens to hundreds of years for sufficient strain energy to build culminating in the release of a large magnitude earthquake. In contrast, for an intra-plate region it may take hundreds of thousands of years for similar levels of compressive stress and strain energy to develop. Thus, due to the paucity of records this type of event is far more difficult to forecast.

The long return period of major earthquakes and the absence of interim perceptible seismic activity in intra-plate regions has led to these areas being referred to as being of low seismicity or low seismic risk. A common misconception follows that this infers weak ground motion while the reality is that strong ground motion can still occur but less frequently. In probabilistic terms there is a much reduced likelihood of intra-plate strong ground motion occurring at a particular time and place than inter-plate. This aspect substantially impacts on building code provisions where the design basis event is prescribed in probabilistic terms, rather than on maximum earthquake potential. Thus for

intra-plate regions the design event magnitude will be smaller than for inter-plate regions (Somerville et al 1998).

The earliest earthquake reported in Australia was in June 1788 at Port Jackson (Sydney) where the First Fleet settlers were shaken by a strong local earthquake lasting for not more than two or three seconds. Since this time small earthquakes have been reported under most of the major Australian cities (AGSO 1999).

The Australian continent lies wholly within the Indo-Australian tectonic plate (refer Figure 2.2.1) and as such is only subjected to intra-plate earthquakes. The closest Australian city to an active plate boundary is Darwin, which is regularly but lightly shaken by earthquakes along the subducting Java Trench in the Banda Sea.

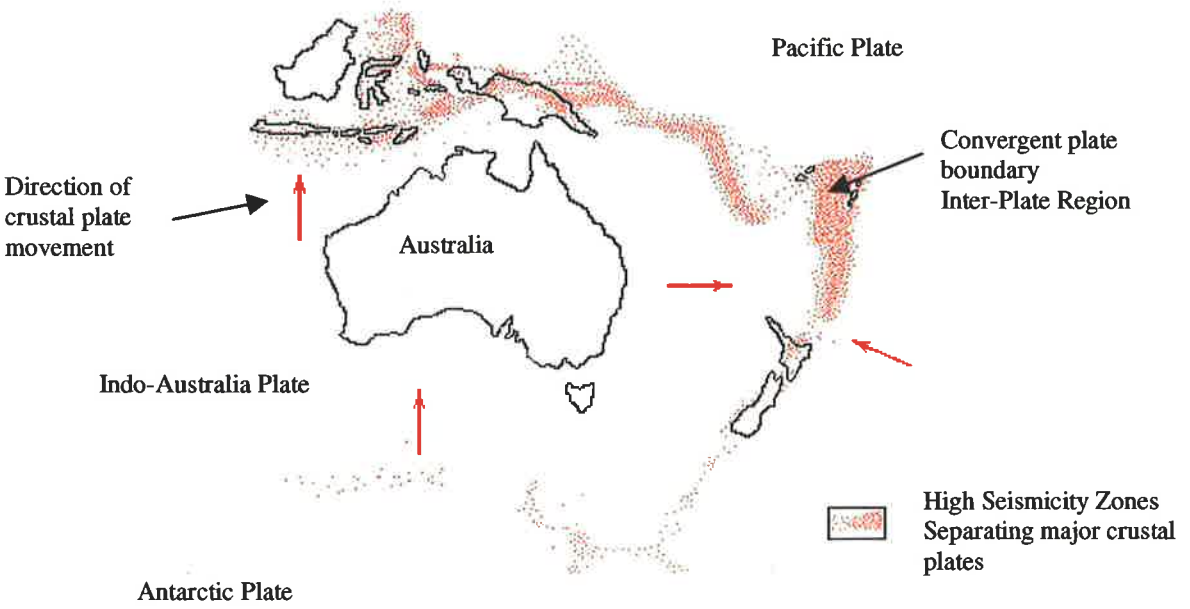

Figure 2.2.1 Australia's Tectonic Location

Since earthquakes only occur in the earth's outer crust where rocks are cold enough to be brittle, in Australia, earthquakes typically only occur to a depth of around 20km (Gibson

1990). This limitation constrains the vertical fault dimension so that for the release of a large amount of strain energy the rupture would need to be very long. By practically limiting the fault length to around 100km the maximum magnitude of earthquake that could be realistically expected in Australia is around M_S 7.5. This assumption is supported by studies of prehistoric Australian fault scarps where no scarp longer than 45km has yet been found (Denham 1992). It is therefore not unreasonable to argue that a maximum credible earthquake of this magnitude be adopted for earthquake risk in Australia.

Over the relatively short-recorded seismic history in Australia the largest known earthquake occurred in 1906 off of the Northwest Coast of the continent with an estimated magnitude of 7.2. On land the 1941 Meeberrie earthquake, which was felt over most of Western Australia, appears to have been the largest having a magnitude of approximately 7 (Denham 1992).

In 1968 a magnitude 6.9 earthquake devastated the Western Australian agricultural township of Meckering. Here although no people died, 85 dwellings were severely damaged being predominantly of unreinforced masonry construction. Later, in 1954, Adelaide was subjected to a damaging magnitude 5.5 earthquake. Here again there were no fatalities however over 30,000 dwellings sustained damage (Irish 1992) costing at the time in excess of 4 million pounds or $91m in 1995 dollars (AGSO 1999). More recently, in 1988, a magnitude 6.8 earthquake having a 35km fault length and maximum surface displacement of 2.0m (AGSO 1999) struck Tennant Creek in the Northern Territory of Australia. Fortunately due to the remoteness of the area there was only moderate damage caused.

By far the most devastating and expensive, although not the largest seismic event in Australia's brief recorded history, was the 1989 Newcastle earthquake. Despite by world standards being only a moderate magnitude 5.6 the earthquake caused massive damage to both property and infrastructure with damage estimates of over a billion dollars at the time of the earthquake (Melchers 1990, Blong 1992). It is also the only earthquake in

recorded Australian history to have been responsible for the loss of life with thirteen people killed and over one hundred injured. Furthermore, it was only the fortunate timing of the event that saved many more from being killed or injured (Melchers 1990).

Attributed to the vastness of the Australian continent it has been fortunate that previous large magnitude Australian earthquakes have occurred far from populated centers causing only relatively low-level property damage. With an ever-increasing population density and aging building stock the potential for earthquake disaster in Australia is becoming a far greater threat to our society so that earthquake hazard must now be fully considered in risk assessment scenarios. To further place the seismic risk of Australian cities into perspective it has been reported (Blong 1993) that a design magnitude event, i.e. a 500 year return period earthquake, in Melbourne or Sydney could result in more than 500 deaths and $8 billion dollars worth of damage to domestic construction alone.

2.3. URM Building Stock in Australia

Due to Australia's modest level of seismicity and the many advantageous characteristics of masonry, the use of URM as a building medium in Australia has been widely embraced. The majority of Australian URM building stock is of either domestic or commercial low-rise construction although some taller buildings, up to 5 stories, have been constructed. For housing, masonry is often used as a veneer although with older homes in the Western states cavity wall construction is more prevalent. Single skin grouted or partially grouted masonry is also popular in the north of Australia (Page 1995). With a large proportion of URM building stock comprising single occupancy housing, multiple occupancy residence (three to four storey 'walk up' flats) and low rise commercial buildings, URM is prevalent in the inner suburban areas of Australian cities. In these areas the population densities are often the highest and combined with the relative older age of the URM building stock the potential seismic vulnerability of these areas is appreciable.

The historical development and implementation of the Australian Earthquake Loading Code provides an insight into the current thinking in Australia on the seismic vulnerability of existing URM building stock. As highlighted in Section 2.2, even though there had been a number of Australian earthquakes greater in magnitude 5.0, the first Australian Earthquake Code, AS2121, was not published until 1979 as a response to the 1968 Meckering earthquake. Due to the lack of prior Australian strong ground motion and research, this standard was based largely on requirements in the 1977 Structural Engineers Association of California (SEAOC) Code and the 1976 Uniform Building Code (UBC). After its release AS2121 was seldom used and with the seismic zone map having most of the country located in 'zone 0', which did not require seismic loading to be considered, very few buildings were designed for earthquake loading. In fact, only the South Australian and Commonwealth Governments actually used the code and in some states with seismic design requirements these were ignored as they were not gazetted by state authorities. It is possible that the misconception that design for wind also provided for earthquakes led to this oversight.

With an increased understanding of earthquakes, AS2121 was due for revision in 1989 when the Newcastle earthquake struck giving impetus and point to the deliberation. The revised standard was again adapted from codes developed by Ameerican institutions such as the Applied Technology Council (ATC), The National Hazard Reduction Program (NEHRP) and SEAOC before being incorporated into the Australian Loading Code in 1993 as the SAA Earthquake Loading Code, AS1170.4-1993. This, the current standard, ensures that for every building constructed in Australia a minimum consideration is given to seismic loading. The level required varies in sophistication from simple detailing to comprehensive dynamic analysis depending on structural category and regularity. For masonry the general detailing provisions are referenced from the respective material standard being the SAA Masonry Code, AS3700-1998. As a consequence of the recent development of earthquake codes almost all of Australia's existing URM building stock was constructed in the absence of mandatory earthquake design requirements.

Unlike other popular methods, masonry construction is labour intensive in nature and consequently quality is particularly sensitive to workmanship. Paradoxically, unlike more modern construction methods, masonry is often not subjected to a high degree of quality control due largely to its traditional background. For these reasons finished product quality has been highly variable and is often not indicative of the designer's assumptions.

For URM buildings having relatively low levels of overburden stress a critical property of masonry is the bond between brick units and mortar known as the flexural tensile strength. This is also possibly the most variable and sensitive property to workmanship with variations of 30% to 35% found to be not unusual. The factors influencing bond strength have been well-documented (Taylor-Firth 1990, Van den Boon 1994, DeVitis 1995, Lawrence 1995, Page 1998) and include the suction of the masonry units, the water retention of the mortar, the mortar ingredients, the use of additives and the method of laying.

A recent study (Nawar 1994) which documented current masonry construction practices on building sites in Sydney identified large gaps between the designers intent and actual practices. Here it was found that over 50% of the sites inspected had serious omissions capable of compromising the long-term performance of the masonry. In a second study (Zsembery 1995) the measurement of flexural bond strength at 19 sites in the Melbourne area was undertaken where a significant variation in the results was also found.

The 1989 Newcastle earthquake highlighted the vulnerability of non seismically designed buildings with a significant proportion of the damage attributed to the lack of consideration to earthquake loading and inadequate standards of URM design, detailing and construction (Melchers 1990, Page 1992). An additional finding was that the real masonry quality was much lower than would have been expected (Page 1992). In many cases damage surveillance reported that in what appeared to be sound outer masonry skins, problems such as inadequately filled bed and perpend joints and inadequate tying or support of one or both of the skins was evident. In older structures poor maintenance and wall tie corrosion also played a significant role in exacerbating the damage. The

presence of weak lime mortars is also thought to have been responsible for a high proportion of the billion dollars worth of damage during the Newcastle earthquake. It followed that the resistance of the effectively pre-cracked URM walls was left to rely solely on stabilising gravity effects.

While deficiencies associated with poor workmanship and maintenance are the responsibility of the Masonry industry as a whole, their existence and consequent influence on structural durability and ductility must be recognised. As the Newcastle situation is not unique in Australia it must be assumed that the same scenario of non-seismically designed buildings in poorly maintained condition, constructed of poor quality materials and concentrated in inner suburban areas where population densities are greatest exist in other Australian cities.

In recognition of the need to strengthen existing buildings with an assessed inadequate seismic resistance the voluntary code 'Strengthening of Existing Buildings for Earthquakes', AS3826-1998, has recently been released in Australia. This requires the designer to consider the same philosophical approach as AS1170.4-1993 by establishing clear load paths for the transmission of vertical and lateral loads. Many existing masonry structures would be economically infeasible to upgrade to a capacity able to withstand the full loads specified in AS1170.4-1993. AS3826-1998 therefore specifies lower threshold values for retrofitting structures based on the buildings use classification being either 33% or 66% of the full AS1170.4-1993 specified loads. In the absence of realistic dynamic analysis methodologies the rationale here is that with the long return period of large magnitude earthquakes, a greater degree of risk is acceptable in existing buildings than that allowed in the design and construction of new buildings.

In the ideal situation structural engineers retained to investigate the seismic resistance of a URM building would have at their disposal tools enabling them to prepare a realistic, neither unduly conservative nor permissive, statement of the seismic resistive capacity of both structural and architectural components. Since the traditional design methodologies inherently provide conservative assessment of the seismic vulnerability of a URM

building, adoption of these techniques may lead to the possibility of incorrectly labeling a seismically adequate building as unsafe. In contrast overestimating the dynamic capacity of elements to resist damaging cycles of seismic excitation could lead to a false and dangerous sense of security. In this context, the benefit of developing better tools to accurately determine the seismic resistance capacity of URM buildings and components is apparent.

The first stage of the current research project was to survey and catalogue URM connection details and overburden stress levels typical of Australian masonry construction. Figures 2.3.1 to 2.3.5 show construction drawings of the most predominantly used URM connections.

Figure 2.3.1 shows a 'cornice' type connection frequently used for internal non-loadbearing URM partition walls. Often return walls are not incorporated into the internal partition walls so that one-way bending predominates. Since the cornice connection provides only horizontal restraint, the wall acts as a propped cantilever under face loading.

Figure 2.3.2 and Figure 2.3.3 show common connection details used in cavity wall construction. Where both brick leaves are laid on flat, the roof truss is typically supported on the internal loadbearing leaf using a 'wooden top plate'. Alternatively, often for economy of material use, the external leaf is laid brick on flat but the internal leaf is brick on edge. In this case the internal leaf is unsuitable for roof support and the roof truss is supported on the outer loadbearing leaf. For either case nails or masonry anchors are used to fix the top plate to the URM wall providing a positive connection to resist horizontal shearing forces. Light gauge steel trusses and wall plates are now also used as an alternative to timber. To resist wind uplift a galvanised strap is typically detailed being fixed to the roof truss and hooked around a support bar in the wall approximately 1.2m below the top (Figure 2.3.3).

Connections shown in Figure 2.3.4 and Figure 2.3.5 are often used between concrete slab and loadbearing masonry elements. As will be discussed in Chapter 3, this type of connection is typically detailed to meet serviceability design criteria.

Since, in general, only one wall leaf of cavity wall construction is loadbearing with the other supporting only its own weight, the loadbearing leaf has a superior lateral strength. Both URM wall leaves are connected via wall ties. The stiffer loadbearing wall therefore must carry the combined inertia load from the dynamic response of both of the URM wall leaves. Past earthquakes, in particular the Newcastle earthquake (Page 1992), have demonstrated that wall ties can corrode thus becoming ineffective or that they may pull out from deteriorated weak lime mortar under lateral loading. This often leads to the weaker non-loadbearing outer leaf acting as an individual element being extremely vulnerable to earthquake damage with a peeling off of the outer leaf commonly reported.

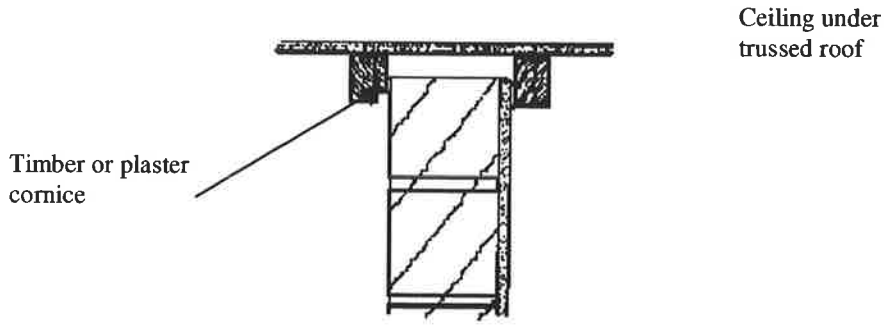

Figure 2.3.1 Internal Partition Wall 'Cornice' Connection Detail

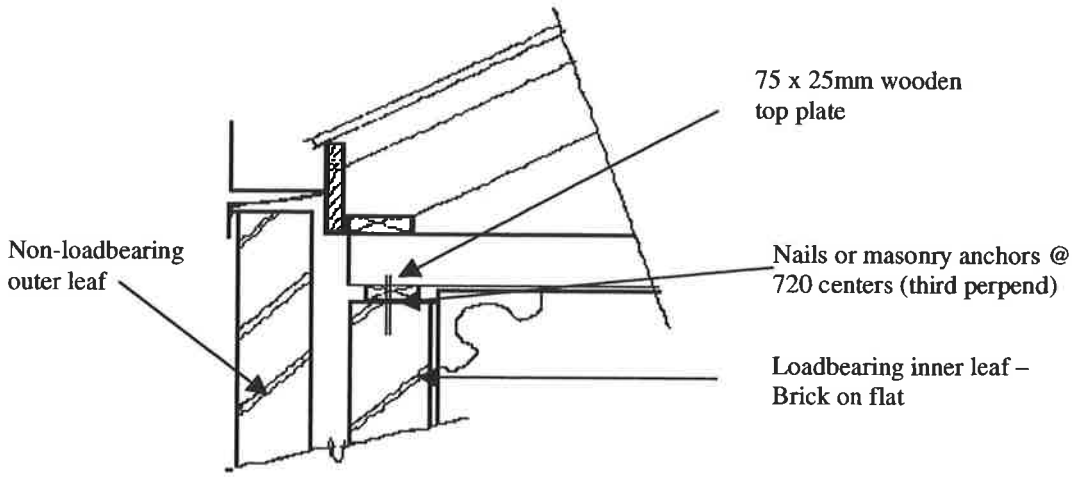

Figure 2.3.2 URM Cavity Wall to Roof Truss Connection Detail (Inner Loadbearing)

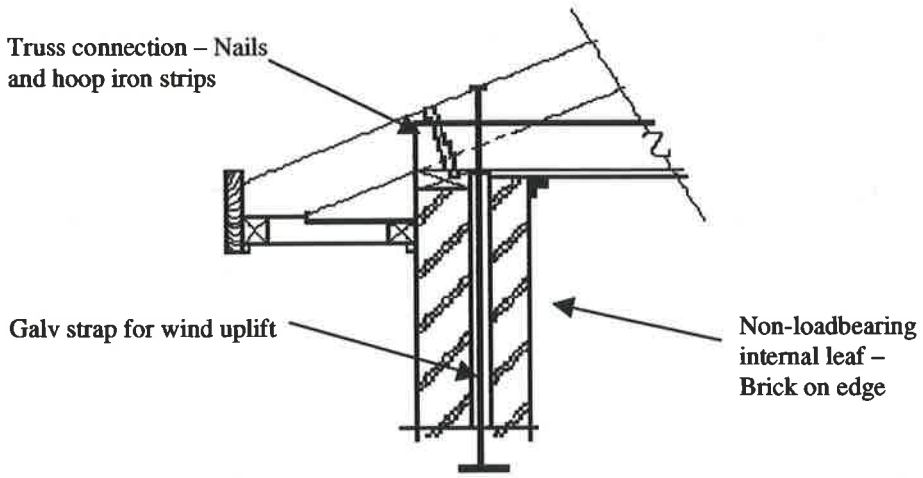

Figure 2.3.3 URM Cavity Wall to Roof Truss Connection Detail (Outer Loadbearing)

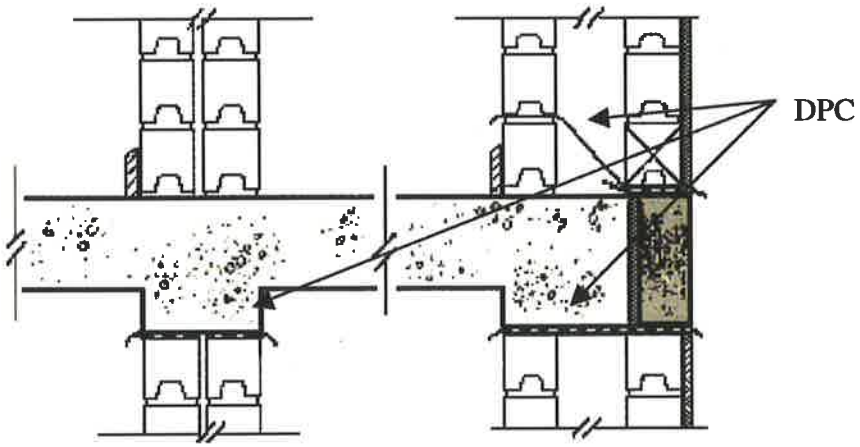

Figure 2.3.4 URM Wall to Inter Story Floor Slab DPC Connection Detail

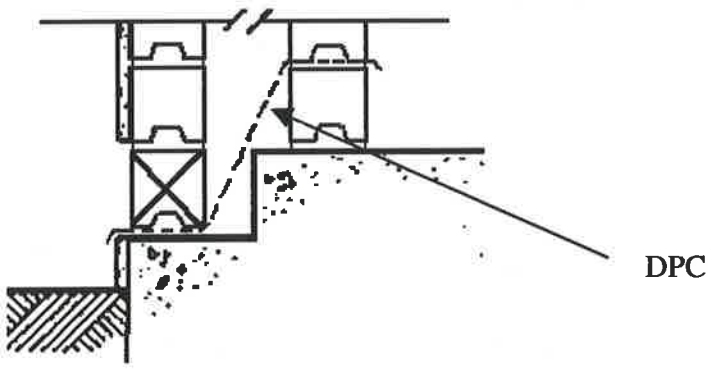

Figure 2.3.5 URM Wall to Ground Floor Slab DPC Connection Detail

A second outcome of this survey was the determination of typical levels of overburden stress in Australia. This involved the analysis of numerous existing two to four story tall URM buildings. Structural configurations included cavity and veneer URM construction, concrete slab and timber floor diaphragms and both light gauge galvanised and heavy tiled roof diaphragms. The conclusion of this survey was that overburden stress typically ranged from 0.4MPa in the lower stories reducing to less than 0.1MPa in the upper stories.

2.4. URM Vulnerability in Moderate Seismicity Regions

2.4.1. Failure Modes of URM Elements (Related to Seismic Load Path)

While the earthquake ground motion itself does not constitute a direct threat to life safety the subsequent failure of man made structures does. During an earthquake a building is subjected to a series of random ground displacements. As the structure reacts to these displacements inertial forces are induced. The structural response to these inertia forces is dependent on the natural frequencies and inherent damping of the building, and its components, which themselves are dependent on the structural mass and stiffness.

To assist in illustrating elemental failure modes within a URM building it is pertinent to describe the path that seismic input energy follows (Priestly 1985, Bruneau 1994, Calvi et al 1996) as is shown in Figure 2.4.1. When subjected to seismic ground motion, the foundation transmits seismic energy to the stiffest elements of the URM building being the in-plane structural walls. The response of the shear walls, which itself is dependent on height, stiffness and overburden stress excite the floor diaphragm, through the wall to floor connection, with a motion that has now been filtered by the shear wall. Following this the floor diaphragm response excites the out-of-plane walls, through the wall to floor connection, such that its dynamic characteristics directly influence the severity of the out-of-plane wall excitation. The input excitation at the top of the face-loaded walls need therefore not necessarily be in phase or even of the same magnitude as the bottom.

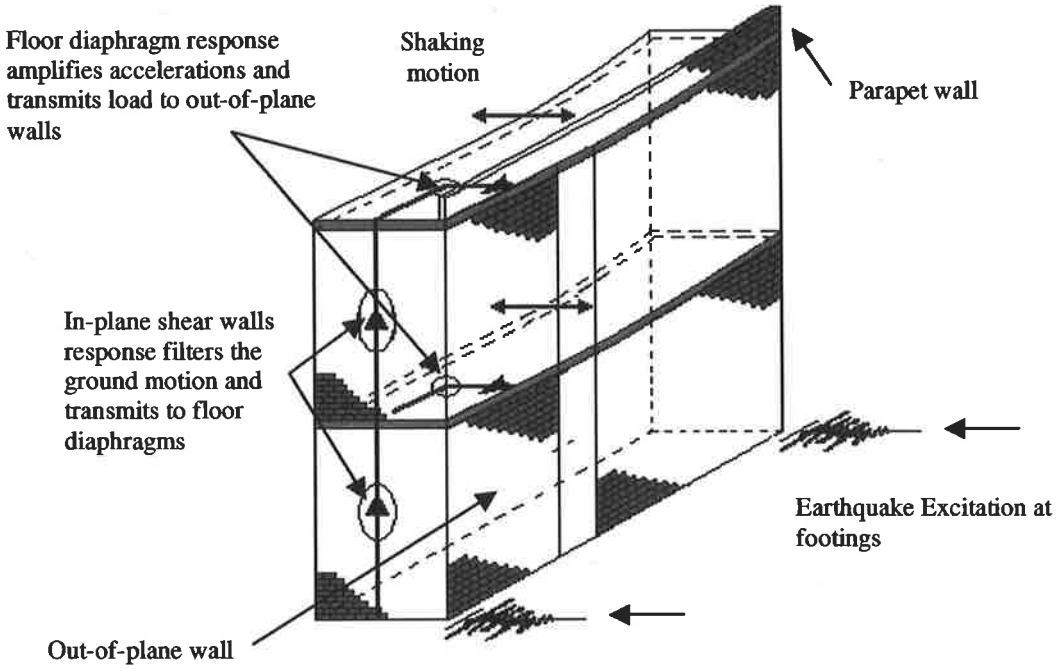

Figure 2.4.1 Seismic Load Path for Unreinforced Masonry Building

2.4.2. Review of the Seismic Performance of URM Buildings

As has been discussed in Section 2.2 the most damaging and therefore relevant earthquake in Australia's recorded history was the 1989 Newcastle earthquake, M_L 5.6. The earthquake intensity in outer Newcastle has been assessed at MM6.0±0.5 (McCue 1990, Melchers 1990) while for inner Newcastle areas the general level of damage was consistent with an intensity of MM7.0±0.5. Mean soft soil amplification factors of 3±1 are therefore considered indicative for the inner areas of Newcastle.

In reviewing damage patterns in Newcastle (Bubb 1990, Donaldson 1990, Loke 1990, Pederson 1990, Melchers 1990, Jordan et al 1990, Page 1990:1992, Griffith 1991, Welhelm 1998) it is apparent that timber housing performed best followed by brick veneer construction and that cavity brick construction was worst affected. It is noted however that the latter mainly consisted of older buildings, many at least 60 years old, and with significant structural deterioration. With few exceptions modern buildings

performed better with damage confined to masonry cladding and infill. The nature of the damage can be summarised as:

- extensive cracking and deterioration of walls due to in-plane racking
- tilting of walls under transverse forces including sliding at damp proof courses
- partial loss of roof support by sliding from support walls
- cracking of walls in flexure under the action of transverse forces
- loss of end walls under transverse forces due to corroded wall ties
- gable end and parapet failures

URM parapet wall failure was the major form of damage in both older and newer buildings and constituted a significant safety hazard both during and after the earthquake. Often the collapse of parapets onto awnings preempted failure of the awnings in turn leading to out-of-plane wall collapse. The most widespread incidence of parapet failure was at the Tighes Hill Campus of the Newcastle Technical College as shown in Figure 2.4.2.

Figure 2.4.2 Parapet Failure, Tighes Hill Campus, Newcastle Technical College

(Newcastle Earthquake Study, The Institution of Engineers, Australia, 1990)

A study (Murphy & Stewart 1993) of 651 Government buildings damaged during the earthquake at 300 different locations found that parapets on buildings founded on alluvium soil appear to have been the most hazardous with 55% of these incurring hazardous damage as opposed to 17% on non-alluvium. This then suggested that the amplified ground motion on the soft alluvium was substantial enough to cause the parapet walls to become unstable. In contrast, on non-alluvium soil areas where there was less ground motion amplification the parapets were less prone to becoming unstable, although base cracking of parapets was still observed.

The Australian experience of URM performing poorly in earthquakes is not unique. However, care must be taken when reviewing overseas URM research papers as the lessons learnt from their experience is typically determined from different standards of URM construction. Often the type of masonry construction and materials being referred to bear little resemblance to materials and practices used in Australia. For example, after both the 1997 Jabalpar, India, M_S 6.0, and 1999 Mexico, M_S 6.7, earthquakes, the collapse and severe damage to URM housing was reported (Jain et al 1997, Alcocer 1999). The implication for poor URM performance is apparent. With poor quality materials such as burnt brick in mud mortar and very weak adobe masonry being the predominantly used building materials, these bear little resemblance to materials used in Australia and as such few lessons can be learnt. Figure 2.4.3 gives an indication of the typical quality of masonry in the Jabalpar earthquake.

Similar examples can be made of Greek (Fardis 1995) and Italian (Spence et al 1999) earthquakes where damage to URM buildings often dating as far back as the middle ages are being reported.

Figure 2.4.3 Masonry Damage During 1997 Jabalpar, India Earthquake

(Jain et al 1997)

An analogy can however be drawn between earthquake damage to URM in some US, New Zealand and Chinese cities where similar URM construction types, materials and seismic design histories to that in Australia exist. For example, like Australia, many of these cities comprise old URM buildings in inner suburban areas that have been designed with little or no consideration for seismic action. Similarly weak lime mortars and poor maintenance are also commonly found. Recent events in seismically active areas where ordinances have been place to upgrade vulnerable URM buildings have also enabled comparisons of retrofitted and un-retrofitted damage to be made.

Selected documented events include: 1933 Long Beach, California (Fatemi 1999), 1935 Helena, Montana (James 1999), 1971 San Fernando, California (Leeds 1972), 1975 Imperial Valley, California and Mexico (Blakie et al 1992), 1983 Colinga, California (Blakie et al 1992), 1983 Borah Peak, Idaho (Reitherman 1985), 1987 Whittier Narrows, California (Deppe 1988, Hart 1988, Moore et al 1988), 1989 Loma Prieta, California (Benuska 1990, Lizundia et al 1994), 1994 Northridge, California (Somers 1996), 1855

and 1942 Wairarapa, Central New Zealand (Grapes & Downes 1997, Blakie et al 1992), 1931 Hawke's Bay, East Coast New Zealand (Blakie et al 1992), 1990 Weber, East Coast New Zealand (Blakie et al 1992), Tangshan, China, 1976 (Yuxian 1979).

2.4.3. Common URM Element Failure Modes

Blakie et al 1992 has presented URM damage data relevant for MM6 to MM8 intensities as could be expected for regions of moderate seismicity although some examples of high intensity shaking to MM10 are also included. At MM7 no URM buildings were reported to collapse as compared with 8% to 45% at MM8. Similarly, around 70% had only slight or no damage at MM7, dropping to 20% at MM8. Where retrofit ordinances had been undertaken URM performance was acceptable with mostly only low level damage. At MM10 severe damage was reported for URM buildings with as many as 75% of multi-storey brick buildings collapsing. Here current retrofit methods were found to be insufficient to prevent failures.

The following paragraphs provide a brief description and review of common failure modes for URM buildings which have been more prevalent during past earthquakes.

Anchorage failures: Anchorage is an important factor as it enables seismic load to pass between walls and the floor or roof diaphragm. In many URM buildings diaphragm joists and beams rest on URM walls, sometimes on special corbels although mostly these are recessed into the wall. Without effective anchorage face loaded exterior walls behave as cantilevers over the total building height thus increasing the risk of face loaded wall failure which may in turn precipitate total collapse. Global structural failure may also occur by slippage of joists and beams from their supports. Where floor diaphragms are positively connected to URM walls these anchors may rupture at the connection points leading to the condition of 'lack of anchorage' as described above.

Anchorage failure has been the most frequent cause of wall and gable collapse in moderate earthquakes however this has often been related to deteriorated or poor quality lime mortar.

Diaphragm flexibility and strength: No instance of complete diaphragm failure was reported for any moderate intensity earthquake although the flexibility of the floor and roof diaphragm has been suggested as a possible cause of wall damage. A particular case is unsecured gable wall ends, which are extremely vulnerable through impact with the roof structure.

As the floor diaphragm response directly excites the out-of-plane walls it is critical to the URM building seismic response. In an attempt to mitigate the effect that diaphragm response has on the dynamic behaviour of URM buildings, research has been undertaken in the United States (ABK 1984). Here fourteen different diaphragms were tested to obtain information on their in-plane static and dynamic, linear and non-linear properties. Eleven of the diaphragms tested were of wood construction and the remaining of steel decking either filled with concrete or not. Results showed that strong diaphragms produced large amplifications of up to 3 to 4 times the input accelerations in the elastic range essentially behaving as 2% damped oscillators. Flexible diaphragms were found to have highly non-linear flexible behaviour with typical amplifications in the order of 2 to 2.25.

Out-of-plane wall failures: When sufficient anchorage exists between the diaphragms and walls, out-of-plane wall behaviour is as a one storey high panel dynamically excited at either end. These panels themselves are susceptible to out-of-plane bending failure and while in-plane failure does not always endanger the gravity load carrying capabilities of the structure out-of-plane failure does. As amplification of the ground motion increases with building height, face loaded walls in the upper stories of URM buildings tend to be at the highest risk of failure. Parapet wall failures are also prone to flexural failure due to the lack of masonry tensile strength.

In moderate magnitude earthquakes cracking of walls loaded in the out-of-plane direction is common. For MM7 intensity shaking there appear to have been very few instances where pure simply supported out-of-plane collapse occurred where walls were adequately supported at the top and bottom. For MM8 intensity areas out-of-plane wall collapse was

a more prevalent cause of URM damage. Although many of these failures would have been instigated by anchorage problems it is possible that a number resulted from excessive out-of-plane displacements at the mid-height of the wall spanning between the diaphragms. At MM10 intensity shaking out-of-plane wall failure was reported as profuse. In some instances, adequately supported out-of-plane walls have survived even this intensity shaking. It was also found that buildings with concrete floors had a lower percentage of damage attributed to increased overburden stress.

Interior partition walls: As generally these walls are only one wythe thick and typically have no overburden other than their own self weight they have been particularly vulnerable even in moderate intensity shaking.

Parapet wall failure: Parapet collapse has been reported in all reviewed earthquakes. For moderate intensity shaking these typically have been responsible for most loss of life.

In-Plane Wall Failures: As seismic load passes through the structural shear wall, in-plane failure may occur if the inertial bending or shear forces induced exceeds the wall capacity. Over the past ten or so years a substantial quantity of experimental and analytical research into in-plane ultimate behavioral properties of URM walls has been reported (König et al 1988, Abrams 1992, Tercelj et al 1992, Pärsenjad et al 1994, Magenes et al 1995, Jankulovski et al 1995, Gambarotta et al 1995, Lafuente et al 1995, Romano et al 1995, Anthoine et al 1995, Zhuge et al 1996). In reviewing this documentation a wide variety of behaviour, which depends on the wall height to length ratio, the applied load and the mechanical properties of the materials constituting the brickwork can be found.

With different combinations of parameters three failure mechanisms have been identified. These include (1) rocking/flexural mechanism, (2) shear-sliding mechanism and (3) shear cracking mechanism typified by double diagonal (X) cracking. The first two failure modes are considered to be favourable as they are capable of significant energy dissipation without compromising the gravity load carrying capacity thus providing an

effective ductility. In contrast the third failure mechanism is considered to be non-favourable as brittle collapse often results. If a stair stepped crack pattern occurs along bed and head joints the element may still possess ductile characteristics as shear forces can still be resisted through friction. Low aspect ratios and high axial loads have been reported to develop diagonal cracking failure, while rocking and sliding were more likely to occur with low axial loads and high aspect ratio walls. Higher mortar strength was also found to inhibit shear cracking failure mechanisms in favour of rocking and sliding failure. Increased axial load was found to increase lateral strength in terms of the maximum load carrying capacity although the seismic performance was also worsened with the undesirable transition from a favourable to non-favourable failure mechanism.

Whether a URM wall element is controlled by flexural or shear, if suitable details are provided the lateral force deflection behaviour will include a significant plateau portion much like an elastic plastic material provided vertical compressive stress is present.

Both diagonal (X) cracking and horizontal cracking at the top and bottom of piers have been commonly reported in most areas of moderate intensity shaking but do not appear to have been responsible for any total building collapse. In contrast, brittle shear failure caused by the diagonal shear (X) cracking failure mechanism was a serious cause of collapse in more intensely shaken regions. For example in the 1976 Tangshan earthquake, M_S 8.0, where shaking intensities reached MM10, hundreds of URM buildings were reported to have failed due to shear failure in loadbearing URM walls. Figure 2.4.4 shows a school in Tangshan damaged by the earthquake where in-plane distress can clearly be seen in the front wall piers and out-of-plane wall failure has occurred at the top end wall.

Figure 2.4.4 Damage to URM Building, Tangshan, China, 1976

(Steinbrugge Collection, Earthquake Engineering Research Center, University of California, Berkeley)

2.4.4. 'Weak Link' URM Failure Modes

In summarising the data presented in Section 2.4.3, for moderate intensity shaking, the 'weak link' failure mode, which predominates for regular URM buildings, is the lack of anchorage between structural elements, in particular between floor/roof diaphragms and URM walls. Typically this has been due to a lack of consideration to lateral loading and in most cases could have been avoided by the provision of positive connections. As will be discussed further in Chapter 3, where the diaphragm is relatively rigid the provision of positive connections may cause serviceability problems and as such friction based connections are often relied upon. Where sufficient anchorage between structural elements has been provided the dominant 'weak link' failure mode is the out-of-plane flexure of URM walls including both simply supported and parapet walls. Tying parapets back to the main structure has proven to be a successful retrofit method for moderate intensity shaking.

In regions of moderate intensity shaking there have been many reported instances of URM buildings that have suffered minimal or no damage at all while other buildings of a similar nature and in the same shaking intensity region have suffered substantial

structural damage. It is therefore clear that provided the 'weak link' failure modes can be avoided URM can be relied upon to behave adequately during moderate earthquakes. Clearly for areas where the probability of stronger intensity shaking is deemed sufficiently high URM construction is not appropriate with the logical alternatives being more ductile methods such as reinforced masonry, reinforced concrete or steel construction.

Analytical research by Klopp 1998 has also identified 'weak link' URM failure modes. This involved the analysis of eleven existing URM buildings in Adelaide using the response spectrum method and equivalent static force requirements of AS1170.4-1993. As a results Klopp reported that the two most likely failure modes for Australian URM construction are:

(1) The limited force capacity of connections between floors and walls. Klopp reported that the code guidelines for connection force capacities between the floors and walls of URM buildings were found to be insufficient being significantly smaller than the requirement determined by elastic response spectrum analysis to AS1170.4-1993. Despite this Klopp also reported that typical forms of positive connection could generally easily meet the earthquake shearing forces induced. Of more concern were connections containing a DPC membrane often found in URM-concrete slab buildings, which rely on friction to transfer horizontal forces. In comparing the calculated connection shear force demand under the AS1170.4-1993 design earthquake, friction coefficients of around 0.3 to 0.4 were required. These values are of about the same magnitude as static friction coefficients reported by Page 1994,1995 for connections containing DPC membranes commonly used in Australian masonry construction. This suggests that friction might sufficiently transfer the shearing forces although this assumes that the full static frictional resistance can be relied upon. This assumption therefore warrants further investigation.

(2) The out-of-plane bending failure of walls of URM buildings. Klopp found that five out of the eleven URM buildings analysed under the AS1170.4-1993 earthquake had bending stresses greater than the simply supported elastic bending capacity of the wall.

Current design practice in Australia would thus indicate failure. As will be discussed in Chapter **5**, however, the resulting cracked condition may not constitute failure or collapse as a reserve dynamic capacity may exist. An additional factor was reported that the stress was more likely to exceed capacity in the upper stories of URM buildings where excitation amplification is a maximum and beneficial overburden stress is at a minimum.

2.5. 'Capacity' Design for Improved Seismic Response

When considering the preservation of life the most important design criterion is the Ultimate Limit State. In Australia only the Ultimate Limit State is considered. Here relatively large inelastic deformations must be accommodated without significant loss of lateral force resistance or the integrity of the structure to support gravity loads. Although non-repairable residual plastic deformations may occur the principal aim is to ensure that collapse is avoided.

The 'Capacity' design strategy has been defined (Paulay 1997) as "*In structures so designed for earthquake resistance, distinct elements of the primary lateral force resisting system are chosen and suitably designed and detailed for energy dissipation under severe imposed deformations. All other elements are then to be protected against actions that could cause failure by providing them with strength greater than that corresponding to the maximum feasible strength in the potential plastic regions.*" In theory the application of the 'Capacity' design principal leads to a benign and tolerant inelastic response with a high degree of protection against the collapse of structures subjected to severe earthquakes.

For framed reinforced concrete structures the 'Capacity' design methodology can be followed by detailing plastic hinge locations in beam elements rather than in columns. Thus, at the Ultimate Limit State a ductile inelastic sway mechanism having strong energy dissipative qualities is formed without the creation of a failure mechanism. In a similar fashion for a URM building the 'Capacity' design methodology can be followed

by the selection of a suitably ductile mechanism capable of dissipating seismic energy without damaging other structural elements due to severe deformations.

As has been discussed in Section 2.4.3 with the correct selection of URM in-plane wall geometry a failure mode capable of inelastic deformation and seismic energy dissipation suitable for 'Capacity' design is possible. Other less desirable failure modes such as out-of-plane bending and anchorage failure must then be protected against. Clearly if the 'Capacity' design principals are to be used effectively for URM it is important that realistic assessment of dynamic capacity of these failure modes is possible.

2.6 Overall Project Aim

As a result of this literature survey the research aim to be addressed within the scope of this report has been determined as providing designers with appropriate tools to avoid the brittle 'weak link' failure modes in the design of new and the assessment of existing URM buildings being:

(1) The limited force capacity of connections between floors and walls, in particular the friction dependent connections containing damp proof course (DPC) membranes and

(2) *the out-of-plane failure of walls in the upper stories of URM buildings.*

The first aim was achieved for the DPC connections through an extensive series of shaking table tests, which provided realistic data on the connections' dynamic capacity. The second aim was achieved by an extensive series of shaking table tests used to develop a better understanding of the physical processes governing the collapse behaviour of face loaded URM walls. From this improved understanding realistic analytical models were developed to provide an accurate and reliable assessment of actual capacity. As these were complex, by necessity, a further refinement was to produce a simplistic rational analysis procedure for practical applications.

Once these 'weak links' have been avoided with adequate seismic load paths developed, carefully designed, detailed and constructed, regular URM buildings have repeatedly shown that they will behave adequately during moderate intensity earthquakes. Further, this allows the 'capacity' design methodology to be more effectively undertaken resulting in an increased effective ductility for URM buildings to be realized.

3. DPC CONNECTIONS IN URM CONSTRUCTION

3.1. Introduction

In general, masonry buildings are constructed utilising a vast array of flashings, damp proof course (DPC) membranes and construction joints aimed at ensuring satisfactory serviceability performance. As highlighted in Section 2.3 for Australian unreinforced masonry (URM) construction, connections between a concrete slab and masonry wall are commonly detailed containing DPC membrane.

Typically, DPC membranes used for URM connections are flexible, manufactured from either embossed polythene or a light gauge aluminium and covered with polythene or bitumen. Normal practice is either to incorporate the membrane laid directly adjacent to the slab with a single mortar layer placed between the membrane and brick or to place it one to two brick courses up from the slab. This configuration is referred to as a standard DPC connection. Alternatively, the membrane may also be sandwiched between two mortar layers although not often used in practice as it is labour intensive. This is referred to as a centered DPC connection. Finally, in some circumstances no mortar is used with the membrane laid directly between the brick and slab or brick and brick. For these connections two layers of DPC membrane are often used back to back. This is referred to as a slip joint connection. Figure 3.1.1 provides a representation of the above three connection configurations.

In masonry construction, connections containing a DPC membrane are generally detailed to fulfil the dual serviceability role of providing an impervious barrier to moisture movement while acting as a plane of separation between structural elements. The latter role prevents distress of the connected elements by limiting the transfer of forces and

strains through the connection, caused by differential movements. While these movements will be discussed further in Section 3.3.2 it is clear that these connections must be capable of satisfying two conflicting horizontal shear requirements. Firstly, they must have the ability to allow for long-term relative movements between structural elements by limiting force transfer. Secondly, they must provide sufficient shear resistance to give lateral support to the wall under short-term earthquake loading. With friction being relied upon for horizontal shear resistance, the frictional properties are therefore critical to the successful application of these connections.

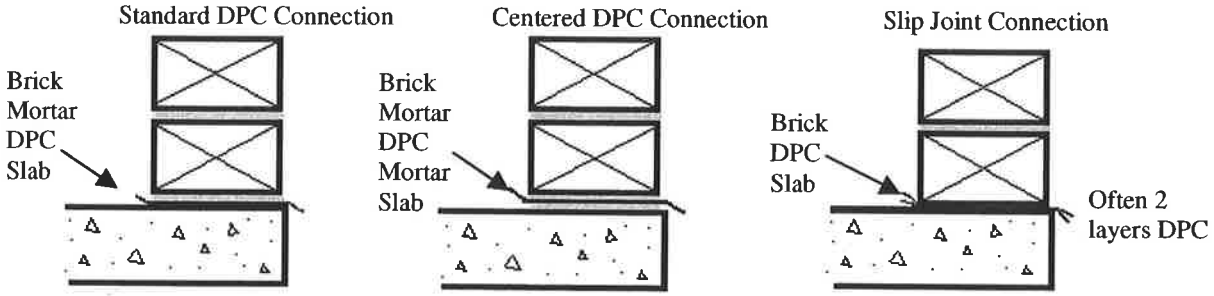

Figure 3.1.1 Types of URM Connection Containing DPC Membranes

This Chapter reviews previous work and relevant literature associated with both serviceability requirements and shear-resisting capacity of URM to concrete slab connections containing DPC membrane material and presents the specific 'weak link' research focus to be further considered within the scope of this project.

3.2. General Friction Review

The shear-resisting behaviour of a URM connection containing a DPC membrane is characterised by Coulomb (dry) friction, which involves rigid bodies in contact along a non-lubricated surface.

3.2.1. Coulomb Friction Behaviour

Investigations (Suh & Turner 1975) into surface topography have shown that the surface of a dry material such as metal, polymer or brickwork is not smooth but made up of many tiny peaks called 'asperities'. Thus, when two surfaces touch the real contact area is much

less than is apparent as only the asperities interact and consequently these govern the frictional behaviour. When a normal stress is applied to the friction plane the real contact area increases along with interaction between the asperities.

The static friction coefficient, $k_{v.static}$, can be defined as the minimal tangential force, F_m, required to initiate tangential motion divided by the normal load acting on the interface, N, as is represented by Equation 3.2.1. Hence, $k_{v.static}$ is governed by adhesion of the touching asperities and has been found to be independent of the apparent contact area, normal load and duration of loading. Once the adhesion force between asperities F_m is exceeded slip at the friction interface follows (refer Figure 3.2.1).

$$k_{v.static} = F_m / N \tag{3.2.1}$$

The plowing of soft surface layers by hard asperities primarily controls the sliding or dynamic friction between solids. On sliding, the magnitude of force required to sustain motion drops from F_m to the lesser dynamic friction force, F_k. This reduction in resistance is caused by less interpenetration of the surface asperities when the surfaces move with respect to one another and is well documented to be generally of the order of 25% (Suh & Turner 1975). Thus, the dynamic friction coefficient, $k_{v\ dynamic}$, is less than the static friction coefficient, $k_{v.static}$.

Both the static and dynamic friction coefficients strongly depend on the nature of the surfaces in contact. As the exact condition of the surface dictates these coefficients they are seldom known within an accuracy of greater than 5% as any foreign material present at the interface, such as corrosion or dirt, will alter the coefficient.

Coulomb friction can be further catagorised by the type of material at the friction plane as classically (e.g. metals) and non-classically behaving (e.g. polymers) friction. Since DPC membranes found in Australian URM construction are commonly produced in both of these materials a brief review of both Coulomb friction behaviours will be presented.

3.2.1.1. Classically Behaving Materials

There are three generally accepted laws of friction for classically behaving materials. These are (i) Friction is proportional to the normal load, (ii) Friction is independent of the apparent area of contact and (iii) Friction is independent of sliding speed.

Once sliding for a classically behaving material has commenced the dynamic friction force, F_k, remains approximately constant provided there is no material degradation (refer Figure 3.2.1).

3.2.1.2. Polymers

The frictional behaviour of polymers differs from that of classically behaving materials in that it does not necessarily obey the classical laws of friction. Since the static friction coefficient for polymers is sensitive to the hydrostatic component of stress it becomes dependent on normal stress. It has been reported (Suh and Turner 1975) that the dynamic friction coefficient for polymers can reduce substantially with increased normal force.

A second difference is that polymer frictional behaviour is very sensitive to sliding velocity caused by the large strain rate and temperature dependence of the flow stress of polymers. In any frictional scenario, as sliding velocities are increased the mechanical work done also increases the interfacial temperature. At a critical velocity/temperature a maximum dynamic friction coefficient is reached, and thus a maximum dynamic frictional resistance force, F_{kp} (refer Figure 3.2.1).

For some polymers F_{kp} has been reported (Rosato et al 1991) to be higher than the original static resistance force, F_m. This is attributed to sliding velocity/temperature increase prior to the maximum coefficient of dynamic friction being reached. As strain rate effects dominate the frictional behaviour the shear force for deformation also increases. After the critical velocity is passed the frictional behaviour is no longer dominated by strain rate increases but softening of the polymer which reduces the dynamic friction coefficient. It has been reported (Corneliussen 1986) that the reduction

of dynamic friction coefficient may be due to a molten film of polymer developing which acts as a lubricant so that a hydrostatic sliding condition prevails.

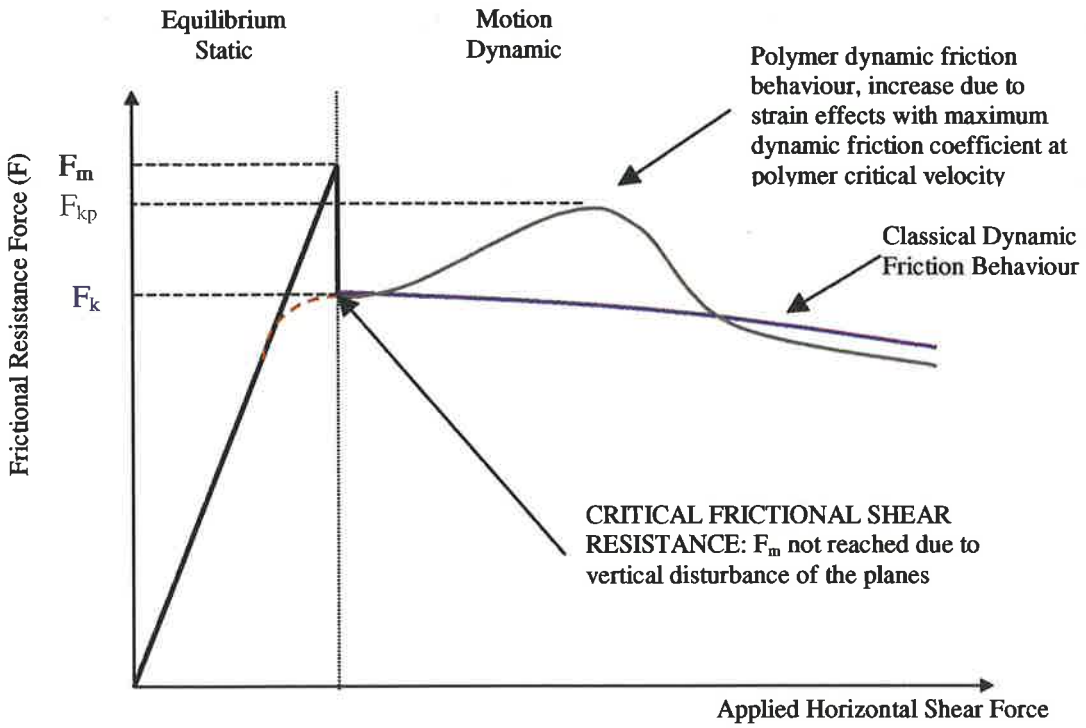

Figure 3.2.1 Diagrammatic Representation: Frictional Resistance vs Applied Shear

3.3. URM Connection: Previous Research

In the following section a review of previous work carried out by other researchers relevant to the serviceability and shear resistance of URM connections is presented.

3.3.1. Plain-Masonry Joint Shear

As URM connections containing DPC are in essence a plain-masonry joint containing a thin flexible DPC membrane, their shear behaviour is closely related to that of a plain-masonry joint. The main differences are firstly that the frictional properties of the DPC-brick, slab or mortar interface rather than the mortar-brick interface must be considered. Secondly, the initial shear bond, caused by mechanical interlock of mortar and brick in a plain-masonry joint, is typically reduced significantly where a DPC membrane is present.

Previous investigators have shown that when an increasing normal compressive stress is applied to brickwork, the horizontal shear strength at a plain-masonry joint increases linearly with compressive stress up to a limiting compressive stress. The widely accepted explanation for this is that the strength of the joint is derived from a combination of initial shear bond and Coulomb friction between the brick and the mortar. Consequently, the relationship between ultimate shear strength, τ_u, and normal compressive stress, σ_c, is often expressed by a Coulomb type relationship, such as that shown in Equation 3.3.1 where τ_o is the initial shear bond and μ is the friction coefficient of the brick-mortar interface.

$$\tau_u = \tau_o + \mu \sigma_c \tag{3.3.1}$$

Hendry and Sinha, 1981 have reported on a series of tests carried out on full-scale and model shear walls built of wire cut bricks in 1:¼:3 lime mortar. It was found that the shear resistance for this type of brickwork was well represented by the Coulomb type relationship shown in Equation 3.3.2 up to a normal compressive stress level of 2MPa.

$$\tau_u = 0.3 + 0.5\sigma_c \tag{3.3.2}$$

Similar results using different brick and mortar combinations have also been reported (Stafford Smith & Carter 1971, Riddington & Ghazali 1990, Magenes & Calvi 1992, Seisun et al 1994, Mullins & O'Conner 1995). Although τ_o (0.1 to 1.19) and μ (0.4 to 1.33) have varied significantly with the type of materials tested, a similar Coulomb type relationship has been obtained for low levels of normal compressive stress.

While the linear Coulomb relationship has been consistently reported for relatively low levels of normal compressive stress the above research has also indicated that the rate of increase in shear strength reduces at higher normal compressive stresses. Where this is the case the value of μ appears to decrease with increasing normal compressive stress. The level at which this reduction begins has generally been reported to be around 2MPa

although this is dependent on the quality of masonry construction and materials considered.

Although initially it was proposed that an average value of μ could be assumed over all normal compressive stress ranges this was questioned as it did not realistically model the true shear behaviour at higher over burden stresses. In recognition of this Riddington and Ghazzali (1990) proposed a hypothesis for the shear failure of plain-masonry joints. Here, similar to the original findings of Hendry and Sinha (1981) and the likes, it was postulated that below a normal compressive stress of around 2MPa, shear failure is initiated by joint slip as predicted by a typical Coulomb relationship. Above this the shear failure mechanism is governed by tensile failure within the mortar and finally at very high compressive stress the compression failure of the brickwork becomes the dominant factor. An experimental investigation was also reported (Riddington & Ghazali 1990) confirming the plain-masonry shear failure hypothesis as represented in Figure 3.3.1.

Also shown in Figure 3.1.1, the plain-masonry joint failure hypothesis (Riddington & Ghazali 1990) can be related to URM connections containing DPC membrane. Since for these connections both the initial shear bond and friction coefficient may be reduced as compared with a plain-masonry joint, the intersection of the DPC joint slip and mortar tensile failure lines will occur at a higher normal compressive stress. For the range of normal compressive stress commonly found in Australian masonry construction, as described Section 2.3 it is therefore unlikely that a mortar tensile failure mechanism would dominate under horizontal load but rather a joint slip mechanism (refer Figure 3.3.1).

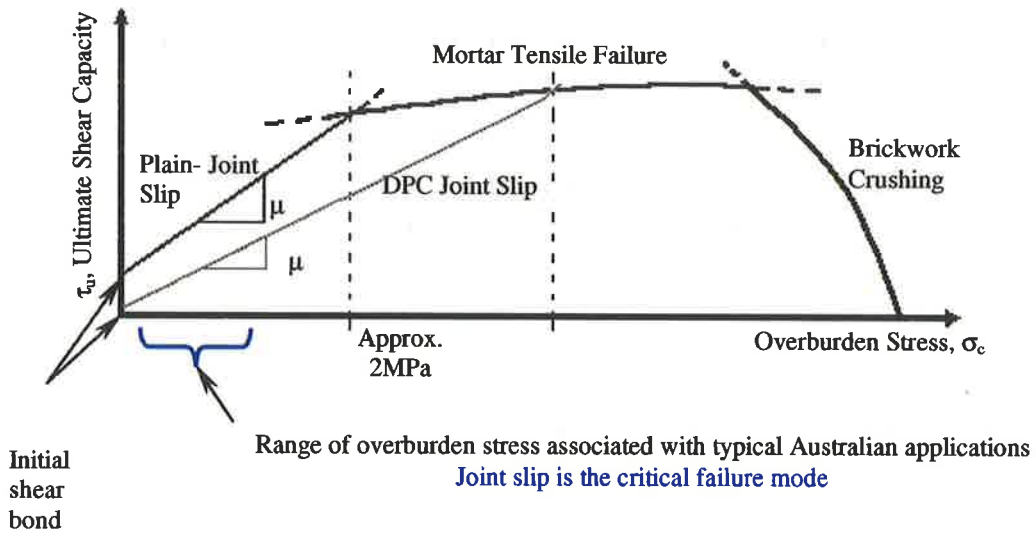

Figure 3.3.1 Shear Failure Hypothesis

(Riddington & Ghazali 1990)

In a real loading scenario masonry elements are rarely subject to only one type of load and are generally in a complex state of stress where in-plane and out-of-plane actions occur simultaneously (Yokel & Fattal 1976). With loading such as earthquake or wind, URM walls can experience cyclic bi-axial stress states being either tension or compression. Dhanasekar (1985) has reported on a series of half scale brick masonry panel tests subjected to bi-axial compression-compression and compression-tension. Here, it was found that mortar joints acted as planes of weakness influencing the failure loads and failure patterns.

3.3.2. Serviceability Requirements

The following section presents a brief summary of previous research associated with serviceability requirements of connections within URM buildings. One such connection serviceability requirement is the prevention of distress caused by differential movement of structural elements. Since movement may be caused by differential movements associated with concrete slab shrinkage, growth/shrinkage of clay/concrete masonry units, thermal movements or foundation settlement, each structural element will behave differently over time. Consequently, each element will induce forces into adjoining

elements. Where the induced force is in shear its magnitude is limited by the shear capacity of the connection joining the structural elements.

It is well documented that concrete, whether it constitutes masonry units or floor slab undergoes shrinkage and creep with time. In contrast the time dependent behaviour of clay masonry is not as well documented and is complicated by the composite nature of the material. It has however been reported (Beard et al 1969) that the time dependent movement of brickwork is caused by one or a combination of thermal movement, moisture movement, chemical expansion or deformation under load. Further research (Beard et al 1969, Cole & Lewis 1974, Wyatt 1976) has reported on studies associated with the movement of brickwork. In general, findings were that all of the walls expanded horizontally and vertically with time and the rate of expansion was maximum during the early life of the wall and decreased with time.

It is therefore clear that there is a conflict between the time dependent behaviour of concrete and clay constructed structural elements. As mentioned in Section 3.1, URM connections containing DPC are typically detailed to fulfil a dual serviceability role, one of which is that the shear resistive capacity is sufficiently low to allow the differential movement between structural elements. Research (Beard et al 1969) has been carried out to determine if this is actually the case as the magnitude of force transmitted by the differential movement is difficult to ascertain. Here the movement of brickwork above and below a lead cored bituminous standard DPC connection at the base of an actual building was measured. It was found that the lack of shear restraint offered allowed the brickwork above the connection to move.

Although not directly related to seismic loading another important aspect of URM building serviceability is the movement of footings supporting masonry walls. Research (Page & Kleenman 1994) has been undertaken to establish parameters influencing wall behaviour under such actions. Here, provided the walls had sufficient strength to resist cracking they were found to bridge the movement of the flexible footings. In practice

masonry walls often do not have sufficient strength to resist cracking and are commonly observed to crack under deformations permitted by flexible footing movement.

3.3.3. Positive Anchorage

As highlighted in Section 0, the lack of anchorage of masonry walls to floor and roof diaphragms contributed to the separation and non-uniform vibration of walls in areas of moderate intensity shaking. This was less prevalent, however, with concrete slab diaphragms, which provided a higher normal compressive stress and increased frictional resistance than in URM buildings with flexible timber diaphragms. Conversely, anchorage through positive connection of concrete slab and URM wall is more likely to create a serviceability conflict due to differential movement whereas this is less likely with the more flexible timber diaphragms.

In order to assess the vulnerability of non-anchored timber diaphragms a non-linear dynamic analysis able to model the friction and impact characteristics of wood joist bearing on a brick wall has been developed (Jones & Cross 1993). Using this model comparisons were made with the dynamic response of a retrofitted building in Gilroy, California having a well anchored timber floor diaphragm which survived the M_s 7.1 Loma Prieta (1989) earthquake. While entire city blocks were demolished in nearby Santa Cruz and another URM building, a Town Hall, two blocks south was severely damaged the Gilroy building sustained very little damage despite roof accelerations of 0.79g. As a result of the analysis it was found that the structural response remained elastic provided the diaphragms and wall were connected. If, however, the joist to wall connections were disconnected the response of the structure moved into the inelastic range. In the latter case two possible failure mechanisms were identified as (1) collapse of the wall in out-of-plane bending and (2) when joists moved sufficiently to cause them to fall from the wall.

Tomazevic et al (1995) have also reported on a series of shaking table tests completed with ¼ - scale, 2 storey masonry and stone houses having both unconnected timber joists supporting a concrete slab and connected timber joists also supporting a concrete slab. It

was found that freely supported wooden floors did not prevent separation of the walls and severe out-of-plane vibration of the wall was noted. Where horizontal steel ties were provided separation of the walls was prevented with ultimate collapse caused by shear failure of the walls in the first story. The input energy needed to cause collapse of the model building with connected timber joists was over two times greater than the case of the model without ties. It was concluded that separation of wall can be prevented by either anchoring wooden floor joists into the wall using steel ties or replacing wooden floors with reinforced concrete slabs.

Buccino and Vitiello (1995) have reported on an experimental investigation on three types of anchorage to assess their pull out resistance. The experiments showed that the shape of the anchorage and quality of the brickwork had a great influence on the resistance to pull out of the anchorage.

implication for test. procedure?

3.3.4. Shear Resistance of URM Connection Containing DPC Membrane

Since the frictional resistance properties of connections containing a DPC membrane are specific to the particular membrane used overseas research data is not strictly applicable for Australian URM construction. This being the case a brief review will be presented for overseas research where applicable with more focus placed on Australian research.

As part of a study of the long term differential movement resistance of DPC connections British researchers (Beard et al 1969) first highlighted the need for an understanding of the frictional resistance of DPC connections. Here it was highlighted that the shear resistance was significantly less than for a plain-masonry joint. This was confirmed by a further experimental study (Hodgkinson & West 1982) which reported on shear tests to determine the shear resistance of British DPC materials.

Experimental investigations (McGinley & Borchelt 1990:1991) have also been undertaken to evaluate static friction coefficients for eight connections containing a DPC membrane commonly found in the United States. Both in-plane and out-of-plane loading

directions were investigated with both concrete and steel supports. For standard DPC connections on a concrete slab, static friction coefficients were found to vary from 0.19 to 0.5. Similar results were reported for steel supports however a significant reduction was noted with the presence of a coating such as galvanising or paint. While it is generally accepted that rougher slip plane surfaces produce higher coefficients of friction this study indicated that both the stiffness of the support material on either side of the membrane as well as the DPC membrane had a significant effect on the friction behaviour. For a given roughness of DPC material, stiffer membranes produced higher friction coefficients and are more likely affected by the properties of the supports. In contrast, for a more flexible DPC the properties of the membrane tended to dominate the frictional behaviour. The in-plane and out-of-plane behaviour was also found to vary significantly which was attributed to the differing surface texture of the brickwork in either direction.

Static friction tests on a series of three-brick high prisms with up to 0.9MPa normal compressive stress have also been reported (Suter & Ibrahim 1992) for DPC materials commonly available in North America. The significance of these tests is that it was first recognised that the location of the DPC membrane within the mortar joint has an effect on the frictional behaviour. As such, standard DPC, centered DPC and slip joint connections were tested. Static friction coefficients were found to range from 0.1 for slip joint connections to 0.6 for the centered DPC connections.

To establish the frictional characteristics of connections containing DPC membranes directly applicable to Australian masonry construction a comprehensive series of static tests (Page 1994:1995) has been reported. The membrane types selected were chosen on the basis of advice from industry to obtain a reasonable representation of common construction practice in Australia. Here both two and three-brick long specimens laid in running bond with standard DPC, centered DPC and slip joint connection configurations were tested. Both in-plane and out-of-plane tests were carried out with normal compressive stress ranging up to 1.5MPa. For the range of compressive stress considered a Coulomb friction relationship was used to describe the shear resistive behaviour. Thus, tests were performed at various normal compressive stress and a linear regression of the

data points used to determine the static friction coefficient and initial shear bond strength. The resulting static friction coefficients are summarised for DPC connections in Table 3.3.1 and slip joint connections in Table 3.3.2.

Table 3.3.1 DPC Connection Static Friction Coefficient Summary (Page 1994)

		In-plane (k_v)		Out-of-Plane (k_v)	
CONNECTION CONFIGERATION	**COMMERCIAL NAME**	**Centered**	**Standard**	**Centered**	**Standard**
Bitumen Coated Aluminium	Standard Alcore	0.41	0.49	0.50	0.47
Bitumen Coated Aluminium	Super Alcore	0.60	0.41	0.57	0.48
Polyethylene/Bitumen Coated Aluminium	Rencourse	0.26	0.26	0.31	0.35
Embossed Polythene	Supercourse 500	0.68	0.59	0.59	0.56
Embossed Polythene	Supercourse 750	0.71	0.58	0.60	0.59

Table 3.3.2 Slip Joint Connection Static Friction Coefficient Summary (Page 1994)

SLIP JOINT CONNECTION CONFIGERATION	**Out-of-Plane (k_v)**
1 Layer of Super Alcor	0.57
2 Layers of Super Alcor	0.48
2 Layers of Galvanised Steel with Molydenum Disulphide Grease	0.06

In conclusion Page reported that for all of the DPC materials considered, with the exception of polyethylene/bitumen coated aluminium (Rencourse), the static friction coefficient could conservatively be taken as 0.3 for earthquake loading. Also, although small shear bond strengths were reported these were generally very small (0MPa to 0.12MPa) and as such would be neglected.

Using similar connection details to the static tests reported by Page (1994:1995), quasi-static (cyclic) shear tests have also been reported (Griffith & Page 1998). These tests were aimed at studying the cyclic performance of the various membranes under repeated

loading cycles, in particular the potential degradation of the materials. Quasi-static tests were performed at velocities of between 50 and 200mm/minute and at three levels of normal compressive stress. A continuous plot of shear force versus shear displacement recorded which resulted in a series of hysteresis curves (refer Figure 3.3.2). From these curves the maximum quasi-static shear resistance force was determined for each level of normal compressive stress as the plateau of the hysteresis loop. The quasi-static friction coefficient was then determined. While the quasi-static friction coefficients determined will be presented in Chapter 0 these were found to be slightly larger than those determined previously by static testing. A second significant finding of this research was that even after many cycles of shear displacement very little degradation in shear capacity was observed indicating that URM connections containing a DPC membrane would perform satisfactorily in service under cyclic loading.

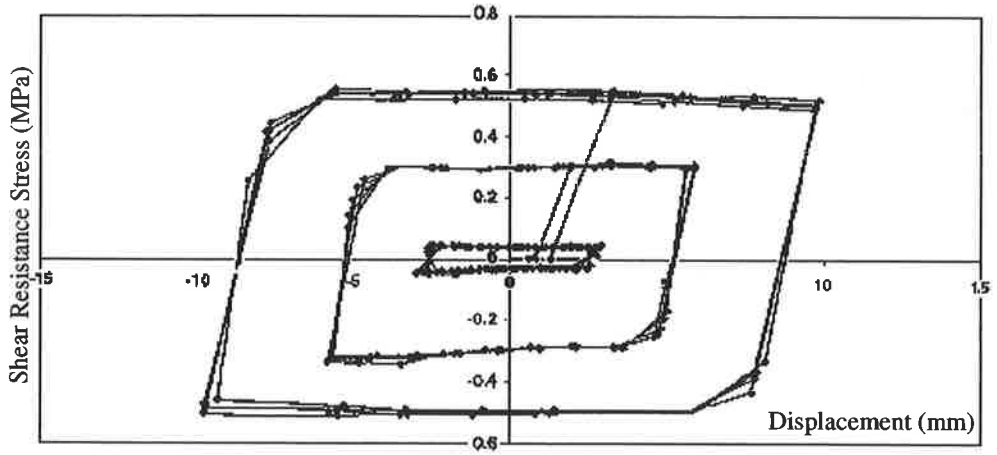

Figure 3.3.2 Results of Typical Quasi-static on DPC Connection

(Griffith & Page 1998)

3.4. Australian Code Provision: URM Connections

The 'SAA Earthquake Loading Code', AS1170.4-1993 requires connections to be capable of transmitting a horizontal force of $10(aS)$ kN/m where a is the acceleration coefficient and S the site factor. To illustrate this requirement, for a firm soil site in Adelaide, a = 0.1g and S = 1.0. Thus, in this case, connections must be capable of transmitting a force of 1kN/m. Research (Klopp 1996) has indicated that this requirement may be inadequate being as little as $1/13^{th}$ of the required shear capacity for a two-storey URM building when subjected to the design magnitude earthquake. Despite this, it was also reported that most typical forms of positive connection would still be sufficient.

As discussed in Section 3.3.3, the positive connection of a concrete diaphragm to a masonry wall may produce a serviceability problem so that URM connections containing DPC are often used. Klopp (1996) therefore also compared the calculated connection shear capacity with experimentally determined (Page 1994:1995) static shear resistance of connection containing DPC membrane. In general he found that the frictional resistance capacity was adequate.

Consequently, although friction is generally not recommended as a method of transferring horizontal loads the AS1170.4-1993 amendment No.1 OCTOBER 1994, now allows friction to be relied upon at connections containing DPC membrane within loadbearing masonry construction. The shear resistance capacity however must still be determined in accordance with the 'SAA Masonry Code', AS3700-1998 as:

$$V_d \leq V_o + V_{1e} \tag{3.4.1}$$

where V_d = *the earthquake induced design shear force*

V_o = *the shear bond strength of the shear section*

$= \phi f'_{ms} A_{dw}$

V_{1e} = *the shear friction strength of the shear section under earthquake actions*

$= 0.9\, k_v\, f_{de}\, A_{dw}$

ϕ = *the capacity reduction factor*

f'_{ms} = *the characteristic shear strength of masonry*

A_{dw} = *the bedded area*

k_v = *friction coefficient*

f_d = *the design compressive stress on the bed joint for earthquake actions*

$= G_g/A_{dw}$

G_g = *the gravity load*

The first term in Equation 3.4.1 represents the basic shear bond strength and the second the frictional component of the capacity. For a plane containing a DPC membrane the shear bond strength is usually negligible as the membrane is generally placed directly onto brick. The shear capacity of the joint is therefore almost solely a function of friction and thus on the friction coefficient, k_v and the design compressive stress at the friction plane, f_d.

Importantly, it must be recognised that the currently recommended friction coefficients are based upon static friction coefficients for URM connections containing DPC membrane. Confirmation was therefore required to determine if these will be indicative of the dynamic friction coefficient under true dynamic excitation.

3.5. Implication of the Dynamic Friction Coefficient

In any seismic event it is well recognised that both horizontal and vertical accelerations occur. For example Glogau (1974) reported that vertical acceleration as large as two thirds of the horizontal were recorded during the 1971 San Fernando earthquake. It is therefore possible that with vertical disturbances at the slip interface of a connection containing a DPC membrane that the maximum static peak tangential force, F_m, may not be reached as the adhesion between the asperities may already be reduced or broken. If this were the case the critical resistance to shear would then be governed by the lower dynamic friction force, F_k, and thus dynamic coefficient of friction, $k_{v\ dynamic}$.

As can be seen in Figure 3.2.1 the frictional behaviour of the polymer up to the static frictional resistance force is similar to that of a classical behaving material. Although for polymers it is possible for the dynamic shear resistance to peak at a critical velocity this value could not be relied upon due to the unpredictability of earthquake excitation. For the above reasons it would therefore be non-conservative to assume a maximum frictional resistance force of either F_m or F_{pk} as it is possible that the critical resistance to shear would come from the lower dynamic friction force, F_k.

3.6. Specific Research Focus

While both static and quasi-static testing has provided data on initial shear bond, static friction coefficients and the potential degradation of the materials, realistic dynamic testing is required to quantify the influence of dynamic loading on the frictional resistance of connections containing DPC membranes. The specific focus of the current research project related to the DPC connection 'weak link' has therefore been the undertaking of dynamic testing for the provision of information regarding the true dynamic behaviour of connections containing DPC membranes commonly found in Australian masonry construction. This experimental testing phase is presented in Chapter 4 where recommendations are made on the applicability of assuming static or quasi-static friction coefficients for the seismic design of connections containing DPC membranes.

4. DYNAMIC SHEAR CAPACITY TESTS ON URM CONNECTION CONTAINING DAMP PROOF COURSE MEMBRANE

4.1. Introduction

As highlighted in Chapter 3, concern that the shear capacity of connections containing DPC membrane under true dynamic loading will be less than under static loading have led to a series of dynamic shear tests being undertaken. The tests described in this Chapter were therefore aimed at determining values of dynamic friction coefficients for connections containing DPC membrane commonly used in Australian masonry construction.

4.2. Dynamic Shear Tests

Dynamic shear tests were conducted on clay brick masonry connections containing a variety of DPC membrane material on the earthquake simulator at the Chapman Structural Testing Laboratory, University of Adelaide. These have included standard DPC, centered DPC and slip joint connection configurations and considered both in-plane and out-of-plane shaking. The main advantages of dynamic testing, as opposed to quasi-static testing, are firstly that true inertial loading can be generated in contrast to displacement-controlled testing. Secondly, a frequency of loading more representative of the frequencies normally associated with earthquake induced loading can be applied.

Since dynamic tests are generally more expensive than quasi-static tests, these were used as 'spot checks' to determine to what extent the quasi-statically determined friction

coefficients were representative of those which could be expected in seismic events. A comparison of dynamic and quasi-statically determined friction coefficients is therefore presented in Section 4.4.

The earthquake simulator at The University of Adelaide consists of a 1400mm x 2000mm shake table mounted on bearing runners and is connected to a 200kN INSTRON load/displacement hydraulic actuator, which is rigidly connected to the laboratory strong floor. The maximum vertical load capacity (on table) of the INSTRON is 66kN and has a maximum horizontal displacement capacity of ±125mm.

4.2.1. Instrumentation

Prior to and during slip, response accelerations of the applied weight, W, above the slip interface and the reference acceleration at the shaking table were recorded. The instruments used to measure these horizontal accelerations were Kistler Servo Accelerometers powered by a servo amplifier.

To determine relative displacements of the test specimen above and below the friction interface, absolute displacements at both the table and concrete slab above the connection were recorded relative to a stationary datum. Table displacements were recorded internally by the INSTRON controller. A Linear Voltage Potentiometer (POT), mounted to a rigid frame connected to the laboratory strong floor, was used to record the absolute response displacement of the unit above the slip interface. The POT used was a Housten Scientific model 1850-050 having a maximum displacement capacity of 500mm and was powered by a 10Volt DC supply.

The 'Microsoft Windows' based data acquisition system 'Visual Designer' was used to collect the four channels of data from the two accelerometers, displacement POT and INSTRON. Data was collected at a period interval of 0.008 seconds (125Hz), which was found to be sufficient to capture all relevant frequencies of the response. Since 'Visual Designer' uses a buffer system to temporarily store data prior to saving to disc, care had to be taken to ensure that the buffer was sufficiently sized to hold data for the full test.

The overall test set up, location of instrumentation and data acquisition is shown schematically in Figure 4.2.1.

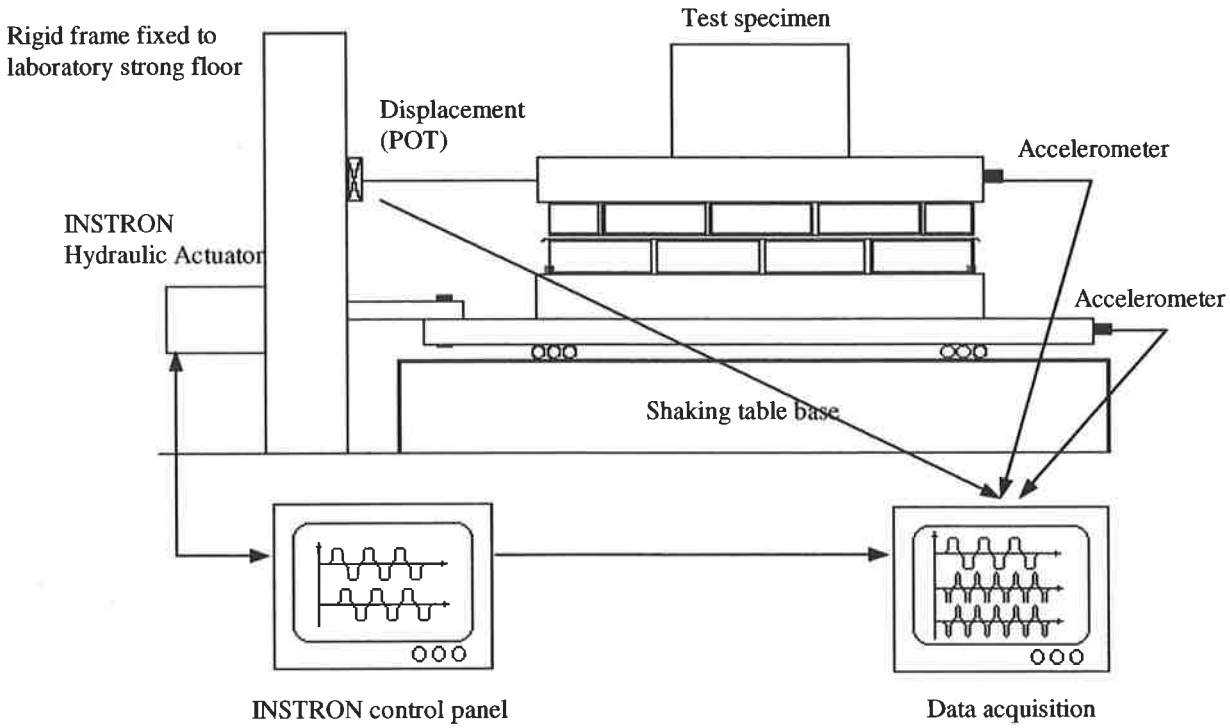

Figure 4.2.1 Schematic URM Connection Containing DPC Dynamic Test Set-up

4.2.2. Damp-Proof Course Membrane and Materials

For the various dynamic connection shear tests undertaken, four different types of DPC membrane were tested, having been selected to match as closely as possible materials used in previous quasi-static tests (Griffith & Page 1998). A brief description of each DPC material tested is given in Table 4.2.1.

It should be noted that both the Polyflash and Dry-Cor membrane were not identical to the products used in quasi-static tests. Although the membranes were produced from similar materials they had a different commercial name and the thickness varied slightly. Despite this it was expected that their frictional behaviour would be similar.

Table 4.2.1 DPC Membrane Test Specimens

Commercial Name	Description	Nominal Thickness
Standard Alcor	Bitumen Coated Aluminium	950 μmm
Super Alcor	Bitumen Coated Aluminium	1550 μmm
Polyflash	Polyethylene/ Bitumen Coated Aluminium	650 μmm
Dry-Cor	Embossed Polythene Plastic	850 μmm

Bricks used to construct the connections were standard 'Red' 3 hole extruded clay bricks. These had the nominal dimensions 230x110x76mm. Mortar was bucket batched using a 1:1:6 cement:lime:sand mix where water was added by the tradesman to achieve a reasonable workability. Including sand absorbed moisture this typically resulted in a total batch water content of approximately 23%. Associated material tests including mortar compressive strength and masonry modulus will be described later in Chapter 6.

4.2.3. Dynamic Test Methodology

As shown in Figure 4.2.2 a concrete slab of dimensions 1000 x 1400 x 100mm was used to support lead ingots above the connection to be tested thus providing a total normal weight, W, at the friction interface. By varying the number of lead ingots the normal compressive force at the friction interface, N (=W), could be varied enabling dynamic shear tests to be carried out at various levels of normal compressive stress.

While an earthquake event comprises a wide range of frequencies, dominant frequencies of around 2-5Hz are not uncommon. For all the dynamic tests reported here inertial loads were induced across the friction interface by applying a representative 2Hz sinusoidal displacement motion to the earthquake platform. The amplitude of the motion was gradually increased until slipping occurred at the connection. Once slip occurred, the dynamic inertia force, F_i, was determined as, $F_i = W \times a_{slip}$, where a_{slip} was the sliding response acceleration sustained by the mass above the friction interface. Since the weight was already in motion it was assumed that initial shear bond was not relevant so that the entire resistance force was due to friction. Therefore, for horizontal equilibrium, equating the inertia force with the dynamic frictional resistance force, F_m, the dynamic

friction coefficient, $k_{v\ dynamic}$ could be determined. As indicated in Figure 4.2.2, $k_{v\ dynamic}$ can be seen to be equal to the response sliding acceleration, a_{slip}, in units of g's.

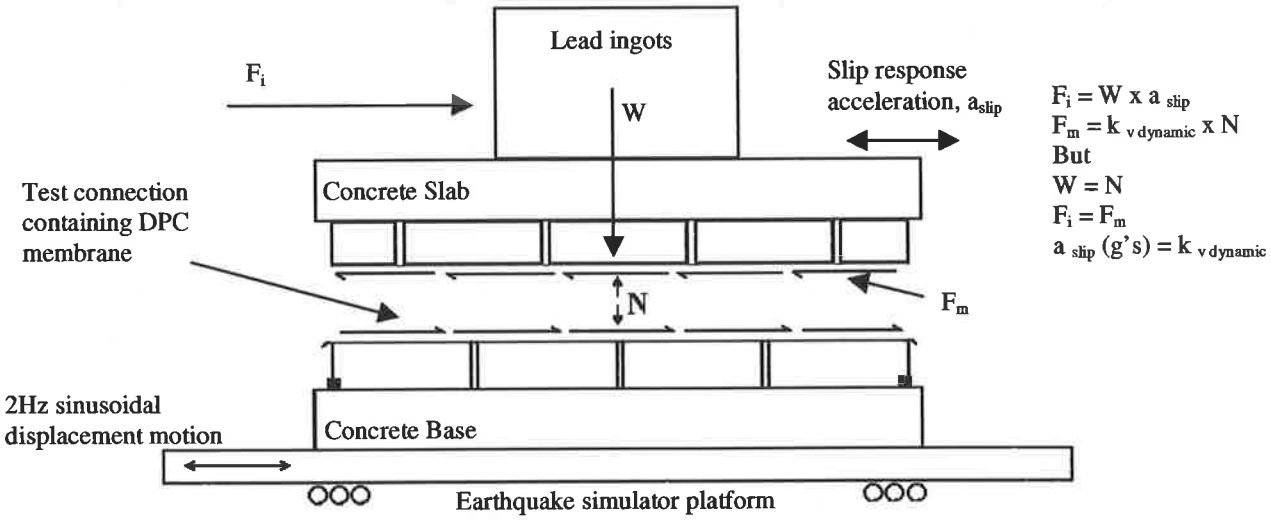

Figure 4.2.2 Test Specimen Free Body Diagram: DPC Connection during Sliding

4.2.4. DPC Connection Tests

For both the standard and centered DPC connection test specimens, two rows of brickwork, four bricks long and two courses high were used to support the concrete slab and lead ingots. The total area of the friction plane was 194,300mm^2. For standard DPC connections the membrane was placed directly on top of the bottom course of bricks and mortar placed on top of the membrane material. For centered DPC connections the membrane was sandwiched between two mortar layers located centrally between the top and bottom course of bricks. The overall layout of a standard DPC test specimen is shown schematically in Figure 4.2.3.

For both the standard and centered connections the following membrane configurations were tested dynamically: 1 layer of Standard Alcor; 1 layer of Super Alcor; 1 layer of embossed plastic; and 1 layer of Polyethylene/ Bitumen Coated Aluminium. Although these four specimen tests were carried out at only one value of vertical compressive stress (0.164MPa) both in-plane and out-of-plane shaking were examined so that a total of eight

tests were undertaken. Figure 4.2.4 shows a photograph of the set up for a standard connection containing 1 layer of Standard Alcor to be tested in the in-plane direction.

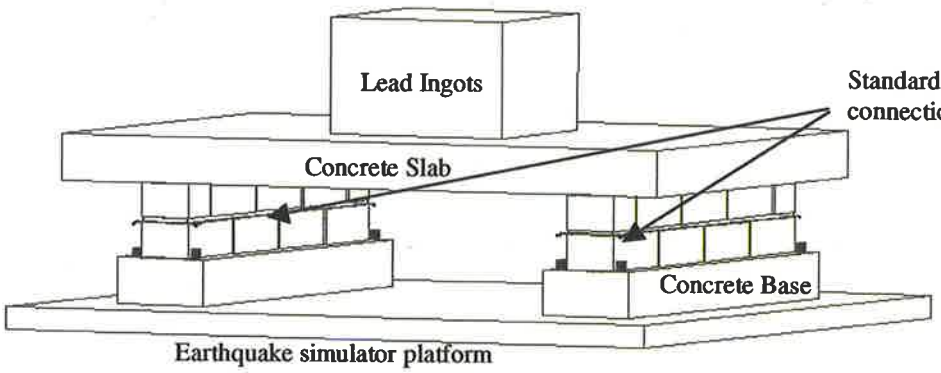

Figure 4.2.3 Dynamic Test Set-up for Standard/Centered DPC Connection

Figure 4.2.4 Photograph of Standard DPC Connection Set up – In-plane

4.2.5. Slip Joint Connection Tests

The slip joint tests were conducted using a similar procedure to that for the DPC connection tests. The main difference was that the concrete slab plus lead weights were supported by four bricks which were bedded directly onto the earthquake simulator using a high strength dental paste. The membrane material was placed between the top of each brick and the underside of the concrete slab. Slip joint connections containing the

following membrane configurations were tested dynamically: 1 layer of Standard Alcor; 2 layers of Standard Alcor; 1 layer of embossed plastic; and 2 layers of greased galvanised steel sheets. The slip joint tests were performed over a range of three normal compression stresses being 0.04, 0.18 and 0.33 MPa conducted only in the in-plane direction. Accordingly, twelve tests were completed. As for the DPC connections multiple confirmatory tests were also undertaken.

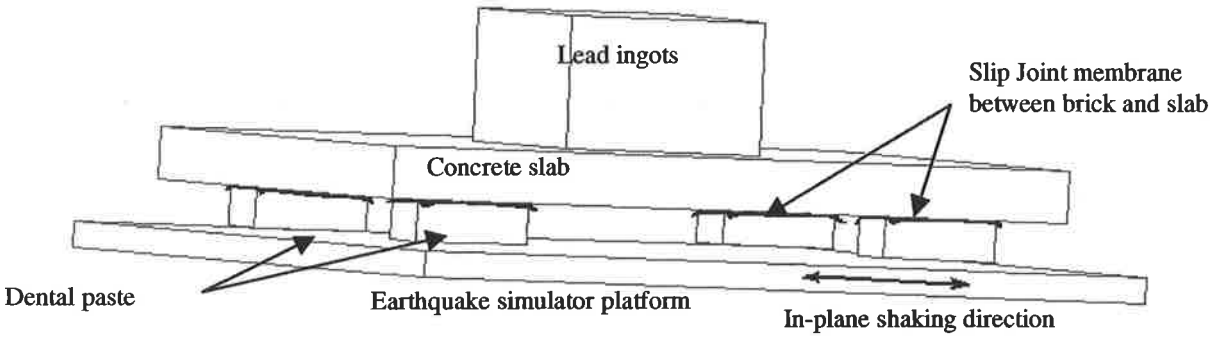

Figure 4.2.5 Schematic Diagram of Dynamic Test Set-up For Slip Joint Connection

Although some polishing of the concrete slab was observed after multiple tests this was not found to greatly reduce the dynamic friction coefficient.

4.3. Results Formulation and Data Analysis

The basic procedure for the formulation of results, including the calculation of the dynamic friction coefficients was the same for both DPC and slip joint connections. This process included:

(1) calibration of raw output data to the required units;
(2) filtering of calibrated data;
(3) determination of the time of first slip;
(4) determination of slip acceleration and corresponding force;
(5) check slip force using displacement amplitude just prior to slip;
(6) plotting of the shear stress versus normal compressive stress; and
(7) determination of the dynamic friction coefficient as the gradient of the shear stress versus normal compressive stress plot.

4.3.1. Data Filtering

Since a 2Hz sinusoidal displacement motion was input to the earthquake platform only frequencies near this were considered to be relevant to the response. Figure 4.3.1 shows a typical Fast Fourier Transform (FFT) of response acceleration data where the 2Hz frequency amplitude is clearly dominant. In order to remove irrelevant noise frequencies from the raw data a Fortran 77 band-pass filter program was specifically developed for these tests (the code is included in Appendix (A)).

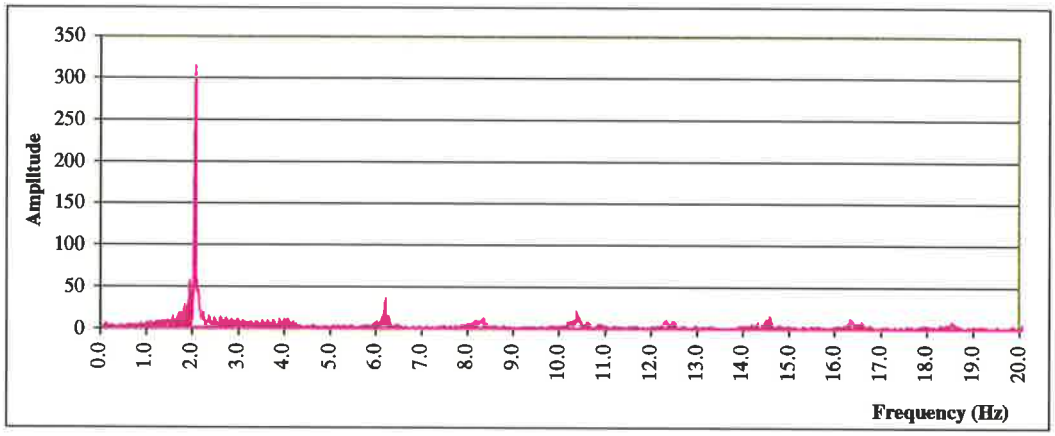

Figure 4.3.1 Dominant Response Acceleration Frequencies

Extensive testing of this filter was undertaken to determine the most suitable band-pass shape and provide an indication of the accuracy of the filter. It was found that a parabolic sided band-pass filter gave the best results although the first and last second of data was found to be slightly corrupted and as such were discarded. Although the filter program allows any band-pass range to be set to best encompass the relevant frequencies full pass was considered between 1.5 and 2.5Hz reducing to zero at 0.5Hz and 3.5Hz respectively (refer Figure 4.3.2).

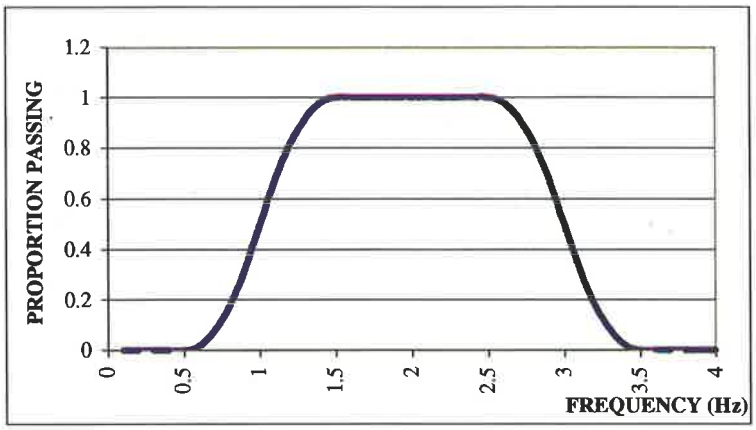

Figure 4.3.2 Parabolic Sided Band Pass Filter - Bandwidth

4.3.2. Dynamic Friction Coefficient Representative Calculation

The following Section provides a representative calculation of the dynamic friction coefficient. Here a slip joint configuration with two layers of Standard Alcor (refer Table 4.2.1), subjected to in-plane shaking with a normal overburden stress of 0.18MPa (N=17.8kN) is used to illustrate the result formulation procedure.

Figure 4.3.3 shows the absolute displacement response of both the connection above and below the slip interface relative to the stationary datum. Prior to 24.5 seconds both the top and bottom units behave as one as the input table sinusoidal displacement motion is gradually increased. At 24.5 seconds the connection's shear resistive capacity is exceeded and slip occurs. From this time on the frictional resistive force is proportional to the dynamic friction coefficient, $k_{v.dynamic}$. Since this is slightly less than the static friction coefficient there is a respective decrease in the sinusoidal response displacement amplitude that the unit above the connection can sustain during sliding. The response accelerations of the unit above the interface are recorded as is shown in Figure 4.3.4. Here a maximum of 0.46g is observed. The dynamic friction coefficient is then determined directly from the slip acceleration as 0.46. From the acceleration response data, hysteresis behaviour can also be developed as shown in Figure 4.3.5. The maximum dynamic frictional resistive force can be determined as the top and bottom plateau of each hysteresis loop as 7.7kN.

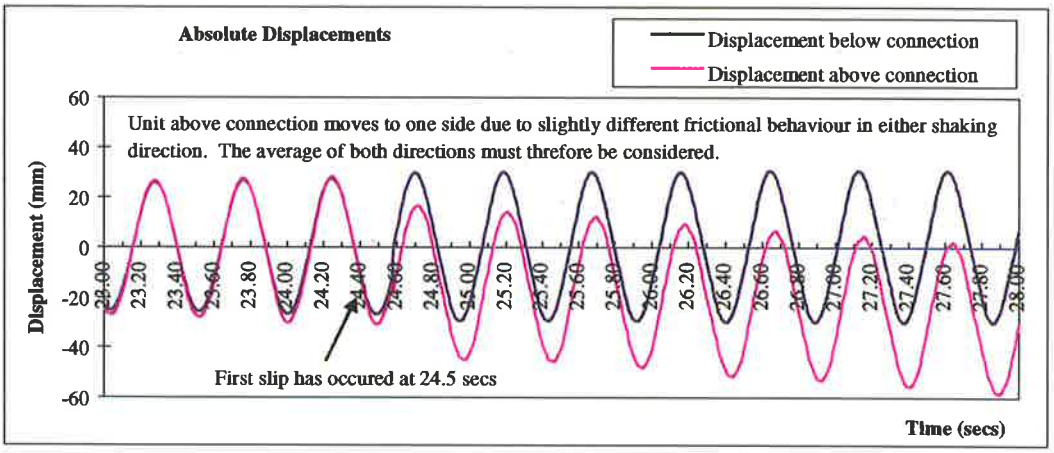

Figure 4.3.3 Relative Connection Displacements

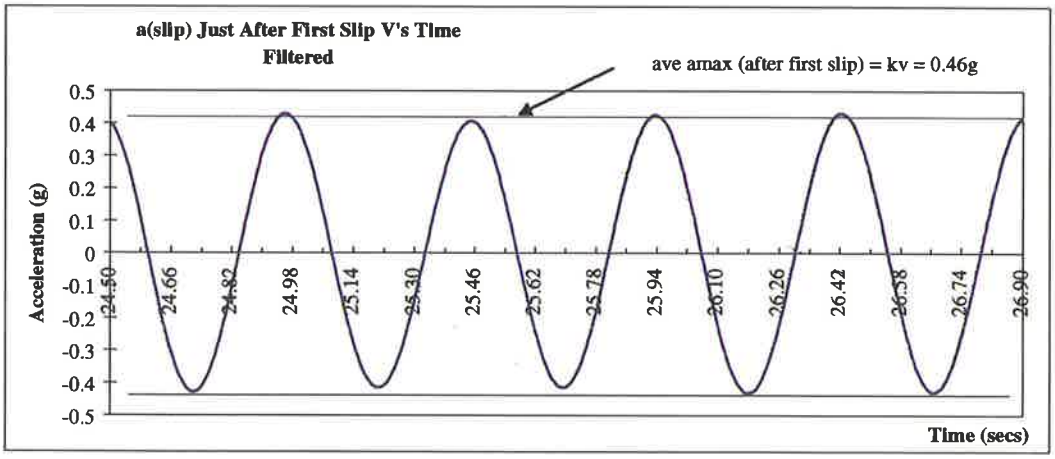

Figure 4.3.4 Response Acceleration above Slip Interface during Slipping

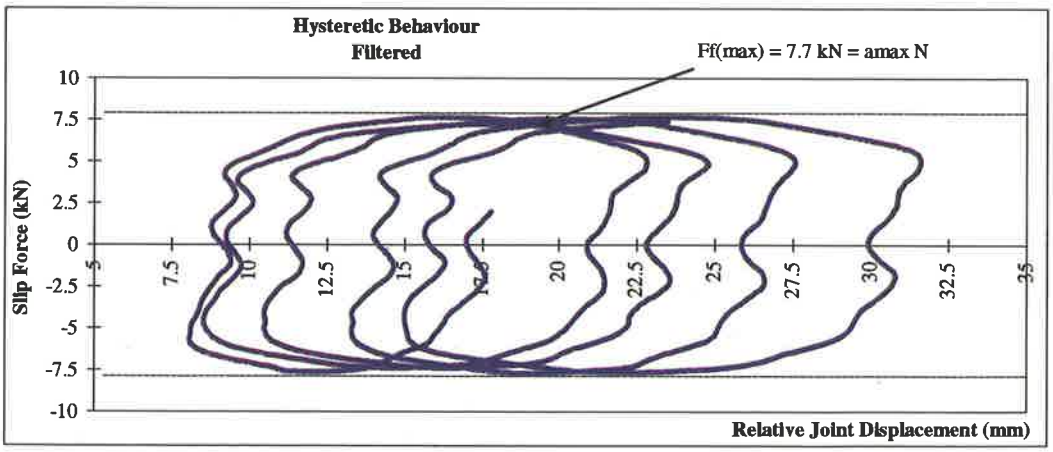

Figure 4.3.5 Hysteresis Behaviour after Slip showing Maximum Shear Resistive Force

4.3.3. Theoretical Check

To check that recorded accelerations were of the correct order the following calculation was undertaken for all tests.

The steady-state displacement response of a single degree of freedom system (SDOF) subjected to harmonic loading is of the form:

$$u(t) = A \sin(\varpi t - \theta) \tag{4.3.1}$$

where $u(t)$ = displacement response

A = Displacement amplitude

ϖ = Angular frequency = $2\pi f$

f = Frequency

θ = Phase angle

By integrating and double integrating this both the velocity v(t), and acceleration a(t) response can be determined respectively as:

$$v(t) = -A \sin(\varpi t - \theta) \tag{4.3.2}$$

$$a(t) = -A\varpi^2 \sin(\varpi t - \theta) \tag{4.3.3}$$

The maximum acceleration therefore occurs when $\sin(\varpi t - \theta) = 1$ and is given as:

$$a_{max} = |-A\varpi^2| = |-A(2\pi f)^2| \tag{4.3.4}$$

For the case of a 2Hz sinusoidal response, the maximum acceleration is related to the amplitude of the displacement response by:

$$a_{max} = |-A(4\pi)^2| = 157.9\ A \quad (mm/s^2)$$

For the example in Section 4.3.2, A at slip = 28.5mm implies

$$a_{max} = 157.9 \times 28.5/(9.81 \times 10^3) = 0.46\ g$$

This agrees thereby confirming that the acceleration data (and hence friction coefficients) were consistent.

4.4. Dynamic Test Results

4.4.1. DPC Connection Dynamic Test Results

Representative DPC connection test data is presented in Appendix (B) in a similar format to that described in Section 4.3.2. A summary of results for standard DPC connection is given below in Table 4.4.1 and presented graphically in Figure 4.4.1. Similarly a summary of results for centered DPC connections is given in Table 4.4.2 and presented graphically in Figure 4.4.2.

Table 4.4.1 Results Summary for Standard DPC Connection Tests

Standard DPC Connection (Ref. Table 4.2.1)	Normal Force (kN)	Normal Stress (MPa)	a_{max} (g)	F_k (kN)	Shear Stress (MPa)	$k_{v.dynamic}$
1 Layer Standard Alcor	31.9	0.164	0.44	14.0	0.072	0.44
1 Layer Super Alcor	31.9	0.164	0.47	15.0	0.077	0.47
1 Layer Polyflash	31.9	0.164	0.37	11.8	0.061	0.37
1 Layer Dry-Cor	31.9	0.164	0.36	11.5	0.059	0.36

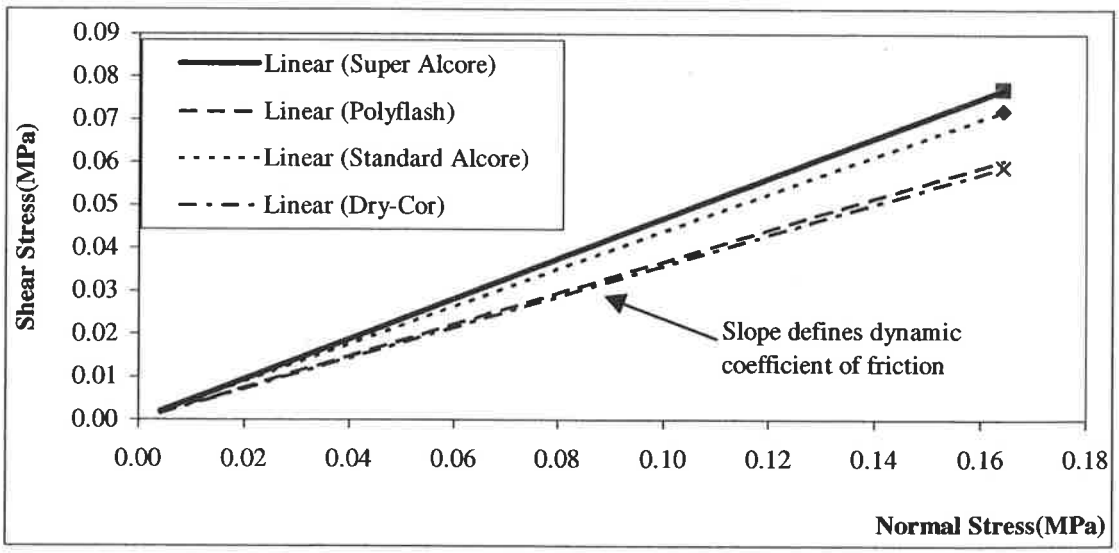

Figure 4.4.1 Graphical Results Summary for Standard DPC Connection Tests

Table 4.4.2 Results Summary for Centered DPC Connection Tests

Standard DPC Connection (Ref. Table 4.2.1)	Normal Force (kN)	Normal Stress (MPa)	a_{max} (g)	F_k (kN)	Shear Stress (MPa)	$k_{v.dynamic}$
1 Layer Standard Alcor	31.9	0.164	0.31	9.9	0.051	0.31
1 Layer Super Alcor	31.9	0.164	0.35	11.2	0.057	0.35
1 Layer Polyflash	31.9	0.164	0.38	12.1	0.062	0.38
1 Layer Dry-Cor	31.9	0.164	0.41	13.1	0.067	0.41

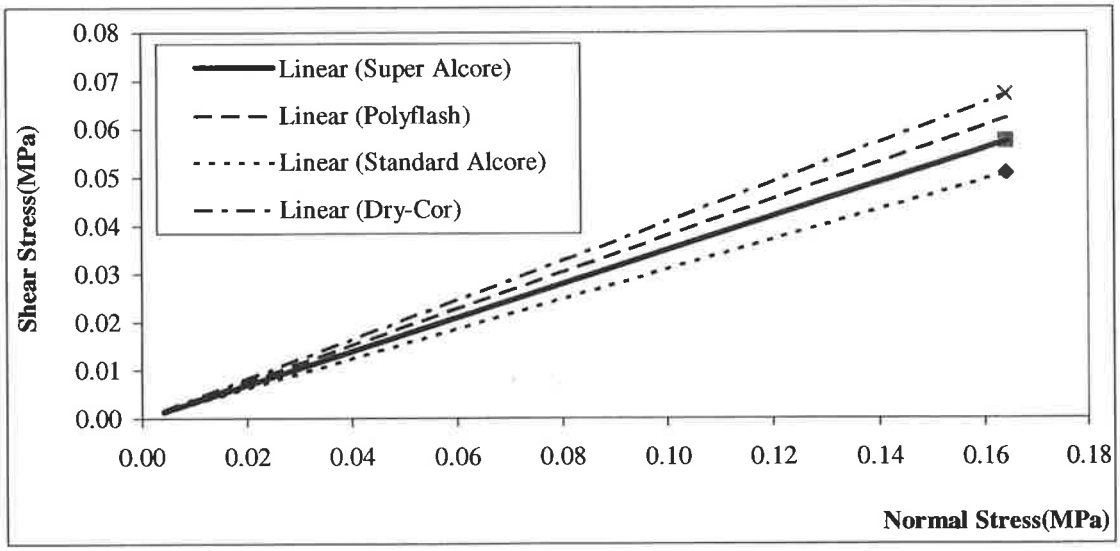

Figure 4.4.2 Graphical Results Summary for Centered DPC Connection Tests

On completion of the dynamic tests the connection was examined to determine at which interface slip had occurred. For centered DPC connections slip was always observed between the mortar and DPC membrane and for standard DPC connections slip was always observed between the brick and DPC membrane.

With the exception of embossed polythene (Dry-Cor) and Polyflash membrane, the dynamic friction coefficient for centered DPC connections were less than for standard DPC connections. In contrast, other researchers (Page 1994) have reported static friction coefficients for centered DPC connections usually greater than for standard DPC

connections. This difference is attributed to a high dependency on workmanship, as any irregularity in the mortar bed below the membrane will significantly impact on the frictional properties of a centered DPC connection. As such, comparison of the frictional behaviour of these connections, with other researcher's results, is difficult.

As mentioned in Section 3.3.4 previous researchers have found that for a given roughness of flashing material, stiffer DPC membranes produce higher coefficients of friction and are more likely to be affected by the properties of the support. The dynamic test results imply that the mortar-DPC sliding plane of the centered DPC connection provided less frictional resistance than the brick-DPC sliding plane of the standard DPC connection. This indicates that the stiffness of the support material on either side of the membrane had a significant effect on the friction behaviour for the relatively stiffer Alcor membranes. Further the Polyflash and embossed polythene, which were less stiff, frictional properties did not appear to be as greatly effected by the properties of the supports but were dominated by the behaviour of the DPC membrane.

4.4.2. Slip Joint Connection Dynamic Test Results

Representative DPC connection test data is presented in Appendix (C) in a similar format to that described in Section 4.3.2. Results of dynamic slip joint shear tests at various levels of normal compressive stress are presented in Figure 4.4.3 to Figure 4.4.5 for out-of-plane loading and Figure 2.4.1 to Figure 4.4.8 for in-plane loading. The dynamic friction coefficient, $k_{v.dynamic}$, is shown as the gradient of the linear regression line. The embossed plastic (Dry-Cor) slip joint connection shear test was only completed at one level of normal compressive stress (0.33MPa) where the dynamic friction coefficient was 0.41. Comparison of the in-plane and out-of plane plots indicated that no significant difference was apparent in the dynamic friction coefficient obtained for the two loading directions. This is attributed to there being no distinct difference in the roughness of the brick for the two directions. Consequently no further distinction will be made with regard to loading direction.

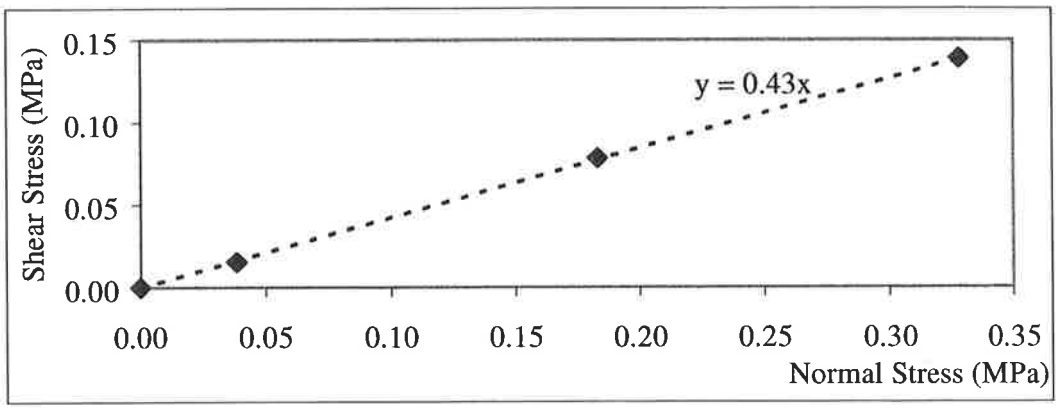

Figure 4.4.3 Out-of-plane Slip Joint – 1 Layer of Standard Alcor

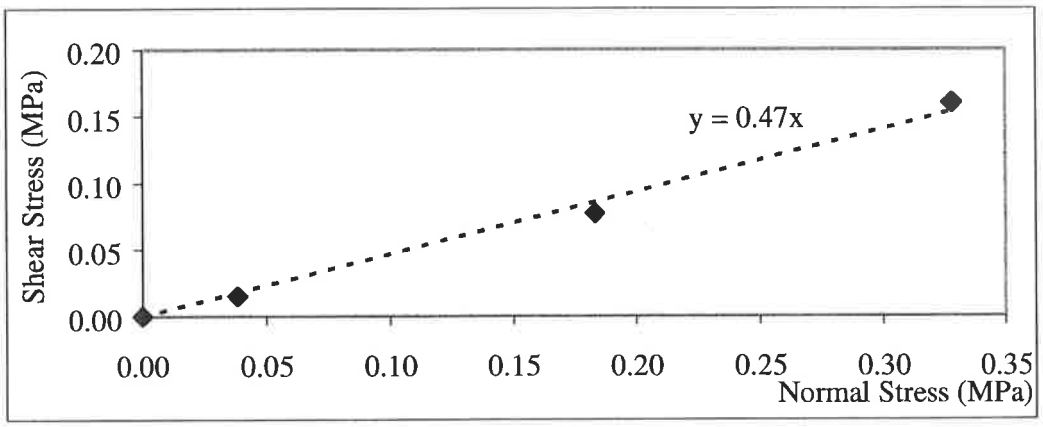

Figure 4.4.4 Out-of-plane Slip Joint Test – 2 Layers of Standard Alcor

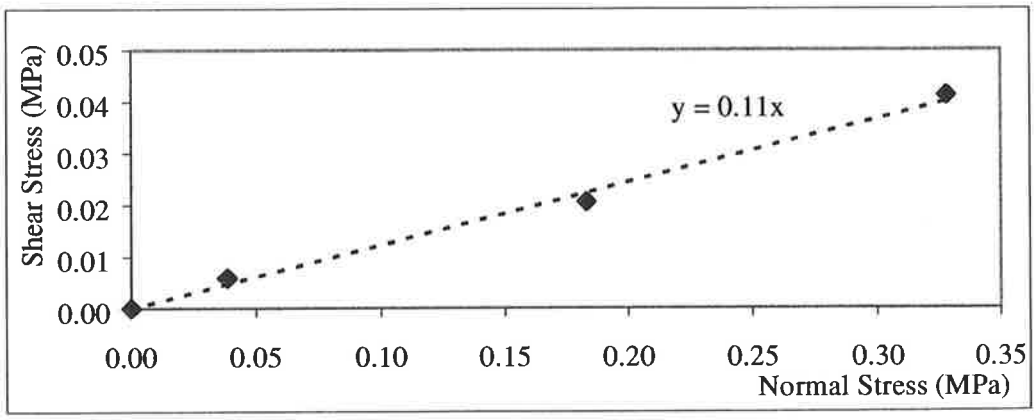

Figure 4.4.5 Out-of-plane Slip Joint Test – 2 Layers of Greased Galvanised Steel

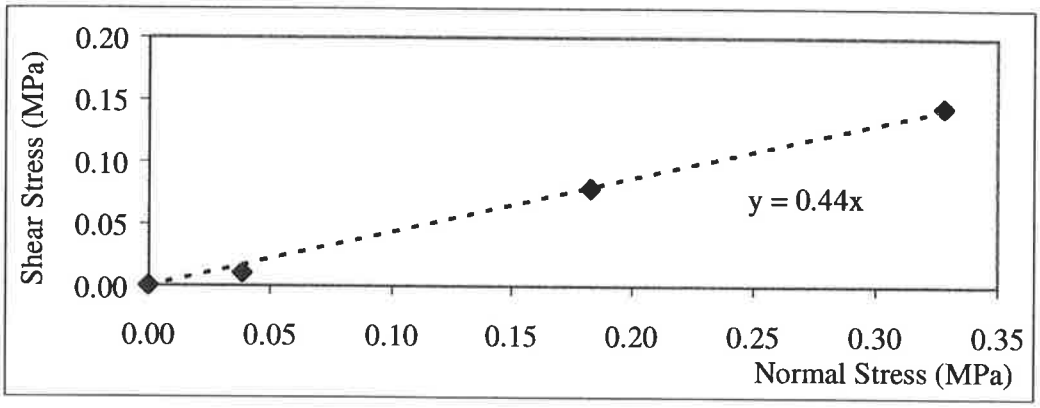

Figure 4.4.6 In-plane Slip Joint Test Results – 1 Layer of Standard Alcor

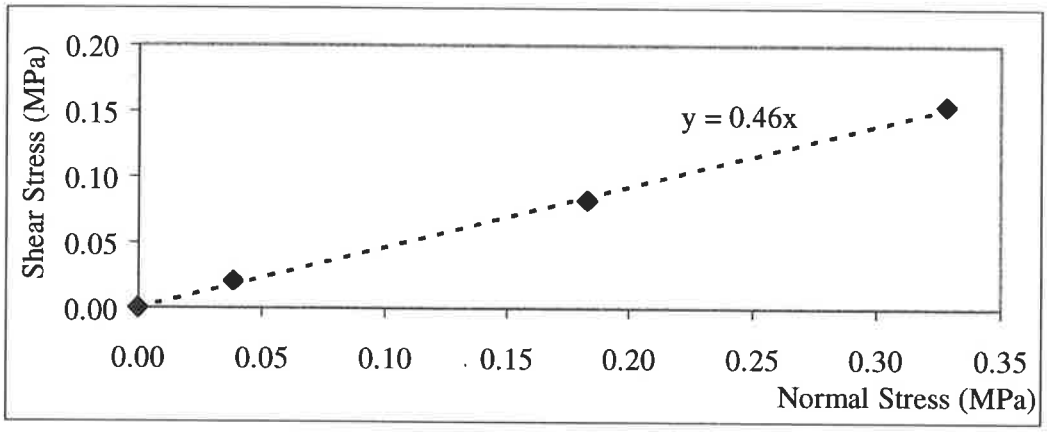

Figure 4.4.7 In-plane Slip Joint Test Results – 2 Layers of Standard Alcor

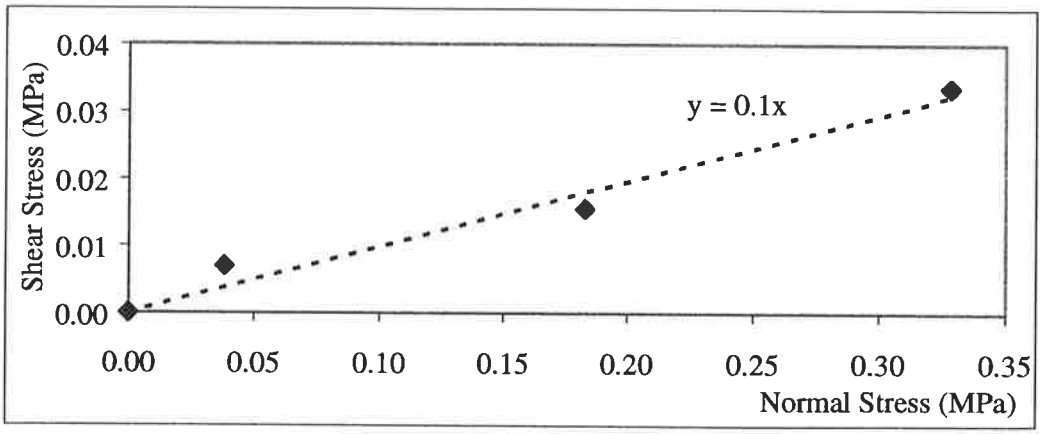

Figure 4.4.8 In-plane Slip Joint Test Results – 2 Layers of Greased Galvanised Steel

4.4.3. Comparison of Dynamic with Static and Quasi-Static Test Results

Table 4.4.3 and Table 4.4.4 respectively present a comparison of friction coefficients for standard DPC and slip joint connections determined statically and quasi-statically by previous research and dynamically as part of the current research project.

Table 4.4.3 Standard DPC Connection Friction Coefficient Comparison

Joint Type	Friction Coefficient, k_v			Dynamic (%) Quasi-Static
	Static Page (1994)	Quasi-static Griffith et al (1998)	Dynamic	
1 layer of Standard Alcor	0.460	0.520	0.43	82%
2 layer of Standard Alcor	0.470	0.569	0.46	81%
1 Layer Dry-Cor (Embossed plastic)	0.304	0.267	0.41*	N/A
2 Layers of Greased Galvanised Steel	0.074	0.108	0.11*	100%

* Not same commercial product as used in the quasi-static tests

Table 4.4.4 Slip Joint Connection Friction Coefficient Comparison

Joint Type	Friction Coefficient, k_v			Dynamic (%) Quasi-Static
	Static Page (1994)	Quasi-static Griffith et al (1998)	Dynamic	
Standard Alcor	-	-	0.44	N/A
Super Alcor	0.527	0.541	0.47	87%
Rencourse/Polyflash	0.259	0.317	0.37*	N/A
Embossed Polythene/Dry-Cor	0.397	0.329	0.36*	N/A

* Not same commercial product as used in the quasi-static tests

Since by necessity the geometry of the quasi-static and dynamic testing apparatus were not identical the direct comparison of results is somewhat limited. However, an indicative comparison of results is still useful. It is of particular interest to note that the value of the dynamic friction coefficient divided by the quasi-static result (as a percentage). For the membrane types, which were common to both sets of tests, the dynamic friction coefficients were greater than or equal to 80% of the quasi-static test value. For all membranes, except the greased galvanised steel, the dynamic friction factor was also found to be greater than the AS3700-1998 code prescribed design value of 0.30.

4.5. Summary and Conclusion: Implication for Design

The results of dynamic shake table tests on DPC and slip joint connections which are typically used in unreinforced masonry construction in Australia have been presented. The main purpose of these tests was to evaluate the connection performance under dynamic loading in order to assess their seismic integrity. Dynamic friction coefficients determined from these tests were then compared with quasi-static friction coefficients determined by previous research (Griffith et al 1998) to assess to what extent the quasi-statically determined friction coefficients represented those which could be expected in seismic events. Here it was found that the dynamic friction coefficients were not more than 20% less than those determined quasi-statically. Further, with the exception of greased galvanised sheets no connection had a friction coefficient less than the AS3700-1998 code prescribed design value of 0.3. Additionally the observed 'seismic strength capacity' of the connections considered were greater than the 'seismic load demand' calculated by Klopp for most of the eleven buildings he analysed.

5. STABILITY OF SIMPLY SUPPORTED URM WALLS SUBJECTED TO TRANSIENT OUT-OF-PLANE FORCES

5.1. Introduction

(Paulay & Priestly 1992) have described the response of masonry walls to out-of-plane seismic excitation as:

"one of the most complex and ill-understood areas of seismic analysis"

Traditionally designers have perceived URM as a brittle form of construction, and thus considered it particularly sensitive to peak ground accelerations. In contrast, recent research has shown that dynamically loaded URM walls may sustain accelerations well exceeding their elastic capabilities (ABK 1985, Bariola 1990, Lam 1995). This apparent anomaly points to our lack of understanding of the true collapse behaviour of URM walls.

The complexity arises from the fact that the response can be highly non-linear as the behaviour is largely governed by stability mechanisms rather than material failure. Not surprisingly, when compared with other areas of structural and earthquake engineering, the current knowledge of the out-of-plane behaviour of masonry walls to seismic loading is sparse.

Figure 5.1.1 shows a typical out-of-plane wall failure in the upper story of a URM building during the 1989 Loma Prieta, California earthquake.

Figure 5.1.1 Out-of-plane Wall Failure during Loma Prieta Earthquake, 1989

The following sections review important aspects of the behaviour of URM walls when subjected to transient out-of-plane forces. Previous experimental and analytical work is discussed and followed by a critical review of the current analysis and design methodologies. This Chapter concludes with both the specific experimental and analytical research focus to be addressed within the scope of this report.

5.2. Fundamentals of Out-of-Plane URM Wall Behaviour

The lateral strength capacity of a simply supported URM walls subjected to out-of-plane loading depends on many variables. Possibly the most fundamental of these is the manner of spanning of the wall between supports. In the simplest case a vertically spanning wall is supported only at the top and bottom so that under out-of-plane loading a vertical one-way bending action develops. Since vertical movement at the top support is not restrained any applied vertical compressive force remains constant regardless of any elongation of the tension face during loading. This type of wall can be related to either loadbearing or non-loadbearing internal URM partition walls (without returns) or very long URM walls where the side boundary conditions do not significantly impact on the wall behaviour.

When return walls or engaged piers are more closely spaced, the wall's response to out-of-plane loading becomes more complicated, consisting of combined vertical and horizontal bending. These walls are therefore referred to as two-way spanning walls and tend to have an increased lateral force resistance capacity over that of a similar sized but one-way spanning wall. Further complications arise since brickwork is strongly anistropic, i.e. behaving differently in orthogonal directions. Depending on the number and nature of supported edges, various cracking patterns are also possible, thus affecting the lateral resistive capacity of the wall. Over the past 30 years a number of static testing programs have been completed on the two-way bending of URM wall panels (Baker 1973, Hendry 1973, West et al 1973:1977, Lawrence 1975:1994, DeVerkey et al 1986, Drysdale et al 1988) resulting in several static analysis techniques. The most recent of these is the Virtual Work Method (Lawrence 1998) where internal and external work are equated. Due to the complexity of the problem, however, as yet no static analysis methodology has been readily evolved into a dynamic analysis procedure.

Another category of URM wall commonly found in Australia is the full infill panel where a masonry wall is constructed within a framed construction without gaps. In this case, under lateral load, elongation of the tension face due to bending can not occur without inducing a large compressive force from the surrounding frame, which acts as a rigid abutment. This results in an arching behaviour where the vertical compressive force increases with mid-height displacement. On further increasing lateral load the vertical compressive forces become sufficiently large to crumble the brickwork at vertical reaction points. This material failure permits further displacement of the wall as its length is reduced until ultimately instability occurs. However, a lateral strength capacity typically much greater than one or two-way bending walls is realised. As the wall's ultimate behaviour is dominated by progressive damage and material failure, a 'quasi-static' analysis is often used to assess the peak lateral capacity of these walls. Various researchers have addressed the out-of-plane behaviour of this type of wall resulting in static arching analysis procedures (Baker 1978, Hendry 1981, Abrams et al 1996). In Australia many infill panels are constructed with a gap at the top, filled with mastic or

sealant, and a gap at the sides with special connectors to allow for brick expansion. This type of wall is therefore a special case of two-way spanning wall.

As a first stage in the development of a method that may also be applicable as a component of the more complicated dynamic two-way behaviour, an understanding of the physical process underlying one-way dynamic action must first be developed. Consequently, the fundamental focus of the current research project has been the experimental and analytical evaluation of the dynamic behaviour of one-way bending URM walls.

For the one-way bending failure of URM walls there are three key contributing phenomenon; (1) tension cracking of the masonry, (2) compression crushing of the masonry at the vertical reactions (including mid-height) and (3) ultimate instability of the wall. Unless the walls have very high compressive axial loading, crushing is rarely significant. Since in Australia overburden stresses are generally relatively low, local crushing at vertical reactions is not a major problem. Hence, cracking and instability of the wall typically dominate the ultimate behaviour.

Another distinguishing aspect of URM walls subjected to out-of-plane forces is whether the loading is a gradual monotonically increasing static load, or a more rapid and reversible dynamic load. This distinction is drawn as 'dynamic stability' concepts, discussed further in Section 5.3.2, contribute to the walls lateral force resistive capacity.

When a one-way spanning wall is dynamically loaded in the out-of-plane direction an inertia load is induced into the masonry wall. Prior to cracking, the wall essentially acts elastically where deformations are relatively small and hence do not significantly impact on the distribution of inertia force. The accelerations felt by the wall can therefore be obtained by averaging the input accelerations at the top and base of the wall. Should the applied accelerations exceed the elastic capacity of the wall, cracks will form at locations of maximum moment i.e. the top and base support and near the mid-height of the wall. If the top and base crack occur first the theoretical position of the span crack will be

determined by the relative value of the induced moment at these locations. These moments can be related to the eccentricity of the vertical reaction forces and are therefore dependent on the connections forming the boundary conditions. Typically, the crack occurs near the mid-height of the wall as the bending moment diagram in this region is usually reasonably flat, generally only varying by 11% from the mid-height to the three quarter height of the wall (Phipps 1994). Practically, the crack will only appear at a mortar joint and will therefore depend on the relative weakness of individual mortar joints in the region of peak stress.

As was discussed in Section 2.3, the 1989 Newcastle earthquake highlighted that the condition of both new and existing URM building stock is generally unknown with poor maintenance and workmanship common place. Further, many existing URM buildings are already cracked due to low strength mortar, settlement of footings, or temperature and moisture changes. Past earthquakes and/or accidental damage may also have previously induced cracking. Despite this many severely cracked masonry buildings are often still standing after earthquakes and have been able to resist strong aftershocks. Following these observations it is pertinent to examine the post-cracked seismic resistance of simply supported URM walls.

5.2.1. Post-cracked Force-Displacement (F-Δ) Relationship

Once cracking occurs three joints are formed at the top, mid-height and base of the wall, such that the portions of the wall above and below the mid-height crack act as free rocking bodies.

The non-linear F-Δ relationship of a face loaded URM wall results from the complex interaction of gravity restoring moments, the movement of vertical reactions with mid-height displacement and P-Δ overturning moments. A common simplification is to approximate the two free bodies as rigid thus having an infinite material stiffness as shown in Figure 5.2.1. Lateral load is initially resisted by gravity restoring moments due to self-weight and applied overburden loads with the vertical reactions at the three joints acting at the extreme compressive faces of the wall. This initial rigid resistance is termed

the 'rigid threshold resistance' force, $R_e(1)$ and is related to wall geometry, overburden and eccentricity of the vertical reactions and thus the wall boundary conditions.

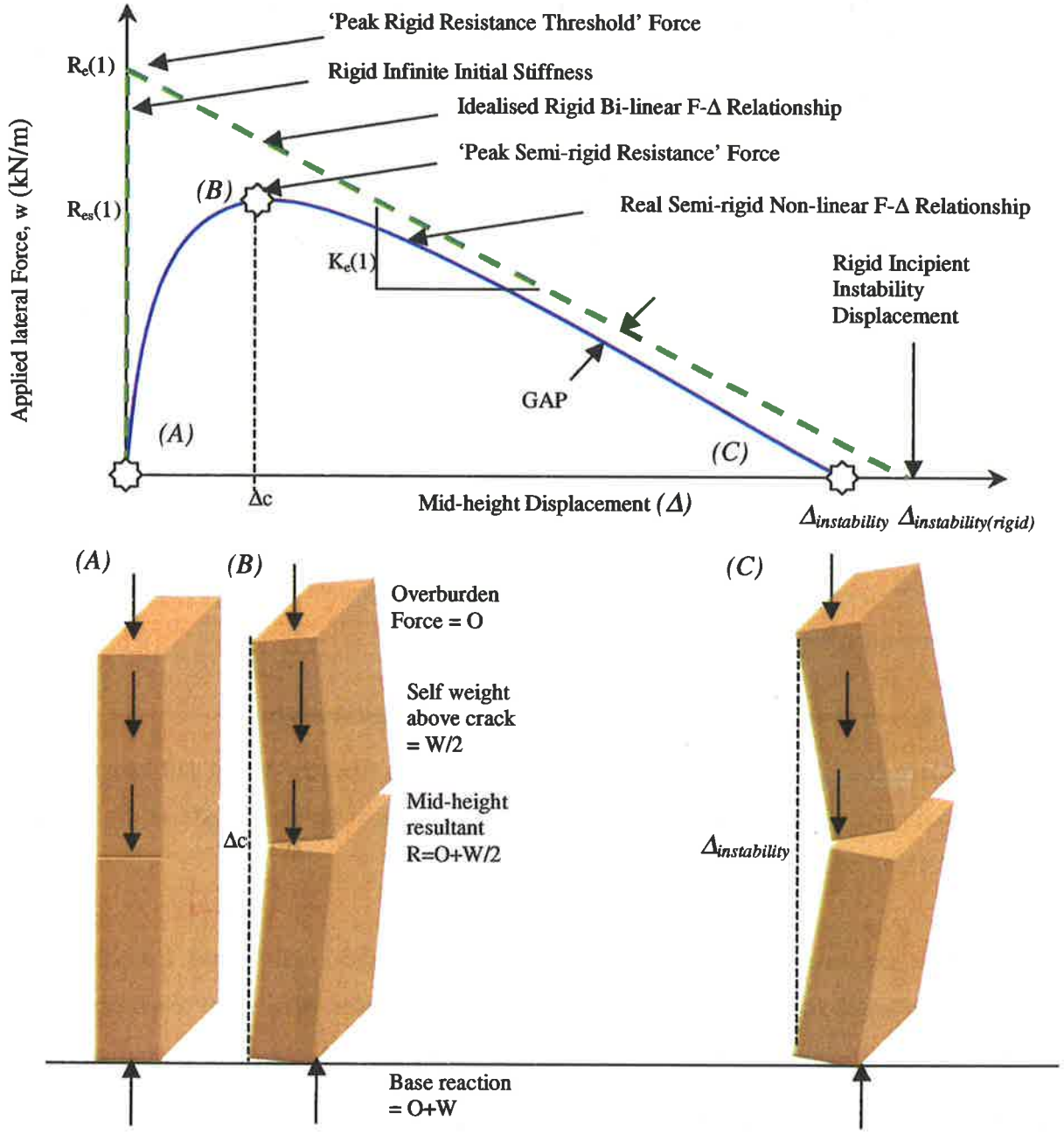

Figure 5.2.1 Real Semi-rigid Non-linear Force-Displacement Relationship

When the lateral force exceeds $R_e(1)$, a mid-height displacement occurs, permitted by the rigid rotation at the three joints. P-Δ effects then reduce the gravity restoring moments as the resultant of the vertical forces above the mid-height crack moves toward the wall's back compressive face. With further displacement P-Δ effects continue to reduce the lateral resistance of the wall creating a negative stiffness arm, $K_e(1)$, of the bi-linear F-Δ relationship (refer Figure 5.2.1). When the vertical force resultant above the mid-height crack moves outside of the wall thickness the resistance to overturning is reduced to zero. The displacement at which this occurs is termed the 'rigid instability displacement', $\Delta_{instability(rigid)}$.

For a real URM wall, the brickwork comprising the two free bodies does not have an infinite stiffness and as such does not behave completely as assumed by the idealised rigid body theory. Instead the real semi-rigid F-Δ relationship for the rocking system is more complicated and non-linear than that of the idealised bi-linear rigid F-Δ relationship.

More realistically, in the vertical position prior to lateral load being applied, all vertical reactions act along the centerline of the wall. Consequently, any applied lateral load will cause a mid-height displacement to occur. This then forces the vertical reactions at the joints to move towards the extreme compressive faces of the wall, thus increasing the gravitational restoring moment lever arm (refer Figure 5.2.1 (A)). The rate at which the reactions move is proportional to the rate of loading and modulus of the brickwork. On further displacement the lateral resistance continues to increase due to the movement of the vertical reactions increasing the gravity restoring moments at a greater rate than the reduction caused by the P-Δ effects. At a critical displacement, Δ_c, when the stabilising effect of these two opposing actions equalize the peak 'semi-rigid resistance threshold' force, $R_{es}(1)$, is realised (refer Figure 5.2.1 (B)). The higher the modulus of brickwork the closer the scenario is to that of the rigid assumption. As a result the closer the critical displacement will occur to the vertical position and the higher the relative value of 'semi-rigid resistance threshold' force. Beyond Δ_c the non-linear relationship approaches the bi-linear rigid relationship as the vertical reactions are forced into the extreme compressive

zones. The curves do not converge, however, due to the finite compressive stress block at the vertical reactions (refer gap Figure 5.2.1). The larger the overburden and the lower the brickwork modulus the larger the gap.

For a static lateral load scenario, beyond the 'threshold resistance', regardless of whether rigid or semi-rigid behaviour is considered, survival of the rocking wall is dependent on the removal or reduction of the static load. Here the wall is said to be in 'unstable equilibrium'. At any displacement, prior to the instability displacement being reached, if the load is statically removed the wall unloading F-Δ relationship will trace back the loading relationship to the vertical position.

As the wall mid-height is displaced its potential energy (PE) is increased with the raising of the wall's center of gravity to a maximum at the incipient instability displacement. Thus, in a dynamic lateral load scenario, survival of a wall beyond the 'threshold limit' is dependent on whether or not the inertia force has sufficient energy to overcome the increased potential energy (PE) so as to further increase the displacement to incipient instability. This energy requirement can be related to the kinetic energy (KE) or velocity of the rocking wall as it passes the static vertical alignment plus any additional input energy that may occur within the failure half cycle. If insufficient energy is available and instability does not take place, the PE which is a maximum at the peak half cycle displacement, is converted back to KE by the gravitational restoring moments. As such, the wall's F-Δ relationship will trace back the loading relationship forming a narrow hysteresis loop due to energy losses in joint rotation. As the wall again passes the static vertical alignment the KE is at a maximum (since the velocity is a maximum) and PE is zero. Again, KE is converted to PE with displacement in the opposite direction. This exchange of energy continues as free vibration until energy losses reduce the total system energy to zero. At this time the wall has returned to the vertical position. Provided the three joints have not degraded through impact or joint dislocation on re-loading, the wall will have a similar F-Δ relationship and dynamic behaviour.

Since the non-linear F-Δ relationship also largely governs the frequency-displacement (*f*-Δ) relationship of a rocking wall system, this is also highly non-linear. The non-linearity can be illustrated by a comparison of secant stiffness at low and high levels of displacement amplitude. Here the secant stiffness is associated with the effective average half cycle secant stiffness. At low displacement amplitude Δ_L, the secant stiffness K_L, is substantially larger than at large displacement amplitude Δ_H, where the secant stiffness is K_H (refer Figure 5.2.2). Since the secant stiffness is directly proportional to the square of the half cycle natural frequency it can be shown that the frequency at low displacement amplitude is relatively large and reduces to zero at the incipient instability displacement. Figure 5.2.2 also shows a schematic *f*-Δ relationship.

The schematic *f*-Δ relationship shown in Figure 5.2.2 is somewhat idealised as it is rare for frequencies near to the incipient instability displacement to occur so that a lower frequencies limit, f_{limit}, is often observed. While it is theoretically possible for frequencies below f_{limit} to occur they are unlikely as the system becomes unstable at these displacements for reasons described below.

As already discussed the F-Δ relationship of URM walls are highly non-linear and as a consequence the responses have no unique natural or resonant frequency. It has however been shown that URM walls undergo larger displacement amplification at certain forcing frequencies. This indicates that they have a unique effective resonant frequency being related to the forcing frequency associated with the largest displacement amplification in a similar fashion to the natural frequency of an elastic system. For the non-linear rocking URM wall systems, the maximum displacement amplification will result when the applied forcing frequency is derived from the average secant stiffness of the half cycle under consideration. Thus, for the critical case where the maximum half cycle displacement reaches the incipient instability displacement, $\Delta_{instability}$, the associated effective resonant frequency, f_{eff}, is related to the average incremental secant stiffness, K_{ave}, determined from the vertical to incipient instability displacements (refer Figure 5.2.2).

During any transient excitation the wall displacement response increases and the response frequencies decrease in accordance with the average half cycle secant stiffness. It is rare for the frequency response to pass through the effective resonant frequency as the likelihood of instability is increased with the increasing displacement amplification. The effective resonant frequency thus provides the observed lower frequency limit so that

$$f_{eff} = f_{limit}$$

The effective resonant frequency therefore also provides the corresponding maximum expected average cycle mid-height displacement, Δ_{limit} before collapse (refer Figure 5.2.2).

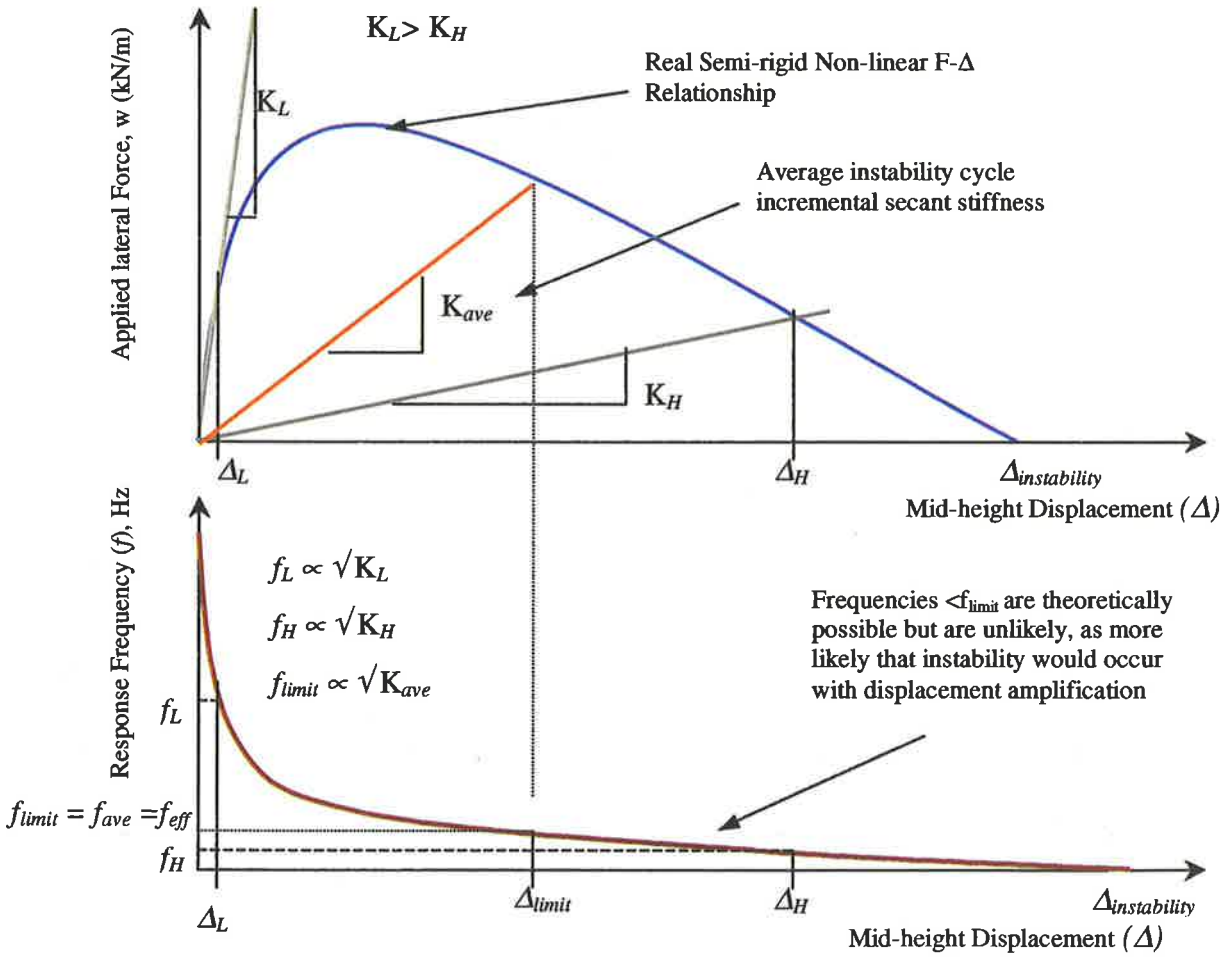

Figure 5.2.2 Post-cracked Frequency-Displacement Relationship

5.2.2. Boundary Condition Impact on Force-Displacement Relationship

The types of wall support comprising the wall boundary conditions are an important aspect that must be considered when assessing out-of-plane URM wall behaviour. To some extent these determine the moment induced into the wall under lateral loading in relation to the eccentricity of the vertical reaction forces at the joints. Typical connections used in Australian masonry construction, such as DPC and 'timber top plate' connections, have been reviewed in Section 2.3.

In URM wall construction, connections to concrete footing beams and floor slabs containing DPC membrane at the top and base wall supports are commonly used to meet serviceability criteria. Consequently, at large mid-height displacements the vertical reactions at the top, middle and base supports will all have been forced to the extreme compressive faces of the wall. Thus, in comparison with other boundary conditions, which do not force the vertical reactions to the wall edge, this scenario provides the greatest 'rigid resistance threshold' force, $R_e(1)$, due to the larger overburden force lever arm providing a maximum restoring moment. In Appendix (D) a generic calculation of the bi-linear F-Δ relationship is presented for the concrete slab support at the top and bottom connections. The generic defining terms Re(1), Ke(1) and $\Delta_{instability\ (rigid)}$ of the rigid bi-linear F-Δ shown in Figure 5.2.2 are summarised in Table 5.2.1 for these boundary conditions as rigid loadbearing simply supported: top and base vertical reactions at the leeward face (LBSSLL).

A second common URM wall support, which is used in single storey URM dwellings, is the connection of the timber roof truss to the masonry wall via a 'timber top plate' where the wall base is set on a concrete slab and DPC connection. As the 'timber top plate' and truss generally provide little rotational support even at large mid-height displacements the top vertical reaction remains near the centerline of the wall, while the middle and base are forced to the extreme compressive faces. With a reduced overburden force lever arm, compared with the concrete slab above case, the 'rigid resistance threshold' force, $R_e(1)$, is also respectively reduced. In Appendix (D) a generic calculation of the bi-linear F-Δ relationship is presented for 'timber top plate' above and concrete slab below boundary

conditions. The generic defining terms Re(1), Ke(1) and $\Delta_{instability\ (rigid)}$ of the rigid bi-linear F-Δ are summarised in Table 5.2.1 for these boundary conditions as rigid loadbearing simply supported: top vertical reaction at the centerline and base vertical reaction at the leeward face (LBSSCL).

Table 5.2.1 also presents the generic defining terms $R_e(1)$, $K_e(1)$ and $\Delta_{instability.rigid}$, for other wall boundary conditions also relevant to Australian masonry construction including rigid parapet (P), rigid non-loadbearing simply supported (NLBSSCL) and rigid loadbearing simply supported at the centerline (LBSSCC). For walls with an applied overburden stress, σ_o, the overburden factor, ψ, is defined as, $\frac{2\sigma_o}{Mg}$, where M is the total wall mass.

Table 5.2.1 Rigid Bi-Linear F-Δ Relationship - Various Boundary Conditions

Support Type	Support Type Abbreviation	$R_e(1)$	$K_e(1)$	$\Delta_{instability}$
Rigid Parapet	(P)	$\frac{h}{gt}$	$\frac{-h}{g}$	t
Rigid Non-loadbearing Simply Supported:base Reaction at the Leeward Face	(NLBSSCL)	$\frac{4.0\ h}{gt}$	$\frac{-4.0h}{g}$	t
Rigid Loadbearing Simply Supported :Top and Bottom Vertical Reaction at the Centerline	(LBSSCC)	$\frac{2.0\ (1+\psi)\ h}{gt}$	$\frac{-4.0\ (1+\psi)h}{g}$	0.5t
Rigid Loadbearing Simply Supported :Top Reaction at Centerline and Base Reaction at The Leeward Face	(LBSSCL)	$\frac{4.0\ (1+¾\psi)\ h}{gt}$	$\frac{-4.0\ (1+\psi)h}{g}$	$\frac{(1+¾\psi)\ t}{(1+\psi)}$ $¾t<\Delta_{instability}<t$
Rigid Loadbearing Simply Supported :Top and Base Vertical Reactions at the Leeward Face	(LBSSLL)	$\frac{4.0\ (1+\psi)\ h}{gt}$	$\frac{-4.0\ (1+\psi)h}{g}$	t

t = thickness of wall

Table 5.2.1 shows that for most of the support conditions, with the exception of LBSSCC and LBSSCL, the mid-height displacement at which static instability occurs is the thickness of the rigid object (t). For the loadbearing simply supported object with top and

bottom vertical reactions at the centerline (LBSSCC) the mid-height displacement at static instability occurs at half the thickness of the rigid object. For the loadbearing simply supported object with the top vertical reaction at the centerline and the base vertical reaction at the leeward face (LBSSCL) the mid-height displacement at which static instability occurs is dependent on the ratio of self-weight to the applied overburden. If the applied overburden is much greater than the self-weight the mid-height instability displacement approaches 75% of the thickness of the rigid object. If the self-weight is much greater than the applied overburden the mid-height instability displacement approaches the thickness of the rigid object. Accordingly the static mid-height instability displacement is always between ¾ t and t.

5.2.3. Un-cracked Force-Displacement Relationship

In the un-cracked state a URM wall behaves essentially elastically where the lateral force resistance increases linearly with displacement. Here the lateral elastic capacity is governed by the tensile strength of the brickwork plus any compressive load due to gravity. Once the elastic capacity has been exceeded, cracking takes place and the wall's lateral force resistive capacity reverts to that of the cracked wall governed by the semi-rigid non-linear F-Δ relationship, as described in Section 5.2.1. The behaviour at cracking is therefore dependent on whether or not the wall's elastic capacity is greater than the post-cracked 'semi-rigid resistance threshold' force, $R_{es}(1)$. For non-loadbearing or low applied overburden force walls the elastic capacity is typically greater than the $R_{es}(1)$. In contrast, for high-applied overburden force walls the tensile strength of the brickwork becomes less significant. Accordingly $R_{es}(1)$ is greater than the elastic capacity. Therefore, to distinguish between the two types of un-cracked behaviour of URM wall they must be catagorised as either low-applied overburden or high-applied overburden force.

5.2.3.1. Low Applied Overburden Force

The first category includes walls where there is no or a low applied overburden force so that the compressive stresses at the critical mid-height cross section are also low. This category of wall could be found as non-loadbearing internal partition walls or as loadbearing walls in low-rise buildings or in the upper stories of multi story buildings.

For this category of wall, prior to cracking the lateral strength is almost entirely governed by the masonry flexural tensile strength, f'_t, so that the elastic capacity is greater than the $R_{es}(1)$ (refer Figure 5.2.3). Thus, once the elastic capacity, $R_{elastic}$, has been exceeded the lateral resistive force reverts back to the lower cracked wall resistance. Therefore, no additional lateral capacity exists beyond cracking and wall survival is reliant on the applied force being reduced to the cracked lateral capacity of the wall.

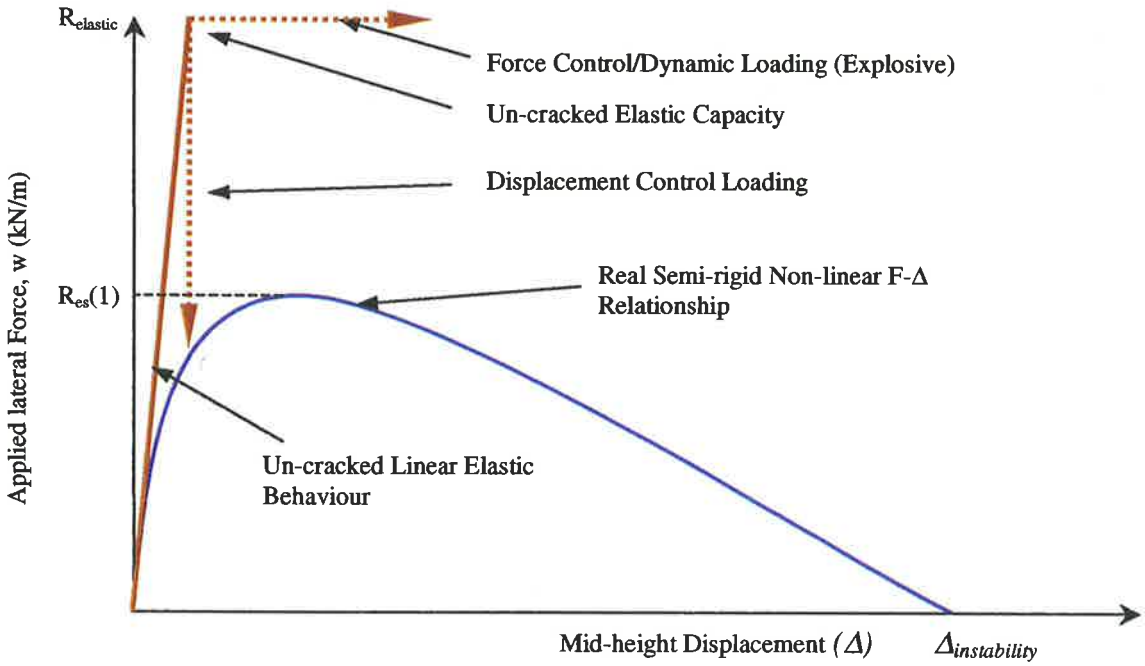

Figure 5.2.3 Un-cracked F-Δ for Low Applied Overburden Stress URM Wall

Where the wall is dynamically loaded, once the elastic capacity has been exceeded the elastic inertia force is typically sufficient to continue to increase the wall displacement (refer Figure 5.2.3). As a result this category of wall generally fail explosively under dynamic loading having no reserve capacity to 'rock'. Consequently, an elastic static analysis will provide a reasonable estimate of the dynamic capacity of this category of wall. Should, however, the wall become cracked at any time during its life this type of elastic static analysis may be highly non-conservative. Alternatively, should high frequency spikes exist within a dynamic excitation these may have sufficient energy to

crack a wall prematurely such that the maximum elastic capacity may not be realised and the elastic static analysis methodology would again be non-conservative.

5.2.3.2. High Applied Overburden Force

The second category of wall is generally found two or more stories below roof level or in upper concrete slab-URM wall construction. Here, where the applied overburden force is larger, compressive stresses at the critical mid-height cross section are correspondingly higher. In this case the benefit provided by the tensile capacity of the brickwork is outweighed by the additional gravity restoring moment resulting from an increased lever arm, as vertical reactions move towards the extreme compressive faces of the wall with increased displacement. Accordingly, cracking of the wall does not alter the wall's ultimate lateral capacity (refer

Figure 5.2.4). Typically, for a dynamic load scenario when the elastic capacity is exceeded the elastic inertia force will not be sufficient to then exceed the 'semi-rigid resistance threshold' force. Therefore, this category of wall behaves similarly to a pre-cracked wall where a reserve capacity due to rocking and 'dynamic stability' concepts must be considered.

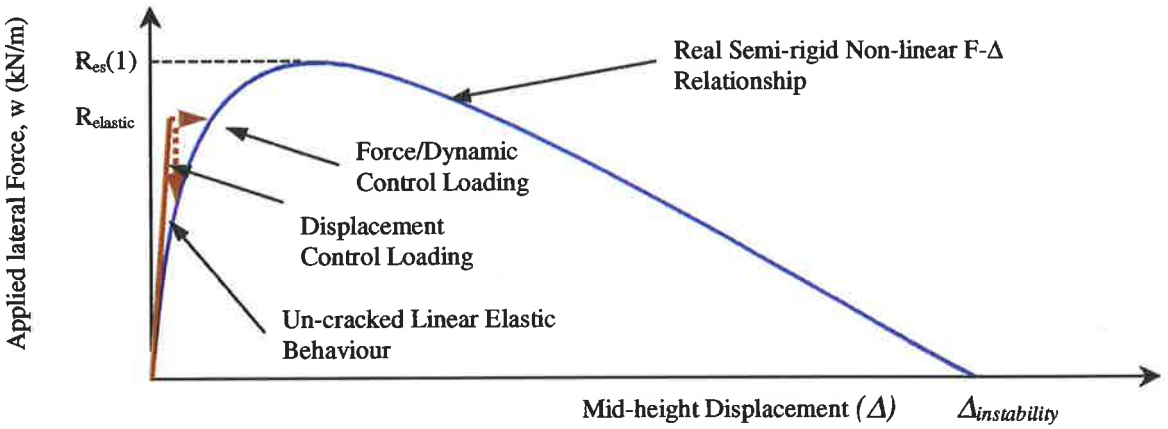

Figure 5.2.4 Un-cracked F-Δ for High Applied Overburden Stress URM Wall

5.3. Previous Research: Experimental Studies

Over the past 30 years or so there have been various experimental studies carried out on both the static and dynamic out-of-plane behaviour of face loaded URM walls. Since earlier research was predominantly concerned with the effect of wind loading these studies mainly considered static loading. More recently, however, the research focus has been placed on seismic loading so that experimental studies have largely involved dynamic loading. The following section provides a brief review of previous works carried out by other researchers relevant to the one-way bending of face loaded URM wall panels.

5.3.1. Static Tests

In the early 1970's the U.S. Building Research Division of the National Bureau of Standards (now the National Institute of Science and Technology, NIST) undertook an extensive experimental study (Yokel et al 1971) on the static one-way out-of-plane bending behaviour of masonry wall panels. In total 192 tests were completed including both single leaf unreinforced brick and concrete block, cavity wall and reinforced masonry. For each type of construction, specimens were subjected to a static vertical compressive load, applied as a point load at the centerline of the top of the wall, followed by a gradually increasing lateral pressure exerted by an inflated air bag. The boundary condition at the base wall support was a steel channel with a fiberboard sheet adjacent to the wall specimen. Boundary conditions were therefore representative of 'timber top plate' above and concrete slab below.

Specimens with both low and high levels of applied overburden force were tested. At low levels it was found that the maximum lateral strength occurred prior to cracking and that this was related to the tensile strength of the masonry. In contrast, at higher levels of applied overburden force additional wall capacity was found after cracking. The reasons for this have been discussed in Section 5.2.3. For walls with moderate levels of overburden force applied, a comparison with simple rigid body theory was found to be consistent. Above 1MPa overburden stress, however, the continuity began to drop away, as crushing of the brickwork at vertical reactions became apparent (refer Figure 5.3.1).

Typical failures for both low and high applied overburden stress are shown in Figure 5.3.2). While the primary objective of this study was the development of appropriate interaction curves for combined bending and axial load, the force-displacement (F-Δ) relationships were also published (refer Figure 5.4.2).

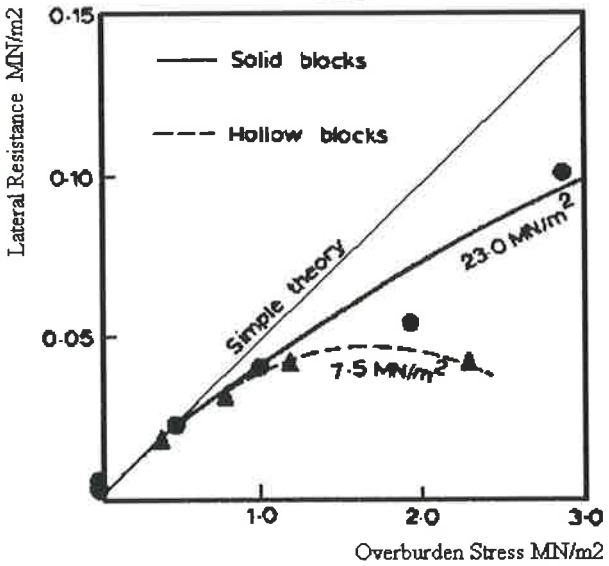

Figure 5.3.1 Comparison of Yokel Study with Simple Rigid Body Theory

(Hendry 1973)

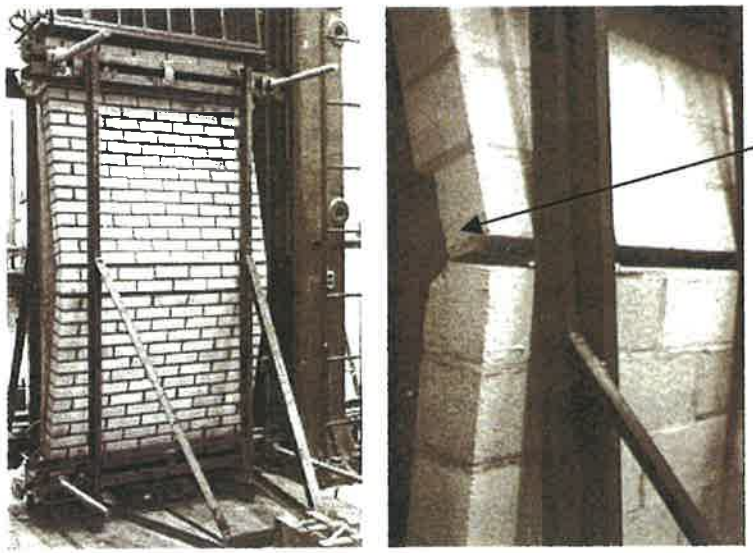

Figure 5.3.2 Typical Lateral Failure of Brick Wall

(Yokel et al 1971)

Later, Yokel and Fattal (1976) performed a similar experimental study to that of Yokel et al (1971) also at the National Bureau of Standards. The main differences between the studies where that for the 1976 tests smaller panel were used having steel half round bars inserted at both top and base boundary conditions. This represented a simply supported wall at its centerline. Since here the movement of vertical reactions was limited to only the center joint, the prediction of the F-Δ relationship was greatly simplified. Experimental F-Δ relationships were again reported (refer Figure 5.4.2). For this case it was observed that both the displacement at which instability occurred and the maximum resistance were reduced in comparison with the Yokel study.

Base and Baker (1973) reported on a series of low overburden force out-of-plane tests. These were aimed at providing fundamental data and an understanding of the action of brickwork under a variety of loading conditions. Here the brickwork specimens were observed to behave essentially elastically in the un-cracked state. A significant reduction in bending strength was reported when brickwork beams were tested under simulated uniform loading as compared with testing under central load over a shorter span. This was attributed to the increased number of mortar joints within the loading span, thus increasing the probability of a weak joint.

West et al (1977) have also performed a series of static out-of-plane tests on wall panels. Here no applied overburden force was considered so that the cracking load was reported to be the maximum load the wall could resist. For these tests the top of the wall was propped against lateral movement and a connection containing a DPC was used at the base to represent as closely as possible the conditions used in practice. It was reported that the material used for the DPC and the way in which it was embedded were important in achieving the full bending strength. Where the shear capacity of the DPC connection was exceeded the full bending strength of the wall was not achieved since slip occurred at the DPC. Further, both vertical and horizontal panels were examined where it was found that the strength in the two orthogonal directions differed. The overall ratios of strength in the direction perpendicular to the bed joint to that parallel joint were reported as being 1.2 to 6.2 with a mean of around 3.

West, Hodkinson and Webb (1973) conducted extensive tests on strip walls demonstrating the relationship between lateral strength and overburden force of storey height walls of various thickness and materials. Support conditions considered were similar to those of concrete slab above and below. Experimental results were reported as being well represented up to a mid-height compressive stress of 1.4 MPa by the simple relationship (refer Figure 5.3.3)

$$p_a = 8\sigma_c/S^2$$

where p_a = *ultimate lateral pressure*

σ_c = *overburden compressive stress*

S = *slenderness ration* = H/t

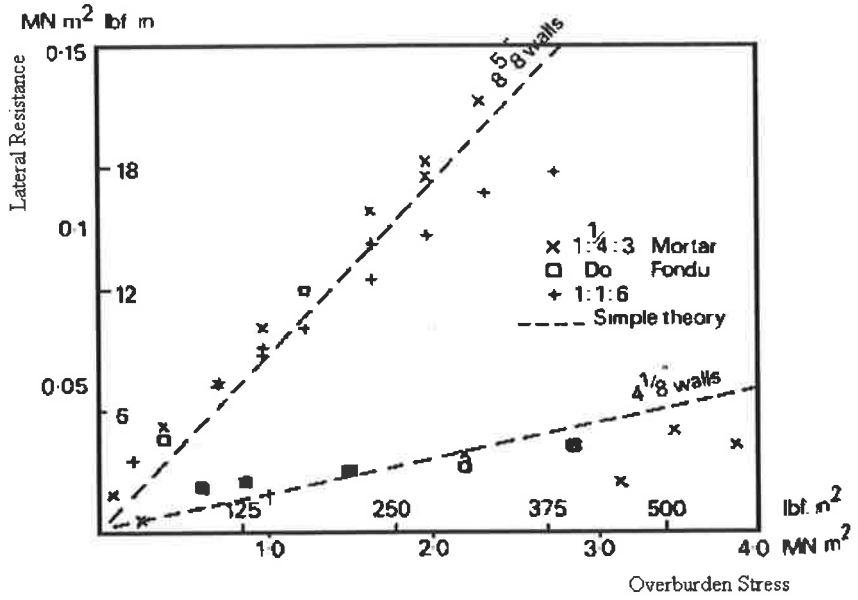

Figure 5.3.3 Comparison of West et al 1973 Tests with Simple Rigid Body Theory

(Hendry 1973)

This relationship was based on the rigid body theory with all vertical reactions pushed to the extreme faces of the wall. Above 1.4 MPa overburden stress, the lateral resistance was again reported to fall away from the linear relationship owing to compression and local crushing. At low overburden force, experimental results tended to exceed the theoretical values because of the tensile strength of the brickwork that is not taken into

account. It was also reported that the lateral strength of a wall with compression is only slightly affected by brick and mortar strengths.

Anderson (1994) reported on the most recent series of static tests where 90 lateral load tests on URM walls with various support conditions were undertaken. Here the behaviour of vertically spanning strip walls was reported to be difficult to predict with post-cracked rigid body theory considered to be a more satisfactory approach for static limit state design. Eccentricity of the vertical load due to rotation of the base of the wall was found to induce a stabilising moment. Consequently it was recommended that the partial fixity moment due to the self-weight acting at an eccentricity of 0.45 of the wall thickness be applied at the base of the wall. The mean height at which the bed joint failed was 0.6 of the vertical span above the base. Failure by sliding was reported at the DPC for some walls with low levels of applied overburden force.

5.3.2. Dynamic Tests

In the early 1980's a consortium of Californian engineers called the ABK Joint Venture (ABK 1984) carried out research into the post-cracking seismic behaviour of URM wall panels. The aim of the research was to develop standards for the renovation of URM buildings in Los Angeles, particularly with respect to wall height-to-thickness ratios (Kariotis et al 1985, Adham et al 1985). The study examined the one-way behaviour of eight specimens of varying construction and geometry under a range of gravity loads. Several dynamic motions were applied at the base and top support, simulating the input motion from the ground or diaphragm anchorage. The base of the wall was allowed to displace without rotation and the top of the wall was free to rotate and to move in the vertical direction without restraint.

It was reported (ABK 1984) that a single horizontal crack typically formed near the mid-height of the test specimen with another forming near its base. The stability of the fully cracked URM wall, shaken by less than critical ground motion intensities, was maintained by gravity load moments applied at the cracked surface. When the center of gravity of the vertical loads, above the cracked surface, lay within the wall thickness

dimension the gravity load moments were found to provide a restoring moment that closed the crack upon reversal of the earthquake displacement motion. This ability to displace without collapse resulted in the walls having a significant reserve capacity above that of the 'semi-rigid threshold' force. The term 'dynamic stability' was used to distinguish this type of behaviour from that which might be expected from static calculations. Correspondingly, a major finding of the study was that neither static elastic nor 'quasi-static' analysis procedures were completely satisfactory to define the dynamic and highly non-linear response of the post-cracked URM walls.

Like the static F-Δ relationship, the hysteretic behaviour was found to have a declining branch and on unloading the hysteretic F-Δ plot traced back along the loading plot.

As a result of this experimental investigation (ABK 1984) key parameters for predicting the failure of URM walls subjected to face loading were identified. These were the wall slenderness, the ratio of the applied gravity load to the wall self weight and the peak input velocities at the base and top of the wall. A further important finding was that although various phase shifts between the top and bottom excitation were examined, input velocities simultaneous in time were found to be the critical case. That is, an in-phase excitation at the top and base of the wall was the critical excitation case.

During the study the effect of vertical ground motion was not considered as it was thought to not have a significant influence on the dynamic stability. This was explained, as the frequency band of vertical motions in seismic events is generally not in the critical frequency band of the horizontal ground motions. That is, the effect of high frequency vertical motions on the restoring moments will not result in a bias of increasing or reducing the restoring moment. This is due to the significantly lower frequency of instability excursions as compared to the typical frequency of vertical seismic motions, especially as the relative excursion of the center part of the wall approaches instability.

Bariola et al (1990) reported on a series of tests where a gradually increasing excitation was applied to the base of parapet URM walls. Here it was reported that prior to cracking

the natural frequency of the wall correlated well with simple elastic beam theory. In the cracked state, however, no unique natural frequency was found as it decreased with increased displacement response. Also, wall slenderness was not found to have a clear influence on the peak acceleration required to cause instability. For walls of the same slenderness wall but with different thickness, the thicker wall appeared to be more stable.

Results of another important dynamic experimental study of out-of-plane URM wall behaviour was recently published by Lam et al (1995). This study focussed on one-way bending of parapet walls with the objective of comparing various analytical approaches with the experimental results. The subject of the experiment was a 1m tall, 110mm thick, clay brick URM wall and was subjected to the El Centro ground motion. Free vibration tests were also used to identify the frequency response and damping characteristics of the cantilevered wall. The un-cracked elastic natural frequency was found to be between 5 and 10 Hz depending on the amplitude of vibration. Once the wall was cracked the rocking frequency was found to decrease from about 4Hz at low amplitude displacements to a lower frequency limit of approximately 1Hz at larger displacements. Although the equivalent viscous damping, ξ, being a measure of energy loss was observed to vary slightly (2.6%-3.4%) with displacement it was reported to be fairly consistently around 3%.

Continuing from their earlier tests Lam et al (1998) have also reported on shaking table tests on parapet walls of different dimensions using harmonic excitations of varying amplitude and frequencies. Here the peak displacement of the wall was correlated to the peak shaking table acceleration and velocity. These relationships were found to be highly dependent on the excitation frequency so that plotting results associated with different forcing frequencies produced large scatters (refer Figure 5.3.4). In contrast, a good linear correlation was obtained between the relative displacement of the wall and the absolute displacement of the shaking table (refer Figure 5.3.5). Typically, the peak relative displacement at the top of the parapet wall was reported to be twice the peak absolute displacement of the table irrespective of the frequency and amplitude of the table motions. Inspection of the test results further showed that the center of gravity of the

wall was displaced by a similar amount to the table so that the response was 180° out of phase with the table motion. In effect the center of gravity position remained effectively stationary in space. Lam et al (1998) therefore postulated that for the harmonic forcing frequencies considered, the 'equal displacement theory' could be adopted. Consequently, wall instability would be predicted when the base displacement equaled half the thickness of the parapet wall.

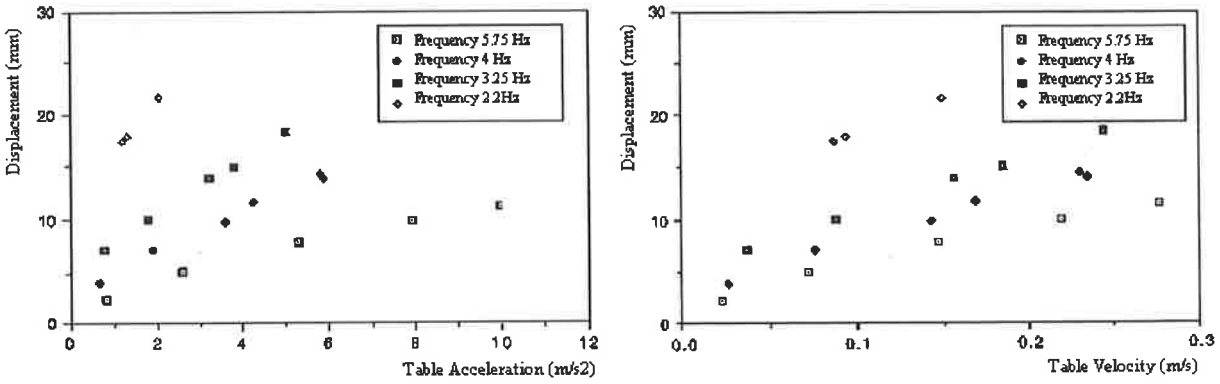

(Harmonic tests on 500mm tall cantilever walls)

Figure 5.3.4 Top of Parapet Wall Disp. Correlated to Table Velocity and Acceleration

(Lam 1998)

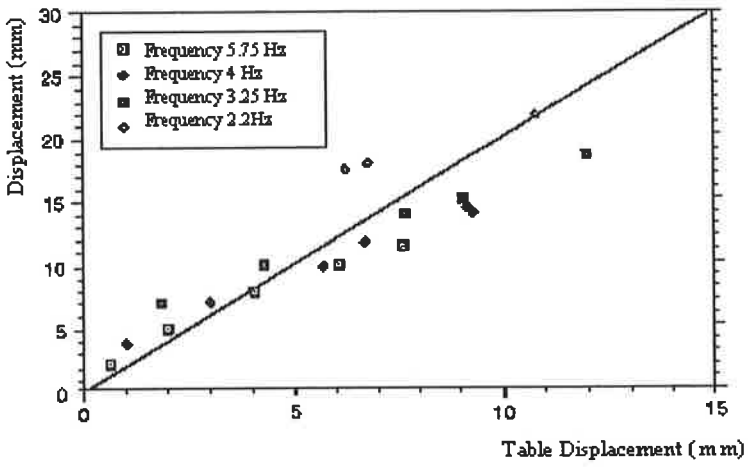

Figure 5.3.5 Top of Parapet Wall Disp. Correlated to Table Disp.

(Lam 1998)

It was noted, however, that the frequencies used were much higher than the effective resonant frequency of the parapet wall tested at large displacements. Consequently, should excitation frequencies closer to those of the wall's effective resonant frequency at large displacements have been used, displacement amplifications greater than unity would have been more likely and the 'equal displacement theory' would not apply.

5.4. Critical Review of Current Analysis Methodologies

As a result of experimental and analytical studies previously carried out, various analysis methodologies have been developed over the years to analyse the one-way out-of-plane seismic capacity of URM walls. The following sections critically review these methodologies highlighting the advantages and limitations of each method.

5.4.1. Quasi-Static Analysis Procedures

The response of a URM wall to earthquake induced base excitations is a complex dynamic process. Analysis, however, is often simplified by considering an instantaneous maximum acceleration occurring at a critical snapshot in time. As such, the peak-input acceleration associated with either the ground motion (PGA) or building response, depending on the location of the wall within the structure, is often used to represent the associated inertia force. Displacements are assumed to be small so prior to failure the induced inertia force is assumed to be uniformly distributed over the height of the wall relative to the distribution of mass.

Alternatively, it is possible to estimate the wall's critical natural frequency, either in the cracked or un-cracked state, thus permitting an estimate of the elastic spectral response acceleration to be determined from an elastic response spectrum. The main limitation here is that the natural frequency of a URM wall is not unique, as described in Section 5.2.1. In addition, for the cracked wall case where response displacements are relatively large, in contrast to the uniformly distributed inertia load assumed above a trapezoidal distributed inertia load is more likely. This is due to the additional triangular inertia force induced by the vibration of the wall over the rectangular inertia force resulting from the motion of the supports.

Regardless of the method used to determine the 'snapshot acceleration' the dynamic action is represented by a 'quasi-static' type analysis. Earthquake design codes and standards typically specify analysis methods based on this 'quasi-static' analysis philosophy. The two most common methods are: (a) the stress based linear elastic (LE) and (b) the rigid body (RB) equilibrium analyses. Both are briefly reviewed in this section.

As described in Section 5.2.3 previous researchers have found that in the un-cracked state URM walls behave essentially elastically. It is possible therefore to utilise the well established linear elastic (LE) analysis methodology to predict at what equivalent lateral inertia force cracking stresses within a URM wall will be exceeded. The fundamental principle is to equate the maximum seismically induced moment at a critical section M_u, to the moment required for the cracking stresses at the leeward face M_e, to be exceeded. Resistance to cracking is provided by both the flexural tensile strength of the brickwork f'_t, and the compressive force at the mid-height of the wall from self-weight and overburden. Figure 5.4.1 shows a representation of the LE analysis for the prediction of the cracking acceleration for a simply supported URM wall. Since elastic deformation prior to cracking in URM walls is generally relatively small the vertical reactions at the top and base supports are assumed to act at the centerline of the wall.

The current seismic design methodology in Australia (AS3700-1998) for the vertical one-way bending of URM walls subjected to transient out-of-plane forces adopts the stress based LE analysis of the un-cracked section. Here a 'Capacity Reduction Factor' of 0.6 is also used in design to allow for the variability in the flexural tensile strength.

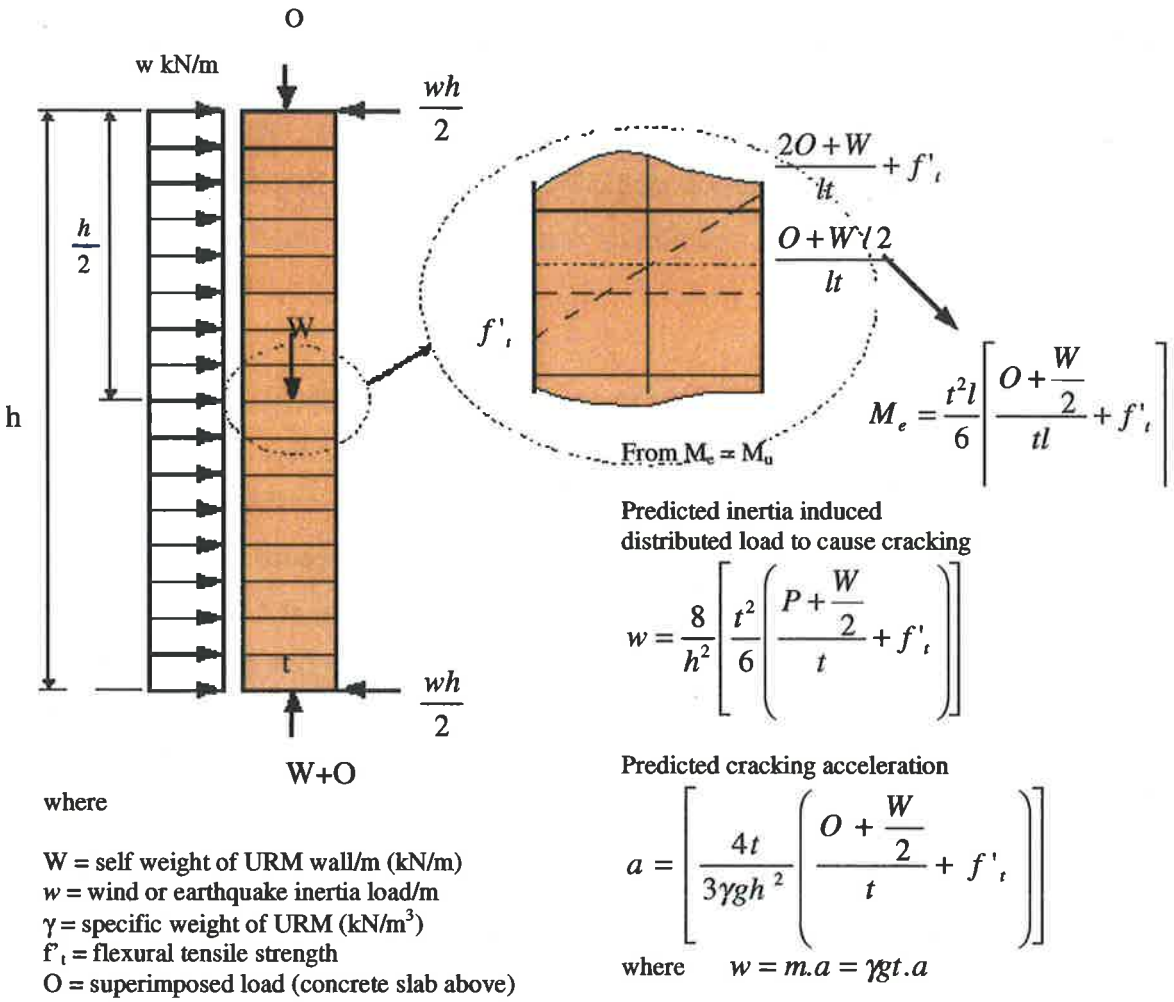

where

W = self weight of URM wall/m (kN/m)
w = wind or earthquake inertia load/m
γ = specific weight of URM (kN/m^3)
f'$_t$ = flexural tensile strength
O = superimposed load (concrete slab above)

Figure 5.4.1 Quasi-Static Linear Elastic Design Methodology

The assumption of an un-cracked wall and elastic stress-strain behaviour is a major limitation of the linear elastic analysis methodology. As highlighted by the Newcastle earthquake much of Australia's older URM building stock may have an appreciably depleted masonry flexural tensile capacity or even be pre-cracked. Also, since the analysis is dependent on a reliable estimate of the highly variable flexural tensile strength of the brickwork at the time of loading it is consequently difficult to accurately predict the cracking capacity. Another major limitation of this method is that the formation of flexural tensile cracks does not necessarily result in failure of the wall as implied. In fact, as discussed in Section 5.2.3, for walls with applied overburden force, this is rarely the case. Instead, after first cracking a small mid-height displacement causes the wall's

neutral axis to be forced in the direction of the compression zone at both mid-height and vertical support reactions. This neutral-axis shift associated with crack propagation can lead to a "tip-toe" situation in which the wall is supported on its edges.

The post-cracked seismic performance of an URM wall is therefore more realistically analysed by the rigid body (RB) equilibrium analysis method, which compares the overturning moment with the restoring moment taken about the rocking edge of the wall. The overturning moment is obtained in the same manner as for LE analysis using the quasi-static methodology, whereas the restoring moment is obtained by consideration of the forces due to self-weight and any overburden acting on the free body above the mid-height crack. This is identical to the method described in Section 5.2.1 for determining the 'rigid threshold resistance' force, $R_e(1)$. A major limitation of this method is that it assumes that the brickwork has an infinite stiffness. In reality, it is semi-rigid and highly dependent on its constituent materials. Correspondingly, the real 'semi-rigid resistance threshold' force, $R_{es}(1)$, can be much lower than $R_e(1)$ as it occurs at a larger displacement where P-Δ effects are more prominent.

To account for the reduced 'resistance threshold' caused by the semi-rigid behaviour of URM walls, Priestly (1985) and Paulay (1992) proposed a method of determining the real non-linear F-Δ relationship. This method is based on first principles of beam theory, and assumes a zero tensile strength for the masonry and simply supported wall at the centerline. The fundamental approach is based on the assumption that the gradient of the linear elastic stress diagram at the critical mid-height section, and thus the wall curvature, is related to the mid-height displacement of the wall. As this relationship is derived through examination of the stress diagram at the cracking displacement the assumed modulus and boundary conditions are important considerations.

A finite element model named the Block-Interface Model has also been developed (Martini 1997) in an attempt to determine the real static post-cracked F-Δ relationship. Here joints are represented by discontinuum elements so that the elastic properties of the mortar and associated local effects at the block mortar interface are neglected with the

mortar joint representing a potential line of failure due to cracking (refer Figure 5.4.2). Here increasing the number of laminations and layers increases the density of the finite element mesh and thus allows more accurate refinement however this also increases the complexity of the model. The finite element Block-Interface approach has the advantage of being able to be implemented using commercial software.

Figure 5.4.2 shows a comparison of experimentally derived F-Δ relationships from the Fattal (1976) and Yokel (1971) studies with those determined analytically by the Block Interface finite element model (Martini 1997) and the Priestly (1986) method.

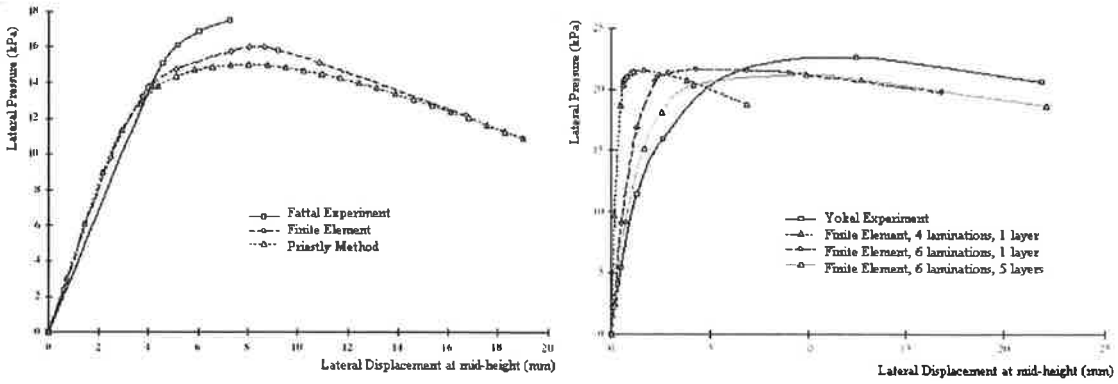

Figure 5.4.2 Experimental and Analytical F-ΔComparison

(Martini 1997)

It must be recognized that none of the previously mentioned 'quasi-static' analyses take into account the time-dependent nature of the response of the wall since only an instantaneous acceleration occurring at a critical snapshot of the response is considered. A URM wall will not necessarily become unstable and collapse should the quasi-static force exceed the resistant capacity of the wall, as the incipient instability displacement may not be reached. As such, the level of seismic loading to cause failure can greatly exceed that predicted by the quasi-static analysis methods (ABK 1985, Bariola 1990, Lam 1995) such that a reserve capacity exists. The quantification of the reserve capacity is reliant on the frequency and amplitude content of the applied excitation so that more realistic dynamic modeling approaches should be used to account for the dynamic behaviour.

5.4.2. Dynamic Analysis Procedures

Although being particularly useful as suitably conservative modern design tools the 'snapshot' quasi-static design methodologies described above may not be appropriate for the review of existing URM structures. In the design of new structures the application of conservative design tools will generally have only minor economic consequence. However, in reviewing existing structures using procedures which do not recognise the additional lateral strength capacity resulting from 'dynamic stability', a more significant economic penalty may be incurred. An example is where the decision to demolish, retrofit or 'leave as is' for a significant monumental URM structure may be in the balance.

In recognition of the problem of assessing the dynamic response by the 'snapshot' principle an alternative analysis method based on the widely recognised 'Equal Energy' procedure has been proposed by (Priestly 1985). The 'Equal Energy' procedure is based on the observation that 'dynamic stability' concepts can be considered by using an equivalent elastic capacity derived by equating the real energy required for instability with that of an elastic system having a stiffness equal to the initial un-cracked stiffness of the wall. Although based on an observation, this simplification has been shown to predict reasonable estimates of peak displacement response for simple systems with relatively short periods (Priestly 1985, Lam 1995). It has been observed however that for systems with very short periods this procedure can provide very un-conservative estimates of lateral dynamic capacity and for systems with longer periods a conservative estimate of lateral dynamic capacity (Priestly 1985, Robertson 1985).

For URM wall dynamic capacity prediction using this method, the potential energy absorptive capacity of a wall undergoing large displacement is first quantified. This is achieved by determining the area under the non-linear F-Δ curve as the wall is pushed from the vertical non-displaced position to that of the incipient instability displacement. The procedure to approximate the F-Δ curve of a simply supported load-bearing URM wall pinned at the centerline for the purpose of applying the equal-energy procedure has been reported in Section 5.4.1. The maximum kinetic energy (KE) demand is then

derived from the maximum spectral velocity as obtained from an elastic response spectrum to compare with the potential energy (PE) capacity. Thus, it is assumed that the wall would remain un-cracked and behave linearly up to the time when the maximum KE is reached (vertical position) and at commencement of the failure half cycle. At this time the wall is assumed to crack and begin to rock as the PE is increased to absorb the KE.

The abrupt transition from the linear elastic response (in the un-cracked state) to the non-linear rocking response (in the cracked state) is a major assumption of the equal energy procedure. In reality, the dynamic behaviour of the wall at the commencement of the failure half cycle is not always linearly elastic. It has been demonstrated by dynamic tests (Lam 1995) that the stiffness and natural period of a URM wall can be highly amplitude dependent even in the un-cracked state. Thus, the "elastic" natural period of vibration of the wall, which governs its spectral velocity (and hence its maximum KE) can not be predicted with certainty. Further, it is possible that the wall may have already cracked and be responding in-elastically prior to the commencement of the failure half cycle. A second major shortcoming of the 'equal energy' method is that ground excitations are also assumed to have stopped once the failure rocking half cycle has commenced. As a result the accumulated effects of multiple pulses on the wall during rocking can not be accounted for as additional input energy into the system within the failure half cycle is not considered.

Figure 5.4.3 presents a comparison of the predicted URM wall acceleration capacity utilising the 'equal energy' method with the previously described quasi-static analyses. As expected the linear elastic analysis provides the most conservative prediction of dynamic lateral capacity for moderate to high overburden stress ranges. For low overburden stress, however, the rigid body analysis is more conservative. For all overburden stress the 'Equal Energy' method provides the least conservative prediction as an allowance is made for 'dynamic stability'. As the effectiveness of the 'equal energy' observation is highly dependent on the system's un-cracked natural frequency the prediction is very sensitive to the selection of elastic modulus. Often a realistic modulus value can result in an extremely un-conservative lateral strength prediction.

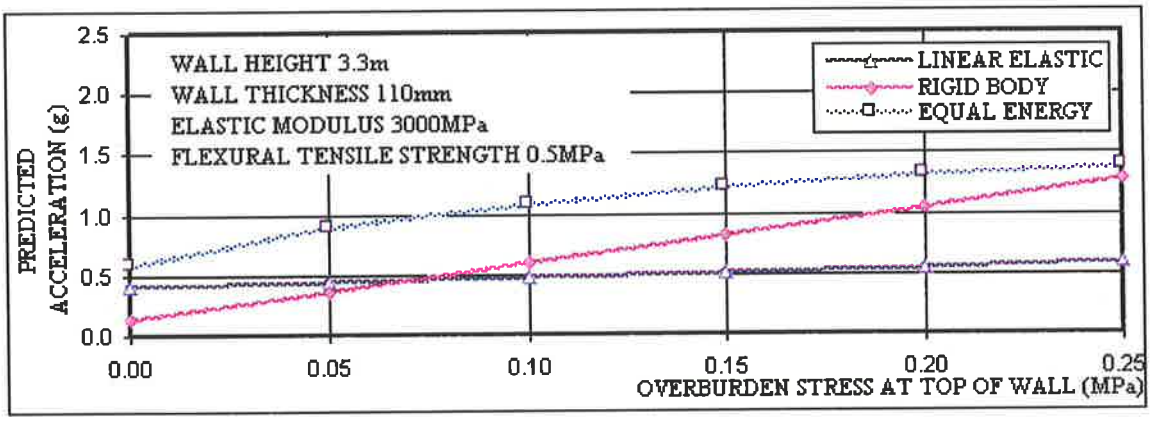

Figure 5.4.3 Comparison of Analysis Predictions

As discussed in Section 5.3.2, Lam (1998) has reported that for harmonic excitations of varying amplitude and relatively high frequencies the center of gravity of a parapet wall effectively remained stationary in space. Consequently, based on an 'equal-displacement' methodology, wall instability could only occur when the table displacement exceeded the incipient instability displacement, which could be related to the thickness of the wall. It was also highlighted that for forcing frequencies closer to the natural frequency of the wall at large displacements that significant displacement amplification was possible so that instability could occur at table displacements less than the incipient instability displacement thus invalidating the 'equal-displacement' methodology for practical applications. To overcome this shortfall a dynamic amplification factor was proposed. While this method is useful for the dynamic analysis subjected to harmonic excitations it is limited for multiple frequency, transient excitations where random pulse arrival will significantly affect the wall response.

The methods described so far have all used a single parameter (acceleration, velocity, or displacement) to predict the effect of the excitation on the response of a URM wall. As a result these methods all have limitations for dynamic analysis although the velocity based dynamic analysis is satisfactory to analyse the response of single pulse excitation and the equal displacement method is suitable for stationary periodic excitations. Unfortunately, general, transient excitations can not be accurately represented by a single parameter so

that Time History Analysis (THA) procedures are required to take into account the effect of the frequency content, duration and pulse arrival details of the excitations.

Although researchers (Housner 1963, Yim et al 1980, Hogan 1989) have reported on analytical studies where explicit mathematical solutions of rigid rocking motion equations have been derived these are limited for applications where the system can not readily be idealised. Further, where transient excitations are considered explicit mathematical representation is not possible. Consequently, to undertake a THA an approximate numerical evaluation of the response integral must be used. This requires an assumption to be made on the motion between consecutive time steps. For example, acceleration may be assumed to be constant or linearly varying thus allowing the basic integration equations to be developed (Clough & Penzien 1993).

Lam (1995B) has reported on the development of specific THA software for the analysis of the dynamic response of a parapet walls to transient excitations using the Constant Average Acceleration Integration technique and a rigid bi-linear F-Δ relationship. To minimise computational time an iterative procedure was not included to model damping but rather an average mass proportional damping coefficient for the response was developed based on an estimate of the response frequency. Nevertheless, despite the approximations made in modelling the F-Δ and damping properties, results from this THA have provided reasonable agreement with experimental results. Similar THA techniques are also currently being developed for the in-plane rocking analysis of URM walls (Magenes & Calvi 1996:1997, Abrams 1998).

In 1992 Blakie et al reported that a simplified Displacement-based (DB) analysis, which compared the displacement demand with capacity, might better predict the seismic capacity of out-of-plane panels. Although approximate, this method has the potential to account for the dynamic behaviour and thus the walls reserve capacity. Similar DB analysis procedures are currently also being developed for the prediction of in-plane rocking capacity of URM walls (Magenes & Calvi 1996:1997).

5.5. Specific Research Focus

Although most URM walls are designed as two-way spanning elements, as a first stage in the development of a method that may also be applicable as an analysis component of dynamic two-way behaviour, an understanding of the physical process underlying one-way dynamic action must first be developed.

While there has been a substantial research effort undertaken on the static loading behaviour of one-way spanning wall panels, dynamic action has not been as well examined. Consequently, simple static analysis procedures have been developed which are capable of predicting cracking and ultimate loads and have been shown to correlate well with experimental results. In contrast, the dynamic behaviour is not well understood.

The few dynamic loading experimental studies that have been previously undertaken have indicated that URM walls have a significant capacity to displace without becoming unstable. As a result they are often observed to have the capability of sustaining inertia forces greater than that predicted by 'quasi-static' methods. This is referred to as the wall's dynamic 'reserve capacity' to rock. Unfortunately, currently available seismic predictive models have been unable to account for this large displacement post-cracked behaviour. Where the 'reserve capacity' to rock is overlooked in analysis a conservative estimate of seismic capacity is made. Although this may be acceptable for the design of new buildings, it may impose serious economic penalties in the analysis of existing structures.

In response to the above shortfall a need was apparent for the development of a rational and simple analysis procedure, encompassing the essence of the dynamic behaviour and thus accounting for a URM wall's 'reserve capacity' to rock. The development of this analysis procedure was adopted as the research focus for the final component of this project.

6. OUT-OF-PLANE SHAKE TABLE TESTING OF SIMPLY SUPPORTED URM WALLS

6.1. Introduction

With the aim of developing a better understanding of the physical processes governing the dynamic collapse behaviour of simply supported URM walls a series of shaking table tests were conducted on the earthquake simulator in the Chapman Structural Testing Laboratory, University of Adelaide. In this experimental study the wall response to harmonic, transient and pulse excitations was examined with the effect of wall variables including thickness, slenderness and the level of overburden stress taken into consideration. In Chapter 7 the resulting dynamic response data is used to confirm the reliability of a specifically developed non-linear Time History Analysis (THA) procedure for modelling the semi-rigid rocking response of URM walls.

To complement the shaking table test data, static push tests and free vibration tests were also conducted. These complementary tests enabled the non-linear force-displacement (F-Δ), frequency-displacement (f-Δ) and damping-frequency (ξ-f) relationships for the rocking wall to be investigated. In Chapter 7, these experimentally derived relationships are used to calibrate the specifically developed non-linear Time History Analysis (THA) program.

For completeness, material tests were conducted even-though the ultimate behaviour of face loaded URM walls, at low levels of overburden, have not previously been found to be particularly dependent on the constituent brickwork material properties. Nevertheless, these results provide an indication of the masonry quality tested.

The following chapter presents a description of the experimental study undertaken highlighting key results and where possible a comparison of experimental results with theory is also presented. A representative cross section of test results is presented in the Appendices E and F.

6.2. General Test Set Up

6.2.1. Test Specimens

In total, 14 one-way spanning URM wall panels were constructed for out-of-plane testing. Where possible, multiple static and dynamic tests were performed on each specimen. Details of each of the wall specimens are presented in Table 6.4.1. The height of the wall panels was limited to 1.5m by the height of the laboratory gantry crane. Consequently, standard 110mm thick wall specimens were constructed at a height of 1.5m giving a slenderness ratio of 13.6. For more realistic slenderness ratios to be examined, 1.5m tall, 50mm thick walls were also constructed. These had a slenderness ratio of 30.

The bricks used were standard extruded clay bricks having the dimensions 76 x 110 x 230mm and had 3 x ϕ45mm holes as shown in Figure 6.2.1. A 10mm mortar joint was adopted for both horizontal and vertical perpends as per normal construction practices in Australia. The average density of the 110mm thick brickwork was determined to be 1800kg/m^3. This was achieved by weighing a representative sample of the brickwork and dividing by its volume. In this way, the mortar which partially filled the brick holes was also taken into account.

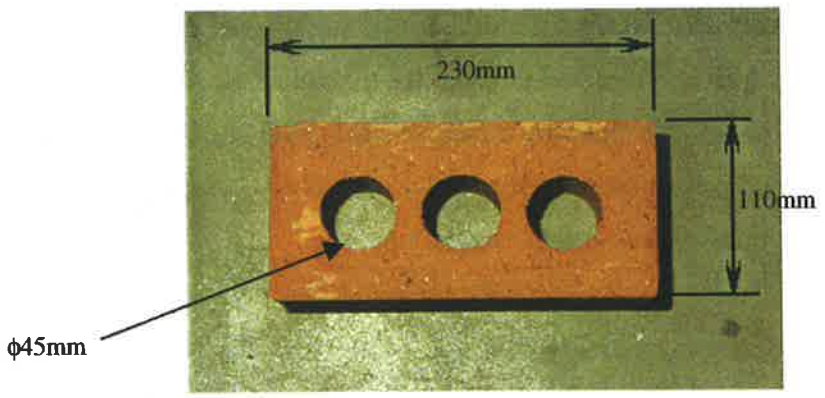

Figure 6.2.1 Standard Three Hole Extruded Clay Brick (110mm)

The 50mm bricks used in these tests were solid having been cut from brick pavers, with dimensions 33 x 50 x 230mm. For the 50mm thick wall specimens, a 5mm mortar joint was adopted. Since wall geometry rather than material properties was considered critical to the rocking behaviour, no attempt was made to model the constituent mortar materials to half scale. The average density of the solid 50mm thick brickwork was measured at 2300kg/m^3.

For all of the wall specimens a typical Australian mix of 1: 1: 6 (cement: lime: sand) mortar was used. Common 'brick' sand and Portland cement were used and water was added until good workability of the mortar was achieved. No air entraining additives were used and to improve consistency between mortar batches, 'bucket batching' was used.

A professional bricklayer was employed to construct the one-way spanning wall specimens. At the base of each wall an embossed polythene membrane DPC connection was used (refer Figure 6.2.2). Wall specimens were constructed in three lots with four 110mm thick walls constructed in March 98 and June 98 and three 50mm thick and 110mm thick walls constructed in September 98. All walls were constructed as a standard veneer with wall ties connected to a timber support frame (refer Figure 6.2.2). This construction method was adopted after preliminary tests showed that the mortar bond could be depleted if wall panels were constructed without lateral support. This was attributed to the fact that lower brick layers were disturbed as the upper layers were

placed thus breaking the bond. Using the timber wall for support overcame this problem by providing stability to the wall panel during construction. An added benefit was that this also prevented accidental damage during curing and provided a more realistic construction technique. After a minimum of 28 days curing time the wall ties were cut and the wall panel carefully lifted onto the shaking table.

Throughout the fabrication of the test walls, two-brick and five-brick prisms and 100x100x100mm mortar cubes were regularly constructed for material testing, as described in Section 6.3.

Veneer wall used for construction

Embossed Polythene DPC connection at base

Figure 6.2.2 Construction of URM Wall Panels

6.2.2. Test Rig

To provide a representative boundary condition at the top of each of the simply supported URM wall panels tested, a braced steel frame was rigidly attached to the shake table with a 'cornice' type support connection used to provide lateral restraint at the top of each brick wall. The 'cornice' support was made up of steel angle and 10mm square, stiff rubber spacers to prevent the wall from binding against the angle at large wall mid-height displacements (refer Figure 6.2.3). Prior to testing the 'cornice' was fitted snuggly to the wall. However, to ensure a minimal vertical restraint due to friction the 'cornice' was not over tightened.

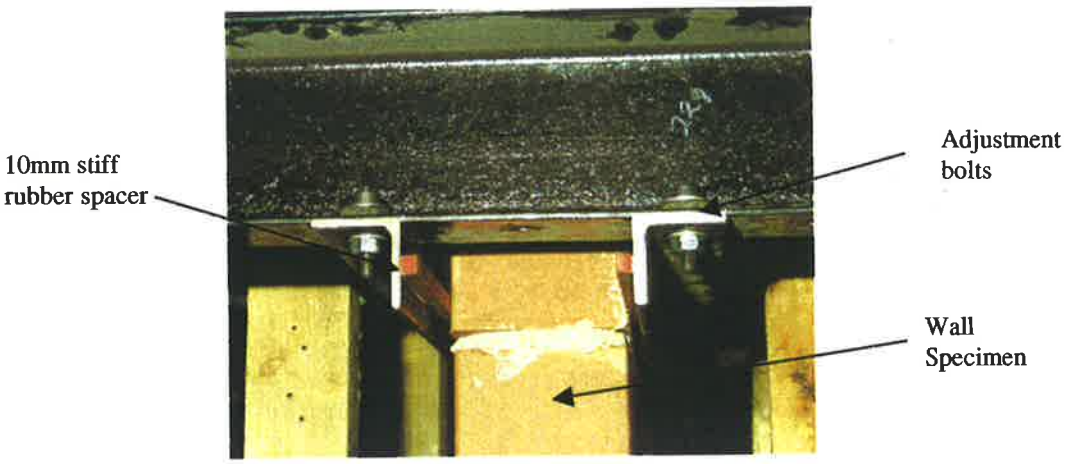

Figure 6.2.3 Top 'Cornice' Support Connection

The stiffness of the braced frame was designed to represent as closely as possible the in-plane stiffness of a URM structural shear wall (refer Figure 6.2.4). As a consequence, any input excitation provided at the table was also applied approximately in phase at the top of the wall. This was confirmed by comparison of the absolute displacements of the table and top of the braced frame for each of the dynamic tests. Using an impulse free vibration test the natural frequency of the braced frame was determined to be approximately 10Hz. For most of the tests this was not in the range of dominant driving frequencies so that the small response amplification recorded at the top support was neglected. For the relatively high un-cracked wall natural frequency tests, however, where the mid-height of the wall specimen was excited using a mallet strike, the black frame natural frequency dominated the response and thus was required to be filtered out. Also, for harmonic tests completed near the frame's natural frequency of 10Hz significant amplification of the base excitation was observed at the top support of the test specimen so that an average input excitation had to be considered.

Preliminary tests showed that it was very difficult, in practice, to apply an overburden force at the top of the test walls in a realistic manner using weights supported by a concrete slab. This method produced large overturning moments at the bearing support rails of the shaking table, leading to a dangerous rocking action during testing that limited the inertia forces that could be induced into the wall. To overcome this problem an

overburden rig was designed which relied on six large springs to develop the required level of overburden stress (refer Figure 6.2.4). The static deflection of the springs could be altered by adjustment of the central thread, thus altering the overburden force at the top of the wall through the base plate of the springs. The overburden test rig therefore had the advantage of permitting easy changes to the overburden force.

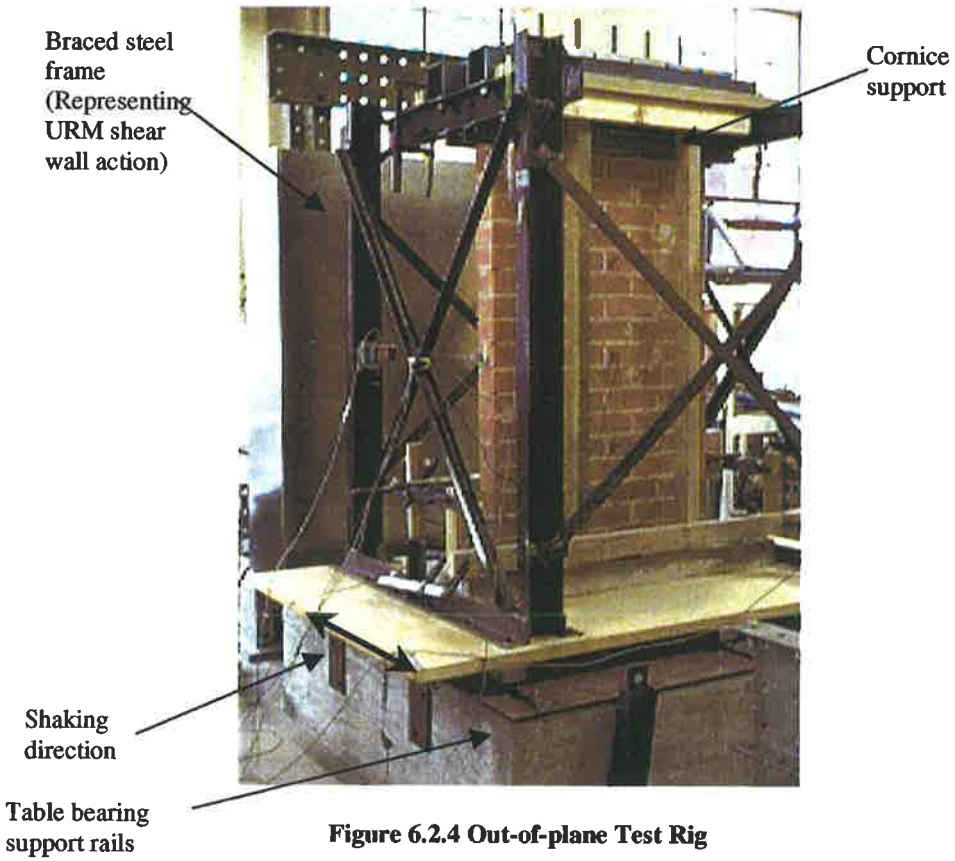

Figure 6.2.4 Out-of-plane Test Rig

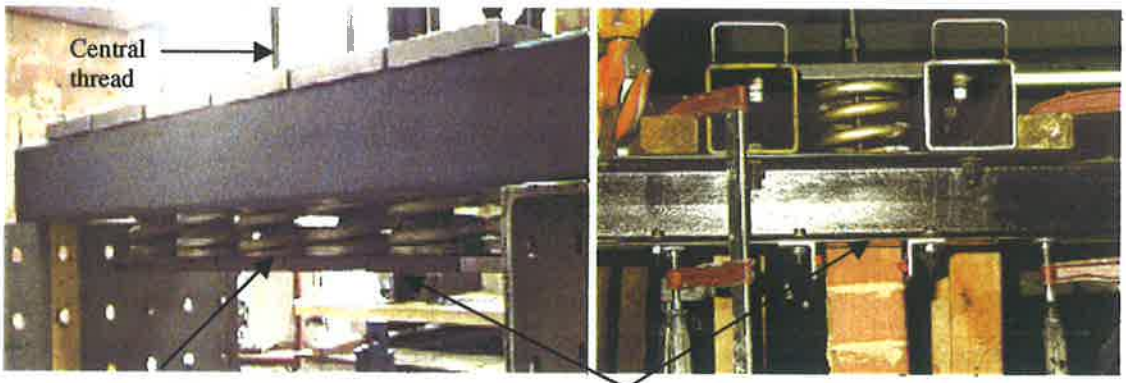

Figure 6.2.5 Overburden Rig

The main disadvantage of using the overburden rig was that with increased mid-height displacement the total wall height also increased slightly thus increasing the static spring deflection and hence overburden force. Accordingly, the desired constant overburden force at the top support was not realised at larger displacements. To overcome this problem springs were selected so that the additional overburden force developed with the expected increase in height was not significant. Further, since the increase in height with mid-height displacement is inversely proportional to the wall slenderness the additional overburden force on the 50mm walls was significantly less than that of the 110mm walls. Correspondingly, for the 50mm wall specimens mid-height displacement changed the mean overburden force by less than ± 5% so that the constant force assumption was acceptable. In contrast, for the 110mm thick wall specimens significant increases in overburden force were observed so that the constant force assumption was only acceptable for mid-height displacements of less than 20% of the wall thickness. Static compression tests were performed on the springs to calibrate the spring coefficients where it was found that a 0.16kN force was developed for each mm of static spring deflection.

Since the situation with overburden represented a vertical continuation of the wall or a supported concrete slab, a point load connection was not used at the top of the wall panels. Thus, the location of the top vertical reaction was governed by the spring base plate, and with increased wall mid-height displacement the top vertical reaction was forced to move to the compressive zone (refer Figure 6.2.6).

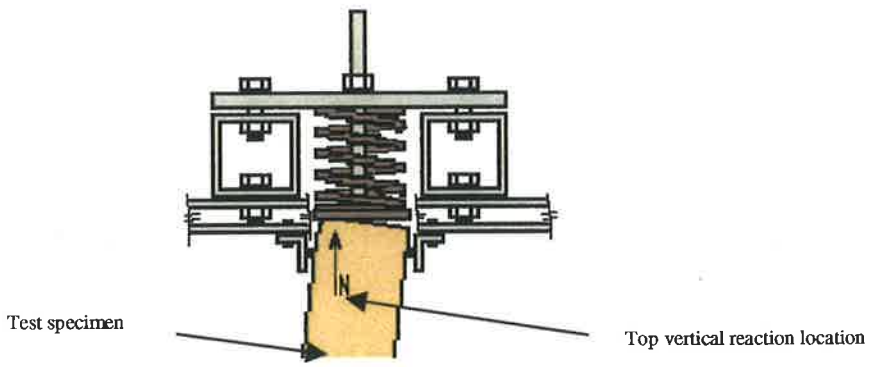

Figure 6.2.6 Top Vertical Reaction – Overburden Test Rig

The test boundary conditions were therefore considered similar to a concrete support slab above and below where the vertical reactions are constant but pushed to the compressive zone with mid-height displacement.

6.2.3. Instrumentation

A total of nine channels of data were recorded for each of the dynamic tests in order to capture the dynamic response characteristics of the rocking URM wall specimens. The instrumentation consisted of five accelerometers, two Linear Voltage Potentiometer Transducers (POT), one Linear Voltage Displacement Transducer (LVDT) and the internal INSTRON hydraulic actuator displacement transducer. For static tests, the same instrumentation was used with the exception of the five accelerometers. Figure 6.2.7 shows the location of the nine instrument points and Table 6.2.1 presents a summary description of the application of each instrument.

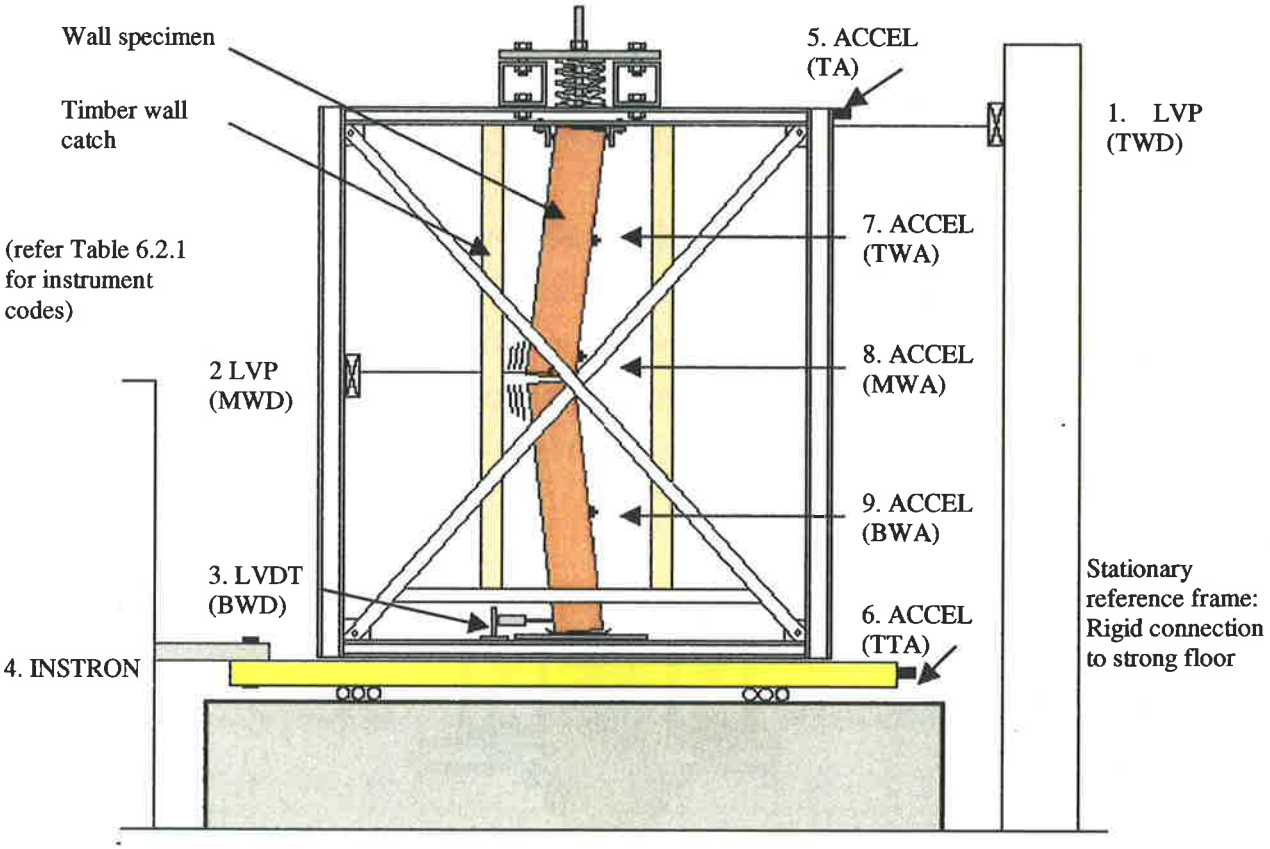

Figure 6.2.7 Out-of-plane Wall Test Instrumentation Locations

Table 6.2.1 Out-of-plane Wall Test Instrumentation Description

Channel No.	Location/Description	Application	Instrument Code
1	Absolute Top Wall Displacement	Top wall displacement excitation	TWD
2	Relative to Frame Mid-height Wall Displacement	Mid-height wall displacement response	MWD
3	Relative to Table Base Wall Displacement	Base slip check	BWD
4	INSTRON internal displacement	Base wall displacement excitation	INSTRON
5	Top Frame Acceleration	Top wall acceleration excitation	TA
6	Table Top Acceleration	Base wall acceleration excitation	TTA
7	Top Wall Acceleration	¾ - wall height acceleration response	TWA
8	Mid-height Wall Acceleration	Mid-height wall acceleration response	MWA
9	Bottom Wall Acceleration	¼ - wall height acceleration response	BWA

One Linear Voltage Potentiometer (POT) was mounted horizontally between the stationary reference frame, connected to the laboratory strong floor, and the braced frame at the level of the top of the simply supported wall specimen to record the total top of wall/frame displacement (TWD). The POT was a Housten Scientific model 1850-050 having a maximum displacement of 500 mm and powered by a 10 Volt DC supply. A similar instrument was used to record the relative mid-height wall response displacement (MWD) between the wall and braced frame. In Chapter 7, the MWD is used for comparison with analytical predictions of the mid-height displacement response of simply supported URM walls using the specially developed THA program. A Schlumberger Linear Voltage Displacement Transducer (LVDT) having a maximum displacement of ±10mm was mounted between the base of the wall specimen, just above the DPC connection, and the shaking table to measure the relative displacement between the wall base and shaking table (BWD). The data from this instrument was only used to ascertain if any sliding at the wall base DPC connection occurred during testing.

Kistler Servo Accelerometers powered by a servo amplifier were used to record the top frame (TA), and tabletop (TTA) accelerations. These accelerometers have a measurable acceleration range of ± 50g and are able to detect accelerations as small as 0.1mm/s^2. These accelerations therefore represented the actual input excitations applied to the wall specimen and are used in Chapter 7 as input for the non-linear THA. The top frame accelerations were also compared with the table accelerations to identify how much amplification of the base excitation was caused by the braced frame's flexibility.

The top (TWA), mid-height (MWA) and bottom (BWA) accelerations were recorded using the 'Analogue Devices' single chip accelerometer, model ADXLO5 which were adhered to the face of the wall at the ¾ -, mid - and ¼ - height respectively. This less expensive semi-disposable accelerometer was selected, as it was possible that should the wall collapse these devices could be sacrificed. These accelerometers have a measurable acceleration range of ± 5g and are able to detect accelerations as small as 0.01g. A limitation of this method was due to the accuracy of the accelerometers being reliant on a horizontal datum. Since the accelerometers were glued to the wall surface they rotated with the rocking of the wall so that as the wall's mid-height displacement increased the accuracy of the data from these accelerometers decreased. For most of the critical response however the accuracy was adequate for the purpose of the tests. Comparison of the BWA and TWA with the mid-height acceleration response was useful in characterising the total dynamic acceleration response profile. The mid-height acceleration response was also later used for comparison with THA predictions.

In a similar fashion to the dynamic tests performed on URM connections containing a DPC membrane, described in Chapter 4, the 'Microsoft Windows' based data acquisition system 'Visual Designer' was used to collect the nine channels of response data. Data was collected at a period interval of 0.01 seconds (100Hz).

Where restoring moments were relatively small, in particular for the non-loadbearing 50mm thick wall specimen, care was taken to ensure that the instrumentation did not influence the test outcome.

6.3. Material Tests

The material tests undertaken have included bond wrench tests to determine the brickwork flexural tensile strength, f'_t, and compression tests of brickwork prisms and mortar cubes to determine the masonry's modulus of elasticity, E_m, and ultimate compressive strength, f'_m, and mortar's compressive strength, f'_c. The following section presents a brief discussion of these tests and their results.

6.3.1. Bond Wrench

The bond wrench test is one of two methods permitted in AS3700-1998, Appendix (D) to determine the flexural tensile strength, f'_t, of the bond between mortar and brick units perpendicular to the bed joints. As described in Section 5.2.3, for un-cracked walls with low levels of overburden, f'_t is often the critical wall parameter for lateral loading. Here the un-cracked elastic lateral force capacity is greater than the cracked force capacity so that at first cracking an explosive dynamic instability is possible.

Two bond wrenches were specifically manufactured for this project being for the 110mm and the 50mm brick specimens. The bond wrench is used to apply a moment to the joint to be tested by applying a load at the end of the lever arm. From the known applied moment, f'_t can be determined with the assumption of an idealised stress distribution across the bed joint. To best approximate this idealised stress distribution the bond wrench design, as shown for the 110mm brick specimen in Figure 6.3.1, was adopted from research undertaken by Samarasinghe et al (1998). This bond wrench specification has since been included in AS3700-1998, Appendix (D). To simplify the procedure strain gauges were adhered to the arm of the bond wrench with peak strains calibrated to the applied force at the loading point. Calibration plots for the two bond wrenches are presented in Appendix (E).

In order to ascertain if the flexural tensile strengths, determined from the two-brick prism tests, were representative of the test specimens, bond wrench tests were also completed on pre-dynamically tested URM wall specimens, as shown in

Figure 6.3.2. For each test specimen three prism and three wall tests were completed. For the pre-dynamically tested walls the vertical perpends on either side of the test joint were cut using a masonry hand saw. Comparison of prism and wall test results showed that the tested walls generally had a slightly greater f'_t. This was attributed to the wall test including a vertical perpend in the course below as shown in Figure 6.3.2.

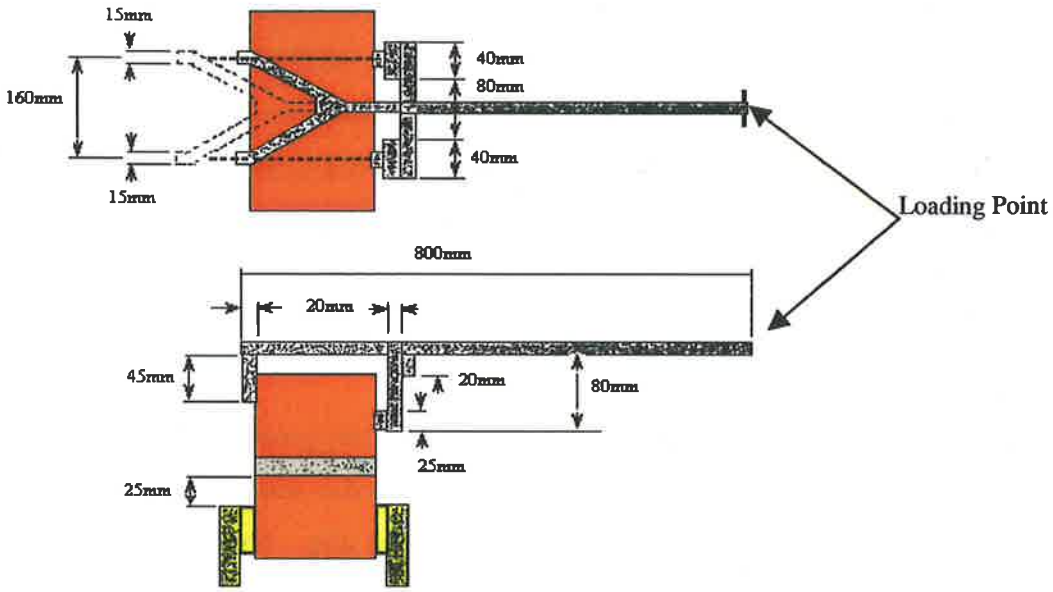

Figure 6.3.1 Bond Wrench Apparatus Dimensions (110mm Brick)

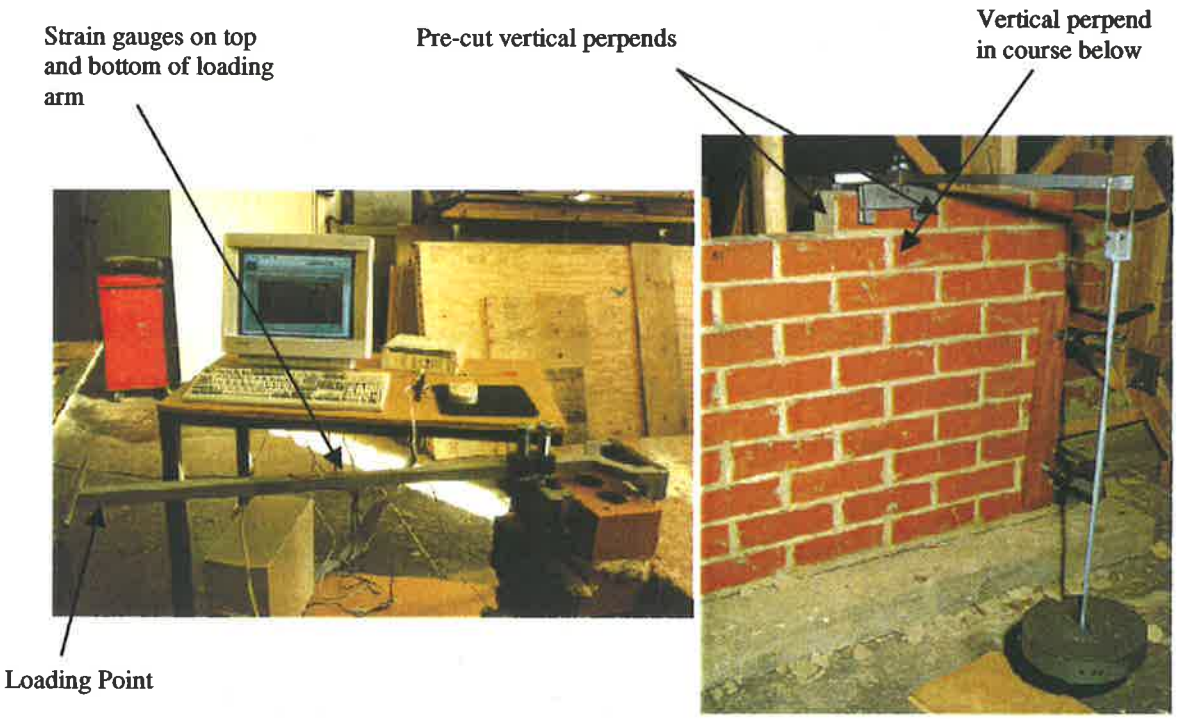

Figure 6.3.2 Bond Wrench Test Set Up

Table 6.3.1 presents a summary of the bond wrench test results showing a range of f'_t between 0.17 and 0.99 MPa with a mean of 0.49MPa and overall standard deviation of 0.15MPa. The characteristic flexural tensile strength (= mean–1.64 x standard deviation) is 0.25MPa. A comparison of this with the design f'_t permitted by AS3700-1998 of 0.2MPa indicates that the design assumption is slightly conservative. A complete list of bond wrench test results is presented in Appendix (E).

Table 6.3.1 Bond Wrench Test Results Summary

Specimen No.	Test	Specimen Thickness	Minimum f'_t	Maximum f'_t	Standard Deviation	Average f'_t (3 tests)
1	Prism	110mm	0.22	0.36	0.07	0.28
	Wall	110mm	0.53	0.72	0.10	0.64
2	Prism	110mm	0.30	0.41	0.06	0.36
	Wall	110mm	0.39	0.54	0.07	0.47
3	Prism	110mm	0.30	0.48	0.10	0.40
	Wall	110mm	0.42	0.53	0.05	0.47
4	Prism	110mm	0.35	0.48	0.07	0.42
	Wall	110mm	0.39	0.84	0.22	0.61
5	Prism	110mm	0.40	0.71	0.17	0.59
	Wall	110mm	0.55	0.99	0.25	0.71
6	Prism	110mm	0.41	0.48	0.04	0.43
	Wall	110mm	0.48	0.53	0.11	0.56
7	Prism	110mm	0.50	0.68	0.09	0.6
	Wall	110mm	0.27	0.53	0.13	0.41
8	Prism	110mm	0.37	0.55	0.09	0.45
	Wall	110mm	0.53	0.63	0.05	0.59
10	Prism	50mm	0.36	0.88	0.30	0.70
11	Prism	110mm	0.17	0.55	0.20	0.32
12	Prism	110mm	0.27	0.32	0.03	0.30
13	Prism	110mm	0.22	0.40	0.10	0.29
14	Prism	50mm	0.56	0.86	0.17	0.76

6.3.2. Modulus of Elasticity

To determine the modulus of elasticity, E_m, for each of the masonry specimens a compressive test was conducted on a five-brick tall prism. Each prism was constructed at the same time and using the same materials as was used for each test wall. After a minimum of 28 days a 2-inch set of Demec points was applied vertically at the center brick and a 8-inch set on the opposite side of the prism thus covering two mortar joints and the center brick. Following this each five-brick prism was carefully placed onto the

base compressive platen of a hydraulic actuator. Dental paste was then applied to the top of the prism before gently lowering the top compressive platen onto the dental paste (refer Figure 6.3.3). This method provided an even loading platform so that stress concentrations at the loading face would be avoided.

A preparatory compressive test was first undertaken to determine the approximate ultimate compressive strength, f'_m, of the prisms. Here strains were not recorded. For the remaining tests Demec strain readings were taken up to approximately 50% of the estimated ultimate load. Each specimen was then loaded to f'_m without further recording of strains (refer Figure 6.3.3 for typical splitting failure). Back calibration of the two Demec readings allowed the strains in a representative sample of brickwork (one brick and one mortar joint) to be determined. This permitted the stress-strain relationship to be determined. The brickwork modulus was then calculated for each specimen as the chord modulus between 5% and 33% of the ultimate brickwork compressive strength, f'_m.

Figure 6.3.3 Five Brick Prism at Ultimate Compressive Load

Table 6.3.2 presents a summary of the modulus test results ranging from 3,300 MPa to 16,000 MPa for the 110mm specimens and 6,700 MPa to 9,800 MPa for the 50mm

specimens. While the results varied significantly the modulus values were typically found to be relatively high as expected of modern masonry. For older masonry constructed with weak lime mortars it is possible that the modulus values would be lower, being in the order of 500MPa to 1,000MPa (Robinson 1985). A complete list of compressive test results for the five-brick prisms is presented in Appendix (E).

Table 6.3.2 Brickwork Modulus Test Results

Specimen No.	Specimen Thickness	Modulus E_m (MPa)	Ultimate Compressive Load (N)	Masonry Compressive Strength, f'_m (MPa)
1	110mm	-	330,000	13
2	110mm	15,000	332,000	13.1
3	110mm	3,300	336,000	13.3
4	110mm	3,300	333,000	13.1
5	110mm	16,000	360,000	14.2
6	110mm	-	338,000	13.4
7	110mm	13,900	313,000	12.4
8	110mm	5,400	245,000	9.7
11	110mm	6,600	359,000	14.2
12	110mm	11,600	397,000	15.7
13	110mm	-	397,000	15.7
AVERAGE	**110mm**	**9,400**	**339,000**	**13.4**
STANDARD DEVIATION		**5,322**	**41,528**	**1.64**
10	50mm	9,800	307,000	26.7
14	50mm	6,700	303,000	26.3
AVERAGE	**50mm**	**8,250**	**305,000**	**26.5**
STANDARD DEVIATION		**2,192**	**2,824**	**0.28**

The masonry modulus of elasticity, E_m, can be represented by the linear relationship

$$E_m = k f'_m$$

where k is a constant. Drysdale et al (1994) reported that from previous experimental studies on clay brick prisms, k generally falls within the range of 210 to 1670. For the 110mm prism tests k was estimated to be 9,400/13.4 = 700 and is therefore within the range of previous experimental results. For the 50mm bricks k was estimated to be 8,250/26.5=310 and is therefore also in the lower range of the proposed values.

6.3.3. Mortar Compressive Strength

Mortar compressive strength, f'_c, is often an important parameter for masonry because it has an influence on the masonry compressive stress, however, it is typically used more as a measure of quality control. For each test specimen three standard 100x100x100mm mortar cubes were produced. After 28 days these were removed from their non-absorptive casing and tested in compression. The typical failure mode was observed to be a pyramidal shape. Due to the relatively high lime and sand content of the mortar as compared to the cement content, the mean f'_c of 5.17MPa was quite low compared with mortars of a higher cement content, ranging from 3.56MPa to 7.16MPa. A complete list of mortar cube compressive test results is presented in Appendix (E)

6.4. Out-of-Plane Testing of Simply Supported URM Walls

To explore the out-of-plane dynamic response of simply supported URM walls harmonic, pulse and transient excitation shaking table tests were conducted. The testing program is best described by grouping the completed tests into the three construction lots of March 98, June 98 and September 98. For both March 98 and June 98, gradually increasing harmonic excitation tests were performed on both cracked and un-cracked 110mm thick URM walls. These harmonic tests were aimed at developing an understanding of the basic physical characteristics governing the dynamic behaviour. Once a basic understanding of the dynamic behaviour was attained, the September 98 test series was designed to further investigate the previously identified specific physical characteristics and examine the influence of excitation frequency and amplitude on the wall's dynamic behaviour. Consequently for the September 98 test series both pulse and real earthquake transient excitations were used.

To complement the dynamic tests and further explore the important physical characteristics of the out-of-plane behaviour of simply supported URM walls, static push and free vibration tests were also undertaken for each wall configuration. Table 6.4.1 presents the full testing program undertaken.

Table 6.4.1 Experimental Phase Test Program

Construction Lot	Specimen No.	Thickness (mm)	Slenderness Ratio	Overburden (MPa)	Dynamic Test
March98	1	110	13.6	0 0	Un-cracked 2Hz Harmonic Excitation Cracked 2Hz Harmonic Excitation
March98	2	110	13.6	0 0	Un-cracked 2Hz Harmonic Excitation Cracked 2Hz Harmonic Excitation
March98	3	110	13.6	0 0	Un-cracked Static Push Test Cracked 2Hz Harmonic Excitation
March98	4	110	13.6	0 0	Un-cracked 2Hz Harmonic Excitation Cracked 2Hz Harmonic Excitation
June98	5	110	13.6	0.15	Un-cracked 10Hz Harmonic Excitation
June98	6	110	13.6	0.15	Un-cracked 7Hz Harmonic Excitation Cracked 7Hz Harmonic Excitation
June98	7	110	13.6	0.15	Un-cracked 7Hz Harmonic Excitation
June98	8	110	13.6	0 0.15 0.15 0	Un-cracked Natural Frequency Un-cracked Static Push Test Cracked Static Push Test Triangular Displacement Impulse
September98	9	50	30	-	Poor Construction - Disregarded
September98	10	50	30	0 0.07 0.07 0 007 0.07 0 0.15	Un-cracked Natural Frequency Un-cracked Static Push Test Cracked Static Push Test Half Sine Displacement Pulse Free Vibration Release Tests Half Sine Displacement Pulse Cracked Static Push Test Half Sine Displacement Pulse
September98	11	110	13.6	0.15 0 0 0	Un-cracked Static Push Test Free Vibration Release Tests Half Sine Displacement Pulse Cracked Static Push Test
September98	12	110	13.6	0 0 0 0	Un-cracked Static Push Test Gaussian Pulse Transient Excitation Cracked Static Push Test
September98	13	110	30	0 0 0 0	Un-cracked Static Push Test Gaussian Pulse Transient Excitation Cracked Static Push Test
September98	14	50	13.6	0 0 0 0.15 0.15 0	Cracked Static Push Test Gaussian Pulse Transient Excitation Gaussian Pulse Cracked Static Push Test Cracked Static Push Test

The following section describes each of the test procedures highlighting key results with a representative cross section of results presented in Appendix (F). Both cracked and un-

cracked 'quasi-static' analyses of the test specimens are presented as these contribute to the understanding of the wall response to dynamic loading.

6.4.1. Data Filter

The band-pass filter program, as described in Section 4.3.1, was used to filter noise from the simply supported URM wall tests.

6.4.2. Un-cracked Natural Frequency of Vibration

In order to investigate the un-cracked natural frequency of vibration for both non-loadbearing simply supported 110mm and 50mm thick wall specimens, a force pulse was applied to the wall mid-height using a rubber mallet. As displacements were too small too measure accurately, being only a fraction of a millimeter, mid-height accelerations were collected using the Kistler Accelerometer. Raw data was then filtered to remove irrelevant noise frequencies and the natural frequency response of the braced steel frame, which tended to dominate the response.

Figure 6.4.1 shows a representative time trace for one of the tests performed on a non-loadbearing 50mm thick wall specimen where the natural frequency of vibration is approximately 19Hz. Similar tests on non-loadbearing simply supported 110mm thick walls indicated that the natural frequency of vibration was approximately 42Hz.

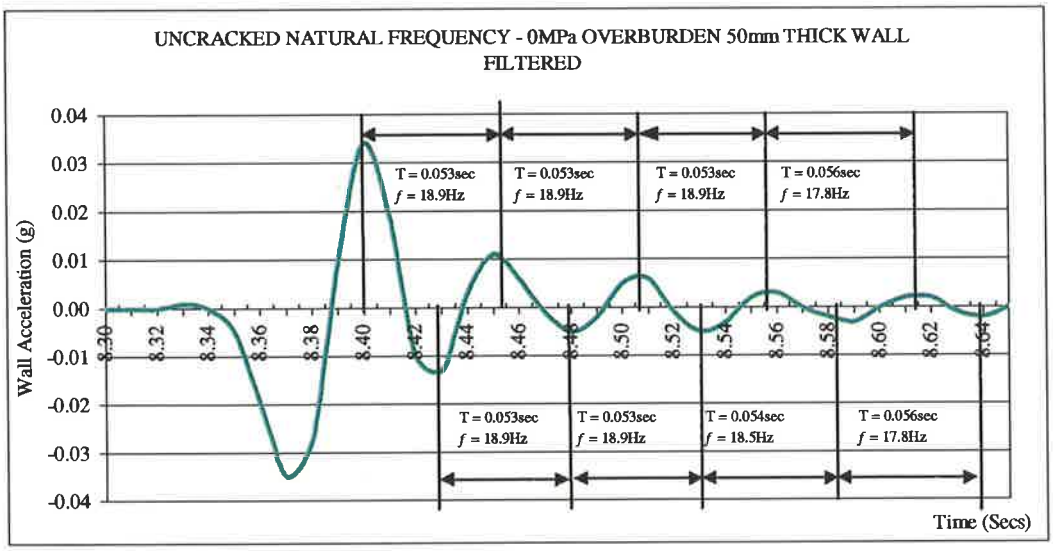

Figure 6.4.1Un-cracked Natural Frequency of Vibration 50mm Non-loadbearing Wall

Unlike the findings of previous researchers (Lam 1995) the elastic natural frequency appeared to be constant over the exponential decay of the wall's mid-height displacement. This therefore supports the theory that URM walls in the un-cracked state behave essentially as an elastically responding material. To further substantiate this a comparison of the empirically determined un-cracked natural frequency with that predicted analytically by simple elastic beam theory is presented in the following section.

6.4.2.1. Comparison with Simple Elastic Beam Theory

From simple beam theory the square of the angular frequency response for a linear elastic, simply supported beam is given by Equation 6.4.1 (Gere & Timonshenco 1990) as,

$$\omega^2 = \pi^4 \left(\frac{E_m I}{mL^4} \right) \tag{6.4.1}$$

where

ω = Angular Frequency = $2\pi f$
f = Natural Frequency
E_m = Elastic Modulus
m =Mass = γt
γ = Material Density
t = Object Thickness
L = Object Length
I = Second Moment of Area = $t^3/12$

Rearranging and substituting into Equation 6.4.2 the natural frequency of an elastic solid beam can be shown to be:

$$f = \frac{t}{L^2}\pi\sqrt{E/48\gamma} \tag{6.4.2}$$

Using the experimentally derived E_m and γ, Equation 6.4.2 predicts the elastic natural frequency for the 50mm brick wall as,

$$f = \frac{0.05}{1.5^2}\pi\sqrt{8.25x10^9/48(2300)} = 19Hz$$

and for 110mm brick wall as,

$$f = \frac{0.11}{1.5^2}\pi\sqrt{9.4x10^9/48(1800)} = 50Hz$$

As these are of the same order as experimentally derived natural frequencies it was concluded that simple beam theory provides a reasonable prediction of the elastic natural frequency of vibration for un-cracked simply supported URM walls without overburden force applied.

6.4.3. Specimen Lateral Capacity Analysis

The predicted lateral acceleration capacity using the 'quasi-static' linear elastic and rigid body analyses, as described in Chapter 5, are shown in Figure 6.4.2 for 110mm thick walls and in Figure 6.4.3 for 50mm thick walls. The range of overburden presented is relevant for Australian masonry construction.

Variable	Height (m)	Thickness (mm)	Effective Modulus (MPa)	Density (kg/m^3)	Flexural Tensile Strength (MPa)
	1.5	110	1000	1,800	0.46

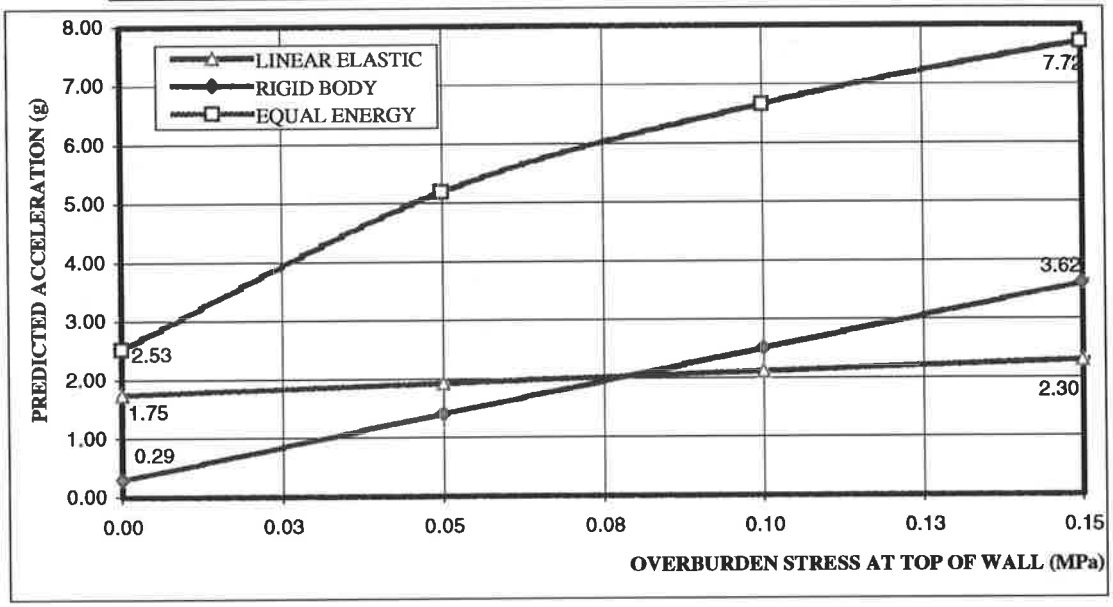

Figure 6.4.2 Current Available Analysis Comparison – 110mm Thick Wall

Variable	Height (m)	Thickness (mm)	Effective Modulus (MPa)	Density (kg/m^3)	Flexural Tensile Strength (MPa)
	1.5	50	5000	2,300	0.73

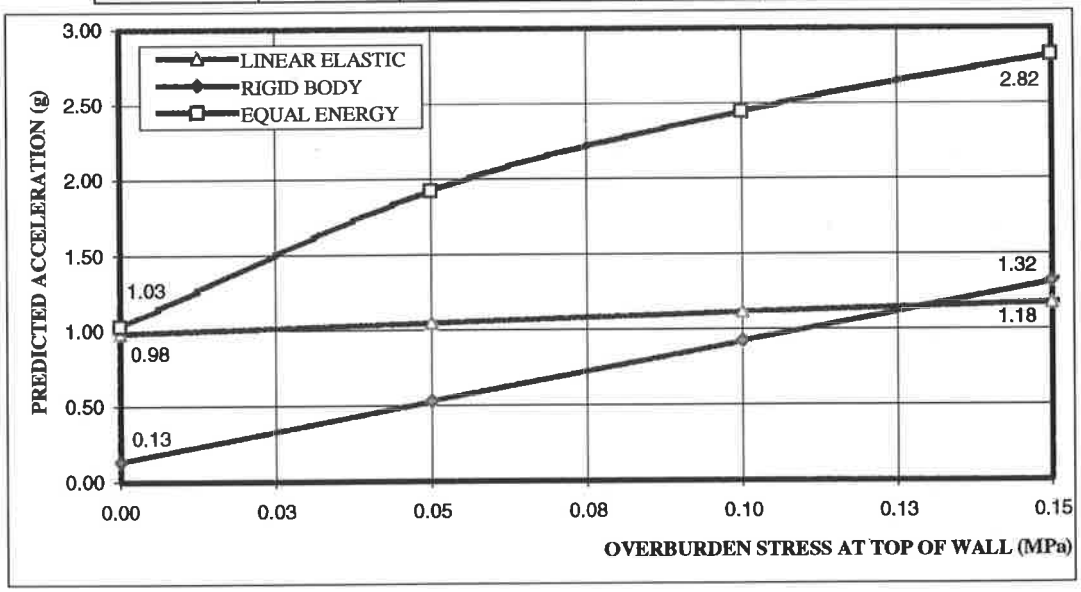

Figure 6.4.3 Current Available Analysis Comparison – 110mm Thick Wall

The predicted lateral acceleration capacity determined by the dynamic 'Equal Energy' method of analysis is also included in the above plots for comparison.

For the 'quasi-static' elastic analysis prediction of the acceleration to cause cracking, the average flexural tensile strength, f'_t, determined from bond wrench tests, presented in Section 6.3.1, was used with vertical reactions assumed to act at the centerline of the wall. For the 'quasi-static' rigid body analysis prediction of the 'rigid resistance threshold' acceleration, vertical reactions were assumed to act at the leeward face of the wall. Lower values of modulus than those determined by five brick prism tests, presented in Section 6.3.2, have been used for the 'Equal Energy' method as it was found that the experimental values provided an unrealistically non-conservative prediction of lateral acceleration capacity. This is because the test walls are relatively stocky and along with the relatively high modulus the system period is lower than appropriate for the 'Equal Energy' observation. Accordingly, the equivalent elastic prediction based on the 'Equal Energy' observation provides a non-conservative estimate of wall's dynamic capacity. By assuming a lower modulus the system period moves into the range were the 'Equal Energy' observation has been shown to be more appropriate so that a reasonable estimate of lateral capacity is achieved. It is therefore apparent that the 'Equal Energy' procedure is not particularly relevant to the test walls however it may be more appropriate for taller walls having a larger elastic period.

Examination of the analysis comparison plots show that for the non-loadbearing test specimens the elastic capacity is greater than the cracked rigid capacity. For walls with larger overburden stress, however, the cracked rigid capacity is larger and thus in theory dominates the behaviour. In all cases the 'Equal Energy' method provides less conservative predictions as an allowance is incorporated for the walls 'reserve capacity' due to dynamic stability concepts.

Table 6.4.2 presents a summary of the analytical results for the wall test specimens. The highlighted analysis results are those which should, in theory, dominate the un-cracked wall behavior.

Table 6.4.2 Analysis of Test Specimen

			Predicted Lateral Acceleration Capacity (g)		
Height (m)	Thickness (mm)	Overburden Stress (MPa)	Un-cracked Linear Elastic Analysis	Cracked Rigid Body Analysis	'Equal Energy' Method
1.5	110	0	**1.75**	0.29	2.53
1.5	110	0.15	2.3	**3.62**	7.72
1.5	50	0	**0.98**	0.13	1.03
1.5	50	0.07	**1.15**	0.65	2.15
1.5	50	0.15	1.18	**1.32**	2.82

6.4.4. Harmonic Excitation Tests

For the March 98 test series, harmonic excitation tests were conducted on 110mm thick simply supported URM walls without applied overburden. For walls that fall within this category the predicted un-cracked elastic lateral acceleration capacity of 1.75g is greater than the cracked 'rigid resistance threshold' acceleration of 0.29g (refer Table 6.4.2). On the basis that the peak 'semi-rigid resistance threshold' acceleration occurs at approximately 20% of the incipient instability displacement, the 'semi-rigid resistance threshold' acceleration was estimated to be approximately 20% less than for the 'rigid resistance threshold' acceleration prediction. Consequently, for walls within this category the cracked semi-rigid lateral acceleration resistance to rocking was estimated at 0.23g.

On examination of the 'quasi-static' analysis results for the un-cracked wall specimens the elastic behaviour was expected to dominate the dynamic response with applied accelerations of up to 1.75g being withstood by the wall. This was then expected to be followed by cracking and an explosive instability as the elastic kinetic and stored strain energy would be sufficient to overcome the potential energy requirement for the wall to become unstable. For pre-cracked walls the non-linear behaviour was expected to dominate the response with accelerations at the wall's effective mass of up to approximately 0.23g withstood prior to rocking, followed by a transient and then steady-state response. Failure of the wall was then expected to only occur when the table amplitude was increased sufficiently so that the maximum steady-state displacement exceeded the incipient instability displacement. The applied acceleration can therefore be

related to the level of displacement amplification and in turn to the wall's dynamic 'reserve capacity'.

To examine the physical dynamic response characteristics for both cracked and un-cracked walls within this category, harmonic tests were conducted on each. In the March 98 test series a gradually increasing 2Hz harmonic excitation was selected for input to the shake table as this was considered representative of what could be expected in URM construction where the ground motion is filtered through the building. Of a more practical concern, at this excitation frequency the predicted lateral accelerations required were also within the capabilities of the shaking table.

Figure 6.4.4 (a) – (c) presents typical results of a 2Hz harmonic test completed on a non-loadbearing and un-cracked 110mm thick simply supported URM wall. The displacement versus time plot, shown in Figure 6.4.4 (a), indicates that prior to t=16 seconds the wall response was elastic and the wall's mid-height displacement responding in phase with the table excitation. At t=16 seconds the wall was observed to crack. The input acceleration at the base and top of the wall at this time was recorded as 0.30g (refer Figure 6.4.4). As the relative elastic mid-height displacements were very small prior to cracking the mid-height response acceleration was un-amplified at 0.3g. As the input base harmonic displacement at this time was 19mm, the measured harmonic input acceleration can be checked using a similar procedure to that outlined in Section 4.3.3 and Equation 4.3.4.

$$a_{max} = |-A\varpi^2| = |-A(2\pi f)^2| = |-A(4\pi)^2| = 157.9\ A \quad (mm/s^2) = 0.0161\ A\ (g)$$
$$= 0.0161(19) = 0.30\ g$$

In contrast to the predicted elastic acceleration capacity the input base acceleration to cause cracking of 0.30g was much lower than the predicted 1.75g. On examination of the wall mid-height acceleration data, high frequency spikes of greater than 2g were observed just prior to cracking. These acceleration spikes were thought to have been a consequence of the wall initially rocking as a single free body and impacting with the top 'cornice' support. The high impact accelerations are thought to have had sufficient

energy to crack the wall prematurely. To further substantiate this on cracking at mid-height and the commencement of rocking as two free bodies the impact at the top support was reduced and the high frequency spikes no longer observed. This finding highlighted the possible non-conservative nature of adopting a stress based elastic analysis procedure for this category of non-loadbearing URM wall.

After the premature cracking the wall's response underwent a transition to steady-state rocking without becoming unstable as the elastic kinetic and stored strain energy were insufficient to overcome the potential energy required to cause instability. Following the transition phase the steady-state mid-height response rocking phase was observed to be 180° out of phase with the table excitation having a mid-height displacement amplification of 45/19 = 2.4. During the steady-state rocking response the ¼ - and ¾ - height accelerations were observed to reduce and the mid-height response acceleration increased (refer Figure 6.4.4(b)). This indicated that the center of gravity (CG) of the two rocking rigid bodies became closer to being stationary in space. Should the excitation frequency have been increased further, according to 'equal displacement theory', the CG would be expected to become completely stationary so that the wall mid-height would have responded at the same displacement as the table. This would therefore reduce the effective mid-height displacement amplification thus increasing the walls dynamic 'reserve capacity'.

Figure 6.4.4 (c) shows the hysteretic acceleration-displacement (a-Δ) behaviour where initially the un-cracked behaviour was observed to be linear. After cracking the dynamic wall behaviour switched to follow the non-linear a-Δ displacement relationship.

Figure 6.4.5 (a) – (c) present typical results of a 2Hz harmonic test completed on a pre-cracked non-loadbearing 110mm thick simply supported URM wall. These show that prior to t=32 seconds the 'semi-rigid threshold resistance' acceleration had not yet been exceeded at the mid-height of the wall so that rocking had not yet commenced. The test wall's dynamic behaviour was however governed by the cracked non-linear a-Δ relationship so that mid-height displacements were observed to be larger than for the un-

cracked wall specimens. Here the wall mid-height was responding in phase with the table motion although some acceleration amplification of the wall mid-height was observed due to the larger displacement response. At t=32 seconds the 'semi-rigid threshold resistance' acceleration was exceeded at the mid-height of the wall. At this time the wall mid-height response acceleration was 0.34g having a displacement amplitude of 21mm. This can again be confirmed using a similar procedure to that outlined in Section 4.3.3 and Equation 4.3.4.

$$a_{max} = |-A\varpi^2| = |-A(2\pi f)^2| = 0.0161(21) = 0.34 \text{ g (wall mid-height).}$$

Following the commencement of rocking a transition period prior to steady-state rocking response phase occurred. During the steady-state rocking response the wall mid-height was again observed to have changed to respond 180° out of phase with the table motion. A displacement amplification of the mid-height response of 37/14=2.6 was observed.

Although not shown experimentally it can therefore be postulated that once a steady-state rocking response had commenced without becoming unstable during the transition period, the amplitude of the 2Hz excitation could then have been increased to 110/2.6 = 42mm prior to the instability displacement being reached. This input displacement excitation corresponds to an input acceleration of 0.67g. Thus, for the 2Hz harmonic excitation this wall would have a 'reserve acceleration' capacity of 0.67-0.33 = 0.34g. Even considering the full predicted dynamic 'reserve capacity' of the wall the 'Equal Energy' prediction of 2.53g remains extremely non-conservative providing a misleading assessment of the wall's acceleration capacity for the excitation being considered.

If the full dynamic 'reserve capacity' is to be relied upon for the assessment of cracked URM walls, as has been proposed by previous researchers (ABK 1984, Priestly 1985), it is important to assess the ability of the rotating mortar joints to sustain repeated loading cycles during rocking. Throughout the March 98 series of harmonic tests on walls without applied overburden, the ability of mortar joints to sustain repeated loading cycles during rocking was found to be very good with only minor degradation observed. As will

be discussed in Section 6.4.5 static push tests have been used to quantify the degradation of the mortar joints caused by dynamic testing.

Table 6.4.3 presents a summary of results for the March 98 test series. A final observation was that for cracked walls the mid-height response acceleration at the commencement of rocking was typically of the order of 1.5 times the estimated 'semi-rigid threshold resistance' acceleration (0.34/0.23=1.5). This suggests that for a pre-cracked simply supported URM wall, during dynamic loading a triangular wall acceleration response relative to the supports is likely, resulting from the larger mid-height response displacements as compared with the base and top of the wall.

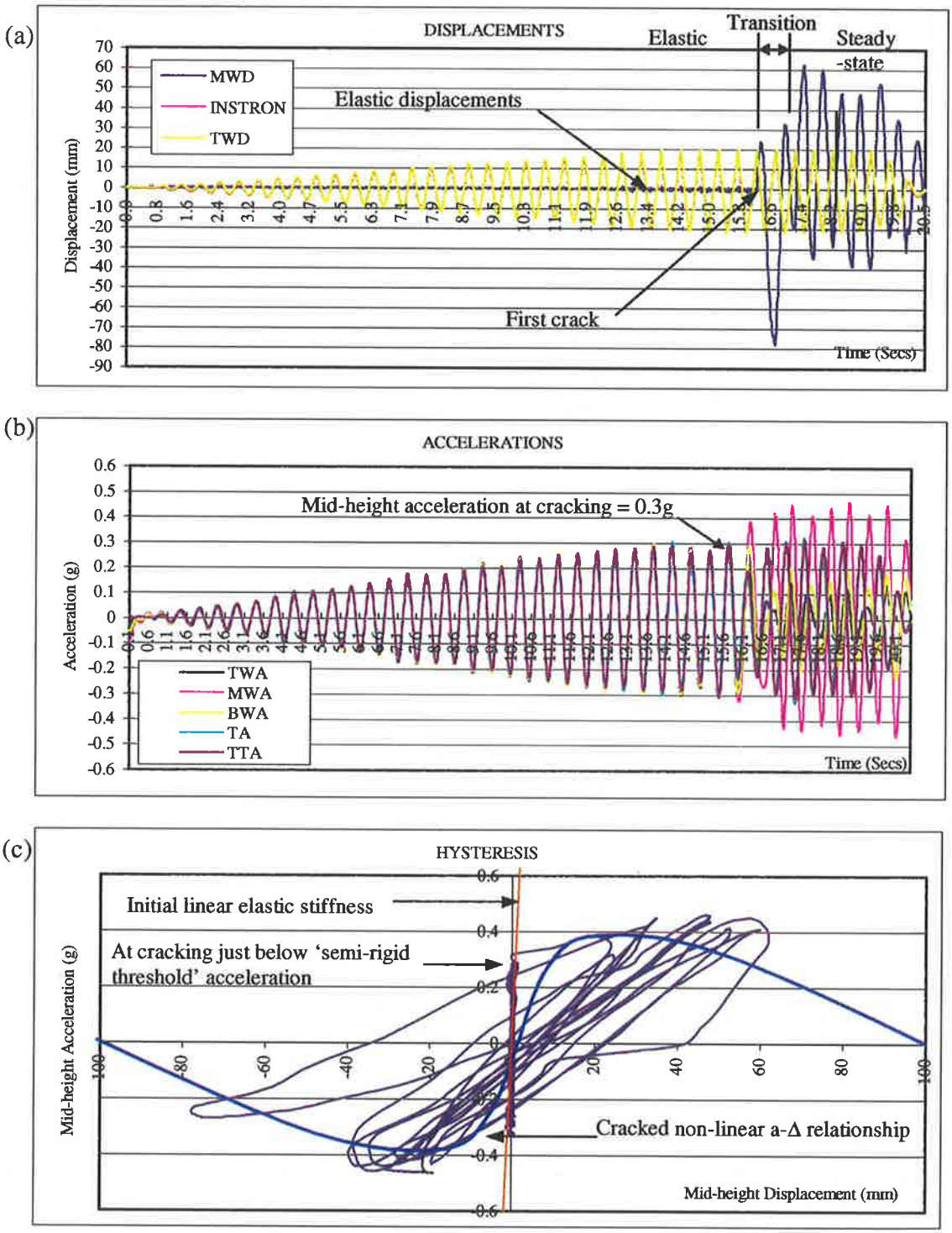

(110mm Wall, 2Hz Harmonic Excitation)

Figure 6.4.4 Un-cracked Non-loadbearing URM Wall Harmonic Excitation Test

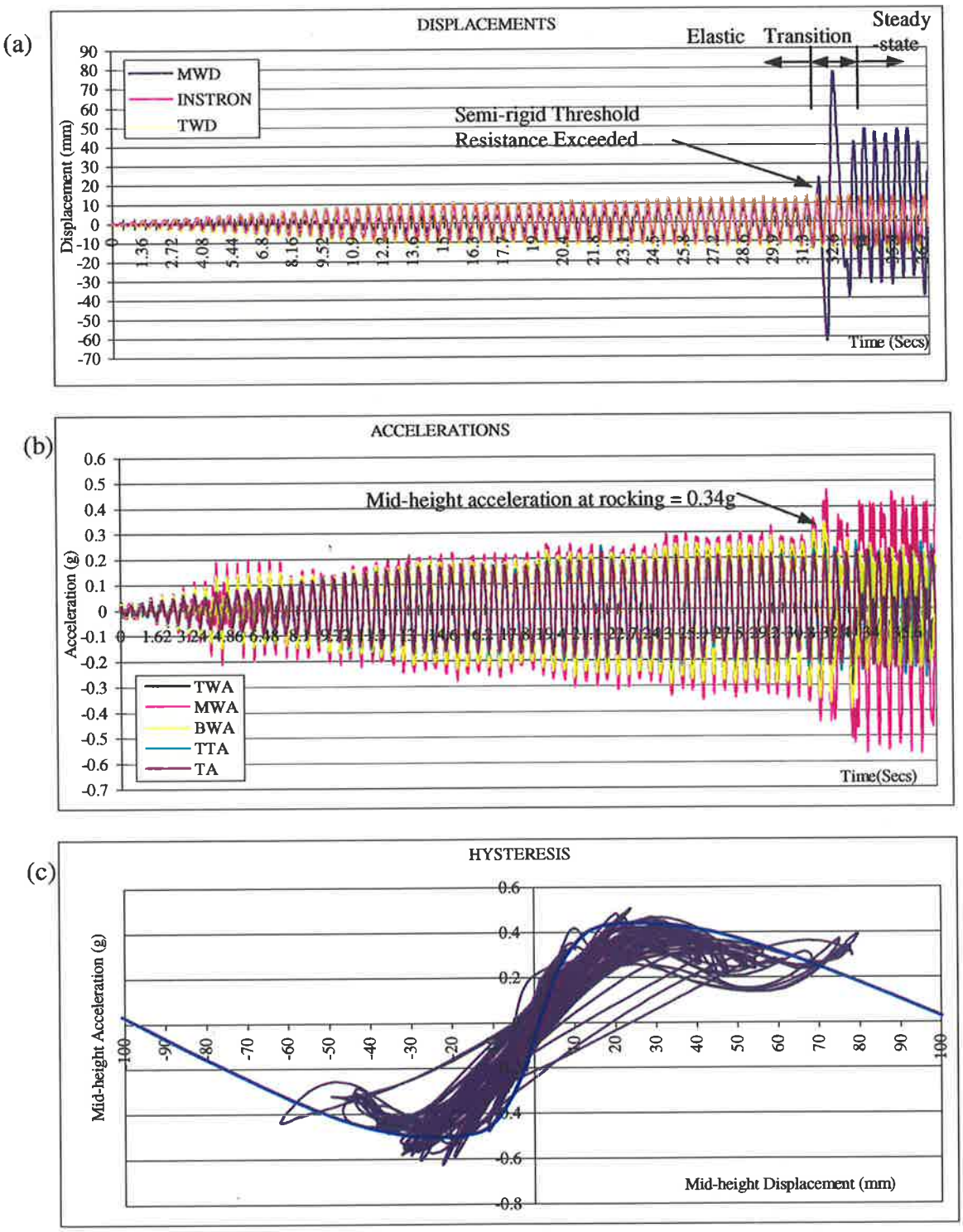

(110mm Wall, 2Hz Harmonic Excitation)

Figure 6.4.5 Pre-cracked Non-loadbearing URM Wall Harmonic Excitation Test

Table 6.4.3 110mm Wall, Non-loadbearing - Harmonic Excitation Test Results

Wall No.	Wall Condition	Predicted 'Quasi-Static' Acceleration Capacity (Refer Table 6.4.2)	Experimental Results	Comment
1	Un-cracked	1.75g	A=20mm (0.32g) (0.32g) 50/20=2.5	Table input at cracking/rocking Mid-height acceleration response at cracking/rocking (no amplification) - High frequency spike (12Hz) >2g prior to cracking Steady-state response displacement amplification
1	Cracked	0.29g (Rigid) 0.23g (Semi-rigid)	A=15mm (0.24g) A=21mm (0.34g) 40/16=2.5	Table input at rocking Mid-height response at rocking - No high frequency spikes observed Steady-state response displacement amplification
2	Un-cracked	1.75g	A=16mm (0.26g) (0.29g)	Table input at cracking/rocking Mid-height acceleration response at cracking/rocking (small amplification) - High frequency spike (12Hz) >2g prior to cracking - Some elastic acceleration amplification - Wall became unstable immediately after cracking (no steady-state response)
2	Cracked (refer Figure 6.4.5)	0.29g (Rigid) 0.23g (Semi-rigid)	A=15mm (0.24g) A=21mm (0.34g) 37/14=2.6	Table input at rocking Mid-height response at rocking - No high frequency spikes observed Steady-state response displacement amplification
3	Cracked	0.29g (Rigid) 0.23g (Semi-rigid)	A=16mm (0.26g) A=22mm (0.35g)	Table input at rocking Mid-height response at rocking - No high frequency spikes observed Mortar drop out prevented steady-state response from occurring
4	Un-cracked (refer Figure 6.4.4)	1.75g	A=19mm (0.30g) (0.30g) 45/19=2.4	Table input at cracking/rocking Mid-height acceleration response at cracking/rocking (no amplification) - High frequency spike (12Hz) >2g prior to cracking Steady-state response displacement amplification
4	Cracked	0.29g (Rigid) 0.23g (Semi-rigid)	A=13mm (0.21g) A=19mm (0.30g) 35/13=2.7	Table input at rocking Mid-height response at rocking - No high frequency spikes observed Steady-state response displacement amplification

For the June 98 test series, harmonic excitation tests were conducted on 110 mm thick simply supported URM walls with 0.15 MPa applied overburden using the spring overburden rig shown in Figure 6.2.5. As described in Section 6.2.2 for mid-height displacements greater than approximately 20% of the wall thickness the additional static spring deflection caused an unacceptable increase in overburden force at the top of the wall. Results were therefore only valid for mid-height displacements less than 20% of the wall thickness. For walls within this category the predicted un-cracked elastic lateral acceleration capacity of 2.3g is less than the cracked 'rigid resistance threshold' acceleration of 3.62g (refer Table 6.4.2). Estimates of the 'semi-rigid resistance threshold' acceleration were approximately 20% less than for the rigid case where the resistance to rocking was estimated to be 2.9 g.

Accordingly, even for the un-cracked wall the non-linear cracked wall behaviour was expected to dominate the dynamic response with cracking of the wall not expected to have significant impact on the dynamic behaviour. Hence, initially elastic behaviour was expected up to applied accelerations of 2.3 g followed by cracking with a slight increase in the wall mid-height displacement response. An increase in applied accelerations up to 2.9 g at the mid-height of the wall was then expected to be applied prior to a transient then steady-state rocking response. As per the previously described March 98 cracked wall response, failure was then expected to only occur when the table amplitude was increased sufficiently so that the maximum steady-state displacement exceeded the instability displacement. This would therefore again be related to the displacement amplification and in turn to the wall's dynamic 'reserve capacity'.

Thus, to examine the physical dynamic response characteristics of both cracked and un-cracked walls within this category, harmonic tests were conducted on each wall specimen. Much higher inertia forces were required for this test series so 7Hz to 10Hz harmonic table excitations were selected. These were still considered to be representative of what could be expected in URM construction due to ground motion. However, since these frequencies were close to the resonant frequency of the braced steel frame some amplification of the base excitation was observed at the top support.

Figure 6.4.6 (a) – (c) present typical results for a 7Hz harmonic test of an un-cracked 110 mm thick simply supported URM wall. The displacement versus time plot shown in Figure 6.4.6 (a) indicates that prior to t=4.4 seconds the wall response was elastic and the mid-height response and table excitation were in phase. At t=4.4 seconds the wall was observed to crack with displacements increasing slightly. However, the mid-height response and table excitation remained in phase (refer Figure 6.4.7) indicating that rocking had not yet commenced. The average input acceleration at the time was recorded as 1.8 g with the mid-height wall acceleration being 2.1 g (refer Figure 6.4.6 (b)). Since the input harmonic displacement at this time was 9mm this can again be confirmed using a similar procedure to that outlined in Section 4.3.3 and Equation 4.3.4.

$$a_{max} = |-A\varpi^2| = |-A(2\pi f)^2| = |-A(14\pi)^2| = 1934.4\ A \quad (mm/s^2) = 0.197\ A\ (g)$$
$$= 0.197(9) = 1.8\ g$$

Following cracking the 7Hz-table excitation amplitude was further increased until at t=19.45 seconds the 'semi-rigid threshold resistance' acceleration was exceeded at the mid-height of the wall. At this time the wall mid-height response acceleration was 4.3g having displacement amplitude of 22 mm. This can again be checked by the following calculation,

$$a_{max} = |-A\varpi^2| = |-A(2\pi f)^2| = 0.197(22) = 4.3g \text{ (wall mid-height).}$$

Following the commencement of rocking a transition period prior to steady-state rocking response phase occurred. During the steady-state rocking response the wall mid-height was again observed to have changed to respond 180° out of phase with the table motion. A displacement amplification of the mid-height response of 25/9=2.77 was observed (refer Figure 6.4.8).

(a)

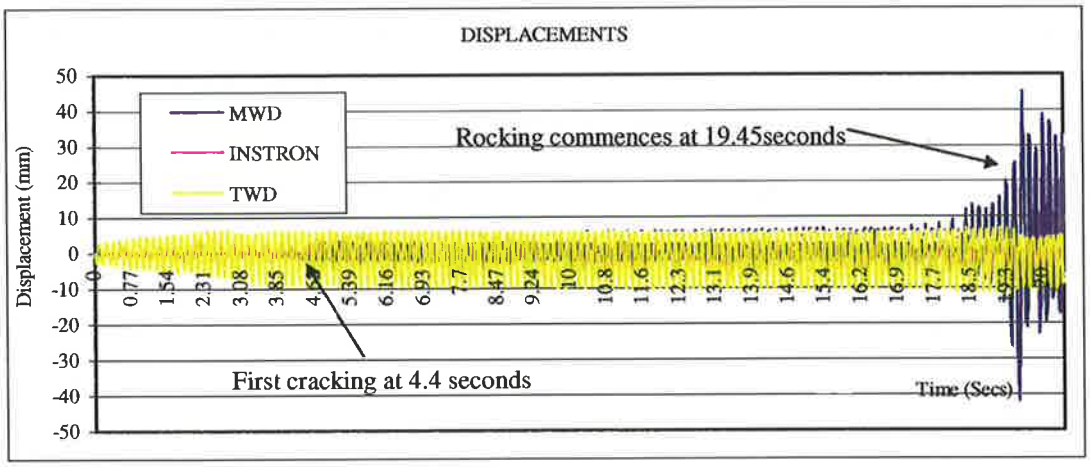

(b)

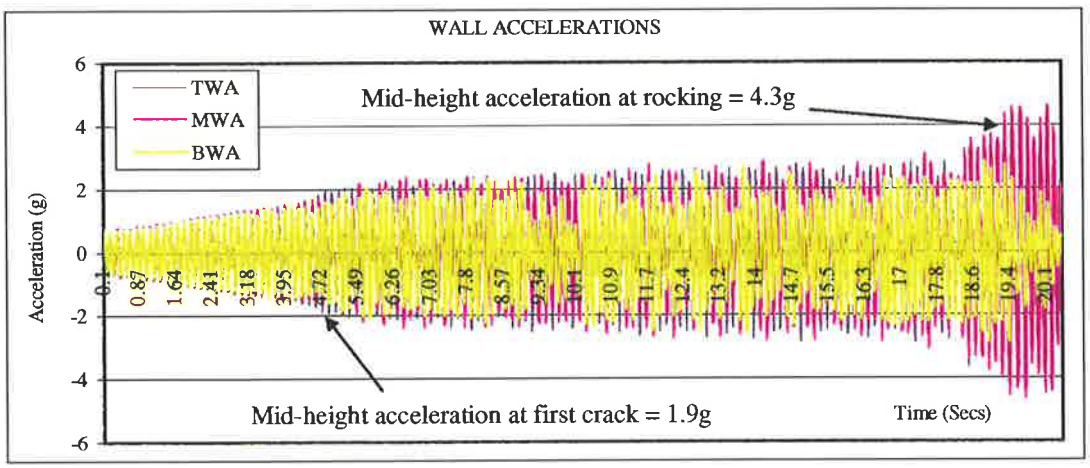

(c)

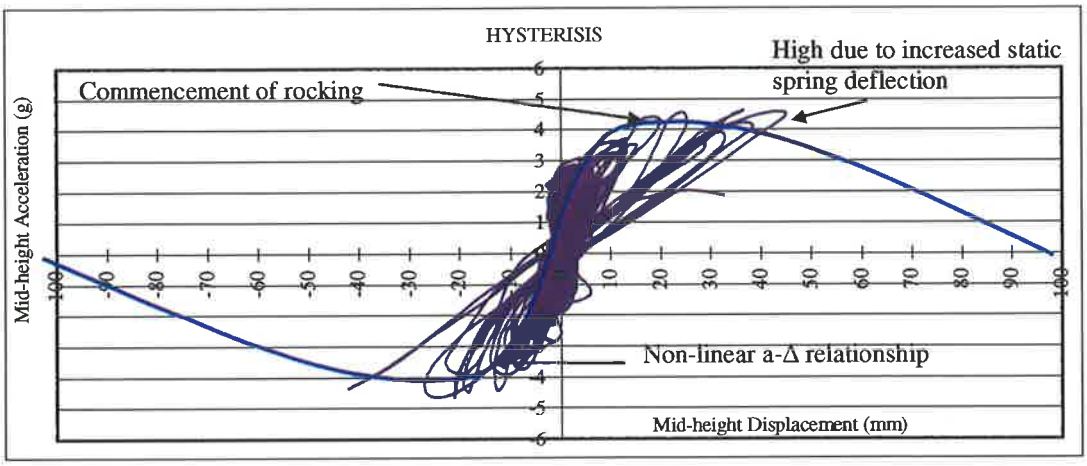

(110mm Wall, 0.15MPa Overburden, 7Hz Harmonic Excitation)

Figure 6.4.6 Un-cracked Non-loadbearing URM Wall Harmonic Excitation Test

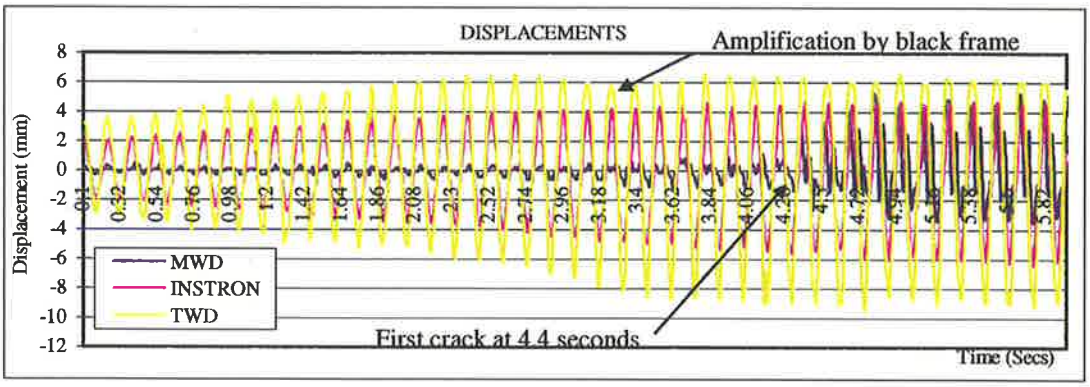

(110mm Wall, 0.15MPa Overburden, 7Hz Harmonic Excitation)

Figure 6.4.7 Un-cracked Non-loadbearing URM Wall – First Cracking

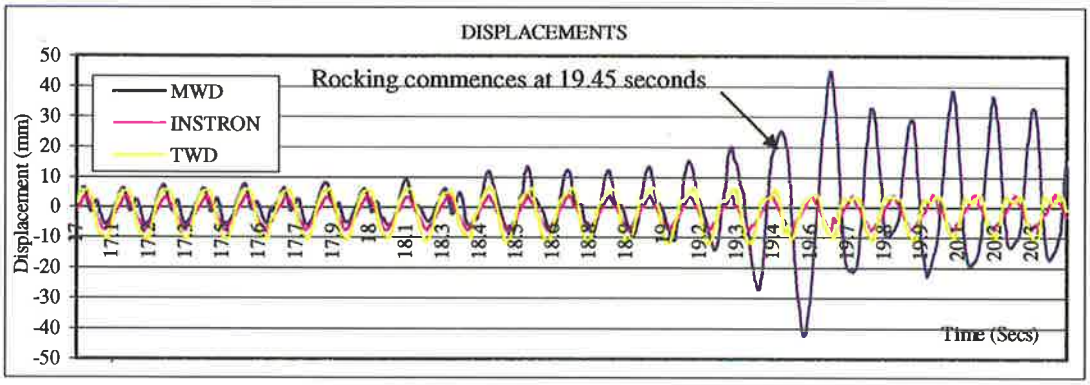

(110mm Wall, 0.15MPa Overburden, 7Hz Harmonic Excitation)

Figure 6.4.8 Un-cracked Non-loadbearing URM Wall – First Rocking

Typically, for the walls tested with applied overburden, once rocking commenced there was a rapid degradation of the mid-height rotation joint. Physically this could be seen as mortar being broken from the rotation joints by the impact of the two free bodies. This was attributed to the rocking frequencies and impact forces being much larger for the loadbearing walls. As a result of the degradation during rocking an increase in displacement and reduction in response acceleration was observed, without further increase in excitation until instability.

Table 6.4.4 presents results of the June 98 test series for 110 mm thick URM wall with 0.15 MPa overburden stress. These walls were subjected to an out-of-plane gradually increasing 7 or 10 Hz harmonic excitation. Consistent with the March 98 tests, a final

observation from this test series was that for cracked walls the mid-height acceleration at the commencement of rocking was again typically of the order of 1.5 times the estimated 'semi-rigid threshold resistance' acceleration.

Table 6.4.4 110mm Wall, 0.15MPa - Harmonic Excitation Test Results

Wall No.	Test	Wall Condition	Predicted 'Quasi-Static' Acceleration Capacity (Refer Table 6.4.2)	Experimental Results	Comment
5	10Hz Harmonic	Un-cracked	2.3g (Cracking) 3.62g (Rigid) 2.9g (Semi-rigid)	A=4mm (1.6g) (2.0g) A=5mm (2.0g) A=10mm (4.1g)	Average support input at cracking Mid-height acceleration response at cracking Average support input at rocking Mid-height response at rocking - Amplification at top support as at black frame resonance
6	7Hz Harmonic	Un-cracked	2.3g (Cracking)	A=6mm (1.2g) (1.6g)	Average support input at cracking Mid-height acceleration response at cracking
6	7Hz Harmonic	Cracked	3.62g (Rigid) 2.9g (Semi-rigid)	A=8mm (1.6g) A=10mm (2.0g)	Average support input (rocking not yet commenced) Mid-height response (rocking not yet commenced)
7	7Hz Harmonic (refer Figure 6.4.7)	Un-cracked	2.3g (Cracking) 3.62g (Rigid) 2.9g (Semi-rigid)	A=9mm (0.18g) (2.1g) A=12mm (2.4g) A=22mm (4.3g) 25/10=2.5	Average support input at cracking Mid-height acceleration response at cracking Average support input at rocking Mid-height response at rocking Steady-state response displacement amplification -Rapid joint degradation during rocking

From both the harmonic March 98 and June 98 test series it was concluded that for most practical cases non-linear cracked behaviour is more relevant to a dynamic loading scenario than the un-cracked properties. Also, from the identified dynamic mid-height non-linear cracked F-Δ relationship, a triangular distribution of horizontal acceleration up the height of the wall assumption relative to the supports has been identified as likely to provide the best approximation of acceleration response.

6.4.5. Static Push Tests

To investigate the out-of-plane non-linear F-Δ behaviour of simply supported URM walls static push tests were conducted on both un-cracked and cracked wall test specimens. The braced steel support frame was used to simply-support the wall panels in these tests. Loading was applied at the wall mid-height using a hand pump driven hydraulic actuator (refer Figure 6.4.9). This was geometrically similar to statically applying the same force at the wall ¼ - and ¾ - height being the center of gravity (CG) of each of the two free bodies. The applied static load was therefore related to the 'quasi-static' assumption of a rectangularly distributed load having a resultant horizontal force at the free body CG.

A calibrated load cell was inserted between the actuator and the wall at mid-height to record the resisting force applied by the wall onto the actuator. This force was recorded for displacements from the vertical position to as near as possible to the incipient instability displacement, where the resisting force was reduced to near zero. The recorded data was that of the 'quasi-static' non-linear F-Δ relationship by means of a rectangular distributed load.

Figure 6.4.9 Static Push Test

A summary of the key results for the static push test and a comparison with static analysis is shown in Table 6.4.5. A representative cross-section of the experimentally derived F-Δ plots is presented in Appendix (F).

Table 6.4.5 Result Summary of Static Push Tests

Construction Lot	Wall No.	Wall State	Thick-ness (mm)	Over-burden (MPa)	Predicted 'Static Capacity' (kN)	Peak Force* (kN)	Disp at Peak Force (mm)	% of Rigid	Comment
March98	3	Un-cracked	110	0	(LE) 2.64 (RB) 0.41	3.18	0.5	-	
June98	8	Un-cracked	110	0.15	(LE) 4.82 (RB) 5.31	5 6.2	0.45 21	-	
June98	8	Cracked	110	0.15	(LE) 2.32 (RB) 5.32	4.36	18.5	82	f'_t=0MPa
September98	10	Cracked	50	0	(LE) 0.07 (RB) 0.11	0.09	6	82	f'_t=0MPa
September98	10	Un-cracked	50	0.075	(LE) 1.07 (RB) 0.59	0.95	0.79	-	
September98	10	Cracked	50	0.075	(LE) 0.29 (RB) 0.62	0.49	8.3	79	f'_t=0MPa
September98	11	Cracked	110	0	(LE) 0.27 (RB) 0.41	0.3	12.6	73	f'_t=0MPa
September98	11	Un-cracked	110	0.15	(LE) 0.27 (RB) 0.41	4.5 5.3	0.66 21.5	-	Increased spring static deflection
September98	12	Un-cracked	110	0	(LE) 2.64 (RB) 0.41	3.0	0.3	-	
September98	12	Cracked	110	0	(LE) 0.27 (RB) 0.41	0.38	8.1	92	f'_t=0MPa
September98	13	Un-cracked	110	0	(LE) 2.64 (RB) 0.59	2.2	0.59	-	
September98	13	Cracked	110	0	(LE) 0.27 (RB) 0.41	0.33	10	81	f'_t=0MPa
September98	14	Cracked	50	0	(LE) 0.07 (RB) 0.11	0.084	8.8	77	f'_t=0MPa -before dynamic
September98	14	Cracked	50	0	(LE) 0.07 (RB) 0.11	0.075	10	68	f'_t=0MPa -after dynamic
September98	14	Cracked	50	0.15	(LE) 0.47 (RB) 1.07	0.71	10	66	f'_t=0MPa

* Real 'Semi-rigid Threshold Resistance' Force
LE = Linear Elastic Analysis
RB = Rigid Body Analysis

Examination of the un-cracked wall static push test results indicated that the linear elastic analysis predicted the 'static' cracking load reasonably well, within the limits of accuracy of the flexural tensile strength prediction.

For the cracked wall specimen tests, the predicted 'rigid threshold resistance' force, $R_e(1)$, determined by rigid body analysis, was observed to overestimate the real 'semi-rigid threshold resistance' by 10% to 40% which was attributed mostly to the real 'semi-rigid' nature of the masonry material. As highlighted in Section 5.3, a simple analytical method has been proposed for predicting the semi-rigid F-Δ relationship (Priestly 1985) based on the assumption of a proportional relationship between the wall curvature and the stress gradient across the critical section. This was not found to represent the current tests well as it overestimated the initial stiffness and 'semi-rigid threshold resistance' force, $R_{es}(1)$. Figure 6.4.10 presents a comparison of the analytical F-Δ prediction for the non-loadbearing 110mm thick specimen no.10 wall and Figure 6.4.11 for the 50mm thick specimen no.11 wall. Here, moduli of elasticity of 1000MPa were used to maintain the initial stiffness and 'semi-rigid resistance threshold' force within reasonable limits. A second shortfall was that the effect of degradation of the mortar joints could not be considered.

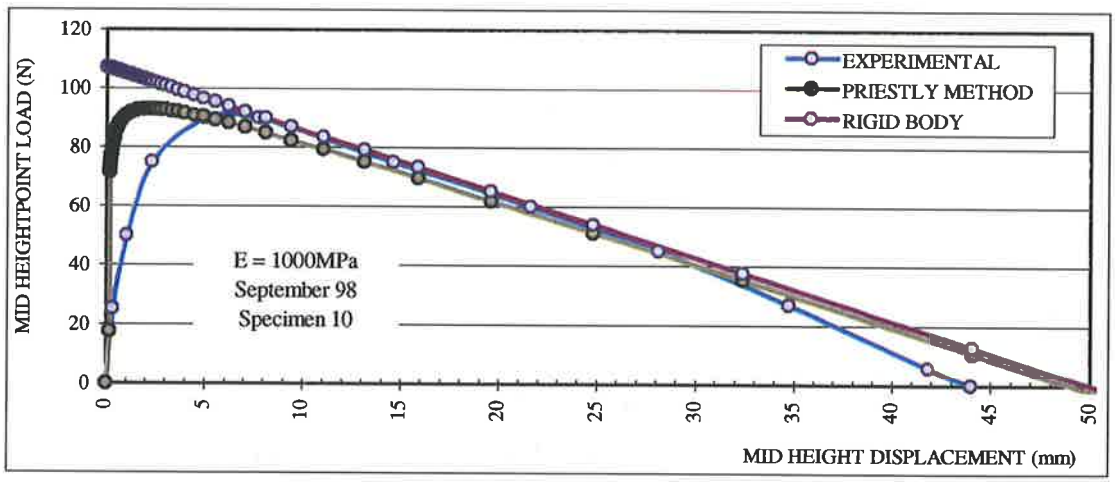

Figure 6.4.10 Comparison of 110mm Specimen Static Push F-Δ with Analytical

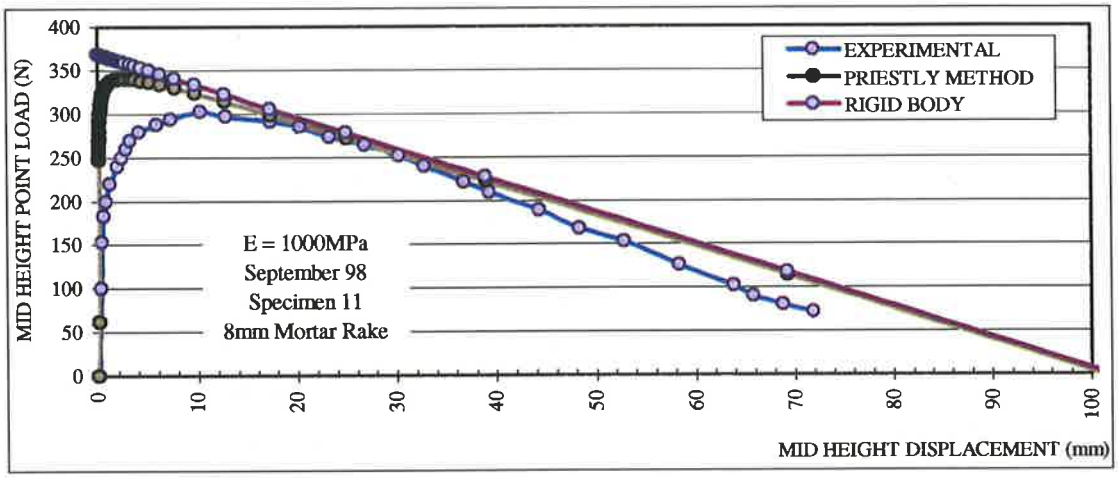

Figure 6.4.11 Comparison of 50mm Specimen Static Push F-Δ with Analytical

After dynamic testing the degradation of rotation joints was observed and related to a flattening of the static F-Δ relationship and thus a lowering of average response frequencies. To quantify this degradation the wall specimens were catagorised throughout the dynamic testing as new, moderately degraded or severely degraded by their appearance as shown in Figure 6.4.12. Using this visual categorisation of the wall specimens, some broad empirically based predictions of the static F-Δ relationship could be made in relation to the idealised bi-linear rigid F-Δ relationship. The empirically determined predictions are discussed further in Chapter 7 as they are related to the modelling of the non-linear force displacement relationship required for THA.

Tests on non-loadbearing 110mm thick walls were also performed having displacements reduced from the incipient instability displacement to investigate the static hysteretic behaviour as presented in Appendix (F). The area encompassed by each hysteresis loop provided an indication of the energy loss per half cycle caused by joint rotation and friction at the connections. The resonant energy loss per cycle method of estimating damping was then used to assess the level of damping within the rocking system. Using this approach the energy dissipated in a vibrational cycle of the wall was equated to that of an equivalent viscous system. It was found that the equivalent single degree-of-freedom (SDOF) equivalent viscous damping (ξ_{SDOF}) was approximately 10%, being of a

similar value to damping results determined in Section 6.4.6 by free vibration tests. However, the accuracy of this method is limited as it only considers the response at resonance. The highly non-linear shape of the F-Δ relationship for URM walls makes the effective half cycle stiffness non-unique so that it is also difficult to use this method.

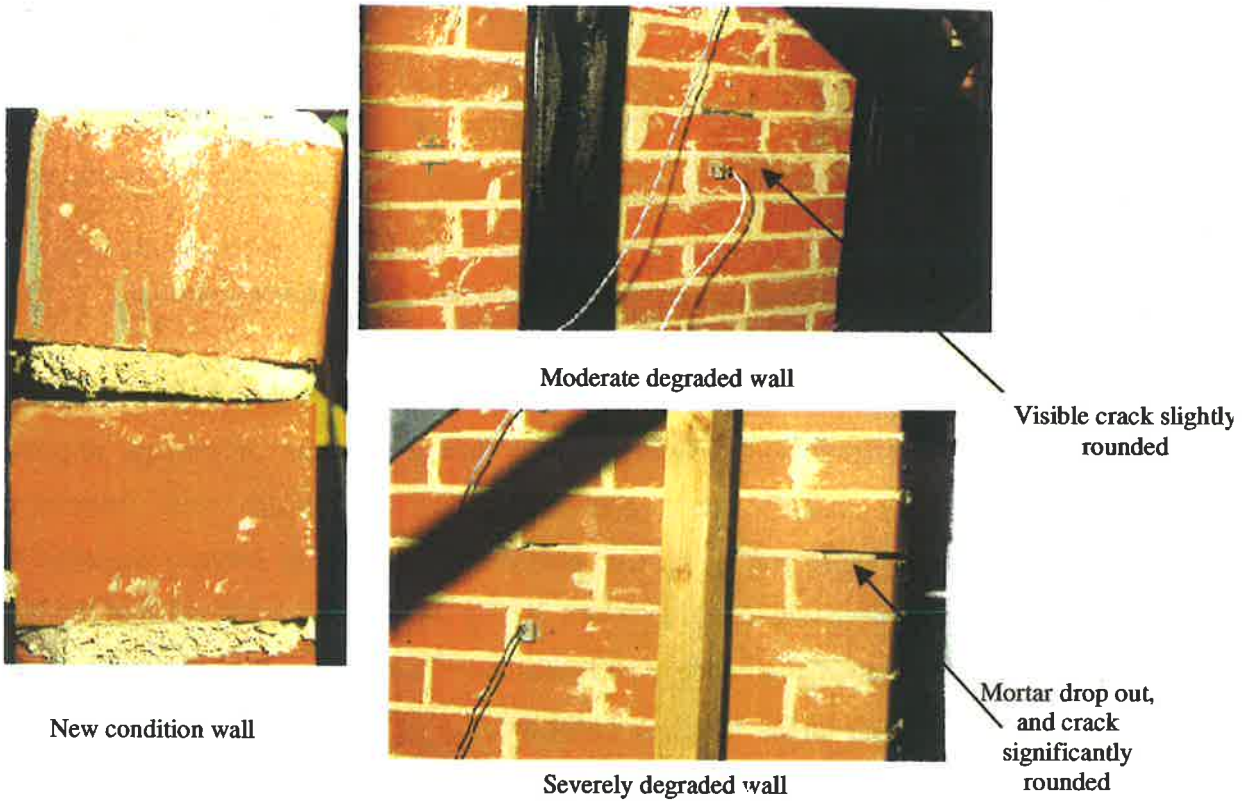

Figure 6.4.12 Mid-height Rotation Joint Condition

From the static push tests on 110 mm walls with a 0.15 MPa overburden, it was confirmed that a significant additional restoring force occurred at large mid-height displacements due to the increased spring deflections. Consequently, for mid-height displacements greater than approximately 20% of the wall thickness the constant force assumption was no longer valid.

In Section 6.4.6 the F-Δ relationships determined by the static push tests have also been used for comparison with dynamic F-Δ relationships, derived in accordance with the assumption of a triangular distribution of acceleration. Here the response of the effective

masses at 2/3 the free body height correlate well with the static push test results. This further supports the use of a triangular distribution of acceleration.

6.4.6. Free Vibration Tests

Free-vibration tests were performed on test specimens which were pre-cracked at mid-height to investigate the physical characteristics of the free vibration response of simply supported URM walls. To enhance the investigation of the free vibration response additional data points have also been derived from the free vibration phase of pulse tests, reported in Section 6.4.7.1. To undertake these tests, the mid-height of the cracked test panel was displaced statically to near the incipient instability displacement. In effect the wall was provided with a degree of potential energy equal to that required to move the wall from its initial vertical position to that of the incipient instability displacement. From this displacement the wall specimens were released and permitted to vibrate freely i.e. to rock between their leeward faces. This vibration resulted from a continuous energy balance comprising an exchange of potential and kinetic energy. During the response the total system energy was exponentially reduced to zero by energy losses associated with the incremental damping at the crack closing impact and support friction. At that time both the potential and kinetic energy are reduced to zero and the vibration ceases with the wall in the vertical position.

The same instrumentation to that described in Section 6.2.3 was used to record both the mid-height displacement and acceleration of the free vibration response. A representative cross-section of the free vibration test results are presented in Appendix (F). For these tests as well as the mid-height acceleration and displacement response the mid-height hysteretic behaviour is also presented. From the free vibration tests the a-Δ relationship and thus the mid-height 'semi-rigid resistance threshold' acceleration and approximate displacement at which this occurred were determined. Further, by adopting the assumption of a triangular distribution of acceleration relative to the supports, the 'semi-rigid resistance threshold' acceleration at the effective mass was determined as 2/3 of the mid-height 'semi-rigid resistance threshold' acceleration. Table 6.4.6 presents a summary of the free vibration release results.

Table 6.4.6 Summary of Release Test Results

Wall No.	Thickness (mm)	Over-burden (MPa)	'Quasi-Static' Rigid Body Acceleration Capacity (Refer Table 6.4.2)	Mid-height 'Semi-rigid Resistance Threshold' Acceleration (g)	Effective Mass 'Semi-rigid Resistance Threshold' Acceleration (g)	Displacement at 'Semi-rigid Resistance Threshold' (mm)
10	50	0	0.13	0.19	0.12	9
10	50	0	0.13	0.18	0.12	8
10	50	0.07	0.65	0.78	0.52	9
11	110	0	0.29	0.35	0.23	15
11	110	0	0.29	0.35	0.23	16
11	110	0	0.29	0.32	0.22	17

As the effective mass 'semi-rigid resistance threshold' acceleration is consistently just below the predicted 'quasi-static' acceleration this further suggests that the assumption of a triangular acceleration distribution and thus effective mass location at the 2/3 free body height, is reasonable.

6.4.6.1. Non-linear Frequency – Mid-Height Displacement Relationship

For all of the free vibration responses analysed, each cycle of the displacement response was considered in turn. In doing so each mid-height response cycle start amplitude, Δ_1, finish amplitude, Δ_2, and cycle period, T were determined as shown by Figure 6.4.13.

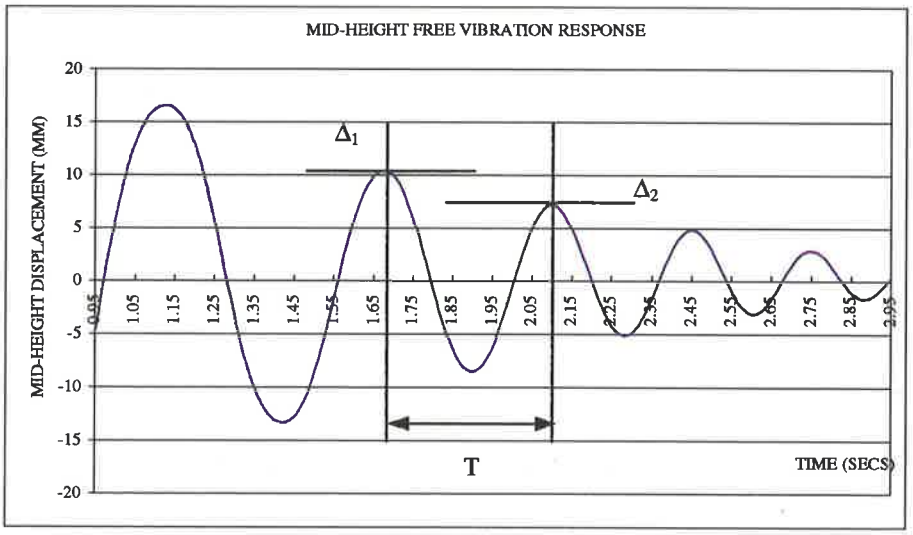

Figure 6.4.13 Free Vibration Calculation

The average cycle amplitude, Δ_a, was determined as,

$$\Delta_a = \frac{\Delta_1 + \Delta_2}{2}$$

and the individual cycle frequency as,

$$f = 1/T$$

Having determined this information for each cycle, the non-linear frequency versus Δ_a relationship was plotted including an exponential or logarithmic line of best fit. Figure 6.4.14 presents this relationship for 50 mm thick specimens at various levels of applied overburden and Figure 6.4.15 for 110 mm thick walls with no applied overburden. A comparison of the empirically derived f-Δ_a relationships with an analytical prediction derived by the comparison of the dynamic equation of motion for a SDOF system and those for the non-linear rocking system is presented in Chapter **7**.

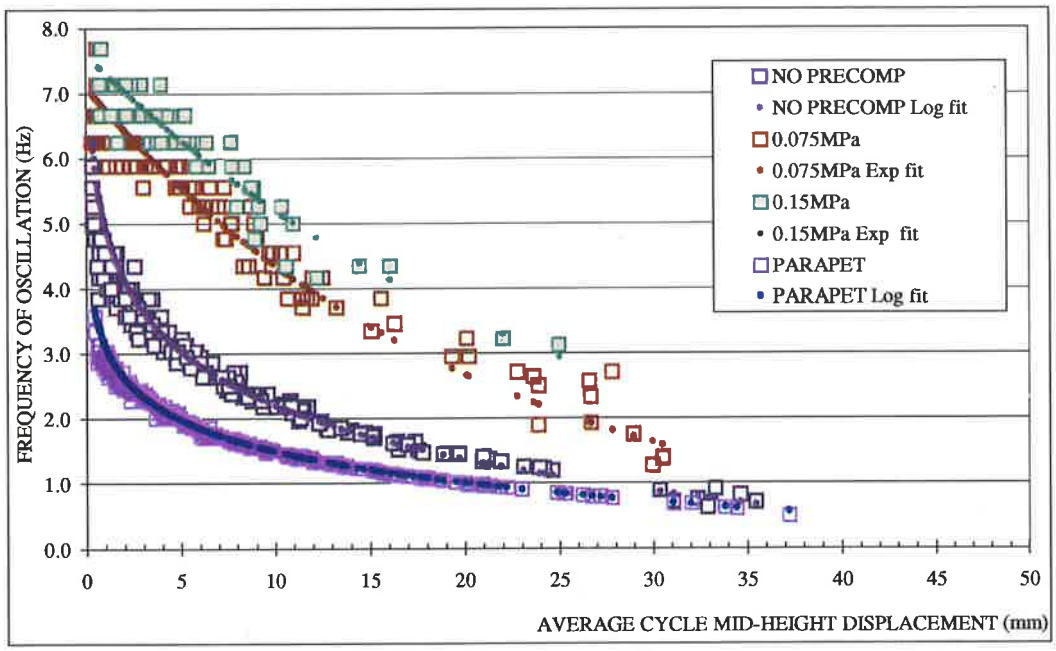

Figure 6.4.14 50mm Specimen Frequency vs Average Cycle Mid-Height Disp.

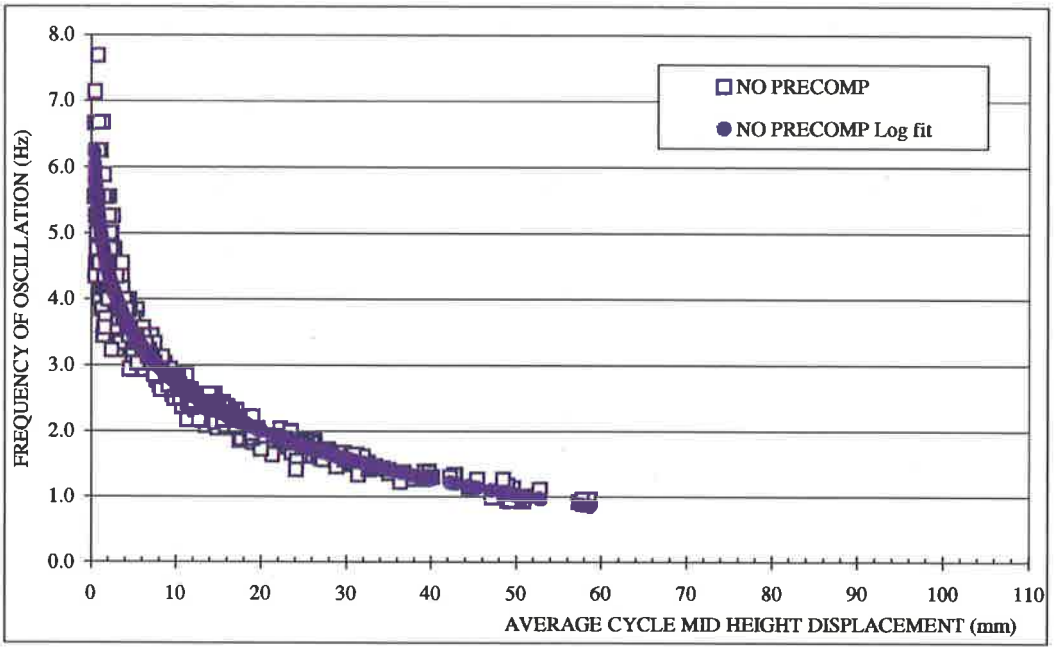

Figure 6.4.15 110mm Specimen Frequency vs Average Cycle Mid-Height Disp.

6.4.6.2. Non-linear Dynamic Force- Mid-Height Displacement Relationship

Rearranging the previously established dynamic relationship (Clough et al 1993)

$$\omega = 2\pi f = \sqrt{\frac{K_a}{M_e}}$$

where ω = cycle angular response frequency

K_a = average cycle secant stiffness

M_e = effective mass of the free body

the average cycle secant stiffness can be written as,

$$K_a = (2\pi f)^2 M_e \qquad (6.4.3)$$

Following from this an estimate of the response force can then be determined as

$$F = K_a \Delta_e = (2\pi f)^2 M_e \Delta_e \qquad (6.4.4)$$

where Δ_e = displacement of the effective mass

Assuming that the acceleration response of each of the rocking free bodies is triangularly distributed relative to the supports, the effective mass is located at 2/3 the height of the free body. Consequently the average effective mass displacement, Δ_e, can be related to the average cycle mid-height displacement, Δ_a, by

$$\Delta_e = \frac{2}{3}\Delta_a$$

Substituting Δ_e back into Equation 6.4.4 the force response at the effective mass can be determined as,

$$F = \frac{2}{3} K_a \Delta_a = \frac{2}{3}(2\pi f)^2 M_e \Delta_a \qquad (6.4.5)$$

This relationship is therefore directly comparable with static test results. From Equation 6.4.5, the dynamic F-Δ relationships at the effective mass for the test specimens have been determined. Each point shown on Figure 6.4.16 shows this relationship for each free vibration response cycle of the 50 mm thick specimens at various levels of applied overburden and is compared with the bi-linear static rigid body F-Δ relationship. The line of best fit has been derived using the line of best fit from the *f*-Δ relationship discussed in Section 6.4.6.1. Similarly, each point shown on Figure 6.4.17 represents the relationship for each free vibration response cycle of the 110 mm thick walls with no applied overburden again compared with the bi-linear static rigid body F-Δ relationship.

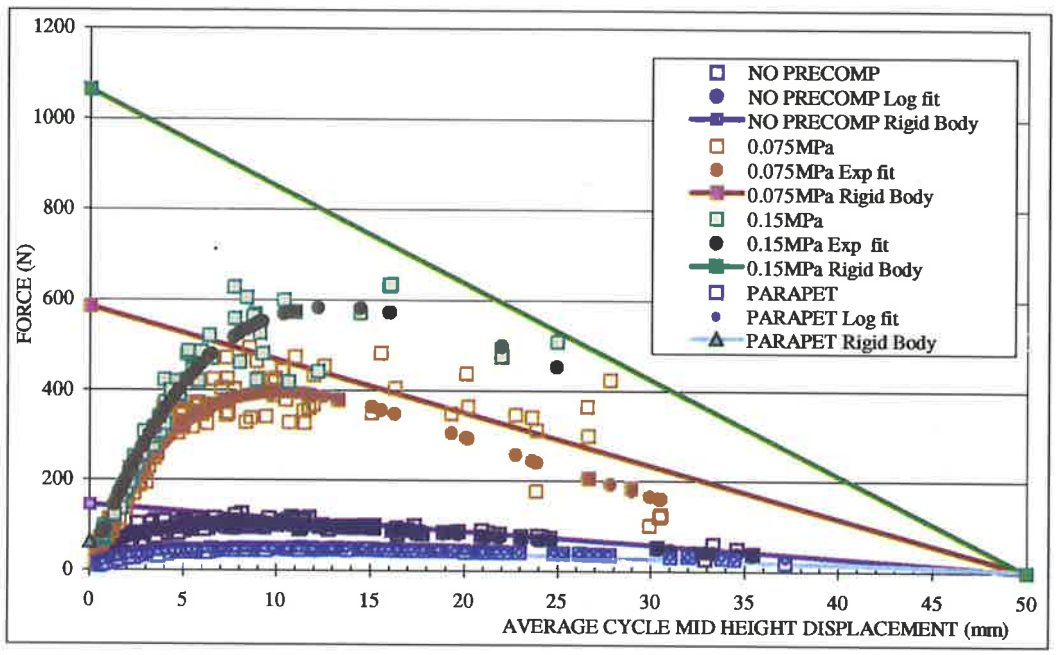

Figure 6.4.16 50mm Wall Dynamic F-Δ Relationships (Various Overburden)

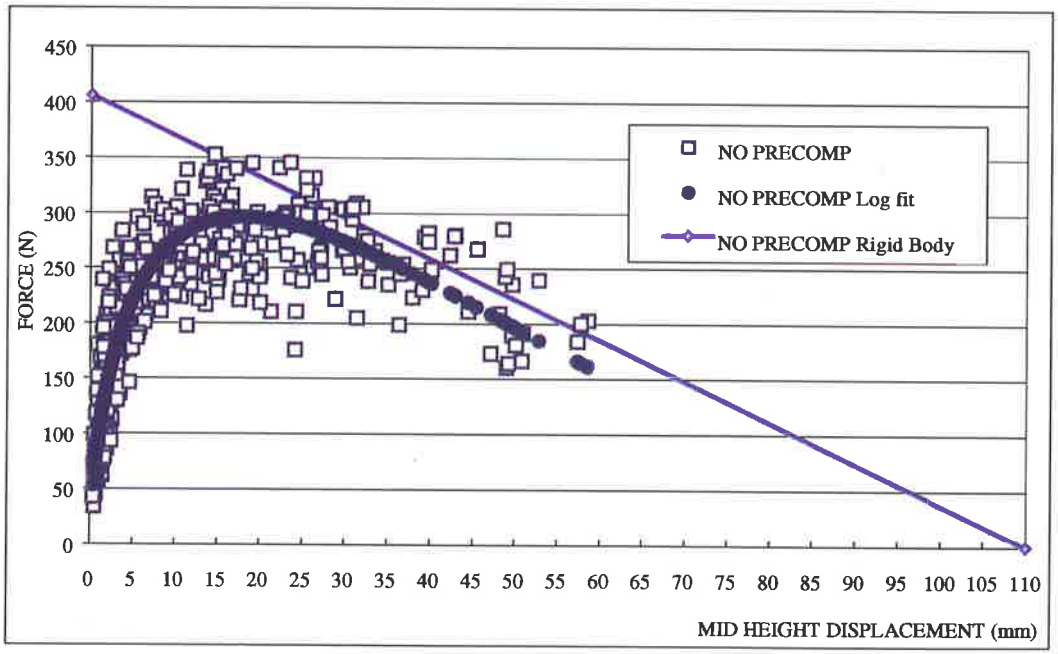

Figure 6.4.17 110mm Wall Dynamic F-Δ Relationship

A comparison of the derived dynamic F-Δ relationships with the results of the static push tests also show a good correlation as presented in Figure 6.4.18 and Figure 6.4.19. This observation further confirms that the assumption of a triangular acceleration response for rocking free bodies relative to the supports provides a reasonable estimate of the true acceleration response.

For the remainder of the analytical modelling of the rocking response of pre-cracked simply supported URM walls, the free body triangular acceleration response assumption is adopted.

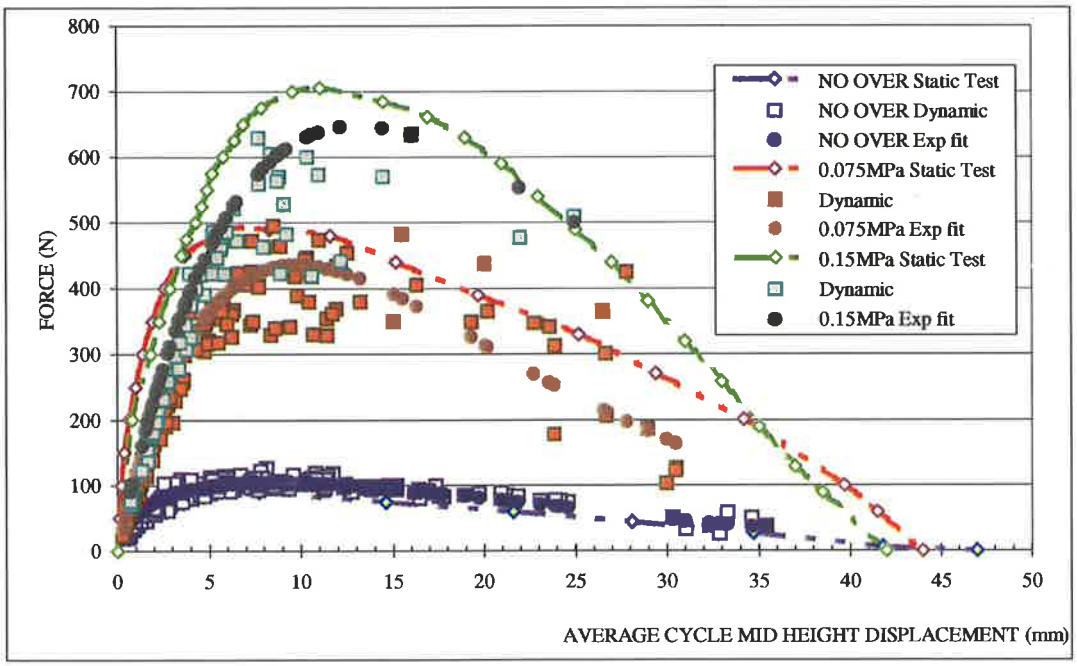

Figure 6.4.18 50mm Wall Comparison of Static and Dynamic F-Δ Relationships

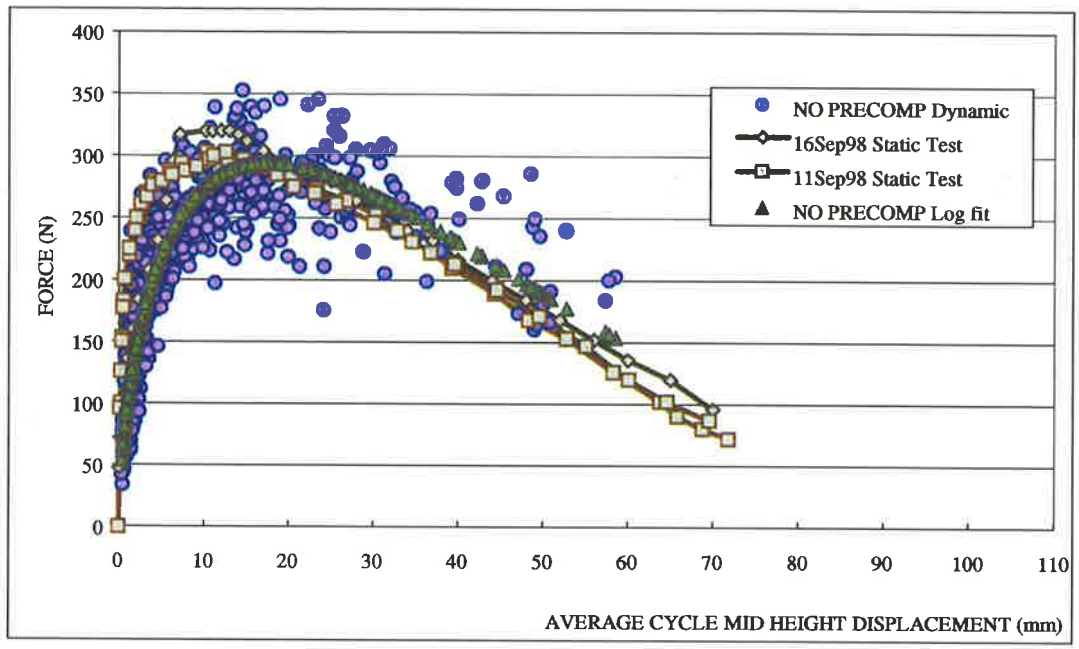

Figure 6.4.19 110mm Wall Comparison of Static and Dynamic F-Δ Relationship

6.4.6.3. Non-linear Damping-Frequency Relationship

As discussed further in Chapter 7, for a single degree-of-freedom (SDOF) system, with 100% of its mass mobilized, the equivalent viscous damping ratio, ξ_{SDOF}, associated with the per cycle energy loss can be estimated for each response cycle (refer Figure 6.4.13) as,

$$\xi_{SDOF} = \frac{\ln\left(\Delta_1 / \Delta_2\right)}{2\pi} \qquad (6.4.6)$$

This estimate can be shown to be reasonable for ξ_{SDOF} less than approximately 20% which is generally the case for building structures. Above this the damped frequency becomes increasingly significant and must be considered. Since the frequency of each response cycle was known, the non-linear ξ_{SDOF} versus frequency relationship was developed. Figure 6.4.20 presents this relationship for the 50 mm wall specimens at various levels of applied overburden and Figure 6.4.22 for non-loadbearing 110 mm wall specimens. For both sets of walls a lowerbound estimate of ξ_{SDOF} of around 5% was observed. This is slightly greater than the 3% observed by (Lam 1995) for tests on

110mm thick parapet walls. A possible reason for this is energy losses associated with the simply supported wall mid-height rotation joint as well as the additional mass due the relative heights of the test walls.

From the non-linear relationship an increase in ξ_{SDOF} at very low response frequency (large displacement oscillations) and at high response frequencies (small displacement oscillations) was observed. Walls having overburden were also observed to typically have relatively higher ξ_{SDOF} values than for walls with small axial loads. The increased energy loss at large displacement oscillations and for walls having overburden can be explained by the increased impact energy loss per half cycle at the closing of the mid-height, top and bottom cracks. The increased energy loss at small displacement oscillation is likely to have been caused by friction losses at the supports becoming proportionally more significant.

A final observation was that the thicker wall specimens tended to have a slightly higher energy loss per cycle although this was not proportional to the ratio of thickness since the density of the two brickwork specimens were not equal.

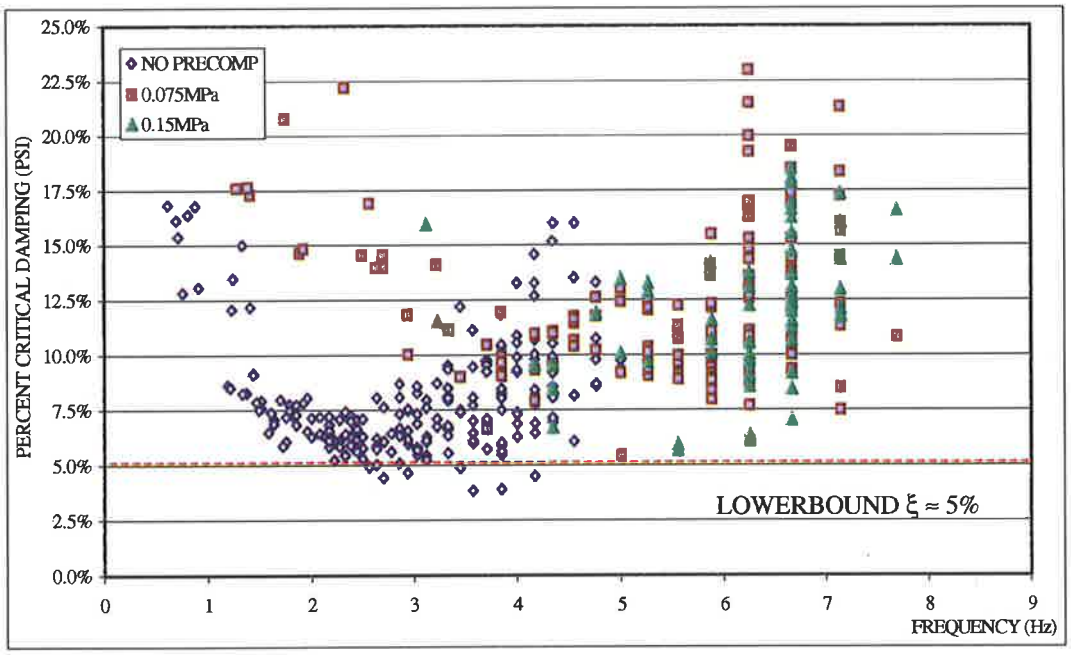

Figure 6.4.20 50mm Wall Non-linear ξ vs Frequency (Various Overburden)

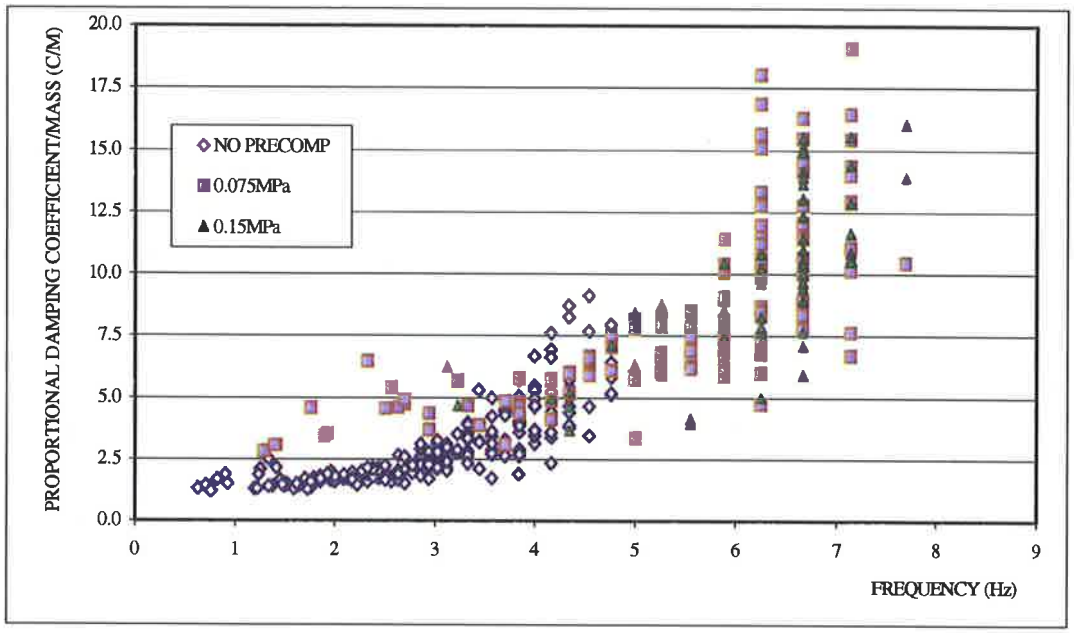

Figure 6.4.21 50mm Wall Non-linear C_{SDOF}/M_e vs Frequency (Various Overburden)

To minimise the effect of the specimen density difference the dynamic relationship (Clough et al 1993)

$$\frac{C_{SDOF}}{M_e} = 4\pi f \xi_{SDOF}$$

was used to derive the ratio of the SDOF proportional damping coefficient, C_{SDOF}, to the effective mass, M_e. This was then plotted against the cycle frequency (refer Figure 6.4.21 and Figure 6.4.23). A comparison of the C_{SDOF}/M_e versus frequency relationship for non-loadbearing 50 mm and 110 mm walls (refer Figure 6.4.23) shows that a good correlation was found between the energy losses in the two rocking systems.

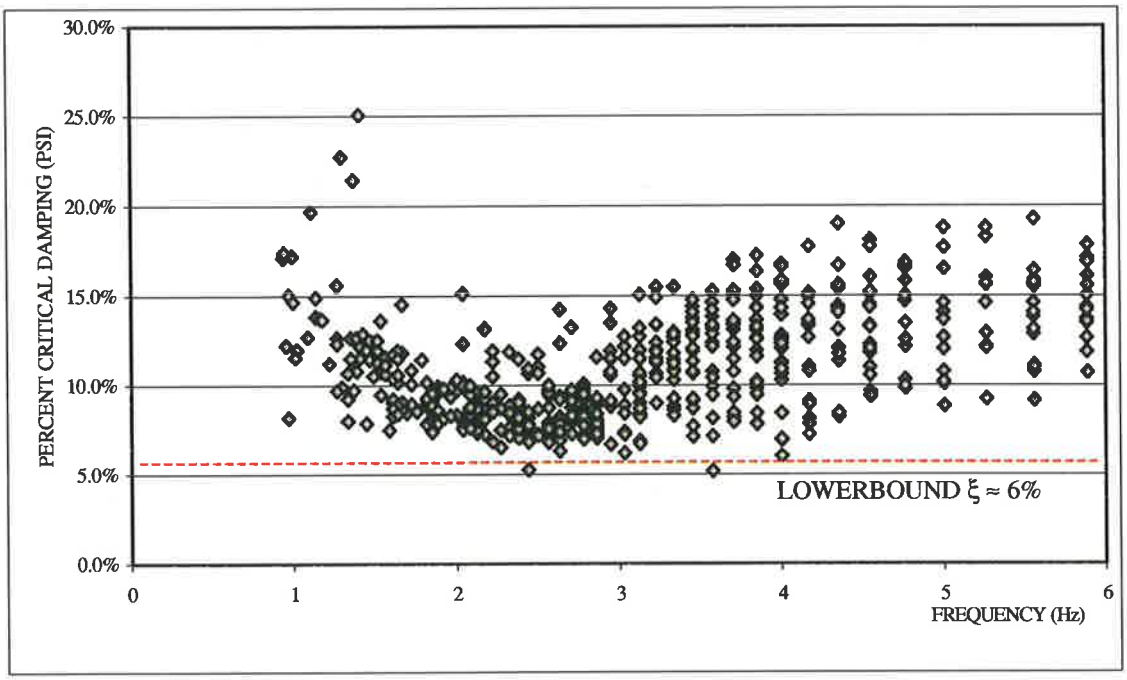

Figure 6.4.22 Non-loadbearing 110mm Wall Non-linear ξ vs Frequency

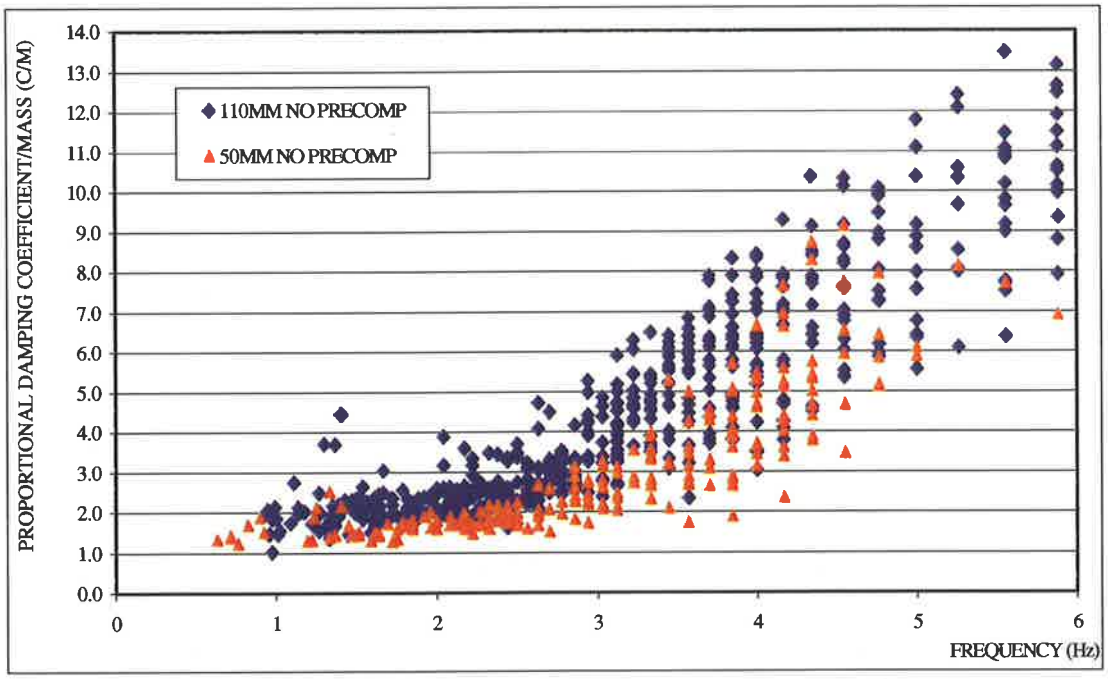

Figure 6.4.23 Non-loadbearing 50mm and 110mm Wall C_{SDOF}/M_e vs Frequency

6.4.7. Transient Excitation Tests

The shaking table input selected for transient excitation tests included both pulse and real earthquake excitations. The range of amplitude and frequency content was selected to permit the rocking wall response to be thoroughly examined over a relevant range of excitation scenario. This allowed critical excitation parameters to be identified and directly related to the wall response. The resulting dynamic data was also used to provide a basis for comparison with analytical response predictions using THA, as discussed in the next chapter.

6.4.7.1. Pulse Tests

As part of the September 98 test series both half-sine (½ SD) and gaussian displacement pulse tests were performed on pre-cracked simply supported URM walls both with and without applied overburden. Instrumentation as described in Section 6.2.3 was used to completely record the dynamic response behaviour of the wall specimens.

The displacement pulse frequencies used for the experimental investigation ranged from 0.5Hz to 3Hz.. This frequency range was selected to cover the lower response frequency limit, f_{limit}, as described in Section 5.2.1, and thus permitted pulse forcing frequency at which the maximum displacement amplification occurred or the effective wall 'resonant frequency' to be approximately identified experimentally. Figure 6.4.24 shows a normalized 0.5Hz input displacement gaussian pulse and Figure 6.4.25 the corresponding acceleration input at the table

For each of the displacement pulse frequencies investigated a normalised displacement pulse was first determined (e.g. refer Figure 6.4.24). The pulse displacement amplitude input to the shaking table was gradually increased, at each frequency level, until rocking and ultimately instability of the wall specimen occurred. The peak pulse displacement (PGD) and acceleration (PGA) were then related to the peak mid-height displacement response of the test specimen. This permitted the identification the displacement amplification (peak mid-height displacement/PGD) of the wall mid-height response. Table 6.4.7 presents a summary of key results of the pulse tests performed.

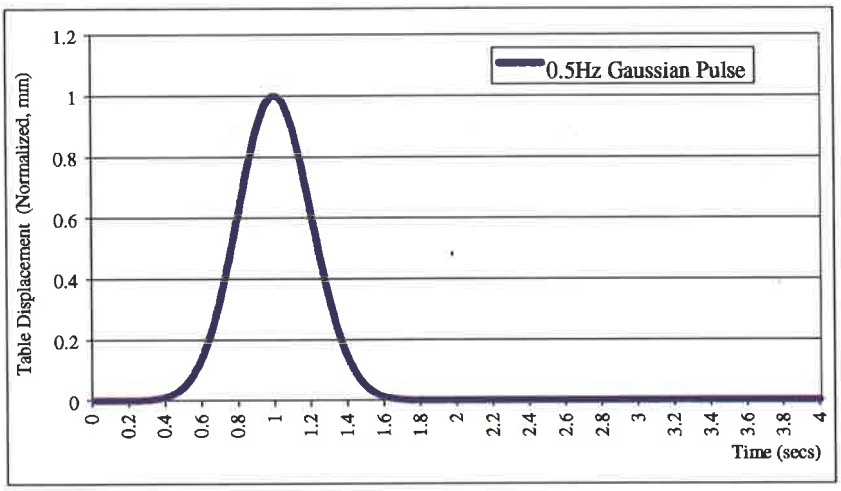

Figure 6.4.24 0.5Hz Normalized Gaussian Displacement Pulse Input

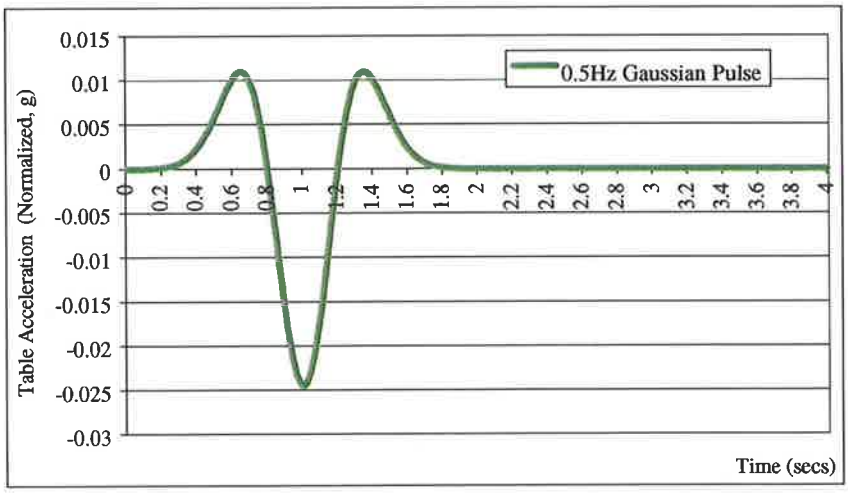

Figure 6.4.25 Corresponding Acceleration Input

On examination of the results it is evident that for each of the wall specimens the maximum displacement amplification is associated with a particular frequency described in Section 5.2.1 as the effective resonant frequency, f_{eff}. For the 1.5m tall, 50mm thick wall without applied overburden, the maximum displacement amplification occurs at pulse frequencies of between 1Hz and 2Hz. With the application of 0.07MPa overburden the effective wall resonant frequency increases to between 2Hz and 3Hz and further to greater than 3Hz with the application of 0.15MPa overburden (refer Table 6.4.7). For the

1.5m tall, 110mm thick wall without applied overburden the effective resonant frequency is similar to that of the 50mm wall at 1Hz to 2Hz (refer Table 6.4.8). A representative cross section of the pulse test results where the mid-height displacement response and input displacements are compared is presented in Appendix (F). The full wall response including ¼ -, mid- and ¾ - height acceleration response is also presented. During the rocking free vibration response phase the mid-height acceleration response is typically approximately twice the ¼ - and ¾ - height acceleration responses.

Table 6.4.7 Summary of Key Pulse Test Results (50mm Walls)

Wall No.	Thick - ness (mm)	Over- burden (MPa)	Pulse Type	Pulse Freq. (Hz)	Peak Pulse Disp. (mm)	Peak Pulse Accel. (mm)	Peak Mid-height Response Accel. (g)	Peak Mid-height Response Disp. (mm)	Mid-height Disp. Amplification
10*	50	0	½ SD	0.5	20	0.1	0.15	5	0.25
10*	50	0	½ SD	0.5	30	0.15	0.18	13	0.43
10*	50	0	½ SD	0.5	40	0.19	0.19	20.5	0.51
10*	50	0	½ SD	0.5	50	0.225	-	50	1.00
10*	50	0	½ SD	1	13	0.135	0.19	46	3.54
10*	50	0	½ SD	1	15	0.155	0.19	31	2.07
10*	50	0	½ SD	1	17	0.175	0.19	31	1.82
10*	50	0	½ SD	1	20	0.2	-	50	2.50
10*	50	0	½ SD	2	10	0.25	0.18	28	2.80
10*	50	0	½ SD	2	13	0.33	0.18	31	2.38
10*	50	0	½ SD	2	15.5	0.39	0.18	32	2.06
10*	50	0	½ SD	2	17.5	0.41	0.18	33	1.89
10*	50	0	½ SD	2	20	0.46	0.18	50	2.50
14	50	0	Gauss	1	5	0.07	0.12	10.5	2.10
14	50	0	Gauss	1	7.5	0.1	0.12	16.5	2.20
14	50	0	Gauss	1	10	0.125	0.12	24	2.40
14	50	0	Gauss	1	12.5	0.15	0.12	33	2.64
14	50	0	Gauss	1	14	0.18	0.12	40	2.86
14	50	0	Gauss	1	15	0.2	-	50	3.33
14	50	0	Gauss	1	16	0.21	-	50	3.13
14	50	0	Gauss	1	14	0.16	0.13	35	2.50
14	50	0	Gauss	1	15	0.175	0.13	40	2.67
14	50	0	Gauss	1	16	0.19	-	50	3.13
14	50	0	Gauss	2	15	0.1	0.09	6	0.40
14	50	0	Gauss	2	21	0.13	0.1	17	0.81
14	50	0	Gauss	2	22	0.15	0.12	23	1.05
14	50	0	Gauss	2	23	0.16	0.13	29	1.26
14	50	0	Gauss	2	24	0.175	0.13	50	2.08
14	50	0	Gauss	0.5	5	0.3	0.13	11	2.20
14	50	0	Gauss	0.5	8	0.6	0.13	13	1.63
14	50	0	Gauss	0.5	10.5	0.7	0.13	15	1.43
14	50	0	Gauss	0.5	13	0.8	0.13	15.5	1.19
14	50	0	Gauss	0.5	15	0.9	0.13	18	1.20
10*	50	0.07	½ SD	0.5	20	0.19	0.5	3	0.15

Continued

Wall No.	Thick - ness (mm)	Over-burden (MPa)	Pulse Type	Pulse Freq. (Hz)	Peak Pulse Disp. (mm)	Peak Pulse Accel. (mm)	Peak Mid-height Response Accel. (g)	Peak Mid-height Response Disp. (mm)	Mid-height Disp. Amplification
10*	50	0.07	½ SD	0.5	30	0.25	0.6	4	0.13
10*	50	0.07	½ SD	0.5	40	0.31	0.6	5.5	0.14
10*	50	0.07	½ SD	0.5	50	0.375	0.6	6.5	0.13
10*	50	0.07	½ SD	0.5	70	0.4	0.6	10	0.14
10*	50	0.07	½ SD	1	10	0.18	0.5	3.5	0.35
10*	50	0.07	½ SD	1	25	0.38	0.7	15	0.60
10*	50	0.07	½ SD	1	30	0.39	0.7	8	0.27
10*	50	0.07	½ SD	1	35	0.4	0.7	10	0.29
10*	50	0.07	½ SD	1	40	0.45	0.7	14	0.35
10*	50	0.07	½ SD	1	50	0.5	0.7	25	0.50
10*	50	0.07	½ SD	1	55	0.8	0.7	37	0.67
10*	50	0.07	½ SD	2	10	0.31	0.7	9	0.90
10*	50	0.07	½ SD	2	15	0.41	0.7	16	1.07
10*	50	0.07	½ SD	2	22.5	0.5	0.7	34	1.51
10*	50	0.07	½ SD	2	25	0.62	0.7	40	1.60
10*	50	0.07	½ SD	3	10	0.7	0.7	21	2.10
10*	50	0.07	½ SD	3	13	0.8	0.7	25	1.92
10*	50	0.07	½ SD	3	16	0.9	0.7	40	2.50
10*	50	0.15	½ SD	0.5	30	0.45	1	7	0.23
10*	50	0.15	½ SD	0.5	40	0.5	1	8	0.20
10*	50	0.15	½ SD	0.5	50	0.55	1	17	0.34
10*	50	0.15	½ SD	0.5	55	0.6	1	11	0.20
10*	50	0.15	½ SD	0.5	57.5	0.7	1	7	0.12
10*	50	0.15	½ SD	1	60	0.75	1	10	0.17
10*	50	0.15	½ SD	1	62.5	0.8	1	36	0.58
10*	50	0.15	½ SD	1	62.5	0.8	1	20	0.32
10*	50	0.15	½ SD	1	65	0.85	1	30	0.46
10*	50	0.15	½ SD	2	20	0.5	1	20	1.00
10*	50	0.15	½ SD	2	22	0.6	1	13	0.59
10*	50	0.15	½ SD	2	28	0.8	1	14	0.50
10*	50	0.15	½ SD	2	30	0.85	1	11	0.37
10*	50	0.15	½ SD	2	32.5	0.95	1	11	0.34
10*	50	0.15	½ SD	2	35	1	1	11	0.31
10*	50	0.15	½ SD	2	37	1.05	1	12	0.32
14	50	0.15	Gaus	0.5	36	N/A	0.9	9	0.25
14	50	0.15	Gaus	0.5	41	N/A	0.9	20	0.49
14	50	0.15	Gaus	0.5	46	N/A	1	24	0.52
14	50	0.15	Gaus	0.5	49	N/A	1	34	0.69

Table 6.4.8 Summary of Key Pulse Test Results (110mm Walls)

Wall No.	Thick - ness (mm)	Over-burden (MPa)	Pulse Type	Pulse Freq. (Hz)	Peak Pulse Disp. (mm)	Peak Pulse Accel. (mm)	Peak Mid-height Response Accel. (g)	Peak Mid-height Response Disp. (mm)	Mid-height Disp. Amplification
11*	110	0	½ SD	1	15	0.16	0.28	8	0.53
11*	110	0	½ SD	1	18	0.2	0.3	13.5	0.75
11*	110	0	½ SD	1	20	0.22	0.3	23	1.15
11*	110	0	½ SD	1	25	0.25	0.3	45	1.80
11*	110	0	½ SD	1	27	0.26	0.3	49	1.81
11*	110	0	½ SD	1	30	0.275	0.31	41	1.37
11*	110	0	½ SD	1	32.5	0.3	0.31	40	1.23
11*	110	0	½ SD	1	37.5	0.32	0.31	62	1.65
11*	110	0	½ SD	1	40	0.33	0.31	72	1.80
11*	110	0	½ SD	1	45	0.35	0.31	82	1.82
11*	110	0	½ SD	2	10	0.2	0.3	20	2.00
11*	110	0	½ SD	2	15	0.25	0.3	40	2.67
11*	110	0	½ SD	2	17.5	0.38	0.3	45	2.57
11*	110	0	½ SD	2	20	0.43	0.3	45	2.25
11*	110	0	½ SD	2	25	0.5	0.3	58	2.32
11*	110	0	½ SD	2	27	0.61	0.3	65	2.41
11	110	0	½ SD	3	8	0.5	0.3	13	1.63
11	110	0	½ SD	3	15	0.8	0.3	26	1.73
11	110	0	½ SD	3	17	0.9	0.3	27	1.59
11	110	0	½ SD	3	18	1	0.3	30	1.67
11	110	0	½ SD	3	16	0.6	0.31	38	2.38
11	110	0	½ SD	3	20	0.65	0.31	49	2.45
11	110	0	½ SD	3	24	0.725	0.31	61	2.54
12	110	0	Gauss	1	16	0.17	0.31	25.5	1.59
12	110	0	Gauss	1	21	0.25	0.31	36	1.71
12	110	0	Gauss	1	26	0.3	0.31	49	1.88
12	110	0	Gauss	1	28	0.35	0.31	54	1.93
12	110	0	Gauss	1	29	0.375	0.31	57	1.97
12	110	0	Gauss	1	30	0.4	0.31	67	2.23
12	110	0	Gauss	1	31	0.425	0.31	73	2.35
12	110	0	Gauss	1	32	0.45	0.31	77	2.41
12	110	0	Gauss	1	31	0.425	0.31	72	2.32
12	110	0	Gauss	1	33	0.85	0.31	80	2.42
12	110	0	Gauss	1	34	0.9	0.31	85	2.50
12	110	0	Gauss	1	35	0.95	0.31	88	2.51
12	110	0	Gauss	1	39	0.52	0.31	58	1.49
12	110	0	Gauss	1	41	0.55	0.31	76	1.85
12	110	0	Gauss	1	44	0.58	0.31	78	1.77
12	110	0	Gauss	1	46	0.61	0.31	68	1.48
12	110	0	Gauss	1	48	0.65	0.31	55	1.15
13*	110	0	Gauss	1	11	0.125	0.3	6	0.55
13*	110	0	Gauss	1	12.5	0.15	0.31	9	0.72
13*	110	0	Gauss	1	15.5	0.175	0.32	15.5	1.00
13*	110	0	Gauss	1	17.5	0.225	0.33	20.5	1.17
13*	110	0	Gauss	1	20	0.25	0.33	26	1.30
13*	110	0	Gauss	1	22.5	0.275	0.33	30.5	1.36
13*	110	0	Gauss	1	25	0.3	0.33	35.5	1.42

Continued

Wall No.	Thick - ness (mm)	Over- burden (MPa)	Pulse Type	Pulse Freq. (Hz)	Peak Pulse Disp. (mm)	Peak Pulse Accel. (mm)	Peak Mid-height Response Accel. (g)	Peak Mid-height Response Disp. (mm)	Mid-height Disp. Amplification
13*	110	0	Gauss	1	27.5	0.325	0.33	40	1.45
13*	110	0	Gauss	1	31	0.35	0.33	45	1.45
13*	110	0	Gauss	1	33	0.4	0.33	57	1.73
13*	110	0	Gauss	1	36	0.45	0.33	65	1.81
13*	110	0	Gauss	1	38	0.5	0.33	55	1.45
13*	110	0	Gauss	1	40	0.55	0.33	50	1.25
13*	110	0	Gauss	1	42.5	0.6	0.33	45	1.06
13*	110	0	Gauss	1	44	0.65	0.33	44	1.00
13*	110	0	Gauss	1	45	0.7	0.33	50	1.11
13*	110	0	Gauss	0.5	50	0.225	0.33	20	0.40
13*	110	0	Gauss	0.5	55	0.25	0.33	24	0.44
13*	110	0	Gauss	0.5	60	0.275	0.33	28	0.47
13*	110	0	Gauss	0.5	65	0.3	0.33	41	0.63
13*	110	0	Gauss	0.5	70	0.35	0.33	85	1.21
13*	110	0	Gauss	0.5	70	0.4	0.33	71	1.01
13*	110	0	Gauss	0.5	75	0.45	0.33	76	1.01
13*	110	0	Gauss	0.5	80	0.5	0.33	74	0.93
13*	110	0	Gauss	0.5	82.5	0.55	0.33	95	1.15
13*	110	0	Gauss	0.5	85	0.575	0.33	69	0.81
13*	110	0	Gauss	0.5	87.5	0.6	0.33	85	0.97
13*	110	0	Gauss	0.5	90	0.625	0.33	76	0.84

* Presented in Appendix (F)

The results also indicated that the wall thickness had only a small impact on the effective resonant frequency but the application of overburden significantly increased the effective resonant frequency. This can be explained, as a change in the wall thickness does not alter the average incremental cycle secant stiffness, K_{ave}, and thus the effective resonant frequency however an increase in overburden does (refer Figure 6.4.26). For a rigid wall this is because an increase in wall thickness does not alter the negative stiffness value, as both of the 'rigid resistance' force, $R_e(1)$, and instability displacement, $\Delta_{instability}$, are increased proportionally. The average incremental secant stiffness and effective resonant frequency therefore remain the same. In contrast, with an increased overburden applied at the leeward face, as was the case for the test specimens, $K_e(1)$ is reduced as $R_e(1)$ increases however $\Delta_{instability}$ does not alter. Thus, the average incremental cycle secant stiffness is increased. This is shown in Figure 6.4.14 where higher response frequencies for the 50mm wall specimens with overburden are observed than without. Where an

increase in overburden is applied at the leeward face of the wall, $R_e(1)$ again increases but to a lesser extent and $\Delta_{instability}$ is reduced to less than the thickness of the wall. The reduction in $\Delta_{instability}$ is dependent on the ratio of overburden to the self weight of the wall (refer Table 5.2.1). Consequently, again the average incremental cycle secant stiffness and thus the effective resonant frequency are increased (refer Figure 6.4.26).

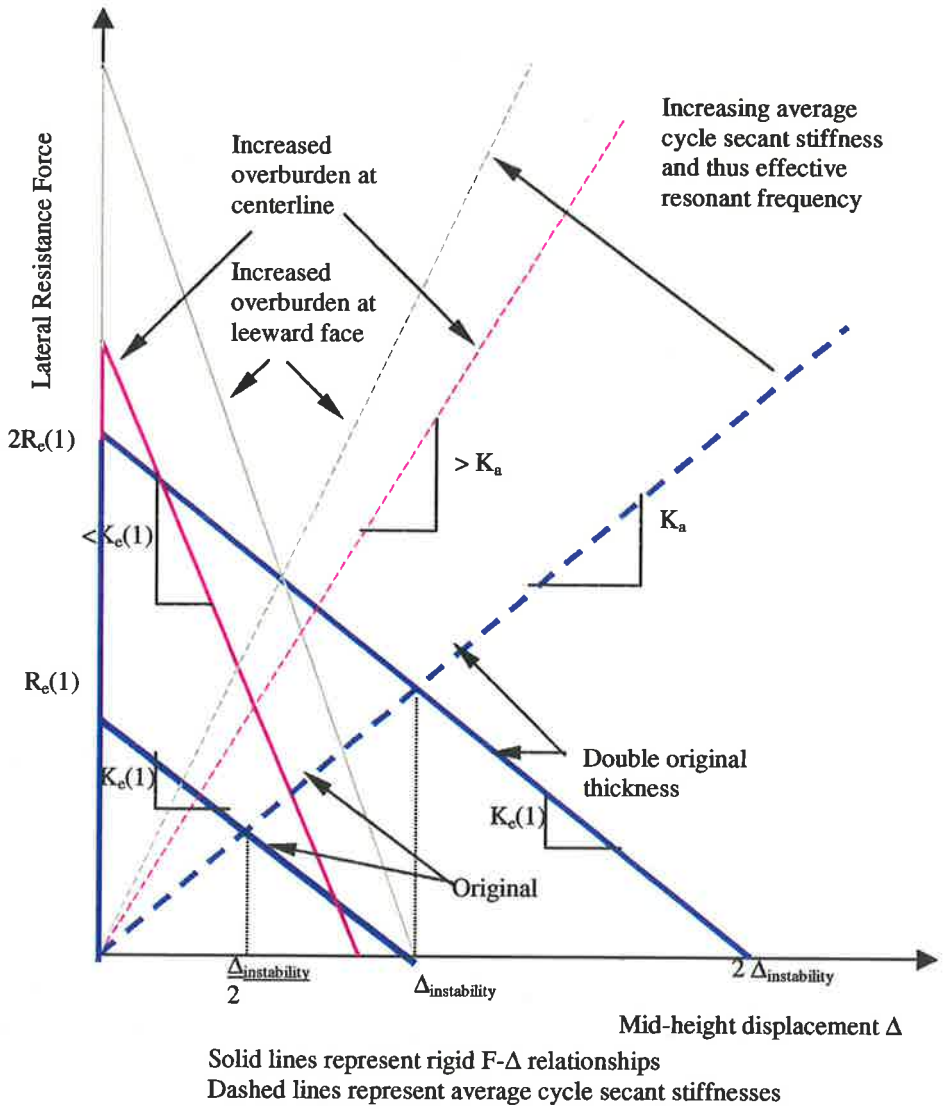

Figure 6.4.26 Effective Resonant Frequency (By Wall Thickness and Overburden)

Experimentally the range of effective resonant frequency observed is due to the changing state of the rotation joints with continued testing and degradation of the rotation joints flattening the F-Δ relationship. As such, there is a corresponding decrease in the average incremental cycle secant stiffness and thus the effective resonant frequency of the wall.

6.4.7.2. Real Earthquake Excitation Tests

To complete the investigation into the response of both loadbearing and non-loadbearing simply supported URM walls to transient excitations, shaking table tests were performed using real earthquake accelerogram records to drive the shaking table. A comparison of recorded table accelerations with the original accelerograms has shown a reasonable level of correlation. Instrumentation as described in Section 6.2.3 was used to capture the dynamic response behaviour of the wall specimens.

To investigate wall response over a range of excitation, relevant real earthquake scenario of both 'low frequency large displacement' and 'high frequency small displacement' excitation were selected. Table 6.4.9 presents a summary of the earthquake excitations used for investigation. By comparison of the PGD and PGA an indication of the type and severity of the earthquake can be attained. For instance it can be seen that the Nahanni aftershock has a relatively high PGA but a small PGD indicating that this earthquake had a dominant high frequency component. This was determined from the power frequency spectrum as approximately 1.75Hz to 2.25Hz. Although traditionally this would therefore not be expected to impact greatly on ductile structures the large accelerations would be expected to impact more severely on stiff brittle structures. The Taft, Pacoima Dam and ElCentro earthquakes typically have higher PGD and similarly large PGA thus indicating a lower dominant frequency in the range of 0.7Hz to 1.1Hz.

In a similar fashion to the pulse tests each earthquake excitation was displacement normalised setting the peak excitation displacement (PGD) to unity. The % of the original excitation could then be related to the PGD input to the table. For each applied excitation the % of the original excitation, was gradually increased until rocking and ultimately instability of the wall specimen occurred. The peak transient excitation

displacement (PGD) and acceleration (PGA) were then related to the peak mid-height displacement of the test specimen.

Table 6.4.9 Earthquake Excitation Description

Transient Excitation Description	**Abbr.**	**100% Peak Ground Displacement (PGD)**	**100% Peak Ground Acceleration (PGA)**
NAHANNI, Canada: Recorded at Iverson during an aftershock of the Nahanni EQ 23rd December 1985 Magnitude 5.5 Epicentral distance 7.5km Soil type rock	NH	4.2mm	2.24m/s^2 (0.23g)
PACOIMA DAM, California: Recorded at Pacoima Dam, downstream during Northridge EQ 17th January 1994 Magnitude 6.6 Epicentral Distance 19km Soil Type: Rock	PD	53.9mm	4.26m/s^2 (0.43g)
ELCENTRO, California: Recorded at ElCentro during the Imperial Valley EQ 18th May 1940 Magnitude 6.6 Epicentral Distance 8km Soil type: Rock Accelerogram component NS	EL	163.0mm	3.42m/s^2 (0.35g)
TAFT, California: Recorded at Kern Country, Taft Lincoln School Tunnel 21st July 1952 Accelerogram component S69E Epicenter 35 00 00N 119 02 00W Seismograph station 35 09 00N 119 27 00W	TF	98.5mm	1.76m/s^2 (0.18g)

A representative cross section of the earthquake excitation results is presented in Appendix (F). Here the mid-height displacement response and input displacements are compared. The full wall response including ¼ -, mid- and ¾ - height accelerations are also presented. The recorded input excitation accelerations at the base and top of the wall specimen are also presented as these are used in Chapter 7 for analytical THA predictions and should be used for future analytical comparison with these experimental results. Table 6.4.10 and Table 6.4.11 present a summary of key results of the earthquake tests performed for the 50mm and 110mm thick walls respectively.

Table 6.4.10 Summary of Key Earthquake Excitation Test Results (50mm Walls)

Wall No.	Thick - ness (mm)	Over-burden (MPa)	Wall Cond -ition	Excitation (refer Table 6.4.9)	PGD (mm)	PGA (g)	Peak Mid-height Response Accel. (g)	Peak Mid-height Response Disp. (mm)	Mid-height Disp. Amp.
12*	110	0	NEW	100% NH	4.2	0.23	0.26	9	2.17
12*	110	0	NEW	200% NH	8.3	0.46	0.26	21	2.53
12*	110	0	NEW	300% NH	12.5	0.69	0.26	28	2.25
12*	110	0	NEW	400% NH	16.6	0.92	0.26	32.5	1.96
12	110	0	MOD	50% EL	81.5	0.18	0.26	16	0.20
12*	110	0	MOD	66% EL	107.6	0.23	-	Failed	-
12	110	0	MOD	80% EL	130.4	0.28	-	Failed	-
12	110	0	MOD	100% TF	98.5	0.18	0.33	31	0.31
12	110	0	NEW	50% PD	27.0	0.22	0.36	32	1.19
12	110	0	NEW	66% PD	35.6	0.28	0.35	65	1.83
12	110	0	NEW	80% PD	43.1	0.34	0.35	80	1.86
12	110	0	NEW	100% PD	53.9	0.43	0.34	105	1.95
13	110	0	NEW	50% PD	27.0	0.22	0.31	51	1.89
13*	110	0	NEW	66% PD	35.6	0.28	0.30	66	1.86
13*	110	0	NEW	80% PD	43.1	0.34	0.32	70	1.62
13*	110	0	NEW	100% PD	53.9	0.43	-	Failed	-
13	110	0	MOD	50% EL	81.5	0.18	0.29	71	0.87
13*	110	0	MOD	66% EL	107.6	0.23	-	Failed	-
13	110	0	MOD	100% EL	163.0	0.35	-	Failed	-
13	110	0	SER	80% PD	43.1	0.34	-	Failed	-

*Presented in Appendix (F)

Table 6.4.11 Summary of Key Earthquake Excitation Test Results (110mm Walls)

Wall No.	Thick - ness (mm)	Over-burden (MPa)	Wall Cond -ition	Excitation (refer Table 6.4.9)	PGD (mm)	PGA (g)	Peak Mid-height Response Accel. (g)	Peak Mid-height Response Disp. (mm)	Mid-height Disp. Amp.
14	50	0	MOD	15% EL	24.5	0.05	0.15	15	0.61
14	50	0	MOD	20% EL	32.6	0.07	-	Failed	-
14	50	0	MOD	25% EL	40.8	0.09	-	Failed	-
14	50	0	MOD	30% EL	48.9	0.11	-	Failed	-
14	50	0	NEW	20% PD	10.8	0.09	0.18	28	2.60
14	50	0	NEW	25% PD	13.5	0.11	-	Failed	-
14	50	0	NEW	30% PD	16.2	0.13	-	Failed	-
14	50	0	NEW	50% TF	49.3	0.09	0.15	13	0.26
14	50	0	MOD	60% TF	59.1	0.11	-	Failed	-
14	50	0	MOD	70% TF	69.0	0.13	-	Failed	-
14	50	0	MOD	50% NH	2.1	0.12	0.05	6	2.88
14	50	0	MOD	70% NH	2.9	0.16	0.1	8.5	2.92
14	50	0	MOD	100% NH	4.2	0.23	0.23	11	2.65
14	50	0	MOD	200% NH	8.3	0.46	0.4	22	2.65
14	50	0	MOD	300% NH	12.5	0.69	0.5	38	3.05
14	50	0.15	SER	100% PD	53.9	0.43	0.9	13	0.24
14	50	0.15	SER	125% PD	67.4	0.54	1.0	38	0.56
14	50	0.15	SER	135% PD	72.8	0.58	1.0	30	0.41
14	50	0.15	SER	150% PD	80.9	0.65	0.9	44	0.54
14	50	0.15	SER	175% PD	94.3	0.75	-	Failed	-

Summary + Conclusions at end of the Chapter?

7. NON-LINEAR TIME HISTORY ANALYSIS DEVELOPMENT

7.1. Introduction

Non-linear time-history analysis (THA) based on time-step integration is the most representative and reliable method of accounting for the time-dependent nature of URM wall response to applied excitations provided that the non-linear (F-Δ) and damping properties are accurately represented in the analytical model.

Time-stepping procedures have been developed for basic linear single degree-of-freedom (SDOF) systems having a known linear stiffness and damping component. This method relies upon an assumption on the response behaviour between consecutive time steps which permits the dynamic response to be estimated from the applied excitation. One such assumption is the 'Newmark' constant acceleration assumption. For the rocking response of 'semi-rigid' URM walls, since both the stiffness and damping properties are highly non-linear and because the entire system mass is not mobilized evenly, the response behaviour does not strictly follow the basic linear SDOF equation of motion. Consequently, to permit the use of time-stepping procedures by substitution of the linear SDOF damping and stiffness components with non-linear damping and stiffness properties, correlation between the non-linear 'semi-rigid' rocking and basic linear SDOF system equations of motion must be established.

The following chapter presents the development of a specialised non-linear THA program for the 'semi-rigid' rocking response of simply supported URM walls. This includes the development of algorithms by comparison of the SDOF and non-linear rocking equations of motion. Consideration to the various support conditions identified for Australian URM construction in Chapter 2 is also provided for in the non-linear THA

program. Calibration of the stiffness and damping properties and confirmation of analytical predictions by comparison with experimental results described in Chapter 6 are also presented.

In the past the use of THA for the analytical prediction of the 'semi-rigid' rocking response of simply supported URM walls has been restricted to commercially available software not designed specifically for URM wall analysis. Consequently these predictions have been limited and have not been adequately confirmed by experimental studies. The main advantage of the current THA program is that it has been designed to specifically take into account the critical non-linear stiffness and damping properties which have been calibrated using the experimental results presented in Chapter 6. The effect of various support conditions and degradation of rotation joints on the non-linear stiffness component was also examined so that analytical comparisons of various realistic situations are possible.

Although THA has limited application in design, as loading scenarios are diverse, it remains a valuable research analysis tool. In Chapter 8 the developed THA program is used to undertake an in-depth parametric study of the 'semi-rigid' rocking response of simply supported URM walls to further investigate the physical parameters which influence URM wall response. Having developed an understanding of these critical parameters a simplified analysis procedure is then proposed and its effectiveness assessed against the more comprehensive THA predictions.

7.2. Brief Description of Basic Linear SDOF System

To permit the use of time-stepping procedures for the highly non-linear 'semi-rigid' rocking response of simply supported URM walls an understanding of the development of the dynamic equation of motion for a basic linear SDOF system is first required. Later this will be expanded into the development of dynamic equations of motion for the non-linear 'semi-rigid' rocking of the simply supported URM walls having various support conditions.

The equation of motion of a dynamic system is a representation of Newton's second law. That is, the rate of change of momentum of any mass particle equals the force acting on it. Together with d'Alemberts principle that a mass develops an inertial force opposing it proportional to its acceleration the equation of motion can be expressed as an equation of dynamic equilibrium. The essential properties governing the displacement response, $\Delta(t)$, of a system subjected to an external excitation, $P(t)$, are its mass, M, stiffness and energy loss mechanism or damping. For a basic linear SDOF system each of these properties is concentrated into a single physical element as shown in Figure 7.2.1. Although the true damping characteristics of real systems are typically very complicated and difficult to define it is common to express the damping of real systems in terms of an equivalent viscous damping, which shows a similar decay rate under free vibration conditions. Therefore, in this case the elastic resistance is provided by the spring stiffness, k, and the energy loss mechanism by the velocity proportional viscous damper, c.

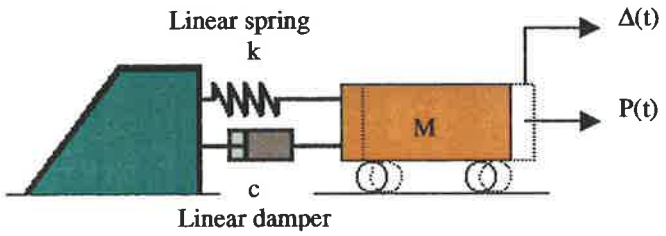

Figure 7.2.1 Basic Linear SDOF System

The motion-resisting forces are therefore the damping force being the product of the damping constant, c, and velocity, $v(t)$, the elastic force being the product of the spring stiffness, k and the response displacement, $\Delta(t)$ and the inertia force in accordance with d'Alambert's principle being the product of the system mass, M and response acceleration, $a(t)$. Equating these motion-resisting forces to the external dynamic loading provides the SDOF equation of motion as,

$$M\,a(t) + c\,v(t) + k\,\Delta(t) = P(t) \qquad (7.2.1)$$

If the loading to be considered is due to ground or support excitation this can be included by expressing the inertial force in terms of the two acceleration components. By rearranging and substituting $\omega^2 = \frac{k}{M}$ the basic linear SDOF system dynamic equation of motion becomes,

$$a(t) + \frac{c}{M} v(t) + \omega^2 \Delta(t) = -a_g(t) \qquad (7.2.2)$$

where ω = un-damped elastic angular natural frequency

By solving the dynamic equation of motion (Equation 7.2.2) it can be shown (Clough and Penzien 1993) that for an under-critically damped system the critical damping coefficient, c_c, is,

$$c_c = 2\,M\,\omega = 4\,M\,\pi f \qquad (7.2.3)$$

where f = un-damped elastic natural frequency

Therefore by definition the SDOF equivalent viscous damping, ξ_{SDOF}, is,

$$\xi_{SDOF} = c/c_c = c/4\,M\,\pi f \qquad (7.2.4)$$

and the SDOF proportional damping coefficient, c_{SDOF},

$$C_{SDOF} = 4\,M\,\pi f\,\xi_{SDOF} \qquad (7.2.5)$$

Further to this by substituting zero initial conditions in to the SDOF dynamic equation of motion solution it can be shown that for ξ_{SDOF} less than approximately 20%,,

$$\xi_{SDOF} = \frac{1}{2\pi} \ln\left(\frac{\Delta_n}{\Delta_{n+1}}\right) \qquad (7.2.6)$$

where Δ_n = peak amplitude at the n^{th} cycle

Δ_{n+1} = peak amplitude at the $(n+1)^{th}$ cycle

It should be noted that both the SDOF based equations 7.2.4 to 7.2.6 were used to determine c and ξ respectively for the experimental rocking wall in Section **6.4.6.2**. Since for the rocking wall the system mass is not mobilized evenly as is assumed above a conversion is required, as will be discussed in Section 7.3.

7.3. Negative Stiffness System Modelled as a Basic Linear SDOF System

In the following discussion a negative stiffness system is defined as a system having a bi-linear F-Δ relationship (refer Figure 7.3.1) comprising an initial infinite stiffness component followed by a negative stiffness component. On application of a force to the negative stiffness system, initially the infinite stiffness governs the behaviour until the 'threshold resistance' force, $R_e(1)$, is exceeded. Following this a negative stiffness, $K_e(1)$, takes effect so that the force resistive capacity is reduced with increased displacement. As described in Chapter 5, for 'semi-rigid' rocking the non-linear F-Δ relationship has a negative stiffness component. It is thus pertinent to first examine the modelling of a negative stiffness system as a basic linear SDOF system to determine if existing time-stepping procedures can be utilised.

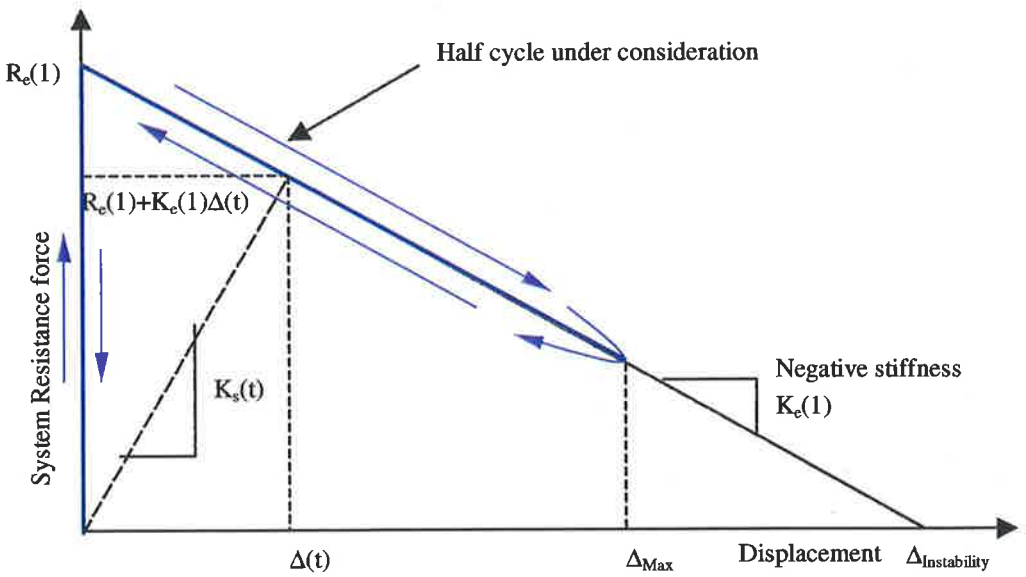

Figure 7.3.1 Negative Stiffness F-Δ Relationship

For all displacements, Δ(t), greater than zero, at any given time the instantaneous secant stiffness, $K_s(t)$, can be derived as,

$$K_s(t)=\frac{R_e(1)}{\Delta(t)}+K_e(1) \quad for\,\Delta(t)>0 \tag{7.3.1}$$

This non-linear instantaneous secant stiffness relationship is then used to derive the non-linear frequency-displacement (f-Δ) relationship for the negative stiffness system which becomes,

$$\omega=2\pi f=\sqrt{\frac{K_s(t)}{M}} \tag{7.3.2}$$

Rearranging this and substituting in the non-linear instantaneous secant stiffness relationship gives the generic response frequency,

$$f=\frac{\sqrt{\frac{R_e(1)}{\Delta(t)}+K_e(1)}}{2\pi} \quad for\,\Delta(t)>0 \tag{7.3.3}$$

Assuming that the entire system mass is evenly mobilized the complete equation of dynamic equilibrium for the negative stiffness system is derived as,

$$Ma(t)+cv(t)+R_e(1)+K_e(1)\Delta(t)=-Ma_g(t) \quad for\,\Delta(t)>0 \tag{7.3.4}$$

By rearranging and substituting the non-linear instantaneous secant stiffness relationship the equation of dynamic equilibrium for a negative stiffness system subjected to a base excitation is,

$$a(t)+\frac{c}{M}v(t)+\frac{K_s(t)}{M}\Delta(t)=-a_g(t) \quad for\,\Delta(t)>0 \tag{7.3.5}$$

Thus, by comparison of the dynamic equation of motion for a basic linear SDOF system (Equation 7.2.2) and for the negative stiffness system (Equation 7.3.5) it can be seen that

a similarity exists provided that the non-linear instantaneous secant stiffness relationship is substituted for the linear stiffness. Thus by adopting this substitution the time-stepping procedure can be applied to the negative stiffness system.

7.4. Rigid Simply Supported Object Rocking Response About Mid-height - Dynamic Equation of Motion

As a second phase in the modelling of the real 'semi-rigid' URM wall rocking response for illustrative purposes we now consider the idealised simply supported rigid rocking scenario. Here, as was the case for the negative stiffness system the idealised rigid F-Δ curve is comprised of a bi-linear F-Δ relationship having an initial infinite stiffness followed by a negative stiffness component due to P-Δ effects (refer Section 5.2.1). The defining terms of the bi-linear F-Δ curve, the 'rigid resistance threshold' force, $R_e(1)$, and negative stiffness $K_e(1)$ are functions of the wall geometry and applied overburden at the top of the simply supported object. Also influencing $R_e(1)$ and $K_e(1)$ are the support conditions as these govern the eccentricity of the vertical reactions.

For the rigid rocking of a simply supported object about it's mid-height it must also be recognised that during the dynamic response the full system mass is not mobilized evenly. Consequently, this must be considered when deriving the systems dynamic equation of motion. As was concluded from the experimental study (Chapter 6) a triangular acceleration distribution relative to the supports provides a good assessment of the rocking object's acceleration response and is thus adopted. This therefore impacts on both the dynamic stiffness and damping components of the dynamic equation of motion.

The following calculation illustrates the derivation of the dynamic equation of motion for a rigid non-loadbearing simply supported wall rocking about a mid-height crack. This is further related to the generic dynamic equation of motion for various rigid rocking objects having other support conditions relevant to Australian masonry construction.
For any rigid rocking object the static bi-linear F-Δ relationship can be generically defined as Equation 7.4.1 where R_e (1) represents the 'rigid threshold resistance' force,

$K_e(1)$ the negative stiffness component ($-R_e(1)/\Delta_{instability}$) and $F_g(t)$ the evenly distributed 'quasi-static' force. Further, the bracketed term represents the instantaneous static secant stiffness, $K_s(t)$ at the mid-height displacement $\Delta(t)$.

$$-F_g(t) = -Ma_g(t) = \left(\frac{R_e(1)}{\Delta(t)} + K_e(1)\right)\Delta(t) \qquad for\ \Delta(t) > 0 \qquad (7.4.1)$$

For a rigid non-loadbearing simply supported wall the static F-Δ relationship is derived as,

$$-F_g(t) = -Ma_g(t) = M\left(\frac{4g}{h}\left[\frac{t}{\Delta(t)} - 1\right]\right)\Delta(t) \qquad for\ \Delta(t) > 0 \qquad (7.4.2)$$

The generic defining terms of the static a-Δ relationship are therefore,

'Rigid Threshold Resistance' force $\qquad R_e(1) = \frac{4gtM}{h}$

Negative Stiffness $\qquad K_e(1) = -\frac{4gM}{h}$

Displacement at static incipient instability $\qquad \Delta_{instability} = -\frac{R_e(1)}{K_e(1)} = t$

Where the load is applied dynamically the acceleration response also comprises a triangular acceleration component, $a_m(t)$, as shown in Figure 7.4.1. The damping component of the equation of motion will be neglected at this stage but will be discussed in more detail following the derivation.

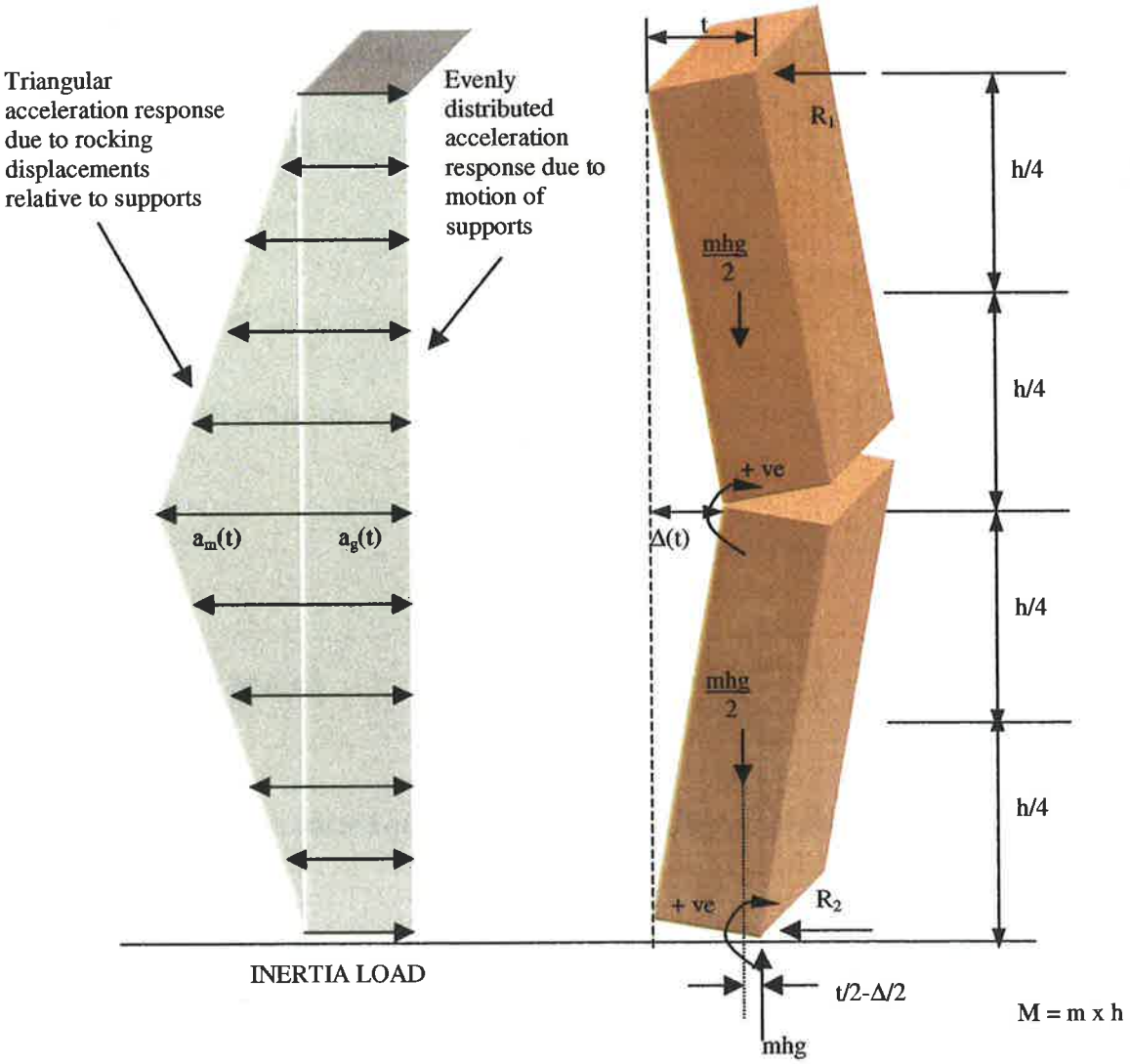

Figure 7.4.1 Non-loadbearing Simply Supported Object at Rocking at Mid-height

The top support horizontal reaction R_1 is determined by taking moments about the base vertical reaction.

$$\sum M_{R_1} \qquad R_1 = -\frac{a_g(t)\,mh}{2} - \frac{a_m(t)\,mh}{4} - \frac{m(t)\,gt}{2} + \frac{m(t)\,g\Delta(t)}{2}$$

Then horizontal equilibrium is used to determine the base support horizontal reaction as,

$$R_2 = -\frac{a_g(t)mh}{2} - \frac{a_m(t)\,mh}{4} + \frac{mgt}{2} - \frac{mg\Delta(t)}{2}$$

Now considering the dynamic equilibrium of the top free body, by taking moments about the mid-height vertical reaction, the mid-height dynamic equation of motion is,

$$a_m(t)+\frac{3}{2}\left(\frac{4g}{h}\left[\frac{t}{\Delta(t)}-1\right]\right)\Delta(t)=-\frac{3}{2}a_g(t) \qquad for\,\Delta(t)>0 \qquad (7.4.3)$$

Writing this in generic terms becomes,

$$a_m(t)+\frac{3}{2}\frac{1}{M_e}\left(\left[\frac{R_e(1)}{\Delta(t)}+K_e(1)\right]\right)\Delta(t)=-\frac{3}{2}a_g(t) \qquad for\,\Delta(t)>0 \qquad (7.4.4)$$

Including the damping component,

$$a_m(t)+\frac{c}{M_e}v(t)+\frac{3}{2}\left(\frac{4g}{h}\left[\frac{t}{\Delta(t)}-1\right]\right)\Delta(t)=-\frac{3}{2}a_g(t) \qquad for\,\Delta(t)>0 \qquad (7.4.5)$$

where the proportional damping coefficient has been measured at the effective mass, M_e, of the responding wall.

In order to continue to use the mid-height wall response as in Chapter **6** rather than the response at the position of the effective mass the damping term must be multiplied by 2/3 to compensate for the relative velocities.

The dynamic equation of motion for the rigid non-loadbearing simply supported object rocking about its mid-height therefore becomes,

$$a_m(t)+\frac{2}{3}\left(\frac{c}{M_e}\right)_{\exp}v(t)+\frac{3}{2}\left(\frac{4g}{h}\left[\frac{t}{\Delta(t)}-1\right]\right)\Delta(t)=-\frac{3}{2}a_g(t) \qquad for\,\Delta(t)>0 \qquad (7.4.6)$$

This can again be rewritten in generic terms as,

$$a_m(t)+\frac{2}{3}\left(\frac{c}{M_e}\right)_{exp} v(t)+\frac{3}{2}\frac{1}{M_e}\left(\frac{R_e(1)}{\Delta(t)}+K_e(1)\right)\Delta(t)=-\frac{3}{2}a_g(t) \qquad for\ \Delta(t)>0 \qquad (7.4.7)$$

and by substituting the instantaneous static secant stiffness, $K_s(t)$, as,

$$a_m(t)+\frac{2}{3}\left(\frac{c}{M_e}\right)_{exp} v(t)+\frac{3}{2}\frac{K_s(t)}{M_e}\Delta(t)=-\frac{3}{2}a_g(t) \qquad for\ \Delta(t)>0 \qquad (7.4.8)$$

Comparing the basic linear SDOF equation of motion (Equation 7.2.2) previously developed for the system shown in Figure 7.2.1 and the generic dynamic equation of motion for rigid rocking objects (Equation 7.4.6) it is evident that the following substitutions can be made to permit the use of time stepping procedures and the mid-height response of the wall.

1. Substitute the linear SDOF proportional damping with 2/3 of the experimentally derived values
2. Substitute the linear stiffness component with the dynamic non-linear instantaneous secant stiffness, $K_{ds}(t)$, represented by 3/2 times the static instantaneous secant stiffness. This is achieved by applying a factor of 3/2 to the static F-Δ relationship.

$$K_{ds}(t)=\frac{3}{2}K_s(t)$$

3. Apply a conversion factor of 3/2 to the applied ground acceleration.

Also from Equation 7.4.7 the theoretical rigid mid-height f-Δ relationship without damping can be derived in accordance with $\omega = 2\pi f = \sqrt{\frac{K_{ds}(t)}{M_e}}$ in generic terms as,

$$f=\frac{\sqrt{\frac{3}{2}\left(\frac{R_e(1)}{\Delta(t)}+K_e(1)\right)}}{2\pi\sqrt{M_e}} \qquad for\ \Delta(t)>0 \qquad (7.4.9)$$

Since each set of support conditions alters the F-Δ relationship by changing the value of $R_e(1)$ and $K_e(1)$ this also influences the dynamic equation of motion. The generic defining terms $R_e(1)$ and $K_e(1)$ are shown in Table 5.2.1 and can be substituted directly into the above equations.

7.5. Semi-rigid URM Loadbearing Wall Dynamic Equation of Motion

As discussed in Chapter 5, the real 'semi-rigid' non-linear F-Δ relationship of a face loaded URM wall results from the complicated interaction of gravity restoring moments, the movement of vertical reactions with increasing mid-height displacement and P-Δ overturning moments. The wall properties that therefore dictate the shape of the curve are wall geometry, support conditions, overburden stress, material modulus and importantly the condition of the mortar joint rotation points. As described in Section 6.4.5 theories have been postulated by previous researchers to define this complex behaviour however these were not found to correlate well with the experimental results as based on simple and often unrealistic support conditions. Consequently a more empirically based method was adopted in this study.

From the experimental study presented in Chapter 6 the real 'semi-rigid' non-linear F-Δ relationship was found to approach that of the idealised rigid bi-linear relationship at large mid-height displacements. This was due to the vertical reactions being pushed nearly to the extreme compressive face of the wall. As the applied overburden was small the influence of the finite compressive stress blocks at vertical reactions was not significant. Since the bi-linear F-Δ relationship is simply a function of geometry, overburden and support conditions, this was used as a basis for development of an approximation of the real non-linear F-Δ relationship.

A parametric study was undertaken to determine which of the non-linear F-Δ relationship properties governed the response behaviour. It was found that the initial stiffness, K_{in}, and 'semi-rigid threshold resistance' force plateau, $R_{es}(1)$, were critical. Thus to model the non-linear F-Δ relationship at smaller mid-height displacements a tri-linear F-Δ

approximation was selected (refer Figure 7.5.1). Since the rigid bi-linear relationship is set the tri-linear approximation is defined by the displacements ratios $\frac{\Delta(1)}{\Delta_{instability}}$ and $\frac{\Delta(2)}{\Delta_{instability}}$, which govern K_{in} and $R_{es}(1)$ respectively. The value of $\frac{\Delta(1)}{\Delta_{instability}}$ and $\frac{\Delta(2)}{\Delta_{instability}}$ are therefore related to material properties, predominantly being the less stiff mortar, and the state of degradation of the rotating mortar joints.

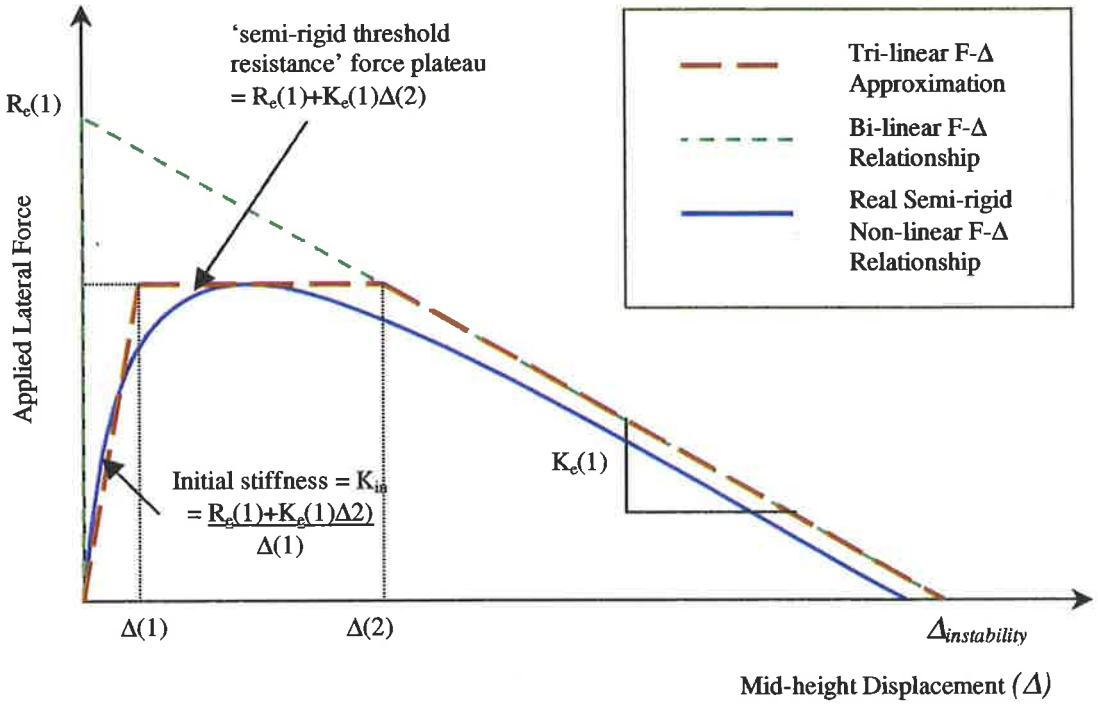

Figure 7.5.1 Tri-linear 'Semi-rigid' Non-linear F-Δ Relationship Approximation

Table 7.5.1 presents the empirically derived defining displacements of the tri-linear approximation from the experimental static push tests presented in Chapter 6. Here the support conditions considered included NLBSSCL and LBSSLL (refer Table 5.2.1), so that $\Delta_{instability}$ was taken as the thickness of the wall. Since the materials used did not change, an increase in degradation of the rotating mortar joints was related to an increase

in both displacement ratios $\frac{\Delta(1)}{\Delta_{instability}}$ and $\frac{\Delta(2)}{\Delta_{instability}}$. This represented a decrease in K_{in} and $R_{es}(1)$ and a corresponding flattening of the 'semi-rigid' non-linear F-Δ relationship (refer Figure 7.5.2). The resulting decrease in the overall response frequencies also led to a decrease in the instantaneous dynamic secant stiffness.

Table 7.5.1 Defining Displacements of the Tri-linear F-Δ Approximation

State of Rotation Joint Degradation	$\frac{\Delta(1)}{\Delta_{instability}}$	$\frac{\Delta(2)}{\Delta_{instability}}$
New	6%	28%
Moderate	13%	40%
Severe	20%	50%

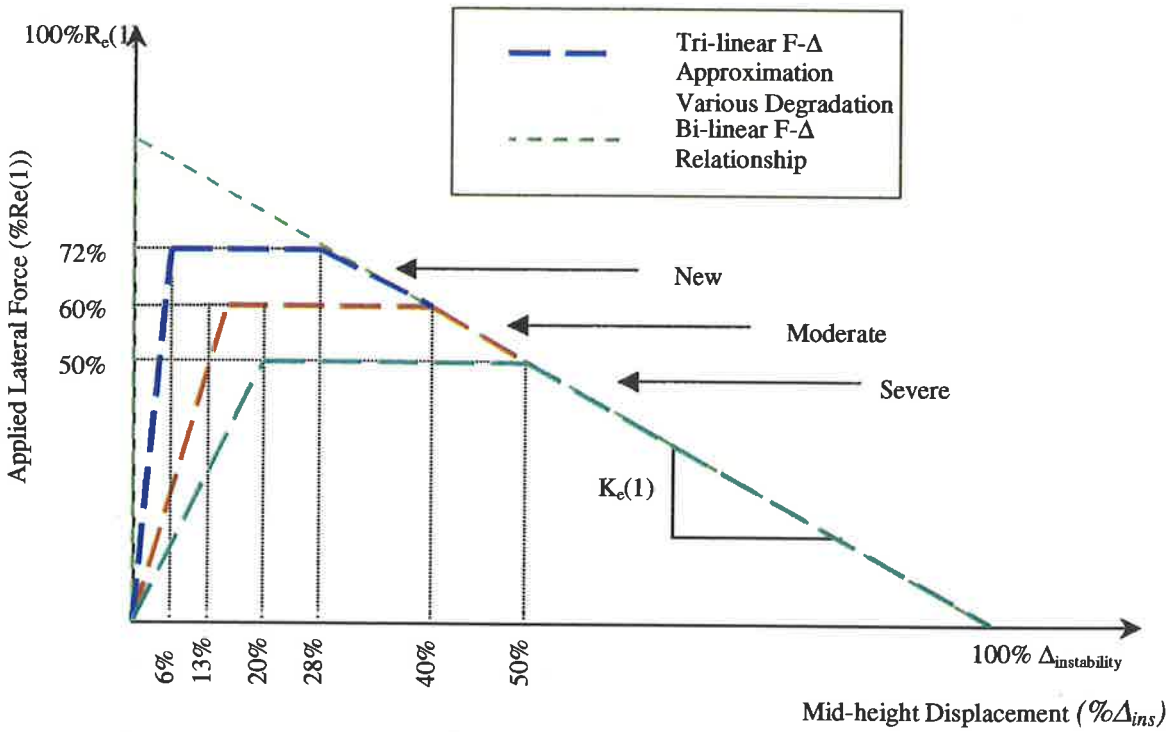

Figure 7.5.2 Tri-linear F-Δ Approximation for Various Wall Degradation

After adopting the tri-linear 'semi-rigid' F-Δ relationship approximation, the rocking response was governed by three discrete equations of motion. At any given time the

governing dynamic equation of motion is dependent on the instantaneous displacement. In generic terms the three governing equations of motion are,

$$a_m(t)+\frac{2}{3}\left(\frac{c}{M_e}\right)_{\exp} v(t)+\frac{3}{2}\frac{1}{M_e}\left(\frac{R_e(1)+K_e(1)\Delta(2)}{\Delta(1)}\right)\Delta(t)=-\frac{3}{2}a_g(t) \qquad for\ 0<\Delta(t)<\Delta(1) \tag{7.5.1}$$

$$a_m(t)+\frac{2}{3}\left(\frac{c}{M_e}\right)_{\exp} v(t)+\frac{3}{2}\frac{1}{M_e}\left(\frac{R_e(1)+K_e(1)\Delta(2)}{\Delta(t)}\right)\Delta(t)=-\frac{3}{2}a_g(t) \qquad for\ \Delta(1)<\Delta(t)<\Delta(2) \tag{7.5.2}$$

$$a_m(t)+\frac{2}{3}\left(\frac{c}{M_e}\right)_{\exp} v(t)+\frac{3}{2}\frac{1}{M_e}\left(\frac{R_e(1)+K_e(1)\Delta(t)}{\Delta(t)}\right)\Delta(t)=-\frac{3}{2}a_g(t) \qquad for\ \Delta(2)<\Delta(t)<\Delta_{instability} \tag{7.5.3}$$

As each stiffness term is represented by the instantaneous dynamic secant stiffness the overall generic dynamic equation of motion again takes the form of Equation 7.4.8. Thus, by comparison with the basic linear SDOF equation of motion (Equation 7.2.2) it is observed that the required substitutions to allow the use of previously developed time-stepping procedures highlighted in Section 7.4 are still applicable. This is provided that the governing dynamic equation of motion at any time is dependent on the instantaneous displacement.

By adopting the tri-linear F-Δ relationship approximation for the 'semi-rigid' rocking response of URM walls allows an estimate of the frequency-displacement response to be made. Since the approximate response is governed by the three dynamic equations of motion, which are dependent on the instantaneous displacement, the frequency response is also dependent on the instantaneous displacement. The relevant instantaneous dynamic secant stiffness can therefore be used to determine the frequency-displacement relationship in accordance with $\omega=2\pi f=\sqrt{\frac{K_{ds}(t)}{M_e}}$. Thus from Equation 7.5.1 to

7.5.3 the generic 'semi-rigid' rocking frequency response can be approximated when neglecting damping as,

$$f = \frac{\sqrt{\frac{3}{2}\left(\frac{R_e(1) + K_e(1)\Delta(2)}{\Delta(1)M_e}\right)}}{2\pi} \qquad for\, 0 < \Delta(t) < \Delta(1) \qquad (7.5.4)$$

$$f = \frac{\sqrt{\frac{3}{2}\left(\frac{R_e(1) + K_e(1)\Delta(2)}{\Delta(t)M_e}\right)}}{2\pi} \qquad for\, \Delta(1) < \Delta(t) < \Delta(2) \qquad (7.5.5)$$

$$f = \frac{\sqrt{\frac{3}{2}\left(\frac{R_e(1) + K_e(1)\Delta(t)}{\Delta(t)M_e}\right)}}{2\pi} \qquad for\, \Delta(2) < \Delta(t) < \Delta_{instability} \qquad (7.5.6)$$

Figure 7.5.3 to Figure 7.5.6 present a comparison of the analytical best fit f-Δ relationship without damping, each derived from Equation 7.5.4, Equation 7.5.5 and Equation 7.5.6 with the experimentally derived f-Δ relationships as presented in Section 6.4.6.1.

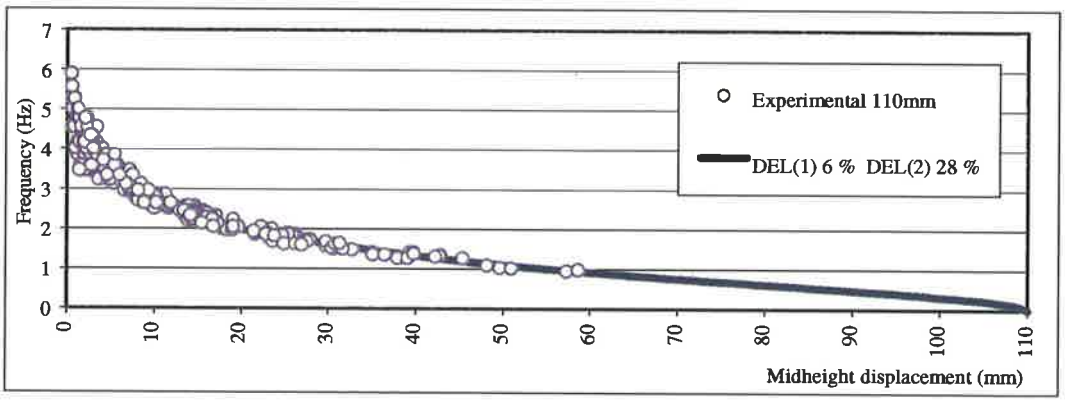

Figure 7.5.3 Analytical vs Experimental F-Δ– 110mm, No Overburden

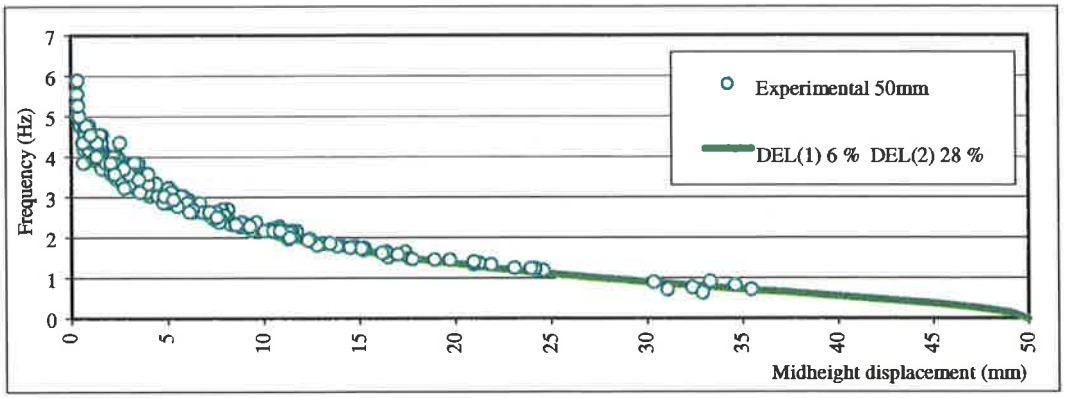

Figure 7.5.4 Analytical vs Experimental F-Δ– 50mm, No Overburden

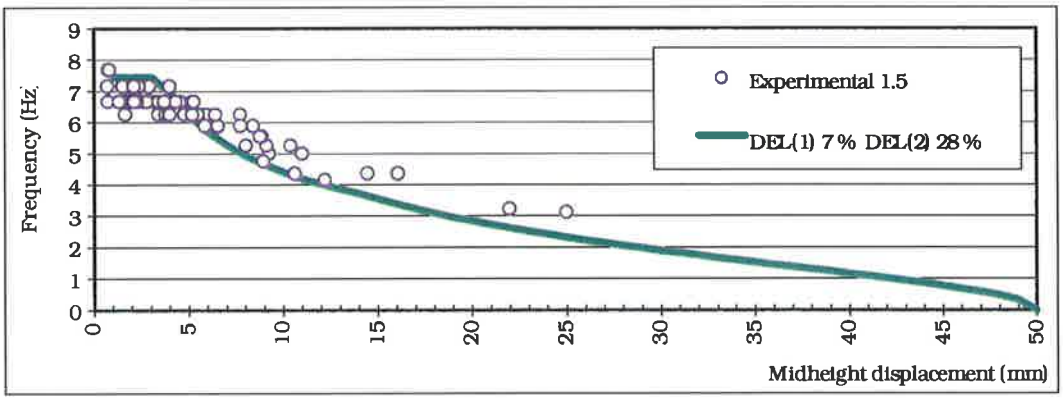

Figure 7.5.5 Analytical vs Experimental F-Δ– 50mm, 0.07MPa Overburden

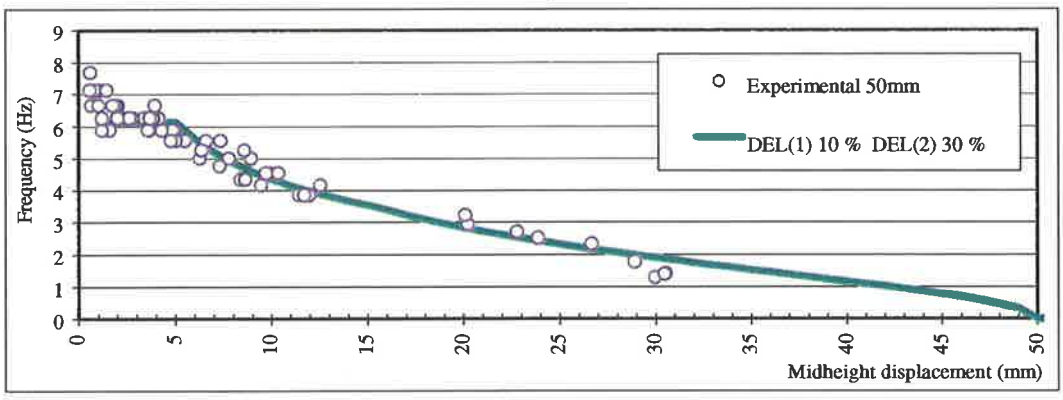

Figure 7.5.6 Analytical vs Experimental F-Δ– 50mm, 0.15MPa Overburden

7.6. Modelling of Non-Linear Damping

Although the F-Δ relationship is the most critical factor for modeling of the rocking frequency response, damping also has an influence on the *f*-Δ relationship. Due to the complex physical nature of damping it is usually represented in a highly idealized fashion as an equivalent viscous (velocity proportional) damping force with a similar decay rate under free vibration conditions to that of the real system being modelled. Thus, the proportional damping coefficient used in formulating the equation of motion (Equation 7.2.2) is selected so that the vibration energy dissipated is equivalent to the energy dissipated in all of the damping mechanisms of the rocking system. For an URM wall these mechanisms would include elastic, friction, impact and joint rotation energy losses. Although not strictly an accurate representation of the system behaviour any disadvantage of using this approximate method is far outweighed by the simplification achieved in applying the equivalent viscous damper.

Commonly the damping in most structures can adequately be modelled by using Rayleigh damping.

Rayleigh damping is a linear combination of both mass and stiffness proportional damping so that,

$$C = \alpha_o M + K\alpha_1 = \alpha_o M + \alpha_1(M\omega^2) = M(\alpha_o + \alpha_1[2\pi f]^2) \qquad (7.6.1)$$

$$\Rightarrow C/M = \alpha_o + \alpha_1[2\pi f]^2$$

By substituting $C/M = 4\pi f\,\xi$ the theoretical Rayleigh equivalent viscous damping becomes,

$$\xi = \frac{\alpha_o}{4\pi f} + \alpha_1 \pi f \qquad (7.6.2)$$

By comparison with experimental results presented in Section 6.4.6.3 and careful selection of α_o, and α_1, Rayleigh damping was found to best represent the physical nature of the real non-linear system damping mechanisms. Figure 7.6.1 presents a comparison

of the experimental equivalent viscous damping versus frequency with that calculated using a theoretical Rayleigh damping (Equation 7.6.2) for a 50 mm thick wall specimen having no applied overburden.

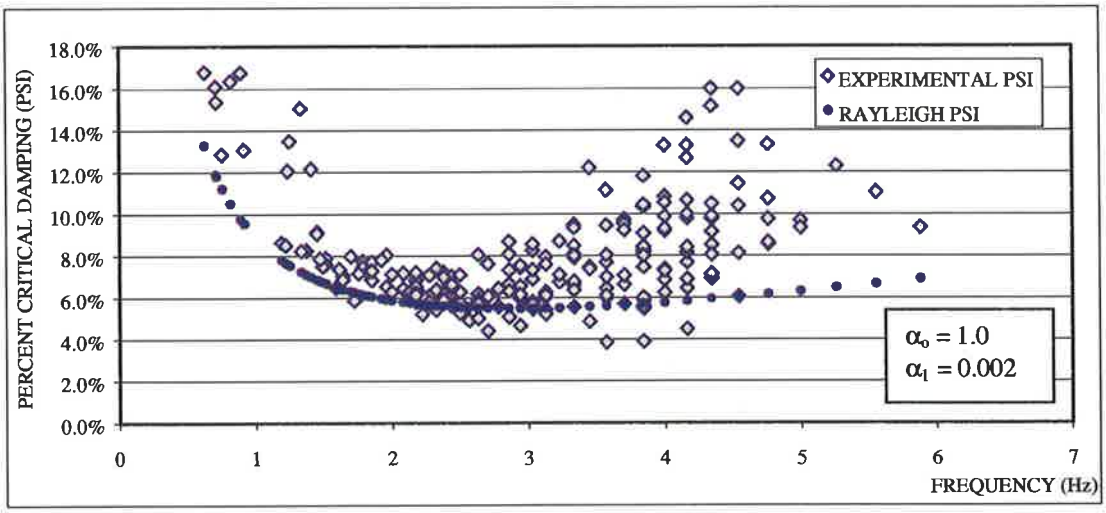

Figure 7.6.1 Experimental ξ vs Rayleigh ξ – 50mm Wall, No Applied Overburden

Although the mass and stiffness proportional damping coefficients were found to be higher for both the 50 mm thick walls with overburden and the 110mm thick walls than the coefficients shown in Figure 7.6.1 these provided a reasonable lower bound estimate of the equivalent viscous damping. Thus to be conservative these coefficients were adopted for the parametric study presented in Chapter 8.

If system damping were truly of the linear viscous form then any set of m consecutive cycles would give the same viscous damping ratio. For the case for rocking of URM walls m consecutive cycles in a high amplitude response section will yield a different damping ratio than that of m consecutive cycles in a lower amplitude section of free response. The equivalent viscous damping ratio is therefore non-linear amplitude or frequency dependent (refer Figure 7.6.1). Thus, we are unable to assume a linear viscous damping within the THA so that either an average proportional damping coefficient or an iterative approach must be invoked into the THA.

While adopting an average proportional damping coefficient method for the entire response is the simplest and least intensive method the main disadvantage is that it requires an average response frequency, f, to be estimated prior to the THA. From this an estimate of c/M is made from Equation 7.6.1. The consequence of this is that the analysis outcome can be subjective as it is related to the assumed average response frequency.

For the iterative approach an initial estimate of the proportional damping is made at the commencement of each half cycle of the response. The instantaneous frequency is then determined at the completion of each half cycle and the resulting proportional damping calculated. This is then tested against the estimated proportional damping at the beginning of the cycle. If the estimate and resulting proportional damping coefficient match then the next half cycle is considered. If not the THA returns to the beginning of the half cycle under consideration and the initial conditions are reset. Another estimate of the proportional damping coefficient is made and the iterative process continues. This iterative process is shown in Figure 7.6.2. The only disadvantage of the iterative method is that the computing time is increased, however, this was not found to be significant for the SDOF system. Comparison of analytical and experimentally response showed that the iterative procedure was the most effective and least sensitive to initial assumptions.

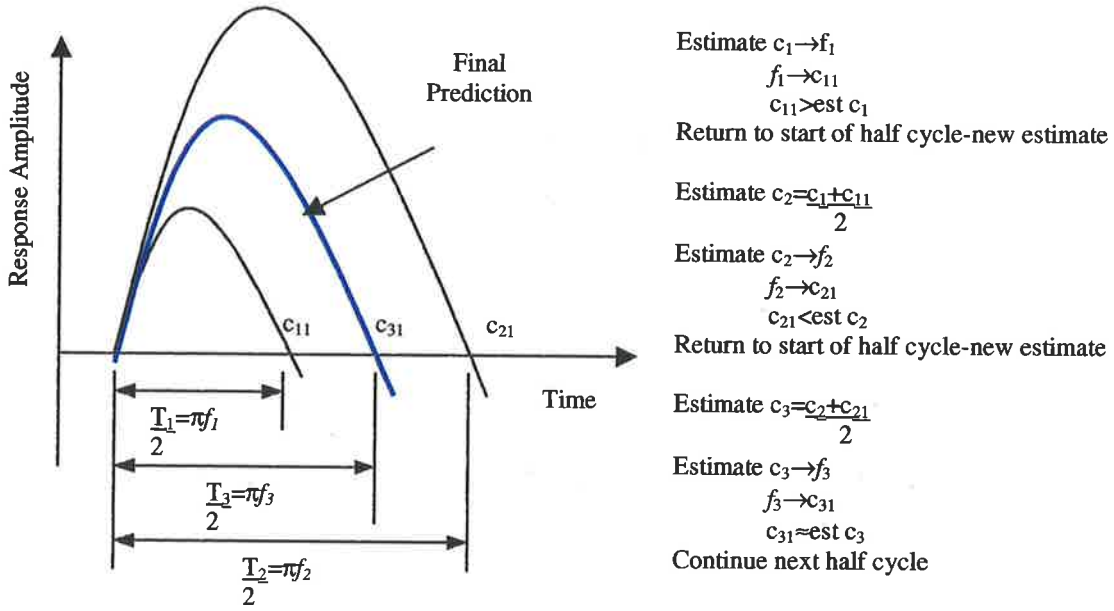

Figure 7.6.2 Iterative Damping

7.7. Event Based Time-Stepping Analysis

Since at any time the dynamic response is dependent on the instantaneous displacement an event based time-stepping analysis was required to distinguish between the governing dynamic equation of motion. As part of the time-stepping procedure the dynamic response was considered by conversion of the static non-linear F-Δ curve into a 'pseudo static' F-Δ relationship. This procedure was based on the constant acceleration assumption between time steps and takes into account the proportional damping. By adopting the tri-linear F-Δ model, the 'pseudo static' F-Δ relationship was made up of the three 'pseudo static' stiffness' being kts1, ktsp and kts2 (refer Figure 7.7.1). To permit the use of the time-stepping procedure as described in Section 7.5 the conversion factor of 3/2 was applied to both the input ground acceleration, $a_g(t)$ and the three 'pseudo static' stiffness'.

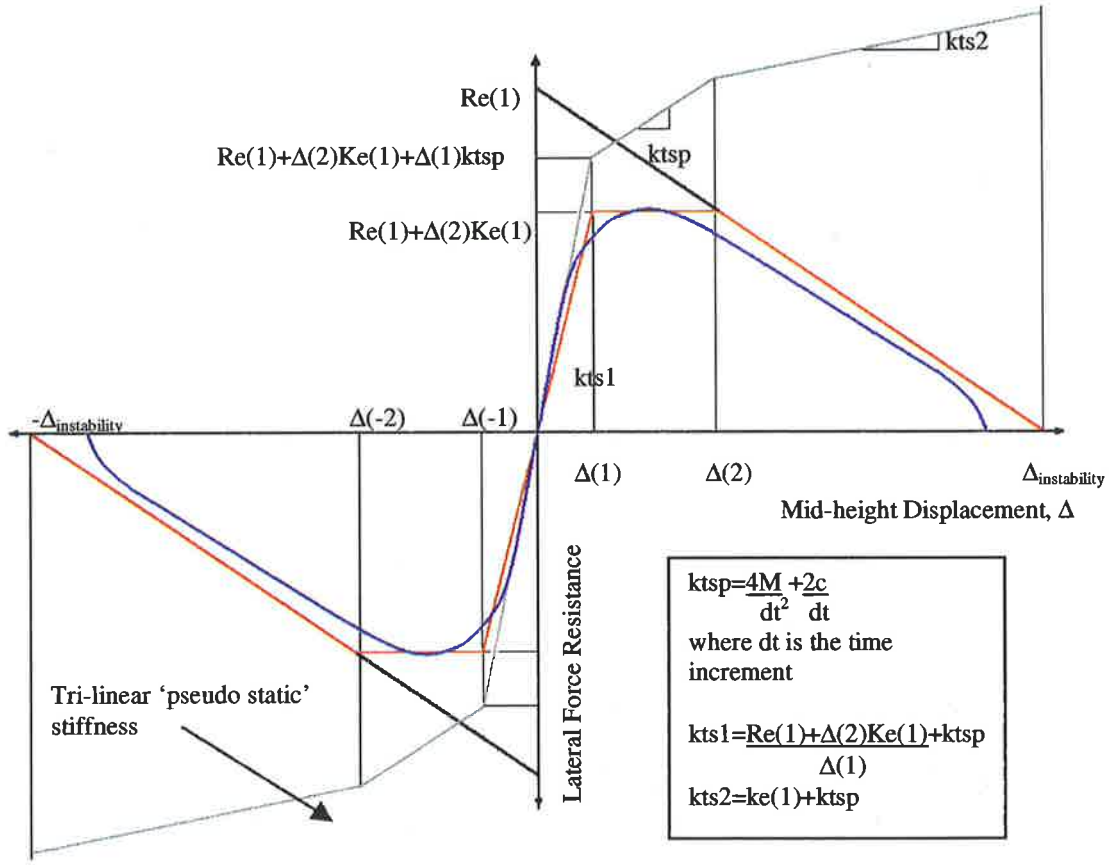

Figure 7.7.1 'Pseudo Static' F-Δ relationship

The time-stepping procedure is then applied to the 'pseudo static' system. The first step is to convert the input excitation, $3/2(a_g(t))$, to an incremental 'pseudo static' force (dps) which takes into account the previous incremental acceleration. Once this has been determined it is used to calculate the incremental 'pseudo static' force displacement using the respective 'pseudo static' stiffness. If $\Delta(\pm1)$ or $\Delta(\pm2)$ is reached within the time increment this is recognised as an event and the dynamic equation of motion and the 'pseudo static' stiffness is updated. Any remaining 'pseudo static' resistance force is then used to determine the remaining incremental displacement according to the new 'pseudo static' stiffness so that the displacement at the completion of the time increment is determined. This process is continued until the incremental 'pseudo static' force and thus the remaining system energy is reduced to zero. Alternatively, if the instability displacement, $\pm\Delta_{instability}$, has been exceeded this indicates failure and the THA process is terminated.

The Fortran 77 program developed to run the non-linear rocking URM wall THA is presented in Appendix (G).

7.8. Comparison of Experimental and Analytical Results

Confirmation of the non-linear time history analysis (THA) software developed for the 'semi-rigid' rocking response of URM walls has been conducted by comparison of analytical results with both pulse and earthquake excitation shaking table test results (refer Chapter 6). Figure 7.8.1 presents an indicative comparison of an analytically and experimentally derived response for a 110mm thick, 1.5m tall wall with no overburden having been subjected to a 1Hz, 37mm amplitude pulse excitation. Further details of the parameters used within the THA are presented in Appendix (H). Figure 7.8.1 (a) provides a comparison of the experimental mid-height displacement, MWD, relative to the shaking table compared with the THA, (u). Figure 7.8.1 (b) provides a comparison of the experimental mid-height acceleration, MWA, compared with the absolute mid-height acceleration derived through THA, (at). Figure 7.8.1 (c) provides a comparison of experimental and analytical hysteretic behaviour.

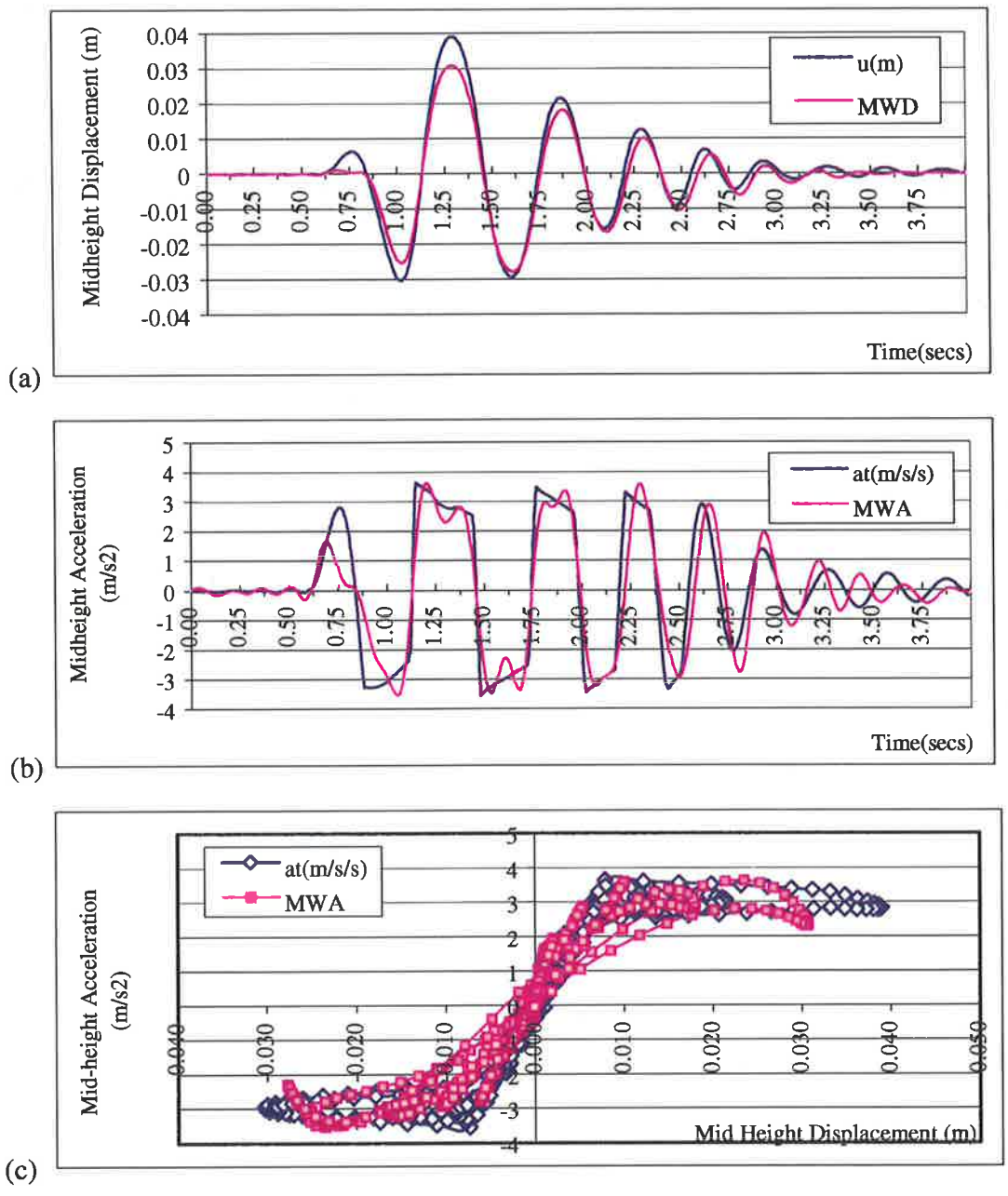

Figure 7.8.1 Comparison of Analytical and Experimental Pulse Test Results

Figure 7.8.2 presents a comparison of the THA and experimental peak mid-height displacements for a non-loadbearing simply supported 110mm thick, 1.5m tall URM wall. For the THA the wall condition was assumed to be moderately degraded. Here it is observed that the peak displacement response for the tested pulse frequencies and amplitudes is well represented by the THA. It is observed that the maximum

displacement amplification occurs for pulse frequencies of around 1Hz to 2Hz. Thus the effective resonant frequency, f_{eff}, for the 110mm thick, 1.5m tall simply supported walls with no applied overburden is also approximately 1Hz.

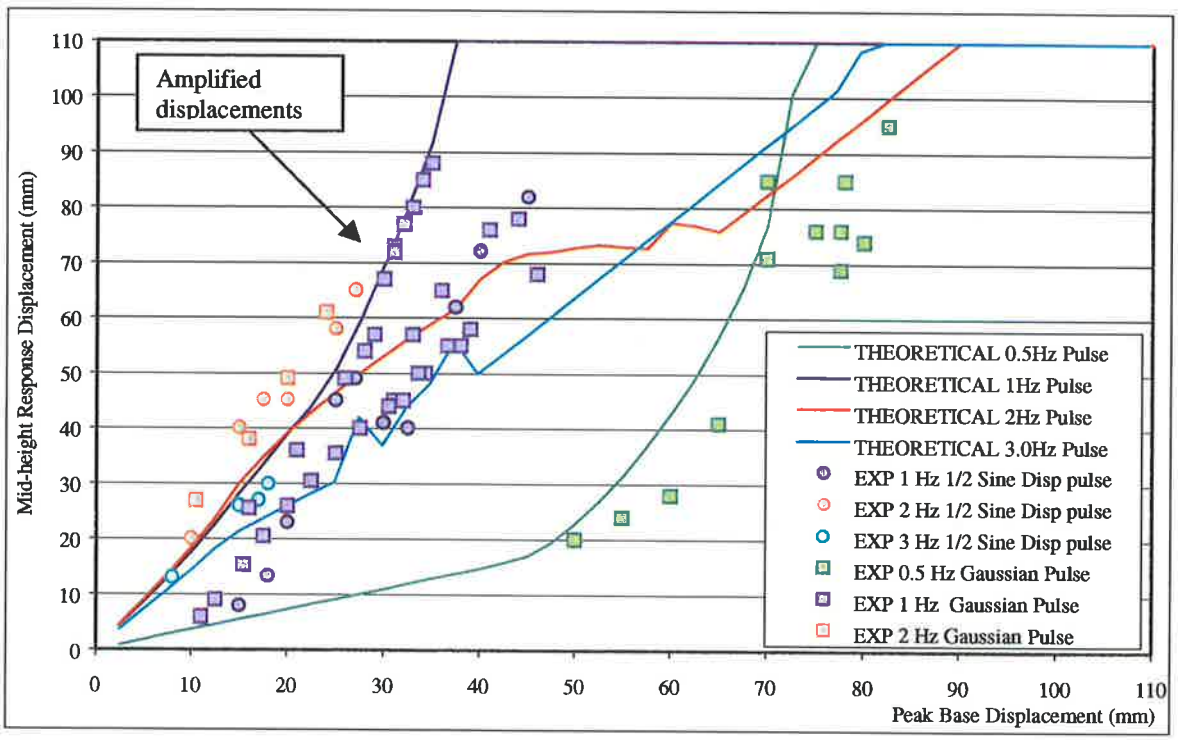

Figure 7.8.2 THA and Experimental Peak Pulse Mid-height Disp. Response

Figure 7.8.3 presents an indicative comparison of an analytically and experimentally derived response for a 110mm thick, 1.5m tall wall with no overburden having been subjected to an earthquake excitation representing 80% of the Pacoima Dam earthquake (refer Table 6.4.9). Further details of the parameters used within the THA are presented in Appendix (H). Figure 7.8.3 (a), (b) and (c) provide comparisons of mid-height displacement, acceleration and hysteretic behaviour respectively.

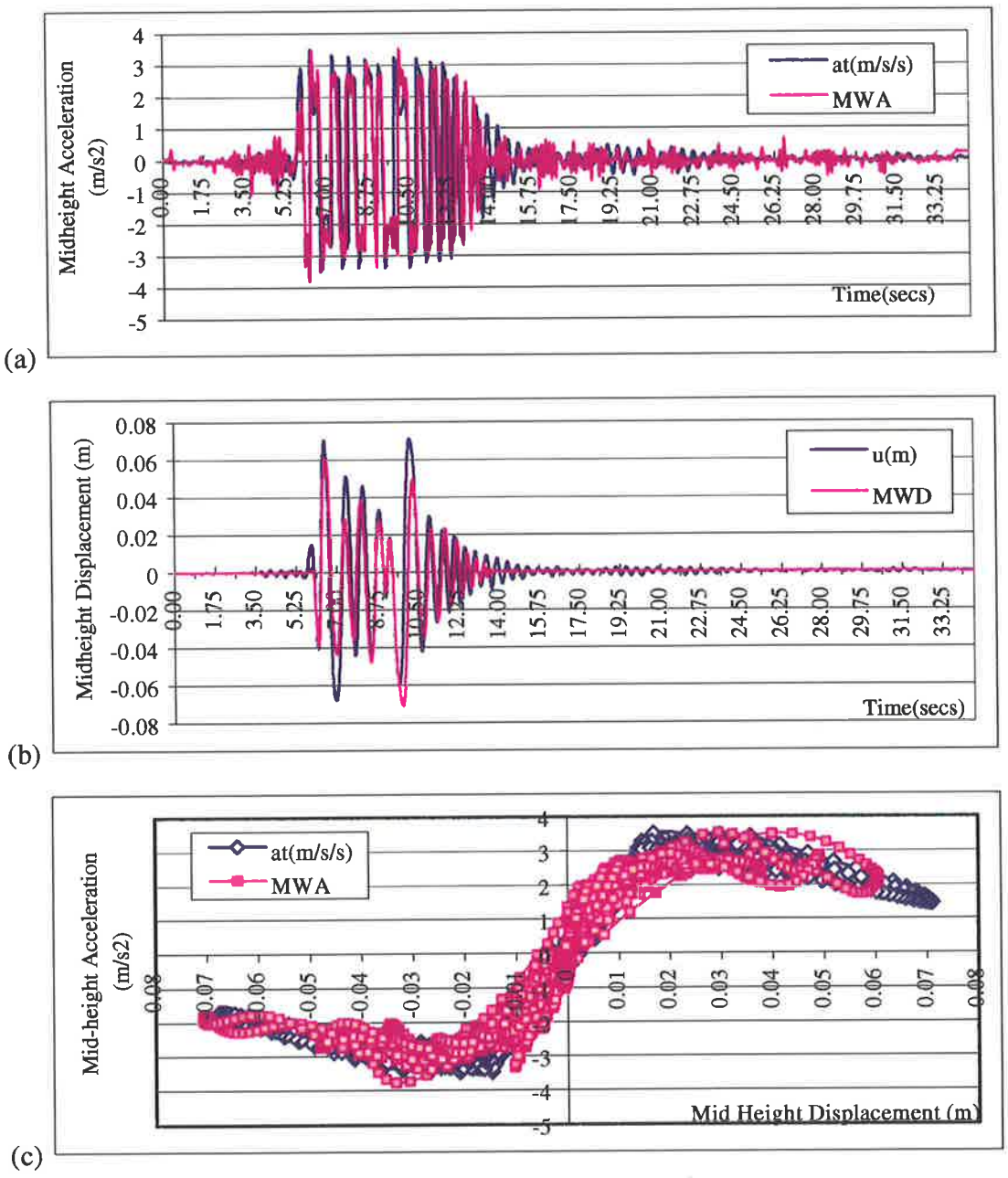

Figure 7.8.3 Comparison of Analytical and Experimental Earthquake Test Results

A representative cross section of analytical and experimental, pulse and earthquake results is presented in Appendix (H). This shows that the THA is capable of accurately predicting both the forced and free vibration rocking response provided that the non-linear (F-Δ) and damping properties are adequately represented in the analytical model.

8. LINEARISED DISPLACEMENT-BASED (DB) ANALYSIS

8.1. Linearised DB Analysis Methodology

The displacement-based (DB) analysis methodology provides a rational means for determining seismic design actions as an alternative to the more traditional 'quasi-static' force-based approach. In the DB procedure the dynamic lateral capacity of a structure is determined on the basis of a comparison of a pre-determined failure displacement with the displacement demand imposed on the structure by a seismic event.

To simplify the DB analysis procedure for highly non-linear systems the 'substitute structure' methodology, proposed by Shibata and Sozen (1976), is often adopted. This involves the substitution of the real structure's stiffness and damping properties with the linear properties of a characteristic elastic SDOF oscillator. Here the characterising linear properties are selected so that the linear and real non-linear systems are likely to reach the failure displacement under the same applied excitation. The elastic system's response to failure, as can be determined from the elastic response spectrum, is therefore representative of the displacement demand on the real structure.

For elastic perfectly plastic systems (refer Figure 8.1.1) the bi-linear F-Δ relationship to the failure displacement is characterised by the elastic stiffness related to the real structure's secant stiffness at the in-elastic failure displacement (Priestly 1996:1997, Judi et al 1998, Edwards et al 1999). Thus, the characterising SDOF oscillator stiffness component is approximated by the lowest secant stiffness analogous with the real structure's dynamic response and is associated with the lowest feasible response frequency. Using this characteristic 'substitute structure' property for elastic perfectly plastic systems and an appropriate level of equivalent viscous damping during the non-

linear response, the linearised DB analysis has been found to provide a reasonable prediction of these system's dynamic lateral capacity.

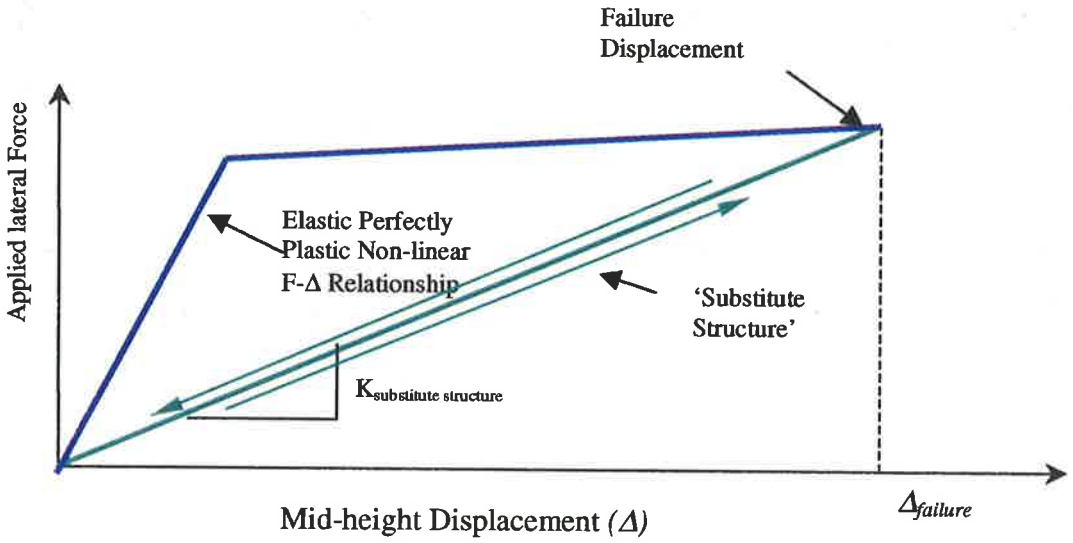

Figure 8.1.1 Linearised DB Analysis for Elastic Perfectly Plastic System

Unlike the more comprehensive non-linear time history analysis (THA), the linearised DB procedure does not provide an accurate representation of the complete dynamic response but rather an indication of the excitation (load) required to reach the pre-defined failure displacement. To illustrate, during the elastic response phase the tangential stiffness is underestimated however during the in-elastic response phase the tangential stiffness is overestimated. As a consequence of this a 'period lag' may develop between the 'substitute structure' and the real system displacement response so that at the critical response cycle the DB analysis initial conditions may not represent the real initial conditions.

The DB analysis effectiveness is dependent on the probability that the 'substitute structure' and real system will reach the pre-determined failure displacement when subjected to the same excitation. It is therefore evident that for the DB analysis to provide a reasonable estimate of the excitation required to cause the structure to reach the failure displacement an integral part of the procedure is the selection of the characteristic

SDOF oscillator or 'substitute structure' linear stiffness. To confirm that the selected 'substitute structure' properties represent the real system at the critical displacement for any linearised DB analysis procedure an extensive comparison of the DB prediction with experimental and THA results was required.

The following chapter presents a proposed linearised DB analysis procedure for the ultimate limit state analysis of simply supported URM walls including a procedure for the definition of the characterising linear SDOF oscillator stiffness. The displacement capacity and damping properties of the simply supported walls are discussed in conjunction with the implication on the modeling of the real structure as a characteristic SDOF oscillator. An extensive comparison of the linearised DB analysis predictions of dynamic lateral capacity with THA and experimental results is then presented to confirm the procedure's suitability.

Similar to the above, a comparison of THA predictions with the existing 'quasi-static' rigid body and 'semi-rigid resistance threshold' force prediction of lateral capacity is also conducted. This highlights the limitations of not considering 'dynamic stability' concepts for the dynamic analysis of simply supported URM walls. Here the 'quasi-static' analysis results are shown to often fall outside of the limiting tolerance assumed for the DB analysis.

8.2. Proposed Linearised DB Analysis

In accordance with the DB procedure, the 'substitute structure' displacement demand relative to the top and bottom wall supports is determined from the response spectral displacement (Δ_{RSD}), as obtained from the corresponding elastic displacement response spectrum and characteristic 'substitute structure' frequency and damping. As is shown by the typical relative elastic displacement response spectrum in Figure 8.2.1, for flexible (low natural frequency) elastic systems the maximum relative displacement imposed by an excitation is equal to the peak ground displacement (PGD). For elastic systems with natural frequencies near to the excitations dominant frequency, displacement

amplification and resonant effects increase the Δ_{RSD} to a maximum greater than the PGD. The displacement amplification is thus defined as Δ_{RSD}/PGD. For elastic systems with natural frequencies greater than the excitation's dominant frequency the Δ_{RSD} and displacement amplification is reduced. For rigid elastic systems with large natural frequencies (i.e. infinite stiffness), Δ_{RSD} approaches zero.

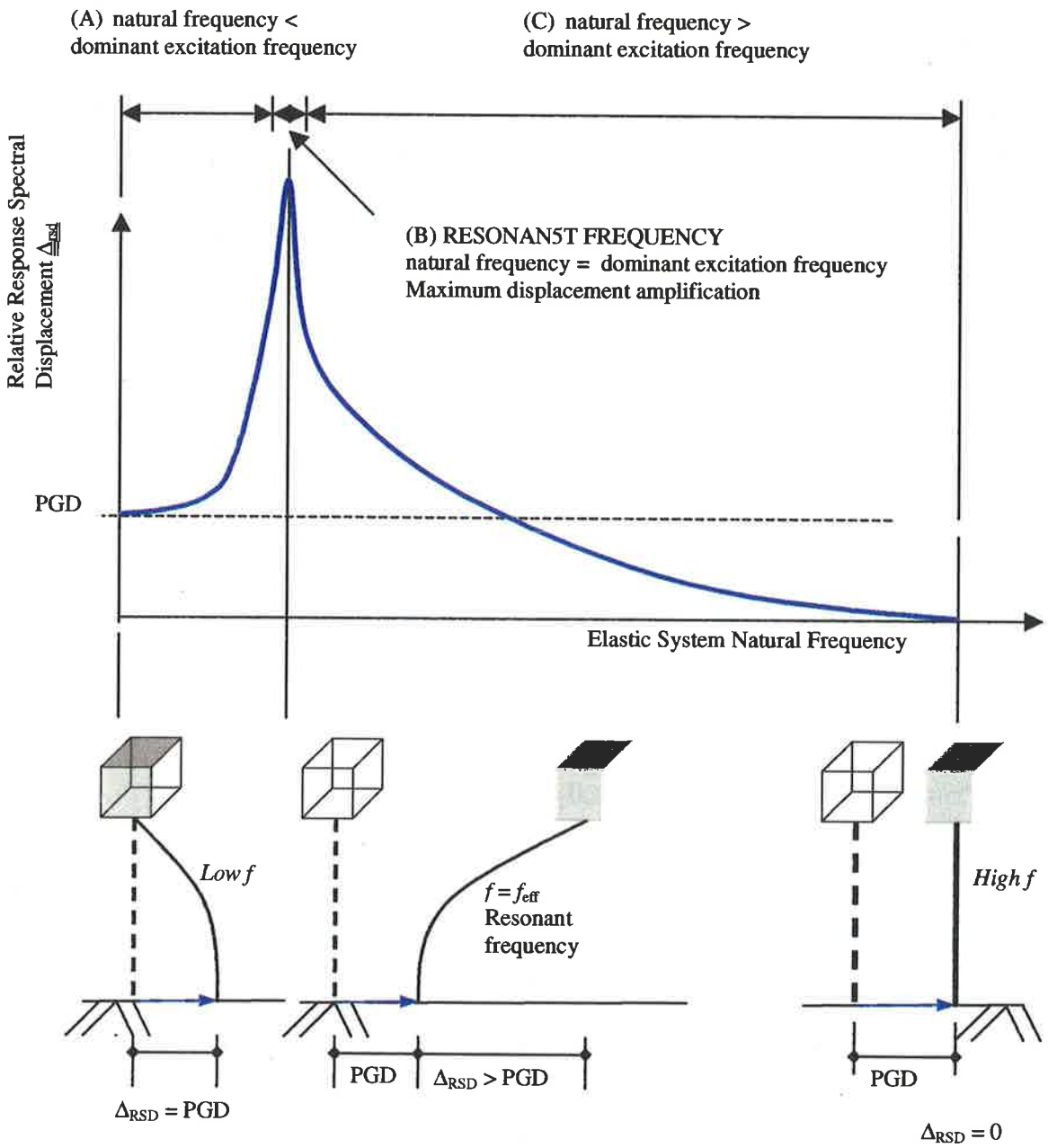

Figure 8.2.1 Typical Elastic Displacement Response Spectrum

This indicates that for ground motions where the dominant frequencies are much greater than the elastic system's natural frequency the system will be safe from failure provided that the PGD does not exceed $\Delta_{instability}$. On the other hand should the dominant ground motion frequency be near that of the natural resonant frequency, the Δ_{RSD} may be significantly amplified above that of the PGD depending on damping. In this case failure may occur under excitations with much lower PGD.

THA and shaking table tests have shown the maximum relative mid-height displacement amplification to be 1.5 to 3.3. This corresponds to a dynamic amplification of 1 to 2.2 at the wall's effective mass, which is the point located at 2/3 of the free body height from the point where the wall is stationary. This suggests that during ground motion with dominant frequencies in the vicinity of the walls resonant frequency the wall will be safe from overturning provided that the PGD does not exceed 0.3 of the wall thickness (0.66/2.2). For design, safety factors would also need to be applied.

8.2.1. Derivation of Characteristic SDOF 'Substitute Structure' Stiffness

Provided that the selected SDOF 'substitute structure' stiffness, K_{eff}, (refer Figure 8.2.2) linearly characterises the real structure for response at the incipient instability displacement the real structure's displacement demand can be determined in accordance with the relative elastic displacement response spectrum. The selection of K_{eff} must therefore be made so that it is probable that the 'substitute structure' and rocking wall system will reach their respective displacement capacity under the same excitation.

Unlike the elastic perfectly plastic system presented in Section 8.1, where the lowest secant stiffness analogous with the real structures dynamic response is used to characterise the non-linear, this is not appropriate for rocking objects as at the failure or instability displacement, $\Delta_{instability}$, the secant stiffness is zero. It was therefore necessary to develop an alternative procedure for deriving the characterising linear stiffness for rocking simply supported URM walls.

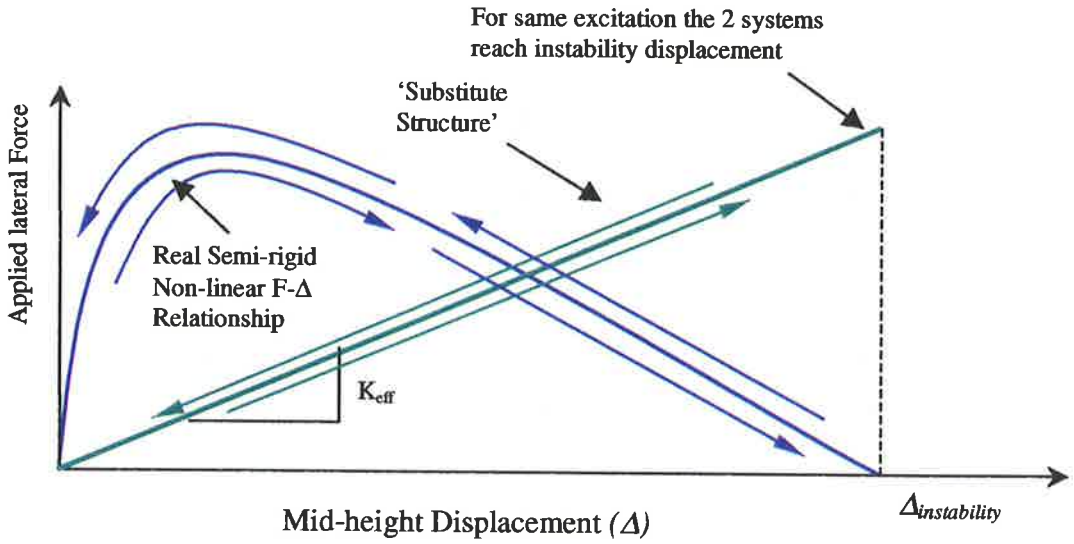

Figure 8.2.2 Linearised DB Analysis Characteristic Stiffness, K_{eff}

During the response of a simply supported URM wall subjected to a transient excitation, it has been observed that incipient instability is most likely to be reached as a consequence of the large displacement amplifications associated with the effective resonant frequency of the wall. This is because unrealistically large ground motions are required at or near resonance to cause the wall response to reach incipient instability. Consequently, the resonant behaviour of the simply supported URM walls should be modelled by the linear 'substitute structure' stiffness. Thus, the characteristic linear stiffness that will most likely best model the real wall behaviour at instability is the real structure's effective resonant frequency. As was discussed in Chapter 5, the effective resonant frequency, f_{eff}, of a simply supported wall is associated with the average incremental secant stiffness, K_{ave}, of the dynamic F-Δ relationship. By again assuming the tri-linear approximation of the static F-Δ relationship $K_{s\ ave}$ is determined in generic terms as,

$$K_{s\ ave} = K_e(1)\left(\frac{\Delta(2)}{\Delta_{instability}} - 1\right)\left(1 + 2\frac{\Delta(2)-\Delta(1)}{\Delta(2)+\Delta(1)} + \frac{\Delta_{instability}-\Delta(2)}{\Delta_{instability}+\Delta(2)}\right) \qquad (8.2.1)$$

Here $K_e(1)$ is defined by Table 5.2.1 and Δ(1) and Δ(2) by Table 7.5.1.

As the average dynamic secant stiffness, $K_{d\ ave} = 3/2\ K_{s\ ave}$ (again assuming a triangular acceleration response relative to the wall supports) an estimate of the effective resonant frequency without considering damping is therefore derived in accordance with $\omega = 2\pi f = \sqrt{\frac{\frac{3}{2}K_{s\,ave}}{M_e}}$ as,

$$f_{eff} = \frac{\sqrt{\frac{3}{2}\frac{K_{s\,ave}}{M_e}}}{2\pi} \tag{8.2.2}$$

Since this estimation of f_{eff} by Equation 8.2.2 does not consider the damping component, the true effective resonant frequency is expected to be slightly higher than the estimation. This is confirmed by comparison with THA in Section 8.3.1.

8.2.2. Simply Supported URM Walls Modelled as a SDOF Oscillator

Prior to DB analysis being applied to a simply supported URM wall the substitutions required for the modeling of the rocking system as an SDOF oscillator must be recognised. These substitutions are required as for SDOF oscillator it is assumed that 100% of the system mass is mobilized whereas for rocking bodies this is not the case. As a result the effective mass location relative to the supports must be considered.

8.2.2.1. Modelled Displacement Capacity

As discussed in Section 5.2.1, for rigid simply supported objects the instability mid-height displacement, $\Delta_{instability}$, is considered to have been reached when the resultant vertical force above the mid-height crack, due to self weight and overburden, is displaced outside of the back mid-height edge of the wall. The mid-height displacement at which this occurs is dependent on the support conditions (Table 5.2.1). For simply supported 'semi-rigid' URM walls with relatively low levels of applied overburden the finite vertical reaction stress blocks are small at large mid-height displacements. Consequently, the rigid incipient instability displacement, $\Delta_{instability}$, can also be assumed for the analysis of 'semi-rigid' simply supported URM walls.

As was discussed in the development of the THA algorithm in Chapter 7, to represent a simply supported rocking object as an SDOF oscillator a triangular acceleration response is appropriate relative to the supports. Consequently, the effective masses of the two rocking free bodies are located at the 2/3 of the free body heights as measured from the supports. The effective displacement capacity of the modelled SDOF 'substitute structure', $\Delta_{\text{eff instability}}$, is therefore reduced to 2/3 of the wall's static mid-height displacement capacity so that:

$$\Delta_{\text{eff instability}} = 2/3\ \Delta_{\text{instability}}$$

8.2.2.2. Modelled Damping Appropriate During Rocking Response

To take into account the reduced response velocity at the effective mass the level of damping associated with the elastic displacement response spectrum is taken as 2/3 that determined experimentally from the mid-height response of the wall. As was presented in Section 6.4.6.3, a lower bound mid-height experimental equivalent viscous damping, ξ_{SDOF}, of approximately 5% was observed for both the 50 mm and 110 mm thick wall specimens (refer Figure 6.4.20 and Figure 6.4.21). For simplicity and to be slightly conservative an equivalent viscous damping of 5% for all frequencies was adopted. The proportional damping coefficient, c, therefore varies linearly with frequency. The corresponding equivalent viscous damping assumed for the DB analysis to determine the elastic RSD was therefore 3% (≈2/3 5%).

8.3. Effectiveness of the Linearised DB Analysis

To test the effectiveness of the proposed DB analysis for face loaded simply supported URM walls an extensive analytical study was conducted using the non-linear THA software ROWMANRY presented in Chapter 7. In this study wall configurations selected for examination included simply supported URM walls 1.5m tall, being representative of the experimental study presented in Chapter 6, 3.3m tall, being a common height found in Australian masonry construction and 4.0m tall, as permitted by the South Australian Housing Code, 1996. For each wall height, wall thickness

considered included 50mm, 110mm and 220mm. Levels of applied overburden included 0MPa, 0.075MPa, 0.15MPa and 0.25MPa being representative of Australian masonry construction. For all wall configurations having applied overburden, the top vertical reaction was assumed to be pushed to the leeward face of the wall so that the mid-height $\Delta_{instability}$ was the thickness of the wall (refer Table 5.2.1) being representative of a concrete slab above boundary condition. Finally, the three levels of mortar joint degradation defined in Section 7.5 were also examined for each of the wall configuration considered. As the tri-linear F-Δ approximation is again used Table 7.5.1 presents the defining displacements $\Delta(1)$ and $\Delta(2)$ associated with each of the three levels of joint degradation.

The first stage in testing the effectiveness of the proposed linearised DB analysis procedure was to determine the estimated effective resonant frequency for each of the wall configurations based on the average cycle secant stiffness to $\Delta_{instability}$, without considering damping in accordance with Equation 8.2.1. Following this, an extensive THA study using gaussian pulse input was conducted to confirm that the estimate of the effective resonant frequency derived was appropriate. A linearised DB analysis was then conducted on each of the simply supported wall configuration subjected to the transient excitations as presented in Table 6.4.9. Here the percentage of the normalised transient excitations required to cause instability of the simply supported URM wall under consideration was predicted. As part of the linearised DB analysis procedure the derived estimate of effective resonant frequency using Equation 8.2.2 was used as the characteristic 'substitute structure' frequency. As discussed in Section 6.4.7.2 the earthquake excitations used were selected to provide a representative cross section of frequency and amplitude contents of plausible ground motions.

Comparison of the DB analysis is then made with results derived using the comprehensive THA software. The following sections present each stage of the study.

8.3.1. Effective Resonant Frequency of Simply Supported URM Walls

The first stage of the study was to determine the effective resonant frequency of the simply supported wall configurations selected. Initially an estimate of effective resonant frequency based on the average static secant stiffness determined from Equation 8.2.1 was made from Equation 8.2.2.

A THA study was then conducted to confirm the effective resonant frequency for the selected wall configurations. This was achieved by running a series of 500 gaussian pulse THA at frequencies ranging from 0.25Hz to 10Hz and amplitudes from 2.5mm to 110mm for each of the wall configurations under consideration. From the resulting RSD versus PGD plot the frequency associated with maximum displacement amplification was identified as the effective resonant frequency. To illustrate, Figure 8.3.1 presents the RSD versus PGD for a 500 gaussian point THA run for a non-loadbearing 3.3m tall, 110mm thick simply supported wall having moderately degraded rotation joints. From this plot it is observed that the maximum mid-height displacement amplification of 110/40 = 2.75 is associated with gaussian pulse frequencies of between 0.75Hz and 1.0Hz. This is compared with the estimated effective resonant frequency derived in accordance with Equation 8.2.2 for the 3.3m tall simply supported URM wall having moderately degraded rotation joints of 0.81Hz. For pulses with a much higher frequency than the system natural frequency (>2.5Hz) it can be seen that the plot converges to a straight line where the PGD is equal to approximately 2/3 of the relative response mid-height spectral displacement. Alternatively this line indicates where the PGD is approximately equal to the Δ_{RSD} measured at the 2/3 free body height being representative of the effective mass location relative to the supports due to the triangular acceleration response. This can be related to the lower part of zone (A) shown in Figure 8.2.1). For these higher frequencies it is evident that instability can only occur when the PGD is equal to or greater than 2/3 of $\Delta_{instability}$ (measured at the mid-height). Accordingly, much higher forces can be withstood by the wall at the higher excitation frequencies than at frequencies near to the effective resonant frequency. This illustrates the dependence of the walls dynamic reserve capacity on the dominant excitation frequency.

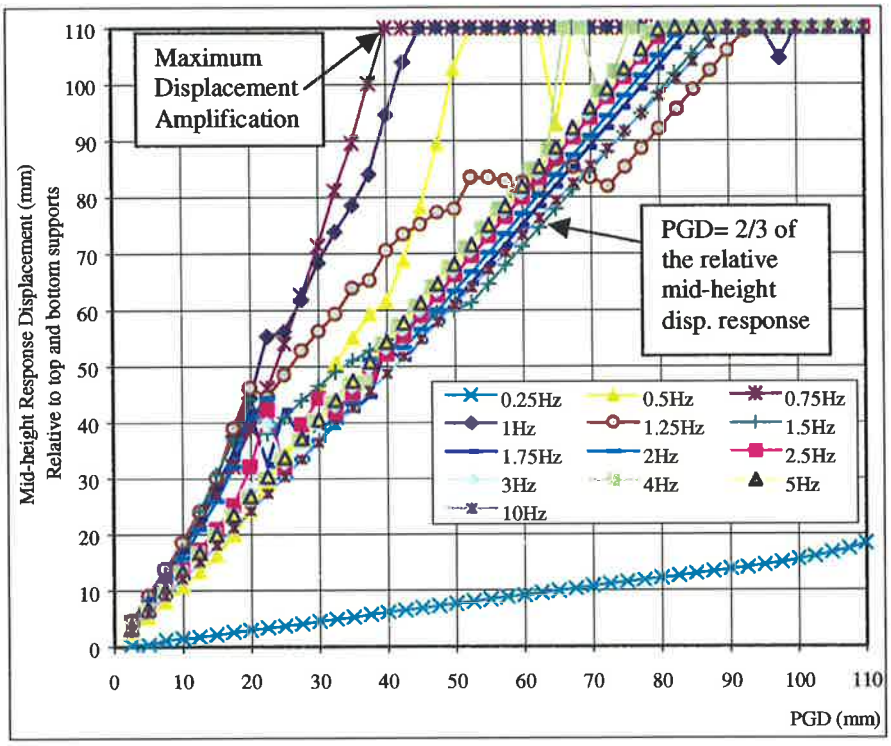

Figure 8.3.1Gaussian Pulse: 3.3m Tall, 110mm Thick, Moderate Degradation THA

As a result of this study it was determined that the effective resonant frequency of simply supported URM walls derived using THA was approximately that predicted from the average secant stiffness to $\Delta_{instability}$ (refer Equation 8.2.1). A slight variation was predicted to be due to the small influence of including damping in the THA increasing the response frequency slightly. In summary, it was found that the frequency derived using Equation 8.2.1 provided a good assessment of the estimate of effective resonant frequency derived from the THA study which itself correlated well with the experimental results (refer Figure 7.8.2). Consequently, it was postulated that the approximate effective resonant frequency for simply supported URM walls determined in accordance with Equation 8.2.2 for use as the characteristic 'substitute structure' frequency is adequate considering the approximations made within the linearisation procedure.

The estimated effective resonant frequency (Equation 8.2.2) determined for the 1.5m, 3.3m and 4.0m height walls at various levels of overburden stress and joint degradation

are presented in Table 8.4.1 to Table 8.4.12. In most cases the effective resonant frequency is associated with the secant stiffness at instantaneous displacements at around 30 to 40% of the incipient instability displacement. The wall thickness was found to have little influence on the effective resonant frequency (the reasons for this are discussed in Section 5.2.1).

By comparison with experimental results it was also found that the analytically derived effective resonant frequencies correlated well with frequencies observed experimentally as the minimum asymptotic frequency, f_{limit}.

8.3.2. Linearised DB Analysis

The second stage of the study was to conduct the linearised DB analysis on each of the simply supported URM wall configurations subjected to the transient excitations presented in Table 6.4.9 including Elcentro, Pacoima Dam, Nahanni and Taft earthquake.

Here the effective resonant frequency determined in the first stage of the study, and the elastic displacement response spectrum at 3% damping (≈2/3x5%) were used to determine the displacement demand on each of the modelled wall configurations. Using the effective resonant frequency as the characterising elastic SDOF stiffness the percent normalised earthquake excitation required for the modelled displacement demand to equal the modelled displacement capacity was determined. This therefore represented the excitation required for ultimate instability of the wall to be reached. For illustrative purposes the linearised DB procedure for the 3.3m tall, 110mm thick wall with 0.075MPa applied overburden stress having moderately degraded rotation joints and subjected to the ElCentro earthquake is described.

Figure 8.3.2 presents the relative elastic displacement response spectrum (3% damping) for the Elcentro earthquake comprised of displacement-normalized spectrum ranging from 25% to 500% in 25% increments. The horizontal line shown at 73mm (110x2/3) displacement is representative of the displacement capacity of the elastic SDOF 'substitute structure' representing the 110mm thick wall both with and without

overburden. The estimate of effective resonant frequency, determined in accordance with Equation 8.2.1 (refer Table 8.4.2) is 1.23Hz. As frequencies greater than the assumed characteristic SDOF oscillator frequency are relevant to the response, to be slightly conservative the lowest percent displacement normalised ElCentro earthquake is adopted from all frequencies greater than the estimated effective resonant frequency. Thus, using the characteristic 'substitute structure' stiffness compatible with the 1.23Hz resonant frequency the percent displacement normalised ElCentro earthquake predicted to cause instability of the wall is determined as 70%.

Results of the linearised DB analysis for all of the considered wall configurations are presented in Table 8.4.1 to Table 8.4.12.

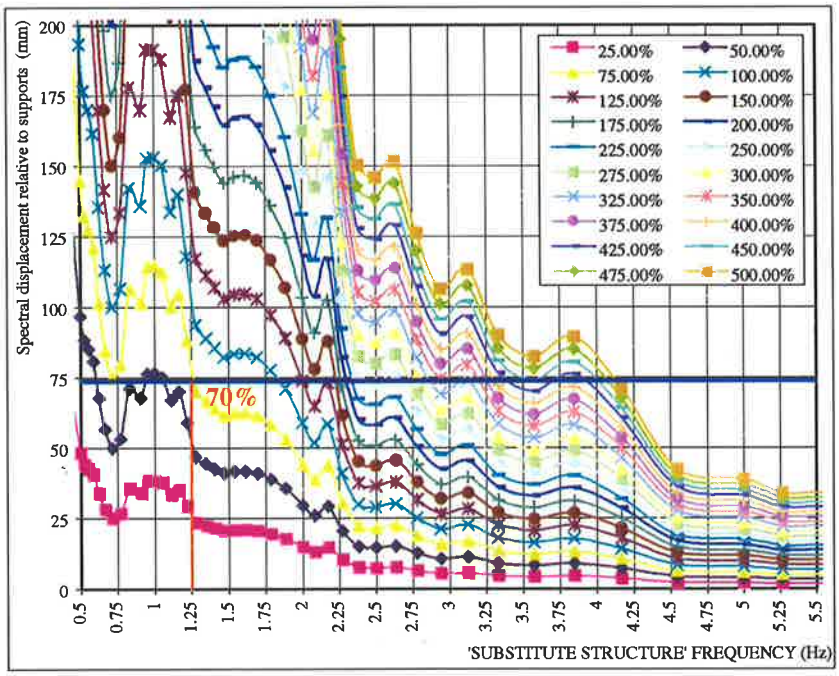

Figure 8.3.2 Relative ElCentro Earthquake Elastic Response Spectrum (3% damping)

8.3.3. THA for Various Transient Excitation

The next stage of the study to test the effectiveness of the DB criterion was to predict the percent displacement normalised earthquake to cause ultimate instability using the non-linear THA software described in Chapter 7. For each wall under consideration a THA was performed gradually increasing the displacement-normalised earthquake by 1% at a

time. Figure 8.3.3, Figure 8.3.4 and Figure 8.3.5 present the peak mid-height displacement result, relative to the supports, for the 1.5m, 3.3m and 4m wall respectively at various overburden and with moderately degraded bed joints subjected to the ElCentro earthquake. From Figure 8.3.4 it can be observed that for the 3.3m wall with 0.075MPa applied overburden stress the THA prediction for ultimate instability is 85% of the displacement normalised ElCentro earthquake. This compares reasonably well with the DB analysis prediction of 70% ElCentro as described in Section 8.3.2. Damping assumed for all THA was Rayleigh damping with the mass proportional coefficient of 1.0 and stiffness proportional coefficient of 0.002 as these represented the lower bound of the experimental results presented in Section 6.4.6.3.

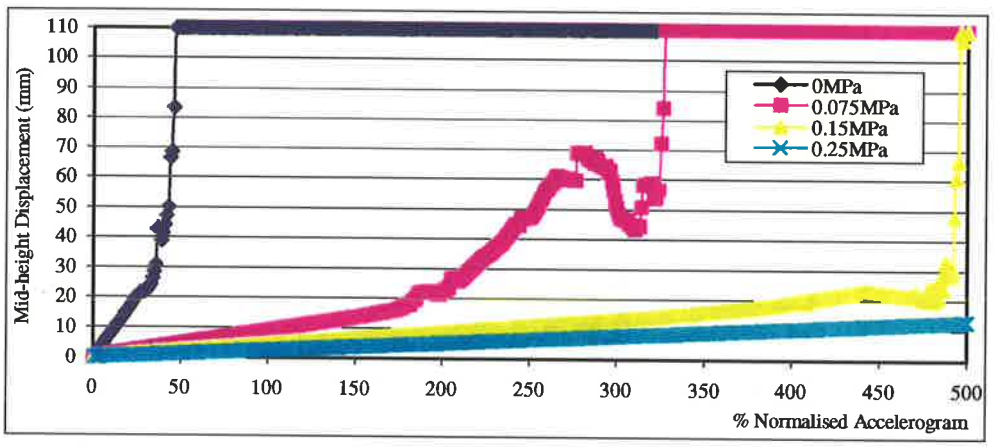

Figure 8.3.3 THA ElCentro Earthquake: 1.5m Tall, Moderate Degradation

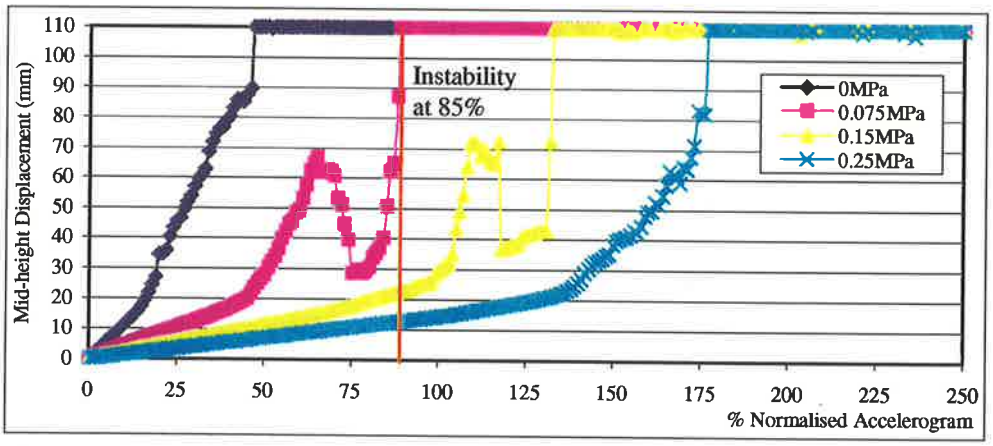

Figure 8.3.4 ElCentro Earthquake: 3.3m Tall, Moderate Degradation

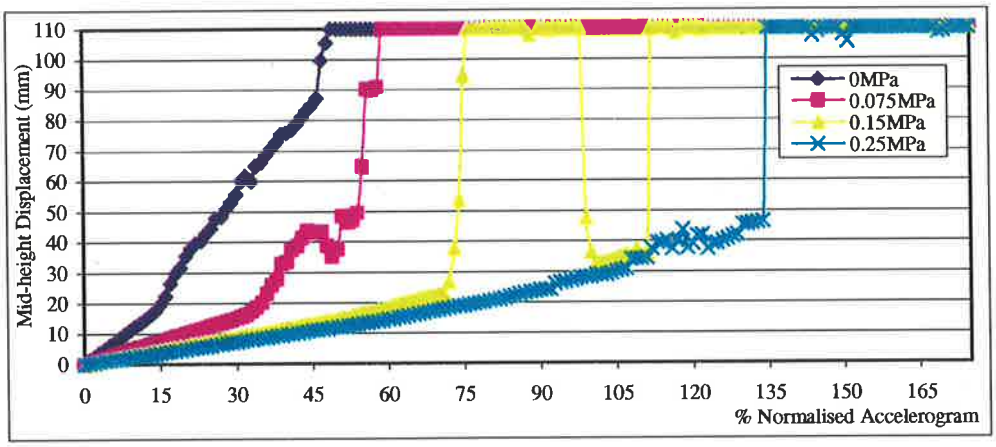

Figure 8.3.5 ElCentro Earthquake: 4.0m Tall, Moderate Degradation

The analysis results for the THA study are presented in Table 8.4.1 to Table 8.4.12.

8.3.4. Comparison of Predictive Model Results

The final stage of the study to test the effectiveness of the DB criterion was to compare the linearised DB and non-linear THA predictions of the percent displacement normalised earthquake to cause ultimate instability as derived in 8.3.2 and 8.3.3 respectively. Figure 8.3.6 graphically presents these comparisons where it is observed that almost all of the results fall within the bounds of the 150% tolerance lines. That is, the linearised DB analysis, using the estimate of effective resonant frequency derived in accordance with Equation 8.2.2 as the characterising 'substitute structure' frequency, will provide an ultimate instability prediction not more than 1.5 times and or less than 2/3 of that predicted by the more comprehensive non-linear THA. The scatter of results observed is a function of the linearisation of the real non-linear stiffness and damping components of the real rocking wall system.

Further to this comparison, the more traditional 'quasi-static' rigid body prediction of lateral resistance capacity and the 'semi-rigid resistance threshold' acceleration (refer Table 8.4.1 to Table 8.4.12) are compared with the THA predictions.

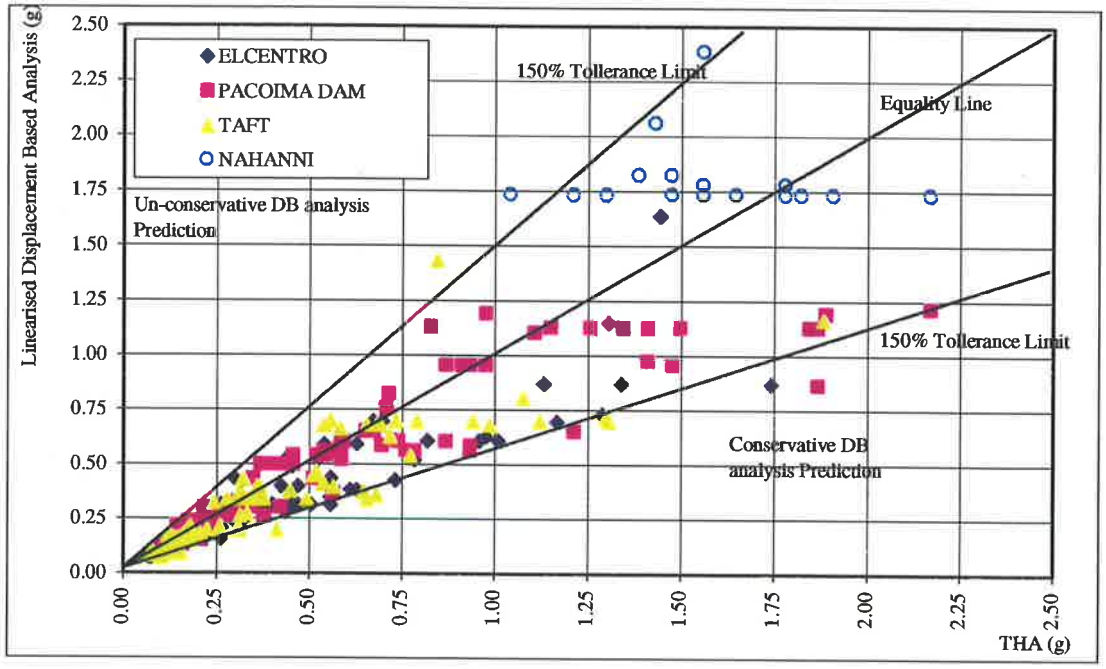

Figure 8.3.6 Comparison of DB Analysis and THA Ultimate Instability Prediction

Figure 8.3.7 presents graphically the comparison of the 'semi-rigid resistance threshold' acceleration with the THA ultimate instability prediction. Here it is observed that for the transient excitations with lower dominant frequencies (Taft, ElCentro and Pacoima Dam) near to the wall's effective resonant frequency the 'semi-rigid resistance threshold' acceleration provides a good prediction of the lateral acceleration capacity of the wall. This is because at these dominant excitation frequencies there is little benefit gained through 'dynamic stability' concepts so that the URM wall's reserve capacity is small. Thus, this 'quasi-static' analysis provides a reasonable prediction of lateral capacity. For excitations having dominant frequencies greater than the effective resonant frequency (Nahanni) the dynamic reserve capacity is far more significant. As this is not accounted for by the 'quasi-static' analysis the ultimate instability prediction is conservative.

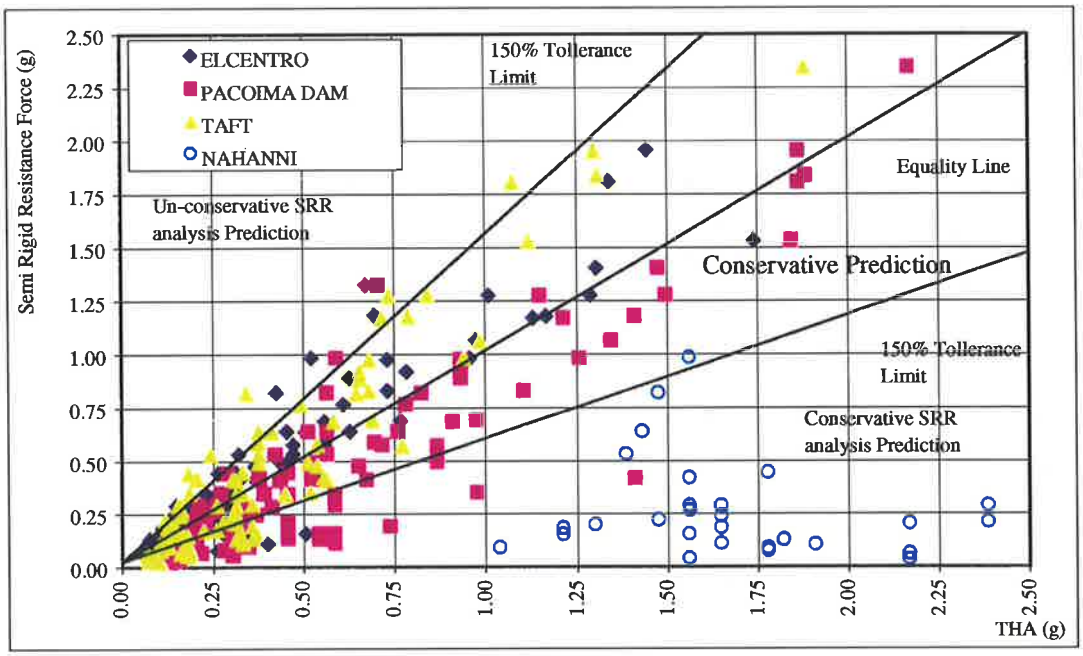

Figure 8.3.7 $R_{es}(1)$ vs THA Ultimate Instability Prediction

Figure 8.3.8 presents graphically the comparison of the 'quasi-static' rigid body ultimate instability prediction. Here it is observed that for the transient excitations with lower dominant frequencies near to the wall's effective resonant frequency the 'quasi-static' rigid body analysis provides an un-conservative prediction of the lateral acceleration capacity of the wall. This is attributed to the overestimation of the 'semi-rigid resistance threshold' force by the rigid assumption and the in-significant wall dynamic reserve capacity. For transient excitations with higher dominant frequencies than the wall's effective resonant frequency, like the 'semi-rigid resistance threshold' force prediction, the 'quasi-static' rigid body analysis provides a conservative prediction of the lateral acceleration capacity of the wall.

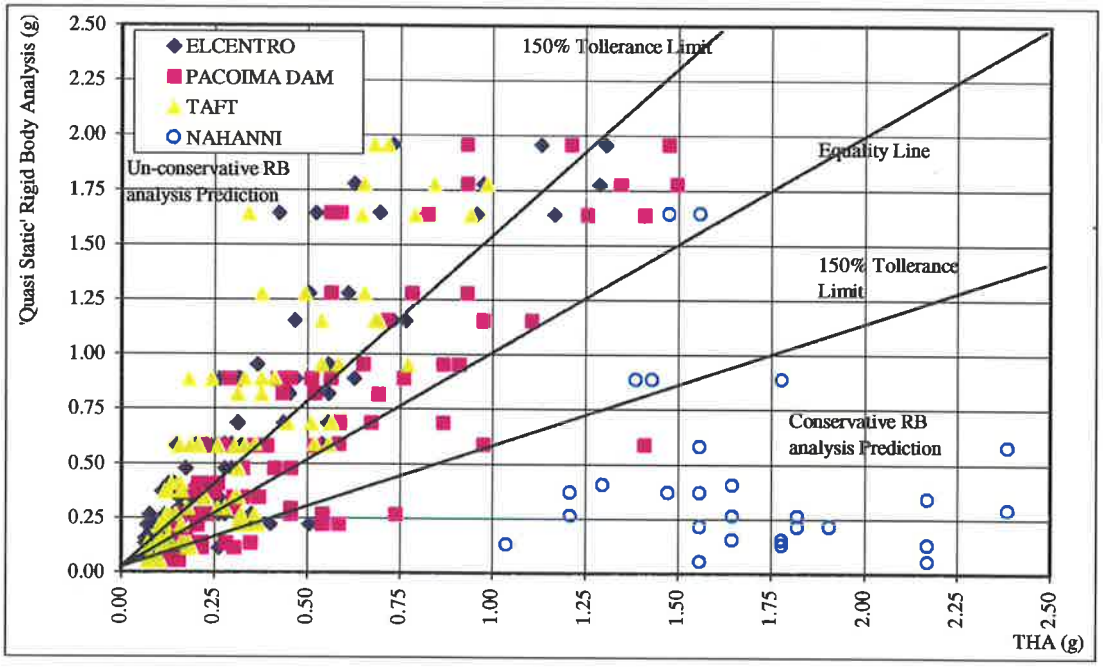

Figure 8.3.8 'Quasi-static' Rigid Body vs THA Ultimate Instability Prediction

8.4. Conclusion

Linearised DB analysis using the wall's effective resonant frequency as the 'substitute structure' natural frequency provides predictions of ultimate instability within ± 50% of the more comprehensive THA. Equation 8.2.1, which represents the generic average secant stiffness to the incipient instability displacement, has been found to provide a reasonable estimate of the simply supported URM walls effective resonant frequency.

The linearised DB analysis therefore provides a rational and relatively straight forward prediction of the dynamic lateral capacity for simply supported URM walls. Since this takes into account the true dynamic behaviour of the rocking wall system, the dynamic reserve capacity for excitations having dominant frequencies greater than the effective resonant frequency is accounted for.

In conclusion the linearised DB analysis using the wall's effective resonant frequency determined in accordance with Equation 8.2.1 as the 'substitute structure' characteristic

frequency provides predictions within limiting tolerances of ± 50% of the more comprehensive THA results. This method therefore provides the most rational and simple approach for assessing the dynamic lateral capacity of simply supported URM walls subjected to transient excitations.

Table 8.4.1 ElCentro Analysis Comparison: 1.5m Height Wall

GEOMETRY		OVER-BURDEN (MPa)	WALL CONDITION			RIGID BODY (g)	SEMI RIGID (g)	THA		DBA		
(t) (mm)	(h) (m)		(refer Figure 6.4.12)	$\Delta(1)$ Δ_{ins}	$\Delta(2)$ Δ_{ins}			%EQ	PGA (g)	f_{eff} (Hz)	>FREQ %EQ	>FREQ PGA (g)
50	1.5	0	NEW	6%	28%	0.13	0.10	**33%**	0.11	**1.45**	**30%**	0.10
50	1.5	0	MOD	13%	40%	0.13	0.08	**19%**	0.07	**1.21**	**25%**	0.09
50	1.5	0	SEV	20%	50%	0.13	0.07	**21%**	0.07	**1.04**	**20%**	0.07
50	1.5	0.075	NEW	6%	28%	0.89	0.64	**130%**	0.45	**2.84**	**140%**	0.49
50	1.5	0.075	MOD	13%	40%	0.89	0.53	**92%**	0.32	**2.36**	**100%**	0.35
50	1.5	0.075	SEV	20%	50%	0.89	0.44	**76%**	0.26	**2.04**	**60%**	0.21
50	1.5	0.15	NEW	6%	28%	1.64	1.18	**500%**	1.74	**3.74**	**200%**	0.70
50	1.5	0.15	MOD	13%	40%	1.64	0.99	**150%**	0.52	**3.12**	**150%**	0.52
50	1.5	0.15	SEV	20%	50%	1.64	0.82	**122%**	0.42	**2.69**	**115%**	0.40
50	1.5	0.25	NEW	6%	28%	2.65	1.91	**NF**	NF	**4.62**	**400%**	1.39
50	1.5	0.25	MOD	13%	40%	2.65	1.59	**NF**	NF	**3.9**	**200%**	0.70
50	1.5	0.25	SEV	20%	50%	2.65	1.33	**193%**	0.67	**3.37**	**200%**	0.70
110	1.5	0	NEW	6%	28%	0.29	0.21	**80%**	0.28	**1.45**	**85%**	0.30
110	1.5	0	MOD	13%	40%	0.29	0.18	**45%**	0.16	**1.21**	**60%**	0.21
110	1.5	0	SEV	20%	50%	0.29	0.15	**45%**	0.16	**1.04**	**45%**	0.16
110	1.5	0.075	NEW	6%	28%	1.95	1.41	**375%**	1.31	**2.84**	**330%**	1.15
110	1.5	0.075	MOD	13%	40%	1.95	1.17	**325%**	1.13	**2.36**	**250%**	0.87
110	1.5	0.075	SEV	20%	50%	1.95	0.98	**210%**	0.73	**2.04**	**123%**	0.43
110	1.5	0.15	NEW	6%	28%	3.62	2.60	**NF**	NF	**3.74**	**425%**	1.48
110	1.5	0.15	MOD	13%	40%	3.62	2.17	**NF**	NF	**3.12**	**325%**	1.13
110	1.5	0.15	SEV	20%	50%	3.62	1.81	**385%**	1.34	**2.69**	**250%**	0.87
110	1.5	0.25	NEW	6%	28%	5.83	4.20	**NF**	NF	**4.62**	**NF**	NF
110	1.5	0.25	MOD	13%	40%	5.83	3.50	**NF**	NF	**3.9**	**425%**	1.48
110	1.5	0.25	SEV	20%	50%	5.83	2.92	**NF**	NF	**3.37**	**425%**	1.48
220	1.5	0	NEW	6%	28%	0.59	0.42	**155%**	0.54	**1.45**	**170%**	0.59
220	1.5	0	MOD	13%	40%	0.59	0.35	**85%**	0.30	**1.21**	**125%**	0.44
220	1.5	0	SEV	20%	50%	0.59	0.29	**80%**	0.28	**1.04**	**85%**	0.30
220	1.5	0.075	NEW	6%	28%	3.91	2.81	**NF**	NF	**2.84**	**NF**	NF
220	1.5	0.075	MOD	13%	40%	3.91	2.35	**NF**	NF	**2.36**	**NF**	NF
220	1.5	0.075	SEV	20%	50%	3.91	1.95	**415%**	1.45	**2.04**	**470%**	1.64
220	1.5	0.15	NEW	6%	28%	7.23	5.21	**NF**	NF	**3.74**	**NF**	NF
220	1.5	0.15	MOD	13%	40%	7.23	4.34	**NF**	NF	**3.12**	**NF**	NF
220	1.5	0.15	SEV	20%	50%	7.23	3.62	**NF**	NF	**2.69**	**NF**	NF
220	1.5	0.25	NEW	6%	28%	11.66	8.40	**NF**	NF	**4.62**	**NF**	NF
220	1.5	0.25	MOD	13%	40%	11.66	7.00	**NF**	NF	**3.9**	**NF**	NF
220	1.5	0.25	SEV	20%	50%	11.66	5.83	**NF**	NF	**3.37**	**NF**	NF

*NF – No Fail within limits of study

Table 8.4.2 ElCentro Analysis Comparison: 3.3m Height Wall

GEOMETRY		OVER-BURDEN (MPa)	WALL CONDITION			RIGID BODY (g)	SEMI RIGID (g)	THA		DBA		
(t) (mm)	(h) (m)		(refer Figure 6.4.12)	Δ(1) Δ_{ins}	Δ(2) Δ_{ins}			%EQ	PGA (g)	f_{eff} (Hz)	>FREQ %EQ	>FREQ PGA (g)
50	3.3	0	NEW	6%	28%	0.06	0.04	**20%**	0.07	**0.96**	25%	0.09
50	3.3	0	MOD	13%	40%	0.06	0.04	**22%**	0.08	**0.81**	25%	0.09
50	3.3	0	SEV	20%	50%	0.06	0.03	**26%**	0.09	**0.7**	25%	0.09
50	3.3	0.075	NEW	6%	28%	0.22	0.16	**32%**	0.11	**1.46**	30%	0.10
50	3.3	0.075	MOD	13%	40%	0.22	0.13	**27%**	0.09	**1.23**	25%	0.09
50	3.3	0.075	SEV	20%	50%	0.22	0.11	**20%**	0.07	**1.06**	20%	0.07
50	3.3	0.15	NEW	6%	28%	0.37	0.27	**54%**	0.19	**1.82**	45%	0.16
50	3.3	0.15	MOD	13%	40%	0.37	0.22	**37%**	0.13	**1.54**	35%	0.12
50	3.3	0.15	SEV	20%	50%	0.37	0.19	**32%**	0.11	**1.33**	30%	0.10
50	3.3	0.25	NEW	6%	28%	0.58	0.42	**93%**	0.32	**2.22**	70%	0.24
50	3.3	0.25	MOD	13%	40%	0.58	0.35	**66%**	0.23	**1.87**	50%	0.17
50	3.3	0.25	SEV	20%	50%	0.58	0.29	**43%**	0.15	**1.62**	40%	0.14
110	3.3	0	NEW	6%	28%	0.13	0.10	**45%**	0.16	**0.96**	45%	0.16
110	3.3	0	MOD	13%	40%	0.13	0.08	**45%**	0.16	**0.81**	45%	0.16
110	3.3	0	SEV	20%	50%	0.13	0.07	**45%**	0.16	**0.7**	45%	0.16
110	3.3	0.075	NEW	6%	28%	0.48	0.34	**80%**	0.28	**1.46**	80%	0.28
110	3.3	0.075	MOD	13%	40%	0.48	0.29	**85%**	0.30	**1.23**	70%	0.24
110	3.3	0.075	SEV	20%	50%	0.48	0.24	**50%**	0.17	**1.06**	55%	0.19
110	3.3	0.15	NEW	6%	28%	0.82	0.59	**160%**	0.56	**1.82**	100%	0.35
110	3.3	0.15	MOD	13%	40%	0.82	0.49	**130%**	0.45	**1.54**	90%	0.31
110	3.3	0.15	SEV	20%	50%	0.82	0.41	**125%**	0.44	**1.33**	80%	0.28
110	3.3	0.25	NEW	6%	28%	1.28	0.92	**225%**	0.78	**2.22**	150%	0.52
110	3.3	0.25	MOD	13%	40%	1.28	0.77	**175%**	0.61	**1.87**	110%	0.38
110	3.3	0.25	SEV	20%	50%	1.28	0.64	**145%**	0.51	**1.62**	90%	0.31
220	3.3	0	NEW	6%	28%	0.27	0.19	**75%**	0.26	**0.96**	90%	0.31
220	3.3	0	MOD	13%	40%	0.27	0.16	**80%**	0.28	**0.81**	90%	0.31
220	3.3	0	SEV	20%	50%	0.27	0.13	**100%**	0.35	**0.7**	90%	0.31
220	3.3	0.075	NEW	6%	28%	0.95	0.69	**160%**	0.56	**1.46**	160%	0.56
220	3.3	0.075	MOD	13%	40%	0.95	0.57	**160%**	0.56	**1.23**	125%	0.44
220	3.3	0.075	SEV	20%	50%	0.95	0.48	**105%**	0.37	**1.06**	90%	0.31
220	3.3	0.15	NEW	6%	28%	1.64	1.18	**335%**	1.17	**1.82**	200%	0.70
220	3.3	0.15	MOD	13%	40%	1.64	0.98	**275%**	0.96	**1.54**	175%	0.61
220	3.3	0.15	SEV	20%	50%	1.64	0.82	**235%**	0.82	**1.33**	175%	0.61
220	3.3	0.25	NEW	6%	28%	2.55	1.84	**455%**	1.58	**2.22**	350%	1.22
220	3.3	0.25	MOD	13%	40%	2.55	1.53	**500%**	1.74	**1.87**	250%	0.87
220	3.3	0.25	SEV	20%	50%	2.55	1.28	**290%**	1.01	**1.62**	175%	0.61

*NF – No Fail within limits of study

Table 8.4.3 ElCentro Analysis Comparison: 4.0m Height Wall

GEOMETRY		OVER-	WALL CONDITION			RIGID	SEMI	THA		DBA		
(t) (mm)	(h) (m)	BURDEN (MPa)	(refer Figure 6.4.12)	Δ(1) Δ_{ins}	Δ(2) Δ_{ins}	BODY (g)	RIGID (g)	%EQ	PGA (g)	f_{eff} (Hz)	>FREQ %EQ	>FREQ PGA (g)
50	4	0	NEW	6%	28%	0.05	0.04	**32%**	0.11	**0.88**	**25%**	0.09
50	4	0	MOD	13%	40%	0.05	0.03	**30%**	0.10	**0.74**	**25%**	0.09
50	4	0	SEV	20%	50%	0.05	0.03	**33%**	0.11	**0.64**	**25%**	0.09
50	4	0.075	NEW	6%	28%	0.16	0.11	**32%**	0.11	**1.26**	**25%**	0.09
50	4	0.075	MOD	13%	40%	0.16	0.09	**19%**	0.07	**1.06**	**22%**	0.08
50	4	0.075	SEV	20%	50%	0.16	0.08	**21%**	0.07	**0.92**	**22%**	0.08
50	4	0.15	NEW	6%	28%	0.26	0.19	**50%**	0.17	**1.55**	**40%**	0.14
50	4	0.15	MOD	13%	40%	0.26	0.16	**34%**	0.12	**1.31**	**35%**	0.12
50	4	0.15	SEV	20%	50%	0.26	0.13	**22%**	0.08	**1.13**	**25%**	0.09
50	4	0.25	NEW	6%	28%	0.40	0.29	**62%**	0.22	**1.01**	**50%**	0.17
50	4	0.25	MOD	13%	40%	0.40	0.24	**41%**	0.14	**1.58**	**40%**	0.14
50	4	0.25	SEV	20%	50%	0.40	0.20	**37%**	0.13	**1.36**	**35%**	0.12
110	4	0	NEW	6%	28%	0.11	0.08	**75%**	0.26	**0.88**	**45%**	0.16
110	4	0	MOD	13%	40%	0.11	0.07	**45%**	0.16	**0.74**	**45%**	0.16
110	4	0	SEV	20%	50%	0.11	0.06	**55%**	0.19	**0.64**	**45%**	0.16
110	4	0.075	NEW	6%	28%	0.34	0.25	**75%**	0.26	**1.26**	**70%**	0.24
110	4	0.075	MOD	13%	40%	0.34	0.21	**55%**	0.19	**1.06**	**50%**	0.17
110	4	0.075	SEV	20%	50%	0.34	0.17	**45%**	0.16	**0.92**	**45%**	0.16
110	4	0.15	NEW	6%	28%	0.58	0.42	**105%**	0.37	**1.55**	**85%**	0.30
110	4	0.15	MOD	13%	40%	0.58	0.35	**75%**	0.26	**1.31**	**75%**	0.26
110	4	0.15	SEV	20%	50%	0.58	0.29	**70%**	0.24	**1.13**	**60%**	0.21
110	4	0.25	NEW	6%	28%	0.89	0.64	**180%**	0.63	**1.01**	**110%**	0.38
110	4	0.25	MOD	13%	40%	0.89	0.53	**135%**	0.47	**1.58**	**90%**	0.31
110	4	0.25	SEV	20%	50%	0.89	0.44	**90%**	0.31	**1.36**	**90%**	0.31
220	4	0	NEW	6%	28%	0.22	0.16	**145%**	0.51	**0.88**	**90%**	0.31
220	4	0	MOD	13%	40%	0.22	0.13	**100%**	0.35	**0.74**	**90%**	0.31
220	4	0	SEV	20%	50%	0.22	0.11	**115%**	0.40	**0.64**	**90%**	0.31
220	4	0.075	NEW	6%	28%	0.69	0.49	**125%**	0.44	**1.26**	**150%**	0.52
220	4	0.075	MOD	13%	40%	0.69	0.41	**160%**	0.56	**1.06**	**90%**	0.31
220	4	0.075	SEV	20%	50%	0.69	0.34	**90%**	0.31	**0.92**	**90%**	0.31
220	4	0.15	NEW	6%	28%	1.15	0.83	**210%**	0.73	**1.55**	**175%**	0.61
220	4	0.15	MOD	13%	40%	1.15	0.69	**220%**	0.77	**1.31**	**160%**	0.56
220	4	0.15	SEV	20%	50%	1.15	0.58	**135%**	0.47	**1.13**	**115%**	0.40
220	4	0.25	NEW	6%	28%	1.78	1.28	**370%**	1.29	**1.01**	**210%**	0.73
220	4	0.25	MOD	13%	40%	1.78	1.07	**280%**	0.98	**1.58**	**180%**	0.63
220	4	0.25	SEV	20%	50%	1.78	0.89	**180%**	0.63	**1.36**	**170%**	0.59

*NF – No Fail within limits of study

Table 8.4.4 Taft Analysis Comparison: 1.5m Height Wall

GEOMETRY		OVER-BURDEN (MPa)	WALL CONDITION			RIGID BODY (g)	SEMI RIGID (g)	THA		DBA		
(t) (mm)	(h) (m)		(refer Figure 6.4.12)	Δ(1) Δ_{ins}	Δ(2) Δ_{ins}			%EQ	PGA (g)	f_{eff} (Hz)	>FREQ %EQ	>FREQ PGA (g)
50	1.5	0	NEW	6%	28%	0.13	0.10	**72%**	0.13	**1.45**	**80%**	0.14
50	1.5	0	MOD	13%	40%	0.13	0.08	**58%**	0.10	**1.21**	**55%**	0.10
50	1.5	0	SEV	20%	50%	0.13	0.07	**40%**	0.07	**1.04**	**45%**	0.08
50	1.5	0.075	NEW	6%	28%	0.89	0.64	**NF**	NF	**2.84**	**190%**	0.34
50	1.5	0.075	MOD	13%	40%	0.89	0.53	**136%**	0.24	**2.36**	**180%**	0.32
50	1.5	0.075	SEV	20%	50%	0.89	0.44	**102%**	0.18	**2.04**	**95%**	0.17
50	1.5	0.15	NEW	6%	28%	1.64	1.18	**NF**	NF	**3.74**	**410%**	0.74
50	1.5	0.15	MOD	13%	40%	1.64	0.99	**NF**	NF	**3.12**	**210%**	0.38
50	1.5	0.15	SEV	20%	50%	1.64	0.82	**191%**	0.34	**2.69**	**190%**	0.34
50	1.5	0.25	NEW	6%	28%	2.65	1.91	**NF**	NF	**4.62**	**500%**	0.90
50	1.5	0.25	MOD	13%	40%	2.65	1.59	**NF**	NF	**3.9**	**455%**	0.82
50	1.5	0.25	SEV	20%	50%	2.65	1.33	**NF**	NF	**3.37**	**310%**	0.56
110	1.5	0	NEW	6%	28%	0.29	0.21	**155%**	0.28	**1.45**	**190%**	0.34
110	1.5	0	MOD	13%	40%	0.29	0.18	**145%**	0.26	**1.21**	**120%**	0.22
110	1.5	0	SEV	20%	50%	0.29	0.15	**100%**	0.18	**1.04**	**120%**	0.22
110	1.5	0.075	NEW	6%	28%	1.95	1.41	**NF**	NF	**2.84**	**420%**	0.75
110	1.5	0.075	MOD	13%	40%	1.95	1.17	**400%**	0.72	**2.36**	**350%**	0.63
110	1.5	0.075	SEV	20%	50%	1.95	0.98	**380%**	0.68	**2.04**	**200%**	0.36
110	1.5	0.15	NEW	6%	28%	3.62	2.60	**NF**	NF	**3.74**	**1000%**	1.79
110	1.5	0.15	MOD	13%	40%	3.62	2.17	**NF**	NF	**3.12**	**550%**	0.99
110	1.5	0.15	SEV	20%	50%	3.62	1.81	**600%**	1.08	**2.69**	**450%**	0.81
110	1.5	0.25	NEW	6%	28%	5.83	4.20	**NF**	NF	**4.62**	**NF**	NF
110	1.5	0.25	MOD	13%	40%	5.83	3.50	**NF**	NF	**3.9**	**NF**	NF
110	1.5	0.25	SEV	20%	50%	5.83	2.92	**NF**	NF	**3.37**	**70%**	0.13
220	1.5	0	NEW	6%	28%	0.59	0.42	**310%**	0.56	**1.45**	**390%**	0.70
220	1.5	0	MOD	13%	40%	0.59	0.35	**290%**	0.52	**1.21**	**260%**	0.47
220	1.5	0	SEV	20%	50%	0.59	0.29	**200%**	0.36	**1.04**	**220%**	0.39
220	1.5	0.075	NEW	6%	28%	3.91	2.81	**NF**	NF	**2.84**	**800%**	1.43
220	1.5	0.075	MOD	13%	40%	3.91	2.35	**1050%**	1.88	**2.36**	**650%**	1.17
220	1.5	0.075	SEV	20%	50%	3.91	1.95	**725%**	1.30	**2.04**	**400%**	0.72
220	1.5	0.15	NEW	6%	28%	7.23	5.21	**NF**	NF	**3.74**	**NF**	NF
220	1.5	0.15	MOD	13%	40%	7.23	4.34	**NF**	NF	**3.12**	**NF**	NF
220	1.5	0.15	SEV	20%	50%	7.23	3.62	**NF**	NF	**2.69**	**810%**	1.45
220	1.5	0.25	NEW	6%	28%	11.66	8.40	**NF**	NF	**4.62**	**NF**	NF
220	1.5	0.25	MOD	13%	40%	11.66	7.00	**NF**	NF	**3.9**	**NF**	NF
220	1.5	0.25	SEV	20%	50%	11.66	5.83	**NF**	NF	**3.37**	**NF**	NF

*NF – No Fail within limits of study

Table 8.4.5 Taft Analysis Comparison: 3.3m Height Wall

GEOMETRY		OVER-BURDEN (MPa)	WALL CONDITION			RIGID BODY (g)	SEMI RIGID (g)	THA		DBA		
(t) (mm)	(h) (m)		(refer Figure 6.4.12)	Δ(1) Δ_{ins}	Δ(2) Δ_{ins}			%EQ	PGA (g)	f_{eff} (Hz)	>FREQ %EQ	>FREQ PGA (g)
50	3.3	0	NEW	6%	28%	0.06	0.04	**53%**	0.10	**0.96**	**50%**	0.09
50	3.3	0	MOD	13%	40%	0.06	0.04	**46%**	0.08	**0.81**	**50%**	0.09
50	3.3	0	SEV	20%	50%	0.06	0.03	**41%**	0.07	**0.7**	**50%**	0.09
50	3.3	0.075	NEW	6%	28%	0.22	0.16	**91%**	0.16	**1.46**	**95%**	0.17
50	3.3	0.075	MOD	13%	40%	0.22	0.13	**66%**	0.12	**1.23**	**95%**	0.17
50	3.3	0.075	SEV	20%	50%	0.22	0.11	**58%**	0.10	**1.06**	**50%**	0.09
50	3.3	0.15	NEW	6%	28%	0.37	0.27	**91%**	0.16	**1.82**	**95%**	0.17
50	3.3	0.15	MOD	13%	40%	0.37	0.22	**66%**	0.12	**1.54**	**95%**	0.17
50	3.3	0.15	SEV	20%	50%	0.37	0.19	**70%**	0.13	**1.33**	**95%**	0.17
50	3.3	0.25	NEW	6%	28%	0.58	0.42	**115%**	0.21	**2.22**	**100%**	0.18
50	3.3	0.25	MOD	13%	40%	0.58	0.35	**104%**	0.19	**1.87**	**95%**	0.17
50	3.3	0.25	SEV	20%	50%	0.58	0.29	**88%**	0.16	**1.62**	**95%**	0.17
110	3.3	0	NEW	6%	28%	0.13	0.10	**102%**	0.18	**0.96**	**110%**	0.20
110	3.3	0	MOD	13%	40%	0.13	0.08	**95%**	0.17	**0.81**	**110%**	0.20
110	3.3	0	SEV	20%	50%	0.13	0.07	**90%**	0.16	**0.7**	**100%**	0.18
110	3.3	0.075	NEW	6%	28%	0.48	0.34	**175%**	0.31	**1.46**	**190%**	0.34
110	3.3	0.075	MOD	13%	40%	0.48	0.29	**175%**	0.31	**1.23**	**145%**	0.26
110	3.3	0.075	SEV	20%	50%	0.48	0.24	**175%**	0.31	**1.06**	**110%**	0.20
110	3.3	0.15	NEW	6%	28%	0.82	0.59	**210%**	0.38	**1.82**	**190%**	0.34
110	3.3	0.15	MOD	13%	40%	0.82	0.49	**210%**	0.38	**1.54**	**190%**	0.34
110	3.3	0.15	SEV	20%	50%	0.82	0.41	**175%**	0.31	**1.33**	**190%**	0.34
110	3.3	0.25	NEW	6%	28%	1.28	0.92	**365%**	0.65	**2.22**	**190%**	0.34
110	3.3	0.25	MOD	13%	40%	1.28	0.77	**275%**	0.49	**1.87**	**190%**	0.34
110	3.3	0.25	SEV	20%	50%	1.28	0.64	**210%**	0.38	**1.62**	**190%**	0.34
220	3.3	0	NEW	6%	28%	0.27	0.19	**200%**	0.36	**0.96**	**210%**	0.38
220	3.3	0	MOD	13%	40%	0.27	0.16	**180%**	0.32	**0.81**	**240%**	0.43
220	3.3	0	SEV	20%	50%	0.27	0.13	**200%**	0.36	**0.7**	**200%**	0.36
220	3.3	0.075	NEW	6%	28%	0.95	0.69	**325%**	0.58	**1.46**	**370%**	0.66
220	3.3	0.075	MOD	13%	40%	0.95	0.57	**430%**	0.77	**1.23**	**300%**	0.54
220	3.3	0.075	SEV	20%	50%	0.95	0.48	**300%**	0.54	**1.06**	**230%**	0.41
220	3.3	0.15	NEW	6%	28%	1.64	1.18	**440%**	0.79	**1.82**	**390%**	0.70
220	3.3	0.15	MOD	13%	40%	1.64	0.98	**525%**	0.94	**1.54**	**390%**	0.70
220	3.3	0.15	SEV	20%	50%	1.64	0.82	**360%**	0.65	**1.33**	**210%**	0.38
220	3.3	0.25	NEW	6%	28%	2.55	1.84	**730%**	1.31	**2.22**	**390%**	0.70
220	3.3	0.25	MOD	13%	40%	2.55	1.53	**625%**	1.12	**1.87**	**390%**	0.70
220	3.3	0.25	SEV	20%	50%	2.55	1.28	**410%**	0.74	**1.62**	**390%**	0.70

*NF – No Fail within limits of study

Table 8.4.6 Taft Analysis Comparison: 4.0m Height Wall

GEOMETRY		OVER-BURDEN (MPa)	WALL CONDITION			RIGID BODY (g)	SEMI RIGID (g)	THA		DBA		
(t) (mm)	(h) (m)		(refer Figure 6.4.12)	Δ(1) Δ_{ins}	Δ(2) Δ_{ins}			%EQ	PGA (g)	f_{eff} (Hz)	>FREQ %EQ	>FREQ PGA (g)
50	4	0	NEW	6%	28%	0.05	0.04	40%	0.07	0.88	50%	0.09
50	4	0	MOD	13%	40%	0.05	0.03	42%	0.08	0.74	50%	0.09
50	4	0	SEV	20%	50%	0.05	0.03	58%	0.10	0.64	40%	0.07
50	4	0.075	NEW	6%	28%	0.16	0.11	70%	0.13	1.26	60%	0.11
50	4	0.075	MOD	13%	40%	0.16	0.09	60%	0.11	1.06	50%	0.09
50	4	0.075	SEV	20%	50%	0.16	0.08	58%	0.10	0.92	50%	0.09
50	4	0.15	NEW	6%	28%	0.26	0.19	82%	0.15	1.55	90%	0.16
50	4	0.15	MOD	13%	40%	0.26	0.16	73%	0.13	1.31	85%	0.15
50	4	0.15	SEV	20%	50%	0.26	0.13	68%	0.12	1.13	50%	0.09
50	4	0.25	NEW	6%	28%	0.40	0.29	86%	0.15	1.01	50%	0.09
50	4	0.25	MOD	13%	40%	0.40	0.24	90%	0.16	1.58	95%	0.17
50	4	0.25	SEV	20%	50%	0.40	0.20	76%	0.14	1.36	90%	0.16
110	4	0	NEW	6%	28%	0.11	0.08	100%	0.18	0.88	110%	0.20
110	4	0	MOD	13%	40%	0.11	0.07	105%	0.19	0.74	105%	0.19
110	4	0	SEV	20%	50%	0.11	0.06	100%	0.18	0.64	80%	0.14
110	4	0.075	NEW	6%	28%	0.34	0.25	170%	0.30	1.26	110%	0.20
110	4	0.075	MOD	13%	40%	0.34	0.21	175%	0.31	1.06	110%	0.20
110	4	0.075	SEV	20%	50%	0.34	0.17	125%	0.22	0.92	110%	0.20
110	4	0.15	NEW	6%	28%	0.58	0.42	170%	0.30	1.55	190%	0.34
110	4	0.15	MOD	13%	40%	0.58	0.35	185%	0.33	1.31	190%	0.34
110	4	0.15	SEV	20%	50%	0.58	0.29	145%	0.26	1.13	110%	0.20
110	4	0.25	NEW	6%	28%	0.89	0.64	230%	0.41	1.01	110%	0.20
110	4	0.25	MOD	13%	40%	0.89	0.53	210%	0.38	1.58	190%	0.34
110	4	0.25	SEV	20%	50%	0.89	0.44	185%	0.33	1.36	190%	0.34
220	4	0	NEW	6%	28%	0.22	0.16	205%	0.37	0.88	220%	0.39
220	4	0	MOD	13%	40%	0.22	0.13	175%	0.31	0.74	210%	0.38
220	4	0	SEV	20%	50%	0.22	0.11	185%	0.33	0.64	150%	0.27
220	4	0.075	NEW	6%	28%	0.69	0.49	285%	0.51	1.26	250%	0.45
220	4	0.075	MOD	13%	40%	0.69	0.41	315%	0.56	1.06	220%	0.39
220	4	0.075	SEV	20%	50%	0.69	0.34	250%	0.45	0.92	210%	0.38
220	4	0.15	NEW	6%	28%	1.15	0.83	380%	0.68	1.55	380%	0.68
220	4	0.15	MOD	13%	40%	1.15	0.69	385%	0.69	1.31	380%	0.68
220	4	0.15	SEV	20%	50%	1.15	0.58	300%	0.54	1.13	380%	0.68
220	4	0.25	NEW	6%	28%	1.78	1.28	470%	0.84	1.01	800%	1.43
220	4	0.25	MOD	13%	40%	1.78	1.07	550%	0.99	1.58	380%	0.68
220	4	0.25	SEV	20%	50%	1.78	0.89	365%	0.65	1.36	380%	0.68

*NF – No Fail within limits of study

Table 8.4.7 Pacoima Dam Analysis Comparison: 1.5m Height Wall

GEOMETRY		OVER-	WALL CONDITION			RIGID	SEMI	THA		DBA		
(t) (mm)	(h) (m)	BURDEN (MPa)	(refer Figure 6.4.12)	Δ(1) Δ_{ins}	Δ(2) Δ_{ins}	BODY (g)	RIGID (g)	%EQ	PGA (g)	f_{eff} (Hz)	>FREQ %EQ	>FREQ PGA (g)
50	1.5	0	NEW	6%	28%	0.13	0.10	**43%**	0.19	**1.45**	**50%**	0.22
50	1.5	0	MOD	13%	40%	0.13	0.08	**33%**	0.14	**1.21**	**50%**	0.22
50	1.5	0	SEV	20%	50%	0.13	0.07	**48%**	0.21	**1.04**	**35%**	0.15
50	1.5	0.075	NEW	6%	28%	0.89	0.64	**118%**	0.51	**2.84**	**100%**	0.43
50	1.5	0.075	MOD	13%	40%	0.89	0.53	**97%**	0.42	**2.36**	**70%**	0.30
50	1.5	0.075	SEV	20%	50%	0.89	0.44	**67%**	0.29	**2.04**	**65%**	0.28
50	1.5	0.15	NEW	6%	28%	1.64	1.18	**NF**	NF	**3.74**	**250%**	1.08
50	1.5	0.15	MOD	13%	40%	1.64	0.99	**136%**	0.59	**3.12**	**140%**	0.61
50	1.5	0.15	SEV	20%	50%	1.64	0.82	**130%**	0.56	**2.69**	**85%**	0.37
50	1.5	0.25	NEW	6%	28%	2.65	1.91	**NF**	NF	**4.62**	**280%**	1.21
50	1.5	0.25	MOD	13%	40%	2.65	1.59	**NF**	NF	**3.9**	**280%**	1.21
50	1.5	0.25	SEV	20%	50%	2.65	1.33	**163%**	0.71	**3.37**	**175%**	0.76
110	1.5	0	NEW	6%	28%	0.29	0.21	**105%**	0.46	**1.45**	**115%**	0.50
110	1.5	0	MOD	13%	40%	0.29	0.18	**105%**	0.46	**1.21**	**125%**	0.54
110	1.5	0	SEV	20%	50%	0.29	0.15	**70%**	0.30	**1.04**	**75%**	0.33
110	1.5	0.075	NEW	6%	28%	1.95	1.41	**340%**	1.48	**2.84**	**220%**	0.95
110	1.5	0.075	MOD	13%	40%	1.95	1.17	**280%**	1.21	**2.36**	**150%**	0.65
110	1.5	0.075	SEV	20%	50%	1.95	0.98	**215%**	0.93	**2.04**	**130%**	0.56
110	1.5	0.15	NEW	6%	28%	3.62	2.60	**NF**	NF	**3.74**	**NF**	NF
110	1.5	0.15	MOD	13%	40%	3.62	2.17	**460%**	2.00	**3.12**	**300%**	1.30
110	1.5	0.15	SEV	20%	50%	3.62	1.81	**430%**	1.87	**2.69**	**200%**	0.87
110	1.5	0.25	NEW	6%	28%	5.83	4.20	**NF**	NF	**4.62**	**NF**	NF
110	1.5	0.25	MOD	13%	40%	5.83	3.50	**NF**	NF	**3.9**	**NF**	NF
110	1.5	0.25	SEV	20%	50%	5.83	2.92	**NF**	NF	**3.37**	**400%**	1.74
220	1.5	0	NEW	6%	28%	0.59	0.42	**325%**	1.41	**1.45**	**225%**	0.98
220	1.5	0	MOD	13%	40%	0.59	0.35	**225%**	0.98	**1.21**	**275%**	1.19
220	1.5	0	SEV	20%	50%	0.59	0.29	**135%**	0.59	**1.04**	**140%**	0.61
220	1.5	0.075	NEW	6%	28%	3.91	2.81	**NF**	NF	**2.84**	**425%**	1.84
220	1.5	0.075	MOD	13%	40%	3.91	2.35	**500%**	2.17	**2.36**	**280%**	1.21
220	1.5	0.075	SEV	20%	50%	3.91	1.95	**430%**	1.87	**2.04**	**260%**	1.13
220	1.5	0.15	NEW	6%	28%	7.23	5.21	**NF**	NF	**3.74**	**NF**	NF
220	1.5	0.15	MOD	13%	40%	7.23	4.34	**NF**	NF	**3.12**	**NF**	NF
220	1.5	0.15	SEV	20%	50%	7.23	3.62	**600%**	2.60	**2.69**	**375%**	1.63
220	1.5	0.25	NEW	6%	28%	11.66	8.40	**NF**	NF	**4.62**	**NF**	NF
220	1.5	0.25	MOD	13%	40%	11.66	7.00	**NF**	NF	**3.9**	**NF**	NF
220	1.5	0.25	SEV	20%	50%	11.66	5.83	**NF**	NF	**3.37**	**NF**	NF

*NF – No Fail within limits of study

Table 8.4.8 Pacoima Dam Analysis Comparison: 3.3m Height Wall

GEOMETRY		OVER-BURDEN (MPa)	WALL CONDITION			RIGID BODY (g)	SEMI RIGID (g)	THA		DBA		
(t) (mm)	(h) (m)		(refer Figure 6.4.12)	Δ(1) Δ_{ins}	Δ(2) Δ_{ins}			%EQ	PGA (g)	f_{eff} (Hz)	>FREQ %EQ	>FREQ PGA (g)
50	3.3	0	NEW	6%	28%	0.06	0.04	29%	0.13	0.96	35%	0.15
50	3.3	0	MOD	13%	40%	0.06	0.04	28%	0.12	0.81	30%	0.13
50	3.3	0	SEV	20%	50%	0.06	0.03	33%	0.14	0.7	30%	0.13
50	3.3	0.075	NEW	6%	28%	0.22	0.16	47%	0.20	1.46	50%	0.22
50	3.3	0.075	MOD	13%	40%	0.22	0.13	36%	0.16	1.23	50%	0.22
50	3.3	0.075	SEV	20%	50%	0.22	0.11	33%	0.14	1.06	35%	0.15
50	3.3	0.15	NEW	6%	28%	0.37	0.27	58%	0.25	1.82	60%	0.26
50	3.3	0.15	MOD	13%	40%	0.37	0.22	46%	0.20	1.54	55%	0.24
50	3.3	0.15	SEV	20%	50%	0.37	0.19	49%	0.21	1.33	50%	0.22
50	3.3	0.25	NEW	6%	28%	0.58	0.42	87%	0.38	2.22	60%	0.26
50	3.3	0.25	MOD	13%	40%	0.58	0.35	63%	0.27	1.87	60%	0.26
50	3.3	0.25	SEV	20%	50%	0.58	0.29	49%	0.21	1.62	55%	0.24
110	3.3	0	NEW	6%	28%	0.13	0.10	80%	0.35	0.96	70%	0.30
110	3.3	0	MOD	13%	40%	0.13	0.08	65%	0.28	0.81	70%	0.30
110	3.3	0	SEV	20%	50%	0.13	0.07	50%	0.22	0.7	70%	0.30
110	3.3	0.075	NEW	6%	28%	0.48	0.34	105%	0.46	1.46	115%	0.50
110	3.3	0.075	MOD	13%	40%	0.48	0.29	95%	0.41	1.23	115%	0.50
110	3.3	0.075	SEV	20%	50%	0.48	0.24	75%	0.33	1.06	75%	0.33
110	3.3	0.15	NEW	6%	28%	0.82	0.59	160%	0.69	1.82	135%	0.59
110	3.3	0.15	MOD	13%	40%	0.82	0.49	120%	0.52	1.54	125%	0.54
110	3.3	0.15	SEV	20%	50%	0.82	0.41	100%	0.43	1.33	115%	0.50
110	3.3	0.25	NEW	6%	28%	1.28	0.92	215%	0.93	2.22	135%	0.59
110	3.3	0.25	MOD	13%	40%	1.28	0.77	180%	0.78	1.87	130%	0.56
110	3.3	0.25	SEV	20%	50%	1.28	0.64	130%	0.56	1.62	130%	0.56
220	3.3	0	NEW	6%	28%	0.27	0.19	170%	0.74	0.96	140%	0.61
220	3.3	0	MOD	13%	40%	0.27	0.16	125%	0.54	0.81	130%	0.56
220	3.3	0	SEV	20%	50%	0.27	0.13	105%	0.46	0.7	115%	0.50
220	3.3	0.075	NEW	6%	28%	0.95	0.69	210%	0.91	1.46	220%	0.95
220	3.3	0.075	MOD	13%	40%	0.95	0.57	200%	0.87	1.23	140%	0.61
220	3.3	0.075	SEV	20%	50%	0.95	0.48	150%	0.65	1.06	150%	0.65
220	3.3	0.15	NEW	6%	28%	1.64	1.18	325%	1.41	1.82	260%	1.13
220	3.3	0.15	MOD	13%	40%	1.64	0.98	290%	1.26	1.54	260%	1.13
220	3.3	0.15	SEV	20%	50%	1.64	0.82	190%	0.82	1.33	260%	1.13
220	3.3	0.25	NEW	6%	28%	2.55	1.84	435%	1.89	2.22	275%	1.19
220	3.3	0.25	MOD	13%	40%	2.55	1.53	425%	1.84	1.87	260%	1.13
220	3.3	0.25	SEV	20%	50%	2.55	1.28	265%	1.15	1.62	260%	1.13

*NF – No Fail within limits of study

Table 8.4.9 Pacoima Dam Analysis Comparison: 4.0m Height Wall

GEOMETRY		OVER-	WALL CONDITION			RIGID	SEMI	THA		DBA		
(t) (mm)	(h) (m)	BURDEN (MPa)	(refer Figure 6.4.12)	Δ(1) Δ_{ins}	Δ(2) Δ_{ins}	BODY (g)	RIGID (g)	%EQ	PGA (g)	f_{eff} (Hz)	>FREQ %EQ	>FREQ PGA (g)
50	4	0	NEW	6%	28%	0.05	0.04	**36%**	0.16	**0.88**	**30%**	0.13
50	4	0	MOD	13%	40%	0.05	0.03	**23%**	0.10	**0.74**	**28%**	0.12
50	4	0	SEV	20%	50%	0.05	0.03	**31%**	0.13	**0.64**	**28%**	0.12
50	4	0.075	NEW	6%	28%	0.16	0.11	**40%**	0.17	**1.26**	**55%**	0.24
50	4	0.075	MOD	13%	40%	0.16	0.09	**32%**	0.14	**1.06**	**35%**	0.15
50	4	0.075	SEV	20%	50%	0.16	0.08	**33%**	0.14	**0.92**	**30%**	0.13
50	4	0.15	NEW	6%	28%	0.26	0.19	**53%**	0.23	**1.55**	**55%**	0.24
50	4	0.15	MOD	13%	40%	0.26	0.16	**37%**	0.16	**1.31**	**50%**	0.22
50	4	0.15	SEV	20%	50%	0.26	0.13	**47%**	0.20	**1.13**	**45%**	0.20
50	4	0.25	NEW	6%	28%	0.40	0.29	**60%**	0.26	**1.01**	**60%**	0.26
50	4	0.25	MOD	13%	40%	0.40	0.24	**48%**	0.21	**1.58**	**55%**	0.24
50	4	0.25	SEV	20%	50%	0.40	0.20	**50%**	0.22	**1.36**	**50%**	0.22
110	4	0	NEW	6%	28%	0.11	0.08	**70%**	0.30	**0.88**	**70%**	0.30
110	4	0	MOD	13%	40%	0.11	0.07	**50%**	0.22	**0.74**	**70%**	0.30
110	4	0	SEV	20%	50%	0.11	0.06	**70%**	0.30	**0.64**	**70%**	0.30
110	4	0.075	NEW	6%	28%	0.34	0.25	**85%**	0.37	**1.26**	**115%**	0.50
110	4	0.075	MOD	13%	40%	0.34	0.21	**75%**	0.33	**1.06**	**75%**	0.33
110	4	0.075	SEV	20%	50%	0.34	0.17	**70%**	0.30	**0.92**	**70%**	0.30
110	4	0.15	NEW	6%	28%	0.58	0.42	**120%**	0.52	**1.55**	**125%**	0.54
110	4	0.15	MOD	13%	40%	0.58	0.35	**90%**	0.39	**1.31**	**115%**	0.50
110	4	0.15	SEV	20%	50%	0.58	0.29	**80%**	0.35	**1.13**	**100%**	0.43
110	4	0.25	NEW	6%	28%	0.89	0.64	**175%**	0.76	**1.01**	**130%**	0.56
110	4	0.25	MOD	13%	40%	0.89	0.53	**130%**	0.56	**1.58**	**130%**	0.56
110	4	0.25	SEV	20%	50%	0.89	0.44	**105%**	0.46	**1.36**	**115%**	0.50
220	4	0	NEW	6%	28%	0.22	0.16	**135%**	0.59	**0.88**	**135%**	0.59
220	4	0	MOD	13%	40%	0.22	0.13	**125%**	0.54	**0.74**	**125%**	0.54
220	4	0	SEV	20%	50%	0.22	0.11	**135%**	0.59	**0.64**	**120%**	0.52
220	4	0.075	NEW	6%	28%	0.69	0.49	**200%**	0.87	**1.26**	**220%**	0.95
220	4	0.075	MOD	13%	40%	0.69	0.41	**155%**	0.67	**1.06**	**150%**	0.65
220	4	0.075	SEV	20%	50%	0.69	0.34	**135%**	0.59	**0.92**	**135%**	0.59
220	4	0.15	NEW	6%	28%	1.15	0.83	**255%**	1.11	**1.55**	**255%**	1.11
220	4	0.15	MOD	13%	40%	1.15	0.69	**225%**	0.98	**1.31**	**220%**	0.95
220	4	0.15	SEV	20%	50%	1.15	0.58	**165%**	0.72	**1.13**	**190%**	0.82
220	4	0.25	NEW	6%	28%	1.78	1.28	**345%**	1.50	**1.01**	**260%**	1.13
220	4	0.25	MOD	13%	40%	1.78	1.07	**310%**	1.34	**1.58**	**260%**	1.13
220	4	0.25	SEV	20%	50%	1.78	0.89	**215%**	0.93	**1.36**	**220%**	0.95

*NF – No Fail within limits of study

Table 8.4.10 Nahanni Analysis Comparison: 1.5m Height Wall

GEOMETRY		OVER-BURDEN (MPa)	WALL CONDITION			RIGID BODY (g)	SEMI RIGID (g)	THA		DBA		
(t) (mm)	(h) (m)		(refer Figure 6.4.12)	$\Delta(1)$ Δ_{ins}	$\Delta(2)$ Δ_{ins}			%EQ	PGA (g)	f_{eff} (Hz)	>FREQ %EQ	>FREQ PGA (g)
50	1.5	0	NEW	6%	28%	0.13	0.10	**240%**	0.55	**1.45**	**400%**	0.91
50	1.5	0	MOD	13%	40%	0.13	0.08	**410%**	0.94	**1.21**	**400%**	0.91
50	1.5	0	SEV	20%	50%	0.13	0.07	**500%**	1.14	**1.04**	**400%**	0.91
50	1.5	0.075	NEW	6%	28%	0.89	0.64	**330%**	0.75	**2.84**	**475%**	1.09
50	1.5	0.075	MOD	13%	40%	0.89	0.53	**320%**	0.73	**2.36**	**420%**	0.96
50	1.5	0.075	SEV	20%	50%	0.89	0.44	**410%**	0.94	**2.04**	**410%**	0.94
50	1.5	0.15	NEW	6%	28%	1.64	1.18	**380%**	0.87	**3.74**	**600%**	1.37
50	1.5	0.15	MOD	13%	40%	1.64	0.99	**360%**	0.82	**3.12**	**550%**	1.26
50	1.5	0.15	SEV	20%	50%	1.64	0.82	**340%**	0.78	**2.69**	**420%**	0.96
50	1.5	0.25	NEW	6%	28%	2.65	1.91	**400%**	0.91	**4.62**	**900%**	2.06
50	1.5	0.25	MOD	13%	40%	2.65	1.59	**NF**	NF	**3.9**	**750%**	1.71
50	1.5	0.25	SEV	20%	50%	2.65	1.33	**NF**	NF	**3.37**	**600%**	1.37
110	1.5	0	NEW	6%	28%	0.29	0.21	**550%**	1.26	**1.45**	**900%**	2.06
110	1.5	0	MOD	13%	40%	0.29	0.18	**900%**	2.06	**1.21**	**900%**	2.06
110	1.5	0	SEV	20%	50%	0.29	0.15	**1050%**	2.40	**1.04**	**900%**	2.06
110	1.5	0.075	NEW	6%	28%	1.95	1.41	**750%**	1.71	**2.84**	**900%**	2.06
110	1.5	0.075	MOD	13%	40%	1.95	1.17	**900%**	2.06	**2.36**	**900%**	2.06
110	1.5	0.075	SEV	20%	50%	1.95	0.98	**750%**	1.71	**2.04**	**900%**	2.06
110	1.5	0.15	NEW	6%	28%	3.62	2.60	**NF**	NF	**3.74**	**1500%**	3.43
110	1.5	0.15	MOD	13%	40%	3.62	2.17	**950%**	2.17	**3.12**	**1200%**	2.74
110	1.5	0.15	SEV	20%	50%	3.62	1.81	**850%**	1.94	**2.69**	**1000%**	2.28
110	1.5	0.25	NEW	6%	28%	5.83	4.20	**NF**	NF	**4.62**	**NF**	NF
110	1.5	0.25	MOD	13%	40%	5.83	3.50	**NF**	NF	**3.9**	**1600%**	3.66
110	1.5	0.25	SEV	20%	50%	5.83	2.92	**NF**	NF	**3.37**	**1300%**	2.97
220	1.5	0	NEW	6%	28%	0.59	0.42	**1100%**	2.51	**1.45**	**1760%**	4.02
220	1.5	0	MOD	13%	40%	0.59	0.35	**1800%**	4.11	**1.21**	**1760%**	4.02
220	1.5	0	SEV	20%	50%	0.59	0.29	**2200%**	5.03	**1.04**	**1760%**	4.02
220	1.5	0.075	NEW	6%	28%	3.91	2.81	**1400%**	3.20	**2.84**	**NF**	NF
220	1.5	0.075	MOD	13%	40%	3.91	2.35	**1300%**	2.97	**2.36**	**1800%**	4.11
220	1.5	0.075	SEV	20%	50%	3.91	1.95	**1600%**	3.66	**2.04**	**1800%**	4.11
220	1.5	0.15	NEW	6%	28%	7.23	5.21	**NF**	NF	**3.74**	**NF**	NF
220	1.5	0.15	MOD	13%	40%	7.23	4.34	**2000%**	4.57	**3.12**	**NF**	NF
220	1.5	0.15	SEV	20%	50%	7.23	3.62	**1700%**	3.88	**2.69**	**1900%**	4.34
220	1.5	0.25	NEW	6%	28%	11.66	8.40	**NF**	NF	**4.62**	**NF**	NF
220	1.5	0.25	MOD	13%	40%	11.66	7.00	**NF**	NF	**3.9**	**NF**	NF
220	1.5	0.25	SEV	20%	50%	11.66	5.83	**NF**	NF	**3.37**	**NF**	NF

*NF – No Fail within limits of study

Table 8.4.11 Nahanni Analysis Comparison: 3.3m Height Wall

GEOMETRY		OVER-BURDEN (MPa)	WALL CONDITION			RIGID BODY (g)	SEMI RIGID (g)	THA		DBA		
(t) (mm)	(h) (m)		(refer Figure 6.4.12)	Δ(1) Δ_{ins}	Δ(2) Δ_{ins}			%EQ	PGA (g)	f_{eff} (Hz)	>FREQ %EQ	>FREQ PGA (g)
50	3.3	0	NEW	6%	28%	0.06	0.04	360%	0.82	0.96	400%	0.91
50	3.3	0	MOD	13%	40%	0.06	0.04	500%	1.14	0.81	400%	0.91
50	3.3	0	SEV	20%	50%	0.06	0.03	NF	NF	0.7	400%	0.91
50	3.3	0.075	NEW	6%	28%	0.22	0.16	360%	0.82	1.46	400%	0.91
50	3.3	0.075	MOD	13%	40%	0.22	0.13	420%	0.96	1.23	400%	0.91
50	3.3	0.075	SEV	20%	50%	0.22	0.11	440%	1.01	1.06	400%	0.91
50	3.3	0.15	NEW	6%	28%	0.37	0.27	360%	0.82	1.82	400%	0.91
50	3.3	0.15	MOD	13%	40%	0.37	0.22	340%	0.78	1.54	400%	0.91
50	3.3	0.15	SEV	20%	50%	0.37	0.19	280%	0.64	1.33	400%	0.91
50	3.3	0.25	NEW	6%	28%	0.58	0.42	360%	0.82	2.22	410%	0.94
50	3.3	0.25	MOD	13%	40%	0.58	0.35	NF	NF	1.87	400%	0.91
50	3.3	0.25	SEV	20%	50%	0.58	0.29	360%	0.82	1.62	400%	0.91
110	3.3	0	NEW	6%	28%	0.13	0.10	1050%	2.40	0.96	900%	2.06
110	3.3	0	MOD	13%	40%	0.13	0.08	NF	NF	0.81	900%	2.06
110	3.3	0	SEV	20%	50%	0.13	0.07	NF	NF	0.7	900%	2.06
110	3.3	0.075	NEW	6%	28%	0.48	0.34	1050%	2.40	1.46	900%	2.06
110	3.3	0.075	MOD	13%	40%	0.48	0.29	600%	1.37	1.23	900%	2.06
110	3.3	0.075	SEV	20%	50%	0.48	0.24	1000%	2.28	1.06	900%	2.06
110	3.3	0.15	NEW	6%	28%	0.82	0.59	1050%	2.40	1.82	900%	2.06
110	3.3	0.15	MOD	13%	40%	0.82	0.49	980%	2.24	1.54	900%	2.06
110	3.3	0.15	SEV	20%	50%	0.82	0.41	1000%	2.28	1.33	900%	2.06
110	3.3	0.25	NEW	6%	28%	1.28	0.92	1050%	2.40	2.22	900%	2.06
110	3.3	0.25	MOD	13%	40%	1.28	0.77	750%	1.71	1.87	900%	2.06
110	3.3	0.25	SEV	20%	50%	1.28	0.64	1000%	2.28	1.62	900%	2.06
220	3.3	0	NEW	6%	28%	0.27	0.19	2050%	4.68	0.96	1760%	4.02
220	3.3	0	MOD	13%	40%	0.27	0.16	2050%	4.68	0.81	1760%	4.02
220	3.3	0	SEV	20%	50%	0.27	0.13	NF	NF	0.7	1760%	4.02
220	3.3	0.075	NEW	6%	28%	0.95	0.69	2050%	4.68	1.46	1760%	4.02
220	3.3	0.075	MOD	13%	40%	0.95	0.57	1600%	3.66	1.23	1760%	4.02
220	3.3	0.075	SEV	20%	50%	0.95	0.48	2000%	4.57	1.06	1760%	4.02
220	3.3	0.15	NEW	6%	28%	1.64	1.18	2050%	4.68	1.82	1800%	4.11
220	3.3	0.15	MOD	13%	40%	1.64	0.98	1800%	4.11	1.54	1800%	4.11
220	3.3	0.15	SEV	20%	50%	1.64	0.82	2000%	4.57	1.33	1760%	4.02
220	3.3	0.25	NEW	6%	28%	2.55	1.84	2100%	4.80	2.22	1800%	4.11
220	3.3	0.25	MOD	13%	40%	2.55	1.53	1500%	3.43	1.87	1800%	4.11
220	3.3	0.25	SEV	20%	50%	2.55	1.28	2050%	4.68	1.62	1800%	4.11

*NF – No Fail within limits of study

Table 8.4.12 Nahanni Analysis Comparison: 4.0m Height Wall

GEOMETRY		OVER-BURDEN (MPa)	WALL CONDITION			RIGID BODY (g)	SEMI RIGID (g)	THA		DBA		
(t) (mm)	(h) (m)		(refer Figure 6.4.12)	Δ(1) Δ_{ins}	Δ(2) Δ_{ins}			%EQ	PGA (g)	f_{eff} (Hz)	>FREQ %EQ	>FREQ PGA (g)
50	4	0	NEW	6%	28%	0.05	0.04	**NF**	NF	**0.88**	**400%**	0.91
50	4	0	MOD	13%	40%	0.05	0.03	**NF**	NF	**0.74**	**400%**	0.91
50	4	0	SEV	20%	50%	0.05	0.03	**240%**	0.55	**0.64**	**400%**	0.91
50	4	0.075	NEW	6%	28%	0.16	0.11	**380%**	0.87	**1.26**	**400%**	0.91
50	4	0.075	MOD	13%	40%	0.16	0.09	**410%**	0.94	**1.06**	**400%**	0.91
50	4	0.075	SEV	20%	50%	0.16	0.08	**NF**	NF	**0.92**	**400%**	0.91
50	4	0.15	NEW	6%	28%	0.26	0.19	**380%**	0.87	**1.55**	**400%**	0.91
50	4	0.15	MOD	13%	40%	0.26	0.16	**280%**	0.64	**1.31**	**400%**	0.91
50	4	0.15	SEV	20%	50%	0.26	0.13	**420%**	0.96	**1.13**	**400%**	0.91
50	4	0.25	NEW	6%	28%	0.40	0.29	**380%**	0.87	**1.01**	**400%**	0.91
50	4	0.25	MOD	13%	40%	0.40	0.24	**380%**	0.87	**1.58**	**400%**	0.91
50	4	0.25	SEV	20%	50%	0.40	0.20	**300%**	0.69	**1.36**	**400%**	0.91
110	4	0	NEW	6%	28%	0.11	0.08	**1050%**	2.40	**0.88**	**900%**	2.06
110	4	0	MOD	13%	40%	0.11	0.07	**NF**	NF	**0.74**	**900%**	2.06
110	4	0	SEV	20%	50%	0.11	0.06	**NF**	NF	**0.64**	**900%**	2.06
110	4	0.075	NEW	6%	28%	0.34	0.25	**1050%**	2.40	**1.26**	**900%**	2.06
110	4	0.075	MOD	13%	40%	0.34	0.21	**500%**	1.14	**1.06**	**900%**	2.06
110	4	0.075	SEV	20%	50%	0.34	0.17	**1000%**	2.28	**0.92**	**900%**	2.06
110	4	0.15	NEW	6%	28%	0.58	0.42	**1050%**	2.40	**1.55**	**900%**	2.06
110	4	0.15	MOD	13%	40%	0.58	0.35	**750%**	1.71	**1.31**	**900%**	2.06
110	4	0.15	SEV	20%	50%	0.58	0.29	**550%**	1.26	**1.13**	**900%**	2.06
110	4	0.25	NEW	6%	28%	0.89	0.64	**1050%**	2.40	**1.01**	**900%**	2.06
110	4	0.25	MOD	13%	40%	0.89	0.53	**1100%**	2.51	**1.58**	**900%**	2.06
110	4	0.25	SEV	20%	50%	0.89	0.44	**800%**	1.83	**1.36**	**900%**	2.06
220	4	0	NEW	6%	28%	0.22	0.16	**NF**	NF	**0.88**	**1760%**	4.02
220	4	0	MOD	13%	40%	0.22	0.13	**NF**	NF	**0.74**	**1760%**	4.02
220	4	0	SEV	20%	50%	0.22	0.11	**NF**	NF	**0.64**	**1760%**	4.02
220	4	0.075	NEW	6%	28%	0.69	0.49	**2000%**	4.57	**1.26**	**1760%**	4.02
220	4	0.075	MOD	13%	40%	0.69	0.41	**1100%**	2.51	**1.06**	**1760%**	4.02
220	4	0.075	SEV	20%	50%	0.69	0.34	**1950%**	4.45	**0.92**	**1760%**	4.02
220	4	0.15	NEW	6%	28%	1.15	0.83	**2000%**	4.57	**1.55**	**1760%**	4.02
220	4	0.15	MOD	13%	40%	1.15	0.69	**1700%**	3.88	**1.31**	**1760%**	4.02
220	4	0.15	SEV	20%	50%	1.15	0.58	**1100%**	2.51	**1.13**	**1760%**	4.02
220	4	0.25	NEW	6%	28%	1.78	1.28	**2000%**	4.57	**1.01**	**1800%**	4.11
220	4	0.25	MOD	13%	40%	1.78	1.07	**1600%**	3.66	**1.58**	**1760%**	4.02
220	4	0.25	SEV	20%	50%	1.78	0.89	**1600%**	3.66	**1.36**	**1760%**	4.02

*NF – No Fail within limits of study

9. SUMMARY AND CONCLUSIONS

This report has presented the findings of an investigation into the weak links in the seismic load path of unreinforced masonry buildings specifically aimed at Australian masonry construction being:

(1) The limited force capacity of connections between floors and walls, in particular the friction dependent connections containing damp proof course (DPC) membranes and

(2) the out-of-plane failure of walls in the upper stories of URM buildings.

The two prime objectives of this investigation were thus to provide designers with the appropriate tools to avoid these brittle 'weak link' failure modes in the design of new and the assessment of existing URM buildings. Once adequate seismic load paths have been developed and these 'weak links' successfully avoided it is expected that carefully designed, detailed and constructed regular URM buildings will behave adequately during moderate intensity earthquakes.

The first of the above objectives was fulfilled by an extensive series of shaking table tests on URM connections containing DPC membrane typical found in Australian masonry construction being aimed at providing data on the connections dynamic capacity applicable (refer Chapter 4). The main purpose of these tests was therefore to evaluate the connection performance under dynamic loading in order to assess their seismic integrity. Dynamic friction coefficients determined from these tests were then compared with quasi-static friction coefficients determined by previous research (Griffith et al 1998) to assess to what extent the quasi-statically determined friction coefficients represented those which could be expected in seismic events. Here it was found that the dynamic friction coefficients were not more than 20% less than those determined quasi-

statically. Further with the exception of greased galvanised sheets no connection had a friction coefficient less than the AS3700-1998 code prescribed design value of 0.3.

The second of the above objectives was achieved by the development of a simplistic rational analysis procedure for face loaded simply supported URM walls for practical applications which considers the essence of the true dynamic response behaviour. Since the simplified procedure was required to be both user friendly and readily codified it was developed from the increasingly popular linearised 'Displacement-based' method. Various boundary conditions for URM walls are often encountered which can significantly impact on the wall's dynamic behaviour. The analysis procedure therefore needed to have the ability of easily accounting for these conditions. Also, with poor quality masonry, lack of maintenance and poor workmanship arising as major issues from previous earthquake reconnaissance documentation, the analysis needed to have the capability of allowing for rotation joint condition over the life of the wall. Both of these requirements were taken into account by modifications to the modelled F-Δ relationship (refer Chapter 8). The following paragraphs briefly describe the steps undertaken to develop this procedure:

To gain a better understanding of the physical process governing the out-of-plane behaviour of URM walls an extensive series of out-of-plane static and dynamic tests were undertaken on one-way spanning wall panels as presented in Chapter 6. Test variables included the level of overburden stress and wall aspect ratio, however, only one set of boundary conditions was examined. Joint degradation was also examined as part of the experimental phase.

A comprehensive THA program was then developed to accurately model the dynamic wall behaviour, as presented in Chapter 7. Here the rocking wall was modelled as a single degree of freedom (SDOF) system having a non-linear spring and frequency dependent damper. The relationships between the real and SDOF systems were determined by comparison of the dynamic equations of motion. The modelled non-linear spring and frequency dependent damper were then calibrated by comparison with experimentally determined F-Δ and f-ξ relationships. Results of the THA were then confirmed by

comparison with experimental results including free vibration tests, single pulse, harmonic and transient excitation tests.
Following confirmation of the THA, results were used to undertake parametric studies to further identify key properties of URM wall behaviour without the expense of continued experimental testing. In total over two hundred thousand THA were completed as part of this process.

The simplified analysis procedure was based on the linearised 'Displacement-based' procedure, used to predict the input excitation required to force the post-cracked URM wall to incipient instability (refer Chapter 8). For the simplified analysis, as most realistic failures are associated with the large displacement amplifications associated with resonance, the characteristic 'substitute structure' linear stiffness was related to the effective resonant frequency of the simply supported wall to permit the wall's resonant behaviour to be modelled. The effective resonant frequency was in turn related to the average incremental secant stiffness of the failure half cycle. Damping was related to a constant lowerbound observed during the experimental phase. As this method linearises a highly non-linear problem it has an inherent degree of inaccuracy for transient excitations where a 'period lag' between the modelled linear SDOF oscillator and the real system. Consequently, the suitability and accuracy of using the simplified method was determined by comparison with THA and experimental results. Although, as expected some result scatter was observed the correlation was substantially better than that of a comparison with 'quasi-static' methods which are currently in use. Therefore, with the provision of suitable safety factors it appears that the proposed linearised DB procedure in conjunction with a 'quasi-statically' determined lowerbound force provides an improved method for assessing the dynamic capacity for the design of new and the assessment of existing URM buildings.

REFERENCES

ABK - A Joint Venture, "Methodology for the Mitigation of Seismic Hazards in Existing Unreinforced Masonry Buildings: The Methodology", Topical Report 08, 1984

ABRAMS, D., DEMPSTER, A., "Seismic Analysis of Masonry Buildings", Elsevier Science Ltd., 1998, Paper reference T126-6

ABRAMS, D., P., " Effects of Scale and Loading Rate with tests of Concrete and Masonry Structures", Earthquake Spectra, Journal of the Earthquake Engineering Research Institute, Volume 12, No.1, 1996, pp.13-28.

ABRAMS, D., P., "A Lesson Learned From Loma Prieta on Vulnerability of URM Construction East of the Rockies", Proceedings of the National earthquake Conference, USA, 1993, pp. 143-151

ABRAMS, D., P., "Strength and Behaviour of Unreinforced Masonry Elements", Proceedings of the 10th World Conference on Earthquake Engineering, Rotterdam, 1992, pp.3475-3480.

ABRAMS, D., P., ANGEL, R., UZARSKI, J., "Out-of-Plane Strength of Unreinforced Masonry Infill Panels", Earthquake Spectra, Vol. 12, No. 4, 1996, pp. 825-844

ABRAMS, D., P., PAVESE, A., MAGENES, G., CALVI, G., M., "Large Scale Seismic Testing of Unreinforced Brick Masonry Building", Proceedings of the 5th National Conference on Earthquake Engineering, Vol. 1, 1994, pp.137-145

ABRAMS, D., P., TENA-COLUNGA, A., "Seismic Behaviour of Structures with Flexible Diaphragms", Journal of Structural Engineering, 1996, pp. 439-445.

ABRAMS, D., P., PAULSON, T., J.," Correlation between Static and Dynamic Response of Model Masonry Structures", Earthquake Spectra, Journal of the Earthquake Engineering Research Institute, Volume 6, No.3, 1990, pp.573-591

ABRAMS, P., D., "USA Masonry Today and Seismic Rehabilitation of Masonry Buildings", Proceedings of the 4th Australasian Masonry Conference, Sydney, 1995, pp.1-13

ADHAM, S., A., "Static and Dynamic Out of Plane Response of Brick Masonry Walls", Proceedings of the 7th International Brick Masonry Conference, Melbourne, 1985, pp.1218-1224

ALCOCER, SERGIO, "June 1999 Mexico Earthquake", National Information Service for Earthquake Engineering, University of California, Berkley, http://www.eerc.berkley.edu/mexico/alcocer.htm, 1999

ANDERSON, C., "Arching Action in Transverse Laterally Loaded Masonry Wall Panels", The Structural Engineer, Vol. 62B, No. 1, 1984, pp. 12-23

ANDERSON, C., "Transverse Laterally Loaded Tests on Single Leaf and Cavity Walls", CIB 3rd International Symposium on Wall Structures, Vol. 1, Warsaw, 1984, pp. 93-103

ANICIC, D., STEINMAN, V., "Tensile Strength of Masonry Walls as a Factor of Earthquake Resistance of Masonry Buildings", CIB 3rd International Symposium on Wall Structures, Vol. 2, Warsaw, 1984, pp. 253-267

ANTHOINE, A., MAGONETTE, G., MAGENES, G., "Shear-Compression Testing and Analysis of Brick Masonry Walls", Proceedings of the 10th European Conference on Earthquake Engineering, Vol. 3, Rotterdam, 1995, pp.1657 - 1662

Applied Technology Council "Tentative Provisions For The Development of Seismic Regulations For Buildings", ACT 3-06

AS/NZS 2904-1995, Damp-proof Courses and Flashings, Standards Australia, Sydney, 1995

ASTANEH-ASL, A., MODJTAHEDI, D., McMULLIN, K., SHEN, J., D'AMORE, E., "Stability of Damaged Steel Moment Frames in Los Angeles", Engineering Structures, Vol. 20, No 4-6, 1998, pp. 425-432

ATC – Applied Technology Council 1988, ATC 3-3-06 "Tentative Provisions for the Development of Seismic Provisions for Buildings", National Bureau of Standards, Washington, DC

AUSTRALIAN GEOLOGICAL SURVEY ORGANISATION, Earthquake Information, http://www.bmr.gov.au/geohazards/quakes, 1999

BACHMANN, H., LINDE, P., WENK, T., "Capacity Design and Nonlinear Dynamic Analysis of Earthquake Resistant Structures", Proceedings of the 10th European Conference on Earthquake Engineering, Vol. 1, Rotterdam, 1995, pp. 11 – 20

BAKER, L., R., "Pre-cracking of Behaviour of Laterally Loaded Behaviour with In-Plane Restraints", Proceedings of The British Ceramic Society, No.27, 1978, pp.129-146

BAKER, L., R., "Structural Action of Brickwork Panels Subjected to Wind Loads", Journal of The Australian Ceramic Society, No. 1, Vol.9, 1973, pp. 8-13

BAKER, L., R., "Variation in Flexural Strength of Brickwork With Beam and Span Loading", Journal of The Australian Ceramic Society, May 1974, No. 2, Vol.10, pp. 28-31

BARIOLA, J., GINOCCHIO, J., F., QUINN, D., "Out of Plane Seismic Response of Brick Walls", Proceedings of the 5th North American Masonry Conference, 1990, pp.429-439

BASE, G., D., BAKER, L., R., "Fundamental Properties of Structural Brickwork", Journal of The Australian Ceramic Society, No. 1, Vol.9, 1973, pp. 1-7

BEARD, R., DINNIE, A., RICHARDS, R., "Movement of Brickwork", Transactions of the British Ceramic Society, Vol. 68, No. 2, 1969, pp. 45-96

BEEBY, A., W., CROOK, R., N., READ, J., B., "Behaviour of Slender Concrete Block Walls Under Vertical Loads", CIB 3rd International Symposium on Wall Structures, Vol. 1, Warsaw, 1984, pp. 123-130

BEER, F., P., JOHNSTON, E., R., "Mechanics for Engineers - Statics", McGraw Hill Book Company, 1987

BELL, D., K., McNAUGHTON, H., DAVIDSON, B., J., "Seismic Evaluation of an Unreinforced Masonry Building", Proceedings of the 1998 Technical Seminar of the New Zealand National Society of Earthquake Engineering, 1998, pp. 175-181

BENEDETTI, D, CARYDIS, P., PEZZOLI, P., "Shaking Table Tests on 24 Simple Masonry Buildings", Earthquake Engineering and Structural Dynamics, Vol. 27, 1998, pp.67-90

BENUSKA, K., L., " Loma Prieta Earthquake Reconnaissance Report", Earthquake Spectra, Journal of the Earthquake Engineering Research Institute, Vol. 6, May 1990, pp.127-149.

BLAKIE, E., L., SPUR, D., D., "Earthquake Vulnerability of Existing Unreinforced Masonry Buildings", EQC, Works Consultancy Services, Wellington, 1992

BLONG, R., J., "Domestic Insured Losses and the Newcastle Earthquake", Proceedings of the Australian Earthquake Engineering Society Conference, Sydney, Australia, 1992, pp. 70-83

BLONG, R., W., "Hazard Micronization of Melbourne", Proceedings of the Earthquake Engineering and Disaster Reduction Seminar, Australian Earthquake Engineering Society, Melbourne, 1993, pp. 107-117

BOLT, B., A., "Intraplate Seismicity and Zonation", Bulletin of the New Zealand National Society for Earthquake Engineering, Vol. 29, No.4, 1996, pp. 221-227

BOUSSABAH, L., BRUNEAU, M., "Review of the Seismic Performance of Unreinforced Masonry Walls", Proceedings of the Tenth World Conference on Earthquake Engineering, Madrid, Spain, 1992

BRITISH GEOLOGICAL GROUP (BGS), http://www.gsrg.nmh.ac.uk, 1999

BROOKS, D., S., "Strength and Stability of Brick Masonry Walls", Research Report No. R30, The University of Adelaide, Department of Civil and Environmental Engineering, 1980

BRUNEAU, M., "Seismic Evaluation of Unreinforced Masonry Buildings - A State of the Art Report", Canadian Journal of Civil Engineering, No. 21, 1994, pp.512-539

BRUNEAU, M., "State-of-the-Art Report on Seismic Performance of Unreinforced Masonry Buildings", American Society of Civil Engineers, Journal of Structural Engineering, Vol. 120, No. 1, 1994, pp. 230-251

BRUNEAU, M., YOSHIMURA, K., "Damage to Masonry Buildings Caused by the 1995 Hyogo-ken (Kobe-Japan) Earthquake", Canadian Journal of Civil Engineering, Vol. 23, No. 3, 1996, pp.797-807

BUBB, C., T., J., "Earthquake Engineering in Australia – Before Meckering and After Newcastle", Bulletin of the New Zealand National Society for Earthquake Engineering, Vol. 32, No.1, 1999, pp.13-20

BUBB, G., "Behaviour of Structures – Council Buildings", Proceedings of the Conference on the Newcastle Earthquake, Newcastle, Australia, 1990, pp.26-27

BUCCINO, F., VITIELLO, E., "Experimental Behaviour and Design Criteria for Anchorage Between Slabs and Brick Walls", Proceedings of the 10th European Conference on Earthquake Engineering, Vol. 3, Rotterdam, 1995, pp. 2255 - 2260

CALVI, G., M., KINGSLEY, G., R., MAGENES, G., "Testing of Masonry Structures for Seismic Assessment", Earthquake Spectra, Volume 12, No.1, 1996.

CALVI, G., M., PAVESE, A., "Application of Dynamic Identification Techniques to a Brick Masonry Building Prototype", Proceedings of the 10th European Conference on Earthquake Engineering, Vol. 3, Rotterdam, 1995, pp. 2413 - 2418

CHOPRA, A., K., "Dynamics of Structures – Theory and Applications to Earthquake Engineering", Prentice-Hall, 1995

CHRISTOPHSEN, A., "Magnitude and Catalogue Completeness Study", Proceedings of the 1999 Technical Seminar of the New Zealand National Society of Earthquake Engineering, 1999, pp. 156-162

CLOUGH, R., W., GÜLKAN, P., MANOS, G., C., MAYES, R., L., "Seismic Testing of Single-Story Masonry Houses: Part 1", Journal of Structural Engineering, Vol. 116, No. 1, 1990, pp. 235-256

CLOUGH, R., W., GÜLKAN, P., MANOS, G., C., MAYES, R., L., "Seismic Testing of Single-Story Masonry Houses: Part 2", Journal of Structural Engineering, Vol. 116, No. 1, 1990, pp. 257-2274

CLOUGH, R., W., PENZIAN, J., "Dynamics of Structures", Second Edition, McGraw-Hill, Inc., 1993

COLE, W., LEWIS, R., "A Note on the Moisture Expansion of Unrestrained Experimental Brick Walls", Journal of the Australian Ceramic Society, November, No.3, Vol.10, 1974, pp.55

Concrete Masonry Association of Australia and South Australian Clay Brick Association Incorporated, "A Guide to Masonry Construction", 1983

CORNELIUSSEN, R., D., "Failure of Plastics", Hanser Publishers, 1986

CORTELL, R., "Numerical Analysis and Dynamic Problems with Negative Stiffness", Computers and Structures, Vol. 61, No. 6, 1996, pp. 1009-1011

CRANSTON, W., B., ROBERTS, J., J., " The Structural Behaviour of Concrete Masonry - Reinforced and Unreinforced", The Structural Engineer, No. 11, Vol. 54, 1976, pp. 423-436

CURTIN, W., G., SHAW, G., BECK, J., K., PARKINSON, G., I., "Masonry Fin Walls", The Structural Engineer, Vol. 62A, No. 7, 1984, pp. 203-210

CURTIN, W., G., SHAW, G., BECK, J., K., BRAY, W., A., "Structural Masonry Designers Manual", Granada Publishing Limited, Great Britain, 1982

DAVIDSON, B., J., BRAMMER, D., R., "Cyclic Performance of Nominally Reinforced Masonry Walls", Proceedings of the 1996 Technical Seminar of the New Zealand National Society of Earthquake Engineering, New Plymouth, 1996, pp. 144-151

DE VEKEY, R., C., BRIGHT, N., J., LUCKIN, K., R., ARORA, S., K., "The Resistance of Masonry to Lateral Loading - Research Results on Autoclaved Aerated Concrete Blockwork", The Structural Engineer, Vol. 64A, No. 11, 1986, pp. 332-340

DEANIN, R., D., "Polymer Structure, Properties and Applications", Cahners Publishing Company, 1972

DENHAM, D., "Intraplate Earthquakes – Why?", Proceedings of the Australian Earthquake Engineering Society Conference, Sydney, Australia, 1992, pp. 3-6

DEPPE, K., "The Whittier Narrows, California Earthquake of October 1, 1987 - Evaluation of Strengthened and Un-strengthened Unreinforced Masonry in Los Angelies City", Earthquake Spectra, Vol. 4, No. 1, 1988, pp. 157-180

DeVITIS, N., PAGE, A., W., LAWRENCE, S., J., "Influence of Age on The Development of Bond Strength", Proceedings of the 4th Australasian Masonry Conference, Sydney, 1995, pp.299-307

DHANASEKAR, M., "Effect of Central Queensland Sands on the Shear Capacity of Concrete Masonry Containing Damp Proof Course", Proceedings of the 5th Australasian Masonry Conference, Gladstone, Queensland, 1998, pp. 75-83

DHANASEKAR, M., PAGE, A.,W., KLEENMAN, P., W., "The Failure of Brick Masonry Under Biaxial Stresses", Proceedings of The Institution of Civil Engineers, Part 2, 1985, pp. 295-313

DHANASEKAR, M., KLEENMAN, P., W., PAGE, A.,W., "Biaxial Stress-Strain Relationships for Brick Masonry", American Society of Civil Engineers, Journal of Structural Engineering, Vol.111, No.5, 1985, pp.1085-1100

DOBBINS, J., J., "Problems of Chronology, Decoration, and Urban Design in the Forum at Pompeii", Proceedings of the American Journal of Archeology, Vol. 98, No.4, 1994

DOHERTY, K., LAM, N., GRIFFITH, M., WILSON, J., "Investigation in the Weak Links in the Seismic Load Path of Unreinforced Masonry Buildings", Proceedings of the 5th Australasian Masonry Conference, Gladstone, Queensland, 1998, pp.115-128

DOHERTY, K., LAM, N., GRIFFITH, M., WILSON, J., "The Modelling of Earthquake Induced Collapse of Unreinforced Masonry Walls Combining Force and Displacement Principals", Proceedings of the 12th World Conference on Earthquake Engineering, Auckland, New Zealand, 2000, Paper 1645

DOHERTY, K., LAM, N., GRIFFITH, M., WILSON, J., "Modelling the Collapse Behaviour of Unreinforced Masonry Walls During the Newcastle Earthquake", Proceedings of Australian Earthquake Engineering Society, Sydney, 1999

DONALDSON, R., J., "Behaviour of Structures – Patterns of Failure in Domestic Buildings After the 1989 Newcastle Earthquake, Proceedings of the Conference on the Newcastle Earthquake, Newcastle, Australia, 1990, pp.39-43

DOWRICK, D., J., RHOADES, D., A., "Magnitude of New Zealand Earthquakes, 1901-1993", Bulletin of the New Zealand National Society for Earthquake Engineering, Vol. 31, No.4, 1998, pp. 260-280

DRYSDALE, R., G., ESSAWY, A., S., "Out-of-Plane Bending of Concrete Block Walls", American Society of Civil Engineers, Journal of Structural Engineering, No. 1, Vol. 114, 1988, pp. 121-133

DRYSDALE, R., G., HAMID, A.,A., BAKER, L., R., "Masonry Structures - Behaviour and Design", Prentice Hall, 1994

EDWARDS, M., LAM, N., WILSON, J., HUTCHINSON, G., "The Prediction of Earthquake Induced Displacement Demand of Buildings in Australia : An Integrated Approach", Proceedings of the 1999 Technical Seminar of the New Zealand National Society of Earthquake Engineering, Rotorua, 1999, pp. 43-50

ETTER, D., M., "Structured Fortran 77 – For Engineers and Scientists", Second Edition, The Benjamin/Cummings Publishing Company, Inc., 1987

EWING, R., D., "Seismic Performance of Low Rise Concrete and Masonry Buildings", Proceedings of the Workshop for the Seismic Performance of Low Rise Buildings, State-of-the-art and Research Needs, Illinois, 1980, pp. 66-75

EWING, R., D., KARIOTIS, J., C., JOHNSON, A., W., "Predictions of Stability for Unreinforced Brick Masonry Walls Shaken By Earthquakes", Proceedings of the 7th International Brick Masonry Conference, Melbourne, 1985, pp.1175-1183.

EWING, R., D., KARIOTIS, J., C., JOHNSON, A., W., "Strength Determination and Shear Failure Modes of Unreinforced Brick Masonry with Low Strength Mortar", Proceedings of the 7th International Brick Masonry Conference, Melbourne, 1985, pp.1327-1337

FAILLA, A., La MENDOLA, L., PIRROTTA, A., "Flexural Cyclic Behaviour of Masonry Walls Subjected to Horizontal Forces", Proceedings of the 11th Conference on Earthquake Engineering, Balkema, Rotterdam, 1998

FARDIS, M., N., "S.O.A. Lecture: Lessons Learnt in Past Earthquakes", Proceedings of the 10th European Conference on Earthquake Engineering, Vol. 1, Rotterdam, 1995, pp. 779 - 788

FATEMI, S., JAMES., C., "The Long Beach Earthquake of 1933", National Information Service for Earthquake Engineering, University of California, Berkley, http://www.eerc.berkley.edu, 1999

GAD, E., DUFFIELD, C., "Investigation into Domestic Brick Veneer Structures When Subjected to Lateral Loading", Proceedings of the Australasian Structural Engineering Conference, Sydney, 1994, pp. 673-678

GAMBAROTTA, L., LAGOMARSINO, S., "Damage Models for the Seismic Response of Brick Masonry Shear Walls. Part I: The Mortar Joint Model and its Applications", Earthquake Engineering and Structural Dynamics, Vol. 26, 1997, pp.423-439

GAMBAROTTA, L., LAGOMARSINO, S., "Damage Models for the Seismic Response of Brick Masonry Shear Walls. Part II: The Continuum Model and its Applications", Earthquake Engineering and Structural Dynamics, Vol. 26, 1997, pp.441-462

GAMBAROTTA, L., LAGOMARSINO, S., MORBIDUCCI, R., "Brittle-Ductile Response of In-plane Loaded Brick Masonry Walls", Proceedings of the 10th European Conference on Earthquake Engineering, Vol. 3, Rotterdam, 1995, pp. 1663 – 1668

GERE, J., H., TIMONSHENCO, S., P., "Mechanics of Materials", PWS-Kent Publishing Co., Boston, 1990

GHAZALI, M., Z., RIDDINGTON, J., R., "Simple Test Method For Masonry Shear Strength", Technical Note No. 505, Proceedings of The Institution of Civil Engineers Part 2, Vol.85, 1988, pp.567-574

GIBSON, G., "An Introduction to Seismology", Proceedings of the Conference on the Newcastle Earthquake, Newcastle, Australia, 1990, pp.6-8

GLOGAU, O., A., "Masonry Performance in Earthquakes", Bulletin of the New Zealand National Society for Earthquake Engineering, Vol.7, No.4, 1974

GRAHAM, K., J., PAGE, A., W., "Testing of Post-Tensioned Hollow Clay Masonry", Proceedings of the 4th Australasian Masonry Conference, Sydney, 1995, pp.228-239

GRAPES, R., DOWNES, G., "The 1855 Wairarapa, New Zealand, Earthquake – Analysis of Historical Data", Bulletin of the New Zealand National Society for Earthquake Engineering, Vol. 30, No.4, 1997, pp. 271-368

GRIFFITH, M., C., "Performance of Unreinforced Masonry Buildings During the Newcastle Earthquake, Australia", Research Report No. R86, The University of Adelaide, Department of Civil and Environmental Engineering, 1991

GRIFFITH, M., C., PAGE, A., W., "On the Seismic Capacity of Typical DPC and Slip Joints in Unreinforced Masonry Buildings", Australian Journal of Structural Engineering, Vol. SE1, No. 2,1998, pp.133-140

GUGGISBERG, R., THURLIMANN, B., "Failure Criterion for Laterally Loaded Masonry Walls", Proceedings of the 5th North American Masonry Conference, Urbana-Champign, 1990, pp. 949-958

GUPTA, A., K., "Response Spectrum Method in Seismic Analysis and Design of Structures", Blackwell Scientific Publications, Boston Oxford, ISBN 0-86542-115-3

GURLEY, C., "Existing Structures – Requirements and Repairs", Proceedings of the Conference on the Newcastle Earthquake, Newcastle, Australia, 1990, pp.107-113

HAMID, A., DRYSDALE, R., G., "Flexural Tensile Strength of Concrete Block Masonry", Journal of Structural Engineering, Vol. 114, No. 1, 1988, pp. 50-66

HART, G., C., KARIOTIS, J., NOLAND, J., L., "The Whittier Narrows, California Earthquake of October 1, 1987 - Masonry Buildings Performance Survey", Earthquake Spectra, Vol. 4, No. 1, 1988, pp. 181-195

HASELTINE, B., A., TUTT, J., N., "The Resistance of Masonry to Lateral Loading – Implications of Research on Design Implications", The Structural Engineer, Vol. 64A, No. 11, 1986, pp. 341-350

HASELTINE, B., A., WEST, H., W., H., TUTT, J., N., " The Resistance of Brickwork to Lateral Loading - Part 2 - Design of Walls to Resist Lateral Loads", The Structural Engineer, 1977, No. 10, Vol. 55, pp. 422-430

HENDRY, A., W., "The Lateral Strength of Unreinforced Brickwork - Discussion", Structural Engineer, No. 8, Volume 51, 1973

HENDRY, A., W., "The Lateral Strength of Unreinforced Brickwork", Structural Engineer, No. 2, Volume 51, 1973

HENDRY, A., W., "Structural Brickwork", The MacMillan Press Ltd, 1981

HJELMSTAD, K., D., WILLIAMSON, E., B., "Dynamic Stability of Structural Systems Subjected to Base Excitation", Engineering Structures, Vol. 20, No. 4-6, 1998, pp. 425-432,

HOGAN, S., J., "On the Dynamics of Rigid-Block Motion Under Harmonic Forcing", Proceedings of the Royal Society of London, A425, 1989, pp. 442-476

HOUSNER, G., W., "The Behaviour of Inverted Pendulum Structures During Earthquakes", Bulletin of the Seismological Society of America", Vol. 53, No.2, 1963, pp. 403-417

HUTCHINSON, G., WILSON, J., PHAM, L., BILLINGS, I., JURY, R., KING, A., "Developing a Common Australasian Earthquake Loading Standard", Proceedings of the Australasian Structural Engineering Conference, Sydney, 1994, pp. 853-857

IRISH, J., L., "Earthquake Damage Functions For Australian Houses and the Probable Maximum Loss for an Insurance Portfolio", Proceedings of the Australian Earthquake Engineering Society Conference, Sydney, Australia, 1992, pp. 61-69

JAIN, S., K., MURTY, C., V., R., ARLECAR, J., SINHA, R., GOYAL, A., JAIN, C., "Some Observations on Engineering Aspects of the Jabalpur Earthquake of 22 May 1997", EERI Special Earthquake Report, http://www.eeri.org/Reconn/, 1997

JAMES, C., HERNANDEZ, L., "Helena, Montana, 1935", National Information Service for Earthquake Engineering, University of California, Berkley, http://www.eerc.berkley.edu, 1999

JANKULOVSKI, E., PARSANEJAD, S., "Analytical Evaluation of In-Plane Resistance of Unreinforced Masonry Walls", Proceedings of the 4th Australasian Masonry Conference, Sydney, 1995, pp.65-70

JOHNSON, M., W., PIEREPIEKARZ, M., R., "Seismic Strengthening Methods for Unreinforced CMU Partition and Infill Systems", Proceedings of the National Earthquake Conference, 1993

JONES, N., P., CROSS, W., B., "Floor and Wall Interaction in Unreinforced Masonry Buildings", Proceedings of the National Earthquake Conference, Vol. 11, 1993, pp. 215-224.

JORDAN, J., W., LUDLOW, J., N., TRUEMAN, E., G., "The Newcastle Earthquake and Heritage Structures", Proceedings of the 5th National Conference on Engineering Heritage, Perth, 1990

JUDI, H., DAVIDSON, B., FENWICK, R., "A Comparison of Force and Displacement Based Design", Proceedings of the 1998 Technical Seminar of the New Zealand National Society of Earthquake Engineering, 1998, pp. 67-74

KARIOTIS, J., C., EWING, R., D., JOHNSON, A., W., ADHAM, S., A., "Methodology for Mitigation of Earthquake Hazards in Unreinforced Brick Masonry Buildings", Proceedings of the 7th International Brick Masonry Conference, Melbourne, 1985, pp.1339-1350

KAUTTO, J., PAGE, A., W., "The Impact of The Earthquake Loading Code on Masonry Housing", Proceedings of the 4th Australasian Masonry Conference, Sydney, 1995, pp.160-170

KELLY, T., E., "Earthquake Resistance of Unreinforced Masonry Buildings", Proceedings of New Zealand National Society for Earthquake Engineering, 1995, pp. 28-35

KING, A., "Earthquake Loads and Earthquake Resistant Design of Buildings", Proceedings of the Australian Earthquake Engineering Conference, Perth, 1998

KLOPP, G., M., "Seismic Design of Unreinforced Masonry Structures", Ph.D. Thesis, Department of Civil and Environmental Engineering, The University of Adelaide, Australia, 1996

KLOPP, G., M., GRIFFITH, M., C., "Dynamic Characteristics of Existing Masonry Buildings", Proceedings of the Pacific Conference on Earthquake Engineering, New Zealand, 1991, pp187-195.

KLOPP, G., M., GRIFFITH, M., C., "Earthquake Design Requirements for Unreinforced Masonry Buildings in Australia - 2 Case Studies", Proceedings of the Australasian Structural Engineering Conference, Sydney, 1994, pp. 841-846

KLOPP, G., M., GRIFFITH, M., C., "Seismic Analysis of Unreinforced Masonry Buildings in Australia - 2 Case Studies", Australian Journal of Structural Engineering, Vol. SE1, No.2, 1998, pp.121-131

KLOPP, G., M., GRIFFITH, M., C., "Seismic Analysis of Unreinforced Masonry Buildings", Australian Journal of Structural Engineering, Vol. SE1, No. 2, 1998, pp.121-131

KLOPP, G., M., GRIFFITH, M., C., "Shaking Table Tests of Unreinforced Masonry Wall Panels", Australian Journal of Structural Engineering, Vol. SE1, No. 2, 1998, pp. 113-130

KLOPP, G., M., GRIFFITH, M., C., "The Design of Unreinforced Masonry Buildings for Earthquake Induced Forces", Pacific Conference on Earthquake Engineering, Australia, 1995, pp. 87-96

KLOPP, G., M., GRIFFITH, M., C., "The Earthquake Design of Unreinforced Masonry Structures In Areas of Low Seismic Risk", Proceedings of the 3rd National Masonry Seminar, Brisbane Australia, 1994, pp. 19.1-19.9

KLOPP, G., M., GRIFFITH, M., C., "The Earthquake Design of Unreinforced Masonry Structures - Are Existing Period Formulae Suitable", Proceedings of the National Earthquake Conference, 1993, pp. 153-162

KÖNIG, G., MANN, W., ÖTES, A., "Experimental Investigations on the Behaviour of Unreinforced Masonry Walls Under Seismically Induced Loads and Lessons Derived", Proceedings of the 9th World Conference on Earthquake Engineering, Tokyo-Kyoto, 1988, Vol.8, pp.1117-1122

KOO, R., CHENG, M., LAM, N., WILSON, J., HUTCHINSON, G., GRIFFITH, M., "Modelling of the Earthquake Ground Motions Generated by the Newcastle Earthquake", Proceedings of the 1999 Australian Earthquake Engineering Conference, Sydney, 1999

KRAWINKLER, H, " Cyclic Loading Histories for Seismic Experimentation of Structural Components", Earthquake Spectra, Journal of the Earthquake Engineering Research Institute, Volume 12, No.1, 1996, pp.1-11

La MENDOLA, L., PAPIA, M., ZINGONE, G., "Stability of Masonry Walls Subjected to Seismic Transverse Forces", Journal of Structural Engineering, 1995, pp. 1581-1587

LAFUENTE, M., GENATIOS, C., LORRAIN, M., "Analytical Studies of Masonry Walls Subjected to Monotonic Lateral Loads", Proceedings of the 10th European Conference on Earthquake Engineering, Vol. 3, Rotterdam, 1995, pp. 1751 – 1755

LAM, N., NURTUG, A., WILSON, J., "Shaking Table Testing of Parapet Walls with Periodic and Transient Excitations", Departmental of Civil and Environmental Engineering, The University of Melbourne, Departmental Report No. RR/STRUCT/98, 1998

LAM, N., WILSON, J., "Estimation of the Site Natural Period from a Borehole Record", Australian Journal of Structural engineering, Vol. SE1, No. 3, 1999, pp. 179-200

LAM, N., WILSON, J., CHANDLER, A., HUTCHISON, G., "Response Spectrum Modelling in Low and Moderate Seismicity Regions Combining Velocity, Displacement and Acceleration Predictions", Earthquake Engineering and Structural Dynamics (under review)

LAM, N., WILSON, J., EDWARDS, M., HUTCHISON, G., "A Displacement Based Prediction of the Seismic Hazard for Australia", Proceedings of the 1998 Australian Earthquake Engineering Conference, Perth, 1998, pp. 20.1 – 20.5

LAM, N., WILSON, J., HUTCHINSON, G., "Building Ductility Demand: Interplate Versus Intraplate Earthquakes", Earthquake Engineering and Structural Dynamics, Vol. 25, 1996, pp. 965-985

LAM, N., WILSON, J., HUTCHINSON, G., "Development of Intraplate Response Spectra for Bedrock in Australia", Proceedings of the 1998 Technical Seminar of the New Zealand National Society of Earthquake Engineering, 1998, pp. 137-144

LAM, N., WILSON, J., HUTCHINSON, G., "Modelling of an Unreinforced Masonry Parapet Wall for Seismic Performance Evaluation Based on Dynamic Testing", Departmental of Civil and Environmental Engineering, The University of Melbourne, Departmental Report No. RR/STRUCT/03/95, 1995

LAM, N., WILSON, J., HUTCHINSON, G., "The Ductility Reduction Factor in the Seismic Design of Buildings", Earthquake Engineering and Structural Dynamics, 27, 1998, pp. 749-769

LAM, N., WILSON, J., HUTCHINSON, G., "The Seismic Resistance of Unreinforced Masonry Cantilever Walls in Low Seismicity Areas", Bulletin of The New Zealand National Society of Earthquake Engineering, Vol. 28, no. 3, 1995, pp. 79-195

LAM, N., WILSON, J., HUTCHINSON, G., "Time-History Analysis for Rocking of Rigid Objects Subjected to Base Excitations", Proceedings of the 14th ACMSM, Hobart, Vol. 1, 1995B, pp.284-289

LAM, N., WILSON, J., KOO, R., HUTCHINSON, G., "Determination of Earthquake Response Spectra in Low and Moderate Seismicity Regions Using New Methodologies", Proceedings of The Australian Earthquake Engineering Conference, Newcastle, Australia, 1999

LAWRENCE, S., J., "Masonry codes and Regulations – Past, Present and Future", Proceedings of the 5th Australasian Masonry Conference, Gladstone, Queensland, 1998, pp. 219-225

LAWRENCE, S., J., "The New AS3700 Approach to Lateral Load", Proceedings of the 5th Australasian Masonry Conference, Gladstone, Queensland, 1998, pp. 227-237

LAWRENCE, S., J., "Flexural Strength of Brickwork Normal to and Parallel to The Bed Joints", Journal of The Australian Ceramic Society, No. 1, Vol. 11, 1975, pp. 5-6

LAWRENCE, S., J., "Lateral Loading of Masonry - An Overview", Proceedings to the 2nd National Masonry Seminar, Brisbane Australia, 1994, pp.20.1-20.9

LAWRENCE, S., J., "Out of Plane Lateral Load Resistance of Clay Brick Panels", Proceedings of the Australasian Structural Engineering Conference, Sydney, 1994, pp. 657-663

LAWRENCE, S., J., PAGE, A., W., "Mortar Bond - A Major Research Program", Proceedings of the 4th Australasian Masonry Conference, Sydney, 1995, pp.31-37

LEEDS, D., "Report on Conference on 1971 San Fernando, Ca., Earthquake", American Society of Civil Engineers, Civil Engineering, Environmental Design and Engineered Construction, 1972, pp. 58-60

LIZUNDIA, B., DONG, W., H., W., REITHERMAN, R., "URM Building Damage Patterns in the Loma Prieta Earthquake: Implications for Improvements in Loss Estimation Methodologies", Proceedings of the 5th National Conference on Earthquake Engineering, 1994, pp.459-468

LIZUNDIA, B., HOLMES, W., T., "Development of Procedures to Enhance the Performance of Rehabilitated URM Buildings: A Summary", Proceedings of the 6th US National Conference on Earthquake Engineering

LOKE, J., Y., O., "Behaviour of Structures – Institutional", Proceedings of the Conference on the Newcastle Earthquake, Newcastle, Australia, 1990, pp.28-32

LOURENCO, P., B., "Computational Strategies for Masonry Structures", Ph.D. Thesis, The Civil Engineering Department, Delft University of Technology, The Netherlands, 1996

LOVEGROVE, R., "A Discussion of 'Yieldlines' in Unreinforced Masonry", The Structural Engineer, Vol. 66, No. 22, 1988, pp. 371-375

MAGENES, G., CALVI, G., M., "Cyclic Behaviour of Brick Masonry Walls", Proceedings of the 10th World Conference on Earthquake Engineering, Rotterdam, 1992, pp. 3517-3522

MAGENES, G., CALVI, G., M., "In-plane Seismic Response of Brick Masonry Walls", Earthquake Engineering and Structural Dynamics, Vol. 26, 1997, pp. 1091-1112

MAGENES, G., CALVI, G., M., "Shaking Table Tests on Brick Masonry Walls", Proceedings of the 10th European Conference on Earthquake Engineering, Vol. 3, Rotterdam, 1995, pp. 2419 - 2424

MAKRIS, N., ROUSSOS, Y., "Rocking Response and Overturning of Equipment Under Horizontal Pulse Type Motions", Pacific Earthquake Research Center, Berkley, University of California, PEER-98/05

MANFREDI, G., MAZZOLANI, S., MASI, A., "Review of Existing in Experimental Testing of Masonry Structures Subjected to Horizontal Loads", Proceedings of the 10th World Conference on Earthquake Engineering, Rotterdam, 1992, pp. 3557-3562

MARTINI, K., "Finite Element Studies in the Two–way Out of Plane Failure of Unreinforced Masonry", Proceedings of the 6th US National Conference on Earthquake Engineering

MARTINI, K., "Research in the Out-of-Plane Behaviour of Unreinforced Masonry", http://urban.arch.Virginia.EDU/struct/pompeii/masonry, 1997

MARTINI, K., "Finite Element Studies in the Out-of-Plane Failure of Unreinforced Masonry", Proceedings on the International Conference on Computing in Civil and Building Engineering, Vol. 1, Korea, 1997

MARZAHN, G., "Dry-stacked Masonry in Comparison with Mortar Jointed Masonry", Leipzig Annual Civil Engineering Report, No. 2, 1997, pp.353-365

MARZAHN, G., "Shear Strength of Grout Dowelled Masonry", Leipzig Annual Civil Engineering Report, No. 2, 1997, pp.335-351

McCUE, K., "Seismicity and Earthquake Hazard in Australia", Proceedings of the Earthquake Engineering and Disaster Reduction Seminar, Australian Earthquake Engineering Society, Melbourne, 1993, pp. 9-14

McCUE, K., "Seismological Aspects of the Newcastle NSW Earthquake of 28 December 1989", Proceedings of the Conference on the Newcastle Earthquake, Newcastle, Australia, 1990, pp.9-13

McGINLEY, W., M., BORCHELT, J., G., "Friction at the Supports of Clay Brick Walls", Proceedings of the 5th North American Masonry Conference, 1990, pp.1053-1066

McGINLEY, W., M., BORCHELT, J., G., "Influence of Materials on the Friction Developed at the Base of Clay Brick Walls", Proceedings of the 9th IBMAC, Berlin, 1991, pp. 292-300

MELCHERS, R., E., (Ed) "Newcastle Earthquake Study", The Institution of Engineers, Australia, 1990

MELCHERS, R., E., "On Intra-plate Earthquakes and Existing Buildings", Transactions of the Institution of Engineers, Civil Engineering, Vol. CE36, No.4, 1994, pp.265-271

MELCHERS, R., MORISON, D., "Structural Response to Typical Intra-Plate Ground Shaking", Research Report No. 107.02.1995, The University of Newcastle, 1995

MERCER, J., CROSS, W., "Simple, Low-Cost Retrofit Procedures for Historic Unreinforced Masonry Buildings", Elsevier Science Ltd, 1998, Paper reference T126-5

MOORE, T., A., KOBZEFF, J., H., DIRI, J., ARNOLD, C., "The Whittier Narrows, California Earthquake of October 1, 1987 - Preliminary Evaluation of the Performance of Strengthened Unreinforced Masonry Buildings", Earthquake Spectra, Vol. 4, No. 1, 1988, pp. 197-215

MULLINS, P., J., O'CONNER, C., "Unreinforced Brick Shear Walls", Proceedings of the 4th Australasian Masonry Conference, Sydney, 1995, pp.71-80

MUQTARIR, M., "Slenderness Effects in Eccentrically Loaded Plain Masonry Walls", Proceedings of the 5th North American Masonry Conference, Urbana-Champign, 1990, pp.1007-1015.

MURPHY, S., A., STEWART, M., G., "Analysis of Public Buildings Damaged in the 1989 Newcastle Earthquake", Australian Civil Engineering Transactions, Vol. CE35, No. 3, 1993, pp.187-201

NAWAR, G., ZOURTOS, K., "Planning and Control of Site Quality with Reference to Special Masonry", Proceedings of the 3rd National Masonry Seminar, Brisbane Australia, 1994, pp.7.1-7.11.

NEHRP, "Recommended Provisions for the Development of Seismic Regulations for New Buildings – Part 1 Provisions", National Hazards Reduction Program, Federal Emergency Management Agency, Washington, DC, 1991

NEHRP, "Recommended Provisions for the Development of Seismic Regulations for New Buildings – Part 2 Commentary", National Hazards Reduction Program, Federal Emergency Management Agency, Washington, DC, 1991

NICHOLS, J., M., TOTOEV, Y., Z., "Background to a Study of Damage Mechanics in Masonry Panels Subjected to Cyclic Loading", Proceedings of the 5th Australasian Masonry Conference, Gladstone, Queensland, 1998, pp. 283-292

NURTUG, A., DOHERTY, K., GRIFFITH, M., LAM, N., WILSON, J., "Research into the Seismic Performance of Unreinforced Masonry Walls", Proceedings of the Australian Earthquake Engineering Conference, Brisbane, Australia, 1997, p. 15-1 - 15-4

OH, K., HARRIS, G., "Seismic Behaviour of Floor to Wall Horizontal Joints of Masonry Buildings using 1/3 Scale Direct Models", Proceedings of the 5th North American Masonry Conference, Illinois, 1990, pp. 81-92

PAGE, A., W., "A Note on the Shear Capacity of Membrane Type Damp Proof Courses", Research Report No. 097.05.1994, The University of Newcastle, 1992

PAGE, A., W., "Behaviour of Structures – Patterns of Failure", Proceedings of the Conference on the Newcastle Earthquake, Newcastle, Australia, 1990, pp.39-43

PAGE, A., W., "The Design, Detailing and Construction of Masonry - The Lessons From the Newcastle Earthquake", Research Report No. 073.03.1992, The University of Newcastle, 1992

PAGE, A., W., "The Design, Detailing and Construction of Masonry – The Lessons From the Newcastle Earthquake", Australian Civil Engineering Transactions, Vol. CE34, No. 4, 1992, pp.343-353

PAGE, A., W., "The New Australian Standard for Masonry Structures (AS3700-1998)", Proceedings of the 5th Australasian Masonry Conference, Gladstone, Queensland, 1998, pp. 303-308

PAGE, A., W., "Unreinforced Masonry Structures - An Australian Overview", Proceedings of the Pacific Conference on Earthquake Engineering, Australia, 1995, pp. 1-16.

PAGE, A., W., KLEEMAN, P., W., STEWART, M., G., MELCHERS., R., E., "Structural Aspects of the Newcastle Earthquake", The Institution of Engineers Australia Structural Engineering Conference, Adelaide, 1990, pp. 305-312

PAGE, A., W., LAWRENCE, S., J., "An Integrated Study of Masonry Bond Strength", Proceedings of the 5th Australasian Masonry Conference, Gladstone, Queensland, 1998, pp. 309-317

PAGE, A., W., "Codes Overview - Connectors and Accessories For Masonry Construction - Strengthening of Existing Buildings For Earthquakes", Proceedings of the 4th Australasian Masonry Conference, Sydney, 1995, pp.97-102

PAGE, A., W., "The Shear Capacity of Membrane Type Damp-Proof Courses in Masonry", Transactions of the Institution of Engineers, Civil Engineering, 1995, Vol. CE37, No.1, pp.29-39

PAGE, A., W., GRIFFITH, M., C., "Seismic Design of Connections in Unreinforced Masonry Buildings', Proceedings of the 1998 Structural Engineers World Conference, San Francisco, CA, USA, 1998

PAGE, A., W., KLEENMAN, P., BRYANT, I., "The Effect of Foundation Hogging and Sagging on Masonry Walls", Proceedings of the Australasian Structural Engineering Conference, Sydney, 1994, pp. 665-671

PAGE, A., W., LAWRENCE, S., "Design of Clay Masonry for Wind and Earthquake", Clay Brick and Paver Institute, 1999, ISBN 0 947160 03 5

PARSANEJAD, S., JANKULOVSKI, E., "Hysteresis Behaviour of Plain Brick Masonry Walls: An Experimental Investigation", Proceedings of the Australasian Structural Engineering Conference, Sydney, 1994, pp.679-683.

PAULAY, T., "Simplicity and Confidence in Seismic Design", Proceedings of the Australian Earthquake Engineering Society Conference, Brisbane, Australia, 1997, pp. 1-1 - 1-12

PAULAY, T., PRIESTLY, M., J., N., "Seismic Design of Reinforced Concrete and Masonry Buildings", J. Wiley, 1992

PEDERSEN, I., "Behaviour of Structures – Major Commercial Buildings", Proceedings of the Conference on the Newcastle Earthquake, Newcastle, Australia, 1990, pp.21-25

PHAM, L., GRIFFITH, M., C., "Review of Building Performance in Recent Earthquakes", Proceedings of the 4th Australasian Masonry Conference, Sydney, 1995, pp.14-20

PHAM, L., LI, C., Q., "Domestic Construction and Serviceability", Proceedings of the Australasian Structural Engineering Conference, Sydney, 1994, pp. 847-851

PHIPPS, M., "Diaphragm and Other Walls of Geometric Cross Section in the UK", Proceedings to the 2nd National Masonry Seminar, Brisbane Australia, 1994, pp.24.1-24.10.

PHIPPS, M., E., "The Design of Slender Masonry Walls and Columns of Geometric Cross-section to Carry Vertical Load", The Structural Engineer, Vol. 65A, No. 12, 1987, pp. 443-447

PHIPPS, M., E., PAGE, A., W., "Developments in Masonry Part 1 - Walls of Geometric Cross-Section", Australian Civil Engineering Transactions, Vol. CE37.(2), 1995, 159-165

PHIPPS, M., E., PAGE, A., W., "Developments in Masonry Part 2 - Reinforced and Prestressed Walling", Australian Civil Engineering Transactions, Vol. CE37. (2), 1995, 167-174

POMONIS, A., SPENCE, R., J., S., COBURN, A., W., "Shaking Table Tests on Strong Motion Damageness Upon Reinforced Masonry", Proceedings of the 10th World Conference on Earthquake Engineering, Vol. 6, Rotterdam, 1992, pp. 3533-3538

POTTER, R, J, "Earthquake and Masonry - An Overview", Proceedings of the 3rd National Masonry Seminar, Brisbane Australia, 1994, pp.15.1-15.11.

POULOS, H., G., "Relationship Between Local Soil Conditions and Structural Damage in the 1989 Newcastle Earthquake", Australian Civil Engineering Transactions, Vol. CE33, No. 3, 1991, pp.181-188

PRIESTLEY, J., N., "Seismic Behaviour of Unreinforced Masonry Walls", Bulletin of the New Zealand National Society for Earthquake Engineering, Vol. 18, No. 2, 1985, pp.191-205.

PRIESTLEY, J., N., ROBINSON, L., M., "Discussion - Seismic Behaviour of Unreinforced Masonry Walls", Bulletin of the New Zealand National Society for Earthquake Engineering, Vol. 19, No. 1, March 1986, pp.65-75.

PRIESTLY, M., J., N., CALVI, G., M., "Concepts and Procedures for Direct Displacement-Based Design and Assessment", Workshop on Seismic Design Approaches for the 21st Century, Slovenia, 1997

PRIESTLY, N., J., "Displacement-Based Seismic Assessment of Existing Reinforced Concrete Buildings", Bulletin of the New Zealand National Society for Earthquake Engineering, Vol.. 29, No.4, 1996, pp.256-271

PUJOL, S., RAMIREZ, J., SARRIA, A., "Coffee Zone, Columbia, January 25 Earthquake, Observations on the Behaviour of Low Rise Reinforced Concrete Buildings", http://www.eeri.org/Reconn/, 1999

RAJAKARUNA, M., P., "Effect of a Damp Proof Course on The Shear Strength of Masonry", Proceedings of the 15th Australasian Conference on The Mechanics of Structures and Materials, Melbourne, Victoria, Australia, 1997, pp. 633-637

RAMIREZ, J., PUGLIESI, R., "The October 9, 1995 Magnitude 7.6 Manzanillo, Mexico Earthquake", EERI Special Earthquake Report, http://www.eeri.org/Reconn/, 1995

RANGAN, B., V., WARNER, R., F., "Large Concrete Buildings", Concrete Design and Construction Series, Longman Group Limited, 1996

REITHERMAN, R., "The Borah Peak, Idaho Earthquake of October 28, 1983 - Performance of Unreinforced Masonry Buildings in Mackay, Idaho", Earthquake Spectra, Vol. 2, No. 1, 1985, pp. 205-224

Report by the Masonry Standards Joint Committee on Building Code Requirements for Masonry Structures (ACI 530-92/ASCE 5-92/TMS 402-92), Specification for Masonry Structures (ACI 530.1-92/ASCE 6-92/TMS 602-92), Commentary on Building Code Requirements for Masonry Structures (ACI 530-92/ASCE 5-92/TMS 402-92) and Commentary on Specifications for Masonry Structures (ACI 530.1-92/ASCE 6-92/TMS 602-92), USA, 1992

RIDDINGTON, J., R., JUKES, P., "A Masonry Joint Shear Strength Test Method", Proceedings of the Institution of Civil Engineers, 104, 1994, pp.267-274

RIDDINGTON, J., R., GHAZALI, M., Z., "Hypothesis for Shear Failure in Masonry Joints", Proceedings of The Institution of Civil Engineers, Part 2, 1990, pp.89-102

RODOLICO, B., DOHERTY, K., LAM, N., GRIFFITH, M., WILSON, J., "Seismic Response Behaviour of Unreinforced Masonry Slender Walls Revealed By Shaking Table Testings and Time-History Analyses", Proceedings of the 16th Australasian Conference on Mechanics of Structures and Materials, Sydney, 1999

ROMANO, F., GANDUSCIO, S., ZINGONE, G., "Analysis of Masonry Walls Subject to Cyclic Loads", Proceedings of the 10th European Conference on Earthquake Engineering, Vol. 3, Rotterdam, 1995, pp. 1675 - 1680

ROSATO, Donald, V., MATTIA, D., P., ROSATO, Dominick, V., "Designing with Composites and Plastics: A Handbook", Van Nostrand Reinhold, 1991

SAA Earthquake Loading Code, AS2121, Standards Association of Australia, Sydney, 1979

SAA Loading Code, Minimum Design Loads on Structures – Part 4 – Earthquake Loads, AS1170.4 - 1993, Standards Australia, Sydney 1993

SAA Masonry Code AS3700-1988, Standards Australia, Sydney 1988

SAA Masonry Code AS3700-1998, Standards Australia, Sydney 1998

SAA Masonry Code Commentary, AS3700 Supplement 1, Standards Australia, Sydney, 1991

SAA Strengthening Existing Buildings for Earthquake, AS3626 – 1998, Standards Australia, Sydney 1998

SAMARASINGHE, W., LAWRENCE, S., J., PAGE, A., W., "Investigations of the Bond Wrench Method of Testing masonry", Proceedings of the 15th Australasian Conference on The Mechanics of Structures and Materials, Melbourne, Victoria, Australia, 1997, pp.651-656

SAMARASINGHE, W., LAWRENCE, S., J., PAGE, A., W., "Standardising the Bond Wrench", Proceedings of the 5th Australasian Masonry Conference, Gladstone, Queensland, 1998, pp. 335-344

SAMARASINGHE, W., PAGE, A., W., HENDRY, A., W., "Behaviour of Brick Masonry Shear Walls", The Structural Engineer, Vol. 59B, No. 3, 1981, pp. 43-48

SCHWARTZ, J., THURLIMANN, B., "Design of Masonry Walls Under Normal Force with Swiss STD.SIA V 177/2", Proceedings of the 5th North American Masonry Conference, Urbana-Champign, 1990, pp.959-969

SCRIVENER, J., C., "Masonry Structures - Earthquake Resistant Design and Construction", Proceedings of the Earthquake Engineering and Disaster Reduction Seminar, Australian Earthquake Engineering Society, Melbourne, 1993, pp. 39-44

SEAOC – Structural Engineers Association of California, "Recommended Lateral Force Requirements and Commentary", Structural Engineers Association of California, Los Angeles, California, 1977

SEISMOLOGY RESEARCH CENTER, Seismology Education, http://www.seis.com.au, 1999

SEISUN, M., PARSENEJAD, S., JANKULOVSKI, E., "Experimental Behaviour of Clay Brick Masonry Subject to Compression and Shear", Proceedings of the Australasian Structural Engineering Conference, Sydney, 1994, pp.691-695.

SHELTON, R., H., "Face Loaded Performance of Masonry Veneer Under Seismic Action", Proceedings of the 4th Australasian Masonry Conference, Sydney, 1995, pp.150-159

SHIBATA, A., SOZEN, M., A., "Substitute-Structure Method for Seismic Design in R/C", Journal of the Structural Division, Proceedings of the American Society of Civil Engineers, Vol. 102, No.ST1, 1976

STAFFORD SMITH, B., S., CARTER, C., "Hypothesis for the Shear Failure of Brick Work", American Society of Civil Engineers, Journal of Structural Engineering, Vol. 120, No. ST4, 1971, pp. 1055-1062

SOMERS, P., " Northridge Earthquake of January 17 1994: Reconnaissance Report, Vol. 2 Unreinforced Masonry Buildings", Earthquake Spectra, Journal of the Earthquake Engineering Research Institute, Vol. 11, 1996, pp.195-217.

SOMERVILLE, M., McCUE, K., SINADINOVSKI, C., "Response Spectra Recommended for Australia", Proceedings of the 1998 Australian Earthquake Engineering Conference, Perth, 1998, pp. 19.1 – 19.3

South Australian Housing Code 1996, Department of Housing and Urban Development, Building Standards and Policy Branch Planning Division, ISBN Number 0 7308 4662 8

SPENCE, R., D'AYALA, D., "Damage Assessment and Analysis of the 1997 Umbria-Marche Earthquakes", Journal of the International Association for Bridge and Structural Engineering, SEI Vol. 9, No. 3, 1999

SUH, N., P., TURNER, A., P., L., "Elements of the Mechanical Behaviour of Solids", Scripta Book Company, 1975

SUTER, G., T., IBRAHIM, K., S., "Shear Resistance of Damp Proof Course Materials in Brick Mortar Joints", Proceedings of the 6th Canadian Masonry Symposium, Canada, 1992, pp. 119-130.

TAYLOR-FIRTH, A., TAYLOR, I., "A Bond Tensile Strength Test for use in Assessing the Compatibility of Brick/Mortar Interfaces", Construction and Building Materials, Vol. 4, No.2, 1990, pp. 58-63

TENA-COLUNGA, A., "Seismic Evaluation of Unreinforced Masonry Structured with Flexible Diaphragms", Earthquake Spectra, Vol. 8, No 2, 1992, pp305-320.

TERCELJ, S., SHEPPARD, P., TURNSEK, V., "The Influence of Frequency on the Shear Strength and Ductility of Masonry Walls in Dynamic Loading Tests", Proceedings of the 10th World Conference on Earthquake Engineering, Rotterdam, 1992, pp. 2992-2997

TIMOSHENKO, S., WOINOWSKY-KRIEGER, S., "Theory of Plates and Shells", Second Edition, McGraw-Hill Book Company, 1959

TOMAZEVIC, M., "Seismic Design of Masonry Structures", Progress in Structural Engineering and Materials, Vol. 1 (1), 1997, pp. 88-95

TOMAZEVIC, M., "Simulation of Seismic Behaviour of Masonry Walls and Buildings by Laboratory Testing", Proceedings of the 10th European Conference on Earthquake Engineering, Vol. 3, Rotterdam, 1995, pp. 2425 - 2434

TOMAZEVIC, M., LUTMAN, M., WEISS, P., "The Influence of Tying the Walls with Steel Ties on the Seismic Behaviour of Historical Stone and Brick Masonry Buildings", Proceedings of the 10th European Conference on Earthquake Engineering, Vol. 3, Rotterdam, 1995, pp. 2249 - 2254

TOMAZEVIC, M., WEISS, P., "Seismic Behaviour of Plain- and Reinforced-Masonry Buildings", American Society of Civil Engineers, Journal of Structural Engineering, Vol. 120, No. 2, 1994, pp. 323-338

UBC, "Uniform Building Code", International Conference of Building Officials, Whittier, California, 1976

VAN DEN BOOM, Th., J., "Experimental Research into Flexural Strength of Masonry", CIB 3rd International Symposium on Wall Structures, Vol. 1, Warsaw, 1984, pp. 9-18

VINTZILEOU, E., "Eurocode 8 - Specific Rules for Masonry Buildings : Presentation/comments", Proceedings of the 10th European Conference on Earthquake Engineering, Vol.4, Rotterdam, 1995, pp. 2963 - 2967

WEST, H., W., H., HODGKINSON, H., R., HASELTINE, B., A., DE VEKEY, R., C., "The Resistance of Masonry to Lateral Loading - Research Results on Brickwork and Aggregate Blockwork Since 1977", The Structural Engineer, Vol. 64A, No. 11, 1986, pp. 320-331

WEST, H., W., H., HODGINSKON, H., R., HASELTINE, B., A., " The Resistance of Brickwork to Lateral Loading - Part 1 - Experimental Methods and Results of Tests on Small Specimens and Full Sized Walls", The Structural Engineer, No. 10, Vol. 55, 1977, pp. 411-421

HODGKINSON, H., R., WEST, W., H., "The Shear Resistance of Some Damp Proof Course Materials", Proceedings of the British Ceramic Society, No.30, 1982, pp.13-22

WEST, W., H., HODGKINSON, H., R., WEBB, W., F., "The Resistance of Brick Walls to Lateral Loading", Proceedings of the British Ceramic Society, No.21, 1973, pp.141-164

WILHELM, P., "Earthquake Repairs to the Christ Church Cathedral, Newcastle NSW", Australian Journal of Structural Engineering, Vol. 1, No.1, 1998

WILSON, J., LAM, N., HUTCJINSON, G., "The Capacity of Unreinforced Masonry Parapet Walls in Domestic Buildings to Withstand Earthquake Induced Loading", Australian Civil Engineering Transactions, Vol. CE. 37, No. 1, 1995, pp. 41-49

WYATT, K., "Restrained Moisture Expansion of Clay Masonry", Journal of the Australian Ceramic Society, November, No.2, Vol.12, 1976, pp34-36

WYLLIE, L., "Seismic Strengthening of Historic Churches", Proceedings of the 6th US National Conference on Earthquake Engineering

YIM, C-S., CHOPRA, A., K., PENZIAN, J., "Rocking Response of Rigid Blocks to Earthquakes", Earthquake Engineering and Structural Dynamics', Vol. 8, 1980, pp. 565-587

YOKEL, F., Y., DICKERS, R., D., "Strength of Loadbearing Masonry Walls", American Society of Civil Engineers, Journal of Structural Engineering, Vol. 120, No. ST5, 1971, pp. 1593-1608

YOKEL, F., Y., FATTAL, G., "Failure Hypothesis for Masonry Shear Walls", American Society of Civil Engineers, Journal of Structural Engineering, Vol. 120, No. ST3, 1976, pp. 515-532

YOUNG, D., T., SOLTAN, E., I., "Optimum Design of Concrete Masonry Loadbearing and Non-Loadbearing Walls", Proceedings of the 5th North American Masonry Conference, Urbana-Champign, 1990, pp.937-948

YTTRUP, P., J., "Design of Earth Masonry Walls For Lateral Loads and The Proposed New Zealand Earth Building Standard", Proceedings of the 4th Australasian Masonry Conference, Sydney, 1995, pp.113-118

YUXIAN, HU., "Some Engineering Features of the Tangshan Earthquake", Proceedings of the 2nd US National Conference on Earthquake Engineering, 1979

ZOUTENBIER, J., "Seismic Response of Unreinforced Masonry Buildings", Masters Thesis, The University of Canterbury, Christchurch, New Zealand, 1986

ZSEMBERY, S., McNEILLY, T., SCRIVENER, J., "A Method for Accurately Batching Mortar", Proceedings of the 4th Australasian Masonry Conference, Sydney, 1995, pp.134-140

APPENDIX (A): Band Pass Filter Program Fortran77 Code

```
PROGRAM filt1
C  Fourier Transform of single real function
     INTEGER n, no, isign
     REAL del, botd, topd
     REAL a(0:16384), ai(0:16384), afdu(0:16384), afdf(0:16384)
     REAL freq(0:16384)
     REAL dell(0:16384)
     CHARACTER *50 XFILE, OFILE
C
     Write(*,*) " "
     Write(*,*) "-----------------------------------------------------"
     Write(*,*) "            BAND PASS FILTER PROGRAM"
     Write(*,*) "                  FILT1"
     Write(*,*) "            FILTERS 1 COLUMN OF DATA"
     Write(*,*) "-----------------------------------------------------"
     Write(*,*) "Type filename of input time domain data file (.csv)"
     Read(*,'(a)') XFILE
     Write(*,*) "Type filename for filtered data output (.csv)"
     Read(*,'(a)') OFILE
     Write(*,*) "Type input data time increment (secs)"
     Read(*,*) del
     Write(*,*) "Type bottom band pass filter frequency"
     Read(*,*) botd
     Write(*,*) "Type top band pass filter frequency (Displacements)"
     Read(*,*) topd
     Open(30,file=XFILE,status='old',err=110)
     no=0
C
C  Here the data array is read from external file XFILE
     Do 1 k=1,16384
       Read(30,*,END=2) a(k)
       ai(k)=a(k)
       no=no+1
   1 Continue
C
     Close(30)
   2 Continue
     n=1
   3 Continue
     If(no.gt.n)then
       n=2*n
       goto 3
     end if
C  Arrays are augmented with zeros to get a function of 2
     Do 4 k=no+1, n
       a(k)=0.0
       ai(k)=0.0
```

```
  4 Continue
C  Transform to frequency domain completed giving data(n) array
     isign=1
     call realft(a,n,isign)
     Do 5 k=1,n
       afdu(k)=a(k)
  5  Continue
C  Frequencies are calculated
     Do 6 j=1,n/2
       Freq(j)=j/(n*del)
  6  Continue
C  Frequency domain data is filtered
C  acceleration band pass filter frequencies
     call genfilt(a,freq,n,botd,topd)
     Do 7 k=1,n
       afdf(k)=a(k)
  7  Continue
C  Realft is called to perform the inverse
C     transform of the filtered data
     isign = -1
     call realft(a,n,isign)
     Do 8 k=1,n
       dell(k)=del*k
       a(k)=2*a(k)/n
  8  Continue
C  Data output
     Open(35,file=OFILE,status='new',err=120)
     Write(35,*) "INPUT FILENAME : ",XFILE
     Write(35,9) del
  9  Format ('SAMPLE RATE USED IS = ',F6.3,' seconds')
     Write(35,10) botd, topd
 10  Format ('Band pass filter range',F5.2,' Hz - '
    +,F5.2,'Hz')
     Write(35,*) " "
     Write(35,*) "FREQUENCY DOMAIN,,,,,TIME DOMAIN"
     Write(35,*) "No.,Frequency,Data,Data,,Time,Data,Data"
     Write(35,*) ",,unfilt,filt,,,unfilt,filt"
     Write(35,12) afdu(1),afdf(1),dell(1),ai(1),a(1)
 12  Format ('1,0,',F15.3,',',F15.3,',,',F15.3,',',F15.3,',',F15.3)
     Write(35,13) freq(n/2),afdu(2),afdf(2),dell(2),ai(2),a(2)
 13  Format ('2,',F15.3,',',F15.3,',',F15.3,',,',F15.3,',',F15.3
    +,',',F11.3)
     Do 14 k=3,n-1,2
       Write(35,15) k,freq(k/2-1/2),afdu(k),afdf(k),dell(k),ai(k),a(k)
       Write(35,15) k+1,freq(k/2-1/2),afdu(k+1),afdf(k+1),dell(k+1)
    + ,ai(k+1),a(k+1)
 15    Format (I4,',',F15.3,',',F15.3,',',F15.3,',,',F15.3,',',F15.3,',
    + ',F15.3)
 14  Continue
     Write(*,*) " "
     Write(*,16) no
 16  Format('Number of input data lines  = ',I10)
     Write(*,17) n
 17  Format('Number of output data lines = ',I10)
     Write(*,*) "PROGRAM RUN COMPLETED"
100 Stop
```

```
 110 Write(*,*) "ERROR OPENING INPUT FILE"
 105 Stop
 120 Write(*,*) "ERROR OPENING OUTPUT FILE"
     END



PROGRAM filt1s
C  Fourier Transform of single real function
     INTEGER n, no, isign
     REAL del, botd, topd, temp
     REAL a(0:16384), ai(0:16384), afdu(0:16384), afdf(0:16384)
     REAL freq(0:16384)
     REAL dell(0:16384)
     CHARACTER *50 XFILE, OFILE, TEXT
C
     Write(*,*) " "
     Write(*,*) "-----------------------------------------------------"
     Write(*,*) "            BAND PASS FILTER PROGRAM"
     Write(*,*) "                  FILT1"
     Write(*,*) "            FILTERS 1 COLUMN OF DATA"
     Write(*,*) "-----------------------------------------------------"
     Write(*,*) "Type filename of input time domain data file (.csv)"
     Read(*,'(a)') XFILE
     Write(*,*) "Type filename for filtered data output (.csv)"
     Read(*,'(a)') OFILE
     Write(*,*) "Type input data time increment (secs)"
     Read(*,*) del
     Write(*,*) "Type bottom band pass filter frequency"
     Read(*,*) botd
     Write(*,*) "Type top band pass filter frequency (Displacements)"
     Read(*,*) topd
     Open(30,file=XFILE,status='old',err=110)
     no=0
C
C  Here the data array is read from external file XFILE
     Do 20 i=1,8
       read(*,*) TEXT
       write(*,*) TEXT
  20  Continue
     Do 1 k=1,16384
       Read(30,*,END=2) temp, a(k)
       ai(k)=a(k)
       no=no+1
   1  Continue
C
     Close(30)
   2  Continue
     n=1
   3  Continue
     If(no.gt.n)then
       n=2*n
       goto 3
     end if
```

```
C  Arrays are augmented with zeros to get a function of 2
     Do 4 k=no+1, n
       a(k)=0.0
       ai(k)=0.0
   4 Continue
C  Transform to frequency domain completed giving data(n) array
     isign=1
     call realft(a,n,isign)
     Do 5 k=1,n
       afdu(k)=a(k)
   5 Continue
C  Frequencies are calculated
     Do 6 j=1,n/2
       Freq(j)=j/(n*del)
   6 Continue
C  Frequency domain data is filtered
C  acceleration band pass filter frequencies
     call genfilt(a,freq,n,botd,topd)
     Do 7 k=1,n
       afdf(k)=a(k)
   7 Continue
C  Realft is called to perform the inverse
C     transform of the filtered data
     isign = -1
     call realft(a,n,isign)
     Do 8 k=1,n
       dell(k)=del*k
       a(k)=2*a(k)/n
   8 Continue
C  Data output
     Open(35,file=OFILE,status='new',err=120)
     Write(35,*) "INPUT FILENAME : ",XFILE
     Write(35,9) del
   9 Format ('SAMPLE RATE USED IS = ',F6.3,' seconds')
     Write(35,10) botd, topd
  10 Format ('Band pass filter range',F5.2,' Hz - '
    +,F5.2,'Hz')
     Write(35,*) " "
     Write(35,*) "FREQUENCY DOMAIN,,,,,TIME DOMAIN"
     Write(35,*) "No.,Frequency,Data,Data,,Time,Data,Data"
     Write(35,*) ",,unfilt,filt,,,unfilt,filt"
     Write(35,12) afdu(1),afdf(1),dell(1),ai(1),a(1)
  12 Format ('1,0,',F15.3,',',F15.3,',,',F15.3,',',F15.3,',',F15.3)
     Write(35,13) freq(n/2),afdu(2),afdf(2),dell(2),ai(2),a(2)
  13 Format ('2,',F15.3,',',F15.3,',',F15.3,',,',F15.3,',',F15.3
    +,',',F11.3)
     Do 14 k=3,n-1,2
       Write(35,15) k,freq(k/2-1/2),afdu(k),afdf(k),dell(k),ai(k),a(k)
       Write(35,15) k+1,freq(k/2-1/2),afdu(k+1),afdf(k+1),dell(k+1)
    + ,ai(k+1),a(k+1)
  15   Format (I4,',',F15.3,',',F15.3,',',F15.3,',,',F15.3,',',F15.3,',
    + ',F15.3)
  14 Continue
     Write(*,*) " "
     Write(*,16) no
  16 Format('Number of input data lines  = ',I10)
```

```
    Write(*,17) n
 17  Format('Number of output data lines = ',I10)
    Write(*,*) "PROGRAM RUN COMPLETED"
 100 Stop
 110 Write(*,*) "ERROR OPENING INPUT FILE"
 105 Stop
 120 Write(*,*) "ERROR OPENING OUTPUT FILE"
    END


SUBROUTINE genfilt(data,freq,n,bot,top)
    INTEGER n
    REAL data(n), freq(n/2)
C  Data in the frequency domain is filtered
    Do 22 i=3,n-1,2
      IF (Freq(i/2-1/2).LT.bot-1.0) THEN
        data(i)=0.0
        data(i+1)=0.0
      ELSEIF (Freq(i/2-1/2).LT.bot-0.5) THEN
        data(i)=(2.0*(Freq(i/2-1/2)-bot+1.0)**2)*data(i)
        data(i+1)=(2.0*(Freq(i/2-1/2)-bot+1.0)**2)*data(i+1)
      ELSEIF (Freq(i/2-1/2).LT.bot) THEN
        data(i)=((-2.0*(Freq(i/2-1/2)-bot)**2)+1)*data(i)
        data(i+1)=((-2.0*(Freq(i/2-1/2)-bot)**2)+1)*data(i+1)
      ELSEIF (Freq(i/2-1/2).LT.top) THEN
        data(i)=data(i)
        data(i+1)=data(i+1)
      ELSEIF (Freq(i/2-1/2).LT.top+0.5) THEN
        data(i)=((-2.0*(Freq(i/2-1/2)-top)**2)+1)*data(i)
        data(i+1)=((-2.0*(Freq(i/2-1/2)-top)**2)+1)*data(i+1)
      ELSEIF (Freq(i/2-1/2).LT.top+1.0) THEN
        data(i)=(2.0*(Freq(i/2-1/2)-top-1.0)**2)*data(i)
        data(i+1)=(2.0*(Freq(i/2-1/2)-top-1.0)**2)*data(i+1)
      ELSE
        data(i)=0.0
        data(i+1)=0.0
      ENDIF
    Data(1)=0.0
    Data(2)=0.0
  22 Continue
    END
```

```
      SUBROUTINE realft(data,n,isign)
          INTEGER isign,n
          REAL data(n)
      CU    USES four1
          INTEGER i,i1,i2,i3,i4,n2p3
          REAL c1,c2,h1i,h1r,h2i,h2r,wis,wrs
          DOUBLE PRECISION theta,wi,wpi,wpr,wr,wtemp
          theta=3.141592653589793d0/dble(n/2)
          c1=0.5
          if (isign.eq.1) then
            c2=-0.5
            call four1(data,n/2,+1)
          else
            c2=0.5
            theta=-theta
          endif
          wpr=-2.0d0*sin(0.5d0*theta)**2
          wpi=sin(theta)
          wr=1.0d0+wpr
          wi=wpi
          n2p3=n+3
          do 11 i=2,n/4
            i1=2*i-1
            i2=i1+1
            i3=n2p3-i2
            i4=i3+1
            wrs=sngl(wr)
            wis=sngl(wi)
            h1r=c1*(data(i1)+data(i3))
            h1i=c1*(data(i2)-data(i4))
            h2r=-c2*(data(i2)+data(i4))
            h2i=c2*(data(i1)-data(i3))
            data(i1)=h1r+wrs*h2r-wis*h2i
            data(i2)=h1i+wrs*h2i+wis*h2r
            data(i3)=h1r-wrs*h2r+wis*h2i
            data(i4)=-h1i+wrs*h2i+wis*h2r
            wtemp=wr
            wr=wr*wpr-wi*wpi+wr
            wi=wi*wpr+wtemp*wpi+wi
      11    continue
          if (isign.eq.1) then
            h1r=data(1)
            data(1)=h1r+data(2)
            data(2)=h1r-data(2)
          else
            h1r=data(1)
            data(1)=c1*(h1r+data(2))
            data(2)=c1*(h1r-data(2))
            call four1(data,n/2,-1)
          endif
          return
          END
      C  (C) Copr. 1986-92 Numerical Recipes Software 51P.
```

APPENDIX (B): Representative DPC Connection Test Results

Direction of Shaking: Out-of-plane
Normal Stress at Slip Face: 0.164MPa (31.9kN)

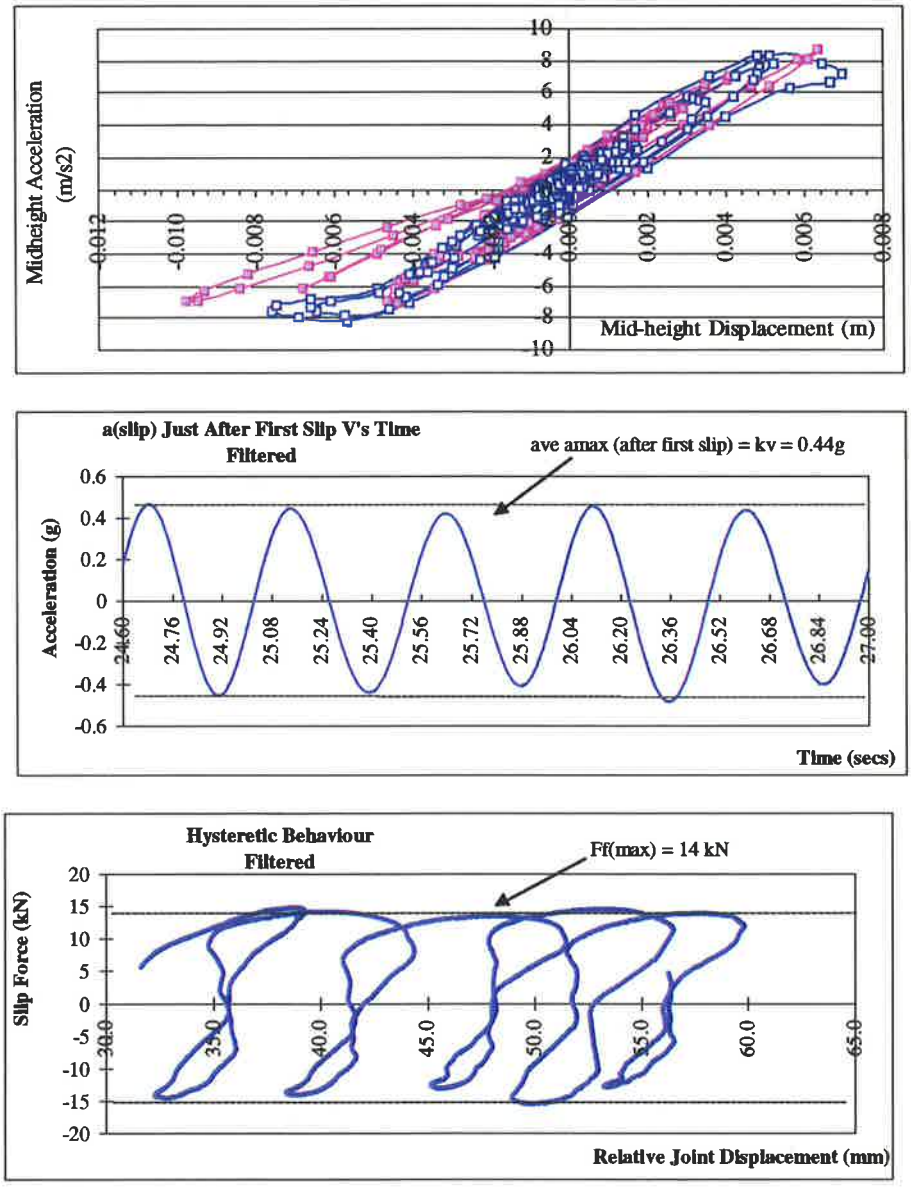

Figure B 1 - Standard DPC Connection One Layer of Standard Alcor

Direction of Shaking: Out-of-plane
Normal Stress at Slip Face: 0.164MPa (31.9kN)

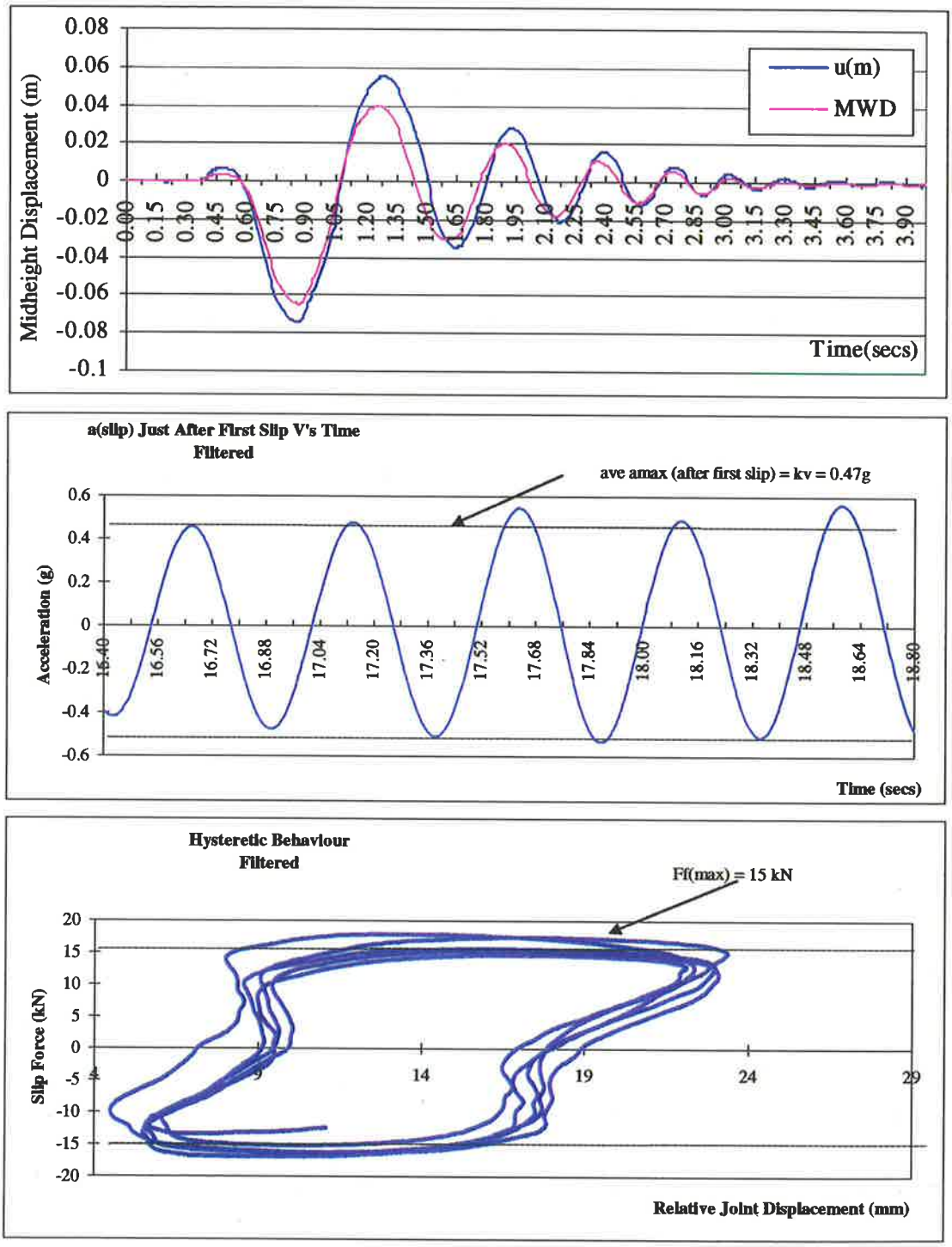

Figure B 2 - Standard DPC Connection One Layer of Super Alcor

Direction of Shaking: Out-of-plane
Normal Stress at Slip Face: 0.164MPa (31.9kN)

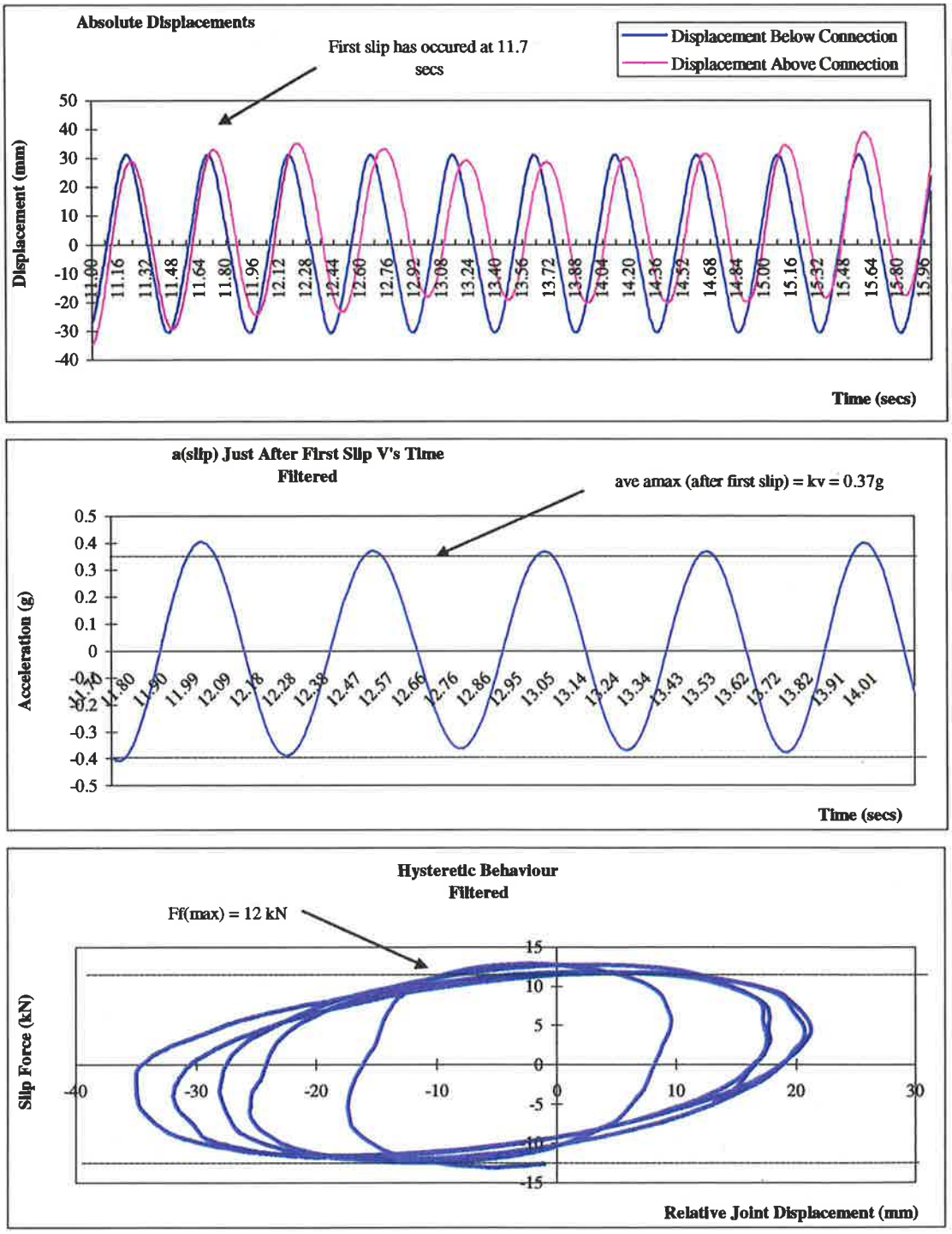

Figure B 3 - Standard DPC Connection One Layer of Polyflash

Direction of Shaking: Out-of-plane
Normal Stress at Slip Face: 0.164MPa (31.9kN)

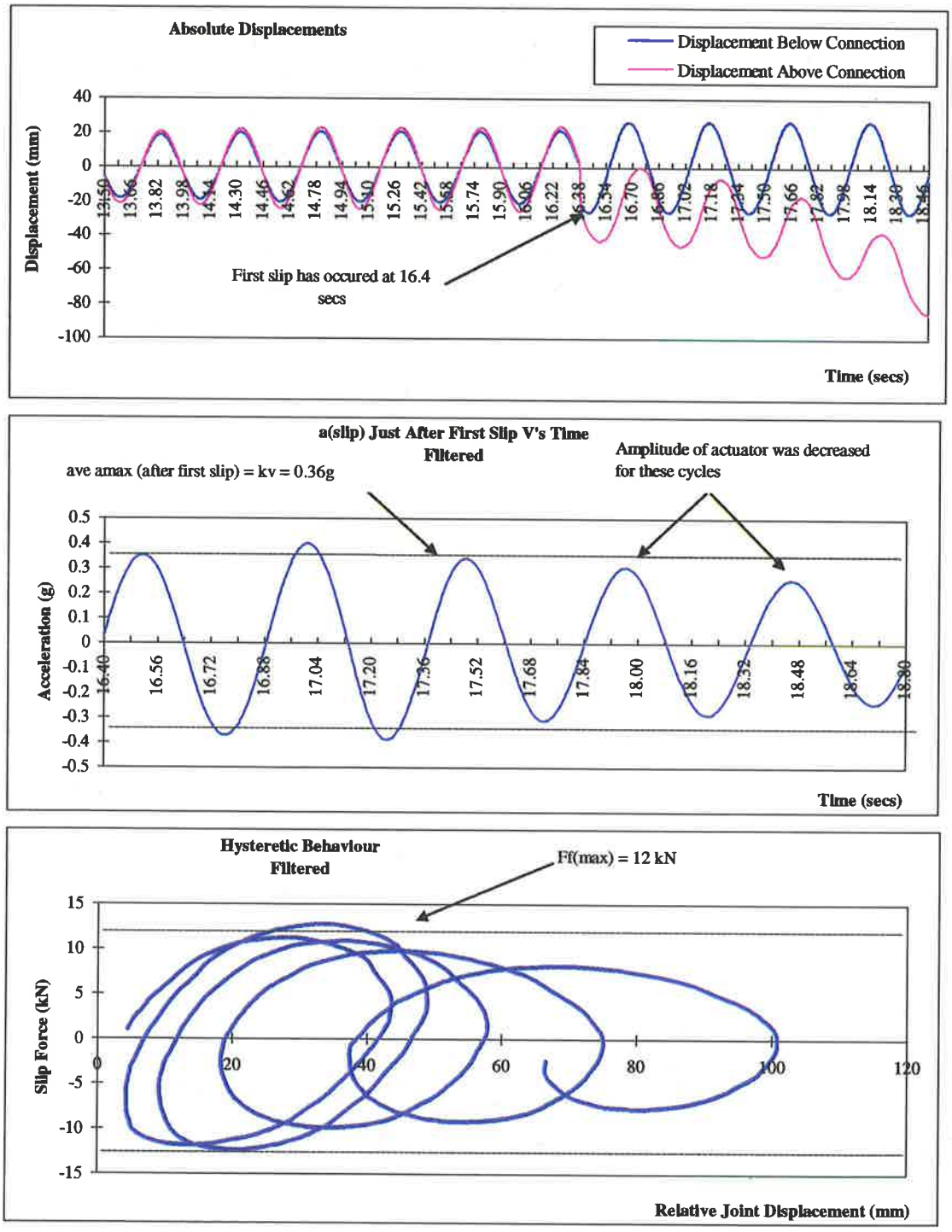

Figure B 4 - Standard DPC Connection One Layer of Dry-Cor (Embossed Polythene)

APPENDIX (C): Representative Slip Joint Connection Test Results

Direction of Shaking: In-Plane
Normal Stress at Slip Face: 0.18 MPa (N=17.8kN)

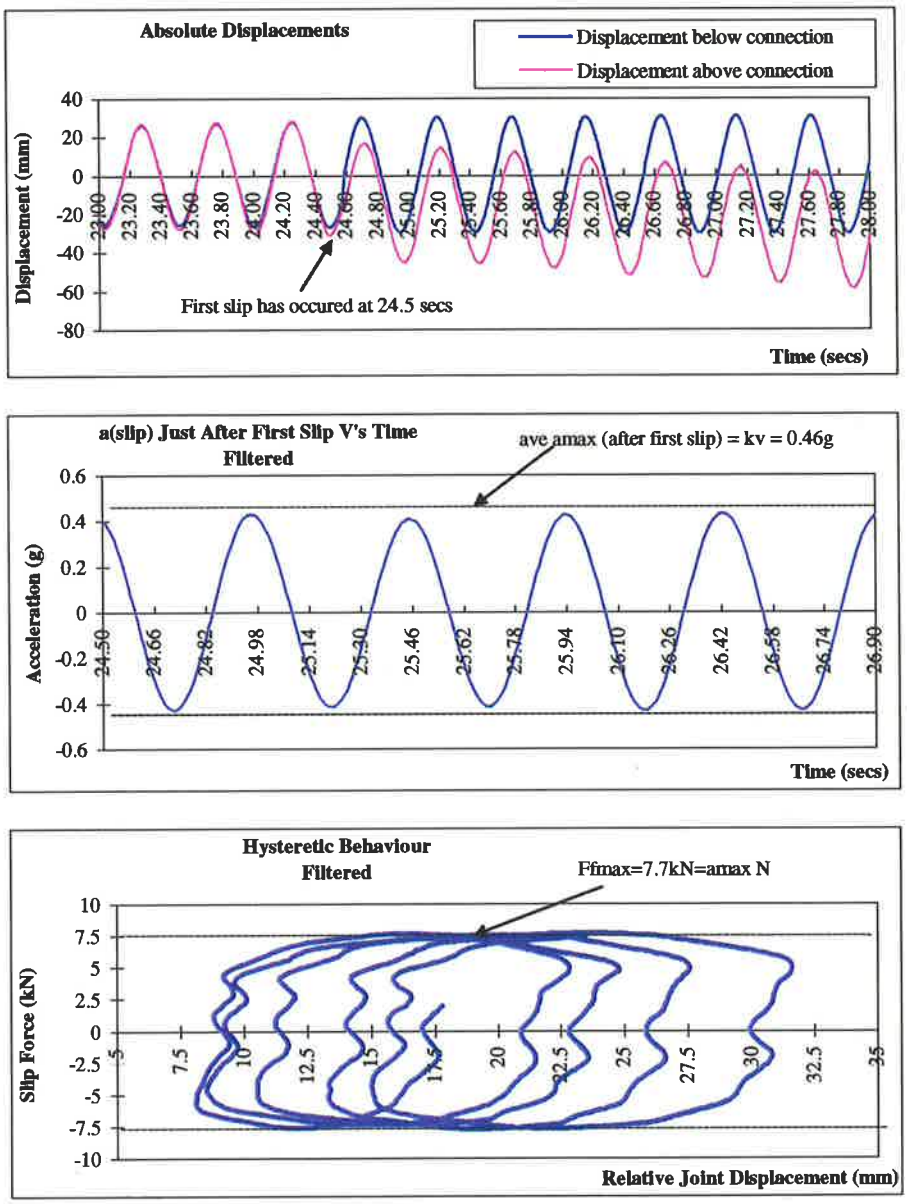

Figure C 1- Slip Joint Two layers of Standard Alcor

Direction of Shaking: Out-of-Plane
Normal Stress at Slip Face: 0.18 MPa (N=17.8kN)

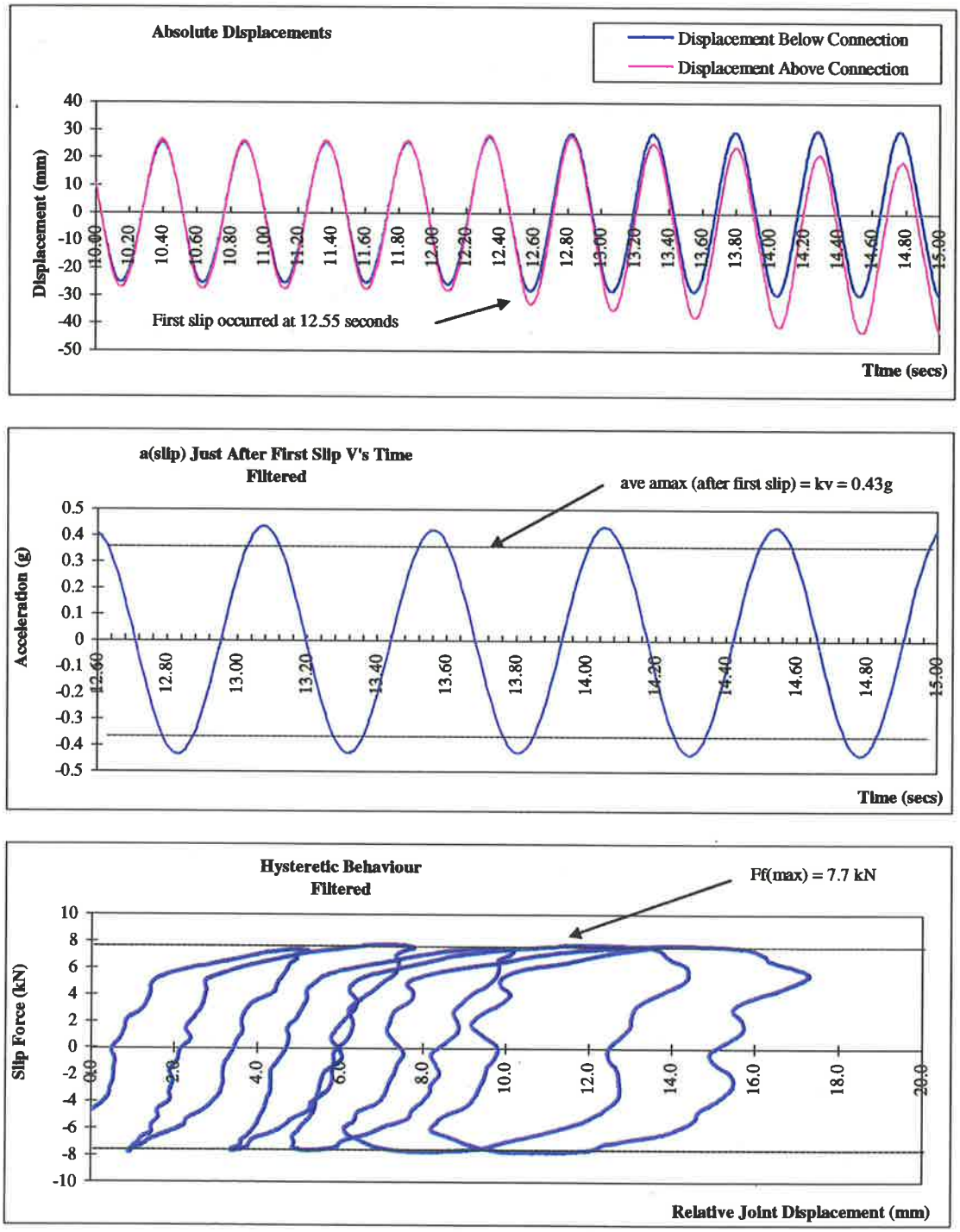

Figure C 2- Slip Joint One layer of Standard Alcor

Direction of Shaking: In-Plane
Normal Stress at Slip Face: 0.18 MPa (N=17.8kN)

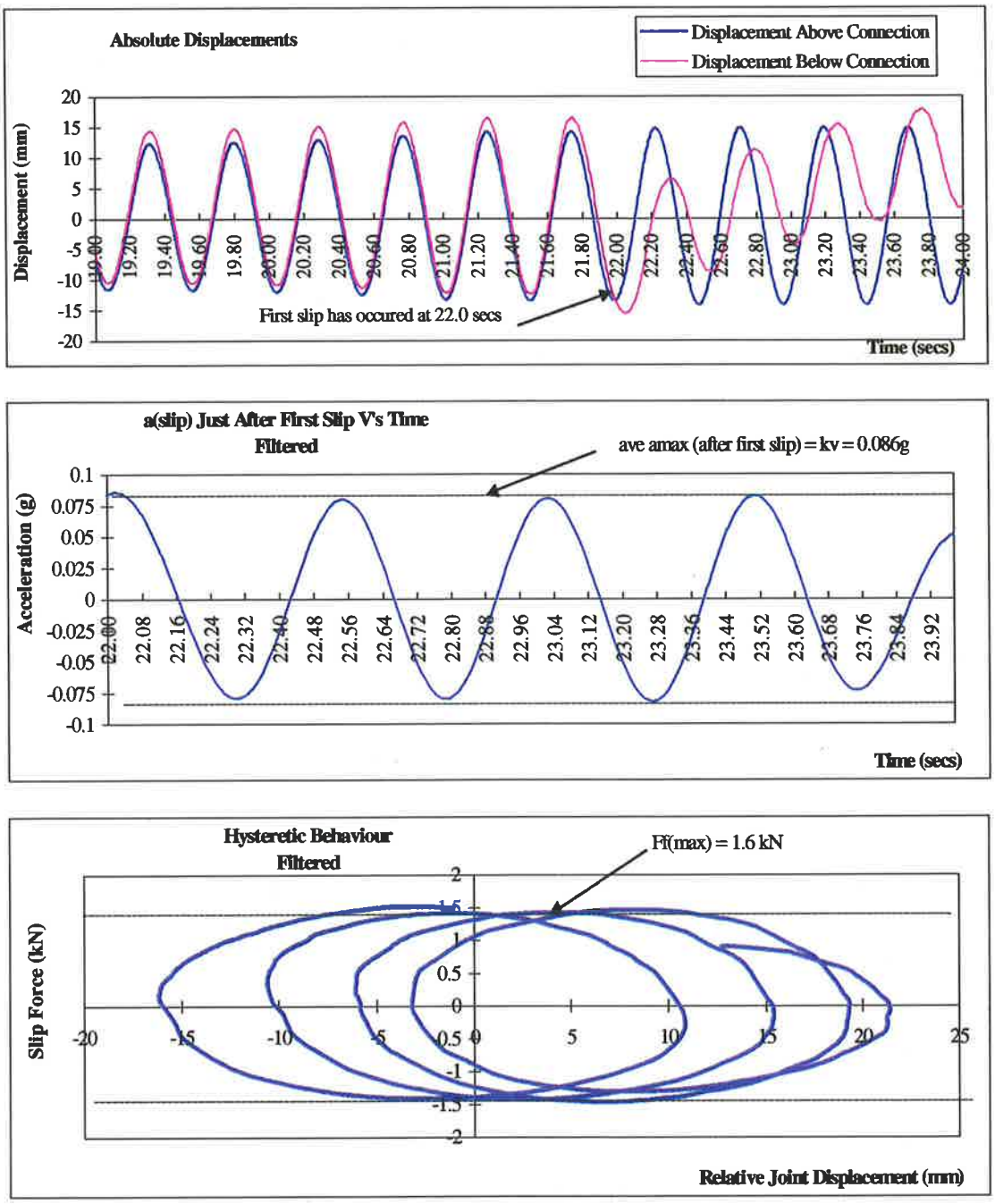

Figure C 3- Slip Joint Two layers of Greased Galvanised Steel

Direction of Shaking: Out-of-Plane
Normal Stress at Slip Face: 0.18 MPa (N=17.8kN)

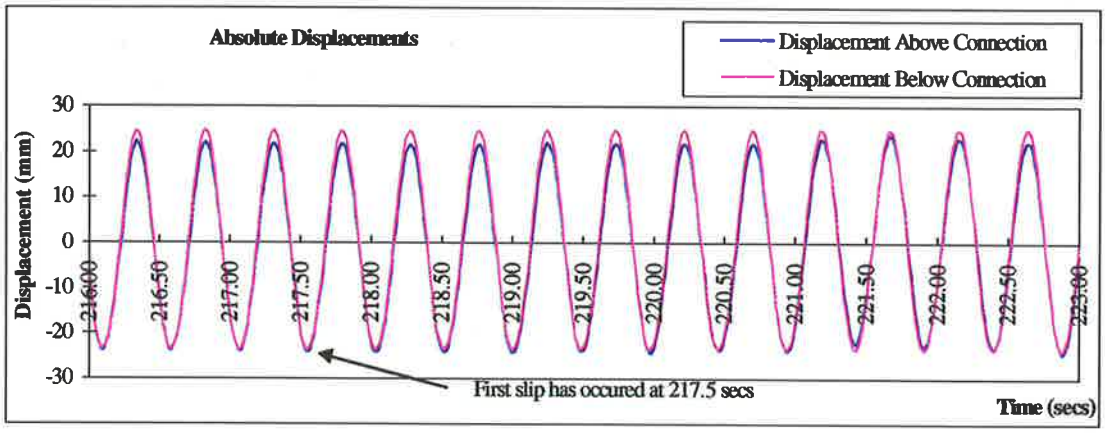

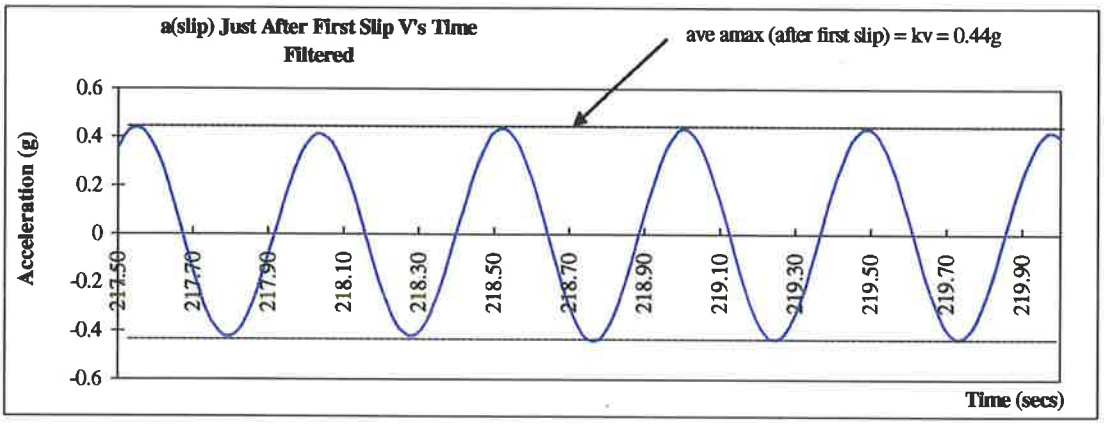

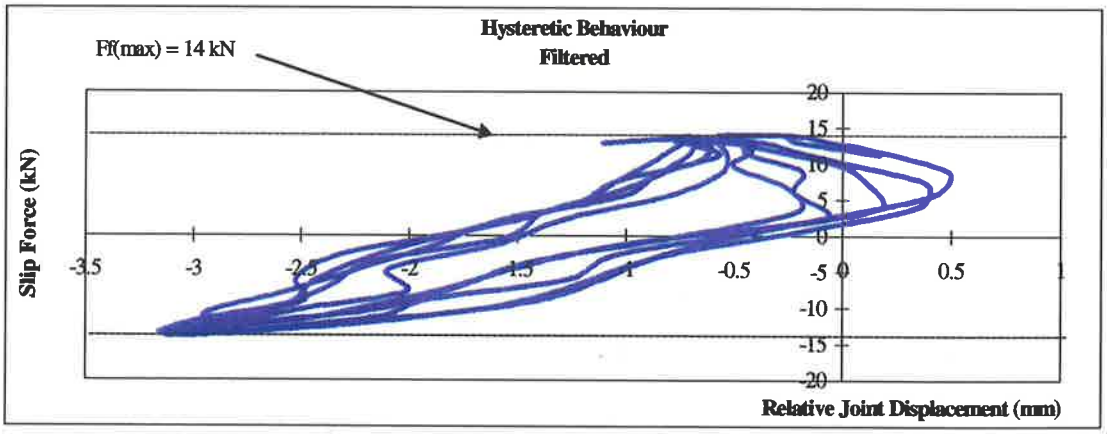

Figure C 4- Slip Joint One layer of Embossed Polythene (Dry-Cor)

APPENDIX (D): Rigid F-Δ - Various Boundary Conditions

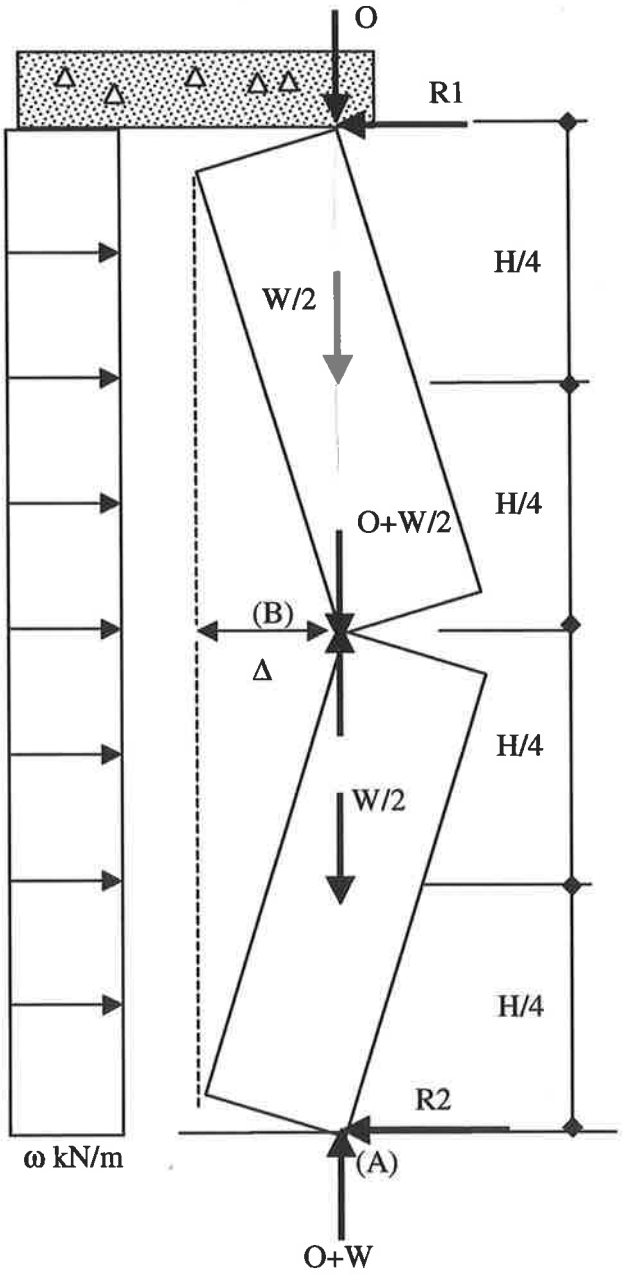

Figure D 1 - Concrete Slab with DPC Connection Above

Taking moments about (A) to determine horizontal reaction forces

$$0 = \frac{\omega h h}{2} - W\left(\frac{t}{2} - \frac{\Delta}{2}\right) - R_2 h$$

$$R_2 = \frac{\omega h}{2} - \frac{W}{2h}(t - \Delta)$$

$$R_1 = \frac{\omega h}{2} + \frac{W}{2h}(t - \Delta)$$

Taking moments about (B) top free body

$$0 = \frac{\omega h^2}{8} + O(t - \Delta) + \frac{W}{2}\left(\frac{t}{2} - \frac{\Delta}{2}\right) - \frac{h}{2}\left(\frac{\omega h}{2} - \frac{W}{2h}(t - \Delta)\right)$$

Rearranging

$$\omega = \frac{8}{h^2}\left(O + \frac{W}{2}\right)(t + \Delta)$$

Maximum resistance occurs when Δ=0

$$\omega_{\max} = \frac{8t}{h^2}\left[O + \frac{W}{2}\right]$$

With the rigid body assumption static instability occurs at a mid height displacement which causes the mid height reaction to move outside of the thickness of the wall. At this point ω=0

$$0 = \frac{8}{h^2}\left(O + \frac{W}{2}\right)(t - \Delta_{ins})$$

Rearranging

$$\Delta_{ins} = \frac{t\left(O + \frac{W}{2}\right)}{\left(0 + \frac{W}{2}\right)} = t$$

CONCRETE SLAB WITH DPC CONNECTION ABOVE - STATIC INSTABILITY

STATIC FORCE-DISPLACEMENT RELATIONSHIP

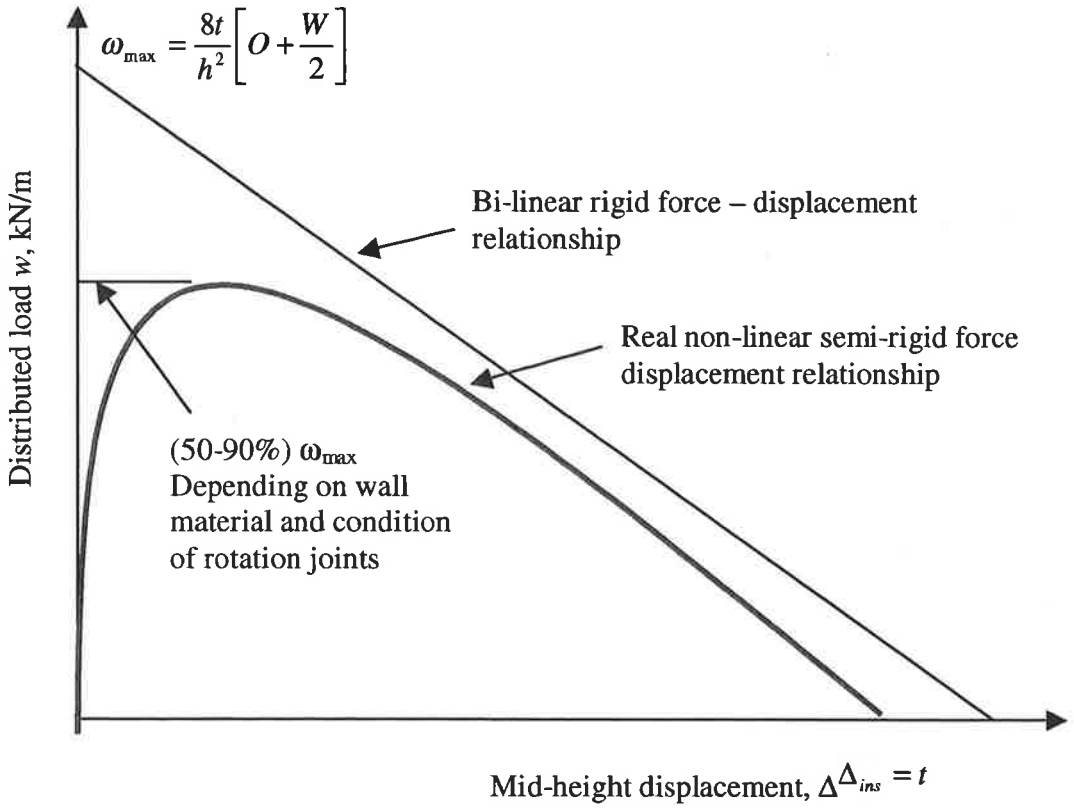

Figure D 2 - Rigid F-Δ Relationship– Top Vertical Reaction at Leeward Face

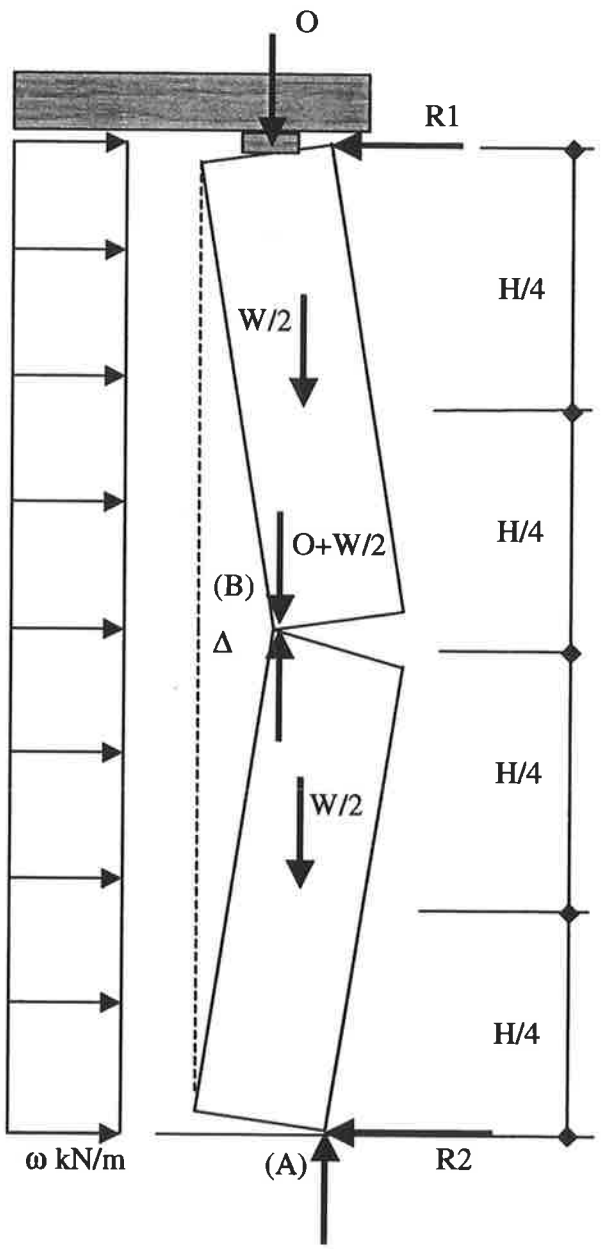

Figure D 3 - Timber Top Plate Above

Taking moments about (A) to determine horizontal reaction forces

$$0 = \frac{\omega h h}{2} - \frac{Ot}{2} - W\left(\frac{t}{2} - \frac{\Delta}{2}\right) - R_2 h$$

$$R_2 = \frac{\omega h}{2} - \frac{Ot}{2h} - \frac{W}{2h}(t - \Delta)$$

$$R_1 = \frac{\omega h}{2} + \frac{Ot}{2h} + \frac{W}{2h}(t - \Delta)$$

Taking moments about (B) top free body

$$0 = \frac{\omega h^2}{8} + O\left(\frac{t}{2} - \Delta\right) + \frac{W}{2}\left(\frac{t}{2} - \frac{\Delta}{2}\right) - \frac{h}{2}\left(\frac{\omega h}{2} - \frac{Ot}{2h} - \frac{W}{2h}(t - \Delta)\right)$$

Rearranging

$$\omega = \frac{4}{h^2}\left[W(t - \Delta) + O(\frac{3t}{2} + 2\Delta)\right]$$

Maximum resistance occurs when Δ=0

$$\omega_{\max} = \frac{4t}{h^2}\left[W + (\frac{3}{2})O\right]$$

With the rigid body assumption static instability occurs at a mid height displacement which causes the mid height reaction to move outside of the thickness of the wall. At this point ω=0

$$0 = \frac{4}{h^2}\left[W(t - \Delta_{ins}) + O(\frac{3t}{2} + 2\Delta_{ins})\right]$$

Rearranging

$$\Delta_{ins} = \frac{t\left(W + \frac{3O}{2}\right)}{(W - 2O)}$$

TIMBER TOP PLATE – STATIC INSTABILITY

STATIC FORCE-DISPLACEMENT RELATIONSHIP

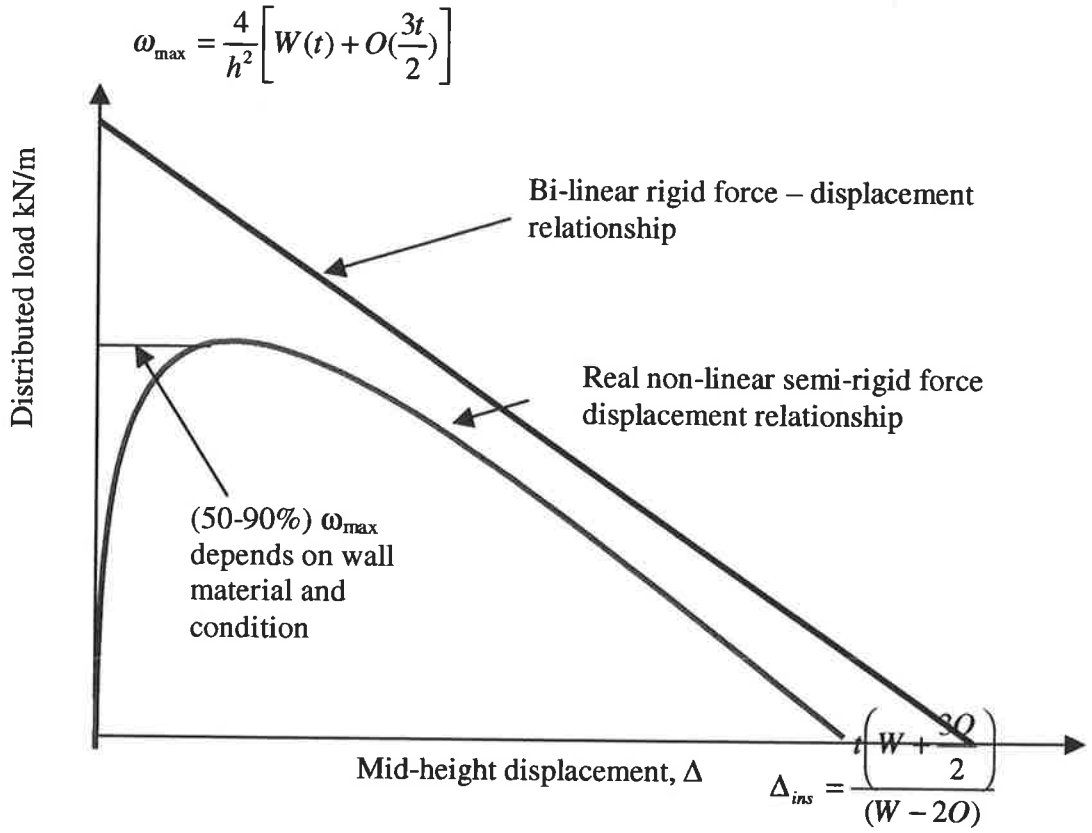

Figure D 4 - Rigid F-Δ Relationship– Top Vertical Reaction at Centerline

APPENDIX (E): Material Test Results

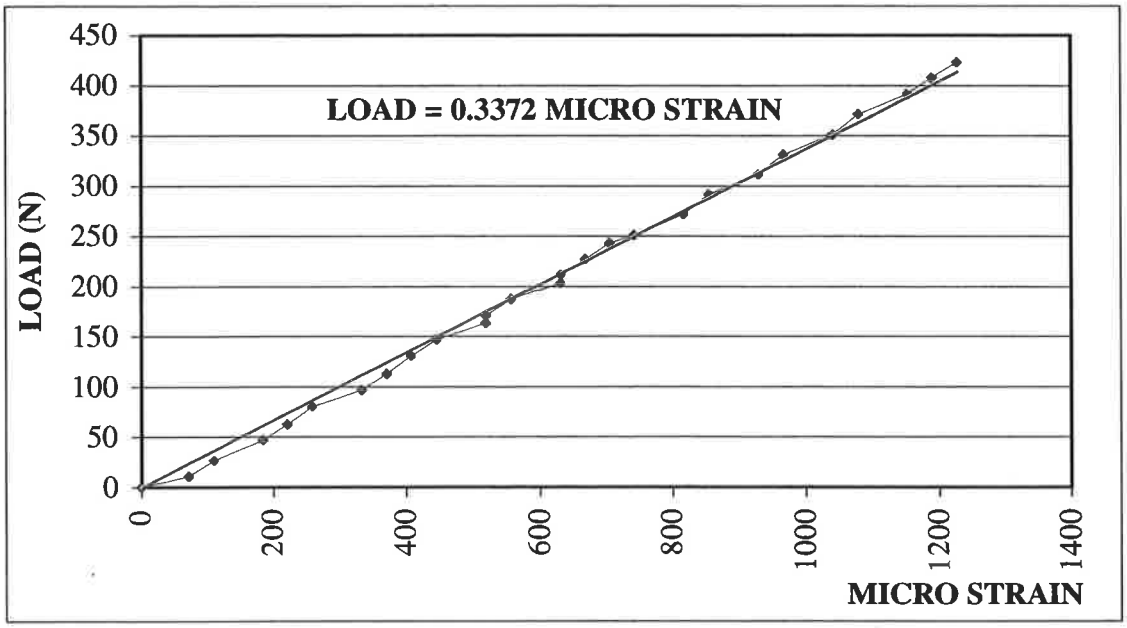

Figure E 1 - Bond Wrench Calibration Plot 110mm Brick Specimen Bond Wrench

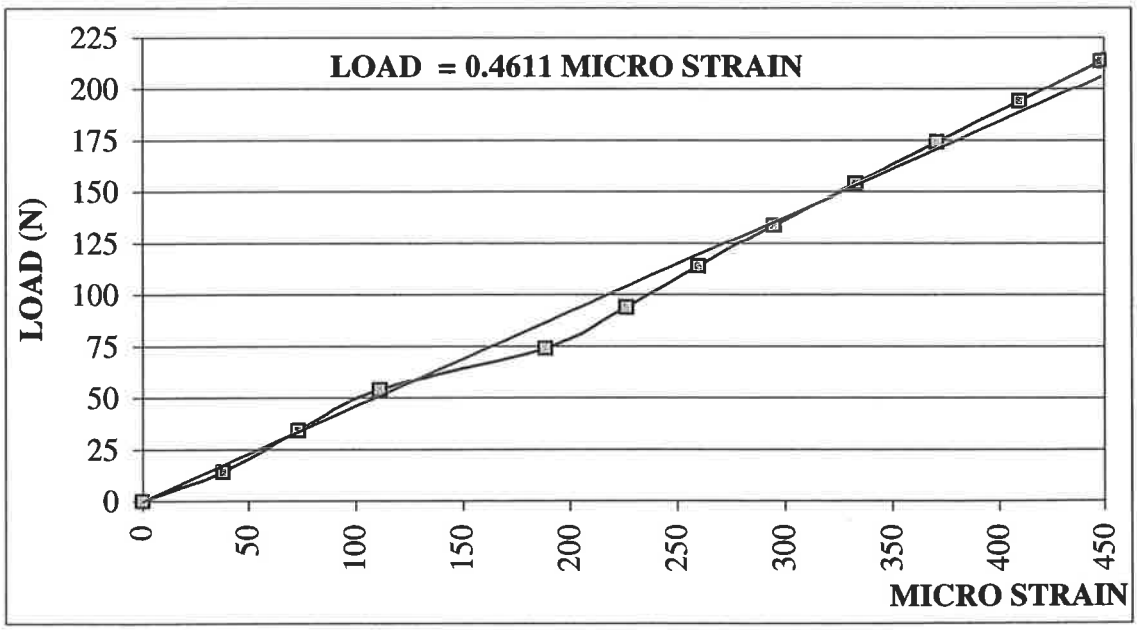

Figure E 2- Bond Wrench Calibration Plot 50mm Brick Specimen Bond Wrench

RESULTS OF BOND WRENCH TESTS

110mm TWO BRICK PRISMS TESTED MARCH 1998 (SERIES 1)

t_u	Brick thickness	110	mm
l	Brick length	230	mm
m_1	Mass bond wrench	4.043	kg
m_2	Mass at lever arm		
m_3	Brick and mortar mass above interface		
d_1	Front brick face to center of gravity	250	mm
d_2	Front brick face to notch	765	mm
Z_d	Elastic modulus	463833	mm^3
A_d	Bedded area	25300	mm^2
F_{sp}	Total compressive force on bedded area		

$$F_{sp} = 9.81(m_1 + m_2 + m_3)$$

M_{sp} Bending moment about the centroid of the bedded area

$$M_{sp} = 9.81m_2\left(d_2 - {}^{t_u}/_{2}\right) + 9.81m_1\left(d_1 - {}^{t_u}/_{2}\right)$$

f_{sp} Flexural strength of the specimen

$$f_{sp} = {}^{M_{sp}}/_{Z_d} - {}^{F_{sp}}/_{A_d}$$

Specimen No.	TEST NO.	micro strain	m^2 kg	m^3 kg	F_{sp} N	M_{sp} Nmm	f_{sp} MPa	Ave MPa	St Dev MPa
1	1		23.5	3.3	302.57	171413.91	0.36		
	2		14.3	3.17	211.04	107334.99	0.22	**0.28**	0.07
	3		17.1	3.62	242.93	126837.27	0.26		
2	1		27.2	3.09	336.81	197184.78	0.41		
	2		24.4	3.05	308.95	177682.50	0.37	**0.36**	0.06
	3		19.7	3.71	269.31	144946.53	0.30		
3	1		19.3	3	258.42	142160.49	0.30		
	2		32.1	3.06	384.58	231313.77	0.48	**0.40**	0.10
	3		28	2.99	343.67	202756.86	0.42		
4	1		22.9	3.14	295.11	167234.85	0.35		
	2		28.8	3.5	356.52	208328.94	0.44	**0.42**	0.07
	3		32.11	3.54	389.39	231383.42	0.48		

OVERALL AVERAGE F_{sp} FOR ALL 4 BATCHES	**0.37**
OVERALL ST DEV FOR ALL 4 BATCHES	0.08
LOWEST BOND VALUE	**0.22**
HIGHEST BOND VALUE	**0.48**

110mm PRE-DYNAMICALLY TESTED WALLS TESTED MARCH 1998 (SERIES 1)

t_u	Brick thickness	110	mm
l	Brick length	230	mm
m_1	Mass bond wrench	4.043	kg
m_2	Mass at lever arm		
m_3	Brick and mortar mass above interface		
d_1	Front brick face to center of gravity	250	mm
d_2	Front brick face to notch	765	mm
Z_d	Elastic modulus	463833	mm^3
A_d	Bedded area	25300	mm^2
F_{sp}	Total compressive force on bedded area		

$$F_{sp} = 9.81(m_1 + m_2 + m_3)$$

M_{sp} Bending moment about the centroid of the bedded area

$$M_{sp} = 9.81m_2\left(d_2 - {}^{t_u}/_{2}\right) + 9.81m_1\left(d_1 - {}^{t_u}/_{2}\right)$$

f_{sp} Flexural strength of the specimen

$$f_{sp} = {}^{M_{sp}}/_{Z_d} - {}^{F_{sp}}/_{A_d}$$

Specimen No.	TEST NO.	micro strain	m_2 kg	m_3 kg	F_{sp} N	M_{sp} Nmm	f_{sp} MPa	Ave MPa	St Dev MPa
1	1		48.01	3.8	347.92	342128.51	0.72		
	2		35.17	3.64	420.39	252696.62	0.53	**0.64**	0.10
	3		44.34	3.18	505.90	316566.59	0.66		
2	1		25.99	3.8	331.90	188757.01	0.39		
	2		31.09	3.5	378.99	224279.02	0.47	**0.47**	0.07
	3		36.19	4.03	434.22	259801.03	0.54		
3	1		35.17	3.5	419.01	252696.62	0.53		
	2		28.03	3.14	345.44	202965.81	0.42	**0.47**	0.05
	3		31.09	3.97	383.60	224279.02	0.47		
4	1		56.57	3.763	631.53	401749.76	0.84		
	2		40.27	3.72	471.20	288218.63	0.60	**0.61**	0.22
	3		25.99	3.925	333.13	188757.01	0.39		

OVERALL AVERAGE F_{sp} FOR ALL 4 BATCHES	**0.55**
OVERALL ST DEV FOR ALL 4 BATCHES	0.14
LOWEST BOND VALUE	**0.39**
HIGHEST BOND VALUE	**0.84**

110mm TWO BRICK PRISMS TESTED JUNE 1998 (SERIES 2)

t_u	Brick thickness	110	mm
l	Brick length	230	mm
m_1	Mass bond wrench	5.36	kg
m_2	Mass at lever arm		
m_3	Brick and mortar mass above interface		
d_1	Front brick face to center of gravity	200	mm
d_2	Front brick face to notch	765	mm
Z_d	Elastic modulus	463833	mm^3
A_d	Bedded area	25300	mm^2
F_{sp}	Total compressive force on bedded area		

$$F_{sp} = 9.81(m_1 + m_2 + m_3)$$

M_{sp} Bending moment about the centroid of the bedded area

$$M_{sp} = 9.81m_2\left(d_2 - {}^{t_u}/_2\right) + 9.81m_1\left(d_1 - {}^{t_u}/_2\right)$$

f_{sp} Flexural strength of the specimen

$$f_{sp} = {}^{M_{sp}}/_{Z_d} - {}^{F_{sp}}/_{A_d}$$

Specimen No.	TEST NO.	micro strain	m^2 kg	m^3 kg	F_{sp} N	M_{sp} Nmm	f_{sp} MPa	Ave MPa	St Dev MPa
5	1	750	25.78	2.984	334.75	187183.33	0.39		
	2	1260	43.31	3.058	507.45	309283.45	0.65	**0.58**	0.16
	3	1360	46.75	3.551	546.01	333224.65	0.70		
6	1	770	26.47	2.982	341.48	191971.57	0.40		
	2	770	26.47	2.985	341.51	191971.57	0.40	**0.42**	0.04
	3	900	30.94	2.974	385.24	223095.13	0.47		
7	1	1200	41.25	2.982	486.48	294918.73	0.62		
	2	1300	44.69	2.984	520.21	318859.93	0.67	**0.59**	0.09
	3	950	32.65	3.502	407.28	235065.73	0.49		
8	1	700	24.06	2.977	317.83	175212.73	0.37		
	2	1050	36.09	3.546	441.43	259006.93	0.54	**0.44**	0.09
	3	800	27.50	3.013	351.90	199153.93	0.42		

OVERALL AVERAGE F_{sp} FOR ALL 4 BATCHES	**0.52**
OVERALL ST DEV FOR ALL 4 BATCHES	0.12
LOWEST BOND VALUE	**0.37**
HIGHEST BOND VALUE	**0.71**

110mm PRE-DYNAMICALLY TESTED WALLS TESTED JUNE 1998 (SERIES 2)

t_u	Brick thickness	110	mm
l	Brick length	230	mm
m_1	Mass bond wrench	5.36	kg
m_2	Mass at lever arm		
m_3	Brick and mortar mass above interface		
d_1	Front brick face to center of gravity	200	mm
d_2	Front brick face to notch	765	mm
Z_d	Elastic modulus	463833	mm^3
A_d	Bedded area	25300	mm^2
F_{sp}	Total compressive force on bedded area		

$$F_{sp} = 9.81(m_1 + m_2 + m_3)$$

M_{sp} Bending moment about the centroid of the bedded area

$$M_{sp} = 9.81m_2\left(d_2 - {}^{t_u}\!/_{2}\right) + 9.81m_1\left(d_1 - {}^{t_u}\!/_{2}\right)$$

f_{sp} Flexural strength of the specimen

$$f_{sp} = {}^{M_{sp}}\!/_{Z_d} - {}^{F_{sp}}\!/_{A_d}$$

Specimen No.	TEST NO.	micro strain	m^2 kg	m^3 kg	F_{sp} N	M_{sp} Nmm	f_{sp} MPa	Ave MPa	St Dev MPa
5	1	1050	36.91	2.984	443.92	264693.30	0.55		
	2	1100	38.67	3.058	461.89	276934.68	0.58	**0.71**	0.25
	3	1900	66.79	3.551	742.59	472796.75	0.99		
6	1	1000	35.15	2.982	426.66	252451.92	0.53		
	2	1300	45.70	2.985	530.14	325900.19	0.68	**0.56**	0.11
	3	900	31.64	2.974	392.10	227969.16	0.48		
7	1	800	28.12	2.982	357.70	203486.40	0.42		
	2	500	17.58	2.984	254.27	130038.13	0.27	**0.41**	0.13
	3	1000	35.15	3.502	431.76	252451.92	0.53		
8	1	1000	35.15	2.977	426.61	252451.92	0.53		
	2	1200	42.18	3.546	501.16	301417.44	0.63	**0.59**	0.05
	3	1150	40.42	3.013	478.69	289176.06	0.60		

OVERALL AVERAGE Fsp FOR ALL 4 BATCHES	**0.57**
OVERALL ST DEV FOR ALL 4 BATCHES	0.17
LOWEST BOND VALUE	**0.27**
HIGHEST BOND VALUE	**0.99**

110mm TWO BRICK PRISMS TESTED SEPTEMBER 1998

t_u	Brick thickness	110	mm
l	Brick length	230	mm
m_1	Mass bond wrench	5.36	kg
m_2	Mass at lever arm		
m_3	Brick and mortar mass above interface		
d_1	Front brick face to notch	200	mm
d_2	Front brick face to center of gravity	765	mm
Z_d	Elastic modulus	463833	mm^3
A_d	Bedded area	25300	mm^2
F_{sp}	Total compressive force on bedded area		

$$F_{sp} = 9.81(m_1 + m_2 + m_3)$$

M_{sp} Bending moment about the centroid of the bedded area

$$M_{sp} = 9.81m_2\left(d_2 - {}^{t_u}/_2\right) + 9.81m_1\left(d_1 - {}^{t_u}/_2\right)$$

f_{sp} Flexural strength of the specimen

$$f_{sp} = {}^{M_{sp}}/_{Z_d} - {}^{F_{sp}}/_{A_d}$$

Specimen No.	TEST NO.	micro strain	m^2 kg	m^3 kg	F_{sp} N	M_{sp} Nmm	f_{sp} MPa	Ave MPa	St Dev MPa
11	1	300	10.55	2.984	185.30	81072.61	0.17		
	2	1050	36.91	3.058	444.65	264693.30	0.55	**0.32**	0.20
	3	450	15.82	3.551	242.59	117796.75	0.24		
12	1	600	21.09	2.982	288.73	154520.88	0.32		
	2	500	17.58	2.985	254.28	130038.13	0.27	**0.30**	0.03
	3	550	19.33	2.974	271.41	142279.50	0.30		
14	1	750	26.36	2.982	340.46	191245.02	0.40		
	2	450	15.82	2.984	237.03	117796.75	0.24	**0.29**	0.10
	3	400	14.06	3.052	220.45	105555.37	0.22		

OVERALL AVERAGE Fsp FOR 3 BATCHES	**0.30**
OVERALL ST DEV FOR 3 BATCHES	0.11
LOWEST BOND VALUE	**0.17**
HIGHEST BOND VALUE	**0.55**

50mm TWO BRICK PRISMS TESTED SEPTEMBER 1998

t_u	Brick thickness	50	mm
l	Brick length	230	mm
m_1	Mass bond wrench	3.5	kg
m_2	Mass at lever arm		
m_3	Brick and mortar mass above interface		
d_1	Front brick face to notch	192	mm
d_2	Front brick face to center of gravity	592	mm
Z_d	Elastic modulus	95833	mm^3
A_d	Bedded area	11500	mm^2
F_{sp}	Total compressive force on bedded area		

$$F_{sp} = 9.81(m_1 + m_2 + m_3)$$

M_{sp} Bending moment about the centroid of the bedded area

$$M_{sp} = 9.81m_2\left(d_2 - {}^{t_u}\!/_{2}\right) + 9.81m_1\left(d_1 - {}^{t_u}\!/_{2}\right)$$

f_{sp} Flexural strength of the specimen

$$f_{sp} = {}^{M_{sp}}\!/_{Z_d} - {}^{F_{sp}}\!/_{A_d}$$

Specimen No.	TEST NO.	micro strain	m_2 kg	m_3 kg	F_{sp} N	M_{sp} Nmm	f_{sp} MPa	Ave MPa	St Dev MPa
10	1	300	14.37	0.9	184.16	85680.95	0.88		
	2	300	14.37	0.9	184.16	85680.95	0.88	**0.70**	0.30
	3	110	5.27	0.9	94.86	35047.85	0.36		
13	1	185	8.86	0.9	130.11	55034.60	0.56		
	2	295	14.13	0.9	181.81	84348.50	0.86	**0.76**	0.17
	3	295	14.13	0.9	181.81	84348.50	0.86		

OVERALL AVERAGE F_{sp} FOR 2 BATCHES	**0.73**
OVERALL ST DEV FOR 2 BATCHES	0.22
LOWEST BOND VALUE	**0.36**
HIGHEST BOND VALUE	**0.88**

RESULTS OF MODULUS TESTS

SPECIMEN No. (2) – 110mm THICK TESTED MARCH 1998

LOAD (N)	DEMEC (1) brick	DEMEC (2) brick/mortar	STRAIN (1) brick	STRAIN (2) brick/mortar	Δ(1) brick	Δ(2) brick/mortar	Δ(comb)	COMB STRAIN	STRESS MPa
0	782	943	0	0	0	0	0	0	0
25000	781	942	0.0000252	0.00001	0.00128	0.002032	0.0012457	0.0000072	0.99
50000	779	930	0.0000756	0.00013	0.00384	0.026416	0.024057	0.0001398	1.98
75000	775	926	0.0001764	0.00017	0.00896	0.034544	0.029040	0.0001688	2.96
100000	767	920	0.000378	0.00023	0.0192	0.046736	0.034941	0.000203	3.95
125000	763	911	0.0004788	0.00032	0.02432	0.065024	0.050084	0.0002911	4.94
150000	758	900	0.0006048	0.00043	0.03072	0.087376	0.068554	0.0003982	5.93
332000	ULTIMATE	5% ULTIMATE		16,600	N				0.66
		33% ULTIMATE		110,556	N				4.37
		Estimate Modulus		15,000 MPa					

SPECIMEN No. (3) – 110mm THICK TESTED MARCH 1998

LOAD (N)	DEMEC (1) brick	DEMEC (2) brick/mortar	STRAIN (1) brick	STRAIN (2) brick/mortar	Δ(1) brick	Δ(2) brick/mortar	Δ(comb)	COMB STRAIN	STRESS MPa
0	988	911	0	0	0	0	0	0	0
25000	995	855	-0.0001764	0.00056	-0.00896	0.113792	0.119295	0.0006935	0.99
50000	994	846	-0.0001512	0.00065	-0.00768	0.13208	0.136797	0.0007953	1.98
75000	993	827	-0.000126	0.00084	-0.0064	0.170688	0.174619	0.0010152	2.96
100000	989	805	-0.0000252	0.00106	-0.00128	0.215392	0.216178	0.001256	3.95
125000	986	780	0.0000504	0.00131	0.00256	0.266192	0.264619	0.001538	4.94
150000	982	765	0.0001512	0.00146	0.00768	0.296672	0.291954	0.001697	5.93
336000	ULTIMATE	5% ULTIMATE		16,800	N				0.66
		33% ULTIMATE		111,888	N				4.42
		Estimate Modulus		3,300 MPa					

SPECIMEN No. (4) – 110mm THICK TESTED MARCH 1998

LOAD (N)	DEMEC (1) brick	DEMEC (2) brick/mortar	STRAIN (1) brick	STRAIN (2) brick/mortar	Δ(1) brick	Δ(2) brick/mortar	Δ(comb)	COMB STRAIN	STRESS MPa
0	796	939	0	0	0	0	0	0	0
25000	795	910	0.0000252	0.00029	0.00128	0.058928	0.0581417	0.0003380	0.99
50000	794	887	0.0000504	0.00052	0.00256	0.105664	0.1040914	0.0006051	1.98
75000	792	864	0.0001008	0.00075	0.00512	0.1524	0.1492549	0.0008677	2.96
100000	789	843	0.0001764	0.00096	0.00896	0.195072	0.189568	0.001102	3.95
125000	786	820	0.000252	0.00119	0.0128	0.241808	0.2339452	0.001360	4.94
150000	782	791	0.0003528	0.00148	0.01792	0.300736	0.289728	0.001684	5.93
333000	ULTIMATE	5% ULTIMATE		16,650	N				0.66
		33% ULTIMATE		110,889	N				4.38
		Estimate Modulus		3,300 MPa					

SPECIMEN No. (5) – 110mm THICK TESTED JUNE 1998

LOAD (N)	DEMEC (1) brick	DEMEC (2) brick/mortar	STRAIN (1) brick	STRAIN (2) brick/mortar	Δ(1) brick	Δ(2) brick/mortar	Δ(comb)	COMB STRAIN	STRESS MPa
0	797	812	0	0	0	0	0	0	0.00
25000	796	810	2.52E-05	0.00002	0.0013	0.004064	0.003277726	1.90565E-05	0.99
50000	795	808	5.04E-05	0.00004	0.0026	0.008128	0.006555451	3.81131E-05	1.98
75000	793	805	0.000101	0.00007	0.0051	0.014224	0.011078903	6.44122E-05	2.96
100000	792	796	0.000126	0.00016	0.0064	0.032512	0.028580629	0.000166166	3.95
125000	780	790	0.000428	0.00022	0.0218	0.044704	0.031337337	0.000182194	4.94
150000	778	781	0.000479	0.00031	0.0243	0.062992	0.048052789	0.000279377	5.93
175000	777	772	0.000504	0.0004	0.0256	0.08128	0.065554515	0.000381131	6.92
200000	775	762	0.000554	0.0005	0.0282	0.1016	0.084301966	0.000490128	7.91
360000	ULTIMATE	5% ULTIMATE		18,000	N				0.71
		33% ULTIMATE		119,880	N				4.74
		Estimate Modulus		16,000 MPa					

SPECIMEN No. (6) – 110mm THICK TESTED JUNE 1998

LOAD (N)	DEMEC (1) brick	DEMEC (2) brick/mortar	STRAIN (1) brick	STRAIN (2) brick/mortar	Δ(1) brick	Δ(2) brick/mortar	Δ(comb)	COMB STRAIN	STRESS MPa
0	911	918	0	0	0	0	0	0	0.00
25000	903	918	0.000202	0	0.0102	0	-0.00629019	-3.6571E-05	0.99
50000	902	916	0.000227	0.00002	0.0115	0.004064	-0.00301247	-1.7514E-05	1.98
75000	893	916	0.000454	0.00002	0.023	0.004064	-0.01008894	-5.8657E-05	2.96
100000	883	916	0.000706	0.00002	0.0358	0.004064	-0.01795168	-0.00010437	3.95
125000	791	915	0.003024	0.00003	0.1536	0.006096	-0.08825691	-0.00051312	4.94
150000	795	910	0.002923	0.00008	0.1485	0.016256	-0.07495182	-0.00043577	5.93
338,000	ULTIMATE	5% ULTIMATE		16,900	N				0.67
		33% ULTIMATE		112,554	N				4.45

Estimate Modulus Unreliable Data No Estimate

SPECIMEN No. (7) – 110mm THICK TESTED JUNE 1998

LOAD (N)	DEMEC (1) brick	DEMEC (2) brick/mortar	STRAIN (1) brick	STRAIN (2) brick/mortar	Δ(1) brick	Δ(2) brick/mortar	Δ(comb)	COMB STRAIN	STRESS MPa
0	812	951	0	0	0	0	0	0	0.00
25000	812	947	0	0.00004	0	0.008128	0.008128	4.72558E-05	0.99
50000	808	945	0.000101	0.00006	0.0051	0.012192	0.009046903	5.25983E-05	1.98
75000	807	940	0.000126	0.00011	0.0064	0.022352	0.018420629	0.000107097	2.96
100000	807	933	0.000126	0.00018	0.0064	0.036576	0.032644629	0.000189794	3.95
125000	804	927	0.000202	0.00024	0.0102	0.048768	0.042477806	0.000246964	4.94
150000	802	918	0.000252	0.00033	0.0128	0.067056	0.059193257	0.000344147	5.93
175000	799	907	0.000328	0.00044	0.0166	0.089408	0.079186434	0.000460386	6.92
200000	797	897	0.000378	0.00054	0.0192	0.109728	0.097933886	0.000569383	7.91
313000	ULTIMATE	5% ULTIMATE		15,650	N				0.62
		33% ULTIMATE		104,229	N				4.12

Estimate Modulus 13,900 MPa

SPECIMEN No. (8) – 110mm THICK TESTED JUNE 1998

LOAD (N)	DEMEC (1) brick	DEMEC (2) brick/mortar	STRAIN (1) brick	STRAIN (2) brick/mortar	Δ(1) brick	Δ(2) brick/mortar	Δ(comb)	COMB STRAIN	STRESS MPa
0	840	918	0	0	0	0	0	0	0.00
25000	835	907	0.000126	0.00011	0.0064	0.022352	0.018420629	0.000107097	0.99
50000	831	893	0.000227	0.00025	0.0115	0.0508	0.043723532	0.000254207	1.98
75000	830	880	0.000252	0.00038	0.0128	0.077216	0.069353257	0.000403217	2.96
100000	829	866	0.000277	0.00052	0.0141	0.105664	0.097014983	0.000564041	3.95
125000	827	849	0.000328	0.00069	0.0166	0.140208	0.129986434	0.000755735	4.94
150000	826	830	0.000353	0.00088	0.0179	0.178816	0.16780816	0.000975629	5.93
175000	823	809	0.000428	0.00109	0.0218	0.221488	0.208121337	0.001210008	6.92
200000	819	786	0.000529	0.00132	0.0269	0.268224	0.25171224	0.001463443	7.91
245000	ULTIMATE	5% ULTIMATE		12,250	N				0.48
		33% ULTIMATE		81,585	N				3.22
		Estimate Modulus		5,400 MPa					

SPECIMEN No. (10) – 50mm THICK TESTED SEPTEMBER 1998

LOAD (N)	DEMEC (1) brick/mortar	STRAIN (1) brick/mortar	DEMEC (1) brick/mortar	STRAIN (1) brick/mortar	DEMEC (1) brick/mortar	STRAIN (1) brick/mortar	DEMEC (1) brick/mortar	STRAIN (1) brick/mortar	Stress MPa
0	898	0	901	0	895	0.000000	898	0.000000	0.00
15000	897.5	0.0000126	898	0.0000756	888	0.000176	895	0.000076	1.30
30000	890	0.0002016	892	0.0002268	884	0.000277	889	0.000227	2.61
45000	884	0.0003528	886	0.000378	882	0.000328	882	0.000403	3.91
60000	880	0.0004536	878	0.0005796	872	0.000580	877	0.000529	5.22
75000	874	0.0006048	873	0.0007056	865	0.000756	868	0.000756	6.52
90000	870.5	0.000693	864	0.0009324	865	0.000756	864	0.000857	7.83
	Test 1 Modulus Estimate	11,300MPa	Test 2 Modulus Estimate	8,400MPa	Test 3 Modulus Estimate	10,400MPa	Test 4 Modulus Estimate	9,100MPa	
307000	ULTIMATE	5% ULTIMATE		15,350	N				1.33
		33% ULTIMATE		102,231	N				8.89
		Average Modulus		9,800 MPa					

SPECIMEN No. (11) – 110mm THICK TESTED SEPTEMBER 1998

LOAD (N)	DEMEC (1) brick	DEMEC (2) brick/mortar	STRAIN (1) brick	STRAIN (2) brick/mortar	Δ(1) brick	Δ(2) brick/mortar	Δ(comb)	COMB STRAIN	STRESS MPa
0	812	901	0	0	0.000000	0.000000	0.000000	0.000000	0.00
25000	811	887	0.0000252	0.00014	0.001280	0.028448	0.027662	0.000161	0.99
50000	809.5	871	0.000063	0.0003	0.003200	0.060960	0.058994	0.000343	1.98
75000	808	857	0.0001008	0.00044	0.005121	0.089408	0.086263	0.000502	2.96
100000	806	844	0.0001512	0.00057	0.007681	0.115824	0.111106	0.000646	3.95
125000	805	831	0.0001764	0.0007	0.008961	0.142240	0.136736	0.000795	4.94
150000	801.5	820	0.0002646	0.00081	0.013442	0.164592	0.156336	0.000909	5.93
359000	ULTIMATE	5% ULTIMATE		17,950	N				0.71
		33% ULTIMATE		119,547	N				4.73
		Estimate Modulus		6,600 MPa					

SPECIMEN No. (12) – 110mm THICK TESTED SEPTEMBER 1998

LOAD (N)	DEMEC (1) brick	DEMEC (2) brick/mortar	STRAIN (1) brick	STRAIN (2) brick/mortar	Δ(1) brick	Δ(2) brick/mortar	Δ(comb)	COMB STRAIN	STRESS MPa
0	807.5	914	0	0	0.000000	0.000000	0.000000	0.000000	0.00
25000	805	908.5	0.000063	0.000055	0.003200	0.011176	0.009210	0.000054	0.99
50000	802.5	900.5	0.000126	0.000135	0.006401	0.027432	0.023501	0.000137	1.98
75000	800	892	0.000189	0.00022	0.009601	0.044704	0.038807	0.000226	2.96
100000	795.5	883	0.0003024	0.00031	0.015362	0.062992	0.053557	0.000311	3.95
125000	793	875	0.0003654	0.00039	0.018562	0.079248	0.067847	0.000394	4.94
150000	788	866	0.0004914	0.00048	0.024963	0.097536	0.082204	0.000478	5.93
397000	ULTIMATE	5% ULTIMATE		19,850	N				0.78
		33% ULTIMATE		132,200	N				5.23
		Estimate Modulus		11,600 MPa					

SPECIMEN No. (13) – 110mm THICK TESTED SEPTEMBER 1998

LOAD (N)	DEMEC (1) brick	DEMEC (2) brick/mortar	STRAIN (1) brick	STRAIN (2) brick/mortar	Δ(1) brick	Δ(2) brick/mortar	Δ(comb)	COMB STRAIN	STRESS MPa
0	900	916	0	0	0.000000	0.000000	0.000000	0.000000	0.00
25000	894	916	0.0001512	0	0.007681	0.000000	-0.004718	-0.000027	0.99
50000	887.5	915	0.000315	0.00001	0.016002	0.002032	-0.007796	-0.000045	1.98
75000	884	912	0.0004032	0.00004	0.020483	0.008128	-0.004452	-0.000026	2.96
100000	880.5	908	0.0004914	0.00008	0.024963	0.016256	0.000924	0.000005	3.95
125000	877	902	0.0005796	0.00014	0.029444	0.028448	0.010364	0.000060	4.94
397000	ULTIMATE	5% ULTIMATE		19,850	N				0.78
		33% ULTIMATE		132,200	N				5.23

Estimate Modulus Unreliable Data No Estimate

SPECIMEN No. (10) – 50mm THICK TESTED SEPTEMBER 1998

LOAD (N)	DEMEC (1) brick/mortar	STRAIN (1) brick/mortar	DEMEC (1) brick/mortar	STRAIN (1) brick/mortar	DEMEC (1) brick/mortar	STRAIN (1) brick/mortar	DEMEC (1) brick/mortar	STRAIN (1) brick/mortar	Stress MPa
0	873	0	811	0	867	0.000000	803	0.000000	0.00
15000	858	0.000378	808	0.0000756	845	0.000554	802	0.000025	1.30
30000	844	0.0007308	802	0.0002268	825	0.001058	801	0.000050	2.61
45000	825	0.0012096	799	0.0003024	814	0.001336	797	0.000151	3.91
60000	818	0.001386	794.5	0.0004158	802	0.001638	794	0.000227	5.22
75000	811	0.0015624	786	0.00063	795	0.001814	790	0.000328	6.52
90000	805	0.0017136	782	0.0007308	788	0.001991	787	0.000403	7.83
105000	794	0.0019908	780	0.0007812	773	0.002369	785	0.000454	9.13
120000	779	0.0023688	776	0.000882	763	0.002621	782	0.000529	10.43
	Test 1 Modulus Estimate	4,400MPa	Test 2 Modulus Estimate	11,800MPa	Test 3 Modulus Estimate	4,000MPa	Test 4 Modulus Estimate	Unreliable Data	
303000	ULTIMATE	5% ULTIMATE		15,150	N				1.32
		33% ULTIMATE		100,900	N				8.77

Average Modulus 6,700 MPa

RESULTS OF COMPRESSIVE MORTAR CUBE TESTS

Series	Specimen No.	Specimen Thickness (mm)	Cube Number (100x100x100mm)	Compressive Strength (MPa)
March1998	1	110	1	5.20
			2	5.02
			3	6.82
March1998	2	110	1	5.88
			2	6.18
			3	5.62
March1998	3	110	1	**7.16**
			2	6.84
			3	6.42
March1998	4	110	1	**7.16**
			2	6.34
			3	6.14
June 1998	5	110	1	6.02
			2	4.30
June 1998	6	110	1	6.06
			2	4.04
June 1998	7	110	1	4.02
			2	4.98
June 1998	8	110	1	5.06
			2	4.32
			3	4.16
September 1998	10	50	1	5.00
			2	5.20
			3	5.48
September 1998	11	110	1	4.68
			2	4.22
			3	4.90
September 1998	12	110	1	5.28
			2	4.94
			3	5.08
September 1998	13	110	1	**3.76**
			2	4.04
			3	3.84
September 1998	14	50	1	4.08
			2	3.56
			3	4.44
			AVERAGE	5.17

APPENDIX (F): Simply Supported Wall Test Results

MARCH 98
SPECIMEN 3

Height	1.485	m
Thickness	110	mm
Length	950	mm
Density	1800	kg/m^3

Applied Overburden	0	MPa
Flexural Tensile Strength, f'_t	460	kPa
Linear Elastic Analysis Prediction	**2.644**	kN
Rigid Body Analysis Prediction	**0.406**	kN

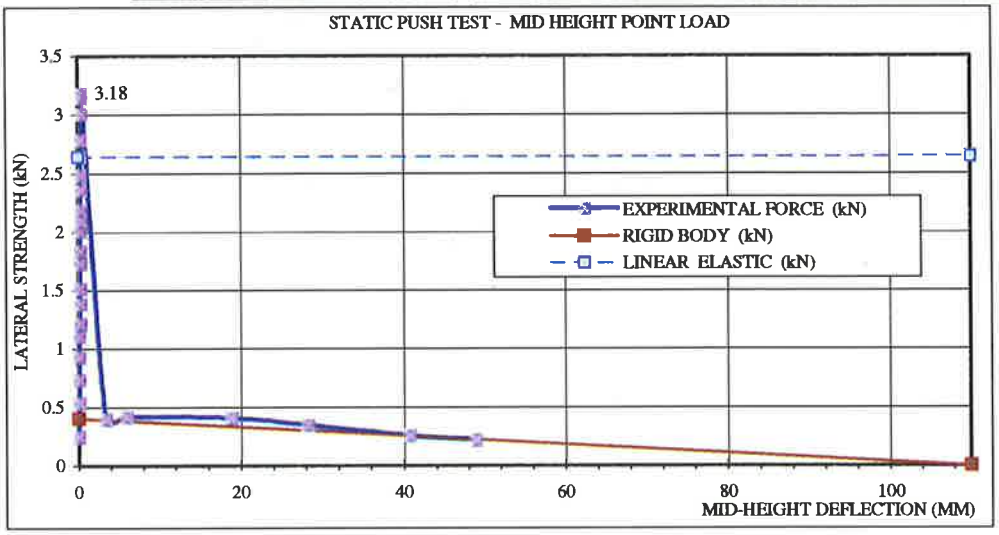

Figure F 1– Static Push Test – Un-cracked, 110mm, No Overburden

JUNE 98
SPECIMEN 8

Height	1.485	m
Thickness	110	mm
Length	950	mm
Density	1800	kg/m^3

Applied Overburden	0.15	MPa
Flexural Tensile Strength, f'_t	460	kPa
Linear Elastic Analysis Prediction	**4.8212**	kN
Rigid Body Analysis Prediction	**5.316**	kN

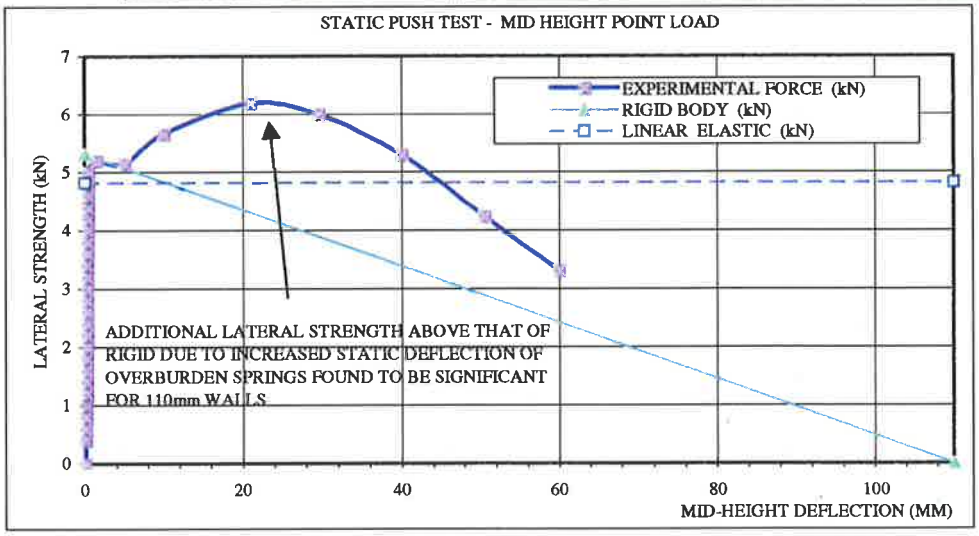

Figure F 2– Static Push Test – Un-cracked, 110mm, 0.15MPa Overburden

JUNE 98
SPECIMEN 8

Height	1.485	m
Thickness	110	mm
Length	950	mm
Density	1800	kg/m^3

Applied Overburden	0.15	MPa
Flexural Tensile Strength, f_t	0	kPa
Linear Elastic Analysis Prediction	2.322	kN
Rigid Body Analysis Prediction	5.316	kN

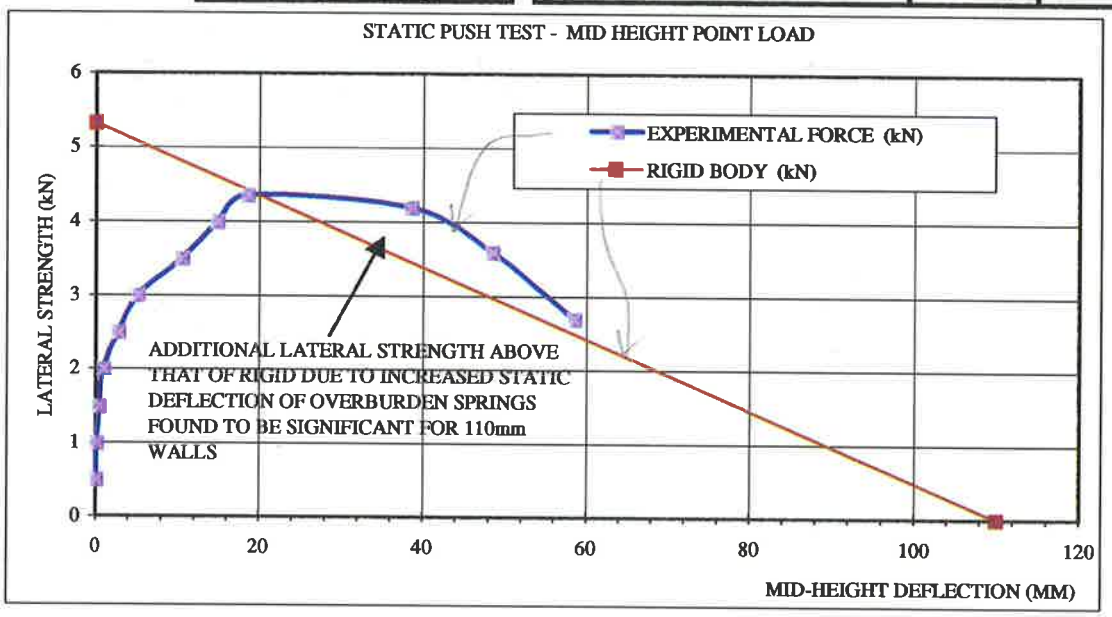

Figure F 3– Static Push Test – Cracked, 110mm, 0.15MPa Overburden

SEPTEMBER 98
SPECIMEN 10

Height	1.485	m
Thickness	50	mm
Length	950	mm
Density	2300	kg/m^3

Applied Overburden	0	MPa
Flexural Tensile Strength, f_t	0	kPa
Linear Elastic Analysis Prediction	0.071	kN
Rigid Body Analysis Prediction	0.107	kN

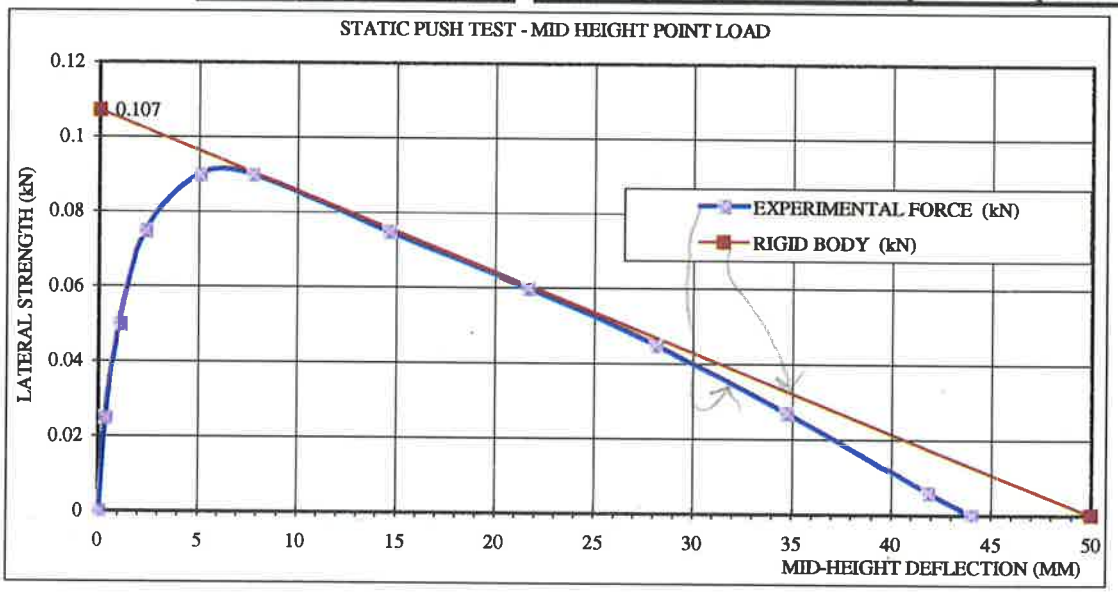

Figure F 4- Static Push Test – Cracked, 50mm, No Overburden

SEPTEMBER 98 SPECIMEN 10			
	Height	*1.485*	m
	Thickness	*50*	mm
	Length	*950*	mm
	Density	*2300*	kg/m^3

Applied Overburden	*0.075*	MPa
Flexural Tensile Strength, f'_t	*750*	kPa
Linear Elastic Analysis Prediction	***1.071***	kN
Rigid Body Analysis Prediction	***0.587***	kN

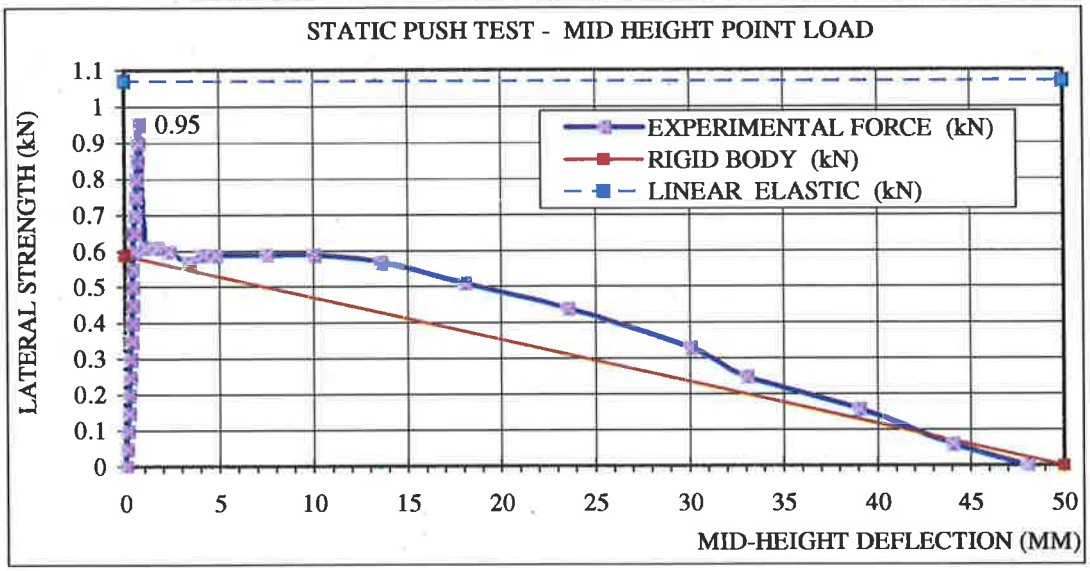

Figure F 5 - Static Push Test – Un-cracked, 50mm, 0.075MPa Overburden

SEPTEMBER 98 SPECIMEN 10			
	Height	*1.485*	m
	Thickness	*50*	mm
	Length	*950*	mm
	Density	*2300*	kg/m^3

Applied Overburden	*0.075*	MPa
Flexural Tensile Strength, f'_t	*0*	kPa
Linear Elastic Analysis Prediction	***0.286***	kN
Rigid Body Analysis Prediction	***0.618***	kN

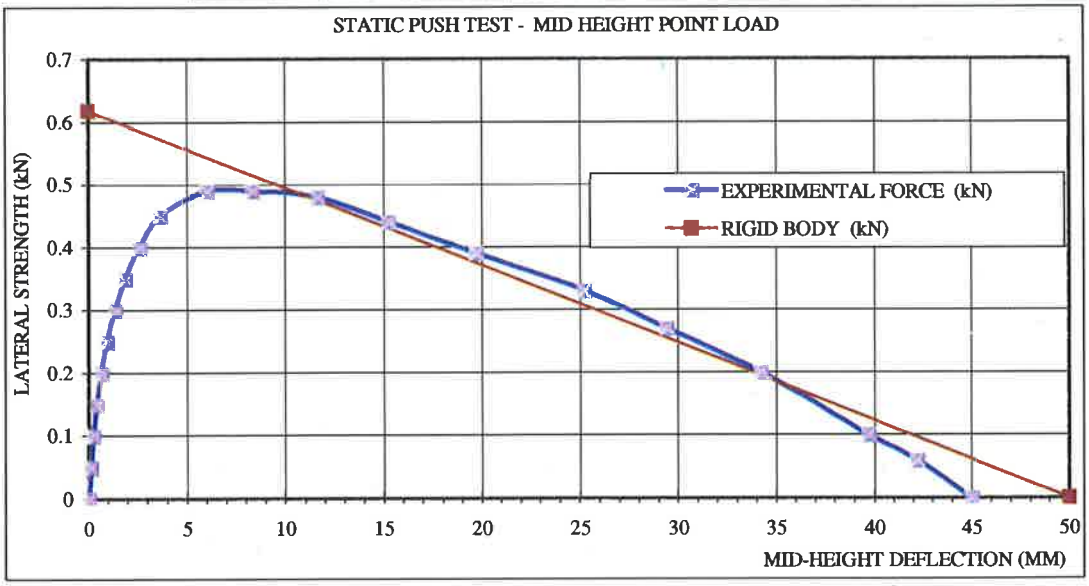

Figure F 6- Static Push Test – Cracked, 50mm, 0.075 Overburden

SEPTEMBER 98
SPECIMEN 11

Height	*1.485*	m
Thickness	*110*	mm
Length	*950*	mm
Density	*1800*	kg/m^3

Applied Overburden	*0*	MPa
Flexural Tensile Strength, f_t	*0*	kPa
Linear Elastic Analysis Prediction	***0.271***	kN
Rigid Body Analysis Prediction	***0.406***	kN

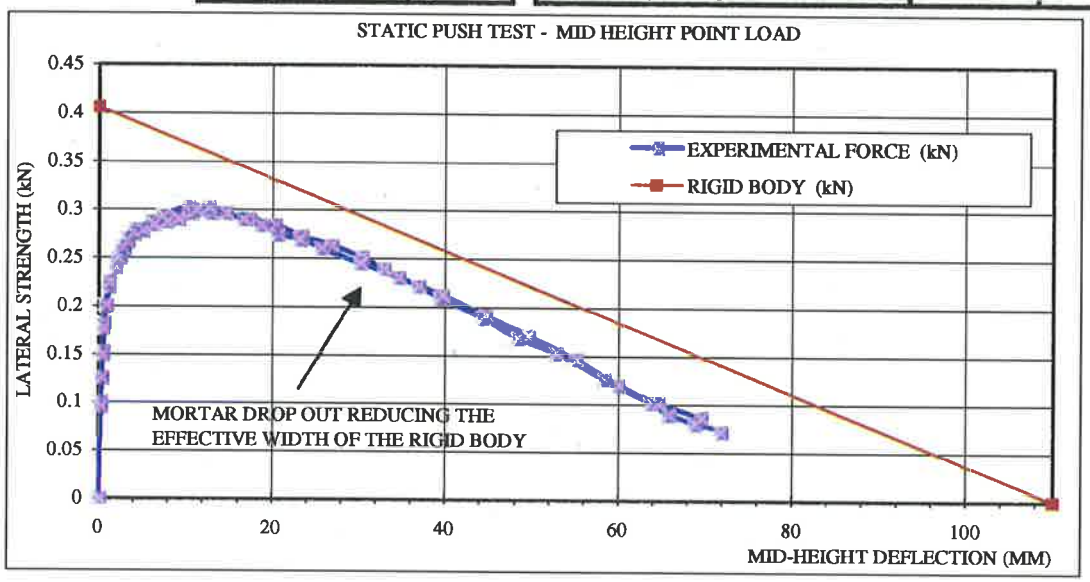

Figure F 7- Static Push Test – Cracked, 110mm, No Overburden

SEPTEMBER 98
SPECIMEN 11

Height	*1.485*	m
Thickness	*110*	mm
Length	*950*	mm
Density	*1800*	kg/m^3

Applied Overburden	*0.15*	MPa
Flexural Tensile Strength, f_t	*460*	kPa
Linear Elastic Analysis Prediction	***4.8212***	kN
Rigid Body Analysis Prediction	***5.316***	kN

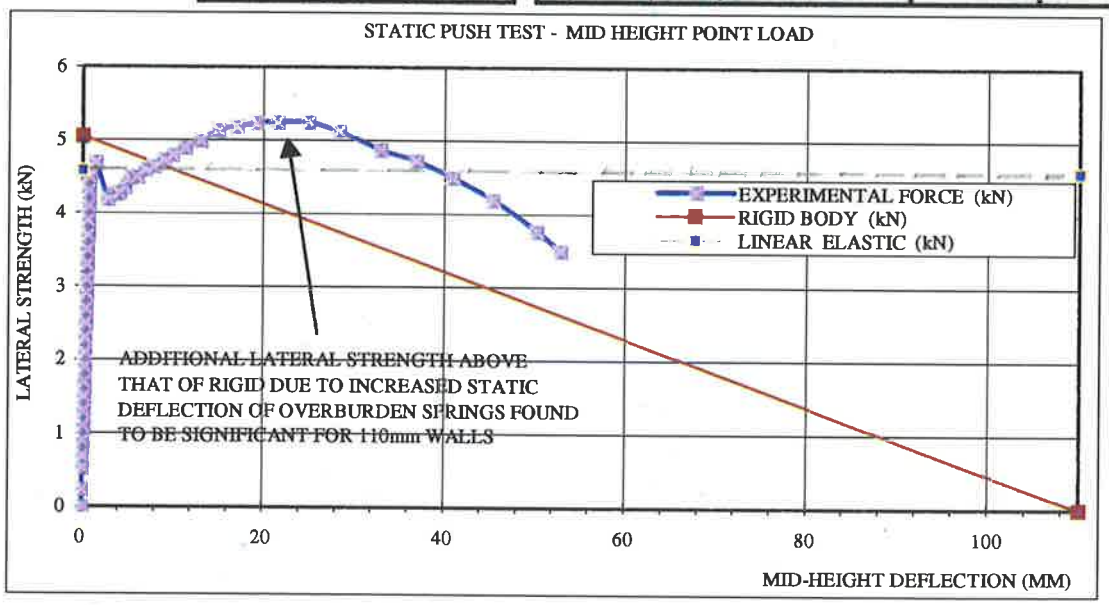

Figure F 8 - Static Push Test – Un-cracked, 110mm, 0.15MPa Overburden

SEPTEMBER 98 SPECIMEN 12	Height	*1.485*	m	Applied Overburden	*0*	MPa
	Thickness	*110*	mm	Flexural Tensile Strength, f_t	*460*	kPa
	Length	*950*	mm	Linear Elastic Analysis Prediction	***2.644***	kN
	Density	*1800*	kg/m^3	Rigid Body Analysis Prediction	***0.406***	kN

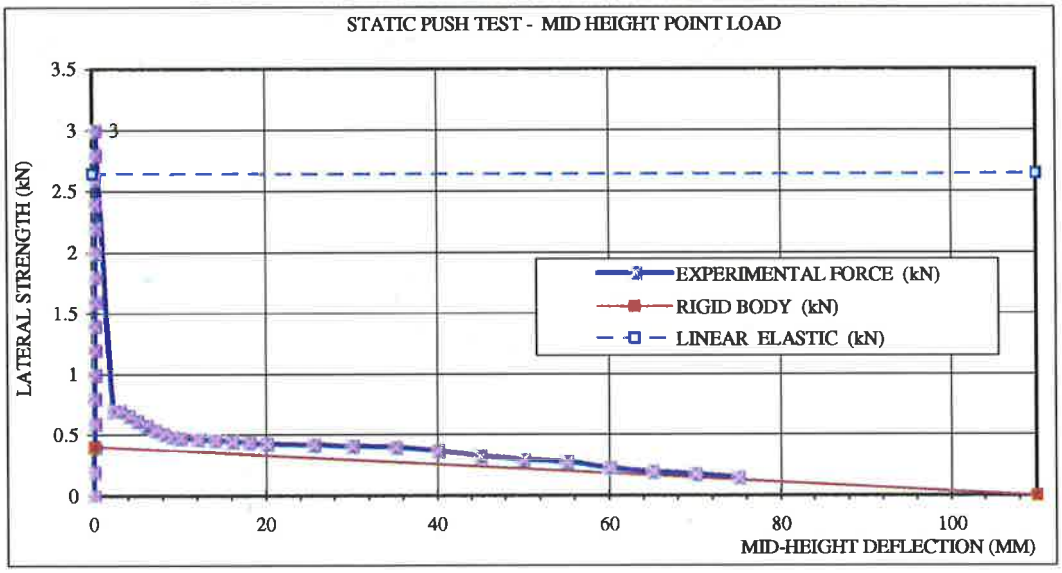

Figure F 9 - Static Push Test – UN-cracked, 110mm, No Overburden

SEPTEMBER 98 SPECIMEN 12	Height	*1.485*	m	Applied Overburden	*0*	MPa
	Thickness	*110*	mm	Flexural Tensile Strength, f_t	*0*	kPa
	Length	*950*	mm	Linear Elastic Analysis Prediction	***0.271***	kN
	Density	*1800*	kg/m^3	Rigid Body Analysis Prediction	***0.406***	kN

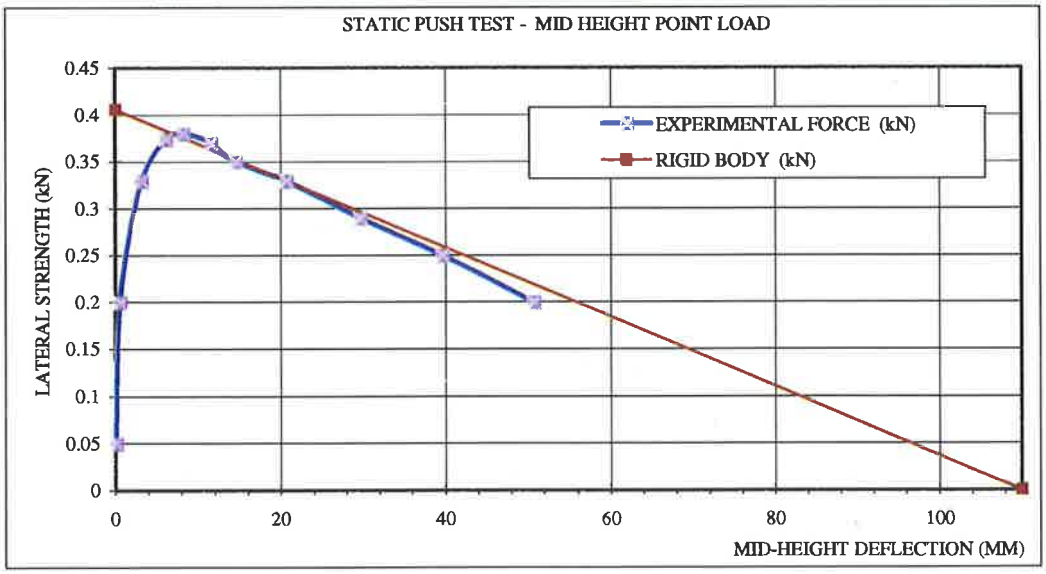

Figure F 10- Static Push Test – Cracked, 110mm, No Overburden

SEPTEMBER 98
SPECIMEN 13

Height	*1.485*	m
Thickness	*110*	mm
Length	*950*	mm
Density	*1800*	kg/m^3

Applied Overburden	*0*	MPa
Flexural Tensile Strength, f_t	*460*	kPa
Linear Elastic Analysis Prediction	***2.644***	kN
Rigid Body Analysis Prediction	***0.406***	kN

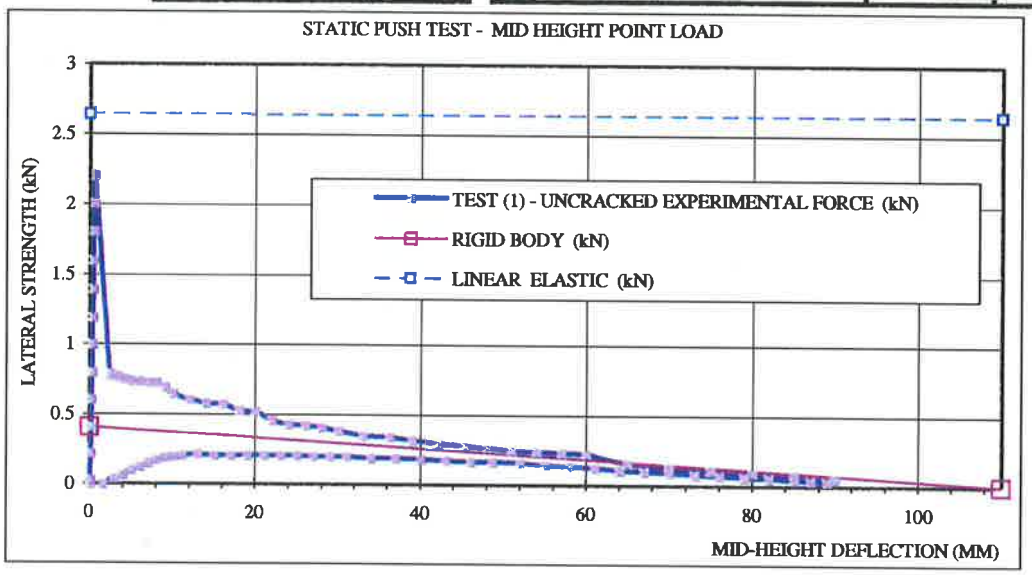

Figure F 11- Static Push Test – Un-cracked, 110mm, No Overburden

SEPTEMBER 98
SPECIMEN 13

Height	*1.485*	m
Thickness	*110*	mm
Length	*950*	mm
Density	*1800*	kg/m^3

Applied Overburden	*0*	MPa
Flexural Tensile Strength, f_t	*0*	kPa
Linear Elastic Analysis Prediction	***0.271***	kN
Rigid Body Analysis Prediction	***0.406***	kN

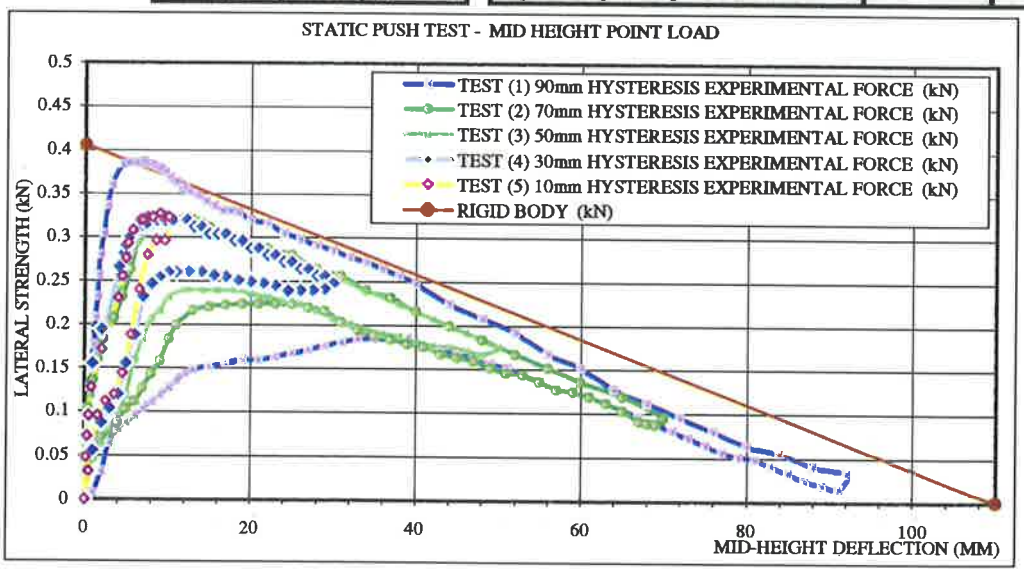

Figure F 12- Static Push Test (Hysteretic) – Cracked, 110mm, No Overburden

SEPTEMBER98 SPECIMEN 13 – RESONANT ENERGY LOSS PER CYCLE

INPUT DATA

$E_{d/2}$	ENERGY DISIPATED IN HALF CYCLE OF ACTUAL STRUCTURE
E_d	ENERGY DISIPATED IN FULL CYCLE OF ACTUAL STRUCTURE
A	ACTUAL MAX VIBRATION AMPLITUDE

DEFINITION OF EFFECTIVE STIFFNESS

A_{eff}	EFFECTIVE MAX VIBRATIONAL AMPLITUDE
F_{eff}	EFFECTIVE MAX RESISTANCE FORCE
K_{eff}	EFFECTIVE CYCLE STIFFNESS
E_{so}	STRAIN ENERGY
p_{si}	DAMPING RATIO FOR MAX VIBRATIONAL AMPLITUDE

DESCRIPTION	$E_{d/2}$	E_d	A_{eff}	F_{eff}	K_{eff}	E_{so}	p_{si}	A
	N	N	mm	N	N/mm	Nmm		mm
MAX DISP. 90	**8213.61**	**16427.23**	**40.00**	**220.00**	**5.50**	**4400.00**	**29.71%**	**90**
MAX DISP. 70	**4026.40**	**8052.79**	**35.00**	**230.00**	**6.57**	**4025.00**	**15.92%**	**70**
MAX DISP. 50	**2946.66**	**5893.32**	**32.00**	**250.00**	**7.81**	**4000.00**	**11.72%**	**50**
MAX DISP. 30	**1761.66**	**3523.31**	**18.50**	**285.00**	**15.41**	**2636.25**	**10.64%**	**30**
MAX DISP. 10	**688.35**	**1376.70**	**6.00**	**320.00**	**53.33**	**960.00**	**11.41%**	**10**

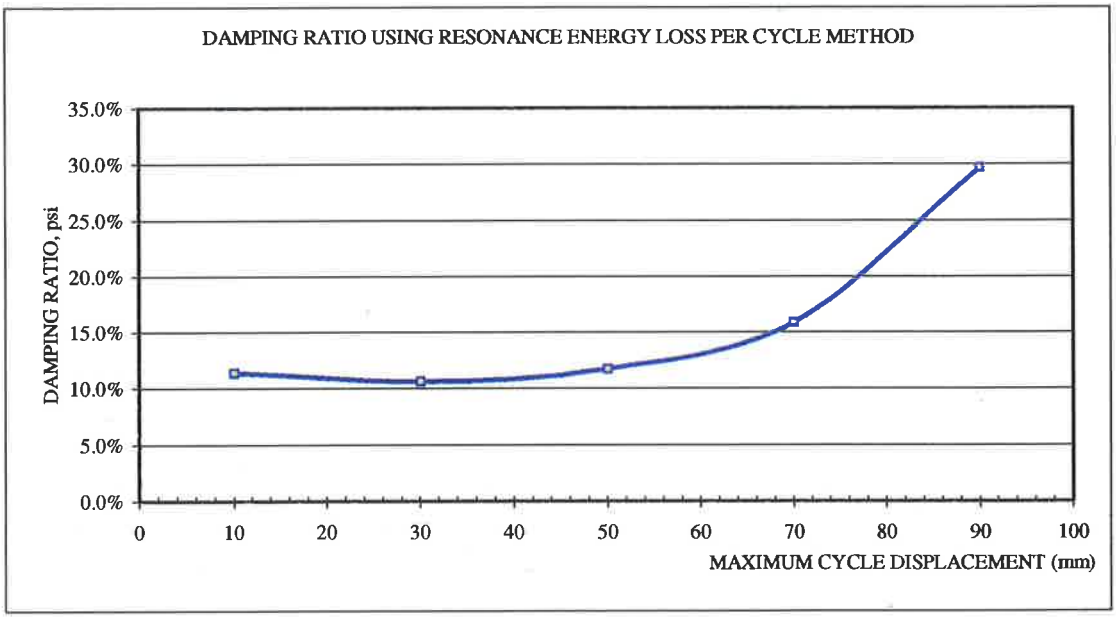

Figure F 13– September98 Specimen 13 – Resonant Energy Loss Per Cycle

SEPTEMBER 98
SPECIMEN 14

Height	*1.485*	m
Thickness	*50*	mm
Length	*950*	mm
Density	*2300*	kg/m^3

Applied Overburden	*0*	MPa
Flexural Tensile Strength, f_t	*0*	kPa
Linear Elastic Analysis Prediction	***0.071***	kN
Rigid Body Analysis Prediction	***0.107***	kN

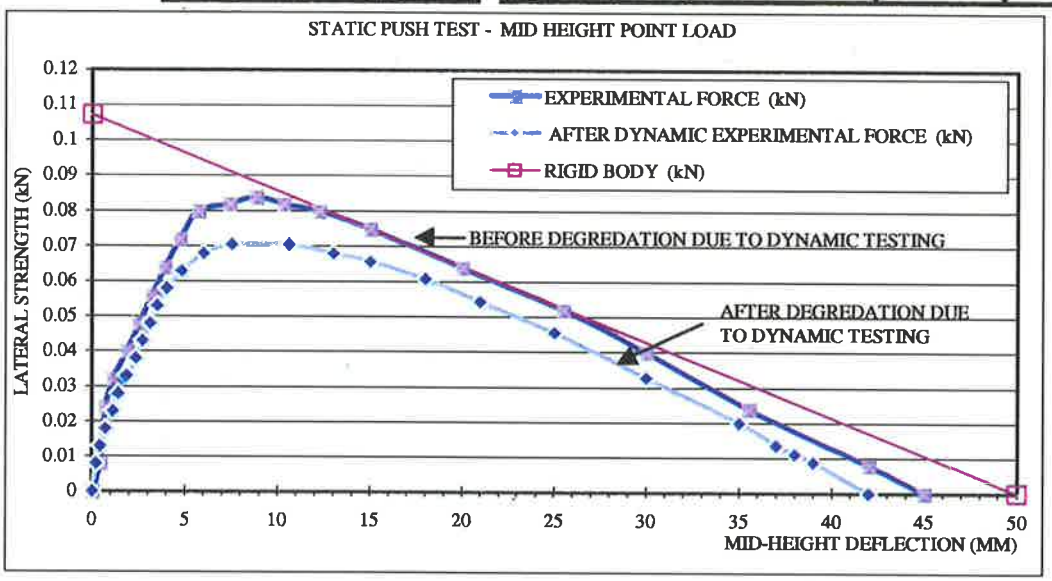

Figure F 14 - Static Push Test – Un-cracked, 110mm, No Overburden

SEPTEMBER 98
SPECIMEN 14

Height	*1.485*	m
Thickness	*50*	mm
Length	*950*	mm
Density	*2300*	kg/m^3

Applied Overburden	*0.15*	MPa
Flexural Tensile Strength, f_t	*0*	kPa
Linear Elastic Analysis Prediction	***0.471***	kN
Rigid Body Analysis Prediction	***1.067***	kN

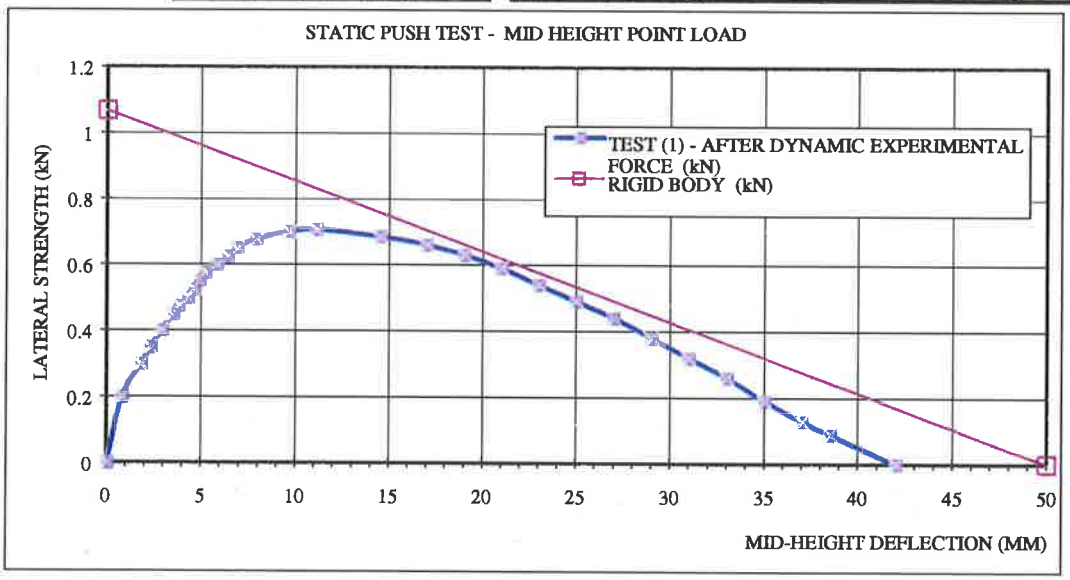

Figure F 15 - Static Push Test – Cracked, 50mm, 0.15MPa Overburden

SIMPLY SUPPORTED URM WALL RELEASE TEST RESULT PLOTS

SEPTEMBER 98 –Specimen (10) - Release Test (1)

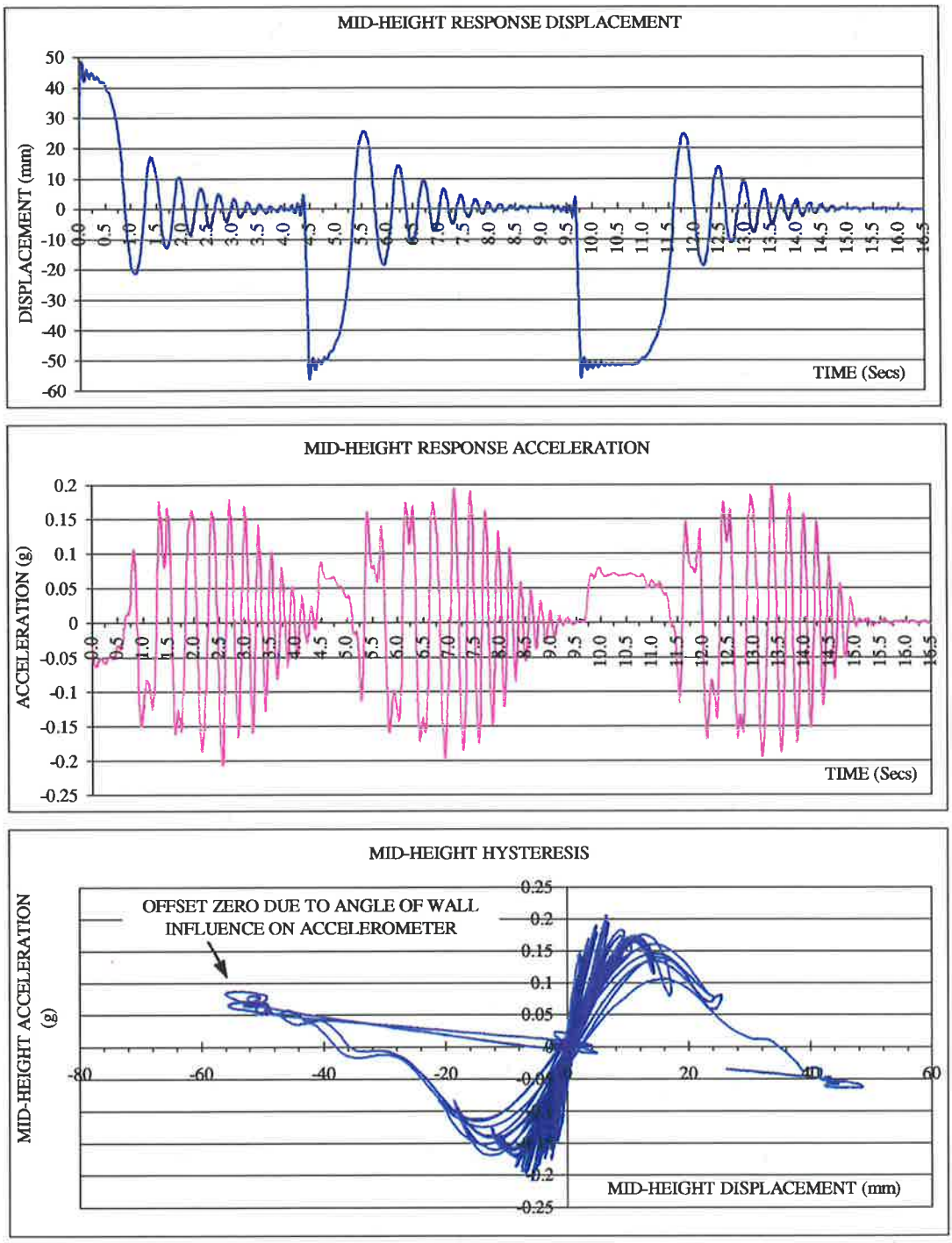

Figure F 16 - Release Test (1) - 50mm, No Overburden

SEPTEMBER 98 –Specimen (1) - Release Test (2)

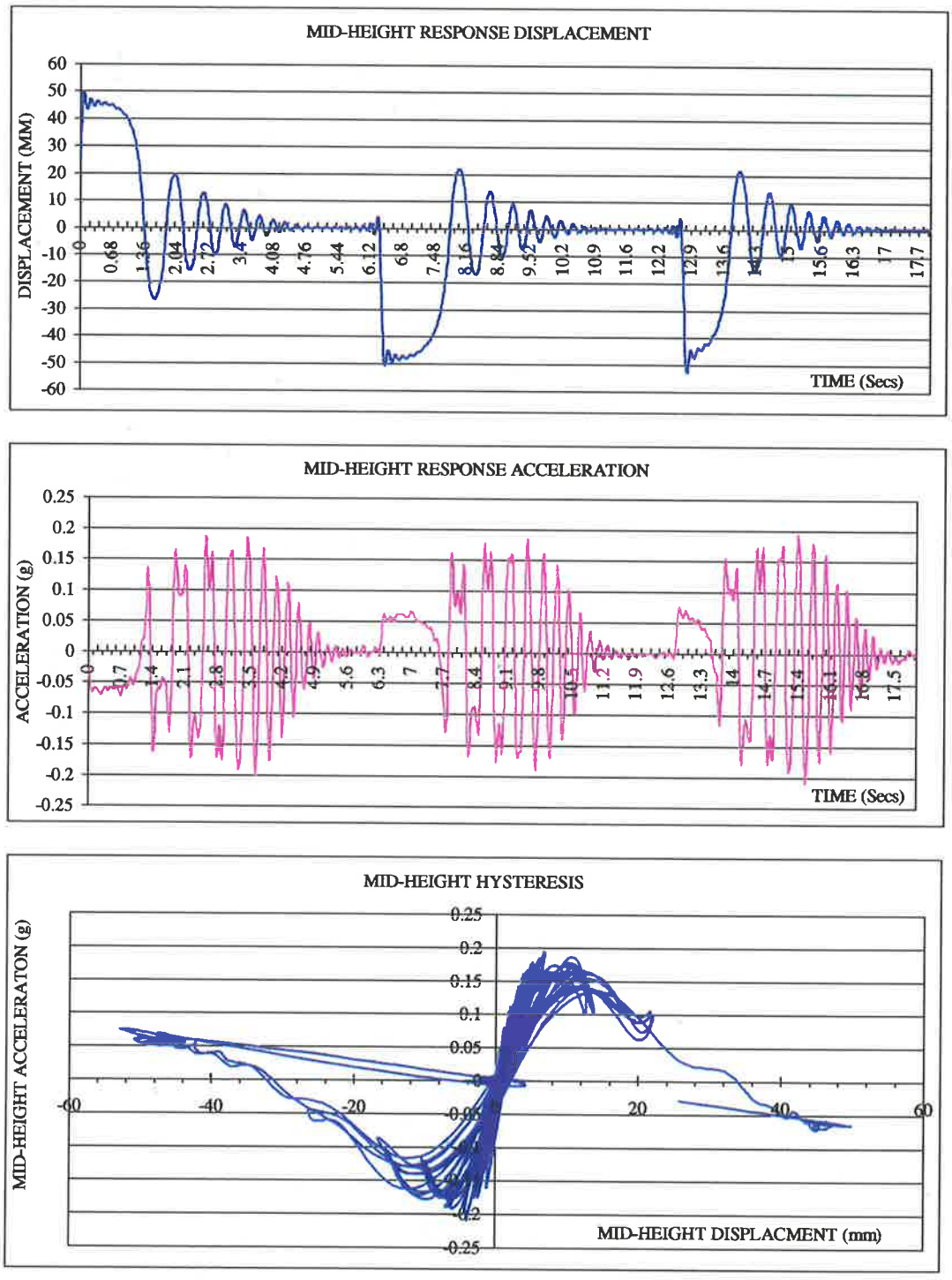

Figure F 17 - Release Test (2) - 50mm, No Overburden

SEPTEMBER 98 –Specimen (1) - Release Test (3)

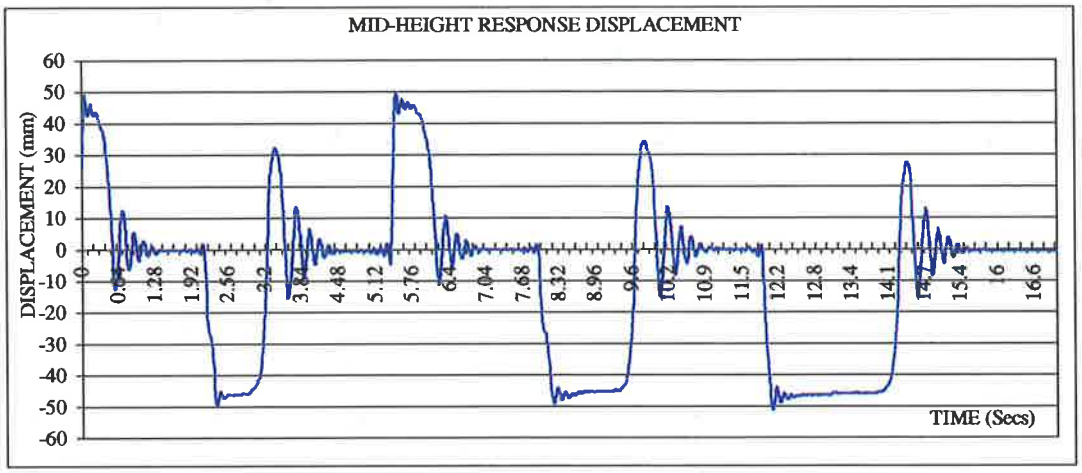

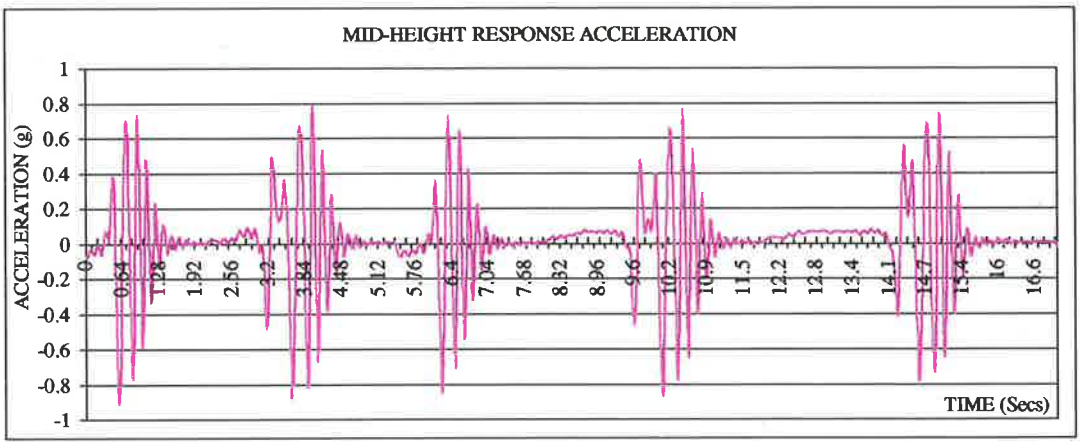

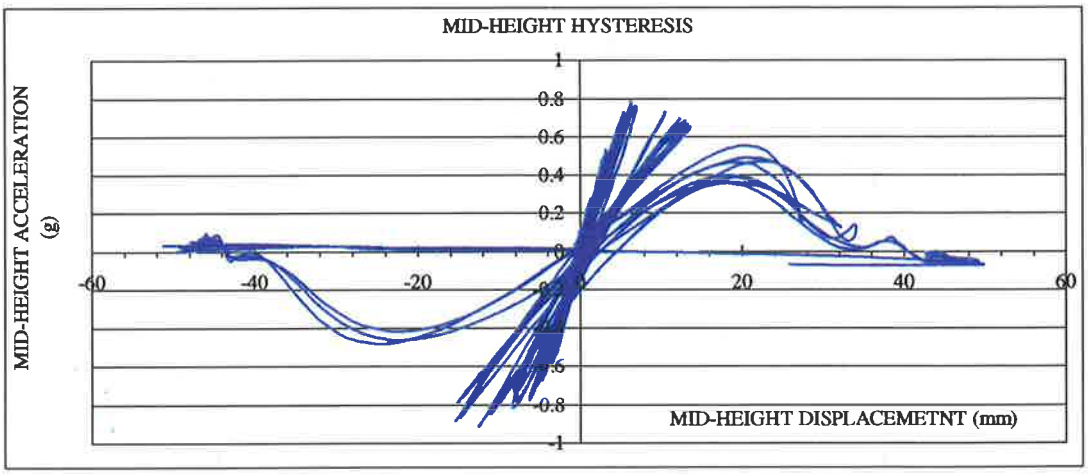

Figure F 18 - Release Test (3) - 50mm, 0.075MPa Overburden

SEPTEMBER 98 – Specimen (11) - Release Test (4)

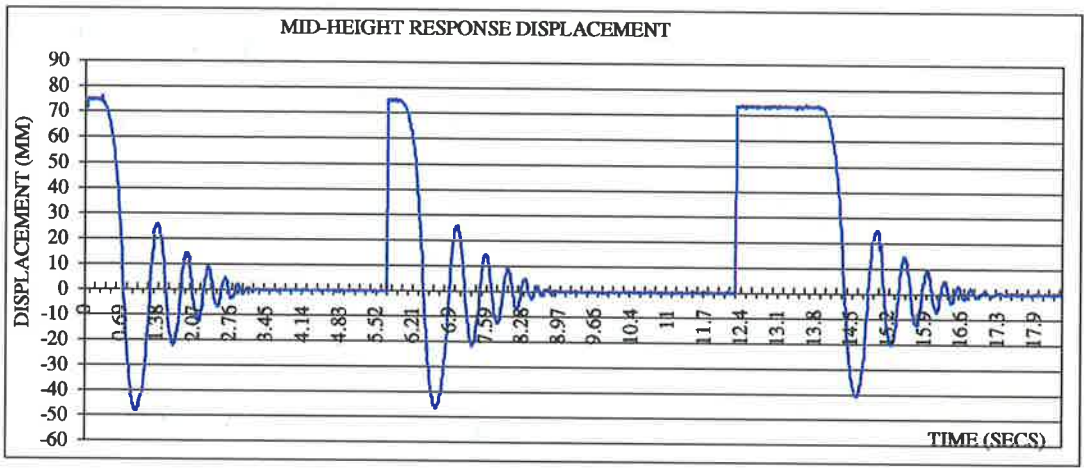

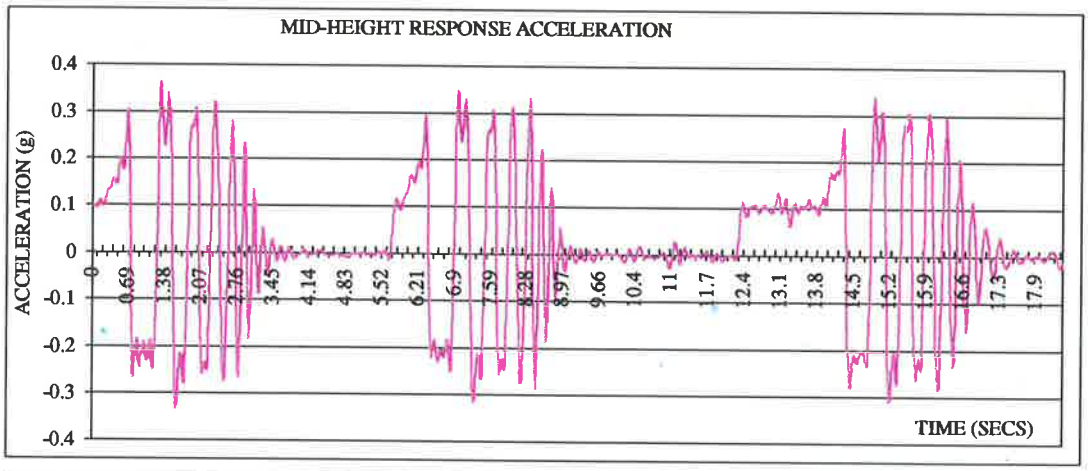

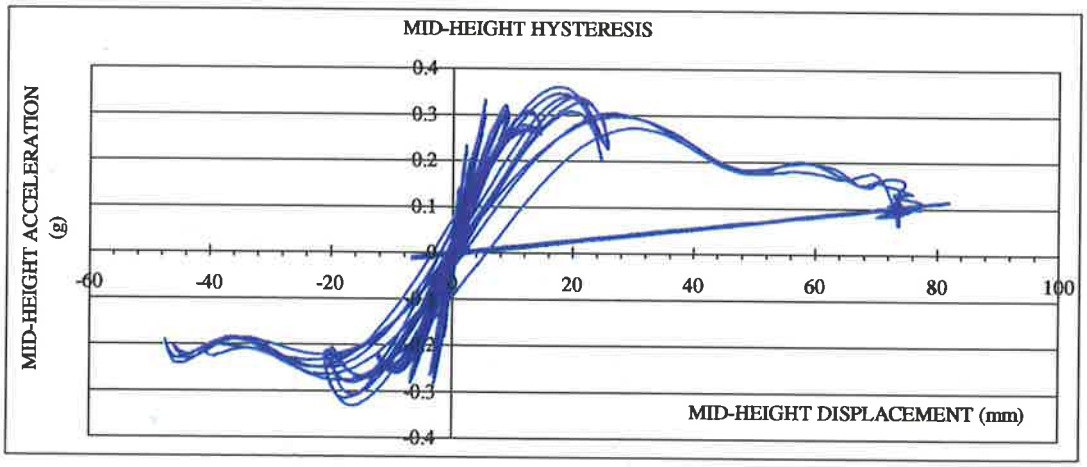

Figure F 19 - Release Test (4) - 110mm, No Overburden

SEPTEMBER 98 –Specimen (11) - Release Test (5)

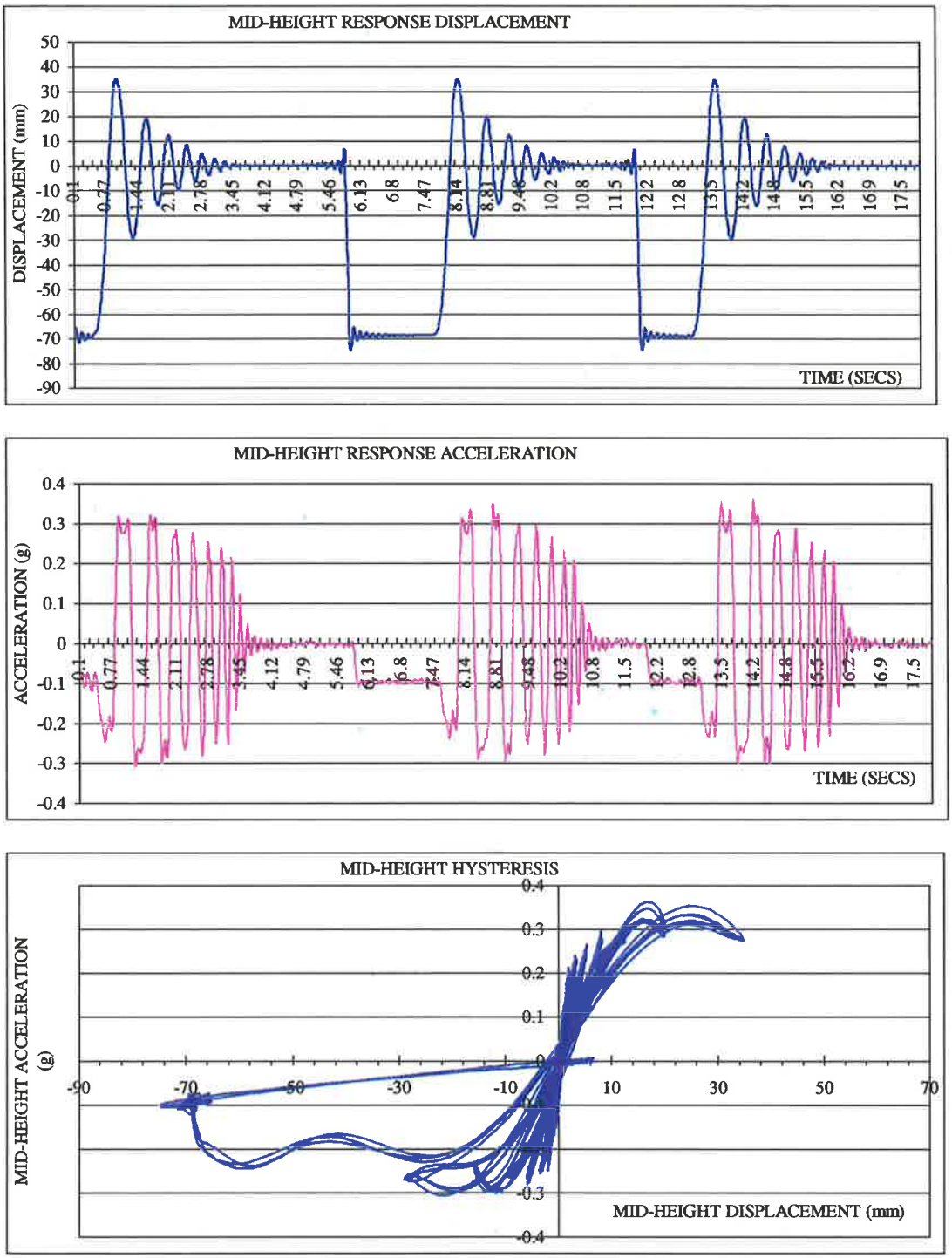

Figure F 20 - Release Test (5) - 110mm, No Overburden

SEPTEMBER 98 –Specimen (11) - Release Test (6)

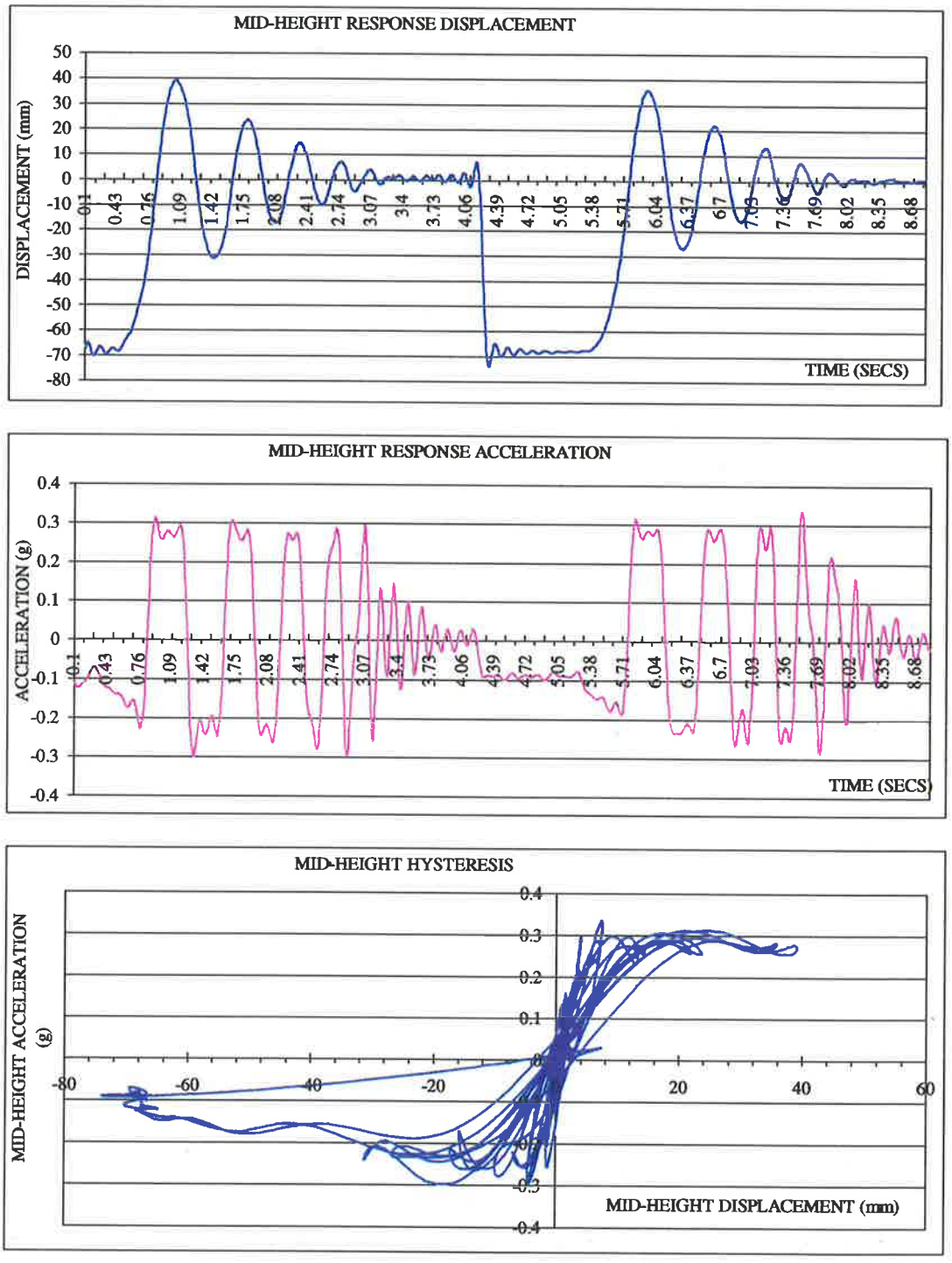

Figure F 21 - Release Test (6) - 110mm, No Overburden

SIMPLY SUPPORTED URM WALL PULSE TEST RESULT PLOTS

SEPTEMBER 98 – Specimen (10) - 0.5Hz Half Sine Displacement Pulse

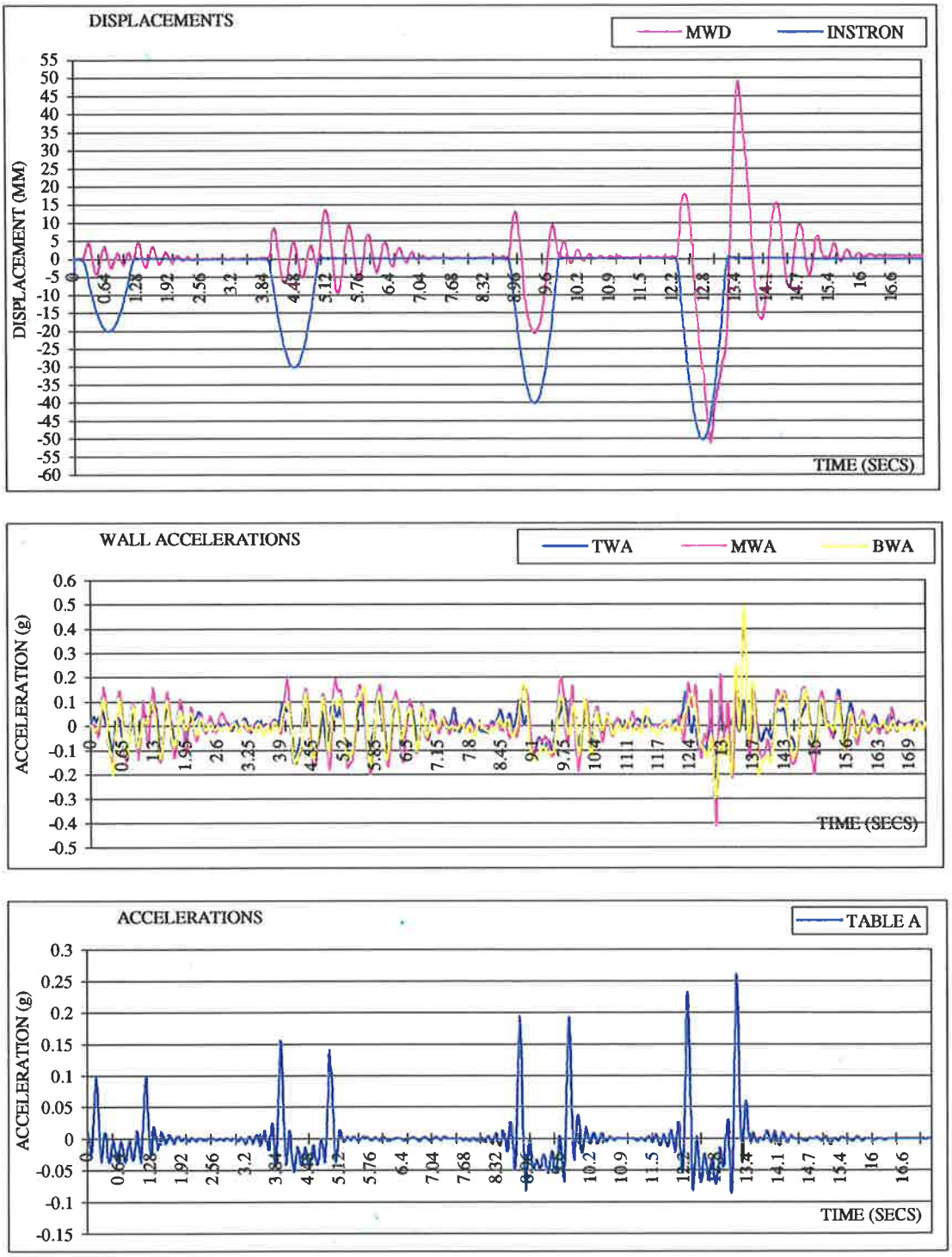

Figure F 22 - 0.5Hz Half Sine Displacement Pulse, 50mm, No Overburden

SEPTEMBER 98 – Specimen (10) - 1.0Hz Half Sine Displacement Pulse

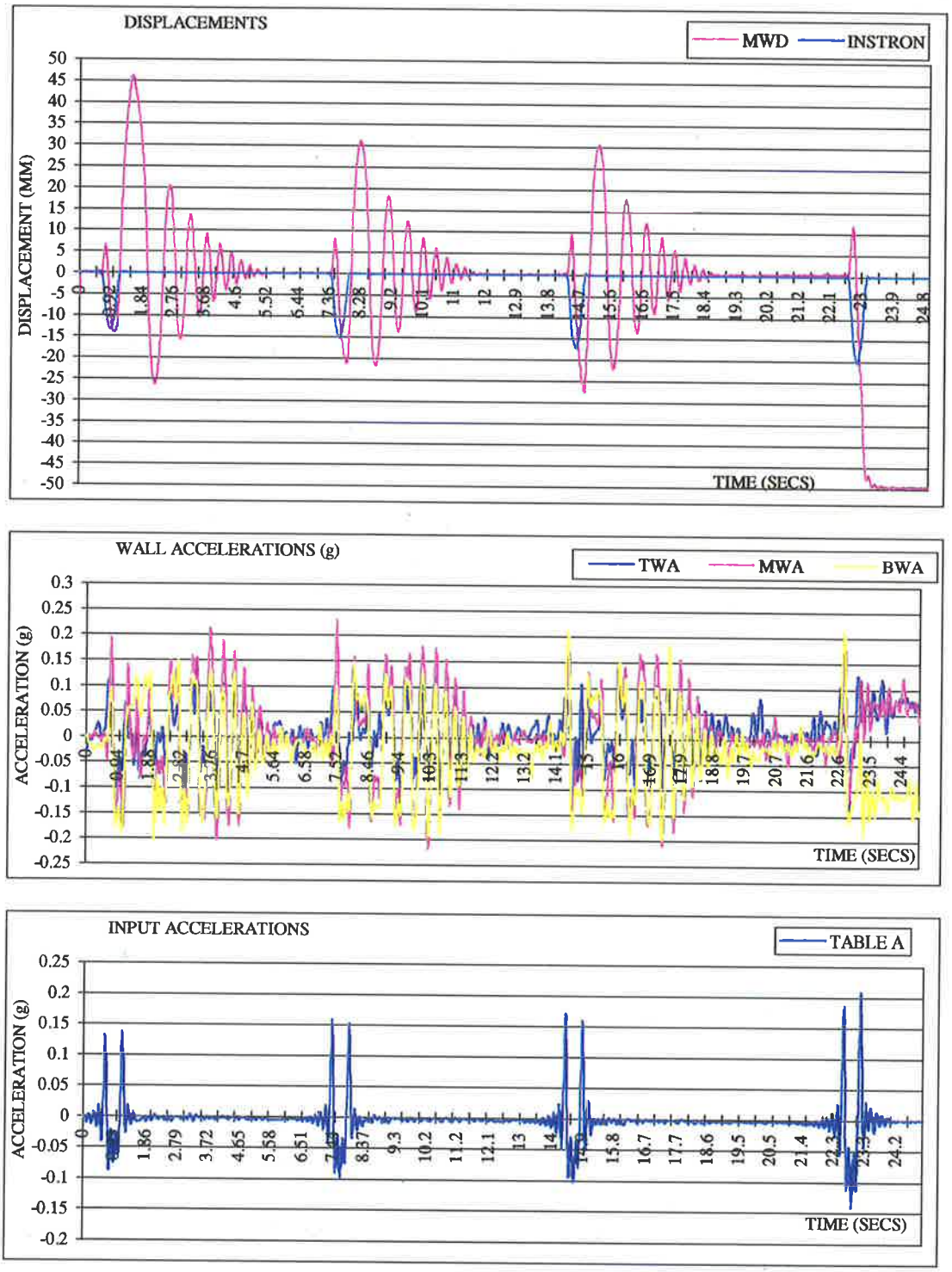

Figure F 23– 1.0Hz Half Sine Displacement Pulse, 50mm, No Overburden

SEPTEMBER 98 – Specimen ((10) - 2.0Hz Half Sine Displacement Pulse

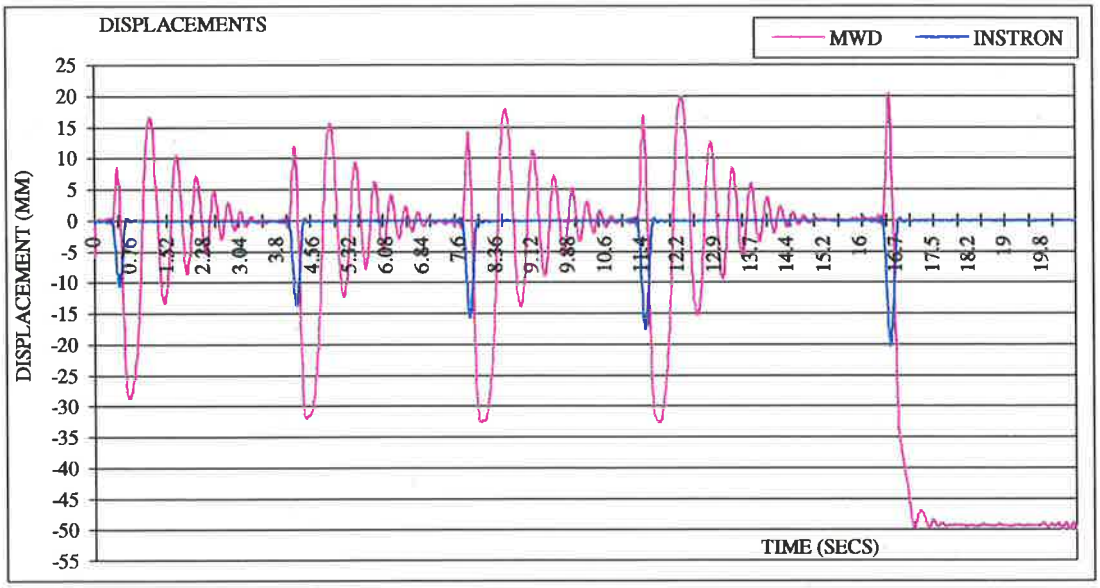

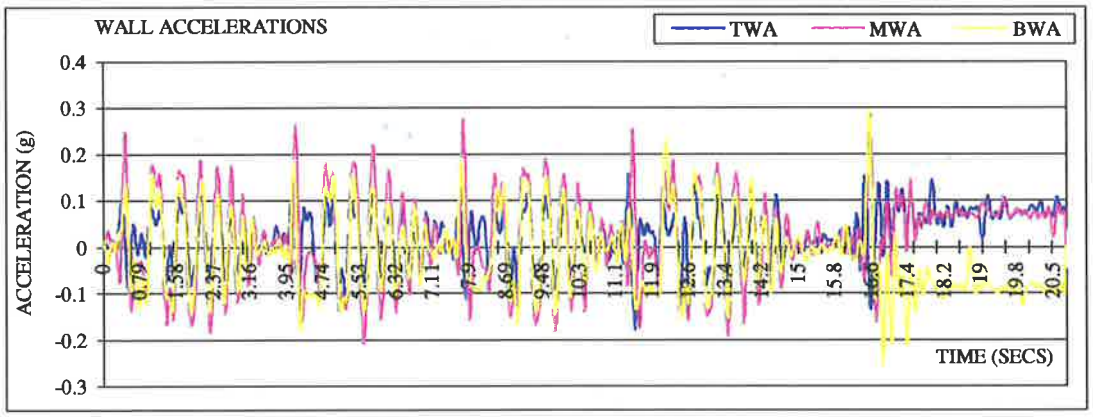

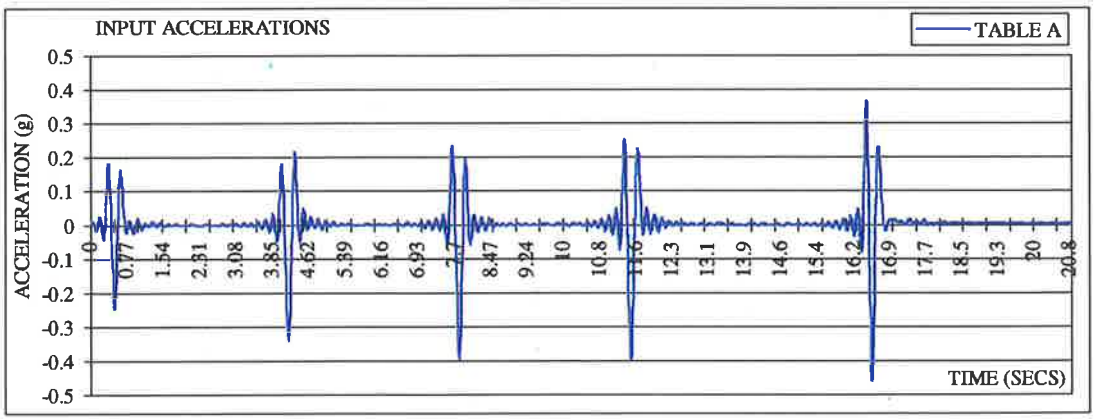

Figure F 24 - 2.0Hz Half Sine Displacement Pulse, 50mm, No Overburden

SEPTEMBER 98 – Specimen (10) - 0.5Hz Half Sine Displacement Pulse

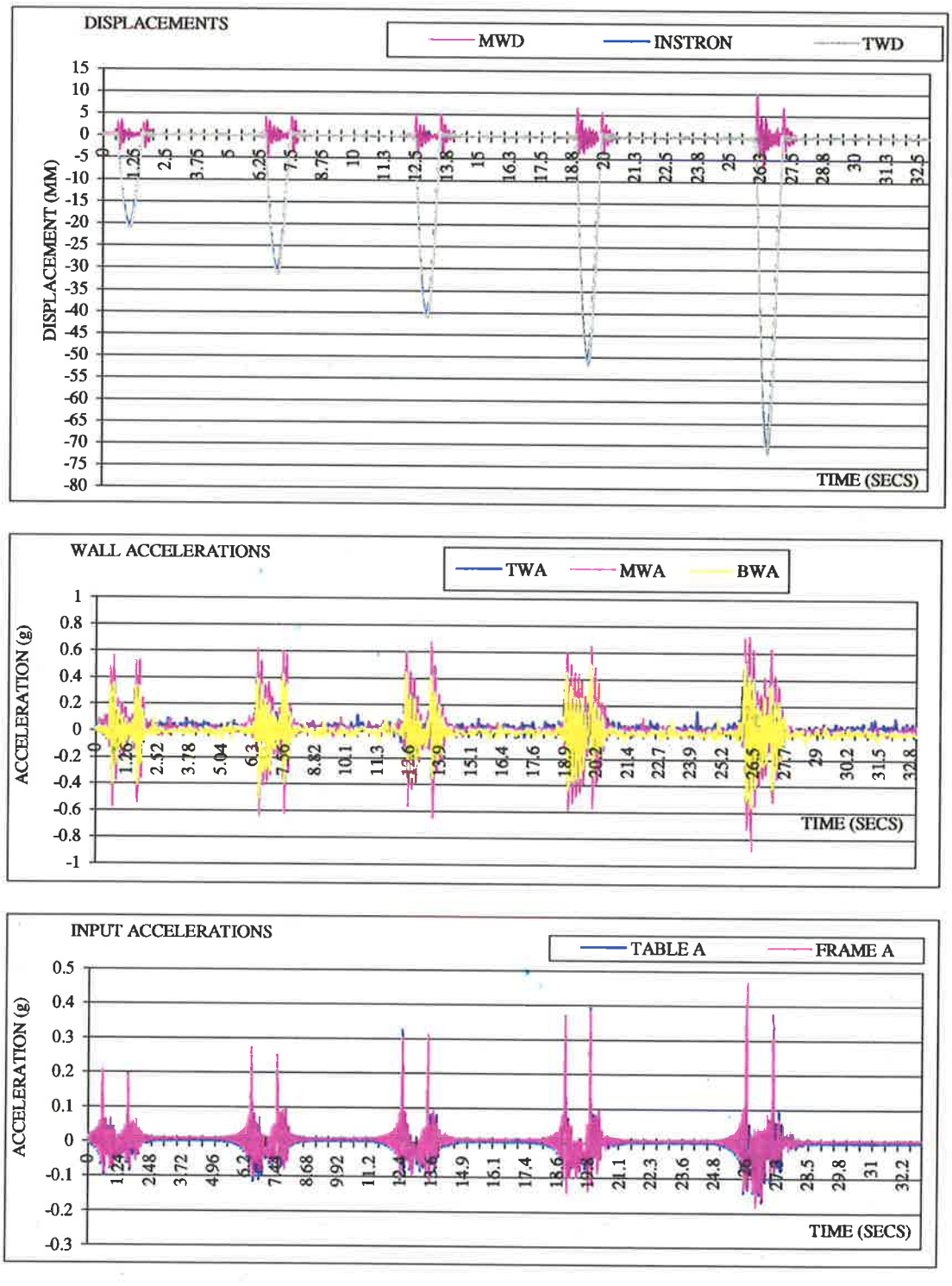

Figure F 25 - 0.5Hz Half Sine Displacement Pulse, 50mm, 0.075MPa Overburden

SEPTEMBER 98 – Specimen (10) - 1.0Hz Half Sine Displacement Pulse

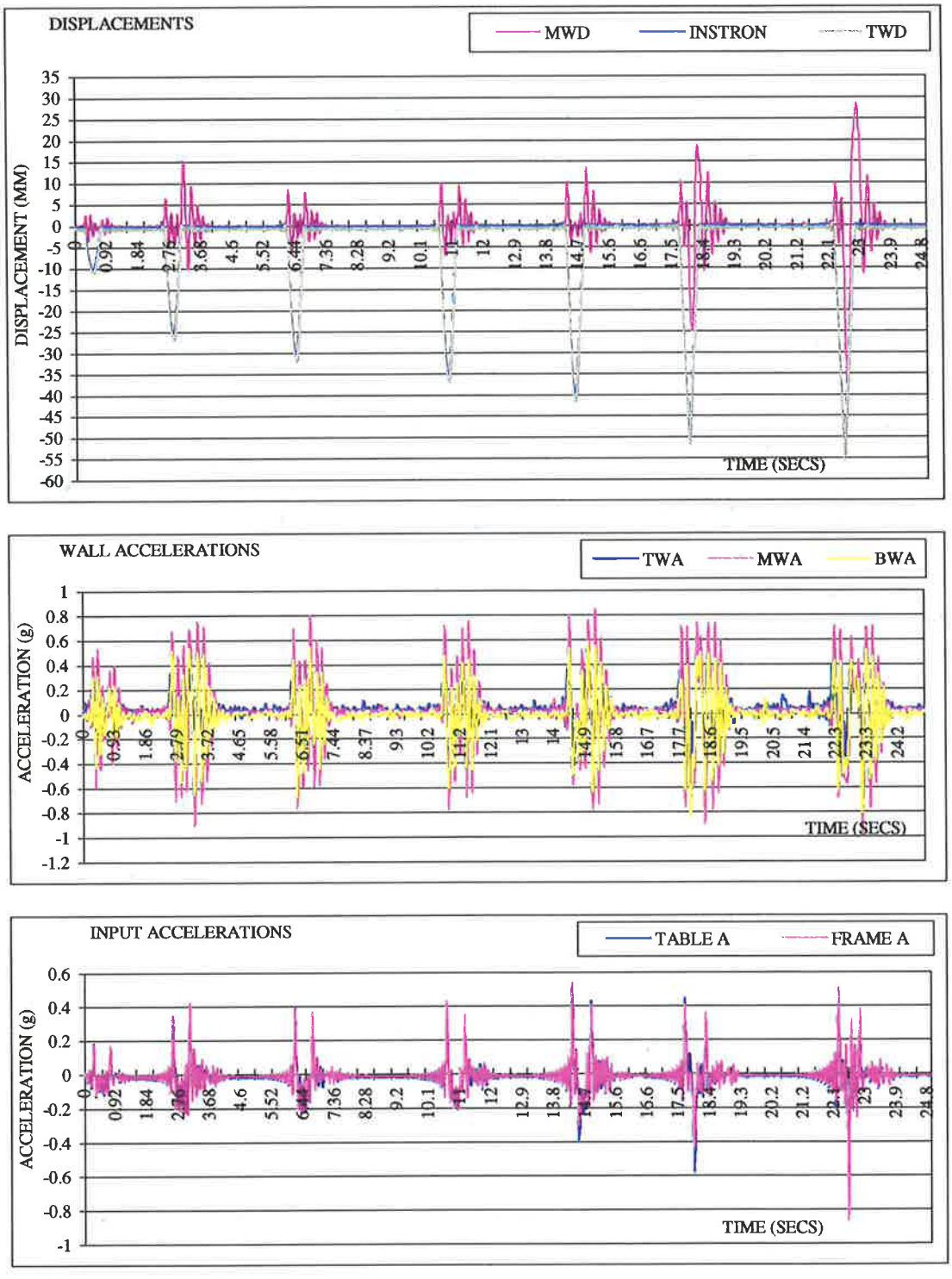

Figure F 26– 1.0Hz Half Sine Displacement Pulse, 50mm, 0.075MPa Overburden

SEPTEMBER 98 – Specimen (10) - 2.0Hz Half Sine Displacement Pulse

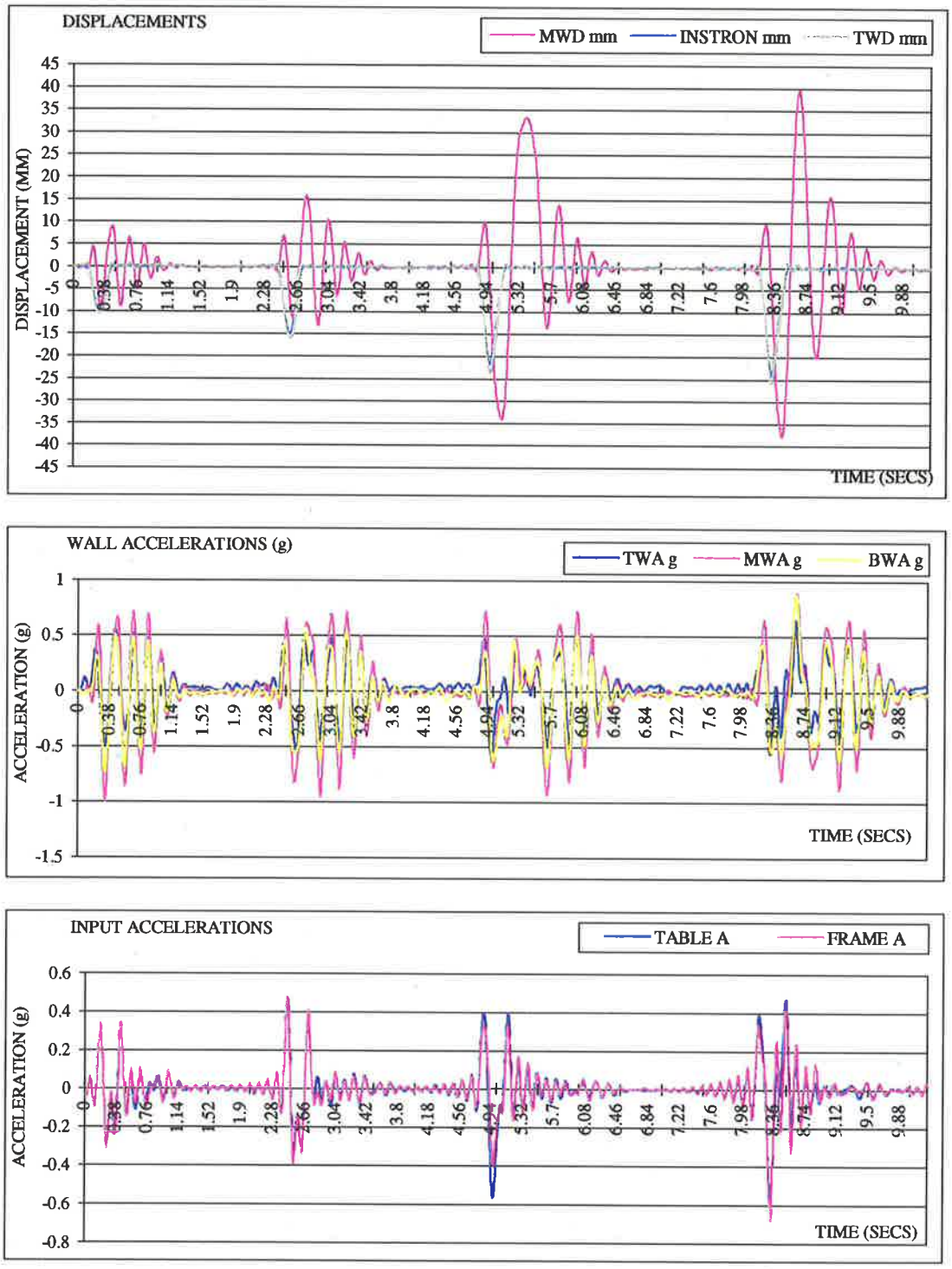

Figure F 27– 2.0Hz Half Sine Displacement Pulse, 50mm, 0.075MPa Overburden

SEPTEMBER 98 – Specimen (10) - 3.0Hz Half Sine Displacement Pulse

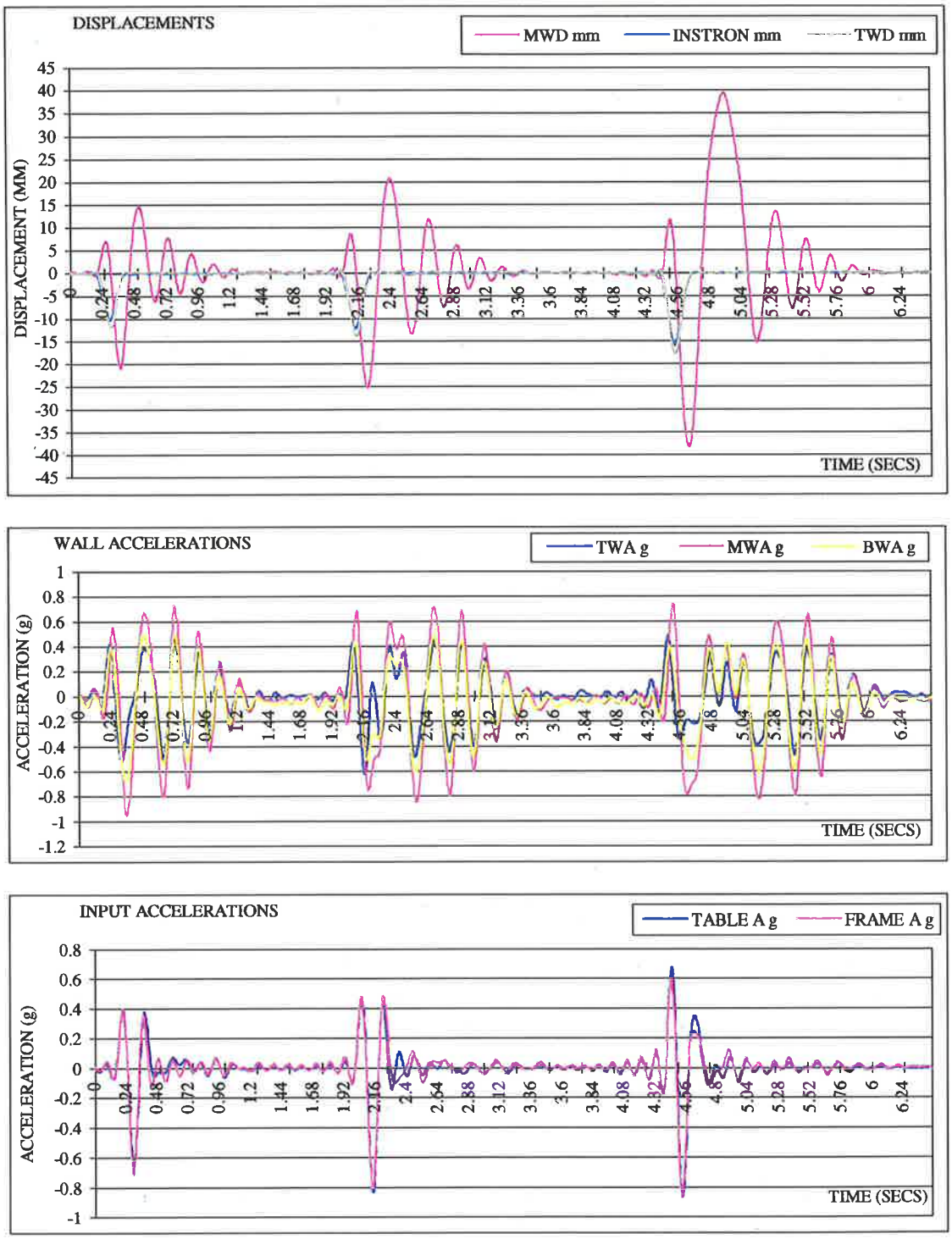

Figure F 28– 3.0 Hz Half Sine Displacement Pulse, 50mm, 0.075MPa Overburden

SEPTEMBER 98 – Specimen (10) - 1.0Hz Half Sine Displacement Pulse

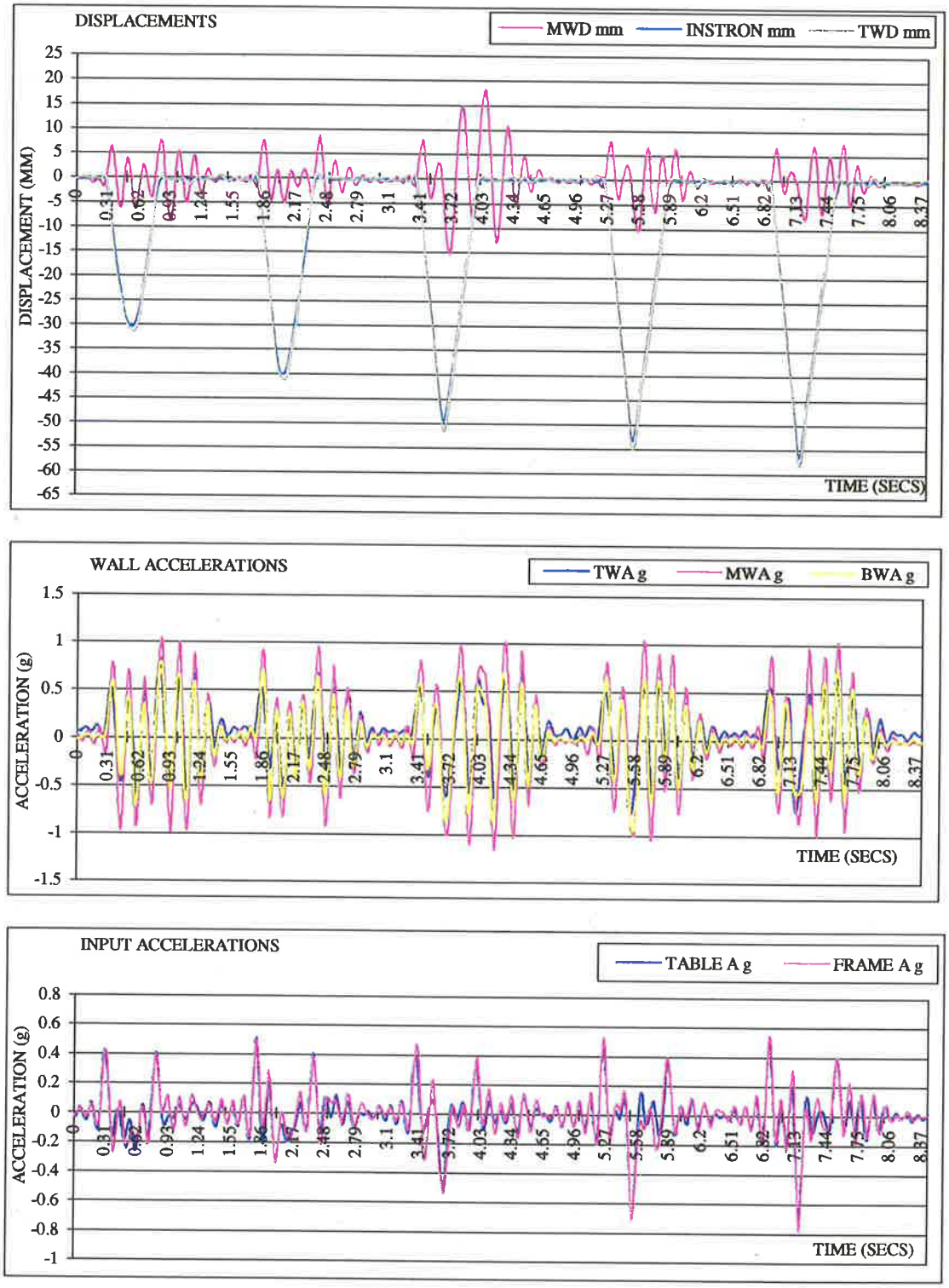

Figure F 29- 0.5Hz Half Sine Displacement Pulse, 50mm, 0.15MPa Overburden

SEPTEMBER 98 – Specimen (10) - 1.0Hz Half Sine Displacement Pulse

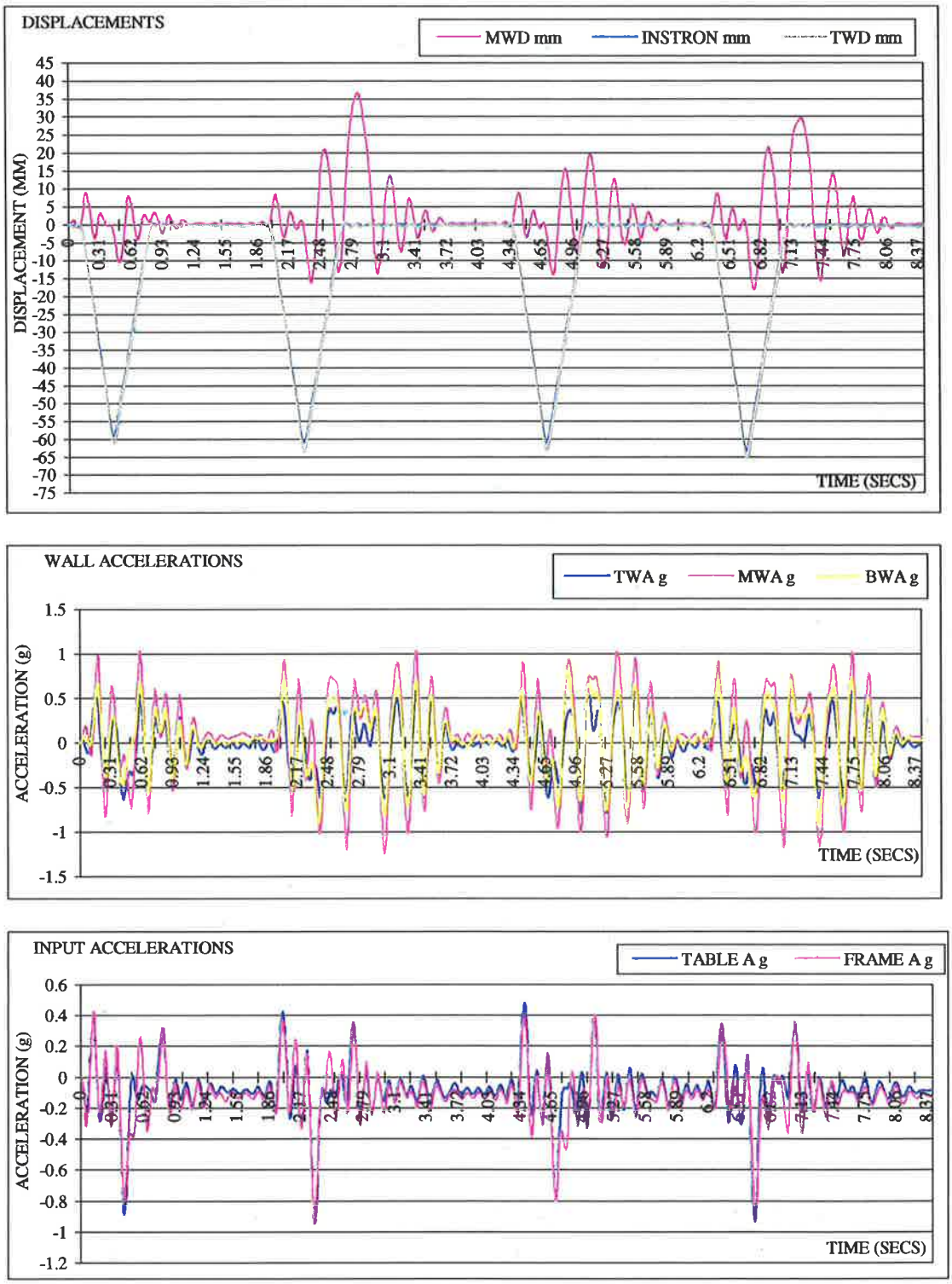

Figure F 30– 1.0Hz Half Sine Displacement Pulse, 50mm, 0.15MPa Overburden

SEPTEMBER 98 – Specimen (10) - 2.0Hz Half Sine Displacement Pulse

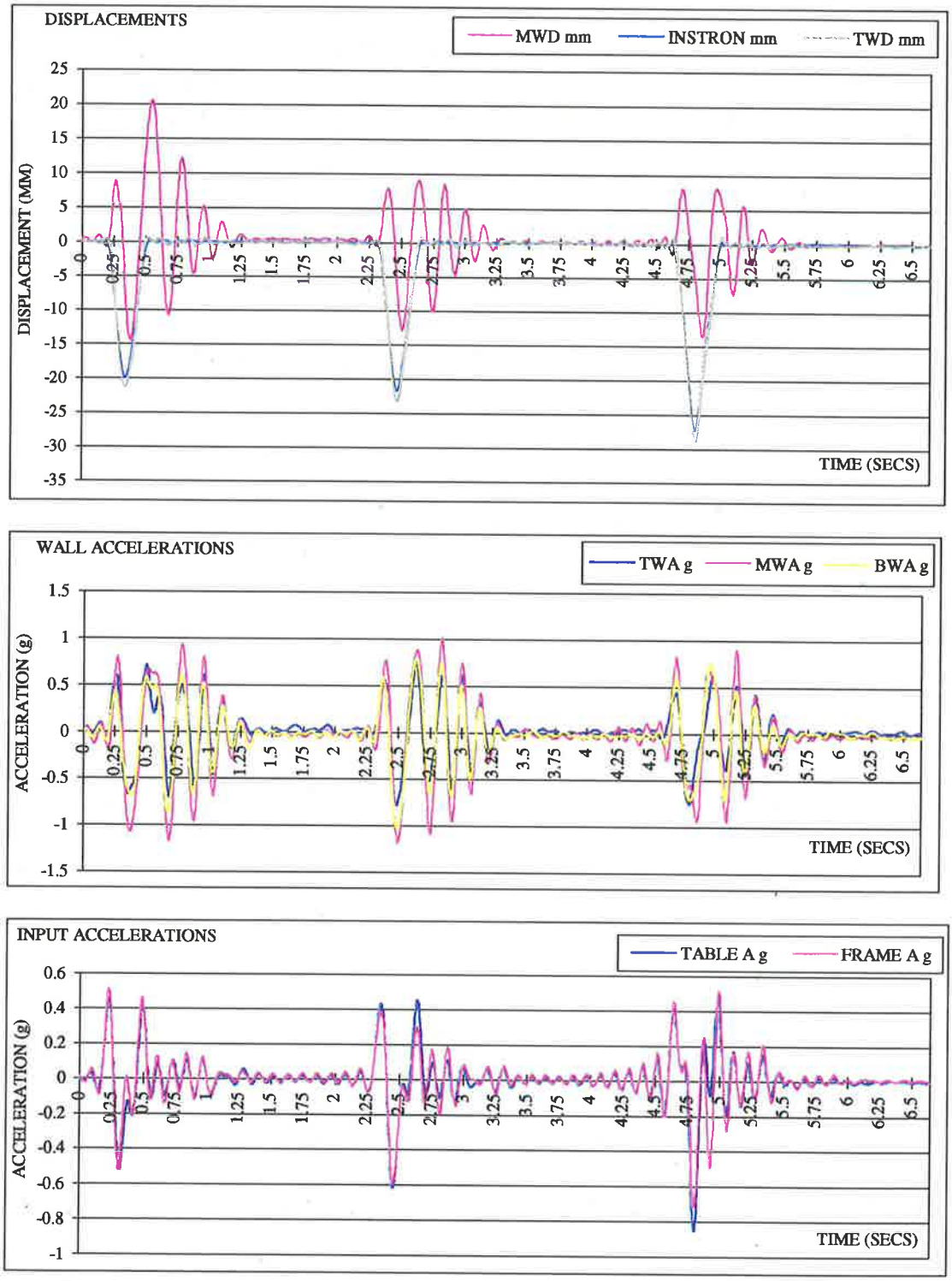

Figure F 31 – 2.0Hz Half Sine Displacement Pulse, 50mm, 0.15MPa Overburden

SEPTEMBER 98 – Specimen (11) - 2.0Hz Half Sine Displacement Pulse

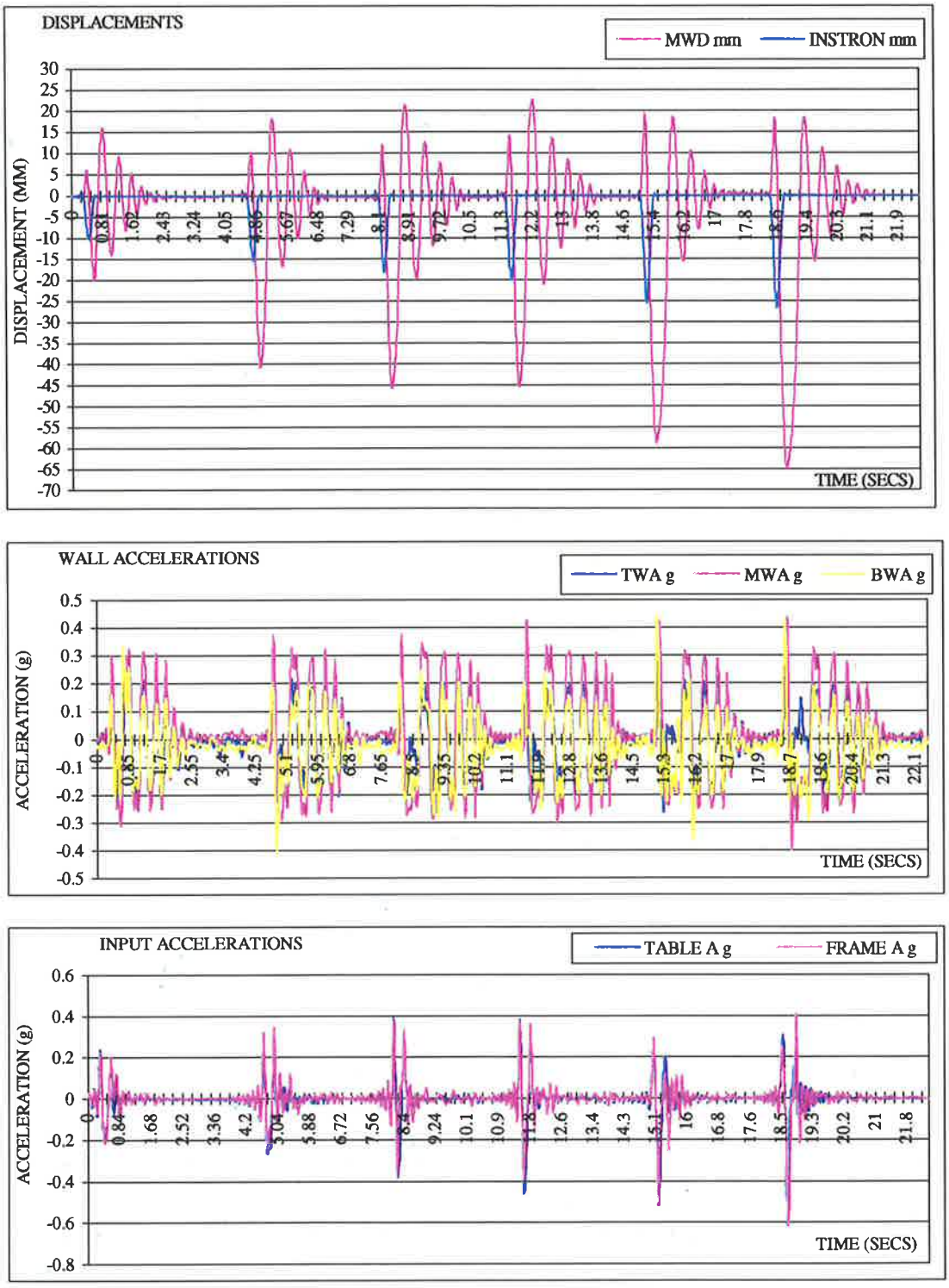

Figure F 35- 2.0Hz Half Sine Displacement Pulse, 110mm, No Overburden

SEPTEMBER 98 – Specimen (11) - 1.0Hz Half Sine Displacement Pulse

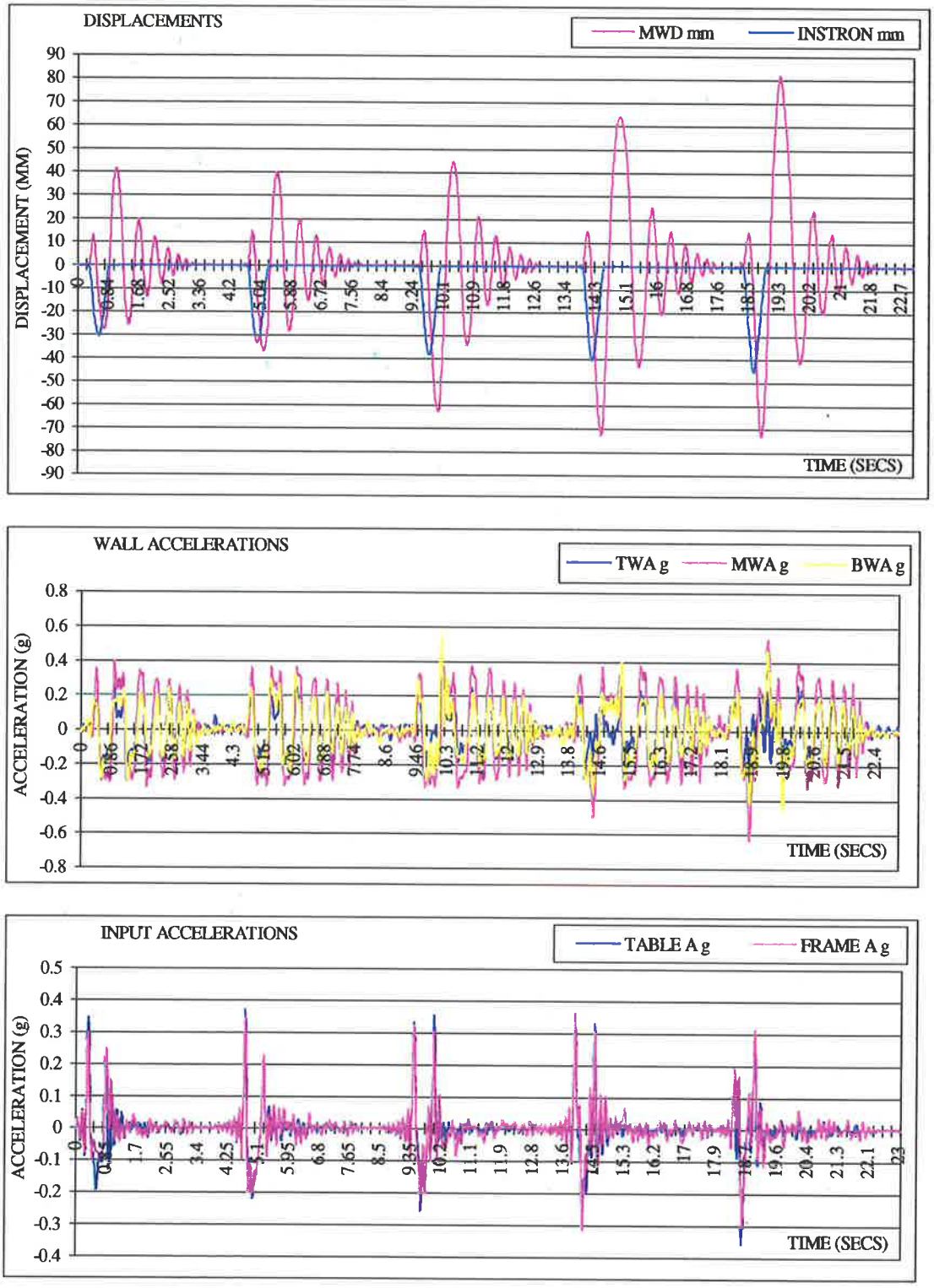

Figure F 34- 1.0Hz Half Sine Displacement Pulse, 110mm, No Overburden

SEPTEMBER 98 – Specimen (11) - 1.0Hz Half Sine Displacement Pulse

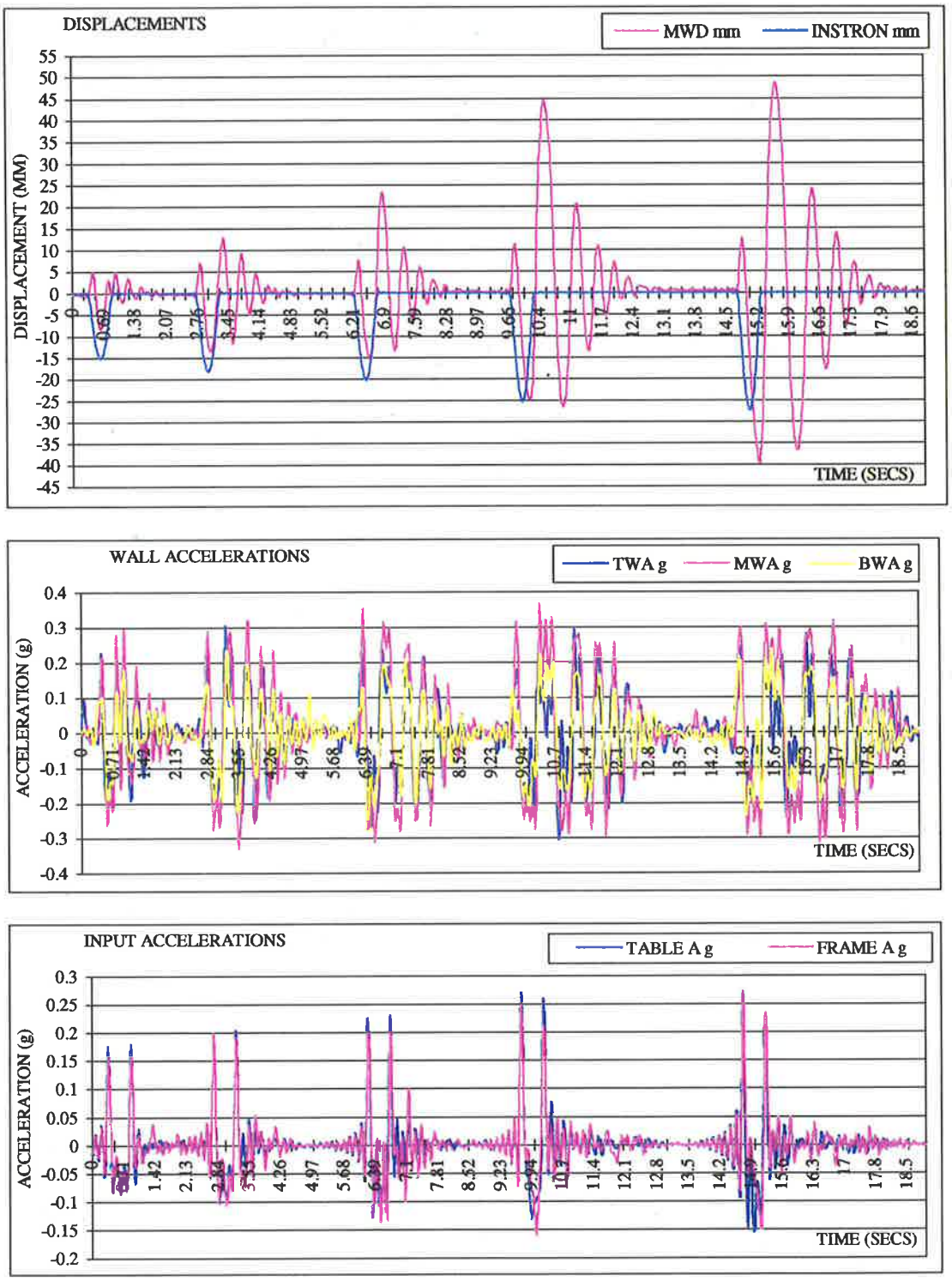

Figure F 33- 1.0Hz Half Sine Displacement Pulse, 110mm, No Overburden

SEPTEMBER 98 – Specimen (10) - 2.0Hz Half Sine Displacement Pulse

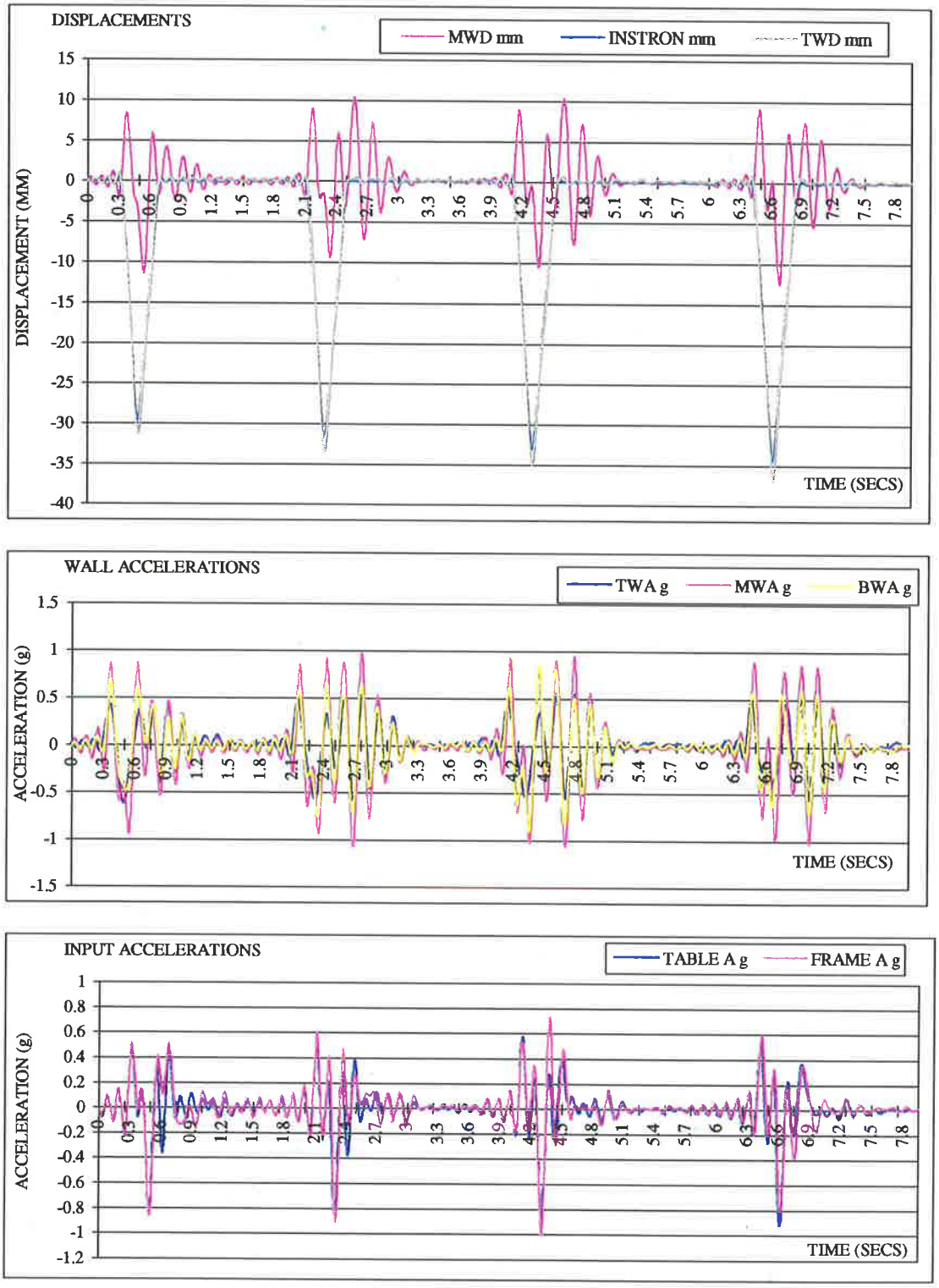

Figure F 32- 2.0Hz Half Sine Displacement Pulse, 50mm, 0.15MPa Overburden

SEPTEMBER 98 – Specimen (13) - 1.0Hz Gaussian Displacement Pulse

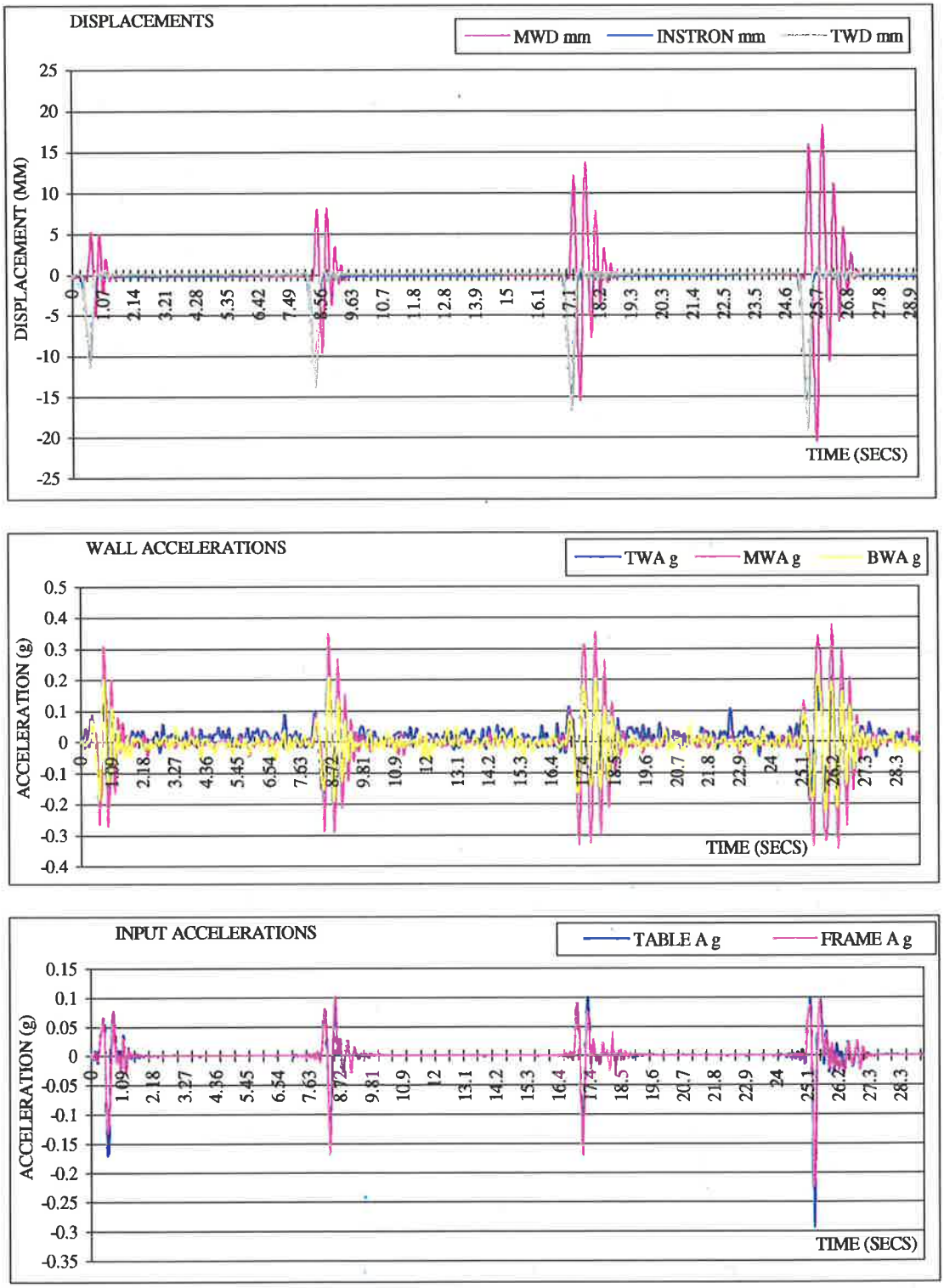

Figure F 36- 1.0Hz Gaussian Displacement Pulse, 110mm, No Overburden

SEPTEMBER 98 – Specimen (13) - 1.0Hz Gaussian Displacement Pulse

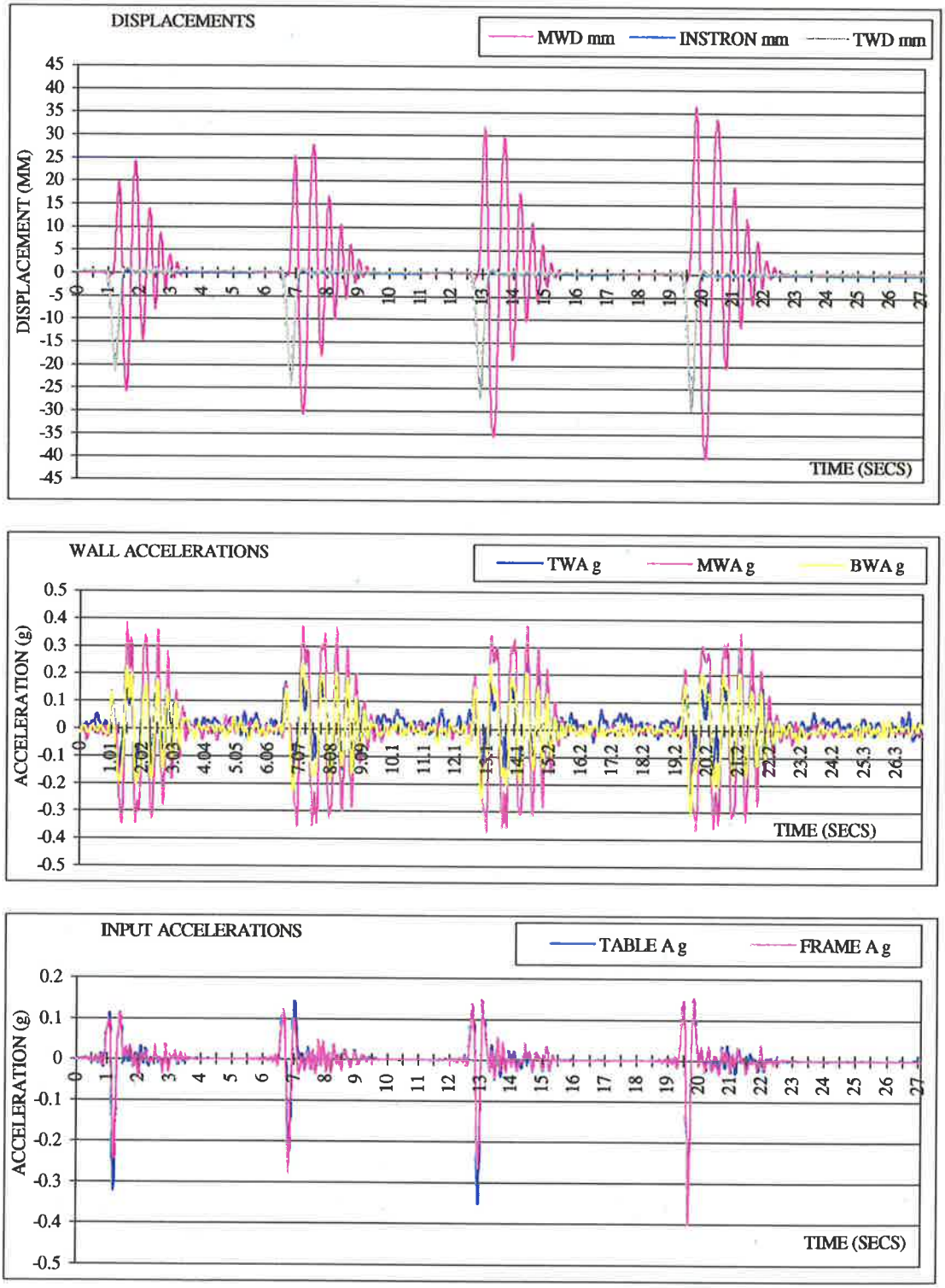

Figure F 37- 1.0Hz Gaussian Displacement Pulse, 110mm, No Overburden

SEPTEMBER 98 – Specimen (13) - 1.0Hz Gaussian Displacement Pulse

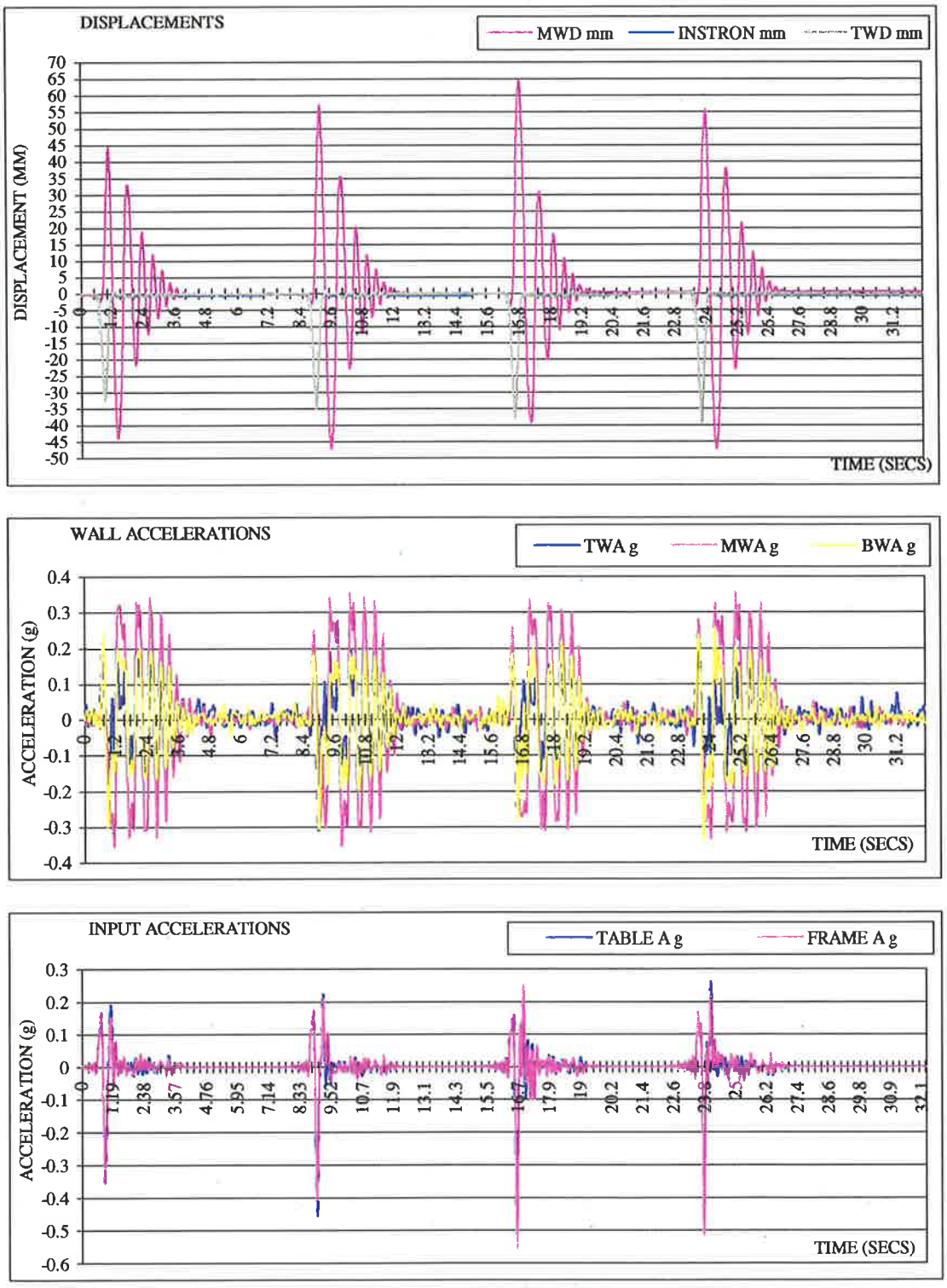

Figure F 38- 1.0Hz Gaussian Displacement Pulse, 110mm, No Overburden

SEPTEMBER 98 – Specimen (13) - 1.0Hz Gaussian Displacement Pulse

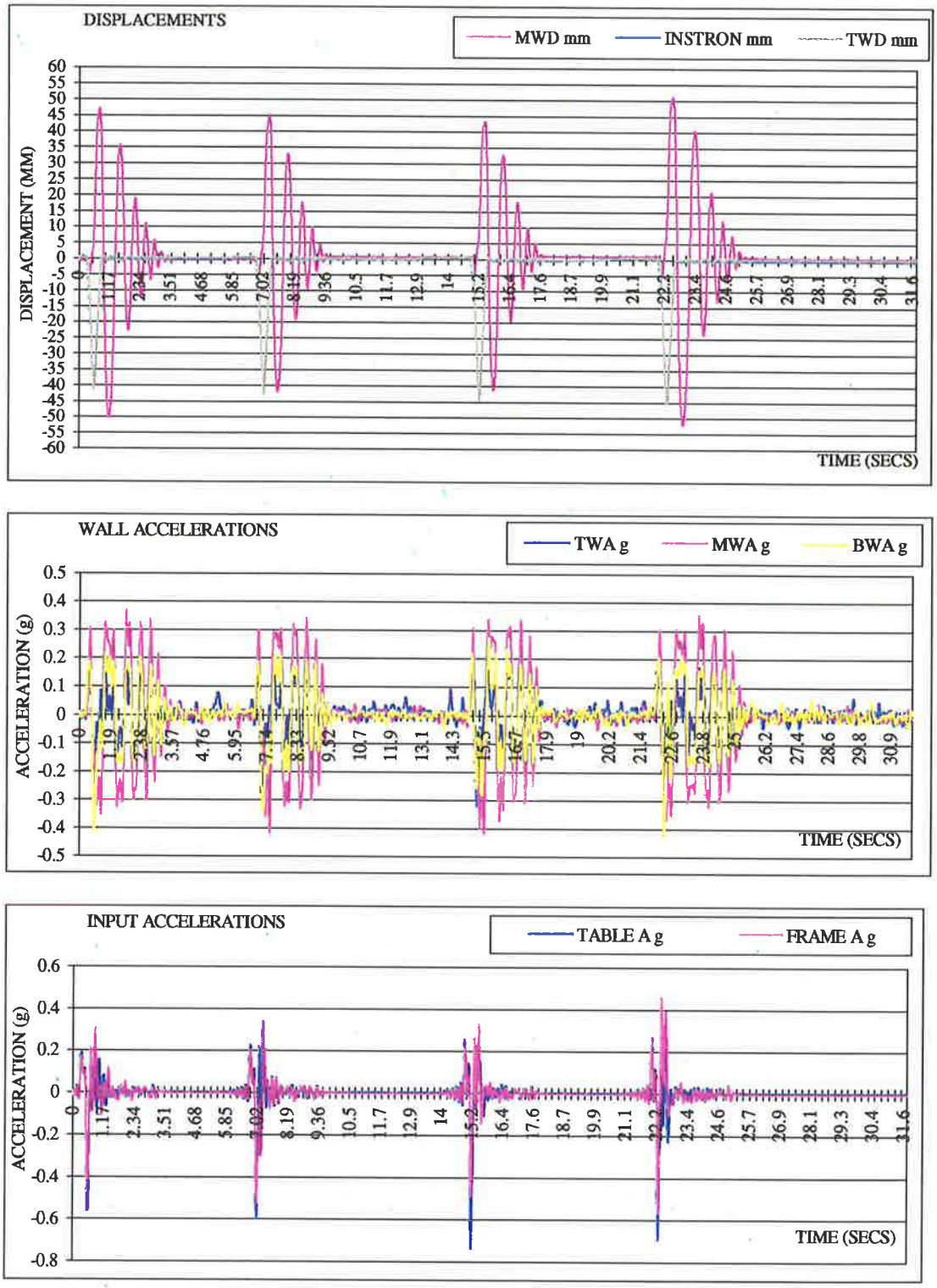

Figure F 39- 1.0Hz Gaussian Displacement Pulse, 110mm, No Overburden

SEPTEMBER 98 – Specimen (13) - 0.5Hz Gaussian Displacement Pulse

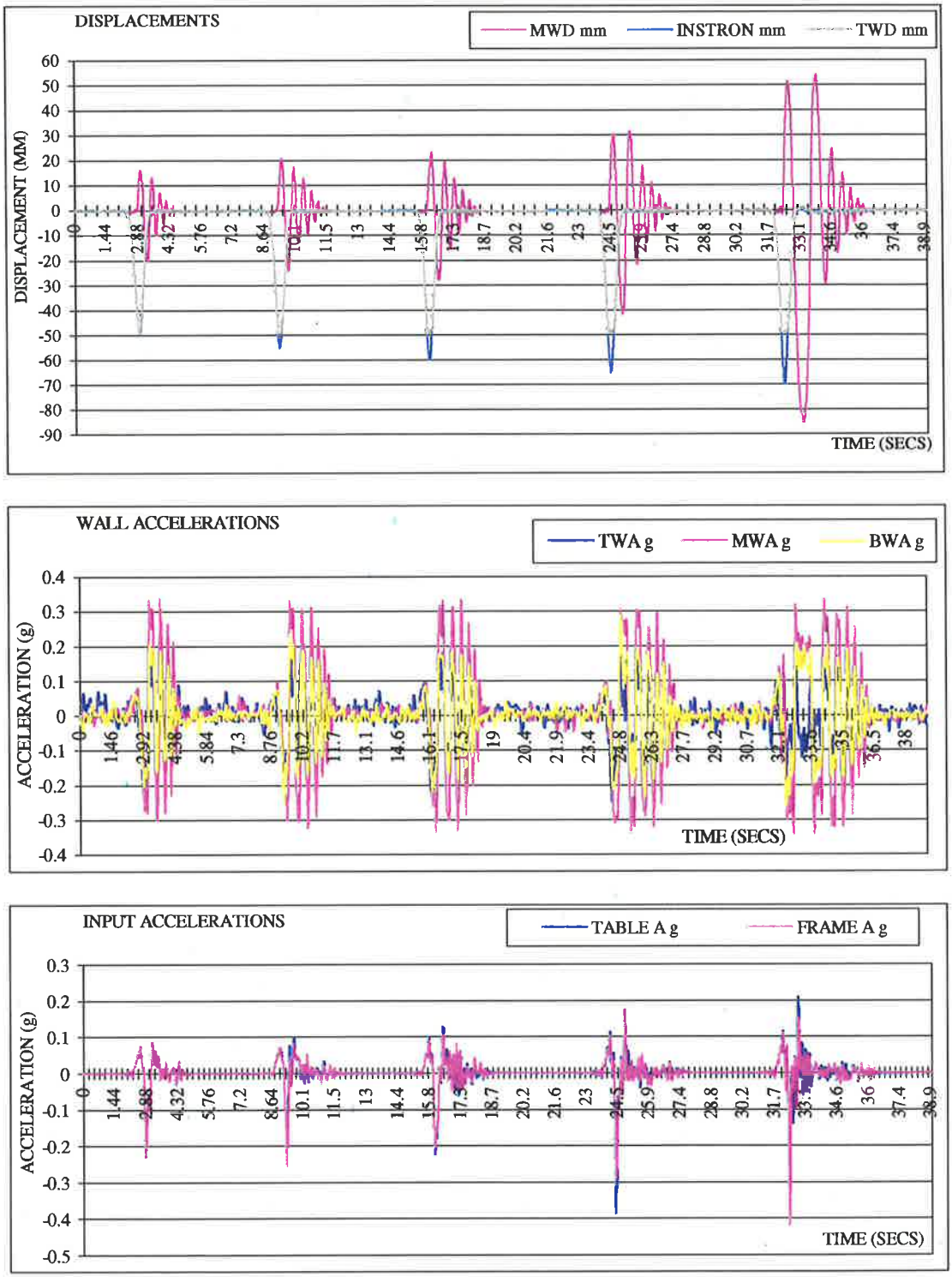

Figure F 40– 0.5Hz Gaussian Displacement Pulse, 110mm, No Overburden

SEPTEMBER 98 – Specimen (13) - 0.5Hz Gaussian Displacement Pulse

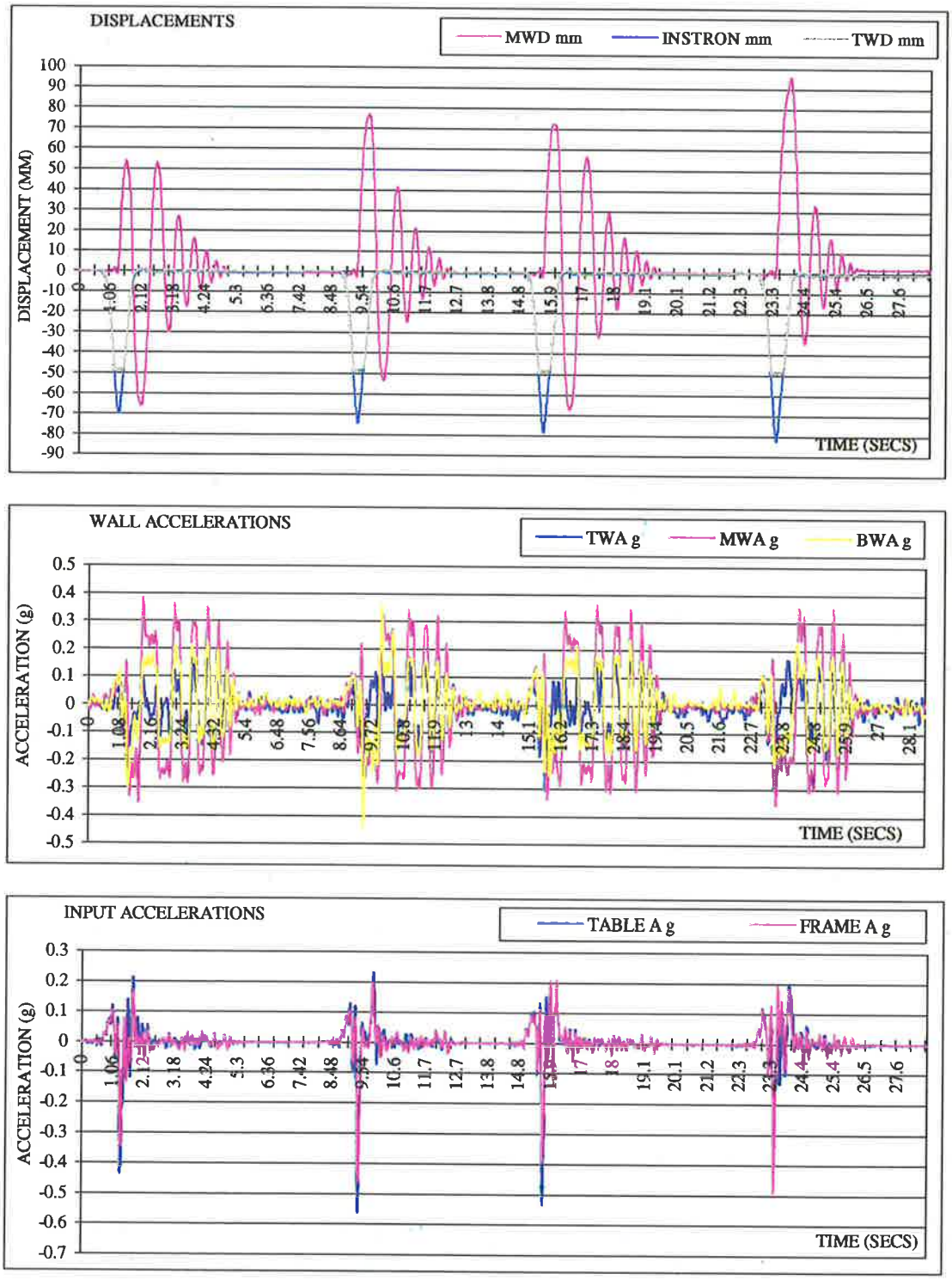

Figure F 41- 0.5Hz Gaussian Displacement Pulse, 110mm, No Overburden

SEPTEMBER 98 – Specimen (13) - 0.5Hz Gaussian Displacement Pulse

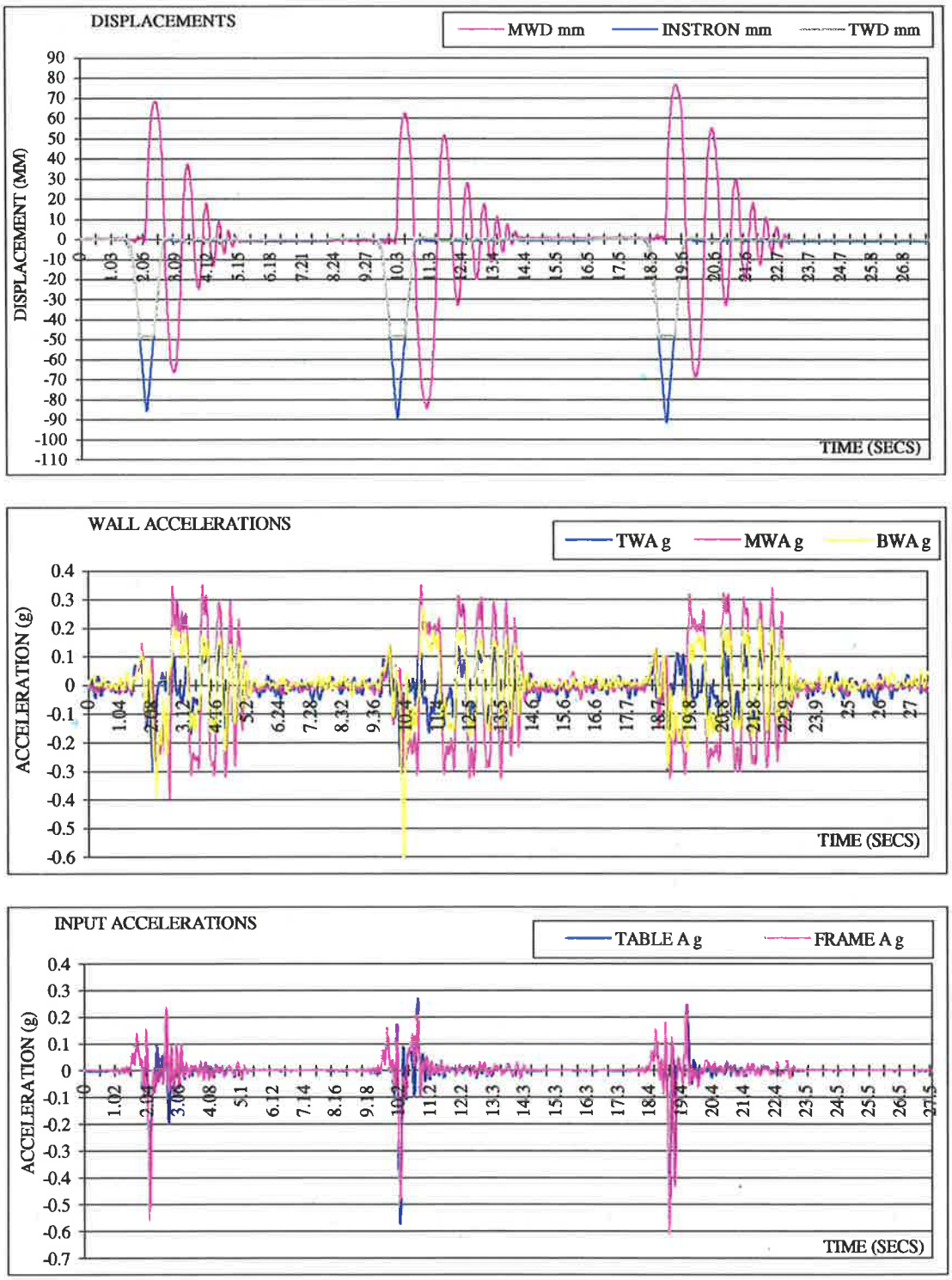

Figure F 42- 0.5Hz Gaussian Displacement Pulse, 110mm, No Overburden

SIMPLY SUPPORTED URM WALL TRANSIENT EXCITATION TEST S

SEPTEMBER 98 – Specimen (12) - 66% Elcentro Earthquake, California (1940)

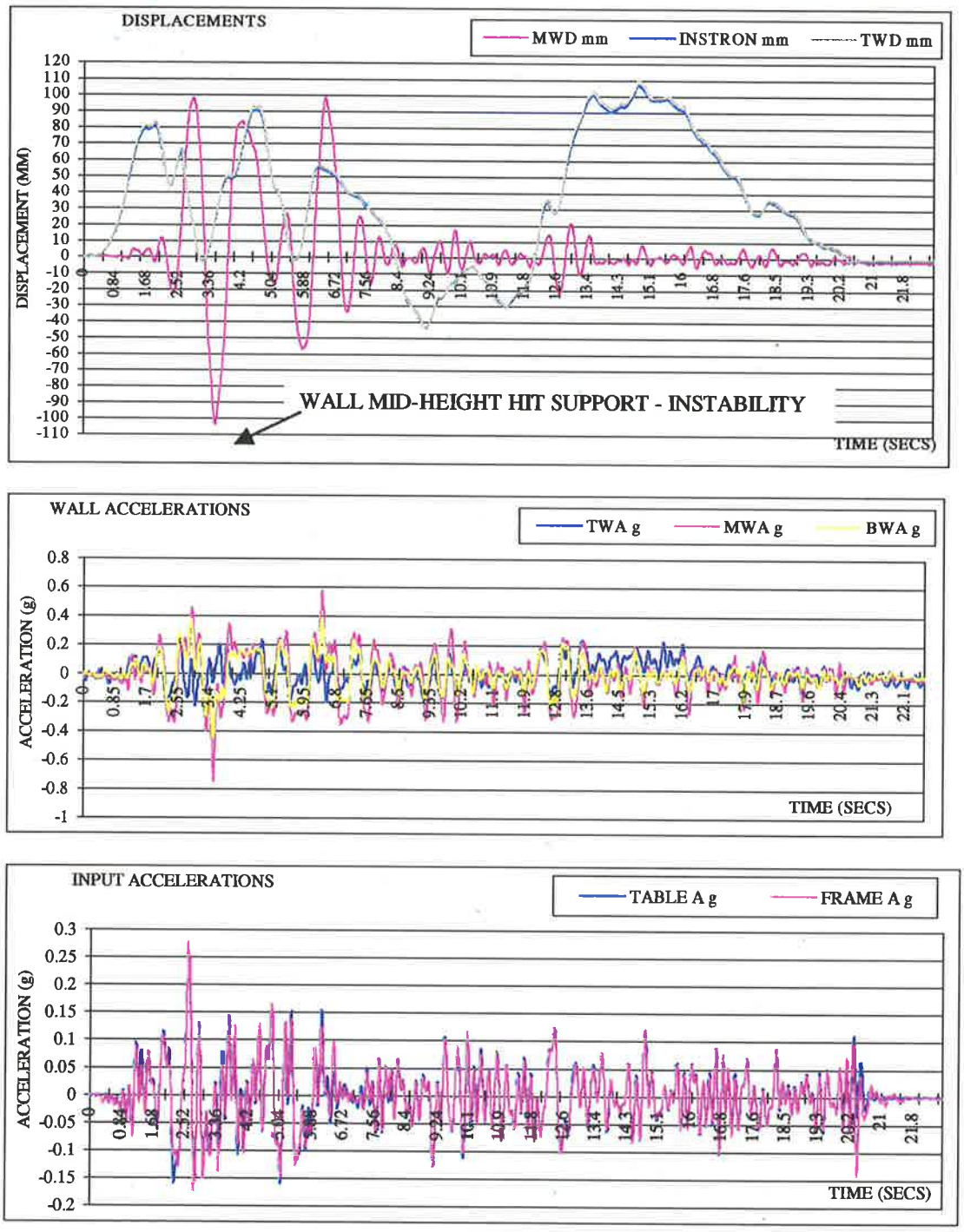

Figure F 43– Transient Excitation Test - 66% Elcentro, 110mm, No Overburden

SEPTEMBER 98 – Specimen (12) - 100% Nahanni Aftershock, Canada (1985)

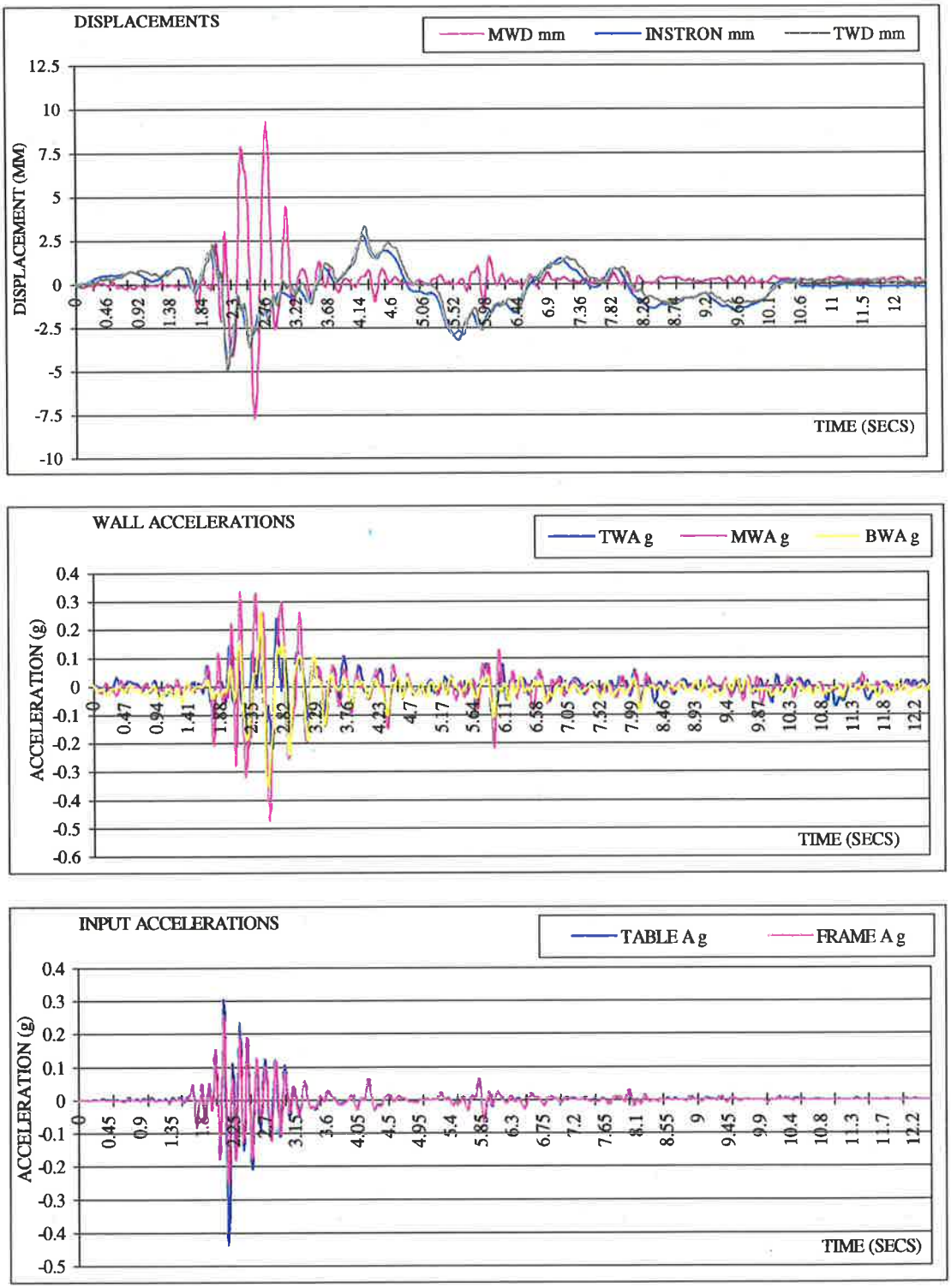

Figure F 44 - Transient Excitation Test - 100% Nahanni, 110mm, No Overburden

SEPTEMBER 98 – Specimen (12) - 200% Nahanni Aftershock, Canada (1985)

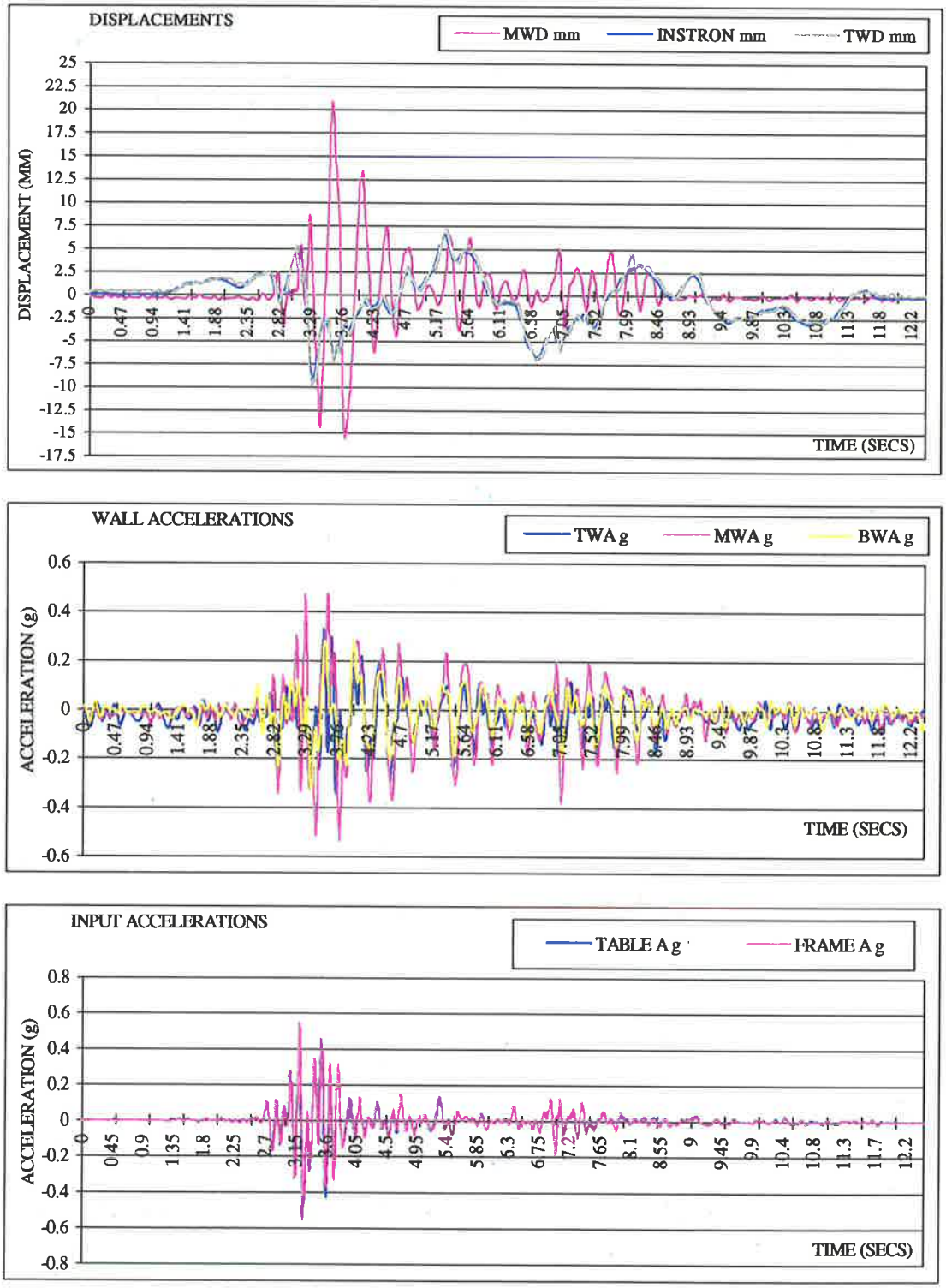

Figure F 45- Transient Excitation Test - 200% Nahanni, 110mm, No Overburden

SEPTEMBER 98 – Specimen (12) - 300% Nahanni Aftershock, Canada (1985)

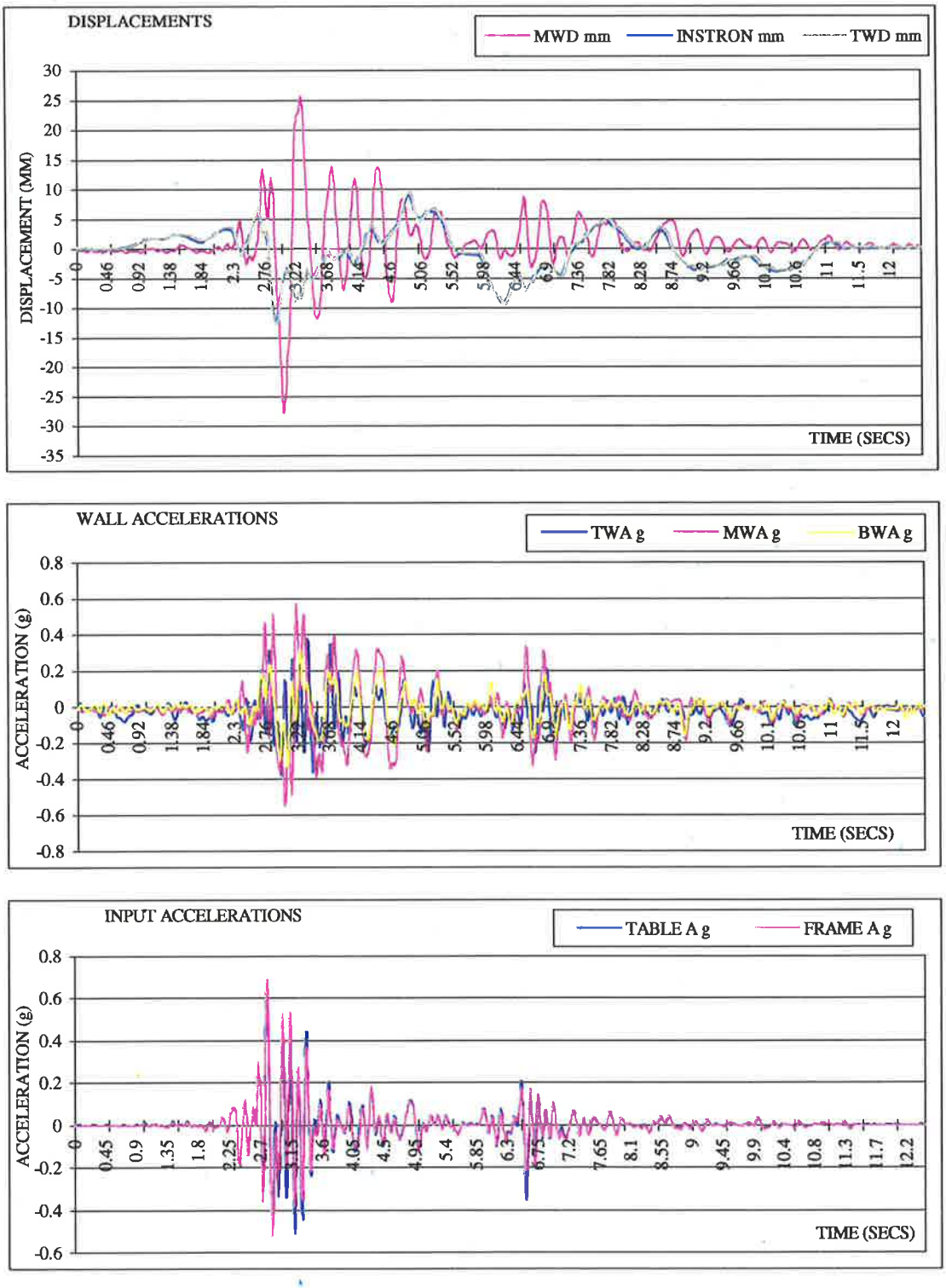

Figure F 46 - Transient Excitation Test - 300% Nahanni, 110mm, No Overburden

SEPTEMBER 98 – Specimen (12) - 400% Nahanni Aftershock, Canada (1985)

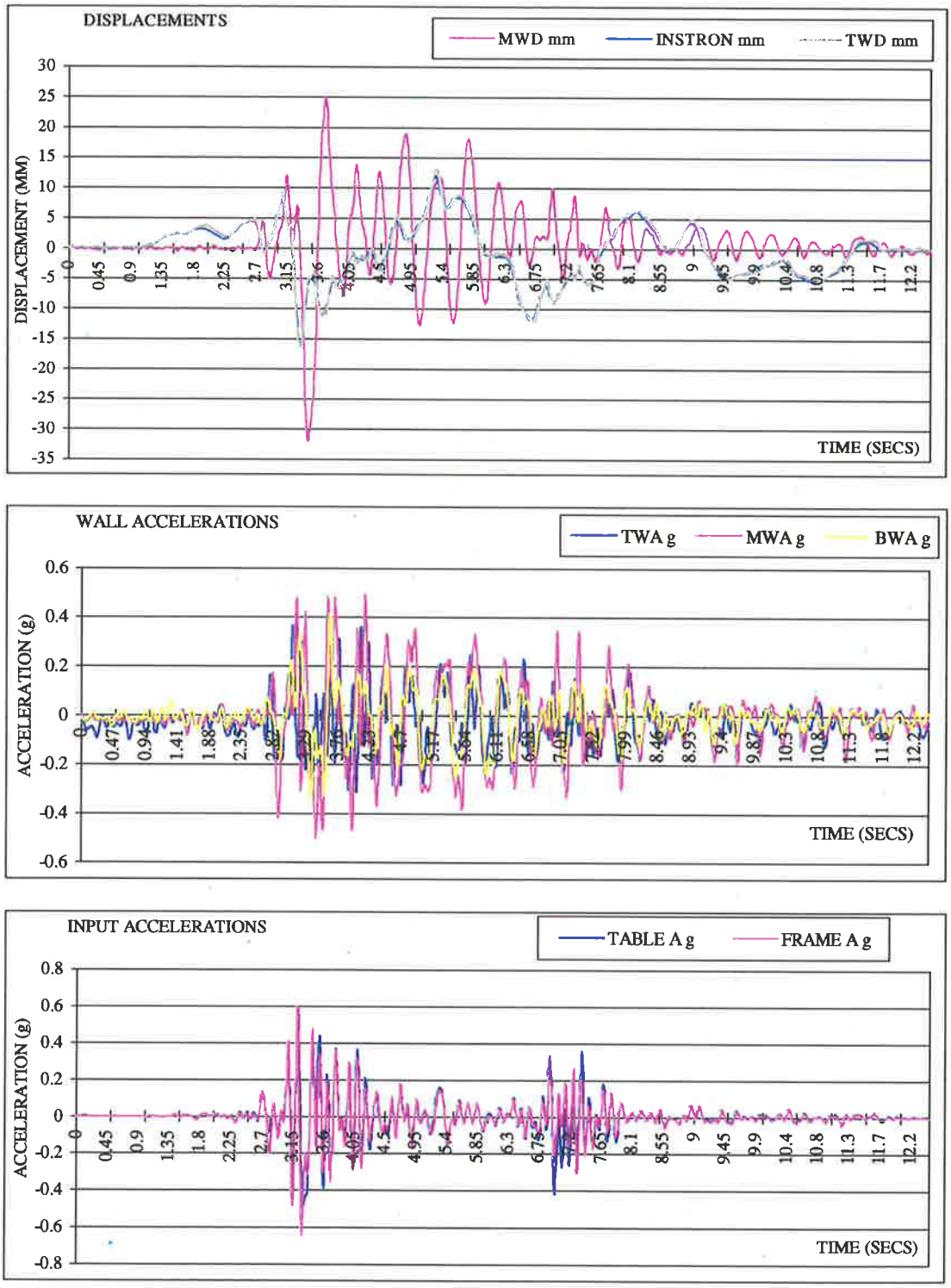

Figure F 47 - Transient Excitation Test - 400% Nahanni, 110mm, No Overburden

SEPTEMBER 98 – Specimen (13) - 66% Elcentro Earthquake, California (1940)

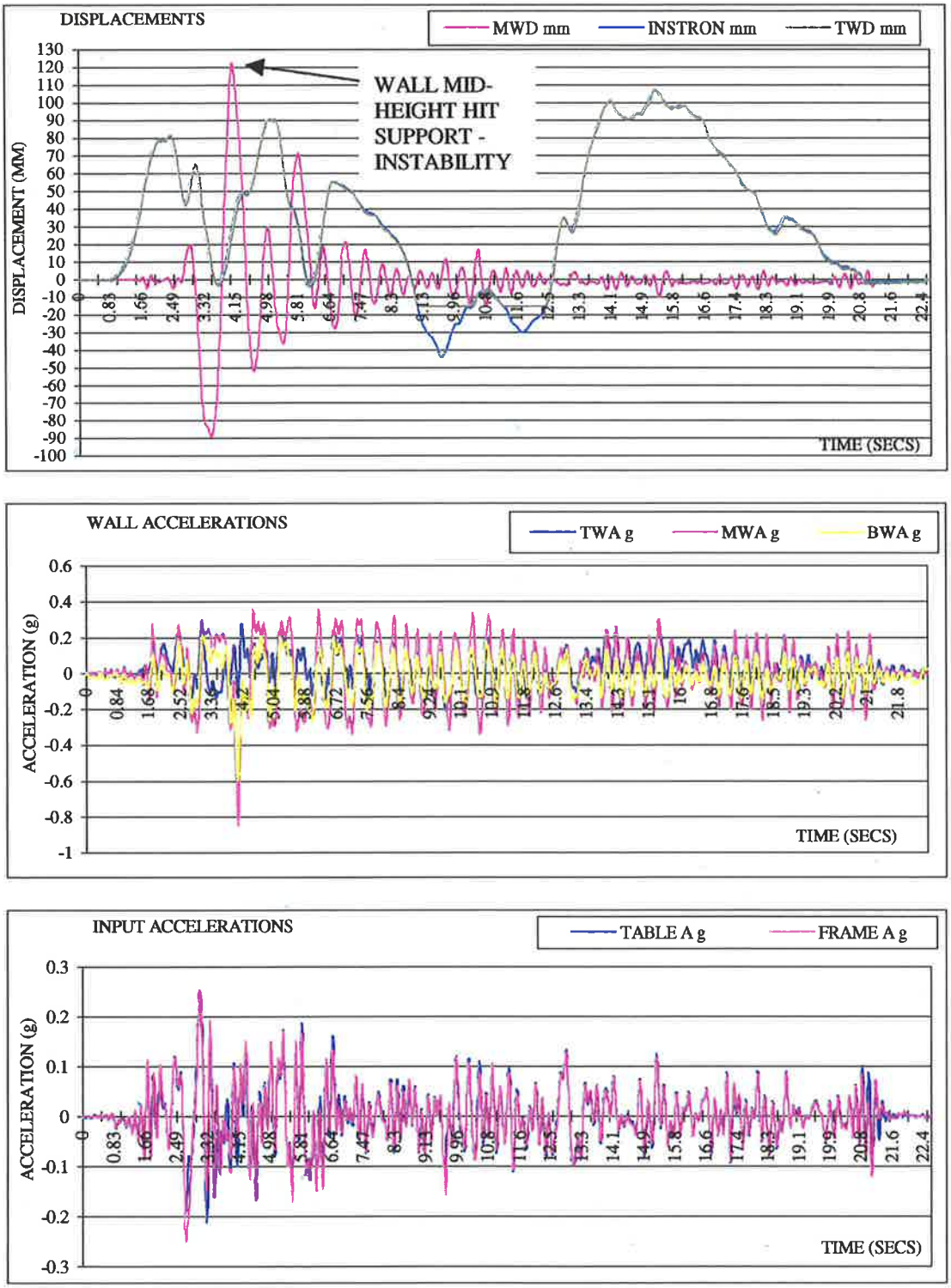

Figure F 48 - Transient Excitation Test – 66% ElCentro, 110mm, No Overburden

SEPTEMBER 98 – Specimen (13) - 66% Pacoima Dam, California (1994)

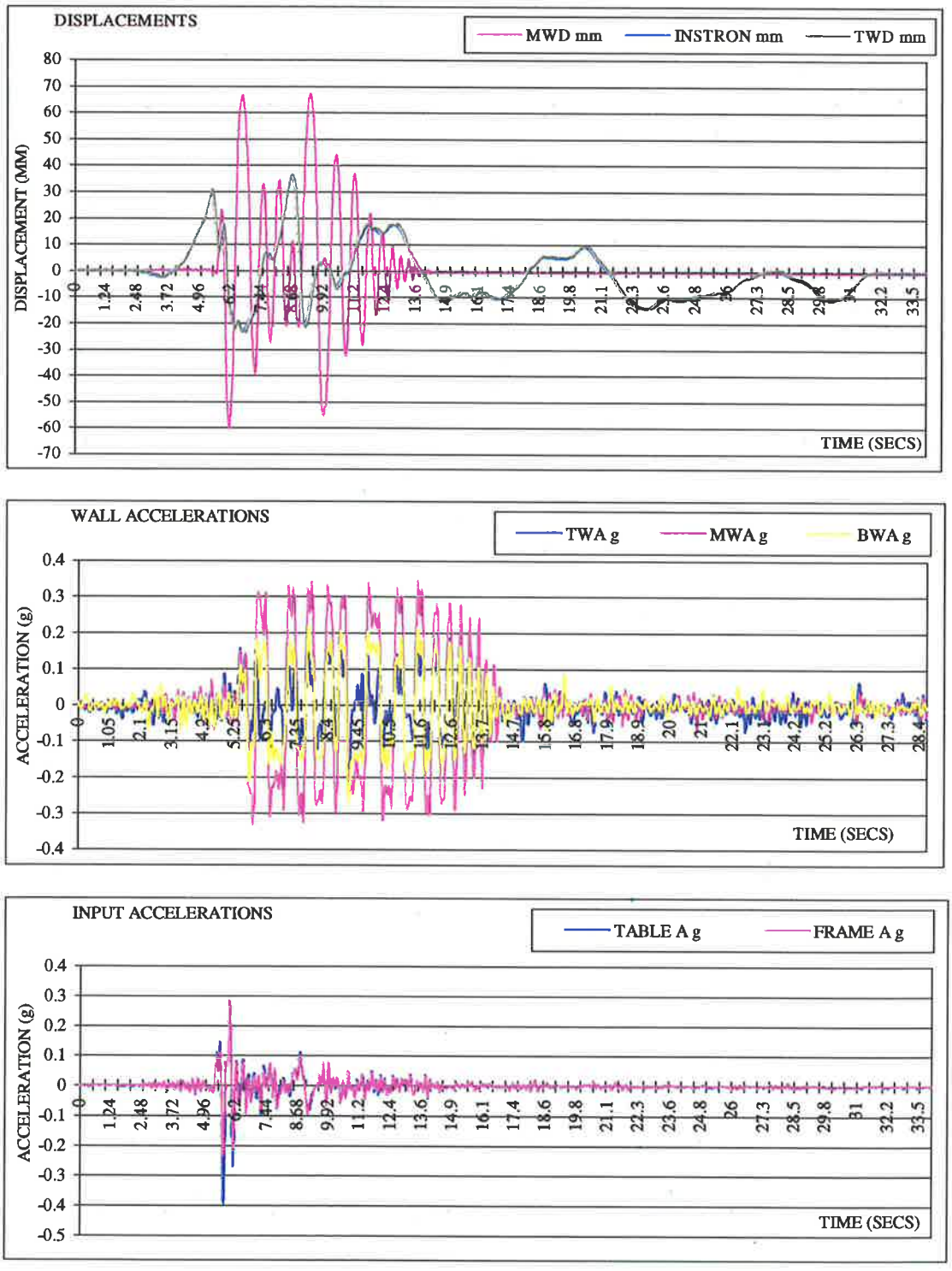

Figure F 49- Transient Excitation Test – 66% Pacoima Dam, 110mm, No Overburden

SEPTEMBER 98 – Specimen (13) - 80% Pacoima Dam, California (1994)

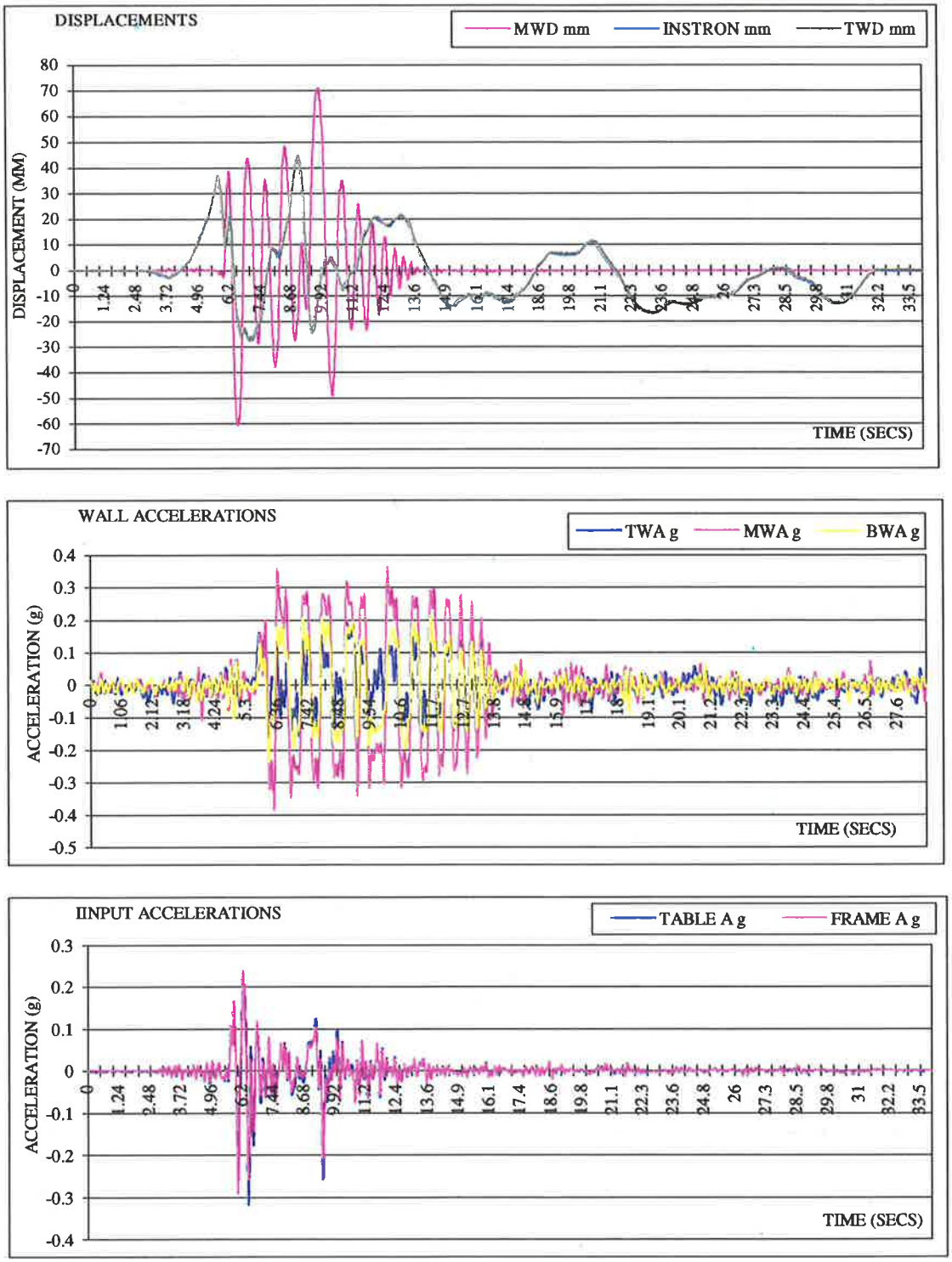

Figure F 50- Transient Excitation Test – 80% Pacoima Dam, 110mm, No Overburden

SEPTEMBER 98 – Specimen (13) - 100% Pacoima Dam, California (1994)

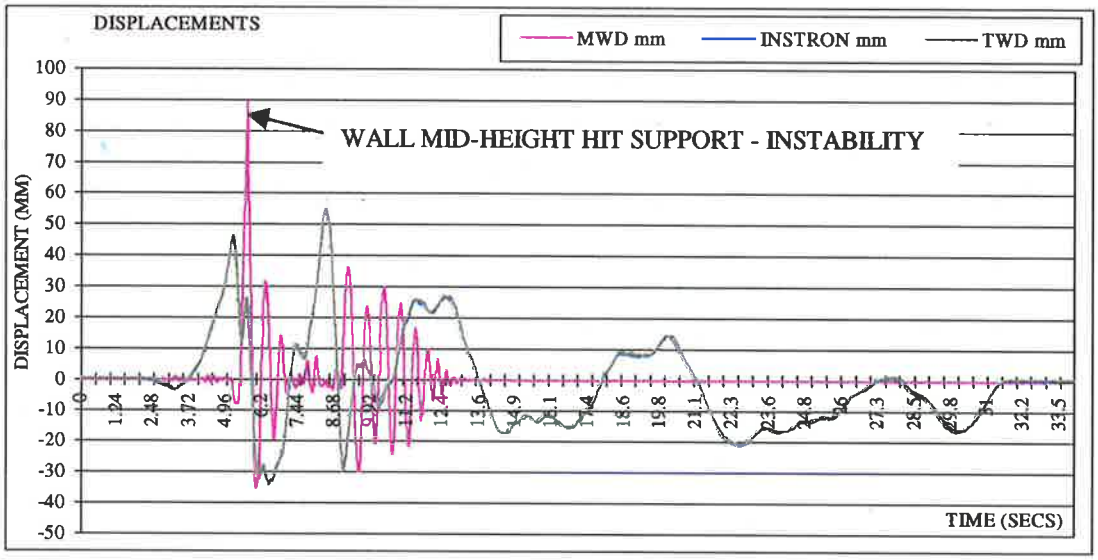

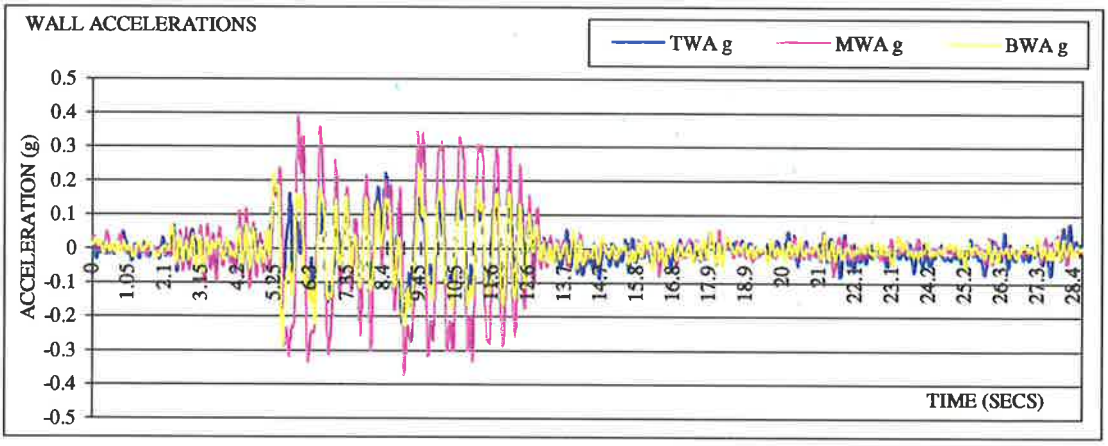

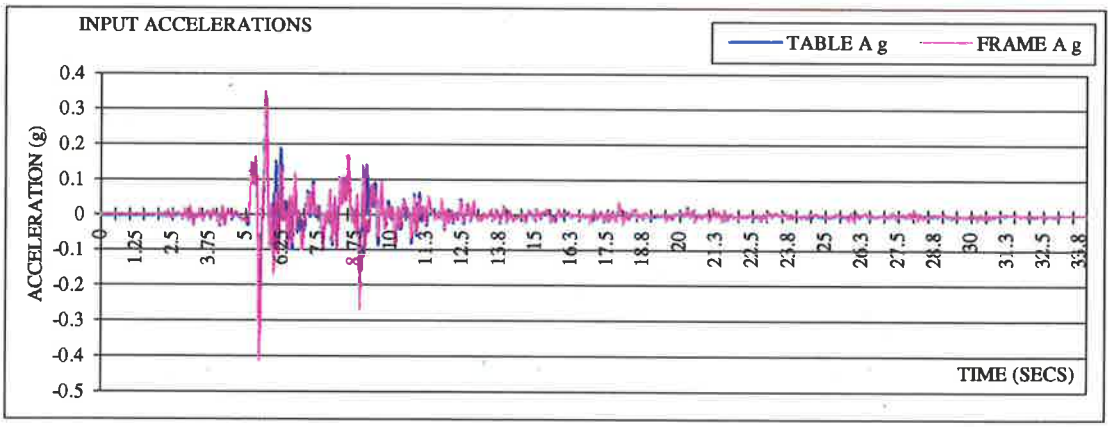

Figure F 51 - Transient Excitation Test – 100% Pacoima Dam, 110mm, No Overburden

APPENDIX (G): Non-linear Time History Analysis ROWMANRY Fortran77 Code

```
Program rowmanry
c  Written February 1999
c  Program "ROWMANRY" was derived from the original program "romain"
c  to determine the rocking behaviour of both rigid and semi rigid
c  objects making allowance for various support conditions
c  The main program drive subroutine is "Row-ray" which
c  determines the displ. time-history of a rocking model
c  using a tri-linear dynamic force displacement profile approximation
c  Rayleigh damping is assumed with an iterative half cycle process used
c  to ensure the proportional damping assumed at the start of each half cycle is appropriate
c  at the end of the half cycle (where the instantaneous frequency is known)
c  An initial damping coefficient of 3 is adopted however with the iterative process
c generally is not critical to the successful running of the program
c  Uniform wall properties are assumed
c  The acceleration data filename ACTIVE, time-step dt and the analysis time
c  segment ta are required as input.
c  The program will produce time-history arrays of the relative
c  displacement u, relative velocity v, and total acceleration at
c  at the top of a free standing object or mid height of a propped cantilever.
c  Maximum u, v and at will be displayed on screen at run time.
c  There is an option to write the time-history series to a new file
c  with the filename designated by the user (char variable ofile).

      character *50 ACTIVE,TEXT,ofile,type
      character *1 yesno
      character  *60 code
      integer NN,NTP,NT,NK,k
      integer IOS,ERL,X,Y,L
      real ts(0:12000),as(0:12000)
      real alpha, dt, ta, ag(0:16384)
      real u(0:16384), v(0:16384), at(0:16384)
      real agmax,umax,vmax,atmax
      real ke(-1:1), re(-1:1),ulimit(-1:1),uy(-2:2),pi,g
      real scale
      real h,t,m
      real HEFFR,HEFFS,gam,PC
      real a0, a1, a0m, a1m
c     real EM,rd
      real PCF
      real PDM
      real ulimrb
      parameter(pi=3.141592654)
      parameter(g=9.806)
c     Rocking is independent of the mass of the object. Thus, a
c     unit mass (1.0kg) has been assumed in subroutine rowray.
      m=1.0
c
      write(*,*)"*****************************************************"
      write(*,*)"              Program ROWMANRY"
      write(*,*)"       For time history rocking analysis of"
```

```
      write(*,*)"    Free Standing or Simply Supported Objects"
      write(*,*)"          Latest Version :  FEBRUARY 1999"
      write(*,*)"*****************************************************"
      write(*,*)"         Units in length - m, time - secs, "
      write(*,*)"           Force – N, Density – kg/m3 "
      write(*,*)"         Stress – MPa unless shown otherwise "
      write(*,*)" "
c     Inputting accelerogram data into ag(t) array
      write(*,*)"Type filename for accel. data [<= 8 Characters]:"
      read (*,'(a)')ACTIVE
      L=INDEX(ACTIVE,' ')
      ACTIVE(L:L+4)='.csv'
c      write(*,2000) ACTIVE(1:L+4)
      write(*,*) " "
      write(*,*)"    --- FOR DEFAULT VALUES [ ] TYPE 0 ---"
      write(*,*) " "
      write(*,*)"Type scaling factor for ground accel. [1.0]:"
      read(*,*)scale
      if(scale.eq.0.0)then
            scale=1.0
            write(*,*) " "
            write(*,*)"-- DEFAULT SCALING FACTOR [1.0] ADOPTED -- "
            write(*,*) " "
      end if
5     write(*,*)"Type time step interval dt [0.01]:"
      read(*,*)dt
      if(dt.eq.0.0)then
            dt=0.01
            write(*,*) " "
            write(*,*) "-- DEFAULT TIME INCREMENT [0.01] SECS ADOPTED --"
            write(*,*) " "
      end if
      open(25,file=ACTIVE,status='old',iostat=IOS,err=1000)
c     Go passed 8 header lines in datafile
      ERL=1
      do 10 k=1,8
            read(25,'(a)',iostat=IOS,err=1010)TEXT
            ERL=ERL+1
10    continue
c     read (25,*,iostat=IOS,err=1010)NN
c     ERL=ERL+1
      NN=0
      do 20 k=0,16384
            read(25,*,iostat=IOS,err=1010,END=3) ts(k),as(k)
            NN=NN+1
            as(k)=scale*as(k)
            ERL=ERL+1
20    continue
3     continue
      close(25)
      write(*,*) " "
      write(*,45) NN
45    format("NUMBER OF DATA POINTS IN INPUT FILE = ",I7)
      write(*,*) " "
c     Data interpolation
      call linter(NN,ts,as,dt,NTP,ag)
```

```
      write(*,*)"Record time is ",real(NTP)*dt,"seconds"
      write(*,*)"Type analysis time [Record time]:"
      read(*,*)ta
      if(ta.eq.0.0)then
            ta=real(NTP)*dt
            write(*,2010) ta
            write(*,*) " "
2010    format('-- DEFAULT : [RECORD TIME',F6.3,'secs] ADOPTED --')
            write(*,*) " "
      end if
      NT=int(ta/dt)
      if (NT.gt.16384)then
            write(*,*)"Required no. of time steps exceed limit of 16384"
            write(*,*)"Retype longer time step or shorter analysis time"
            goto 5
      else
      end if
      if(NT.gt.NTP)then
c       Augment ag(k>=NTP) with zeros
            do 30 k=NTP,NT-1
                  ag(k)=0
30          continue
      else
      end if
41    continue
      write(*,*)"-------------------------------------------------------"
      write(*,*)"        OBJECT RIGIDITY CLASSIFICATION"
      write(*,*)"       Is the object to be analysed either :"
      write(*,*)"         (Type corresponding number)"
      write(*,*)" "
      write(*,*)"(1) RIGID eg steel library bookshelves"
      write(*,*)"(2) SEMI RIGID eg simply supported URM wall"
      write(*,*)"                parapet URM wall"
      write(*,*)"-------------------------------------------------------"
      read(*,*) X
      if(X.ne.1.AND.X.ne.2)goto 41
4     continue
c     Definition of support conditions
      write(*,*)"-------------------------------------------------------"
      write(*,*)"       DEFINITION OF VERTICAL SUPPORT CONDITIONS"
      write(*,*)"          What support conditions exist :"
      write(*,*)"          (Type corresponding number)"
      write(*,*)" "
      write(*,*)"(1) Free standing object, base reaction at LF"
      write(*,*)"(2) SS non loadbearing, base reaction at LF"
      write(*,*)"(3) SS loadbearing, top & bottom reactions at CL"
      write(*,*)"(4) SS loadbearing, top reaction at CL, bottom reaction
     + at the LF"
      write(*,*)"(5) SS loadbearing, top & bottom reaction at LF"
      write(*,*)" "
      write(*,*)"where        SS = simply supported"
      write(*,*)"             LF = leeward face of object"
      write(*,*)"             CL = center line of object"
      write(*,*)"-------------------------------------------------------"
      read(*,*) Y
      if(Y.ne.1.AND.Y.ne.2.AND.Y.ne.3.AND.Y.ne.4.AND.Y.ne.5)goto 4
```

```
c
c    Inputing structural parameters
     gam=0.0
c
     write(*,*)"Type total height of the object (m) :"
     read(*,*)h
     write(*,*)"Type total thickness of the object (mm) :"
     read(*,*)t
     t=t/1000.0
c
     if(Y.ge.3)then
c  Loadbearing simply supported requires overburden stress and density
          write(*,*)"Type the overburden stress at top of object (MPa)"
          read(*,*)PC
       write(*,*)"Type object density [1800 kg/m3] :"
       write(*,*)"[Masonry density approximately 1500 - 2500 kg/m3]"
          read(*,*) gam
          if(gam.eq.0.0)then
        gam=1800.0
           write(*,*) " "
       write(*,*)"-- DEFAULT OBJECT DENSITY [1800kg/m3] ADOPTED --"
          write(*,*) " "
          end if
c  Calculation of overburden stress factor
          PCF=2.0*PC*1E6/(h*gam*g)
     else
          PC=0.0
          PCF=0.0
     end if
c
     if(Y.eq.1)then
          type="Free standing object base reaction at LF"
c  Stiffness and resistance acceleration conversion factors
          HEFFS=1.0
          HEFFR=1.0
          write(*,*) " "
          write(*,1)HEFFS
          write(*,2)HEFFR
          write(*,*) " "
1      format(" Stiffness  coefficient (HEFFS) = ",f7.3)
2      format(" Resistance coefficient (HEFFR) = ",f7.3)
     end if
     if(Y.eq.2)then
       type="SS non loadbearing (LF)"
          HEFFS=4.0
          HEFFR=4.0
          write(*,*) " "
          write(*,1)HEFFS
          write(*,2)HEFFR
          write(*,*) " "
     end if
     if(Y.eq.3)then
       type="SS loadbearing top & bottom (CL)"
          HEFFS=4.0*(1+PCF)
          HEFFR=2.0*(1+PCF)
          write(*,*) " "
```

```
          write(*,1)HEFFS
          write(*,2)HEFFR
          write(*,*) " "
      end if
      if(Y.eq.4)then
       type="SS loadbearing top (CL) bottom (LF)"
          HEFFS=4.0*(1+PCF)
          HEFFR=4.0*(1+0.75*PCF)
          write(*,*) " "
          write(*,1)HEFFS
          write(*,2)HEFFR
          write(*,*) " "
      end if
      if(Y.eq.5)then
       type=" SS loadbearing top & bottom (LF)"
          HEFFS=4.0*(1+PCF)
          HEFFR=4.0*(1+PCF)
          write(*,*) " "
          write(*,1)HEFFS
          write(*,2)HEFFR
          write(*,*) " "
      end if
c     Apply SDOF conversion factor to ag which does not include the factor
      do 60 k=0,NTP-1
            ag(k)=1.5*ag(k)
60    continue
c
3000  Continue
c     Set first half cycle iteration approx proportional damping
      alpha=3.0
c     Set the proportional damping experimental to SDOF conversion factor
      PDM=2.0/3.0
      write(*,*)"Type mass proportional damping coefficient. :"
      read(*,*)a0
c     Modify a0 to fit SDOF model
      a0m=PDM*a0
      write(*,*)"Type stiffness proportional damping coefficient. :"
      read(*,*)a1
c     Modify a1 to fit SDOF model
      a1m=PDM*a1
c
c     Rigid body complete instability displacement (mm)
      ulimrb=t*1000.0*HEFFR/HEFFS
c     Side eccentricities are t/2 as uniform properties assumed
c     Calculation of the rigid body resistance acceleration
      re(1)=1.5*HEFFR*g*t/h
      re(-1)=-1.0*re(1)
c     Calculation of the rigid body negative stiffness
      ke(1)=-1.5*HEFFS*g/h
      ke(-1)=ke(1)
c
c
c     Completely rigid objects
      if(X.eq.1)then
c     Setting the rocking displacements to a nominally small value (>0)
            uy(1)=1.E-4
```

```
            uy(-1)=1.E-4
            uy(2)=1.E-4
            uy(-2)=1.E-4
            ulimit(1)=ulimrb
            ulimit(-1)=-1*ulimit(1)
        end if
c
c   Semi rigid objects
        if(X.eq.2)then
            write(*,*) " "
            write(*,*)"Type disp. rocking expected to commence (mm)"
            write(*,*)"(This disp. dictates the initial rocking stiffness"
            write(*,*)" and must be greater than zero)"
            read(*,*)uy(1)
            uy(1)=uy(1)/1000.0
            uy(-1)=-1.0*uy(1)
            write(*,*) " "
            write(*,*)"Type disp. at start negative stiffness (mm)"
            write(*,*)"(This disp. dictates the peak rocking resistance"
         write(*,*)" plateau as it is the point of intersection of"
            write(*,*)" the semi rigid and rigid body force disp profiles)"
            read(*,*)uy(2)
            uy(2)=uy(2)/1000.0
            uy(-2)=-1.0*uy(2)
            write(*,*)"Type complete instability disp (mm) [RIGID]"
            write(*,71) ulimrb
71      Format("Less than or equal to ",F6.2," (mm) - RIGID -")
            read(*,*) ulimit(1)
            if(ulimit(1).eq.0.0)then
              ulimit(1)=ulimrb
              write(*,*) " "
              write(*,72) ulimrb
72        format('--DEFAULT INSTABILITY DISP[',F6.2,'] mm] ADOPTED--')
              write(*,*) " "
            end if
            ulimit(1)=ulimit(1)/1000.0
            ulimit(-1)=-1*ulimit(1)
        end if
c
c   Doing the actual computations
        call rowray(1.0,alpha,re,uy,ke,ulimit,NT,dt,ag,u,v,at,code,a0m
       +,a1m)
c   Finding the maximum out of each array
        call fndmax(NT,16384,ag,agmax)
        call fndmax(NT,16384,u,umax)
        call fndmax(NT,16384,v,vmax)
        call fndmax(NT,16384,at,atmax)
c
c   Outputting the key results to screen(system output)
        write(*,*)" "
        write(*,22)code
22      format("ANALYSIS CONCLUSION : ",a60)
c   If the code message does not begin with "M" for "Model"
c   go straight to the end of the program.
        if(ichar(code(1:1)).ne.77)goto 1100
        write(*,*)"Analysis results summary: "
```

```
      write(*,21)"Max. rel. displ.  = ",umax
      write(*,21)"Max. rel. velocity = ",vmax
      write(*,21)"Max. total accel.  = ",atmax
21    format(a21,1x,f9.6)
c
c     Setting effective parameters back to original
      uy(1)=1000.0*uy(1)
      uy(2)=1000.0*uy(2)
      t=t*1000.0
c
c     Reporting the time-history output
      write(*,*)"Time-history results can be written to a file"
      write(*,*)"Type y/n to indicate if file is wanted:"
      read(*,'(a)')yesno
      if(ichar(yesno).eq.110)goto 3010
      write(*,*)"Specify output filename [<= 8 characters]:"
      read(*,'(a)')OFILE
      L=INDEX(OFILE,' ')
      OFILE(L:L+4)='.csv'
c     write(*,*) OFILE(1:L+4)
      open(15,file=ofile,iostat=IOS,ERR=1020)
      write(*,*)"Type no. of time steps for every reported results"
      read(*,*)NK
      write(15,*)"*********************************************************
     +*********************"
      write(15,*)"                  Program ROWMANRY"
      write(15,*)"          For time history rocking analysis of"
      write(15,*)"        Free Standing or Simply Supported Objects"
      write(15,*)"              Latest Version :  FEBRUARY 1999"
      write(15,*)"*********************************************************
     +*********************"
      write(15,*)"Output filename :          ",ofile
      write(15,17)"Accelerogram data from :    ",ACTIVE
17    format(a23,1x,a13)
      write(15,18)scale
18    format("Accelerogram scaling factor selected =  ",f7.3)
      write(15,*)" "
c     Echo input data
      write(15,*)"INPUT DATA SUMMARY FOR: "
      write(15,*)type
      write(15,*)" "
      write(15,11)h
11    format("Height of object = ",f7.3," m")
      write(15,13)t
13    format("Object width = ",f7.3," mm")
      write(15,9)PC
9     format("Overburden stress at top of object = ",f7.3," MPa")
      write(15,*)" "
      write(15,*)"Tri-linear force disp profile data"
      write(15,16)uy(1)
16    format("Disp 1 selected for initial stiffness = ",f5.2," mm")
      write(15,26)uy(2)
26    format("Disp 2 selected for maximum force plateau = ",f5.2," mm")
      write(15,1)HEFFS
      write(15,2)HEFFR
      write(15,*) " "
```

```
      write(15,*) "Proportional damping data"
      write(15,27)a0
27    format(" Mass proportional damping coeff. = ",f7.4)
      write(15,28)a1
28    format(" Stiffness proportional damping coeff. = ",f7.4)
      write(15,*)" "
      write(15,*)" "
      write(15,22)code
      write(15,12) ta, dt
12    format('Analysis time =',f7.4,'secs time inc =',f5.4,'secs')
      write(15,*)"Legend:,ag = input ground acceleration"
      write(15,*)",u = relative displacement"
      write(15,*)",v = relative velocity"
      write(15,*)",at = total acceleration"
      write(15,*)" "
      write(15,*)"Time,ag(m/s/s)
     +    ,u(m),v(m/s),at(m/s/s)"
c     Printing the maximum out of each array
      write(15,42)"Maxim :",agmax,umax,vmax,atmax
42    format(a6,',',f7.3,',',f9.6,',',f7.3,',',f8.4)
      write(15,*)"Time,ag(m/s/s)
     +    ,u(m),v(m/s),at(m/s/s),experimental u(m)"
c     Printing the time-history arrays
      do 40 k=0,NT-1,NK
       write(15,51)real(k)*dt,ag(k),u(k),v(k),at(k)
51     format(f6.3,',',f7.3,',',f9.6,',',f7.3,',',f8.4)
40     continue
      close(15)
3010  write(*,*)"Type y/n to continue analysis:"
      read(*,'(a)')yesno
      if(ichar(yesno).eq.110)then
            goto 100
      else
c     Re-Setting effective parameters
            t=t/1000.0
            goto 3000
      end if
100   write(*,*)"Program completed"
      stop
c
c     Error messages
1000  write(*,1001)"opening file ",ACTIVE
1001  format("Error in ",a13,a12)
      goto 1100
1010  write(*,1002)"reading file",ACTIVE,ERL
      goto 1100
1002  format("Error in ",a13,a12,"at line ", i5)
1020  write(*,1001)"opening file ",ofile
      goto 1100
1100  write(*,*)"Program aborted"
      stop
      end
```

```
Subroutine rowray(m,pc,re,uy,ke,ulim,NT,dt,ag,uf,v,at,code,a0m
     + ,a1m)
c    Rowray was originally derived from Rotha including a
c    tri-linear static force displacement relationship
c    Iterative half cycle procedure to determine Rayleigh damping
c    coefficient for current instantaneous frequency
c    uy(1) is the initial positive rocking displacement
c    uy(-1) is the initial negative rocking displacement
c    uy(2) is the secondary positive rocking displacement
c    uy(-2) is the secondary negative rocking displacement
c    re(1) is the completely rigid positive rocking resistance
c    re(-1) is the completely rigid negative rocking resistance
c    ke(1) is the rigid body stiffness for +ve rocking
c    ke(-1) is the rigid body stiffness for -ve rocking
c    ulim(1) is the +ve ultimate displacement
c    ulim(-1) is the -ve ultimate displacement
c
c    Declaration of parameters
     character*60 code
     integer NT
     real m, pc
     real ke(-1:1), re(-1:1), uy(-2:2), ulim(-1:1)
     real ag(0:16384),dt
     real u(0:16384), uf(0:16384)
     real v(0:16384),at(0:16384)
c    Declaration of local variables
     integer Jevent, k, j, p, e, d, X, Y
     integer f, I, l, px
     real ry(-1:1)
     real du, dv, da, a, dag, dps
     real kts1, ktsp, kts2
     real f1,f2,f3
     real t0,t1,t2,t3,t4
     real pi, p1
     real a1m, a0m
     real dpsx, dpsy, nc, jx, jy
     real ay, ax
     parameter(pi=3.141592654)
c
c    Initialise conditions
     u(0)=0.
     uf(0)=0.
     v(0)=0.
     a=0.
     ag(0)=0.
     at(0)=0.
     Jevent=0
     uyy=0.0
     t0=0.0
     t1=0.0
     t2=0.0
     t3=0.0
     t4=0.0
     j=0
     e=0
     d=0
```

```
      p=0
      x=0
      y=0
      f=0
      I=1
      px=0
      code="Model did not rock"
c
5     continue
      if(e.eq.1)then
c     Reset time step at start of iteration
          I=y
      end if
      if(d.eq.1)then
c     Reset time step at start of iteration
          I=x
      end if
c
c      open(unit=1,file='out.dat',status='new')
c      write(1,*) "NT I(=x) pc"
c      write(1,*) NT, I, pc
c     u(k) is the displ. obtained at the end of each time step, and
c     uyy is the displ. calculated and updated within the time step.
c     Time history computation do-loop
c
      do 10 k=I,NT-1
          if(f.ne.1)then
c     Determine pseudo-static force for each time-step except
c     on iteration where returned to previous zeroed conditions
            dag = ag(k) - ag(k-1)
            f1  = m*dag
            f2  = m*((4.*v(k-1)/dt)+2.*a)
            f3  = 2. * pc * v(k-1)
            dps = f2+f3-f1
            uyy=u(k-1)
          else
c     Reset flag for returned to previous zeroed conditions
            f=0
          end if
c     Time step counter for time between zero crossings
          t0=t0+dt
          if(dps.eq.0.0)then
            u(k)=uyy
            goto 25
          end if
c       BEGIN EVENT ITERATION :
c
c       Determine the dynamic stiffness profile for the
c       particular proportional damping coefficient
c
c       Determine pseudo-static stiffness (Jevent 1 rocking stiffness)
          ktsp=(4.*m/(dt**2.))+(2.*pc/dt)
c       Rocking threshold acceleration
          ry(1)=re(1)+ke(1)*uy(2)+ktsp*uy(1)
          ry(-1)=re(-1)+ke(-1)*uy(-2)+ktsp*uy(-1)
c       Determine Jevent 0 rocking stiffness
```

```
          kts1=ry(1)/uy(1)
c       Determine Jevent 2 rocking stiffness
          kts2=ktsp+ke(1)
c         write(1,*)"kts1 ktsp kts2"
c         write(1,*) kts1, ktsp ,kts2
c
15      continue
c       NON ROCKING (DISP INCREASING OR DECREASING)
          if(Jevent.eq.0)then
            du=dps/kts1
            uyy=uyy+du
c         POSITIVE DIRECTION
            if(dps.gt.0.0)then
c           ROCKING NOT COMMENCED-NO EVENT
              if(uyy.lt.uy(1))then
                u(k)=uyy
c           STAGE 1 ROCKING LEVEL REACHED-WITH EVENT
              else
                dps=kts1*(uyy-uy(1))
                uyy=uy(1)
                Jevent=1
                code="Model rocked within limits"
                goto 15
              end if
c         NEGATIVE DIRECTION
            else
c           ROCKING NOT COMMENCED-NO EVENT
              if(uyy.gt.uy(-1))then
                u(k)=uyy
c           STAGE 1 ROCKING LEVEL REACHED-WITH EVENT
              else
                dps=kts1*(uyy-uy(-1))
                uyy=uy(-1)
                Jevent=-1
                code="Model rocked within limits"
                goto 15
              end if
            end if
          else
c         POSITIVE STAGE 1 ROCKING
            if(Jevent.eq.1)then
              du=dps/ktsp
              uyy=uyy+du
c           INCREASING DISPLACEMENT
              if(dps.gt.0.0)then
c             STAGE 2 ROCKING LEVEL NOT YET REACHED
                if(uyy.lt.uy(2))then
                    u(k)=uyy
                else
c             STAGE 2 ROCKIN LEVEL REACHED
                    dps=ktsp*(uyy-uy(2))
                    uyy=uy(2)
                    Jevent=2
                    code="Model rocked within limits"
                    goto 15
                end if
```

```
            else
c         DECREASING DISPLACEMENT
c          NO EVENT
              if(uyy.gt.uy(1))then
                    u(k)=uyy
              else
c          WITH EVENT
                    dps=ktsp*(uyy-uy(1))
                    uyy=uy(1)
                    Jevent=0
                    code="Model rocked within limits"
                    goto 15
              end if
            end if
          end if
c       NEGATIVE STAGE 1 ROCKING
          if(Jevent.eq.-1)then
            du=dps/ktsp
            uyy=uyy+du
c         INCREASING DISPLACEMENT
            if(dps.lt.0.0)then
c           STAGE 2 ROCKING LEVEL NOT YET REACHED
              if(uyy.gt.uy(-2))then
                    u(k)=uyy
              else
c           STAGE 2 ROCKING LEVEL REACHED
                    dps=ktsp*(uyy-uy(-2))
                    uyy=uy(-2)
                    Jevent=-2
                    code="Model rocked within limits"
                    goto 15
              end if
            else
c         DECREASING DISPLACEMENT
c          NO EVENT
              if(uyy.lt.uy(-1))then
                    u(k)=uyy
              else
c          WITH EVENT
                    dps=ktsp*(uyy-uy(-1))
                    uyy=uy(-1)
                    Jevent=0
                    code="Model rocked within limits"
                    goto 15
              end if
            end if
          end if
c       POSITIVE STAGE 2 ROCKING
          if(Jevent.eq.2)then
            if(kts2.le.0.0)goto 1000
            du=dps/kts2
            uyy=uyy+du
c         INCREASING DISPLACEMENT
            if(dps.gt.0.0)then
c           COMPLETE INSTABILITY NOT REACHED
              if(uyy.lt.ulim(1))then
```

```
                u(k)=uyy
            else
c       COMPLETE INSTABILITY REACHED
c   Update pc and return to initial conditions
                if(px.eq.0)then
                  p1=pc
                end if
c   Vary proportional damping to try and achieve convergence
                if(px.lt.50)then
                  pc=p1-real(px)*0.02*p1
                end if
                if(px.eq.50)then
                  pc=p1
                end if
                if(px.gt.50)then
                  pc=p1+(real(px)-50.0)*0.02*p1
                end if
                if(px.eq.101)then
                  write(*,*)"Iteration limit reached-NO CONVERGENGE"
                  u(k)=uyy
                  v(k)=0.0
                  at(k)=0.0
                  do 38 l=I,k
                    uf(l)=u(l)
38            continue
c  Set remaining final displacement store to zero
                  do 41 l=k+1,NT-1
                    uf(l)=0.0
                    v(l)=0.0
                    at(l)=0.0
41            continue
                    goto 1000
                end if
                dps=dpsx
                j=jx
                a=ax
                uyy=0.0
                jevent=0
                px=px+1
                d=1
                f=1
c           write(1,*)"dpsx initial cond at"
c           write(1,*) dpsx, x
c   Restart iteration with new predicted proportional damping coefficient
                goto 5
             end if
c       DECREASING DISPLACEMENT
            else
c         NO EVENT
              if(uyy.gt.uy(2))then
                u(k)=uyy
c         WITH EVENT
              else
                dps=kts2*(uyy-uy(2))
                uyy=uy(2)
                Jevent=1
```

```
                code="Model rocked within limits"
                goto 15
              end if
             end if
            end if
c       NEGATIVE STAGE 2 ROCKING
            if(Jevent.eq.-2)then
             if(kts2.le.0.0)goto 1000
             du=dps/kts2
             uyy=uyy+du
c         INCREASING DISPLACEMENT
            if(dps.lt.0.0)then
c          COMPLETE INSTABILITY NOT REACHED
              if(uyy.gt.ulim(-1))then
                u(k)=uyy
              else
c          COMPLETE INSTABILITY REACHED
c     Update pc and return to initial conditions
                if(px.eq.0)then
                 p1=pc
                end if
                if(px.lt.50)then
                 pc=p1-real(px)*0.02*p1
                end if
                if(px.eq.50)then
                 pc=p1
                end if
                if(px.gt.50)then
                 pc=p1+(real(px)-50.0)*0.02*p1
                end if
c             write(1,*)"Complete instability"
                if(px.eq.101)then
                 write(*,*)"Iteration limit reached-NO CONVERGENGE"
                 u(k)=uyy
                 v(k)=0.0
                 at(k)=0.0
                 do 35 l=I,k
                  uf(l)=u(l)
35            continue
c   Set remaining final displacement store to zero
                 do 42 l=k+1,NT-1
                  uf(l)=0.0
                  v(l)=0.0
                  at(l)=0.0
42            continue
                 goto 1000
                end if
                dps=dpsy
                j=jy
                a=ay
                uyy=0.0
                jevent=0
                px=px+1
                e=1
                f=1
c             write(1,*)"dpsy  initial cond at"
```

```
c           write(1,*) dpsy, y
c     Restart iteration with new predicted proportional damping coefficient
                    goto 5
                end if
c         DECREASING DISPLACEMENT
              else
c           NO EVENT
                if(uyy.lt.uy(-2))then
                    u(k)=uyy
c           WITH EVENT
                else
                    dps=kts2*(uyy-uy(-2))
                    uyy=uy(-2)
                    Jevent=-1
                    code="Model rocked within limits"
                    goto 15
                end if
              end if
            end if
          end if
c
c     Zero crossings, instantaneous frequency and
c     Rayleigh damping
c
c     Identify zero crossing from neg to pos
          if(t0.ne.t2)then
            if(u(k).gt.0.0.AND.u(k-1).le.0.0)then
c           write(1,*) "neg pos zero cross"
              t1=dt*u(k-1)/(u(k-1)-u(k))
              t2=dt*u(k)/(u(k)-u(k-1))
              t0=t0-dt+t1
              j=j+1
              if(j.gt.1)then
                if(d.ne.1)then
c     Provided not prior to first half cycle or reiteration determines
c     Rayleigh damping of completed half cycle response
                    nc=(a0m+a1m*pi*pi/(t0**2))
c     Setting the maximum proportional damping coefficient for
c     Frequency range of interest
                    if(nc.gt.10.0)then
                      nc=10.0
                    end if
c             write(1,*) "period outcome predicted iteration k"
c             write(1,*) t0, nc, pc, p, k
                    if(nc.gt.1.1*pc.OR.nc.lt.0.9*pc.AND.p.lt.1000)then
c     Limit on iterations to 1000
c     Compares Rayleigh damping with initial prediction
c     If out of the specified bounds a reiteration is required
c     with new predicted proportional damping coefficient predicted below
c             write(1,*) "REITERATE - new pc"
                      pc=0.5*nc+0.5*pc
c             write(1,*) pc
c     Reset the initial conditions to the start of the current cycle
                    dps=dpsy
                    j=jy
                    a=ay
```

```
c               write(1,*)"dps j a"
c               write(1,*) dps, j, a
                        uyy=0.0
                        jevent=0
c     Iteration number
                        p=p+1
                        e=1
                        f=1
c     Restart iteration with new predicted proportional damping coefficient
                        goto 5
                       else
c               write(1,*) "PC-NC within limits"
                        if(p.gt.99)then
c                write(*,*)"Iteration limit exceeded"
                        end if
                        p=0
                        px=0
                        e=0
c     Setting the predicted proportional damping for the next half cycle
c     to the successful proportional damping of the current half cycle
                        pc=3.0
c     Transfer successful iteration to final displacement store
                        do 20 l=I,k-1
                          uf(l)=u(l)
20              continue
                      end if
                 end if
                else
c     Transfer displacements prior to first half cycle to final disp store
                 do 21 l=I,k-1
                       uf(l)=u(l)
21           continue
              end if
              t0=t2
c     Set the initial conditions for the next half cycle
c     The zero value for the dps depend on the new u(k) location
             if(u(k).lt.uy(1))then
              dps=kts1*u(k)
             else
              if(u(k).lt.uy(2))then
                    dps=uy(1)*kts1+(u(k)-uy(1))*ktsp
              else
                    dps=uy(1)*kts1+(uy(2)-uy(1))*ktsp+(u(k)-uy(2))
              end if
             end if
             uyy=0.0
             Jevent=0
c     Store the initial conditions for the next half cycle
             dpsx=dps
             jx=j-1
             ax=a
             x=k
c          write(1,*) "dpsx jx x k u(k)"
c          write(1,*) dpsx, jx, x, k, u(k)
               goto 15
             end if
```

```
        end if
c
c   Identify zero crossings from pos to neg
        if(t0.ne.t4)then
         if(u(k).lt.0.0.AND.u(k-1).ge.0.0)then
c       write(1,*) "pos neg zero crossing"
          t3=dt*u(k-1)/(u(k-1)-u(k))
          t4=dt*u(k)/(u(k)-u(k-1))
          t0=t0-dt+t3
          j=j+1
          if(j.gt.1)then
           if(e.ne.1)then
c   Provided not prior to first half cycle or reiteration determines
c   Rayleigh damping of completed half cycle response
                nc=(a0m+a1m*pi*pi/(t0**2))
                if(nc.gt.10.0)then
                 nc=10.0
                end if
c           write(1,*)"t0 nc pc p k"
c           write(1,*) t0, nc, pc, p, k
                if(nc.gt.1.1*pc.OR.nc.lt.0.9*pc.AND.p.lt.1000)then
c   Limit on iterations to 1000
c   Compares Rayleigh damping with initial prediction
c   If out of the specified bounds a reiteration is required
c   with new predicted proportional damping coefficient predicted below
c           write(1,*) "REITERATE - new pc"
                pc=0.5*nc+0.5*pc
c           write(1,*) pc
c   Reset the initial conditions to the start of the current cycle
                dps=dpsx
                j=jx
                a=ax
c           write(1,*)"dps j a"
c           write(1,*) dps, j, a
                uyy=0.0
                jevent=0
c   Iteration number
                p=p+1
                d=1
                f=1
c           write(1,*) "new dps j x d f"
c           write(1,*) dps, j, x, d, f
c   Restart iteration with new predicted proportional damping coefficient
                goto 5
               else
c           write(1,*) "PC-NC within limits"
                if(p.eq.100)then
                 write(*,*)"Iteration limit exceeded"
                end if
                p=0
                px=0
                d=0
c   The successful predicted proportional damping for the current half cycle
c   becomes the first approximation for the next half cycle
                pc=3.0
c   Transfer successful iteration to final displacement store
```

```
                    do 22 l=I,k-1
                     uf(l)=u(l)
22              continue
                      end if
                end if
               else
c  Transfer displacements prior to first half cycle to final disp store
                do 23 l=I,k-1
                      uf(l)=u(l)
23          continue
             end if
             t0=t4
c    Set the initial conditions for the next half cycle
c    The zero value for the dps depend on the new u(k) location
             if(u(k).gt.uy(-1))then
              dps=kts1*u(k)
             else
              if(u(k).gt.uy(-2))then
                    dps=uy(-1)*kts1+(u(k)-uy(-1))*ktsp
              else
                    dps=uy(-1)*kts1+(uy(-2)-uy(-1))*ktsp+(u(k)-uy(-2))
              end if
             end if
             uyy=0.0
             Jevent=0
c    Store the initial conditions for the next half cycle
             dpsy=dps
             jy=j-1
             ay=a
             y=k
             goto 15
            end if
           end if
c
c      Sub-step iteration ends
25      du  = u(k) - u(k-1)
        dv  = 2.*(du/dt) - 2.*v(k-1)
        v(k) = v(k-1) + dv
        da=-2.*a+(2.*dv/dt)
        a   = a + da
        at(k)= ag(k) + a
c
c      if(k.lt.NT)then
c       write(1,*) "j p k u(k)"
c       write(1,*) j, p, k, u(k)
c      end if
c
10   continue
     return
1000  code="Model beyond limits - possible iterative instability"
     return
1100  code="Invalid results, dt too large"
     return
     end
```

```
subroutine fndmax(N,dim,x,max)
c    Subroutine to find the absolute max. value of a
c    single dimension array x
c    declaration of parameters
     integer N,dim
     real x(0:dim),max
c    declaration of local variables
     integer I
     max=0.
     do 10 I=0,N-1
              if(abs(x(I)).ge.abs(max))then
                max=abs(x(I))
              else
              end if
10         continue
     return
     end
```

```
subroutine linter(NN,T,A,DT,NG,G)
c    This subroutine interpolates linearly between uneven sample points.
c    The interpolated data are then generated at a specified sample interval
c
c    declaration of parameters
     integer NN,NG
     real T(0:12000),A(0:12000),DT,G(0:16384)
c    declaration of local variables
     integer J,K
     real S
c
     NG=int((T(NN-1)-T(0))/DT)+1
     G(0)=A(0)
     J=0
     do 50 K=1,NG-1
55         if(K*DT.lt.T(J+1))then
           S=K*DT-T(J)
           G(K)=A(J)+S*(A(J+1)-A(J))/(T(J+1)-T(J))
           else
           J=J+1
           goto55
           end if
50         continue
     return
     end
```

APPENDIX (H): Non-linear Time History Analysis Experimental Confirmation

****

Program ROWMANRY .
For time history rocking analysis of
Free Standing or Simply Supported Objects
Latest Version : FEBRUARY 1999

****

Accelerogram data from 1 Hz 16mm Amplitude Pulse
Accelerogram scaling factor selected = 1.000
INPUT DATA SUMMARY FOR:
SS non- loadbearing base reaction at LF
Height of object = 1.500 m
Object width = 110.000 mm
Overburden stress at top of object = 0.000 MPa

Trilinear force disp profile data
Δ(1) selected for initial stiffness = 7.00 mm
Δ(2) selected for maximum force plateau = 33.00 mm

Stiffness coefficient (HEFFS) = 4.0
Resistance coefficient (HEFFR) = 4.0

Proportional damping data
Mass proportional damping coeff. = 1.5000
Stiffness proportional damping coeff. = 0.0050

ANALYSIS CONCLUSION : Model rocked within limits
Analysis time = 4.0100secs time inc =.0100secs

Legend:
ag = input ground acceleration u = relative displacement
v = relative velocity at = total acceleration

Time	$a_g(t)$ (m/s^2)	Δ(t) (m)	v(t) (m/s)	a(t) (m/s^2)
Maximum	3.545	0.038978	0.471	3.6385

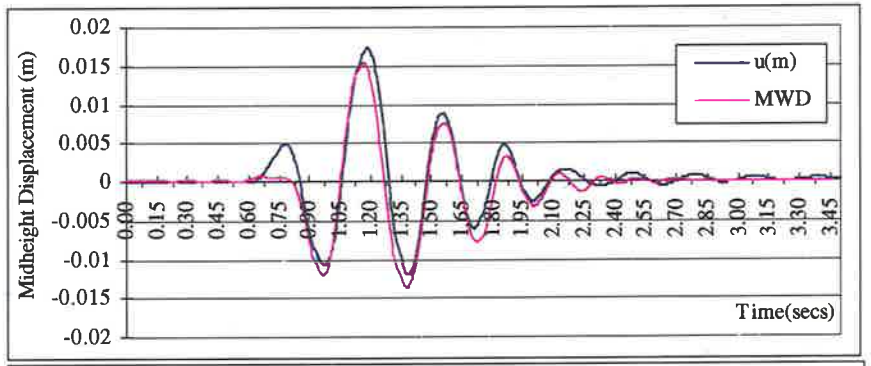

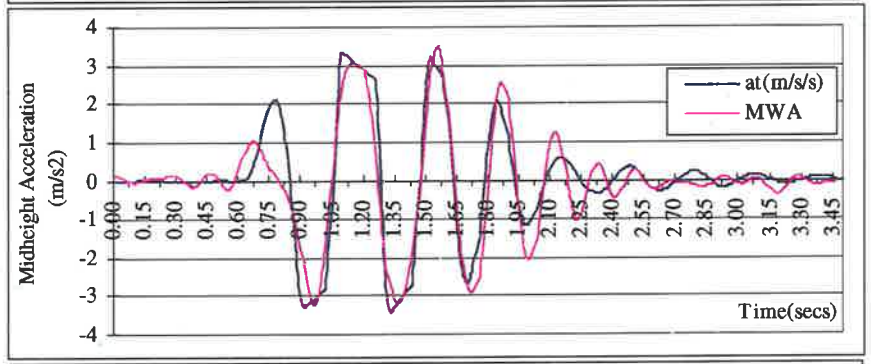

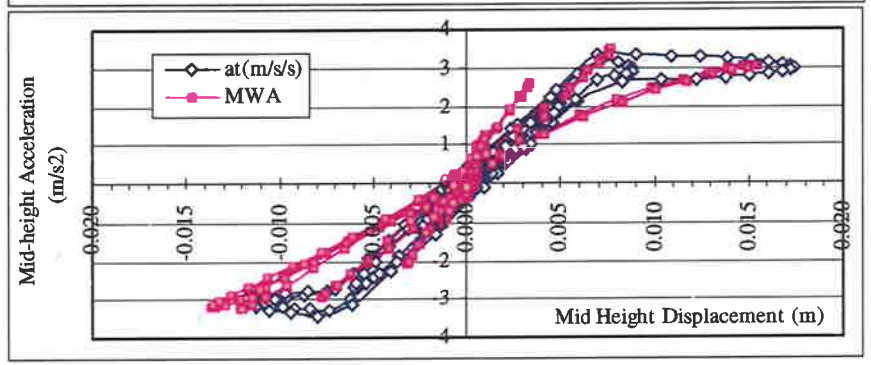

****

Program ROWMANRY
For time history rocking analysis of
Free Standing or Simply Supported Objects
Latest Version : FEBRUARY 1999

****

Accelerogram data from 1 Hz 24mm Amplitude Pulse
Accelerogram scaling factor selected = 1.000
INPUT DATA SUMMARY FOR:
SS non- loadbearing base reaction at LF
Height of object = 1.500 m
Object width = 110.000 mm
Overburden stress at top of object = 0.000 MPa

Trilinear force disp profile data
Δ(1) selected for initial stiffness = 7.00 mm
Δ(2) selected for maximum force plateau = 33.00 mm

Stiffness coefficient (HEFFS) = 4.0
Resistance coefficient (HEFFR) = 4.0

Proportional damping data
Mass proportional damping coeff. = 1.4000
Stiffness proportional damping coeff. = 0.0040

ANALYSIS CONCLUSION : Model rocked within limits
Analysis time = 4.0100secs time inc =.0100secs

Legend:
ag = input ground acceleration u = relative displacement
v = relative velocity at = total acceleration

Time	$a_g(t)$ (m/s^2)	Δ(t) (m)	v(t) (m/s)	a(t) (m/s^2)
Maximum	3.545	0.038978	0.471	3.6385

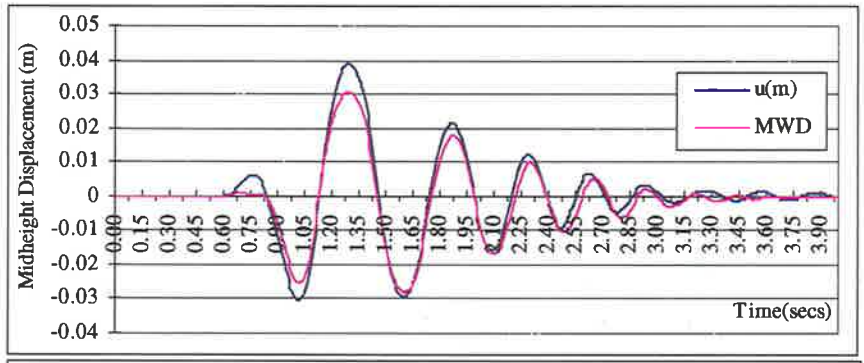

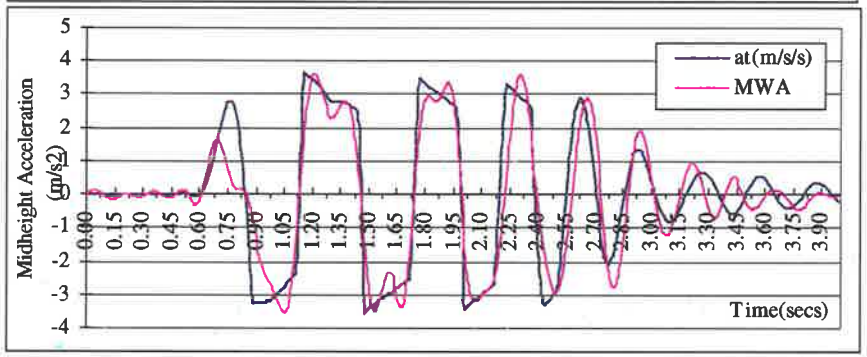

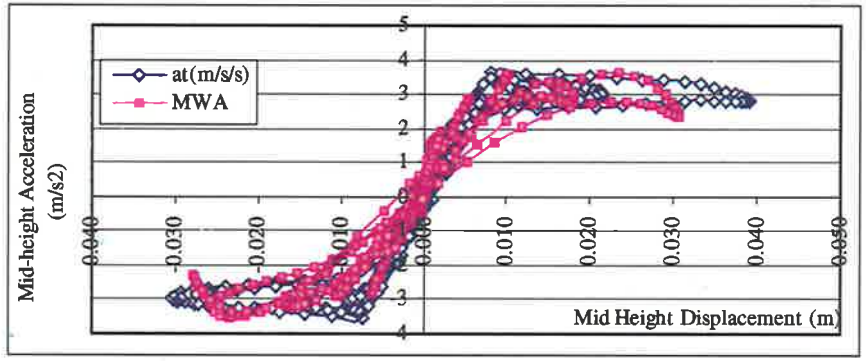

****

Program ROWMANRY
For time history rocking analysis of
Free Standing or Simply Supported Objects
Latest Version : FEBRUARY 1999

****

Accelerogram data from 1 Hz 37mm Amplitude Pulse
Accelerogram scaling factor selected = 1.000
INPUT DATA SUMMARY FOR:
SS non- loadbearing base reaction at LF
Height of object = 1.500 m
Object width = 110.000 mm
Overburden stress at top of object = 0.000 MPa

Trilinear force disp profile data
Δ(1) selected for initial stiffness = 5.50 mm
Δ(2) selected for maximum force plateau = 25.00 mm

Stiffness coefficient (HEFFS) = 4.0
Resistance coefficient (HEFFR) = 4.0

Proportional damping data
Mass proportional damping coeff. = 1.5000
Stiffness proportional damping coeff. = 0.0050

ANALYSIS CONCLUSION : Model rocked within limits
Analysis time = 4.0100secs time inc =.0100secs

Legend:
ag = input ground acceleration u = relative displacement
v = relative velocity at = total acceleration

Time	$a_g(t)$ (m/s^2)	Δ(t) (m)	v(t) (m/s)	a(t) (m/s^2)
Maximum	7.516	0.073902	0.613	4.0328

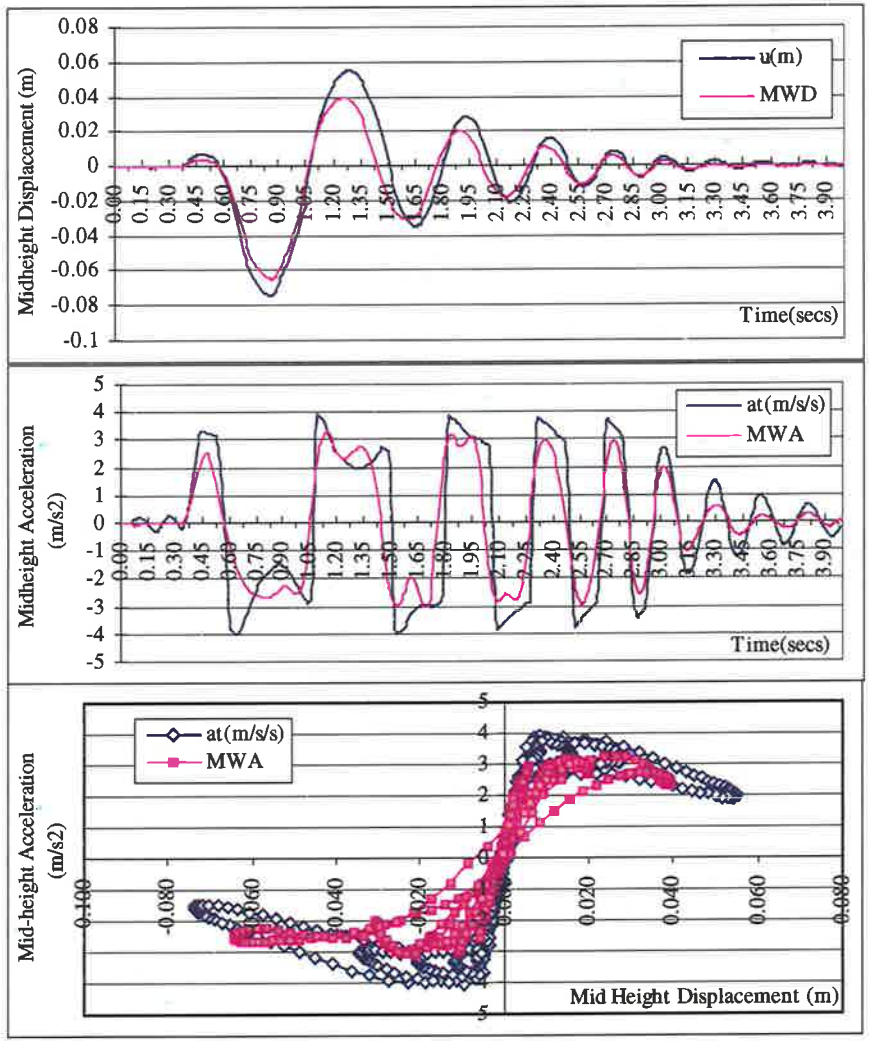

****

Program ROWMANRY
For time history rocking analysis of
Free Standing or Simply Supported Objects
Latest Version : FEBRUARY 1999

****

Accelerogram data from ½ Hz 40mm Amplitude Pulse
Accelerogram scaling factor selected = 1.000
INPUT DATA SUMMARY FOR:
SS loadbearing top & bottom reaction at LF
Height of object = 1.500 m
Object width = 50.000 mm
Overburden stress at top of object = 0.075 MPa

Trilinear force disp profile data
Δ(1) selected for initial stiffness = 5.00 mm
Δ(2) selected for maximum force plateau = 15.00 mm

Stiffness coefficient (HEFFS) = 21.735
Resistance coefficient (HEFFR) = 21.735

Proportional damping data
Mass proportional damping coeff. = 3.0000
Stiffness proportional damping coeff. = 0.0060

ANALYSIS CONCLUSION : Model rocked within limits
Analysis time = 3.0100secs time inc =.0100secs

Legend:
ag = input ground acceleration u = relative displacement
v = relative velocity at = total acceleration

Time	$a_g(t)$ (m/s^2)	Δ(t) (m)	v(t) (m/s)	a(t) (m/s^2)
Maximum	4.78	0.005211	0.202	7.6747

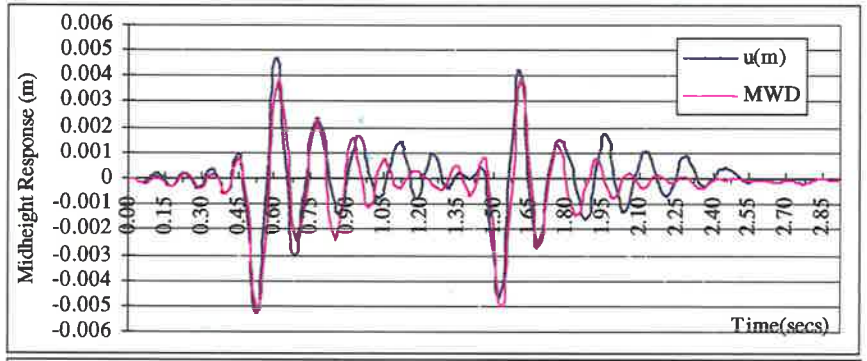

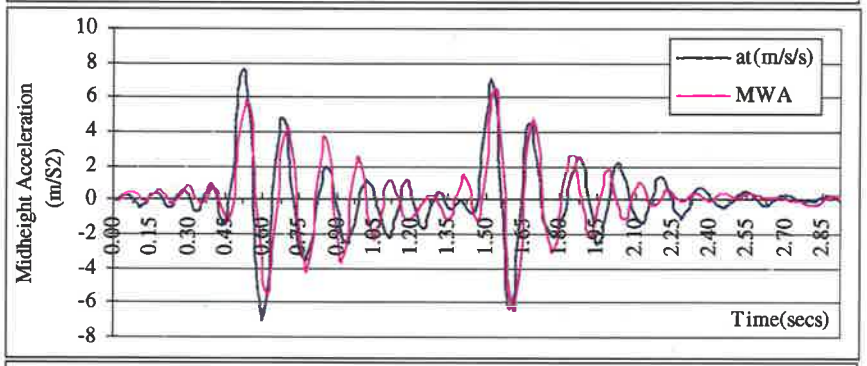

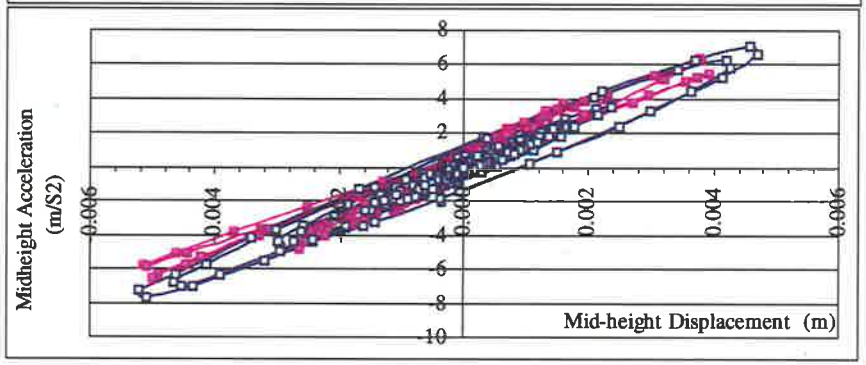

****

Program ROWMANRY
For time history rocking analysis of
Free Standing or Simply Supported Objects
Latest Version : FEBRUARY 1999

****

Accelerogram data from ½ Hz 60mm Amplitude Pulse
Accelerogram scaling factor selected = 1.000
INPUT DATA SUMMARY FOR:
SS loadbearing top & bottom reaction at LF
Height of object = 1.500 m
Object width = 50.000 mm
Overburden stress at top of object = 0.075 MPa

Trilinear force disp profile data
Δ(1) selected for initial stiffness = 5.00 mm
Δ(2) selected for maximum force plateau = 15.00 mm

Stiffness coefficient (HEFFS) = 21.735
Resistance coefficient (HEFFR) = 21.735

Proportional damping data
Mass proportional damping coeff. = 3.0000
Stiffness proportional damping coeff. = 0.0060

ANALYSIS CONCLUSION : Model rocked within limits
Analysis time = 3.5100secs time inc =.0100secs

Legend:
ag = input ground acceleration u = relative displacement
v = relative velocity at = total acceleration

Time	$a_g(t)$ (m/s^2)	Δ(t) (m)	v(t) (m/s)	a(t) (m/s^2)
Maximum	6.398	0.007558	0.285	8.3396

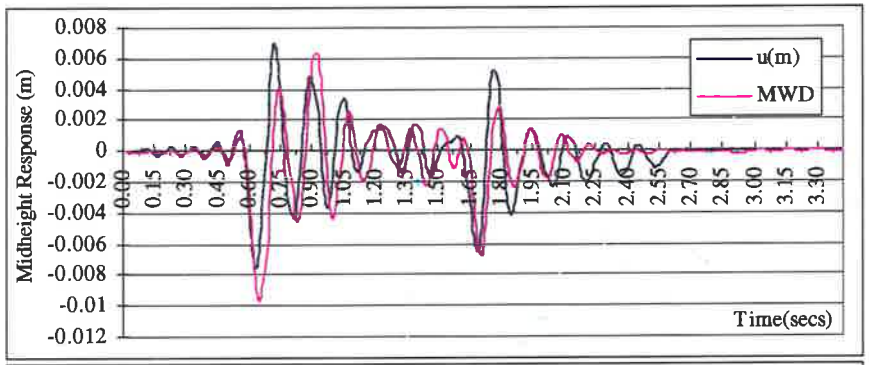

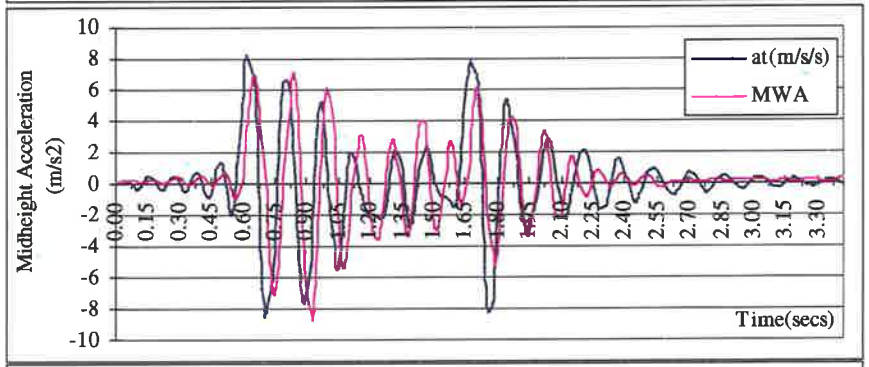

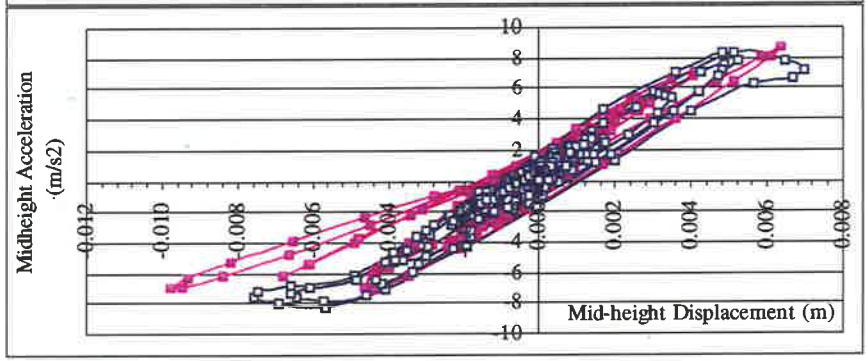

****
Program ROWMANRY
For time history rocking analysis of
Free Standing or Simply Supported Objects
Latest Version : FEBRUARY 1999
****

Accelerogram data from 1 Hz 30mm Amplitude Pulse
Accelerogram scaling factor selected = 1.000
INPUT DATA SUMMARY FOR:
SS loadbearing top & bottom reaction at LF
Height of object = 1.500 m
Object width = 50.000 mm
Overburden stress at top of object = 0.075 MPa

Trilinear force disp profile data
Δ(1) selected for initial stiffness = 4.75 mm
Δ(2) selected for maximum force plateau = 14.00 mm

Stiffness coefficient (HEFFS) = 21.735
Resistance coefficient (HEFFR) = 21.735

Proportional damping data
Mass proportional damping coeff. = 3.0000
Stiffness proportional damping coeff. = 0.0060

ANALYSIS CONCLUSION : Model rocked within limits
Analysis time = 2.0100secs time inc =.0100secs

Legend:
ag = input ground acceleration u = relative displacement
v = relative velocity at = total acceleration

Time	$a_g(t)$ (m/s^2)	Δ(t) (m)	v(t) (m/s)	a(t) (m/s^2)
Maximum	5.839	0.008718	0.283	9.4562

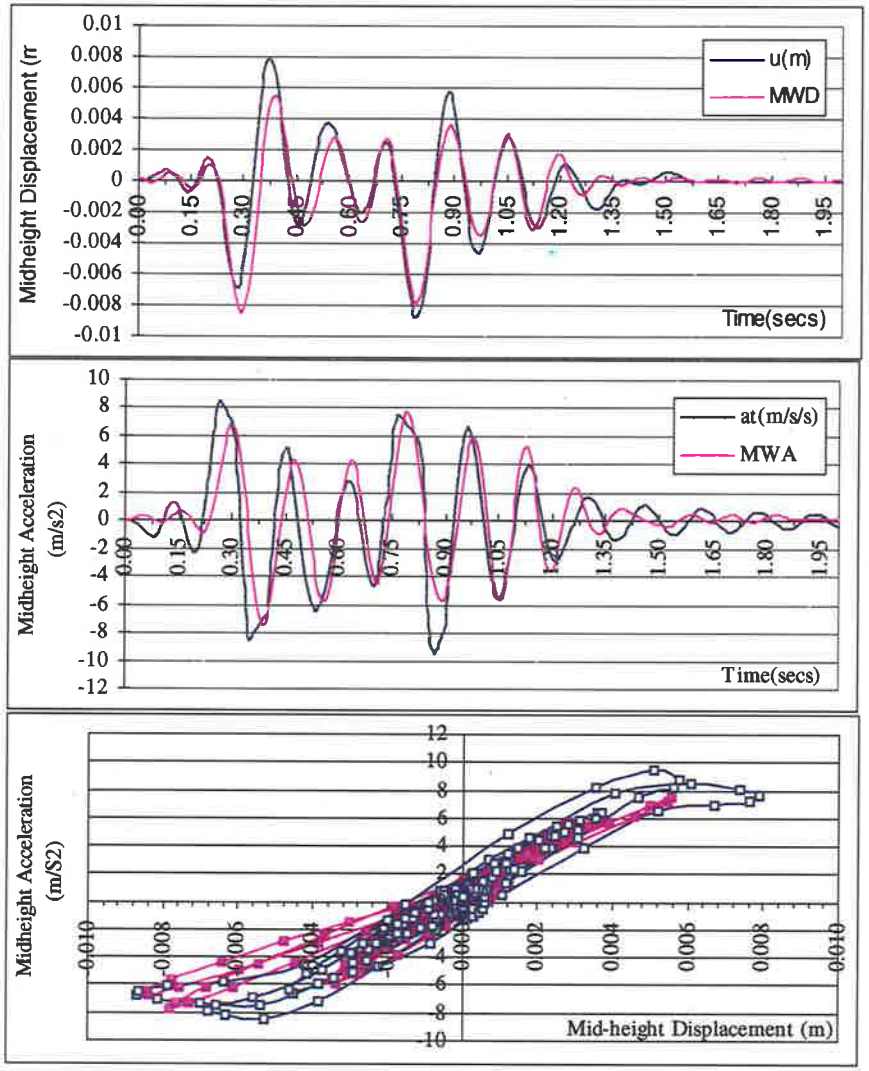

****

Program ROWMANRY
For time history rocking analysis of
Free Standing or Simply Supported Objects
Latest Version : FEBRUARY 1999

****

Accelerogram data from 1 Hz 50mm Amplitude Pulse
Accelerogram scaling factor selected = 1.000
INPUT DATA SUMMARY FOR:
SS loadbearing top & bottom reaction at LF
Height of object = 1.500 m
Object width = 50.000 mm
Overburden stress at top of object = 0.075 MPa

Trilinear force disp profile data
Δ(1) selected for initial stiffness = 4.75 mm
Δ(2) selected for maximum force plateau = 13.50 mm

Stiffness coefficient (HEFFS) = 21.735
Resistance coefficient (HEFFR) = 21.735

Proportional damping data
Mass proportional damping coeff. = 3.0000
Stiffness proportional damping coeff. = 0.0025

ANALYSIS CONCLUSION : Model rocked within limits
Analysis time = 3.9400secs time inc =.0100secs

Legend:
ag = input ground acceleration u = relative displacement
v = relative velocity at = total acceleration

Time	$a_g(t)$ (m/s^2)	Δ(t) (m)	v(t) (m/s)	a(t) (m/s^2)
Maximum	8.531	0.030496	0.575	9.2466

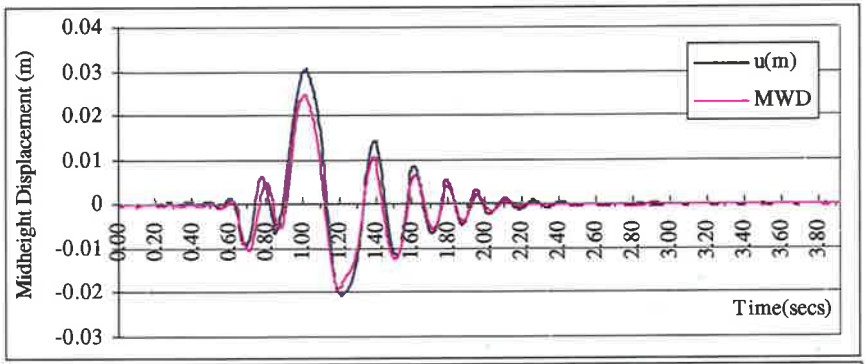

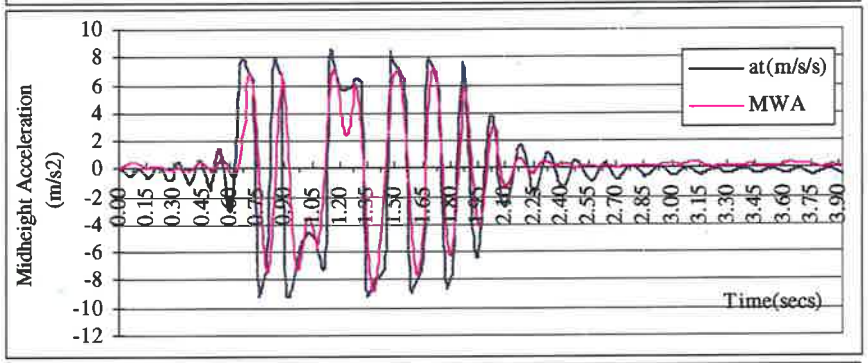

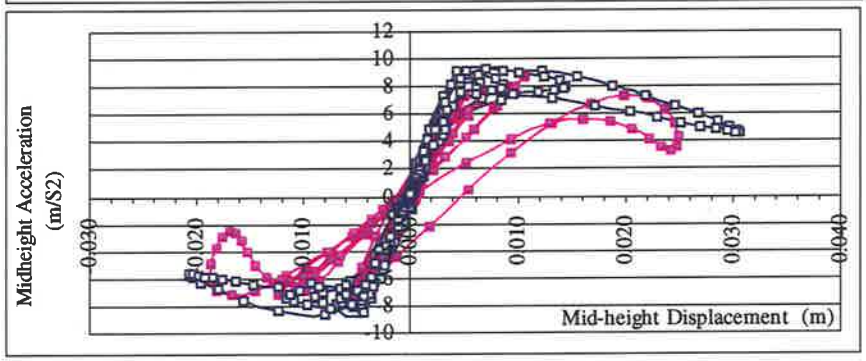

****

Program ROWMANRY
For time history rocking analysis of
Free Standing or Simply Supported Objects
Latest Version : FEBRUARY 1999

****

Accelerogram data from 2 Hz 15mm Amplitude Pulse
Accelerogram scaling factor selected = 1.000
INPUT DATA SUMMARY FOR:
SS loadbearing top & bottom reaction at LF
Height of object = 1.500 m
Object width = 50.000 mm
Overburden stress at top of object = 0.075 MPa

Trilinear force disp profile data
Δ(1) selected for initial stiffness = 4.75 mm
Δ(2) selected for maximum force plateau = 13.50 mm

Stiffness coefficient (HEFFS) = 21.735
Resistance coefficient (HEFFR) = 21.735

Proportional damping data
Mass proportional damping coeff. = 3.0000
Stiffness proportional damping coeff. = 0.0060

ANALYSIS CONCLUSION : Model rocked within limits
Analysis time = 2.2100secs time inc =.0100secs

Legend:
ag = input ground acceleration u = relative displacement
v = relative velocity at = total acceleration

Time	$a_g(t)$ (m/s^2)	Δ(t) (m)	v(t) (m/s)	a(t) (m/s^2)
Maximum	6.972	0.023191	0.479	10.1605

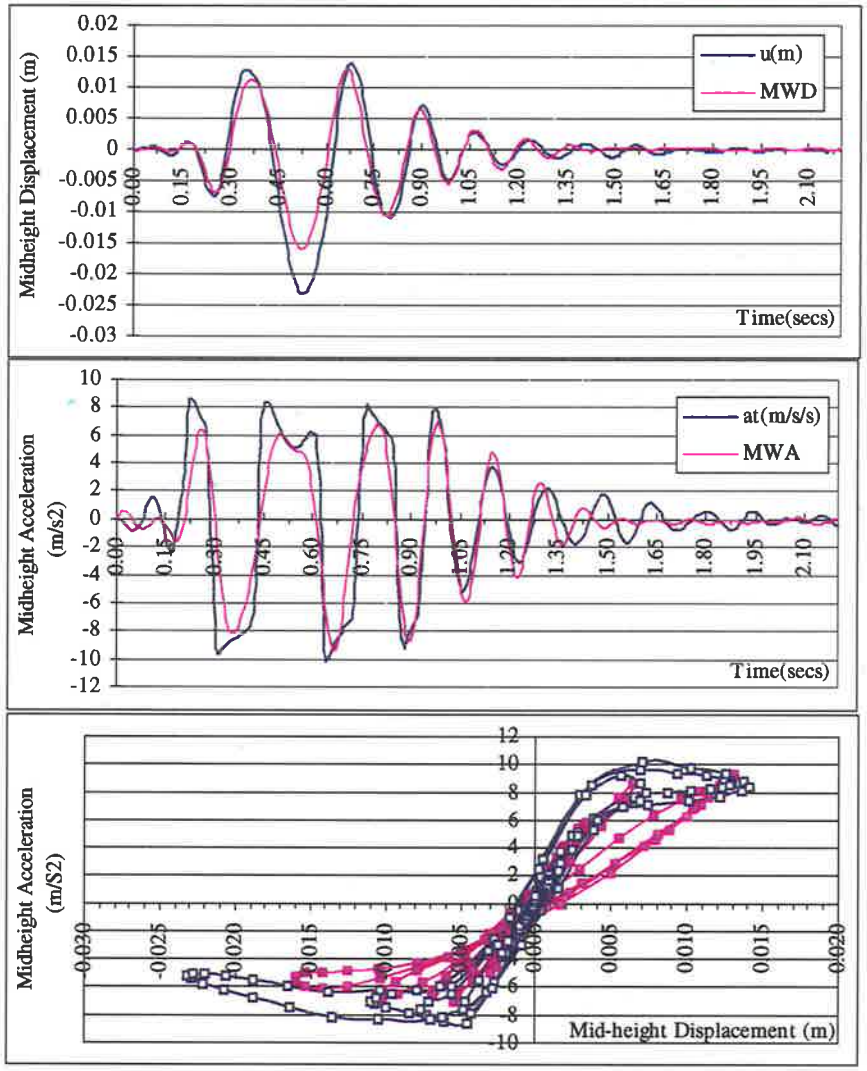

****

Program ROWMANRY
For time history rocking analysis of
Free Standing or Simply Supported Objects
Latest Version : FEBRUARY 1999

****

Accelerogram data from 1 Hz 30mm Amplitude Pulse
Accelerogram scaling factor selected = 1.000
INPUT DATA SUMMARY FOR:
SS loadbearing top & bottom reaction at LF
Height of object = 1.500 m
Object width = 50.000 mm
Overburden stress at top of object = 0.15 MPa

Trilinear force disp profile data
Δ(1) selected for initial stiffness = 7 mm
Δ(2) selected for maximum force plateau = 21 mm

Stiffness coefficient (HEFFS) = 39.471
Resistance coefficient (HEFFR) = 39.471

Proportional damping data
Mass proportional damping coeff. = 2.0000
Stiffness proportional damping coeff. = 0.0050

ANALYSIS CONCLUSION : Model rocked within limits
Analysis time = 1.6600secs time inc =.0100secs

Legend:
ag = input ground acceleration u = relative displacement
v = relative velocity at = total acceleration

Time	$a_g(t)$ (m/s^2)	Δ(t) (m)	v(t) (m/s)	a(t) (m/s^2)
Maximum	6.266	0.008301	0.306	12.0173

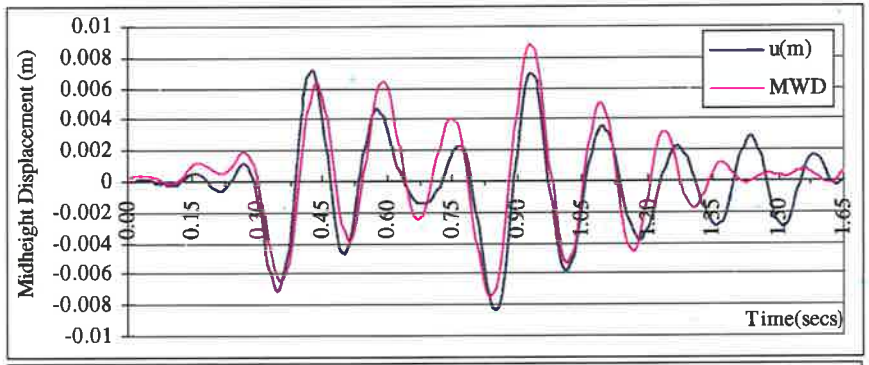

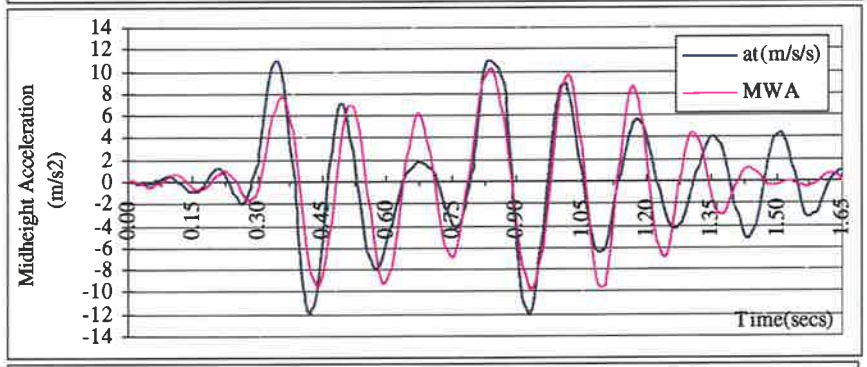

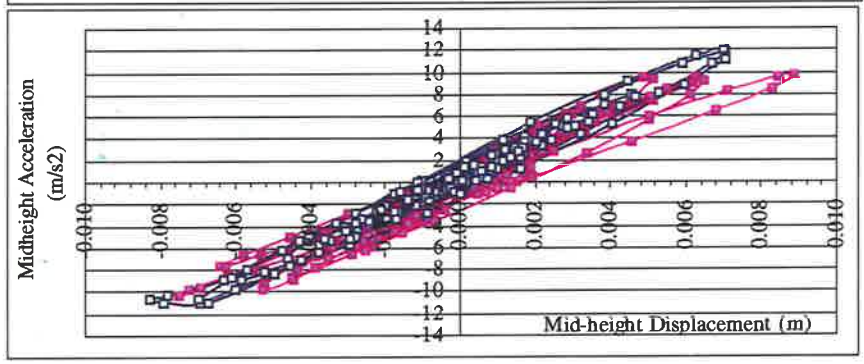

****

Program ROWMANRY
For time history rocking analysis of
Free Standing or Simply Supported Objects
Latest Version : FEBRUARY 1999

****

Accelerogram data from 1 Hz 50mm Amplitude Pulse
Accelerogram scaling factor selected = 1.000
INPUT DATA SUMMARY FOR:
SS loadbearing top & bottom reaction at LF
Height of object = 1.500 m
Object width = 50.000 mm
Overburden stress at top of object = 0.15 MPa

Trilinear force disp profile data
Δ(1) selected for initial stiffness = 8 mm
Δ(2) selected for maximum force plateau = 23 mm

Stiffness coefficient (HEFFS) = 39.471
Resistance coefficient (HEFFR) = 39.471

Proportional damping data
Mass proportional damping coeff. = 2.0000
Stiffness proportional damping coeff. = 0.0050

ANALYSIS CONCLUSION : Model rocked within limits
Analysis time = 2.0500secs time inc =.0100secs

Legend:
ag = input ground acceleration u = relative displacement
v = relative velocity at = total acceleration

Time	$a_g(t)$ (m/s^2)	Δ(t) (m)	v(t) (m/s)	a(t) (m/s^2)
Maximum	7.487	0.020974	0.535	12.966

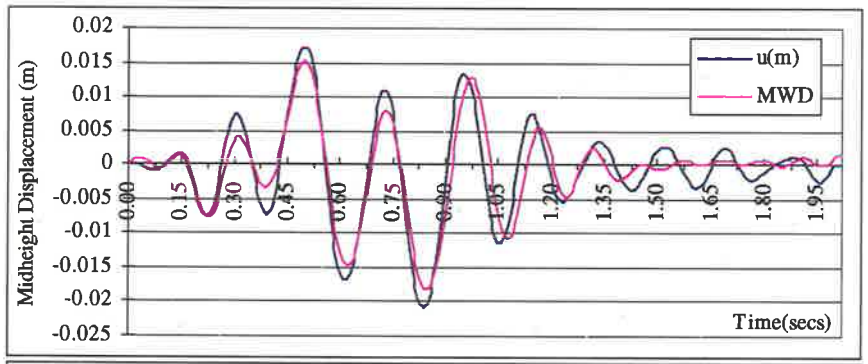

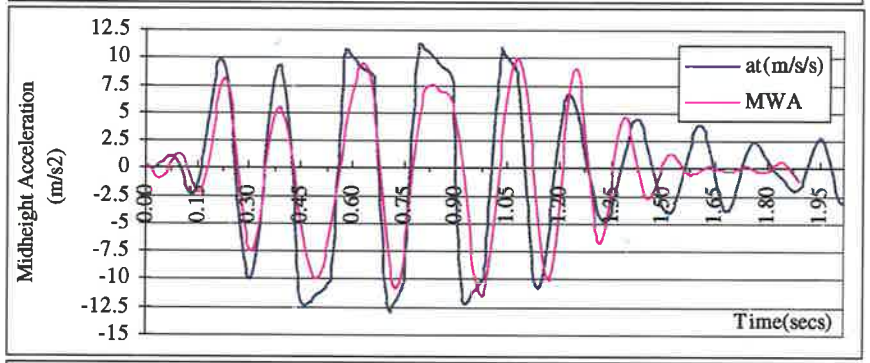

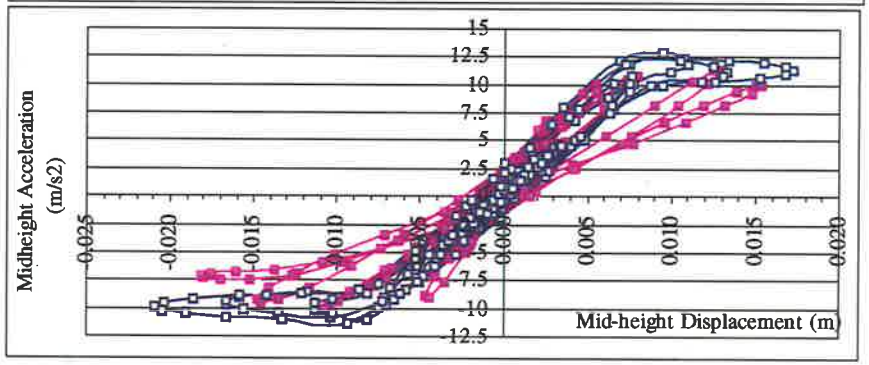

****

Program ROWMANRY
For time history rocking analysis of
Free Standing or Simply Supported Objects
Latest Version : FEBRUARY 1999

****

Accelerogram data from 2 Hz 20mm Amplitude Pulse
Accelerogram scaling factor selected = 1.000
INPUT DATA SUMMARY FOR:
SS loadbearing top & bottom reaction at LF
Height of object = 1.500 m
Object width = 50.000 mm
Overburden stress at top of object = 0.15 MPa

Trilinear force disp profile data
Δ(1) selected for initial stiffness = 7.2 mm
Δ(2) selected for maximum force plateau = 23 mm

Stiffness coefficient (HEFFS) = 39.471
Resistance coefficient (HEFFR) = 39.471

Proportional damping data
Mass proportional damping coeff. = 2.0000
Stiffness proportional damping coeff. = 0.0060

ANALYSIS CONCLUSION : Model rocked within limits
Analysis time = 1.7600secs time inc =.0100secs

Legend:
ag = input ground acceleration u = relative displacement
v = relative velocity at = total acceleration

Time	$a_g(t)$ (m/s^2)	Δ(t) (m)	v(t) (m/s)	a(t) (m/s^2)
Maximum	7.605	0.020093	0.567	12.532

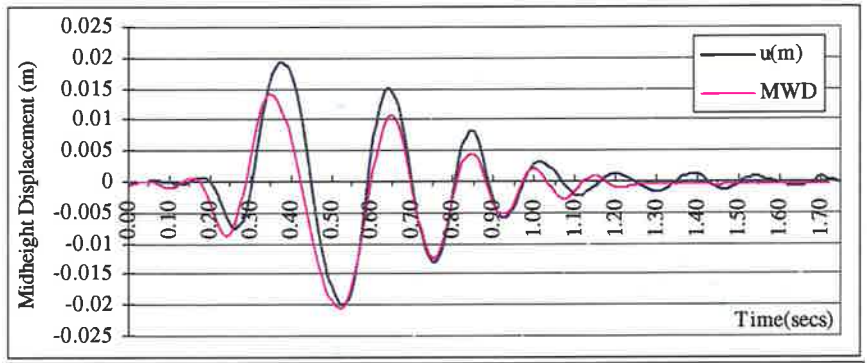

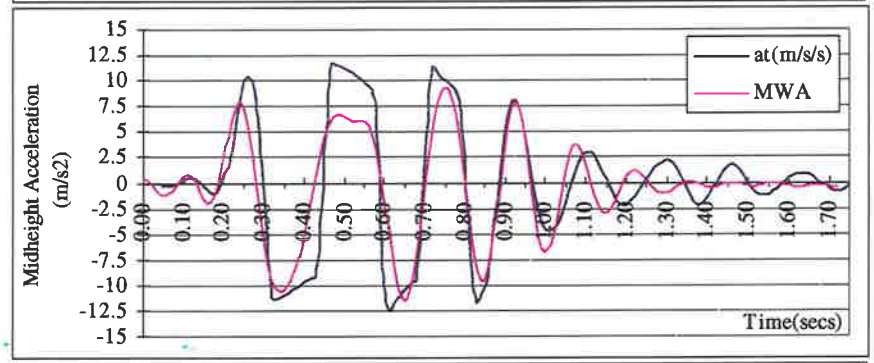

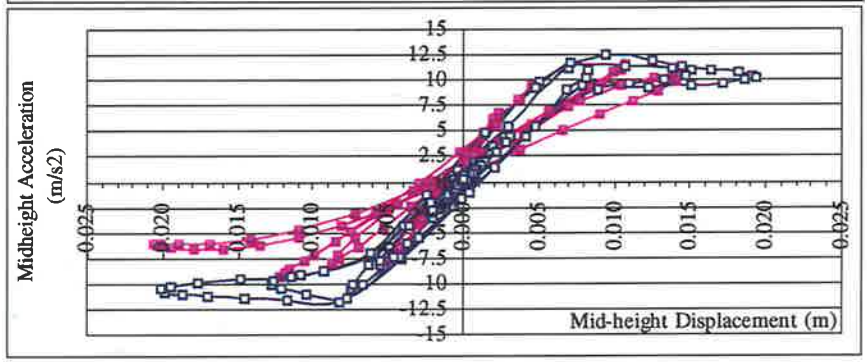

****

Program ROWMANRY
For time history rocking analysis of
Free Standing or Simply Supported Objects
Latest Version : FEBRUARY 1999

****

Accelerogram data from 80% Pacioma Dam E/Q
Accelerogram scaling factor selected = 1.000
INPUT DATA SUMMARY FOR:
SS non- loadbearing base reaction at LF
Height of object = 1.500 m
Object width = 110.000 mm
Overburden stress at top of object = 0.000 MPa

Trilinear force disp profile data
Δ(1) selected for initial stiffness = 15.00 mm
Δ(2) selected for maximum force plateau = 35.00 mm

Stiffness coefficient (HEFFS) = 4.0
Resistance coefficient (HEFFR) = 4.0

Proportional damping data
Mass proportional damping coeff. = 1.000
Stiffness proportional damping coeff. = 0.0030

ANALYSIS CONCLUSION : Model rocked within limits
Analysis time = 34.9600secs time inc =.0100secs

Legend:
ag = input ground acceleration u = relative displacement
v = relative velocity at = total acceleration

Time	$a_g(t)$ (m/s^2)	Δ(t) (m)	v(t) (m/s)	a(t) (m/s^2)
Maximum	3.545	0.038978	0.471	3.6385

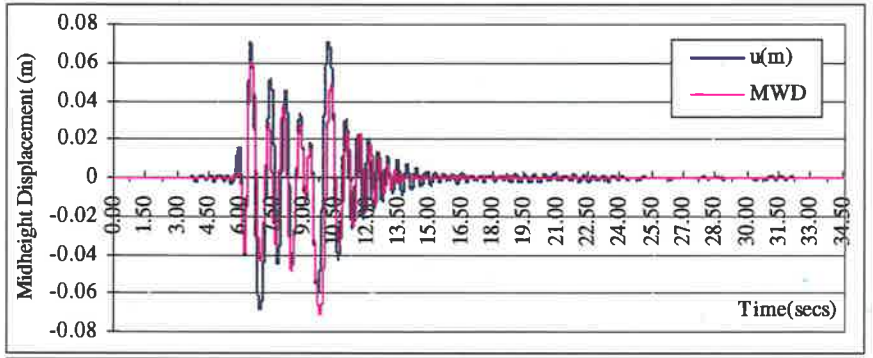

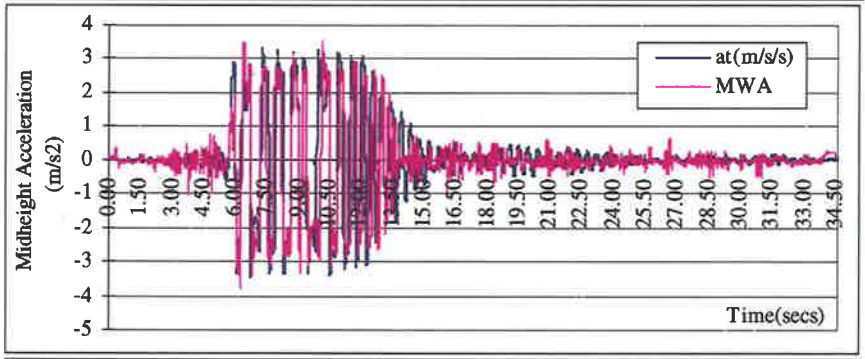

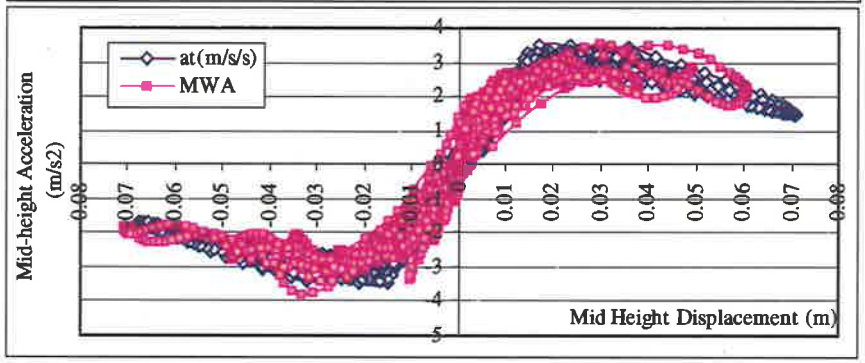

****

Program ROWMANRY
For time history rocking analysis of
Free Standing or Simply Supported Objects
Latest Version : FEBRUARY 1999

****

Accelerogram data from 50% Pacioma Dam E/Q
Accelerogram scaling factor selected = 1.000
INPUT DATA SUMMARY FOR:
SS non- loadbearing base reaction at LF
Height of object = 1.500 m
Object width = 110.000 mm
Overburden stress at top of object = 0.000 MPa

Trilinear force disp profile data
Δ(1) selected for initial stiffness = 12.00 mm
Δ(2) selected for maximum force plateau = 35.00 mm

Stiffness coefficient (HEFFS) = 4.0
Resistance coefficient (HEFFR) = 4.0

Proportional damping data
Mass proportional damping coeff. = 1.500
Stiffness proportional damping coeff. = 0.0050

ANALYSIS CONCLUSION : Model rocked within limits
Analysis time = 34.9600secs time inc =.0100secs

Legend:
ag = input ground acceleration u = relative displacement
v = relative velocity at = total acceleration

Time	$a_g(t)$ (m/s^2)	Δ(t) (m)	v(t) (m/s)	a(t) (m/s^2)
Maximum	3.059	0.044787	0.453	3.521

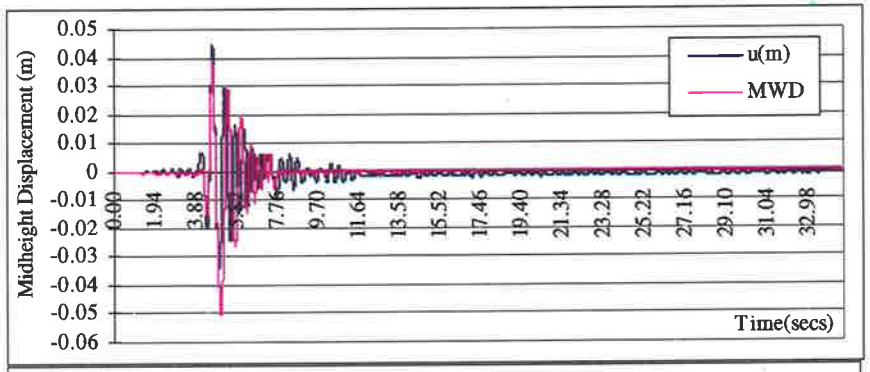

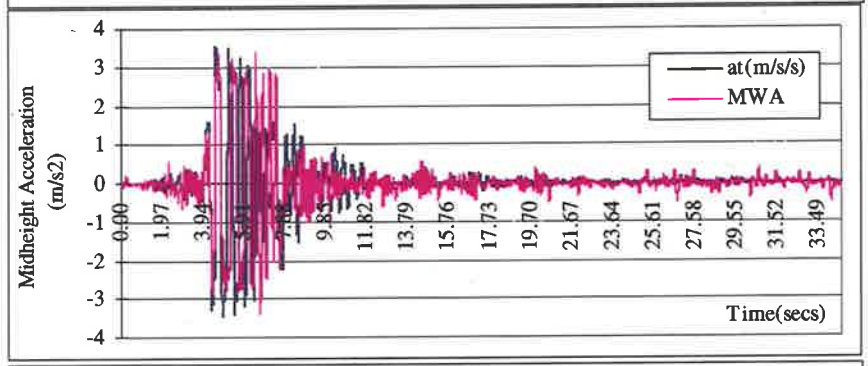

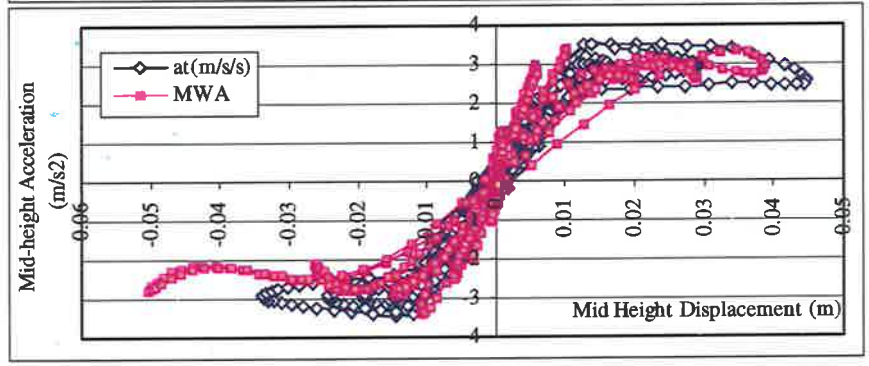

****
Program ROWMANRY
For time history rocking analysis of
Free Standing or Simply Supported Objects
Latest Version : FEBRUARY 1999
****

Accelerogram data from 66% ElCentro E/Q
Accelerogram scaling factor selected = 1.000
INPUT DATA SUMMARY FOR:
SS non- loadbearing base reaction at LF
Height of object = 1.500 m
Object width = 110.000 mm
Overburden stress at top of object = 0.000 MPa

Trilinear force disp profile data
Δ(1) selected for initial stiffness = 15.00 mm
Δ(2) selected for maximum force plateau = 35.00 mm

Stiffness coefficient (HEFFS) = 4.0
Resistance coefficient (HEFFR) = 4.0

Proportional damping data
Mass proportional damping coeff. = 1.750
Stiffness proportional damping coeff. = 0.0060

ANALYSIS CONCLUSION : Model rocked beyond limits
Analysis time = 22.4600secs time inc =.0100secs

Legend:
ag = input ground acceleration u = relative displacement
v = relative velocity at = total acceleration

Time	$a_g(t)$ (m/s^2)	Δ(t) (m)	v(t) (m/s)	a(t) (m/s^2)
Maximum	3.986	Failed	0.706	4.0053

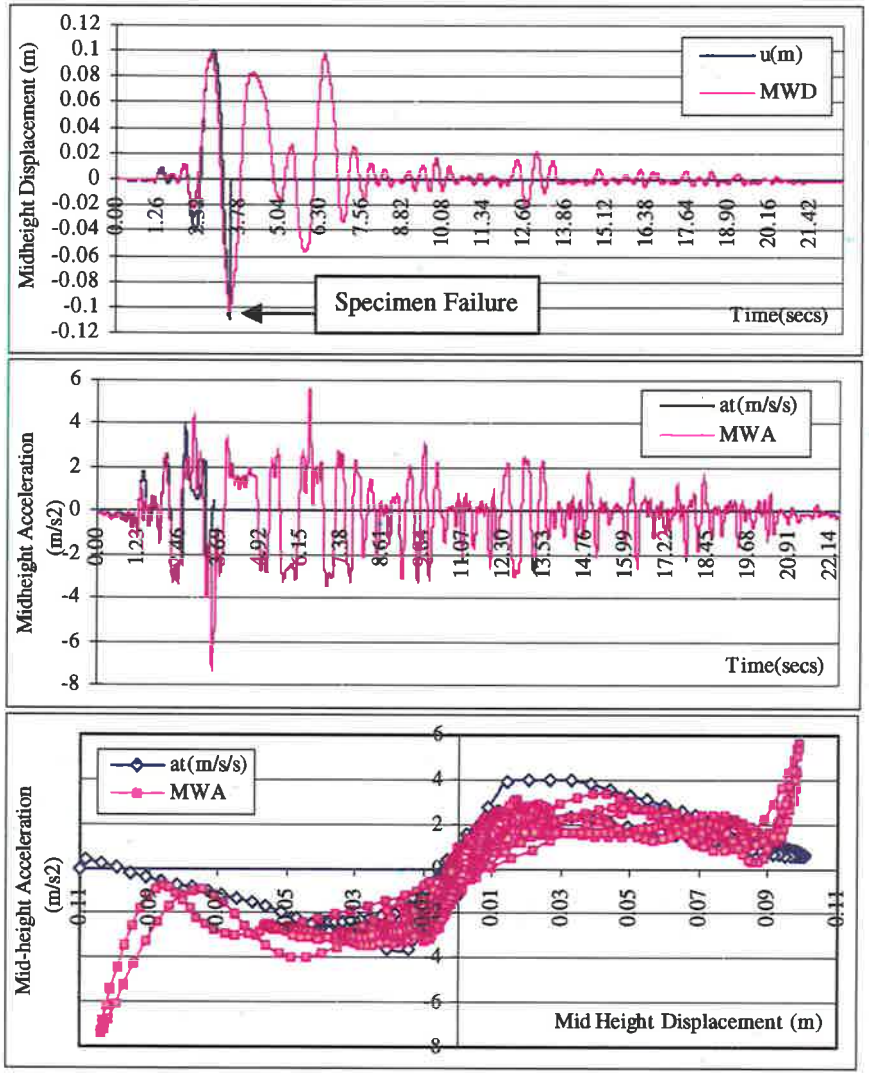

****

Program ROWMANRY
For time history rocking analysis of
Free Standing or Simply Supported Objects
Latest Version : FEBRUARY 1999

****

Accelerogram data from 100% Nahanni Aftershock
Accelerogram scaling factor selected = 1.000
INPUT DATA SUMMARY FOR:
SS non- loadbearing base reaction at LF
Height of object = 1.500 m
Object width = 110.000 mm
Overburden stress at top of object = 0.000 MPa

Trilinear force disp profile data
Δ(1) selected for initial stiffness = 5.00 mm
Δ(2) selected for maximum force plateau = 25.00 mm

Stiffness coefficient (HEFFS) = 4.0
Resistance coefficient (HEFFR) = 4.0

Proportional damping data
Mass proportional damping coeff. = 4.000
Stiffness proportional damping coeff. = 0.0060

ANALYSIS CONCLUSION : Model rocked within limits
Analysis time = 12.4200secs time inc =.0100secs

Legend:
ag = input ground acceleration u = relative displacement
v = relative velocity at = total acceleration

Time	$a_g(t)$ (m/s^2)	Δ(t) (m)	v(t) (m/s)	a(t) (m/s^2)
Maximum	6.413	0.012088	0.248	4.6692